Issue

Alert me when new journal issues are available. Add TOC Alert

November 2003 (Vol. 41, Issue 6)

previous issue | next issue

Imaging of the Acute Abdomen
Guest Editor: E.J. Balthazar

View Selected Abstracts Display: without preview

CONTENTS
pages v-viii
PDF (28 KB)

Forthcoming Issues
page ix
PDF (18 KB)

Preface

Imaging of the acute abdomen
by Balthazar EJ
pages xi-xii
Full Text | PDF (51 KB)

Impact of multislice CT on imaging of acute abdominal disease
by Kundra V, Silverman PM
pages 1083-1093
Full Text | PDF (413 KB)

Radiologic diagnosis of gastrointestinal perforation
by Rubesin SE, Levine MS
pages 1095-1115
Full Text | PDF (1077 KB)

The acute right lower quadrant: CT evaluation
by Macari M, Balthazar EJ
pages 1117-1136
Full Text | PDF (1541 KB)

Adult intussusception: Diagnosis and clinical relevance
by Huang BY, Warshauer DM
pages 1137-1151
Full Text | PDF (710 KB)

CT of acute abdominal aortic disorders
by Bhalla S, Menias CO, Heiken JP
pages 1153-1169
Full Text | PDF (763 KB)

Blunt injury to mesentery and small bowel:: CT evaluation
by Hanks PW, Brody JM
pages 1171-1182
Full Text | PDF (603 KB)

Spontaneous intraperitoneal hemorrhage: Imaging features
by Mortele KJ, Cantisani V, Brown DL, Ros PR
pages 1183-1201
Full Text | PDF (1230 KB)

- **Ultrasound and CT evaluation of emergent gallbladder pathology**
  by Bennett GL, Balthazar EJ
  pages 1203-1216
  Full Text | PDF (1153 KB)
- **Interventional approach to pancreatic fluid collections**
  by Ferrucci JT, Mueller PR
  pages 1217-1226
  Full Text | PDF (833 KB)
- **Ultrasonography of the acute abdomen: Gastrointestinal conditions**
  by Puylaert JBCM
  pages 1227-1242
  Full Text | PDF (1423 KB)
- **MR imaging in abdominal emergencies**
  by Pedrosa I, Rofsky NM
  pages 1243-1273
  Full Text | PDF (1376 KB)
- **Selective role of nuclear medicine in evaluating the acute abdomen**
  by Zuckier LS, Freeman LM
  pages 1275-1288
  Full Text | PDF (845 KB)
- **Complications of liver transplantation:: imaging and intervention**
  by Federle MP, Kapoor V
  pages 1289-1305
  Full Text | PDF (1140 KB)
- **Cumulative Index 2003**
  pages 1307-1335
  PDF (155 KB)

View Selected Abstracts

Display: without preview

Current Issue

Alert me when new journal issues are available. Add TOC Alert

January 2004 (Vol. 42, Issue 1) previous issue

Arthritis Imaging

Guest Editor: B.N. Weissman

View Selected Abstracts Display: without preview

CONTENTS
pages v-viii
PDF (28 KB)

FORTHCOMING ISSUES
page ix
PDF (19 KB)

Preface

Arthritis imaging
by Weissman BN
page xi
Full Text | PDF (121 KB)

An update on the pathogenesis and epidemiology of osteoarthritis
by Felson DT
pages 1-9
Full Text | PDF (266 KB)

Radiographic evaluation of osteoarthritis
by Gupta KB, Duryea J, Weissman BN
pages 11-41
Full Text | PDF (1516 KB)

MR imaging for surgical planning and postoperative assessment in early osteoarthritis
by Azer NM, Winalski CS, Minas T
pages 43-60
Full Text | PDF (1238 KB)

MR imaging of the diabetic foot
by Schweitzer ME, Morrison WB
pages 61-71
Full Text | PDF (694 KB)

Cysts, geodes, and erosions
by Bancroft LW, Peterson JJ, Kransdorf MJ
pages 73-87
Full Text | PDF (760 KB)

Advanced imaging of early rheumatoid arthritis
by Tehranzadeh J, Ashikyan O, Dascalos J
pages 89-107
Full Text | PDF (1083 KB)

Measurement of structural abnormalities in arthritis using radiographic images
by Sharp JT
pages 109-119
Full Text | PDF (353 KB)

- **Spondyloarthropathies: ankylosing spondylitis and psoriatic arthritis**
  by Bennett D L, Ohashi K, El-Khoury GY
  pages 121-134
  Full Text | PDF (792 KB)
- **Monoarticular arthritis**
  by Mohana-Borges AVR, Chung CB, Resnick D
  pages 135-149
  Full Text | PDF (692 KB)
- **Imaging of articular disorders in children**
  by Buchmann RF, Jaramillo D
  pages 151-168
  Full Text | PDF (1742 KB)
- **Gout: a clinical and radiologic review**
  by Monu JU V, Pope TL
  pages 169-184
  Full Text | PDF (766 KB)
- **Calcium pyrophosphate dihydrate and calcium hydroxyapatite crystal deposition diseases: imaging perspectives**
  by Steinbach LS
  pages 185-205
  Full Text | PDF (1082 KB)
- **Avascular necrosis and bone marrow edema syndrome**
  by Watson RM, Roach NA, Dalinka MK
  pages 207-219
  Full Text | PDF (481 KB)
- **Nerves in a pinch: imaging of nerve compression syndromes**
  by Hochman MG, Zilberfarb JL
  pages 221-245
  Full Text | PDF (1123 KB)
- **Index**
  pages 247-255
  PDF (146 KB)

View Selected Abstracts

Display: without preview

CONTENTS

Preface **xi**
Emil J. Balthazar

Impact of Multislice CT on Imaging of Acute Abdominal Disease **1083**
Vikas Kundra and Paul M. Silverman

With the advent of multislice CT, higher resolution and more diagnostic images are now available. By transitioning from axial to single-slice helical to now multislice CT scanners, imaging time has been reduced from minutes to seconds. In addition, collimation width and computing time have decreased. Increased coverage is now obtained with thinner slices and higher image quality. Although multislice CT has had significant impact in evaluating the entire body, it has been particularly useful for abdominal imaging.

Radiologic Diagnosis of Gastrointestinal Perforation **1095**
Stephen E. Rubesin and Marc S. Levine

Perforations of the gastrointestinal tract have many causes. Holes in the wall of gastrointestinal organs can be created by blunt or penetrating trauma, iatrogenic injury, inflammatory conditions that penetrate the serosa or adventitia, extrinsic neoplasms that invade the gastrointestinal tract, or primary neoplasms that penetrate outside the wall of gastrointestinal organs. This article provides a radiologic approach for investigating the wide variety of gastrointestinal perforations. General principles about contrast agents and studies are reviewed, and then perforations in specific gastrointestinal organs are discussed.

The Acute Right Lower Quadrant: CT Evaluation **1117**
Michael Macari and Emil J. Balthazar

This article describes the CT imaging findings of patients presenting with acute right lower quadrant pain. The focus is on appendicitis and current imaging techniques and controversies. The remainder of the article evaluates the most common conditions causing right lower quadrant pain other than appendicitis that can be diagnosed with CT.

Adult Intussusception: Diagnosis and Clinical Relevance **1137**
Benjamin Y. Huang and David M. Warshauer

Adult intussusception is a rare entity. Unlike intussusceptions in childhood, most adult intussusceptions are caused by a definable pathologic lesion, with a significant proportion

caused by malignancy, particularly among those involving the colon. Before the advent of noninvasive imaging, most adult intussusceptions were diagnosed surgically or at autopsy, but modern imaging techniques have proved useful in diagnosis and in directing appropriate therapy. Until recently, adult intussusception had been considered primarily a surgical condition, but recent data in the radiologic literature suggest that there may be a substantial number of transient, nonneoplastic enteroenteric intussusceptions diagnosed by CT, which do not require operative treatment.

CT of Acute Abdominal Aortic Disorders **1153**
Sanjeev Bhalla, Christine O. Menias, and Jay P. Heiken

Aortic aneurysm rupture, aortic dissection, penetrating atherosclerotic ulcer, acute aortic occlusion, traumatic aortic injury, and aortic fistula represent acute abdominal aortic conditions. Because of its speed and proximity to the emergency department, helical CT is the imaging test of choice for these conditions. MR imaging also plays an important role in the imaging of aortic dissection and penetrating atherosclerotic ulcer. Ultrasound is helpful when CT is not readily available and the patient is unable or too unstable to undergo MR imaging. Because CT is the dominant imaging method for diagnosing acute abdominal aortic conditions, this article focuses on CT techniques and manifestations of this group of acute abdominal disorders.

Blunt Injury to Mesentery and Small Bowel: CT Evaluation **1171**
Patrick W. Hanks and Jeffrey M. Brody

CT is widely used in the evaluation of trauma patients. Although the sensitivity for CT detection of solid organ injury is 90% or better, hollow viscous injury has historically been more difficult to identify. Diagnosis of small bowel and mesenteric injury often requires special attention to subtle findings. This article discusses the role of CT in the diagnostic approach to blunt trauma victims, the points of controversy regarding the CT examination technique, the CT findings related to small bowel and mesenteric injury, and the accuracy of imaging diagnosis.

Spontaneous Intraperitoneal Hemorrhage: Imaging Features **1183**
Koenraad J. Mortele, Vito Cantisani, Douglas L. Brown, and Pablo R. Ros

Spontaneous, nontraumatic, intraperitoneal bleeding is a rare but worrisome clinical condition, potentially fatal, which may be related to a vast array of underlying causes. Accurate diagnosis of the cause, organ of origin, extent, and prognosis of this condition can be established with different imaging modalities, such as ultrasound, CT, and MR imaging. This article summarizes the clinical aspects and pathogenesis of the entities causing spontaneous intraperitoneal hemorrhage. The corresponding radiologic features of these conditions are highlighted. Finally, recommendations to perform the imaging modality of choice for each of the abnormalities and key features are provided.

Ultrasound and CT Evaluation of Emergent Gallbladder Pathology **1203**
Genevieve L. Bennett and Emil J. Balthazar

This article provides a review of ultrasound and CT findings in acute conditions of the gallbladder. Although ultrasound or hepatobiliary scintigraphy are usually the initial imaging examinations of choice to evaluate most suspected cases of acute gallbladder pathology, the role of CT in the evaluation of abdominal pain continues to expand. CT allows for more comprehensive evaluation of the abdomen and pelvis and can identify other inflammatory processes that clinically may simulate gallbladder pathology.

In many instances, CT may be the initial diagnostic procedure performed; it is important to become familiar with the spectrum of CT findings in emergent gallbladder disorders. Furthermore, CT plays an important role in the evaluation of associated complications of these disorders, facilitating prompt diagnosis and appropriate management.

Interventional Approach to Pancreatic Fluid Collections **1217**
Joseph T. Ferrucci III and Peter R. Mueller

Interventional radiologic catheter drainage may be an effective therapeutic approach to fluid collections complicating acute pancreatitis. Pancreatic pseudocysts and abscess are the most common conditions requiring radiologic intervention. Imaging guidance is best performed under CT control allowing precise definition of access route, catheter placement, and response. Access routes are chosen to avoid traversing vital intervening structures, especially the pleural space, colon, and small bowel. Optimal results are achieved with the use of large-bore multihole catheters, prolonged duration of drainage, and careful collaboration with the surgical team.

Ultrasonography of the Acute Abdomen: Gastrointestinal Conditions **1227**
Julien B.C.M. Puylaert

Although multislice, helical CT is increasingly replacing ultrasonography for the evaluation of patients with acute abdominal pain, ultrasound does have certain specific advantages over CT. This article discusses the advantages of ultrasound in imaging of the acute abdomen, exploring such areas as appendicitis, ileocecal Crohn's disease, infectious ileocolitis and infectious ileocecitis, mesenteric lymphadenitis, cecal carcinoma, sigmoid diverticulitis, right-sided colonic diverticulitis, and perforated peptic ulcer.

MR Imaging in Abdominal Emergencies **1243**
Ivan Pedrosa and Neil M. Rofsky

The use of MR imaging in the emergency setting is evolving. Clear indications include situations in need of contrast media when iodinated contrast cannot be administered or to facilitate assessments in pregnant patients and children when exposure to ionizing radiation is considered unacceptable. The availability of rapid, motion immune sequences now makes MR imaging a feasible study in less cooperative patients extending the range of patients for whom a diagnostic study can be achieved. Further investigations are needed to identify the diagnostic algorithms for which this favorable use holds true.

Selective Role of Nuclear Medicine in Evaluating the Acute Abdomen **1275**
Lionel S. Zuckier and Leonard M. Freeman

Evaluation of the acute abdomen has evolved with the introduction of the high-resolution imaging techniques of CT, ultrasound, and MR imaging, leaving scintigraphic examinations a limited although important role based on their noninvasive, physiologic, and functional nature. Bleeding studies can be used to localize noninvasively sites of bleeding to regions of the large or small bowel. Pertechnetate studies accurately localize sites of ectopic gastric mucosa. Biliary scintigraphy is helpful in diagnosing patients with acute presentation of biliary disease and is invaluable in analyzing complicated postcholecystectomy patients. Vascular and traumatic injury of the solid organs can be studied by various functional techniques including biliary and renal scintigraphy. A niche for infectious imaging has been found in the evaluation of acute appendicitis.

Complications of Liver Transplantation: Imaging and Intervention **1289**
Michael P. Federle and Vibhu Kapoor

Orthotopic liver transplantation is the accepted treatment for end-stage liver disease. Improvements in surgical techniques and medical therapy have resulted in reduced mortality and some types of complications. Patients are, however, still at risk for a variety of vascular, biliary, neoplastic, and other complications, the signs and symptoms of which are often nonspecific. Radiologists can play a key role in diagnosis and management of these complications, as reviewed in this article.

Cumulative Index 2003 **1307**

FORTHCOMING ISSUES

January 2004

Arthritis Imaging
Barbara N. Weissman, MD, *Guest Editor*

March 2004

Emergency Ultrasound
Vikram Dogra, MD, *Guest Editor*

May 2004

Cardiac Imaging
Martin Lipton, MD, and
Lawrence Boxt, MD, *Guest Editors*

RECENT ISSUES

September 2003

Advances in Renal Imaging
Philip J. Kenney, MD, *Guest Editor*

July 2003

Women's Imaging: Obstetrics and Gynecology
Deborah Levine, MD, *Guest Editor*

May 2003

Multislice Helical CT of the Thorax
Phillip M. Boiselle, MD, *Guest Editor*

RADIOLOGIC
CLINICS OF
NORTH AMERICA

Radiol Clin N Am 41 (2003) xi–xii

Preface
Imaging of the acute abdomen

Emil J. Balthazar, MD
Guest Editor

The only constant in life is change.

—Buddha

It has been over 10 years since the publication of the last issue of the *Radiologic Clinics of North America* devoted entirely to imaging acute abdominal disorders. Significant advances in technology, new applications, changed protocols, and considerable accumulated experience have prompted an update of this important clinical subject.

The purpose of this new issue is twofold. First, acute abdominal conditions that can be diagnosed and evaluated rapidly by relatively noninvasive imaging examinations are reviewed. I have tried to avoid overlaps and duplications while maintaining the relevance of the topic by focusing on pertinent, potentially life-threatening abdominal conditions. Second, this issue provides an abbreviated but comprehensive presentation of new applications of imaging modalities—such as multidetector (multislice) CT, sonography, and MR imaging—that were previously not available or were not commonly used in the evaluation of patients with acute abdominal complaints.

After perusing through this issue, readers will no doubt notice that radiologists, based on their experience and established beliefs, tend to address similar clinical challenges by different means using various imaging modalities or distinctly idiosyncratic technical protocols. Theoretically, the selection of a given imaging modality or a protocol should be based mainly on their reported accuracy, sensitivity, and specificity, as might be expected. In reality, however, the selection process is strongly influenced by past experience and skills, the quality and availability of equipment, and the cost of examination, and is therefore often institutionally dependent. In the seventeenth century, Francis Bacon and the French philosopher René Déscartes identified observation and analysis, respectively, as the primary tools that are essential in the effort to acquire reliable scientific knowledge. The process of gathering data and analysis, however, can be biased, tinted by our own prejudices, and is not always trustworthy. In the words of historian Jacque Barzun: ''Observation is rarely neutral; it rests on preconceptions and preperceptions.''

I hope that this issue describes what is presently available and what is considered current state-of-the-art in the imaging of acute abdominal conditions. A compendium of imaging choices and protocols are described, mainly reflecting the experience and convictions of different authors. I found these recommendations very useful; however, they are not axioms—and are certainly not perennial—but are susceptible to incessant changes and refinements. It is your responsibility as the reader, based on your skills, experience, and local factors, to select the appropriate imaging modality and the required protocol that, in your best judgment, will better serve the interest of your patients.

0033-8389/03/$ – see front matter
doi:10.1016/S0033-8389(03)00142-8

In pursuing my goals, I have been joined and helped by a distinguished group of leading academic radiologists, all experts in their field, to whom I extend my affection and gratitude. I am also indebted to Barton Dudlick, our efficient senior editor, for helping us make this project a reality.

Emil J. Balthazar, MD
Department of Radiology
New York University School of Medicine
560 First Avenue, NB3 W39
New York, NY 10016, USA
E-mail address: emiljmd@aol.com

RADIOLOGIC
CLINICS OF
NORTH AMERICA

Radiol Clin N Am 41 (2003) 1083–1093

Impact of multislice CT on imaging of acute abdominal disease

Vikas Kundra, MD, PhD*, Paul M. Silverman, MD

Division of Diagnostic Imaging, Department of Radiology, The University of Texas, M.D. Anderson Cancer Center, Box 57, Houston, TX 77030, USA

With the advent of multislice CT (MSCT), higher resolution and more diagnostic images are now available. By transitioning from axial to single-slice helical to now MSCT scanners, imaging time has been reduced from minutes to seconds. In addition, collimation width and computing time have decreased. Increased coverage is now obtained with thinner slices and higher image quality. Although MSCT has had significant impact in evaluating the entire body, it has been particularly useful for abdominal imaging.

For example, different phases of enhancement can now be separated more succinctly. Reduced breath-hold times have resulted in more diagnostic scans by curtailing motion artifact. Thinner slices have decreased Z-axis blurring to allow evaluation of minute structures, such as blood vessels. Increased computing speed has also shortened reconstruction and reformation times, enabling selection of the optimal plane for the structure in question. Clinically, imaging findings on CT increase the certainty of diagnosis or offer an alternative diagnosis to guide patient management [1].

Technology

In simple terms, MSCT allows acquisition of multiple slices with a single gantry rotation (Fig. 1). New high heat capacity tubes have significantly reduced the need for cooling; thus, x-rays can be delivered continuously. With MSCT, the point source is projected onto multiple detectors, currently up to 16, in the Z axis instead of the single detector of prior systems. Therefore, more data are acquired with a single gantry rotation.

For image acquisition, generally three major detectors designs are used: (1) matrix, where all detectors are of the same size; (2) adaptive array, where they vary from thinner inside to thicker outside; and (3) hybrid, where usually two sizes are used with the thinner detectors located centrally [2]. The first two support submillimeter to 5-mm acquisitions modes, whereas the latter supports submillimeter to 8-mm acquisition modes

Multislice scanners alter the acquisition thickness by varying the number of detectors used (Fig. 2). For example, a four-slice scanner using the matrix design has a Z-axis width of 20 mm subdivided into 16 equal parts of 1.25 mm each. The beam is collimated to excite a certain number of rows. Slices are acquired in groups of four. If the central four rows are used, four slices of 1.25-mm thickness are obtained for total coverage of 5 mm. If the central eight are used, every two detectors are summed resulting in a slice thickness of 2.5 mm. If the central 12 are used, every three detectors are summed resulting in a slice thickness of 3.75 mm. If all detectors are used, every four are summed resulting in 5-mm slices covering 20 mm in the Z axis. For submillimeter resolution, the beam is collimated across detectors.

With the new 16-slice scanners, 16 slices may be obtained with a single gantry rotation, including at submillimeter resolution. This does not increase the speed of acquisition for 5-mm slices compared with a four-

* Corresponding author.
E-mail address: vkundra@di.mdacc.tmc.edu (V. Kundra).

0033-8389/03/$ – see front matter
doi:10.1016/S0033-8389(03)00117-9

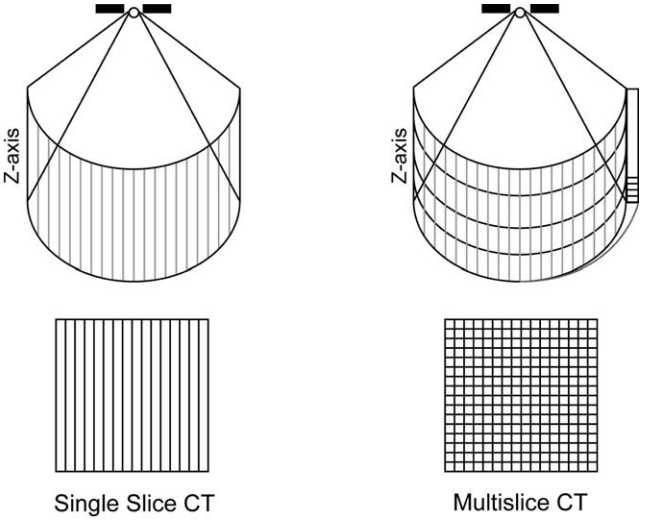

Fig. 1. Single-slice versus MSCT. Instead of a single detector in the Z axis used in single-slice CT, MSCT has multiple detectors in the Z axis, providing a greater number of images per gantry rotation.

slice scanner (4 × 5 mm = 20 mm) because the maximum width for detection in the Z axis is 20 mm. It does, however, increase coverage when thinner slices are used. For example, at 1.25-mm collimation, a four-slice scanner covers 5 mm per gantry rotation (4 × 1.25 mm = 5 mm), whereas a 16-slice scanner covers 20 mm per gantry rotation (16 × 1.25 mm = 20 mm).

In addition to varying collimation at the time of acquisition, slice thickness may also be varied by manipulating how the data are reconstructed. Although slices can be reconstructed at thicker widths than those acquired, they cannot be reconstructed thinner. Thus, it is important to select the thinnest acquisition width needed at the time of scanning.

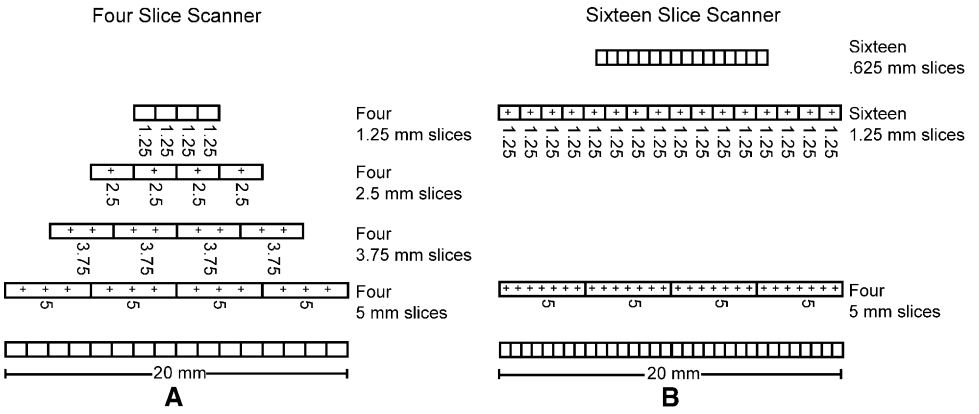

Fig. 2. Matrix detector. (*A*) In the matrix configuration, the Z axis is divided into equal parts. For a four-slice scanner, 20 mm in the Z axis is covered by 16 detectors each measuring 1.25 mm. The X-ray beam is collimated to expose the central 4, 8, 12, or 16 detectors. At the time of acquisition, data from the detectors may be added, resulting in slices of varying thickness. For example, by exposing the central eight detectors and combining data from every two, four 2.5-mm slices are obtained. (*B*) With a 16-slice scanner, 16 different acquisitions may be obtained at submillimeter resolution with a single gantry rotation. In terms of area in the Z axis, 1.25-mm slices cover 20 mm instead of 5 mm by four-slice scanners. Because the total detector width is the same, there is no difference in Z-axis coverage if 5-mm slices are acquired.

As with single-slice helical scanning, MSCT is performed while the patient table is moving through the scanner. On a single-slice scanner, pitch is defined as

$$\frac{\text{Table motion per gantry rotation}}{\text{Collimation thickness}}$$

For example, if the table travels 7.5 mm during one gantry rotation and the image thickness is set at 5 mm, the pitch is 7.5 mm/5 mm = 1.5:1 or 1.5.

On a multislice scanner the definition varies per manufacturer. Pitch may be defined as [3]

$$\frac{\text{Table motion per gantry rotation}}{\text{Total active detector width (x-ray beam collimation)}}$$

This is termed "beam pitch" [4]. For example, if the table travels 7.5 mm during one gantry rotation and four 1.25-mm thick slices are chosen, the total active detector width is 5 mm (4 × 1.25 mm) and the pitch is 7.5 mm/5 mm = 1.5:1 or 1.5.

General Electric defines pitch as [4]

$$\frac{\text{Table motion per gantry rotation}}{\text{Single image slice thickness}}$$

This is termed "slice pitch" [4]. In the previous example, pitch equals 7.5 mm/1.25 mm = 6. With this definition, pitch is increased by a multiple of four.

To calculate the distance that the patient travels per rotation, the gantry rotation speed is multiplied by the table speed. For example, in the previous example, if the gantry makes one complete rotation in 0.8 seconds, this translates to a table speed of 9.375 mm per second (7.5 mm/1 rotation × 1 rotation/0.8 seconds = 7.5 mm/0.8 seconds).

To cover a patient's liver measuring 21 cm takes 22 seconds (21 cm/0.9375 cm/second). If the beam pitch is 1.5 (six-slice pitch), the entire liver may be scanned with 1.25-mm slices during a comfortable breathhold. If greater coverage is desired, the slice thickness or table speed may be increased. For example, acquiring 5-mm slices and increasing the gantry speed to 15 mm/second results in a beam pitch of 0.75 (15 mm per rotation/20 mm total active detector width [4 × 5]) or three-slice pitch (15 mm per gantry rotation/5 mm slice thickness). At one gantry rotation per 0.8 seconds, 18.75 mm are covered per second (15 mm/0.8 second). Thus, a patient's entire 50-cm abdomen and pelvis can be covered with 5-mm slices in 26 seconds (50 cm/1.875 cm/second), again a comfortable breathhold. The 21-cm liver may be covered in 11 seconds with 5-mm slices.

The rapid image acquisition time allows one to control more tightly sampling of a contrast bolus (Fig. 3). With shorter scan duration, the peak of a bolus may be sampled rather than its shoulders. In addition, a tighter bolus may be used. For example, increasing the contrast injection rate decreases the duration of the contrast peak to match more closely the shorter scan time. Another strategy for obtaining a compact bolus is to decrease the volume of contrast instilled. The rate of contrast injection has been increasing [5]. A rate of 2.5 to 3 mL/second is routinely used in many clinical practices, but for hypervascular lesions, 5 to 6 mL/second is common. With faster scanning, these values will likely increase, but safety has to be evaluated concurrently.

With a more compact bolus and shorter sampling time, different phases of enhancement may be distin-

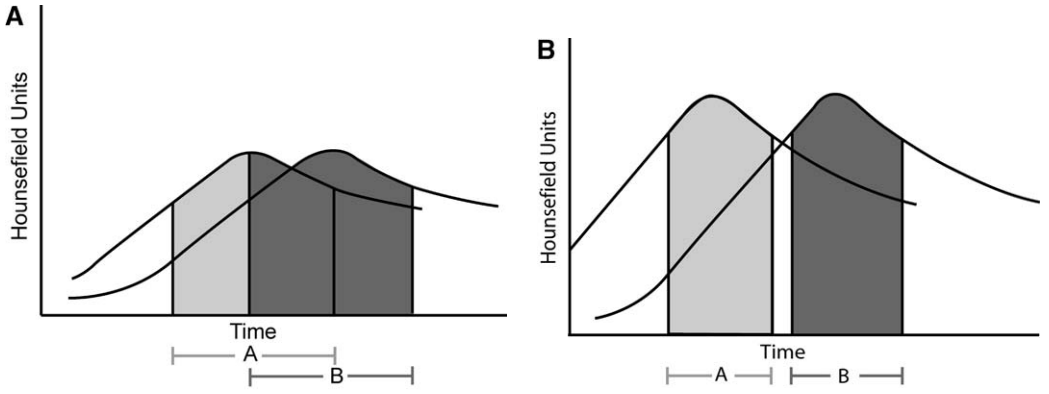

Fig. 3. Contrast bolus. With MSCT, faster acquisition times allow more rapid sampling of a contrast bolus. Phases of enhancement are better separated. (*A*) The longer acquisition time of single-slice CT limits differentiation of the two phases of enhancement. (*B*) The shorter scan time of MSCT allows better separation of phases of enhancement. In addition, further separation may be achieved by using faster rates of contrast injection that result in higher peaks of enhancement for a shorter period of time.

guished. For the liver, the appropriate delay after contrast injection separates different phases of enhancement for optimal lesion characterization. For example, delays may include 15, 30, and 70 seconds for arterial, late arterial, and portal venous phases, respectively [6].

The optimal window for liver imaging varies, however, with the volume of contrast injected [7]. In addition to volume, the amount of iodine injected influences lesion detection [8]. Using a dual-phase protocol, it has been noted that higher concentrations of iodine provide better arterial enhancement and superior mean enhancement of the hypervascular lesion, hepatocellular carcinoma; however, subjectively, lesion detection was not improved [9]. Comparing 370 mg iodine/mL with 300 mg iodine/mL intravenous contrast, Awai et al [10] found no difference in hepatic enhancement; however, hepatocellular carcinoma to liver contrast was improved on the first phase of a triple-phase protocol, but not second or third phase. In comparison, for the portal venous imaging phase, the total amount of iodine instilled influences lesion detectability [8]. Decreasing volume and increasing injection rate need to be balanced by increased iodine concentration to retain conspicuity of hypovascular lesions. As these parameters are adjusted, the delay in scanning after bolus injection needs reassessment.

Because of patient variability, standard delay values become less useful as scan time decreases. Instead, a control within each patient is required. There are primarily two methods for timing the delay after a bolus injection: a test bolus or computer-automated scanning technology. With the former, a mini bolus is instilled and then the site of interest is sampled repeatedly to determine the delay to peak enhancement. The true bolus then follows. With the latter, a cursor is placed over a site of interest or the aorta and once enhancement reaches a predefined threshold, scanning begins. Because no test bolus is used, the examination time is decreased and additional contrast is avoided. For portal-venous phase imaging, a threshold of 50 HU is efficacious when using computer-automated scanning technology [11].

In terms of contrast usage, MSCT results in decreased volume, increased concentration, increased rate, and shorter scan duration. Thereby, phases of enhancement are better separated. To ease interpretation of the many images generated, one can take advantage of soft copy viewing.

Because of ever-increasing computer speed and with near isotropic acquisition, images may be reformatted in any desired plane. Postprocessing can aid detection and characterization of lesions, particularly those involving the vasculature. Increasing speeds also benefit computationally intensive techniques, such as virtual colonography and virtual cystography.

Clinical impact

Because of greater speed of coverage and thinner slices, MSCT has impacted imaging of all organs in the body. When making protocols specific to a disease entity or area of interest, there are three main choices with MSCT compared with single-slice CT [12]. One may cover the same anatomic area with the same collimation in a shorter time period. One may cover the same anatomic area with narrower collimation without decreasing scan time. Although this increases radiation exposure, greater anatomic detail results. Lastly, one may cover the same area with narrower collimation in a shorter time period. The ability of MSCT to perform thinner slices and to cover the area of interest in a single breathhold has improved imaging of the abdomen and pelvis. Increased computer speed and PACS workstations augment MSCT by allowing multiplanar reconstructions and cine-viewing, which is particularly helpful for tubular or fairly constant structures, such as the aorta or spine. These different planes and three-dimensional rendering can also aid treatment planning, such as for radiation therapy or surgery. In addition, MSCT allows retrospective reconstruction to the thinnest initially acquired slices, providing more viewing options for better lesion characterization.

Trauma

In blunt abdominal trauma, clinical findings can be equivocal or misleading in 20% to 50% of patients. In addition, physical examination is reliable in no more than 16% of patients in the presence of head injury [13,14]. Imaging has become a centerpiece of evaluation of trauma and MSCT has had a major impact in this realm. Because of its speed, images of the head, cervical spine, chest, abdomen, and pelvis may be obtained rapidly. When needed, a single bolus of contrast is often adequate for the entire evaluation. Tomographic imaging can augment fracture evaluation and, if needed, focused thin slices may be obtained. Instead of secondary signs, such as a widened mediastinum, injury to the aorta may be visualized more directly. Organ injury and hemorrhage may be identified.

In the acute setting, a multimodality approach is beneficial for patient evaluation. For hemoperitoneum,

ultrasound is the modality of choice in an unstable patient who cannot be moved. With the current CT technology, however, examinations can be performed rapidly in many traumatic situations. CT has high sensitivity for detecting parenchymal injuries of the solid organs [15,16]. The most commonly injured organs in blunt trauma are the spleen and liver. CT is up to 98% accurate at detecting splenic injuries [17]. Fig. 4 demonstrates splenic contusion and pseudoaneurysm after blunt abdominal trauma. In approximately 5% of blunt trauma victims, bowel and mesenteric injuries are found [18]. PACS workstations speed interpretation and reconstructed images can guide interpretation and therapy, such as surgery. They also aid following tubular structures, such as the bowel or vessels. Decreased intravascular volume may manifest as a flattened or small inferior vena cava or the generalized bowel edema of shock bowel. This is especially seen in the pediatric population when volume is depleted secondary to blood loss. Vascular injury may be identified by a vascular blush [19] within organs, contrast extravasation, or by direct visualization of the vessels. Thinner slices can show vessels to better advantage and can guide any future catheterization that may be necessary. Acute bleeds are most often manifested by high-density material in the peritoneal space. In some cases, however, acute hemorrhage can be water density and mimic ascites. In the setting of trauma in a patient without any reason for ascites, such fluid should be viewed with suspicion [20].

With knife or gunshot wounds, again hemoperitoneum and solid organ damage may be noted. The path of the object guides the anatomic structures that deserve particular attention. For blunt trauma, additional delayed imaging can identify potentially clinically silent complications, such as splenic or hepatic rupture, a posttraumatic biloma, or bowel devascularization [21].

For a general survey of the abdomen for trauma, thicker 7.5-mm slices are often adequate; however, if further definition is needed, thinner slices may be helpful. If the initial acquisition is performed at 3.75 mm, it may be reconstructed at 7.5 mm for the survey and if more detail is needed, the thinner slices may be examined. MSCT can provide flexibility for initial and retrospective review of the traumatic injury.

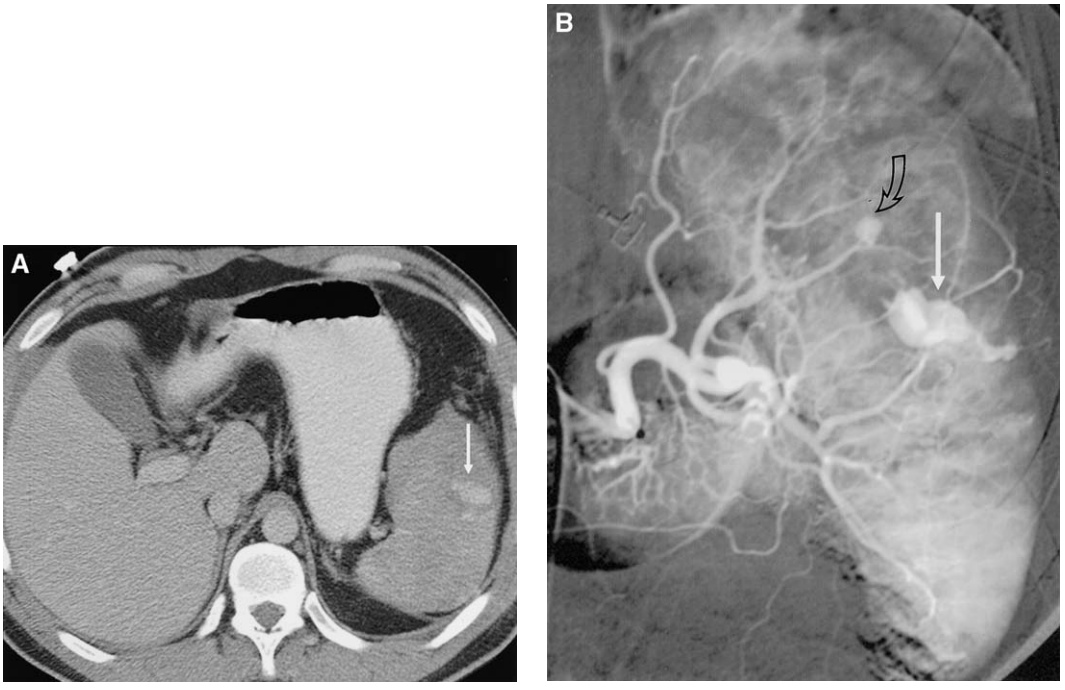

Fig. 4. Splenic contusion and pseudoaneurysm formation associated with recent blunt abdominal trauma. (*A*) Axial CT image of the upper abdomen demonstrates an area of decreased attenuation and a central collection of contrast material at the lateral aspect of the spleen (*arrow*). (*B*) Selective splenic artery angiogram confirms the development of a pseudoaneurysm (*solid arrow*). A second smaller pseudoaneurysm also is detected (*open arrow*).

Abdominal pain

As with trauma, abdominal pain is most often evaluated with thicker 5- to 7.5-mm slices. This is usually adequate for more common diseases, such as diverticulitis, appendicitis, bowel obstruction, and abscess. Less common findings, such as retroperitoneal hemorrhage and secondary signs of bowel rupture, can also be identified with thicker slices. The increased speed of MSCT, however, improves the examination by limiting motion. In addition, the patient is more comfortable having to spend less time on the scanner.

Among causes of abdominal pain, MSCT has had a significant impact on evaluation of renal colic. Unlike gallstones, almost all renal stones are calcified. CT is very useful for their identification [22–24]. Visualizing smaller, less than 5 mm stones is aided by thinner sections, which limit volume averaging artifacts that may obscure the lesion. In addition, PACS workstations simplify following tubular structures, such as the ureters. This is particularly helpful in the pelvis where the curvature of the ureters makes them more difficult to track. CT for stone disease has virtually replaced the intravenous urogram in many institutions and now low-radiation CT approaches are being explored [25]. Sometimes, however, it may still be difficult to separate a small stone from a phlebolith. Contrast may demonstrate a delayed nephrogram or identify the point of obstruction.

A new adaptation for evaluating the urinary system is CT urography [26,27]. Here, MSCT demonstrates clear advantages over single-slice CT. For imaging the ureters, slices as thin as approximately 1 mm may be acquired. The kidneys, ureters, and bladder are obtained in one breathhold. To aid lesion conspicuity, the examination is often performed after hydration and during the excretory phase to opacify the ureters. Although there is increased radiation exposure, for a more complete examination of the urinary excretory system, multiple phases of enhancement may be obtained. Renal lesions, such as cysts, may be differentiated from malignancy by comparing Hounsfield units of preintravenous and postintravenous examinations. Visualization of the upper tracts may be aided further by compression [26]. For examining the ureters in particular, slices may be reconstructed again as thin as approximately 1 mm. The initial thin acquisition results in superior reconstructed and reformatted images. The coronal plane mimics the intravenous urogram (Fig. 5) by demonstrating both ureters in a few slices. Evaluation may be aided further by three-dimensional reconstructions. Urinary tract abnormalities are depicted in a format familiar to clinicians.

Liver and bile ducts

Instead of 20 to 25 seconds required by single-slice CT, MSCT allows coverage of the liver in 4 to 12 seconds, depending on the organ's size, collimation, and gantry rotation speed. This allows better separation of the different phases of contrast enhancement. Foley et al [6] described a triple-phase protocol for separating arterial, late arterial, or portal vein inflow, and hepatic venous phases. With no or minimal confounding venous blood flow, the arterial phase demonstrates normal variants and tumor vasculature, which guides surgery, such as liver transplants and resection; and guides minimally invasive procedures, such as chemoembolization [28]. Hypervascular lesions demonstrate greatest contrast from surrounding liver parenchyma during the second phase [6]. Because these lesions get their supply from the hepatic artery and there is an expected delay between contrast in the feeding vessel and the tumor, the authors favor the term ''late arterial'' for the second phase. Theoretically, pooling of contrast from an active hemorrhage should also be visible at this time. The delay between the first and second phases is approximately 15 seconds. With MSCT, this is easily achievable. However, the 20 to 25 seconds needed to acquire images through the liver by single-slice CT causes overlap between the phases. In addition, thinner slices may be obtained with MSCT, which improves visualization, particularly of vessels. In the third hepatic venous phase, the arteries are no longer distinguished, but the hepatic veins are seen. Now, the hepatic parenchyma attenuation is relatively increased allowing visualization of hypovascular lesions and injuries, such as a laceration. The last phase corresponds to the timing conventionally used for an abdomen-pelvis survey.

Increased spatial resolution of MSCT caused by decreased motion artifact and thinner slices has also improved imaging of bile ducts. Using 2.5-mm collimation and a 70-second delay after intravenous contrast injection, Zandrino et al [29] were able to assess the site of biliary obstruction in 86% of patients. Biliary contrast agents may also aid evaluation [30–32].

Pancreas

MSCT also has enabled greater separation of the phases of pancreas enhancement. Instead of a dual-phase protocol often used on single-slice scanners, McNulty et al [33] have described a triple-phase protocol consisting of a 20-, 35-, and 60-second delay after intravenous contrast injection. The timing corre-

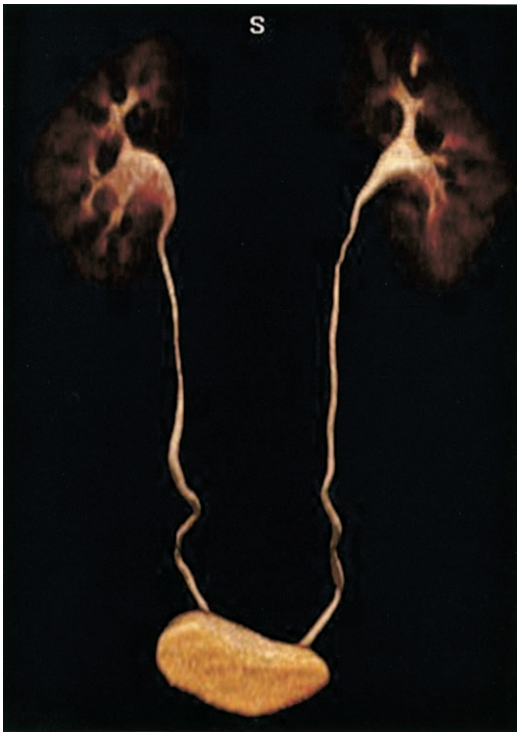

Fig. 5. Multislice (multidetector) CT examination with reconstructed volume-rendered image of the entire urinary tract. (Courtesy of Gary Israel, MD, New York, NY.)

sponds to the arterial, pancreas parenchyma, and portal venous phases, respectively. The delay for the phases is quite similar to that described for the triple-phase protocol of the liver [6]. For the most common pancreas tumor, adenocarcinoma, no significant difference in contrast ratio between the tumors and pancreatic parenchyma was discerned among the latter two phases [33]. In comparison, Imbriaco et al [34] describe no change in pancreatic adenocarcinoma detection using a dual-phase or a single caudocranial acquisition 50 seconds after intravenous contrast injection. The number of patients was too small, however, to differentiate reliably which method was superior for staging. The early phases may be helpful for detecting hypervascular lesions, such as neuroendocrine tumors [35]. Because of better depiction of vascular involvement, tumor staging is improved using thin-slice CT [36]. Because of enhancement in the portal-venous phase, pancreatic injury, such as laceration, may be identified as a hypoattenuating lesion. Pancreatitis and its associated complications, such as necrosis, pseudocysts, and venous thrombosis, can be seen on the later phase as part of an abdominal survey.

Vascular system

The speed of MSCT allows coverage of the entire aorta and common iliac arteries in a comfortable breathhold (Fig. 6), resulting in decreased misregistration and respiratory artifacts. Compared with single-slice CT, Rubin et al [37] found that four-slice CT resulted in CT angiography that was 2.6 times faster, required less intravenous contrast, and provided thinner sections. This improves direct visualization of pathology, such as an aortic dissection or aneurysm. Planning and follow-up evaluation of endovascular stents grafts are also augmented [38]. Acquiring multiple phases can aid evaluation of venous pathology, such as thrombosis.

In addition, the high resolution of MSCT allows direct visualization of branch vessels. For example, stenosis of the renal arteries may be quantified. Stenoses of the superior mesenteric artery resulting in

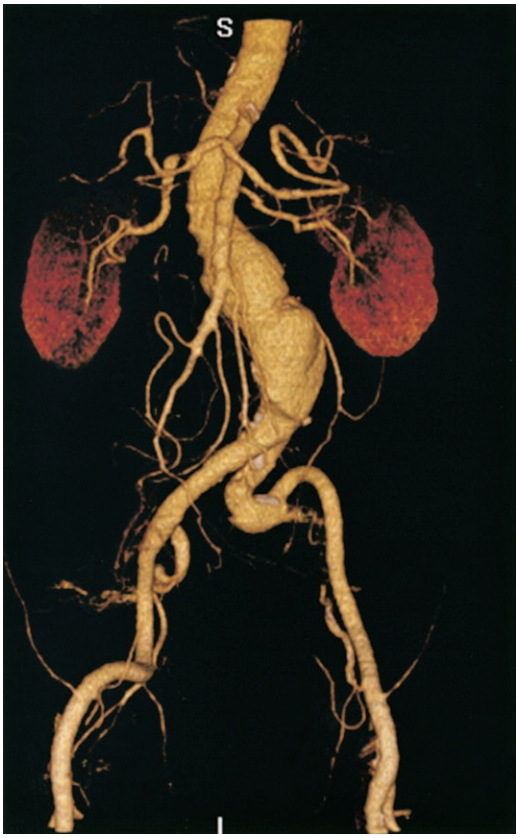

Fig. 6. Multislice CT examination with volume-rendered shaded surface reconstruction of the entire abdominal aorta and its major branches. (Courtesy of Gary Israel, MD, New York, NY.)

mesenteric ischemia may also be identified. In addition, defining vessel anatomy and its variants can guide surgical planning. In the setting of organ transplants, MSCT can be used to evaluate the living donor and then to follow the transplant in the recipient.

Obtaining near isotropic volumes results in exquisite reconstructions whose plane may be maximized for the vessel in question. For stenosis, it often is better to evaluate a plane axial to the artery. Cine-viewing by PACS simplifies following these tubular structures over long distances.

Compared with traditional angiography, CT angiography has greater safety, greater patient acceptance, lower cost, and lower radiation exposure [39,40]. In addition, CT allows visualization of adjacent soft tissue. Extrinsic lesions impacting the vasculature can be seen directly.

Pediatric imaging

One of the major difficulties in imaging pediatric patients has been motion. Particularly, children in the preteenage years are often frightened of the experience and may cry during the examination. Movement is frequently overcome by sedating the patient, usually with the help of an anesthesia team. This increases the number of individuals required to complete the examination, however, and can cause delay. In an emergency setting speed may be critical. Compared with single-slice CT, for covering the same volume, a four-slice CT is at least two times as fast with comparable image quality or three times as fast with diagnostically comparable image quality [41]. With MSCT, scan times have decreased to the point that the duration of sedation or anesthesia is minimized or often not needed at all [42]. An added benefit is reduction in the potential risks of sedation. In addition, there is increased patient throughput and greater efficiency of the sedation team. Significantly, the acquired images are of high diagnostic quality and contain minimal motion artifact.

Little patient cooperation is needed to obtain such useful images. For example, if a 22.5 mm per rotation table speed is used, the 15-cm abdomen and pelvis of a small child may be covered in approximately 5 seconds. In addition, images of the head, chest, abdomen, and pelvis may be obtained rapidly for evaluation of injury, for example, after trauma.

Thinner slices also may be advantageous in children to visualize their comparatively smaller anatomy. Thinner collimation, however, can lead to higher radiation exposure. If a child has an illness and requires multiple rounds of imaging, exposure may become significant. Again attention to table speed and collimation can limit exposure, but with smaller patients one can also adjust the milliampere and kilovolt (peak), because less radiation is needed to penetrate their smaller body.

Pitfalls and concerns

Radiation dose

Compared with single-slice CT, the radiation dose is greater when using multislice scanners [3,12]. One reason is that the source-to-detector distance is decreased in many MSCT scanners compared with single-slice scanners. Another reason is that MSCT requires a more constant beam across all of the detectors, which often translates into sampling the center of a larger fan with deposition of excess radiation at the edges. With single-slice scanners, image thickness and collimation setting have been associated with each other resulting in a rule of thumb that dose is proportional to slice thickness. With multislice scanners, however, slice thickness can be altered during reprocessing. Instead, one needs to be aware of collimation and pitch. For example, a 5-mm slice may be acquired at 5-mm collimation or by combining four 1.25-mm acquisitions. The former requires fewer tube rotations and results in less radiation exposure. Similarly, for the same kilovolt (peak) and milliampere, narrower collimation for a given pitch results in higher radiation than a wider collimation. This is because the number of rotations needed to cover the given area is greater and there is more overlap of the beam with the thinner collimation. Increasing the table motion per gantry rotation for the same collimation also decreases dose, but this needs to be balanced by the quality of the image.

The increased dose is more of a concern for pediatric patients who are still developing organs, including teenage girls with developing breasts [43]. Radiation dose becomes more of a concern with serial examinations (eg, in patients with cancer). To decrease total dose, new tube tracking techniques collimate the x-ray beam to the detector width.

Pitch and contrast

Increasing the pitch increases slice broadening, introducing noise in the image. At thicker collimation and table speeds (ie, 5-mm thick slices in 6:1 or 30 mm per gantry rotation) helical or star-like artifacts are encountered about bony and soft tissue interfaces [12]. With faster rotation speeds, the number of trajectories used for the reconstruction decreases causing aliasing

or streak artifacts. This is part of the problem at high-contrast interfaces, such as between soft tissue and bone or between a contrast bolus and soft tissue. Increasing bolus concentration and rate leads to streak artifacts, limiting evaluation of the axilla, usually, and at times, the subclavicular area. Using high concentrations, it is difficult to evaluate the lumen of all veins traversed by the bolus on its way to the right side of the heart. This can make it difficult to find the tip of a central venous catheter.

Phase of enhancement

Arterial or early arterial phase results in inhomogenous enhancement of the spleen, which may simulate pathology, such as splenic fracture or infection. A more homogeneous appearance, however, is normally found on delayed examinations.

For the kidney, the portal-venous phase of an abdomen-pelvis survey corresponds to the corticomedullary phase of the kidney. At this phase, the appearance of the kidneys may mimic a striated nephrogram. In addition, pathology, such as a cyst, is often more difficult to discern. A delayed examination in the excretory phase results in more homogenous enhancement of normal renal parenchyma. Delayed images may also be valuable in the pelvis. An unopacified bladder can mimic a pelvic fluid collection. Additionally, poor opacification of the iliac veins or even the inferior vena cava can mimic thrombus. Delayed scans are helpful in demonstrating that the low attenuation area represents flow artifact from unopacified blood.

Thinner slices

Although smaller lesions can be found with thinner slices, the relevance of such findings may be suspect. For example, approximately 80% of liver lesions smaller than 0.5 cm are benign, even in the setting of cancer [44]. Following such findings can increase health care costs and patient anxiety.

Another phenomenon noted in MSCT scanners is increased Hounsfield values in small (< 1.5 cm) lesions, such as in the kidneys. This occurs even when collimation is less than 50% of the lesion size. The Hounsfield value increases with greater enhancement in adjacent tissue. The phenomenon is more pronounced in subcentimeter lesions [45–47]. There is variability, however, in the magnitude of this artifact among MSCT scanners from different manufacturers [48]. Nevertheless, the presumption that thinner slices obtained by MSCT are just as quantitative as thicker slices obtained by conventional single-slice CT may need to be reassessed. The criteria for lesion characterization may need to be adjusted with multislice scanners, particularly if Hounsfield measurements are the basis of a diagnosis, such as with renal lesions and some adrenal lesions.

Summary

The increased speed, greater coverage, and thinner slices of MSCT are exciting developments in radiology, and these feature should only improve with newer generation multislice scanners. The impact of this technology on abdominal imaging has just begun.

Acknowledgments

The authors thank Mary Carr for help in preparation of this article and Kelly Duggan for assistance with Figs. 1–3.

References

[1] Rosen MP, Sands DZ, Longmaid III HE, et al. Impact of abdominal CT on the management of patients presenting to the emergency department with acute abdominal pain. AJR Am J Roentgenol 2000;174:1391–6.
[2] Fox SH. An introduction to multislice detector technology. Helical CT Today 1999;6:3–4.
[3] McCollough CH, Zink FE. Performance evaluation of a multi-slice CT system. Med Phys 1999;26:2223–30.
[4] Silverman PM, Kalender WA, Hazle JD. Common terminology for single and multislice helical CT. AJR Am J Roentgenol 2001;176:1135–6.
[5] Silverman PM, Kohan L, Ducic I, et al. Imaging of the liver with helical CT: a survey of scanning techniques. AJR Am J Roentgenol 1998;170:149–52.
[6] Foley WD, Mallisee TA, Hohenwalter MD, et al. Multiphase hepatic CT with a multirow detector CT scanner. AJR Am J Roentgenol 2000;175:679–85.
[7] Chambers TP, Baron RL, Lush RM, et al. Hepatic CT enhancement: comparison of ionic and nonionic contrast agents in the same patients. Radiology 1994;190:721–5.
[8] Freeny PC, Gardner JC, vonIngersleben G, et al. Hepatic helical CT: effect of reduction of iodine dose of intravenous contrast material on hepatic contrast enhancement. Radiology 1995;197:89–93.
[9] Hanninen EL, Vogl TJ, Felfe R, et al. Detection of focal liver lesions at biphasic spiral CT: randomized double-blind study of the effect of iodine concentration in contrast materials. Radiology 2000;216:403–9.
[10] Awai K, Takada K, Onishi H, et al. Aortic and hepatic enhancement and tumor-to-liver contrast: analysis of

the effect of different concentrations of contrast material at multi-detector row helical CT. Radiology 2002; 224:757–63.
[11] Silverman PM, Roberts S, Tefft MC, et al. Helical CT of the liver: clinical application of an automated computer technique, Smartprep, for obtaining images with optimal contrast enhancement. AJR Am J Roentgenol 1995;165:73–8.
[12] Nelson RC, Silverman PM. Multislice CT: a new era, basic technical aspects, and clinical capabilities. Helical CT Today 2000;6:1–2.
[13] Schurink GW, Bode PJ, van Luijt PA, et al. The value of physical examination in the diagnosis of patients with blunt abdominal trauma: a retrospective study. Injury 1997;28:261–5.
[14] Ferrera PC, Verdile VP, Bartfield JM, et al. Injuries distracting from intra-abdominal injuries after blunt trauma. Am J Emerg Med 1998;16:145–9.
[15] Becker CD, Mentha G, Terrier F. Blunt abdominal trauma in adults: role of CT in the diagnosis and management of visceral injuries. Part 1: Liver and spleen. Eur Radiol 1998;8:553–62.
[16] Becker CD, Mentha G, Schmidlin F, et al. Blunt abdominal trauma in adults: role of CT in the diagnosis and management of visceral injuries. Part 2: Gastrointestinal tract and retroperitoneal organs. Eur Radiol 1998;8:772–80.
[17] Brasel KJ, DeLisle CM, Olson CJ, et al. Splenic injury: trends in evaluation and management. J Trauma 1998; 44:283–6.
[18] Allen GS, Moore FA, Cox Jr CS, et al. Hollow visceral injury and blunt trauma. J Trauma 1998;45:69–75 [discussion: 75–8].
[19] Gavant ML, Schurr M, Flick PA, et al. Predicting clinical outcome of nonsurgical management of blunt splenic injury: using CT to reveal abnormalities of splenic vasculature. AJR Am J Roentgenol 1997;168: 207–12.
[20] Levine CD, Patel UJ, Silverman PM, et al. Low attenuation of acute traumatic hemoperitoneum on CT scans. AJR Am J Roentgenol 1996;166:1089–93.
[21] Poletti PA, Wintermark M, Schnyder P, et al. Traumatic injuries: role of imaging in the management of the polytrauma victim (conservative expectation). Eur Radiol 2002;12:969–78.
[22] Fielding JR, Steele G, Fox LA, et al. Spiral computerized tomography in the evaluation of acute flank pain: a replacement for excretory urography. J Urol 1997; 157:2071–3.
[23] Dalrymple NC, Verga M, Anderson KR, et al. The value of unenhanced helical computerized tomography in the management of acute flank pain. J Urol 1998; 159:735–40.
[24] Smith RC, Verga M, McCarthy S, et al. Diagnosis of acute flank pain: value of unenhanced helical CT. AJR Am J Roentgenol 1996;166:97–101.
[25] Meagher T, Sukumar VP, Collingwood J, et al. Low dose computed tomography in suspected acute renal colic. Clin Radiol 2001;56:873–6.
[26] Caoili EM, Cohan RH, Korobkin M, et al. Urinary tract abnormalities: initial experience with multi-detector row CT urography. Radiology 2002;222:353–60.
[27] McTavish JD, Jinzaki M, Zou KH, et al. Multi-detector row CT urography: comparison of strategies for depicting the normal urinary collecting system. Radiology 2002;225:783–90.
[28] Sahani D, Saini S, Pena C, et al. Using multidetector CT for preoperative vascular evaluation of liver neoplasms: technique and results. AJR Am J Roentgenol 2002;179:53–9.
[29] Zandrino F, Benzi L, Ferretti ML, et al. Multislice CT cholangiography without biliary contrast agent: technique and initial clinical results in the assessment of patients with biliary obstruction. Eur Radiol 2002;12: 1155–61.
[30] Caoili EM, Paulson EK, Heyneman LE, et al. Helical CT cholangiography with three-dimensional volume rendering using an oral biliary contrast agent: feasibility of a novel technique. AJR Am J Roentgenol 2000; 174:487–92.
[31] Soto JA, Velez SM, Guzman J. Choledocholithiasis: diagnosis with oral-contrast-enhanced CT cholangiography. AJR Am J Roentgenol 1999;172:943–8.
[32] Kwon AH, Uetsuji S, Ogura T, et al. Spiral computed tomography scanning after intravenous infusion cholangiography for biliary duct anomalies. Am J Surg 1997; 174:396–401 [discussion: 402].
[33] McNulty NJ, Francis IR, Platt JF, et al. Multi–detector row helical CT of the pancreas: effect of contrast-enhanced multiphasic imaging on enhancement of the pancreas, peripancreatic vasculature, and pancreatic adenocarcinoma. Radiology 2001;220:97–102.
[34] Imbriaco M, Megibow AJ, Camera L, et al. Dual-phase versus single-phase helical CT to detect and assess resectability of pancreatic carcinoma. AJR Am J Roentgenol 2002;178:1473–9.
[35] Stafford-Johnson DB, Francis IR, Eckhauser FE, et al. Dual-phase helical CT of nonfunctioning islet cell tumors. J Comput Assist Tomogr 1998;22:335–9.
[36] Loyer EM, David CL, Dubrow RA, et al. Vascular involvement in pancreatic adenocarcinoma: reassessment by thin-section CT. Abdom Imaging 1996;21:202–6.
[37] Rubin GD, Shiau MC, Leung AN, et al. Aorta and iliac arteries: single versus multiple detector-row helical CT angiography. Radiology 2000;215:670–6.
[38] Armerding MD, Rubin GD, Beaulieu CF, et al. Aortic aneurysmal disease: assessment of stent-graft treatment-CT versus conventional angiography. Radiology 2000;215:138–46.
[39] Lawrence JA, Kim D, Kent KC, et al. Lower extremity spiral CT angiography versus catheter angiography. Radiology 1995;194:903–8.
[40] Rubin GD, Shiau MC, Schmidt AJ, et al. Computed tomographic angiography: historical perspective and new state-of-the-art using multi detector-row helical computed tomography. J Comput Assist Tomogr 1999; 23(suppl 1):S83–90.
[41] Hu H, He HD, Foley WD, et al. Four multidetector-

row helical CT: image quality and volume coverage speed. Radiology 2000;215:55–62.
[42] Pappas JN, Donnelly LF, Frush DP. Reduced frequency of sedation of young children with multisection helical CT. Radiology 2000;215:897–9.
[43] Bhatia S, Robison LL, Oberlin O, et al. Breast cancer and other second neoplasms after childhood Hodgkin's disease. N Engl J Med 1996;334:745–51.
[44] Schwartz LH, Gandras EJ, Colangelo SM, et al. Prevalence and importance of small hepatic lesions found at CT in patients with cancer. Radiology 1999;210: 71–4.
[45] Fleischmann D, Rubin GD, Paik DS, et al. Stair-step artifacts with single versus multiple detector-row helical CT. Radiology 2000;216:185–96.
[46] Heneghan JP, Spielmann AL, Sheafor DH, et al. Pseudoenhancement of simple renal cysts: a comparison of single and multidetector helical CT. J Comput Assist Tomogr 2002;26:90–4.
[47] Coulam CH, Sheafor DH, Leder RA, et al. Evaluation of pseudoenhancement of renal cysts during contrast-enhanced CT. AJR Am J Roentgenol 2000;174:493–8.
[48] Birnbaum BA, Maki DD, Chakraborty DP, et al. Renal cyst pseudoenhancement: evaluation with an anthropomorphic body CT phantom. Radiology 2002;225: 83–90.

RADIOLOGIC CLINICS OF NORTH AMERICA

Radiol Clin N Am 41 (2003) 1095–1115

Radiologic diagnosis of gastrointestinal perforation

Stephen E. Rubesin, MD[a,b,*], Marc S. Levine, MD[a,b]

[a]*Department of Radiology, University of Pennsylvania School of Medicine, Philadelphia, PA 19104, USA*
[b]*Department of Radiology, Hospital of the University of Pennsylvania, 3400 Spruce Street, Philadelphia, PA 19104, USA*

Perforations of the gastrointestinal tract have many causes. Holes in the wall of gastrointestinal organs can be created by blunt or penetrating trauma, iatrogenic injury, inflammatory conditions that penetrate the serosa or adventitia, extrinsic neoplasms that invade the gastrointestinal tract, or primary neoplasms that penetrate outside the wall of gastrointestinal organs. This article provides a radiologic approach for investigating the wide variety of gastrointestinal perforations. General principles about contrast agents and studies are reviewed, and perforations in specific gastrointestinal organs are discussed.

General principles

Oral contrast agents

Barium sulfate is a white crystalline powder of varying particle size. The largest particles in a cup of high-density barium are only about 18 μm in diameter [1], so even these largest barium particles can enter tiny perforations. Barium sulfate is not water-soluble. When combined, barium sulfate and water form a suspension. This lack of solubility explains why a preprepared barium suspension forms layers in its stored container. The radiologist must aggressively shake the barium container to resuspend the heavy barium particles. A tiny portion of barium sulfate is absorbed from the gastrointestinal tract. About 2×10^{-7} of the ingested barium is absorbed and excreted in the urinary tract [2]. High-density barium adheres to the mucosa of bowel. When high-density barium enters a perforation, it also adheres to the perforation site. In contrast, low-density barium preparations barely coat the mucosa and primarily fill the bowel lumen.

Water-soluble contrast agents fill the lumen of the gastrointestinal tract without coating the mucosa. Ionic water-soluble contrast agents are solutions containing at least 60% iodine, a concentration of about 282 to 292 mg/mL [1]. The osmolality of ionic water-soluble contrast agents is about 1400 to 1500 mOsm/kg [1], about five times that of serum. Ionic water-soluble contrast agents draw fluid into the lumen and prevent fluid from being resorbed. These contrast agents may also stimulate peristalsis and induce diarrhea. Water-soluble contrast agents have decreased radiographic density in comparison with most barium preparations. Nonionic contrast agents have an iodine concentration of about 300 mg/mL. Most of these agents have an osmolality of 600 to 710 mOsm/kg and are still hyperosmolar relative to serum.

When a perforation of the pharynx, esophagus, stomach, or duodenum is suspected, a contrast study initially uses an ionic water-soluble contrast agent (eg, Gastroview) [3]. The contrast agents for studying a patient with a suspected perforation of the small bowel or colon are discussed later. Water-soluble iodinated contrast agents do not incite an inflammatory reaction in the mediastinum or peritoneum [4–6]. They also are resorbed quickly from these sites. Ionic water-soluble contrast agents are associated with a theoretical risk of inducing pulmonary edema if aspirated into the pulmonary alveoli because of their hyperosmolality [7,8]. Most cases of pulmonary edema related to the use ionic contrast agents,

* Corresponding author. Department of Radiology, Hospital of the University of Pennsylvania, 3400 Spruce Street, Philadelphia, PA 19104.

E-mail address: rubesin@oasis.rad.upenn.edu (S.E. Rubesin).

0033-8389/03/$ – see front matter
doi:10.1016/S0033-8389(03)00100-3

however, have been reported in children who aspirated Hypaque, Renografin, and oil-based iodinated contrast agents, not Gastrografin or Gastroview [9–11]. At the authors' institution, there has not been a case of pulmonary edema resulting from aspirated Gastroview or Gastrografin. Nevertheless, if there is a strong suspicion of aspiration, the study is initially performed with a nonionic water-soluble contrast agent (eg, Omnipaque) and swallowing is assessed fluoroscopically before using Gastroview [12]. Other radiologists advocate the use of barium as the initial contrast agent if a perforation of the pharynx or esophagus is suspected and there is serious clinical concern about aspiration [13].

Once a water-soluble contrast study does not show a leak in the upper gastrointestinal tract, the patient is asked to swallow high-density barium [14,15]. Water-soluble contrast agents are inferior to barium suspensions in the diagnosis of leaks. Water-soluble contrast agents are thinner, do not coat the mucosa, and run through rather than fill the lumen of the gastrointestinal tract. Barium suspensions are superior in the diagnosis of leaks because they have greater radiographic density and adhere to extraluminal tracks. As a result, about 25% to 50% of esophageal perforations not demonstrated with water-soluble contrast agents can be demonstrated with barium suspensions given immediately after negative or equivocal water-soluble contrast studies [16–18]. One disadvantage of barium suspensions in the diagnosis of upper gastrointestinal perforations is that they can potentially incite a granulomatous reaction in the mediastinum that is exacerbated by swallowed oral flora [4]. The authors, however, have not encountered any cases of barium-induced mediastinitis or inflammatory reaction in the neck over the last 20 years. Another potential disadvantage of barium suspensions is that follow-up studies can be more difficult to interpret if barium persists in the region of the leak.

Radiologic modalities

CT and luminal contrast studies are the two primary modalities used to evaluate gastrointestinal perforations. CT is far superior for the demonstration

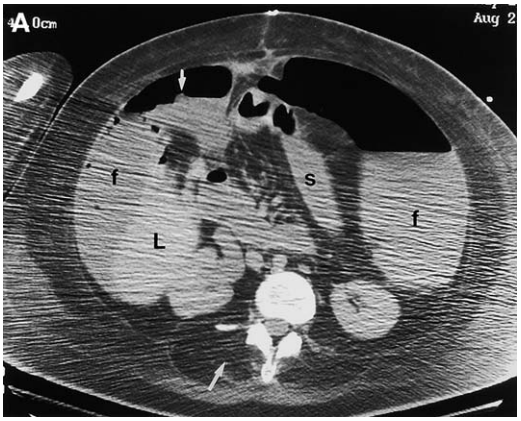

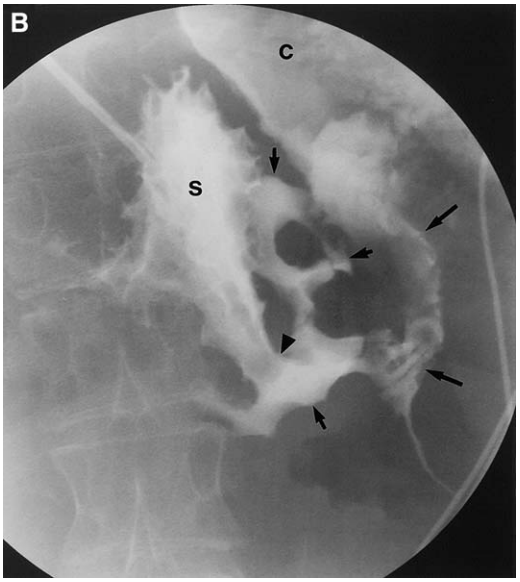

Fig. 1. A 20-year-old man with muscular dystrophy and continuing abdominal distention 7 days after near-total colectomy with ileorectal anastomosis. (*A*) Unenhanced CT through level of mid-stomach (s), lower liver (*L*), and kidneys shows a massive amount of fluid (f) and gas in the right and left intraperitoneal spaces. Several CT findings suggest that the ascitic fluid is not "simple ascites" and that there is the possibility of peritonitis. The fluid level in the right perihepatic space is not level (*short arrow*) and scattered bubbles are present. Note marked atrophy and fatty replacement of the muscles. For example, the paraspinous muscles are of fatty attenuation (*long arrow*). Streak artifact is present because the patient was unable to move his arms and they are by his sides. (*B*) Gastroview was injected into the stomach (s) by an indwelling nasogastric tube. A hole in the greater curvature (*arrowhead*) is seen, with subsequent filling of irregular tracks of contrast (*short arrows*) in the perigastric tissue, then with free flow of fluid (*long arrows*) into a collection (c) in the left subdiaphragmatic space. This case illustrates how CT indicates the presence of an extraluminal process, but that the contrast study may identify the site of leak.

of extraluminal air, fluid, or abscess. CT is often inferior to luminal contrast studies in demonstrating the location, site of origin, or etiology of a gastrointestinal perforation (Fig. 1). In patients who have not had surgery, CT is an excellent modality for detecting the extraluminal changes associated with a perforation (Fig. 2). In immediate postoperative patients or patients with penetrating trauma, however, the presence of a collection or extraluminal air does not necessarily indicate that luminal perforation has occurred or is currently present. For example, most patients with trauma to the chest and CT-demonstrated pneumothorax or pneumomediastinum do not have an esophageal perforation. In some cases, an esophagram may be required to exclude esophageal perforation. Most immediately postoperative patients with pneumoperitoneum do not have a gastrointestinal perforation, but only persistent intraperitoneal gas

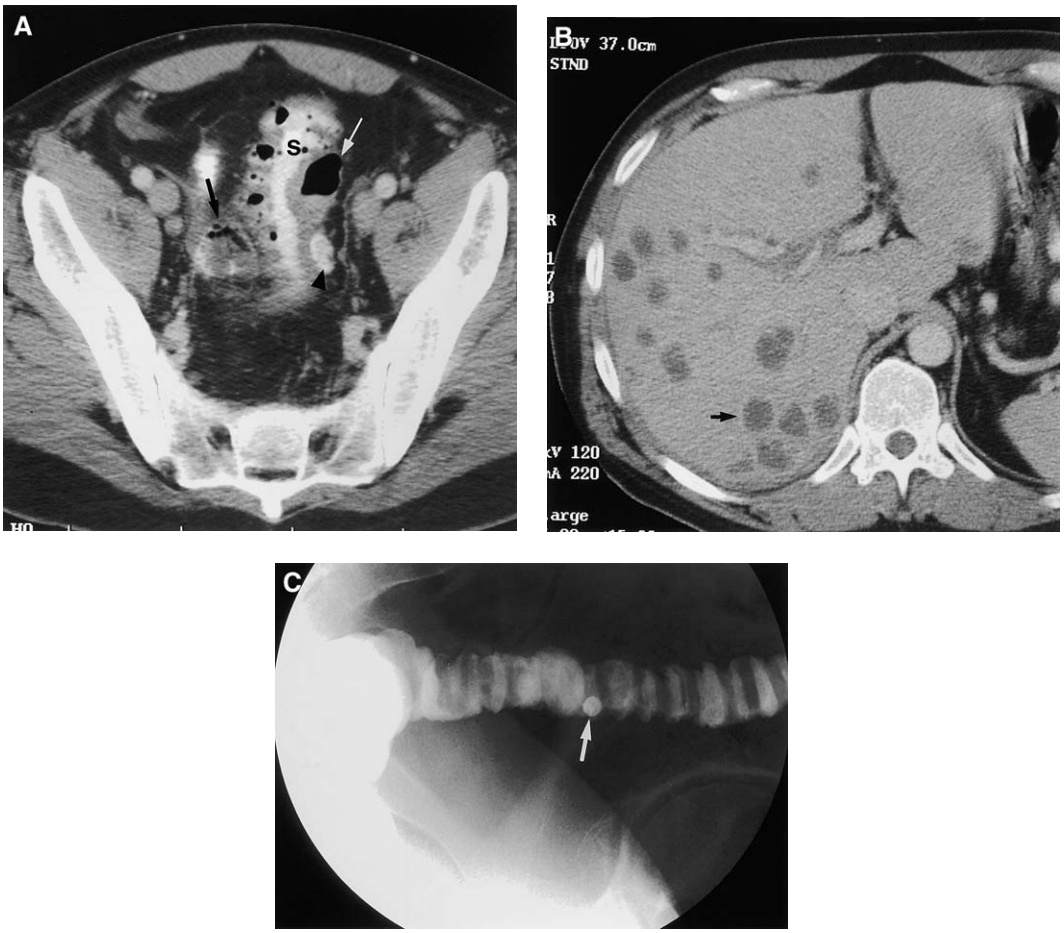

Fig. 2. A 47-year-old man with left lower quadrant pain and fever for 2 weeks. (*A*) CT through pelvis shows multiple diverticula arising from the contrast-filled sigmoid colon (s). A 3 × 2 cm collection (*white arrow*) with an air-debris level lies lateral to the sigmoid. Contrast partially fills a second 1.5 × 1 cm collection (*arrowhead*) lateral to the sigmoid colon. A 2-cm area of soft tissue attenuation and bubbles (*black arrow*) lies to the right of the sigmoid. Fluid tracking into the sigmoid mesentery makes it appear thick. (*B*) CT through the liver reveals many low-attenuation (35 HU) lesions with minimal peripheral enhancement (representative abscess identified by *arrow*). (*C*) Water-soluble contrast enema performed less than 12 hours after the CT scan shows circular muscle thickening and mild narrowing of the colon and one diverticulum (*arrow*), but no contrast enters the pericolic collections. A contrast enema diagnosis of diverticulitis is not possible. At surgery, smoldering diverticulitis was found, associated with many small liver abscesses. This case demonstrates the usual superiority of CT in demonstrating the extent of extraluminal disease and, in particular, the pericolic disease in patients with diverticulitis. The peridiverticular abscesses are examples of extraluminal perforations that have been sealed off from the lumen and may not fill with contrast during a contrast study. The CT also demonstrates a complication of diverticulitis (liver abscess) that is not detected by contrast enema alone.

after surgery. A CT-demonstrated postoperative abscess may be caused by persistence of the inflammatory reaction, continuing or previous perforation at the treated site, or continuing or sealed off anastomotic or staple line leak. Determination of the cause of a postoperative abscess may require a luminal contrast study (see Fig. 1; Fig. 3). Luminal contrast studies are not infallible for diagnosing leaks, because a leak may have sealed off by the time a contrast study is performed (see Fig. 2).

Plain radiographs are inferior to both CT and contrast studies for detection of most diseases that cause perforation. A full plain radiographic series of the abdomen (erect chest and erect and supine abdominal radiographs) is inferior to CT in demonstration of free intraperitoneal gas. Furthermore, many seriously ill patients are evaluated radiographically only in the supine position. Supine abdominal radiographs can demonstrate free intraperitoneal gas in only about 60% of patients with free intraperitoneal gas on a full abdominal series (Fig. 4) [19]. Given the superiority of CT to plain radiographs, CT has been proposed as the initial radiologic test to evaluate patients with acute abdominal pain [20]. At the authors' institution the scout of the CT or a digital scout image is used before a contrast study, rather than obtaining an abdominal series. Plain radiographs are sometimes helpful, however, in demonstrating the distribution of bowel gas and various tubes or surgical clips and staple lines. Plain radiographs are also valuable for follow-up of adynamic ileus or obstruction.

For suspected perforation, the authors suggest that either a CT or water-soluble contrast study be performed, depending on the suspected site, type of disease, and clinical history. These two modalities are clearly complimentary in detection and characterization of gastrointestinal perforation. In general, if a pharyngeal or esophageal perforation is strongly suspected, the authors start with a luminal contrast study. If the patient has a clinical history that strongly suggests a perforation (ie, recent surgical anastomosis, pain after endoscopy) the authors start with a luminal contrast study if the anastomosis or trauma is all but in the mid small bowel (Fig. 5). Otherwise, if the history is of abdominal pain, fever, draining abdominal wound, or leukocytosis, the authors prefer to start with a CT to obtain a global picture that a luminal contrast study cannot achieve. It is always safer to start with CT, because the low-density CT contrast does not ruin a subsequent luminal contrast

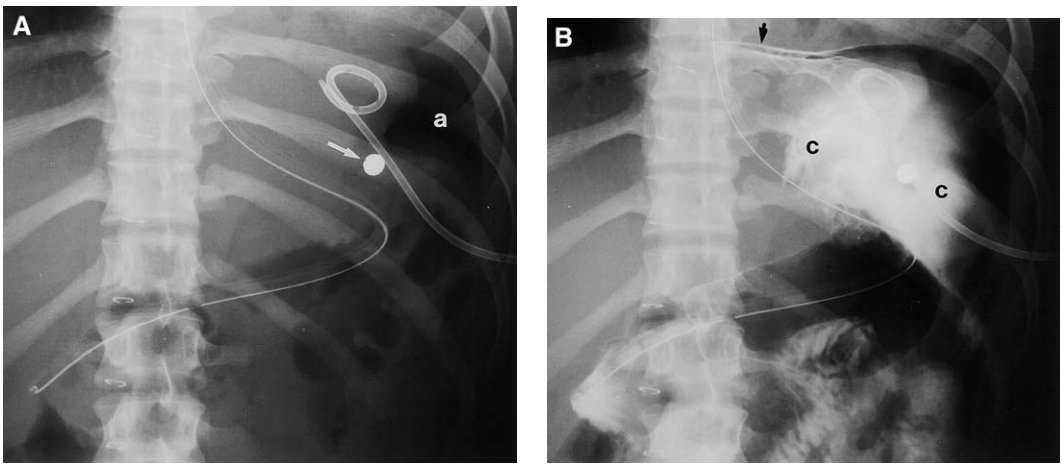

Fig. 3. A 19-year-old man with history of gunshot wound to the abdomen resulting in exploratory laparotomy with splenectomy. Three days postoperative, a CT showed a left subphrenic abscess. One day later, the abscess was drained by a pigtail catheter using ultrasound guidance. (*A*) Plain radiograph of the abdomen obtained 6 days after initial surgery shows the pigtail drainage catheter, a bullet fragment (*arrow*), and a triangular-shaped air collection in the left subdiaphragmatic space (a). (*B*) An upper gastrointestinal series (GI) was performed because of continuing fever and copious drainage from the pigtail catheter. Overhead radiograph from an upper GI series using water-soluble contrast shows an amorphous contrast collection (c) with contrast outlining the left subdiaphragmatic space (*arrow*). A leak in the gastric fundus was shown on fluoroscopic images. At repeat surgery, a perforation of the gastric fundus was oversewn. This case is an example of a contrast study demonstrating a leak, resulting in explanation of plain radiograph or CT findings. This case also demonstrates that in a postoperative patient it is difficult to determine whether CT findings of an abscess represent continuing presence of a known inflammatory process, an untreated leak caused by the original disease, or a postoperative complication.

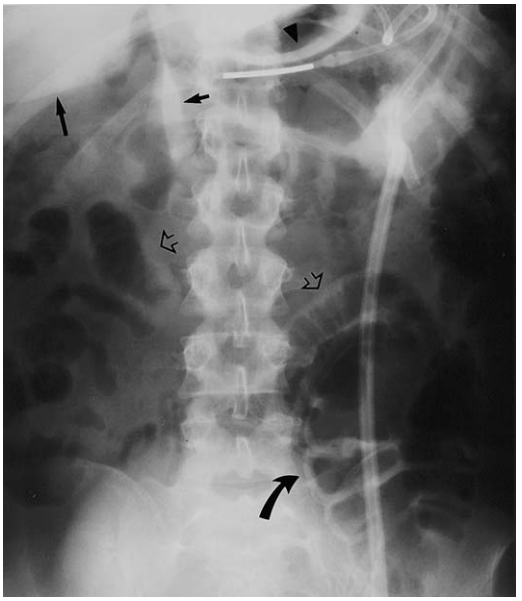

Fig. 4. Plain film findings of free intraperitoneal gas on supine radiograph. Supine plain radiograph of abdomen shows several signs of free intraperitoneal gas. The falciform ligament (*short arrow*) is outlined by free air as a linear density coursing from the edge of the liver toward the umbilicus. The edge of the liver (*long arrow*) is sharply outlined by free intraperitoneal gas. Rigler's sign is the outlining of a bowel wall by gas within the lumen of the bowel and free intraperitoneal gas outside the bowel wall. A Rigler's sign involving the sigmoid colon (*curved arrow*) and several small bowel loops (*open arrows*) is seen. Air in the left posterior perihepatic space results in a Rigler's sign involving the lesser curvature of the stomach (*arrowhead*). The free intraperitoneal gas was caused by recent gastrostomy tube placement.

study, as the high-density luminal contrast agent ruins a subsequent CT.

Perforations of the pharynx and esophagus

Spontaneous esophageal perforation

Spontaneous esophageal perforation is known as "Boerhaave's syndrome," originally described by Boerhaave in 1724 [21]. In contrast, Mallory-Weiss tears are linear lacerations confined to the mucosa and submucosa at or near the gastroesophageal junction [22]. The pathogenesis of both Mallory-Weiss tears and Boerhaave perforations is a sudden, rapid increase in intra-abdominal pressure, most commonly caused by severe retching and vomiting. Although the vomiting episodes are usually related to alcoholic binges, any cause of severe emesis can result in a traumatic tear or perforation. Esophageal perforation can also result from other causes of rapidly elevated intra-abdominal pressure including seizures, childbirth, blunt trauma, and severe straining at stool [23]. Patients with Mallory-Weiss tears typically present with upper gastrointestinal bleeding after an episode of violent retching. Mallory-Weiss tears account for 5% to 15% of all upper gastrointestinal bleeds. In contrast, patients with Boerhaave's syndrome are severely ill, with mediastinitis, sepsis, and shock developing after an episode of severe retching.

In patients with Boerhaave's syndrome, CT may demonstrate an extraluminal collection of gas and fluid, but may not be able to determine the site of perforation. An upper gastrointestinal series may demonstrate a 1 to 4 cm in length, vertically oriented tear in the distal esophagus just above the gastroesophageal junction, with extravasation of contrast material into a lower mediastinal collection (Fig. 6). Although Boerhaave's tears are usually on the left side of the distal esophagus, they occasionally may be located on the right side of the distal esophagus or even in the cervical esophagus [24].

Foreign body perforation

Most foreign bodies that are swallowed pass spontaneously, especially if they are small and smooth [25]. Large or sharp foreign bodies may lodge in the pharynx or esophagus and cause acute dysphagia, however, after an episode of gagging or choking. Large foreign bodies that occlude the laryngeal aditus may cause severe dyspnea. Small fragments of glass are often trapped in the interstices of the palatine tonsils, whereas bone fragments are often trapped in the tips of the piriform sinuses, above the cricopharyngeus or in the upper cervical esophagus [26].

A plain radiograph of the neck should be obtained with the patient in the lateral position during phonation of the sound "Eee." Radiopaque fragments of glass or bone can often be demonstrated in the palatine tonsils and hypopharynx, respectively, but some fish bones and glass fragments are not radiopaque. Plain radiographic signs of perforation include subcutaneous emphysema, pneumothorax, and pneumomediastinum. Focal or diffuse widening of the retropharyngeal space may indicate abscess formation. A water-soluble contrast swallowing study should initially be performed to diagnose a perforation. If a perforation is not seen with a water-soluble contrast agent, high-density barium is then given.

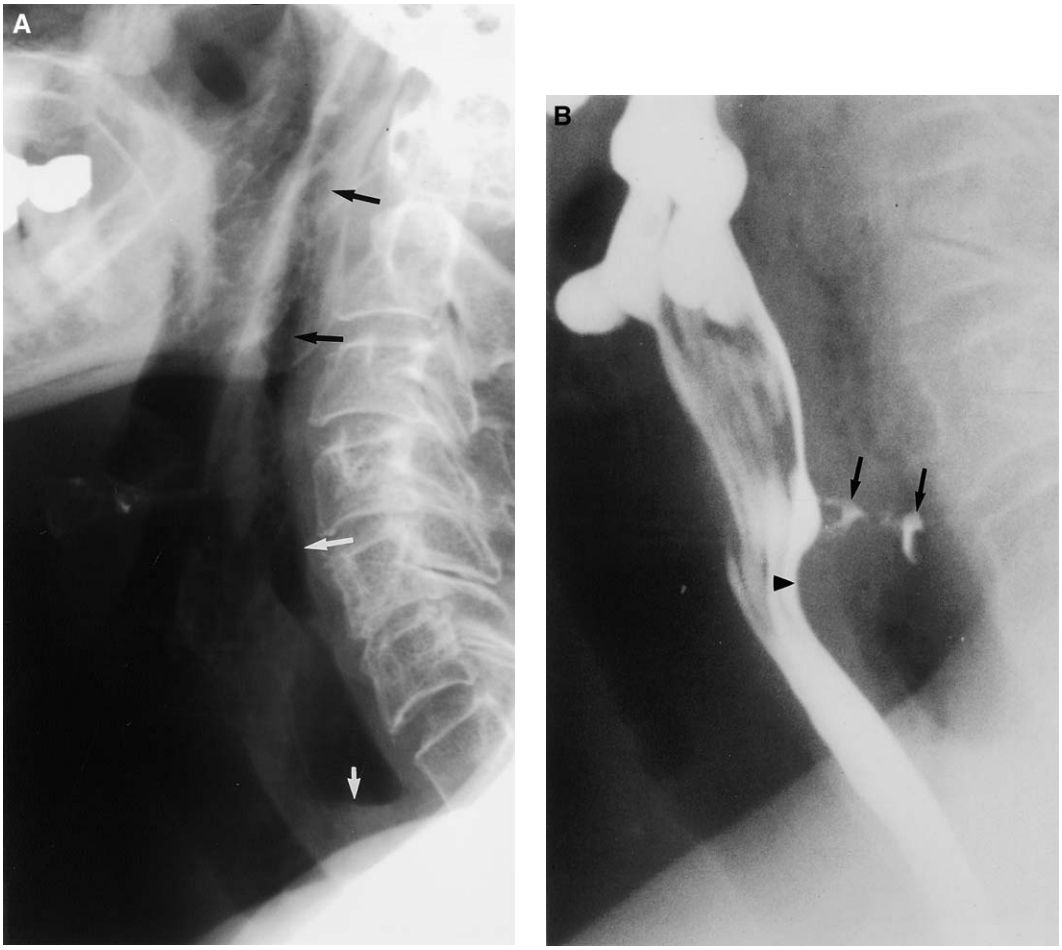

Fig 5. An 81-year-old woman with neck pain after a difficult upper endoscopy. (*A*) Scout radiograph of the neck shows a large amount of air in the retropharyngeal space (*long arrows*), extending from the nasopharynx to the cervical esophagus. An air-fluid level (*short arrow*) is seen at the level of the C-7 vertebral body. (*B*) Close-up from a spot radiograph obtained during swallowing shows a track of contrast (*arrows*) extending into the retropharyngeal space. The track arises from a perforation just above the indentation of the cricopharyngeus muscle (*arrowhead*). Fluoroscopic images showed incomplete opening of the cricopharyngeus muscle.

Leaks from the pharynx or esophagus may be manifested by linear or focal extraluminal collections of contrast, often parallel to the pharyngeal or esophageal wall. Erosions or superficial mucosal tears usually are missed on contrast studies. The authors have not found the use of a barium-coated cotton ball to be helpful for diagnosing nonradiopaque foreign bodies.

Iatrogenic perforations

Endoscopic procedures are responsible for most nonsurgical iatrogenic perforations of the pharynx and esophagus (see Fig. 5; Fig. 7). Perforations related solely to intubation are usually located in the lower piriform sinus or region of the cricopharyngeal muscle. Perforations also are prone to occur at sites of pharyngeal or esophageal narrowing, such as cervical esophageal webs; outpouchings, such as Zenker's diverticulum; or areas of extrinsic compression by osteophytes or the aortic arch. Endoscopic procedures, such as dilatation of the lower esophageal sphincter for achalasia, sclerotherapy, laser coagulation of tumors, or stent placement, are also associated with a substantial risk of esophageal perforation [27,28]. At the authors' institution, contrast studies are obtained on routine basis after all endoscopic procedures for achalasia and stent placement. Perforations may not

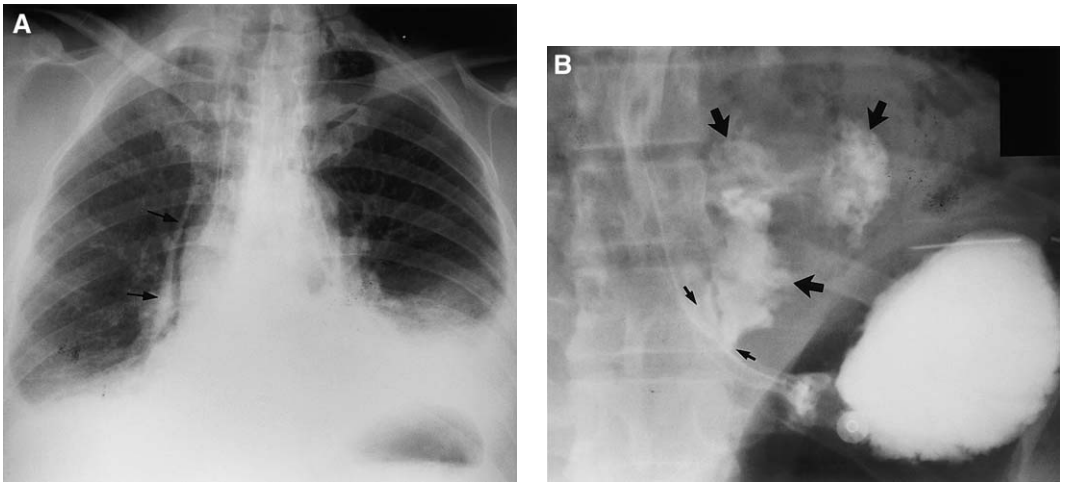

Fig. 6. Boerhaave's syndrome. (*A*) Radiograph obtained in frontal position shows right-sided pneumomediastinum (*arrows*) and a left pleural effusion. (*B*) Water-soluble contrast examination shows contrast flowing from the left lateral wall of the distal esophagus (*small arrows*) into the left side of the mediastinum (*large arrows*). (*From* Levine MS. Miscellaneous abnormalities of the esophagus. In: Gore RM, Levine MS, Laufer I, editors. Textbook of gastrointestinal radiology. Philadelphia: WB Saunders; 1994. p. 517.)

become clinically apparent until several days after surgery [29].

Postoperative esophageal perforation

An anastomotic or staple line leak is the most common serious complication of esophageal surgery. Anastomotic leaks may result in mediastinitis, abscess formation, and sepsis. Esophageal anastomoses are more prone to leak than other gastrointestinal anastomoses because the esophagus lacks a serosa [30]. The esophageal mucosa also tends to retract from a cut margin because there is considerable mobility between the squamous mucosa, submucosa, and muscularis propria [30]. At the authors' hospital, most patients undergo routine contrast studies of the esophagus 6 to 8 days after esophageal surgery to exclude an anastomotic leak that is not causing symptoms or is masked by routine postoperative complaints. Delayed esophageal perforations may also occur [31]. If there is any clinical suspicion of a leak during the postoperative period, an upper gastrointestinal series should be performed. A postoperative chest radiograph that shows pneumomediastinum, a widened mediastinum, subcutaneous air, or an enlarging pleural effusion should also suggest the possibility of an anastomotic or staple line leak [32].

When performing postoperative upper gastrointestinal contrast studies, overhead or fluoroscopically obtained scout images are obtained with the patient in the frontal and right and left posterior oblique positions with the radiographs centered so that the region of the expected anastomosis is demonstrated. When contrast studies are performed on patients after esophagogastrectomy, the radiologist should look for laryngeal penetration, leaks or obstruction at the anastomosis, leaks along the stomach if a gastric tube has been created, obstruction where the stomach passes through the diaphragm, leaks or obstruction at the pyloroplasty or pyloromyotomy, and leaks or obstruction at the jejunostomy tube site if a jejunostomy tube has been placed [33]. Water-soluble contrast agents should initially be used. If no leak is seen, high-density barium should then be administered to the patient. This can be a very difficult examination for both the patient and the radiologist, because postoperative patients are often immobile; unable to stand; and are connected to numerous intravenous lines, monitors, and chest tubes. The patient should be studied in as erect a position as possible and at least once in a recumbent position to ensure that the anastomosis and upper gastric body are bathed in contrast.

Perforations of the stomach

Peptic ulcer disease

Gastric and duodenal ulcers may perforate freely into the intraperitoneal space or into the lesser sac and

Fig. 7. A 71-year-old woman with fever and pain after upper GI endoscopy. Spot radiograph from a water-soluble upper GI series shows a hole (*long black arrow*) just above the esophagogastric junction and contrast beginning to spread (*short black arrows*) into the paraesophageal space. Note the air collection (*white arrow*) that has not yet filled with contrast. A distal esophageal perforation was repaired surgically.

retroperitoneum. Ulcers on the anterior wall of the stomach or duodenal bulb may perforate into the intraperitoneal space, resulting in peritonitis and localized abscesses (Fig. 8). A large percentage of perforated gastric and duodenal ulcers, however, seal off rapidly. As a result, free intraperitoneal gas can be detected on plain abdominal radiographs in only about two thirds of patients with perforated ulcers [34]. When a perforated ulcer is suspected, the upper gastrointestinal study should initially be performed with a water-soluble contrast agent. Extravasation of contrast material into the peritoneal space is detected in only about 50% of patients with a perforated ulcer [35]. About one-half of anterior wall perforations flow freely into the intraperitoneal space; the other half form walled-off collections [35].

Ulcers on the posterior wall of the stomach and duodenum may perforate into pancreas, lesser omentum, transverse mesocolon, liver, spleen, biliary tree, or colon (Fig. 9). Posterior wall peptic ulcers most commonly perforate into the pancreas, resulting in pancreatitis or true abscess formation. Ulcers that perforate into the biliary tree or colon also may lead to fistula formation. An abscess in the left lobe of the liver or spleen may result from posterior wall penetrating ulcers. Less than one-half of patients with penetrating posterior wall ulcers have free intraperitoneal gas on plain radiographs or extravasation of water-soluble contrast agent from the lumen of the stomach or duodenum. Many of these leaks seal off, so that contrast studies only reveal the underlying ulcer on the posterior wall of the stomach or duodenal bulb. As a result, CT may be the first modality to suggest the diagnosis of a perforated posterior wall peptic ulcer [36–38]. Small bubbles of gas or pockets of fluid may be seen trapped near the wall of the stomach or duodenum; near the surface of the pancreas; or in the mesenteries near the duodenal bulb and stomach (ie, the hepatogastric and hepatoduodenal ligaments) (Fig. 10). Small bubbles of air also may be detected in the greater or lesser peritoneal sac. CT may also reveal evidence of pancreatitis, especially in the pancreatic head, or ascites with or without peritoneal enhancement that suggests peritonitis.

Gastrocolic fistulas

The stomach is connected to the transverse colon by the proximal portion of the greater omentum, also known as the "gastrocolic ligament." Any inflammatory or neoplastic disease may spread to and from the stomach to the colon by this ligament. Currently, the most common cause of a fistula between the stomach and transverse colon is a benign gastric ulcer related to the use of a nonsteroidal anti-inflammatory agent [39]. Crohn's disease of the transverse colon and adenocarcinoma of the stomach or transverse colon, however, can also result in the development of gastrocolic fistulas [40,41].

Postoperative perforations

Anastomotic leaks and staple line dehiscences after surgery for peptic ulcer disease are less common than leaks after esophageal surgery. Surgeons frequently choose to oversew a perforated ulcer because there is less than a 20% recurrence rate

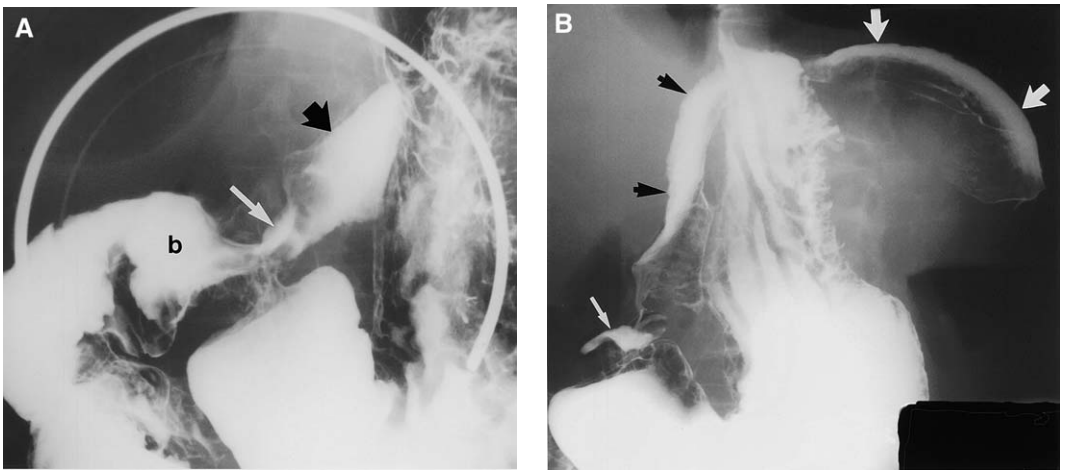

Fig. 8. Perforated ulcer, anterior wall, duodenum in a 64-year-old man with several weeks of mild right upper quadrant abdominal pain. (*A*) Spot radiograph from upper GI shows and ovoid barium collection (*white arrow*) probably representing the duodenal ulcer, just distal to the pylorus. A triangular-shaped extraluminal collection (*black arrow*) is filled with barium. The duodenal bulb (b) is deformed. (*B*) Spot radiograph with patient in right posterior oblique position shows deformity of the duodenal bulb (*thin white arrow*), a large barium-filled track (*black arrows*) anterior to the stomach, and barium spreading into the left subdiaphragmatic space (*thick white arrows*) to outline the spleen.

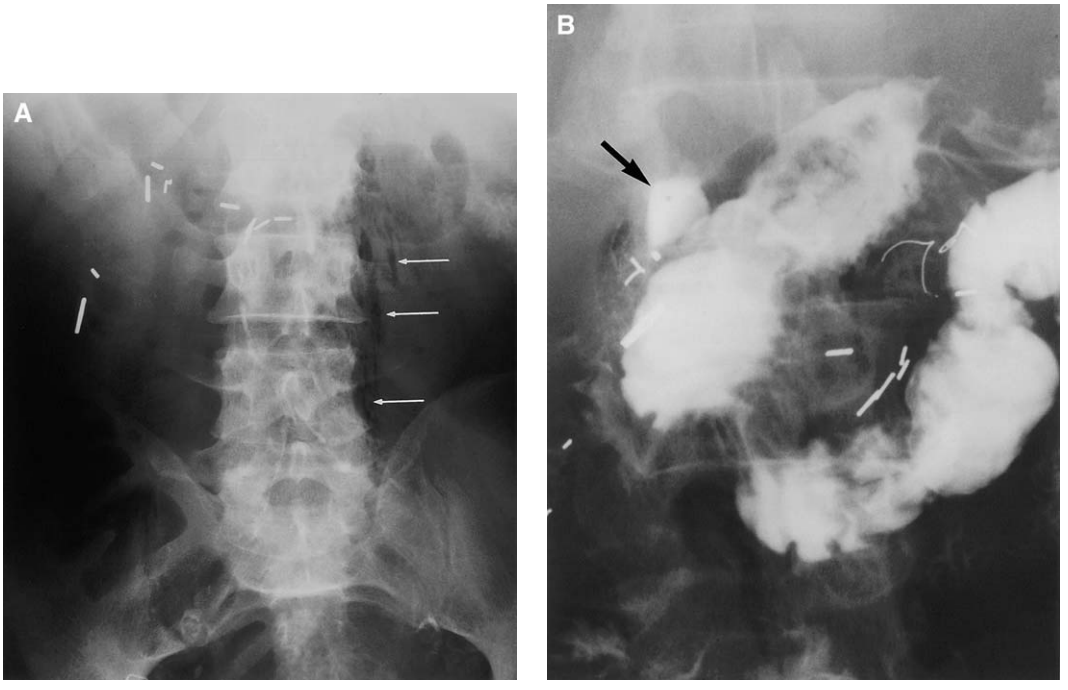

Fig. 9. Perforated posterior wall duodenal ulcer in 64-year-old man with abdominal pain. (*A*) Plain radiograph of abdomen shows linear streaks of gas (*arrows*) in the left retroperitoneum. (*B*) Spot radiograph from water-soluble upper GI series with patient in a steep left posterior oblique position shows a triangle-shaped collection (*arrow*) distal to the apex of the duodenal bulb, just as the second portion of the duodenum enters the retroperitoneum. This collection enlarged on later films. This case is an example of how a duodenal perforation can spread to both sides of the retroperitoneum.

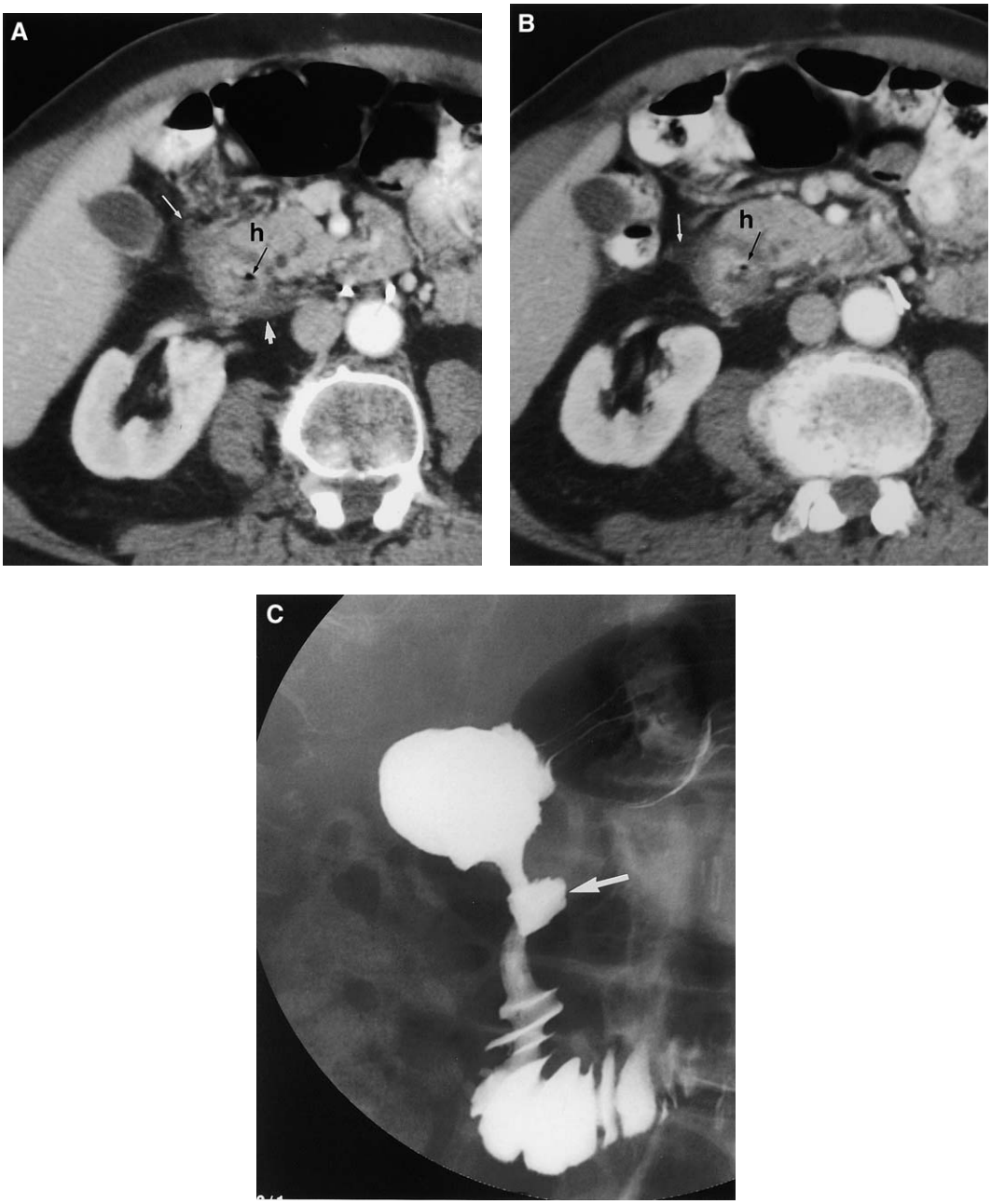

Fig. 10. An 82-year-old man with 30-lb weight loss and mild upper mid-abdominal pain. (*A,B*) Two images from a CT scan at the level of the pancreatic head (h) show that the wall of the duodenum is mildly thickened and of low attenuation. The CT diagnosis was ''thick duodenal wall, recommend endoscopy.'' In retrospect, there is stranding of the periduodenal fat (*thin white arrows*) and a small amount of fluid posterior to the duodenum (*thick white arrow*). A tiny bubble of gas is seen medially (*black arrows*). (*C*) Endoscopy was negative. Digital spot radiograph from a subsequent single-contrast small bowel follow-through shows a 1.5-cm ulcer (*arrow*) just proximal to the papilla of Vater and thickened folds throughout the second part of the duodenum. A repeat endoscopy confirmed the postbulbar ulcer. This case illustrates the difficulty of CT diagnosis in the region of the duodenum and the complementary value of contrast studies for demonstration of small holes in the GI tract. It is unknown if the bubble of gas demonstrated on the CT scan represents the ulcer or the lumen of the duodenum.

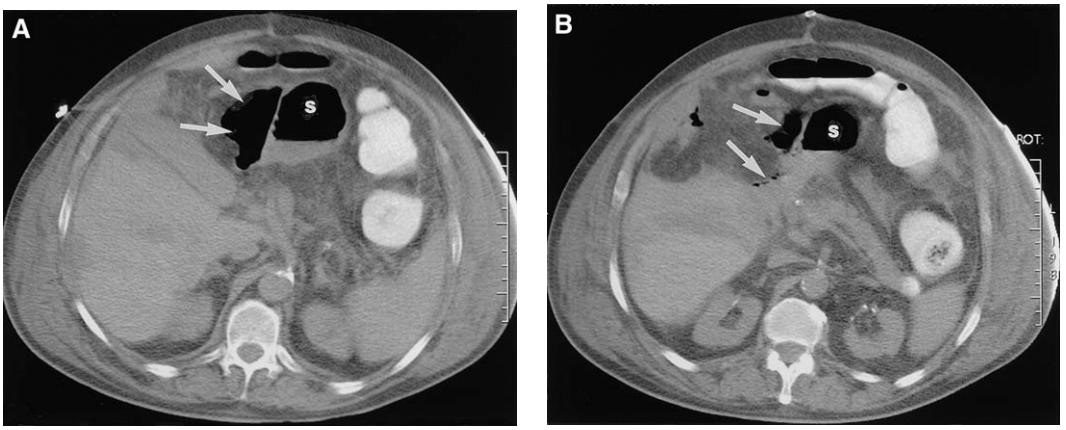

Fig. 11. Duodenal bulb leak following Grahm plication of perforated peptic ulcer in a 73-year-old-man with renal insufficiency. (*A*, *B*) Axial images of the upper abdomen reveal large amounts of extravasated air adjacent to the distal stomach and duodenal bulb (*arrows*). S = stomach. Proved at surgery.

with therapy [42]. At the authors' hospital, upper gastrointestinal contrast studies are performed on a routine basis to exclude leaks after oversewing peptic ulcers. Patients with symptoms after other forms of peptic ulcer surgery also undergo postoperative studies. A postoperative upper gastrointestinal study should initially be performed with an ionic water-soluble contrast agent, followed by high-density barium if no leak is identified.

Anastomotic leaks may be detected at gastroenteric or enteroenteric anastomoses. Leaks may also occur at the oversewn proximal duodenal stump after Billroth II surgery or after Grahm plication of perforated duodenal ulcers (Fig. 11). The postoperative contrast examination may show contrast material outside the expected lumen of the bowel filling a collection or fistula. CT also is useful for demonstrating the size and location of an abscess cavity or guiding percutaneous drainage of an abscess collection.

Anastomotic or staple line dehiscence also may occur after vertical banded gastroplasty or gastric bypass procedures for morbid obesity [43,44]. Perforation of a gastric pouch may also be caused by gastric hyperacidity, ischemia, or an indwelling tube [42–44]. Transmural necrosis may develop 24 to 36 hours after surgery, resulting in a delayed postoperative perforation. Given the difficulty of the surgical procedures performed in patients with morbid obesity, predischarge postoperative contrast studies are routinely performed on these patients at the authors' hospital, first with ionic water-soluble contrast agent, followed by high-density barium if no leak is initially seen.

Perforations of the small intestine

Ischemia and infarction

Small intestinal ischemia has a wide spectrum of etiologies and severity [45]. The most serious complication of small intestinal ischemia is transmural necrosis and perforation, leading to peritonitis, with possible sepsis and death. The most common form of small intestinal ischemia in hospitalized patients is splanchnic vasoconstriction related to hypovolemia and hypotension. Such drugs as digitalis, dopamine, vasopressin, and cocaine can result in severe splanchnic vasoconstriction. Superior mesenteric arterial occlusion may result from embolism caused by atrial fibrillation, cardiac valve disease, left ventricular thrombus related to myocardial infarction, and left atrial myxoma. Other etiologies include atherosclerosis, blunt or penetrating abdominal trauma, mesenteric vascular compression or twisting caused by adhesions (Fig. 12), internal hernias, midgut volvulus, and tumors in the small bowel mesentery [45]. Mesenteric venous occlusion usually occurs secondary to thrombosis related to portal hypertension, surgery, trauma, oral contraceptives, and various hypercoagulable states.

In patients with ischemia, plain radiographs may demonstrate dilated small bowel loops with air-fluid levels; thickening of valvulae conniventes and the bowel wall; pneumatosis in a linear or speckled configuration; and, rarely, portal venous gas. CT is superior to plain radiographs in demonstrating these findings [46,47]. On an unenhanced CT scan, bowel

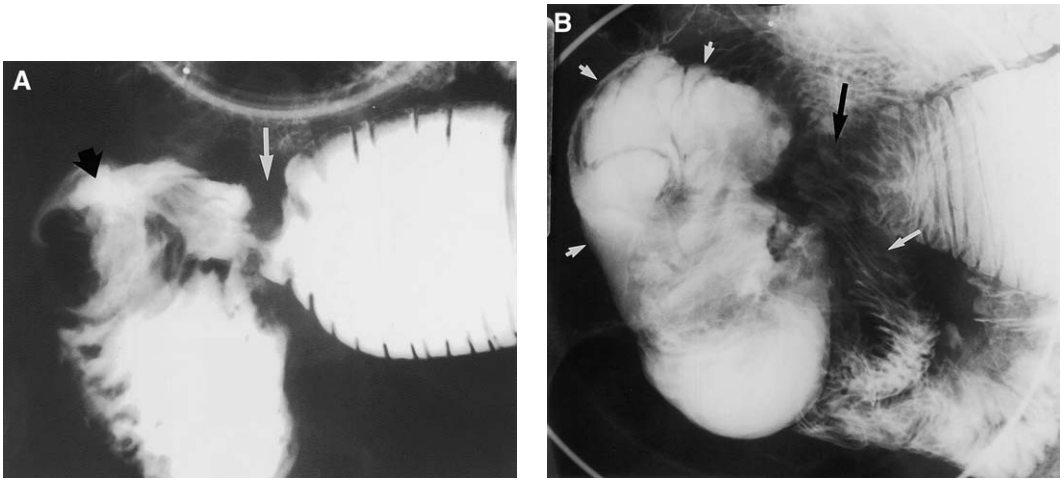

Fig. 12. A 71-year-old woman with abdominal pain and distention after resection for sigmoid carcinoma and repair of colovesical fistula. (*A*) Spot radiograph performed early in the single-contrast phase of enteroclysis centered on the head of the barium column shows a focal band-like narrowing (*white arrow*) and an abnormal loop of jejunum with a questionable 7-mm ulcer manifested as a double density (*black arrow*). (*B*) Spot radiograph of the same loop obtained later in the enteroclysis (after methylcellulose injection) shows a well-circumscribed but amorphous barium collection (*small white arrows*) surrounding the area of the loop. No valvulae are seen in the barium collection. The area of the band is collapsed (*large black arrow*). A collapsed small bowel loop (*large white arrow*) is now seen distally. The enteroclysis diagnosis is now a partial closed loop obstruction underneath an adhesive band with possible perforation. At surgery, an abscess cavity (the amorphous barium collection) was found. The jejunum had ulcerated and perforated because of ischemic necrosis developing in this partially closed-loop obstruction underneath an adhesive band.

wall thickening may be of increased attenuation, reflecting blood within the lamina propria and submucosa [48]. Absent or delayed enhancement of the bowel wall may be detected after injection of intravenous contrast material [48]. The small bowel mesentery may also have increased attenuation caused by vascular engorgement or obstruction or leaking of intestinal contents into the interloop spaces. If a closed loop obstruction is the cause of the ischemia, CT may demonstrate the twisting of the bowel at the site of the adhesive band or internal hernia. Mesenteric vessels converge to a point near the band or entrance to the hernia. The small intestinal loops may be aligned in a U-shaped or radial configuration.

Blunt trauma

Blunt abdominal trauma may result in rapid elevation of intraluminal pressure and intestinal perforation. CT may demonstrate bowel wall thickening, pneumatosis, and pneumoperitoneum with or without extravasation of oral contrast material [49]. A focal fluid collection in the small bowel mesentery may be visualized adjacent to an injured small bowel loop. Direct small intestinal trauma and perforation may also occur during distention of the balloon on the tip of an enteroclysis catheter [50].

Inflammatory conditions

CT is the method of choice for the evaluation of suspected perforations and abscesses related to foreign bodies and inflammatory conditions of the small bowel. Among the most common inflammatory etiologies are perforated diverticula and Crohn's disease. Small bowel diverticula are commonly located in the duodenum or proximal jejunum and seen less frequently in the terminal ileum. Acute inflammation may lead to free perforations and peritonitis or sealed off perforations with abscesses. On CT imaging the distended diverticulum can be visualized, associated with adjacent inflammatory stranding and extraluminal air (Fig. 13). In Crohn's disease, abscesses may be closely related to the bowel wall or may extend well beyond the bowel wall into adjacent structures [51]. Inflammatory stranding and changes in the small bowel mesentery adjacent to thick-walled segments of bowel are not specific for perforation in patients with Crohn's disease. Although fistulas may be detected with CT [52], barium studies (either small bowel follow-through or enteroclysis) are superior for

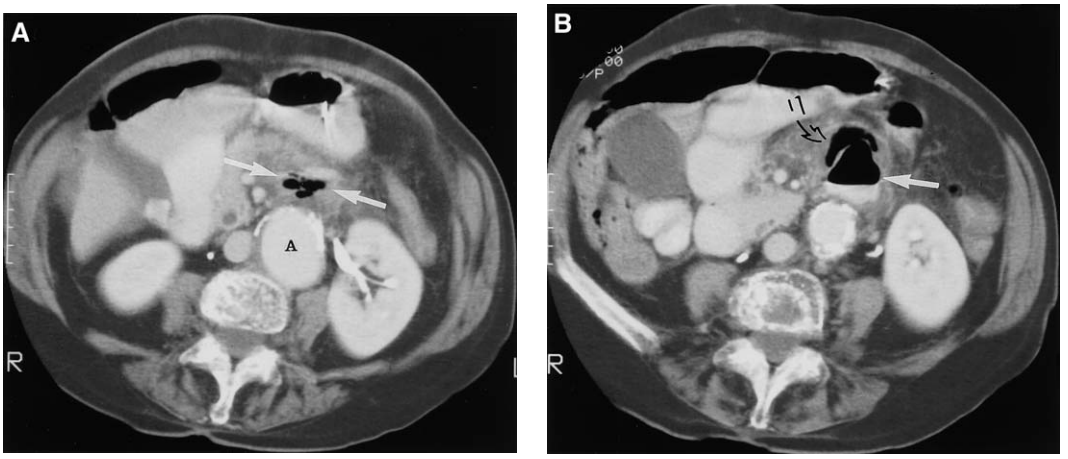

Fig. 13. Perforated duodenal diverticulum in a 71-year-old woman with acute abdominal complaints. (*A*) Axial image in the upper abdomen shows small bubbles of extraluminal air (*arrows*) with adjacent mesenteric inflammatory changes. Note the abdominal aortic aneurysm (*A*). (*B*) An adjacent caudal image reveals the distended distal duodenal diverticulum (*solid arrow*) and extravasation of air anterior to the diverticulum (*open arrow*). Surgically proved.

demonstrating fistulas. Walled-off abscesses also can be seen adjacent to the small bowel in patients with jejunal diverticulitis [53].

Perforating tumors

Primary non-Hodgkin's lymphomas and malignant stromal tumors of the small bowel may invade the adjacent small bowel mesentery. If these tumors become necrotic, a cavity forms within the mesenteric tumor. The cavity may communicate with the bowel lumen. Some of these lesions also show true perforation into the intraperitoneal space [54]. CT may reveal a large cavitary mass with a wall of varying thickness. The adjacent small bowel wall may be thickened by tumor. The small intestine is one of the many sites of involvement by late-stage posttransplant lymphoproliferative disorder. Ulceration with subsequent perforation may occur in loops affected by posttransplant lymphoproliferative disorder, most frequently in the jejunum [55]. Rarely, perforation with abscess formation can also be seen in patients with ectopic pancreas complicated by pancreatitis [56].

Postoperative small intestine

Water-soluble contrast agents are hyperosmolar, draw fluid into the lumen of the intestine, and prevent fluid resorption, resulting in a lower iodine concentration and less radiographic visibility. Water-soluble contrast agents are diluted further if the postoperative small intestine is dilated. It may be very difficult to demonstrate a leak from an enteroenterostomy during a small bowel follow-through performed with water-soluble contrast material, especially if the leak is a considerable distance from the stomach and the intestine is dilated. The ability to demonstrate a small intestinal leak may also be compromised by overlapping loops of small intestine. Fortunately, small bowel anastomoses do not leak very frequently. Leaks from the proximal jejunum can be evaluated adequately by performing a water-soluble contrast study, either by having the patient drink contrast or by injecting a nasogastric tube with water-soluble contrast. If a suspected leak from a mid small bowel anastomosis needs to be evaluated, a CT scan should initially be performed to ascertain if there are any CT findings to suggest a leak, such as intraperitoneal fluid or air bubbles, enhancing peritoneal surfaces, interloop abscesses, or an abscess or inflammatory changes at the staple line. If there is a low suspicion of a leak or the likelihood that the leak is walled-off, barium study should be performed. Rarely, patients with suspected mid small intestinal leaks may be evaluated by enteroclysis with water-soluble contrast agents, but only when the bowel is not dilated, so the contrast is not diluted.

Ileocolic anastomoses or distal enteroileal anastomosis are best evaluated by a retrograde approach through the rectum using a water-soluble contrast enema. The duodenal stump of the afferent loop of a Billroth II procedure or Roux-en-Y procedure may be difficult to visualize by per-oral studies. If an indwelling duodenal tube is present, the duodenum can

be evaluated by the tube. If a biliary tube is present, the duodenum may be evaluated by this tube. If no tube is present, CT may be performed. In some patients, the authors have performed a nuclear medicine scan with a biliary agent to assess for leakage of contrast agent from the duodenum and Roux-en-Y loop.

Leaks related to a recently placed jejunostomy tube may not be seen after injection of the J-tube with contrast material. The tip of the tube may be a considerable distance from its site of entry into the bowel wall. If contrast does not reflux retrograde toward the site of jejunostomy tube entry into the bowel wall, leaks may be missed [57]. J-tube leaks are often best demonstrated from above by contrast material that is swallowed or administered by a nasogastric-gastrostomy tube injection.

Ileal pouches are frequently created as fecal reservoirs proximal to an ileoanal anastomosis in patients who have undergone total colectomy for ulcerative colitis or familial adenomatous polyposis syndrome. This is usually performed as a two-stage procedure because of a very high pouch leak rate. In the first stage, an ileoanal pouch is created and an ileostomy is performed to divert the fecal stream from the operative site. About 6 weeks later, the diverting ileostomy is taken down as a second-stage procedure. The authors routinely perform a water-soluble contrast study of the pouch before the diverting ileostomy is taken down. A Foley catheter is placed in the anal canal. If injection of water-soluble contrast material (Gastroview) reveals no evidence of a leak at the ileoanal anastomosis, the catheter is advanced into the ileal pouch. Water-soluble contrast is then injected into the pouch. Possible sites of a leak include the ileoanal anastomosis and the staple lines of the pouch and at the stump of the pouch [58]. CT may be helpful for showing an abscess and inflammatory stranding of the fat in the presacral space or elsewhere in the pelvis [59], but CT is inferior to contrast enema for showing the size and location of the leak.

Perforations of the colon

Rectal and colonic perforations

Rectal perforation may result from foreign bodies inserted into the rectum, including those inserted for eroticism and during criminal assault. Deep rectal biopsies, polypectomy, improper cleansing enema, or thermometer placement may also lead to rectal perforation. Rectal perforations that occur below the peritoneal reflexion lead to retroperitoneal air dissection and have a more benign clinical course compared with the intraperitoneal perforations. Small rectal perforations that occur in an otherwise healthy patient heal spontaneously without the need of surgical intervention.

Although all intraperitoneal gastrointestinal perforations are grave abdominal emergencies, colonic perforations that often result in peritonitis caused by fecal contamination are particularly dreadful. Colonic perforations are commonly seen in clinical practice. They can be classified into perforations that occur at the site of a localized pathologic process (diverticulitis, carcinoma, foreign bodies) and cecal perforations that occur secondary to distal colonic obstructions. The obstructive process, often carcinoma or sigmoid volvulus, leads to severe colonic distention mostly when the ileocecal valve is competent and the colon cannot decompress. Cecum having the largest transverse diameter develops high intraluminal pressures and the highest wall tension that leads to diastatic perforation (Fig. 14). According to Laplace's law, wall tension = intraluminal pressure × radius, and explains why cecum is a common site of perforation. Risk of

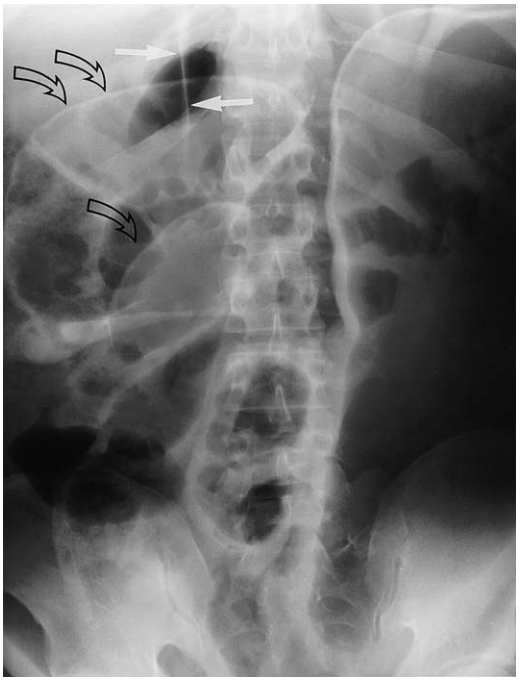

Fig. 14. Cecal perforation caused by sigmoid volvulus in 67-year-old man. Conventional supine abdominal film demonstrates the falciform ligament (*solid arrows*) and Rigler's double wall sign (*open arrows*) indicative of free intraperitoneal air. Proved at surgery.

cecal perforation is high when there is rapid colonic distention, when the cecum reaches 12 cm in diameter, and when the intraluminal cecal pressures are above 20 mg Hg [60].

Perforation during barium enema examination or colonoscopy

Most perforations related to barium enema occur in diseased portions of the colon or because of insufflation of an enema tip balloon [61,62]. Perforation of the colon is rare, occurring during about 1 in 10,000 barium enema examinations. The mortality rate for barium enema is about 1 in 50,000 [63]. In contrast, the perforation rate of colonoscopy is 10 to 20 times that of barium enema, with a perforation rate of about 0.2% and a mortality rate of 0.02% [64,65]. Distention of the enema tip balloon is usually not necessary, because with encouragement, most patients can hold the barium and air in the rectum. The authors find that it is necessary to insufflate the enema balloon in only about 5% to 10% of patients. The enema balloon is inflated only after a normal rectum has been demonstrated by the barium column. Relative contraindications for enema balloon insufflation include suspected colitis; a history of pelvic radiation; chronic mucosal prolapse syndromes (ie, solitary rectal ulcer syndrome); suspected rectovaginal fistula; known rectal mass; or perianal inflammatory diseases, such as Crohn's disease or hidradenitis suppurativa. Tears related to the enema tip usually result in contained leakage of barium, depicted radiographically as linear streaks of barium in a submucosal location paralleling the course of the rectal wall.

There also is a risk of colonic perforation if a barium enema is performed immediately after polypectomy or large forceps biopsy. These procedures can create a mucosal tear or complete transmural perforation of the colon. A barium enema should be postponed for about 1 week after an endoscopically performed polypectomy, mucosal cautery, or large forceps biopsy through a rigid sigmoidoscope [66,67]. A barium enema can be performed after a small forceps biopsy through a flexible sigmoidoscope or colonoscope.

Diverticulitis

Diverticulitis with formation of a pericolic abscess is a classic example of local gastrointestinal perforation. Because diverticula extend into the pericolic fat, inflammation with subsequent microscopic perforation of a diverticulum usually leads to a pericolic inflammatory process with possible abscess formation. The inflammatory process can spread longitudinally as pericolic tracks or into adjacent organs as fistulas. Only rarely does diverticulitis result in free intraperitoneal perforation.

CT is the modality of choice for the demonstration of an acute pericolic inflammatory process [68–71]. Diverticulitis is manifested by disruption of the pericolic fat by linear streaks of soft tissue attenuation or focal fluid collections (see Fig. 2). CT may reveal bubbles of extraluminal gas or fluid tracking along the sigmoid mesentery. A heterogeneous soft tissue mass with or without air bubbles, fluid, or air-fluid levels indicates that a true abscess has formed. An intramural fluid collection may be seen if an intramural abscess is present. In about 10% of cases it is difficult to determine whether the perforation is caused by diverticulitis or a perforated colon cancer [72]. CT demonstration of diverticula or thickening of the bowel wall because of circular muscle hypertrophy indicates that diverticular disease is present, but does not prove that the pericolic inflammatory process or abscess is caused by diverticulitis. If there is abrupt transition of focal wall thickening, local lymphadenopathy, or a wall thickness greater than 1.5 cm, the possibility of a perforated colon cancer should be considered [72,73]. It is also difficult to distinguish diverticulitis from perforation related to a foreign body unless CT demonstrates a high-attenuation foreign body, such as a chicken bone. The CT diagnosis of acute diverticulitis is based on the presence of a pericolic inflammatory process and the absence of a demonstrable foreign body or tumor mass. If a focal mass is present, endoscopy or a contrast enema should be performed after treatment to exclude a perforated colon cancer.

Before the advent of CT, contrast enemas were often performed in patients with suspected diverticulitis. A definitive diagnosis of diverticulitis on contrast enemas depends on the demonstration of extraluminal air or contrast filling tracks or collections in the pericolic space (Fig. 15) [74]. Contrast enemas are inferior to CT in assessing both the presence and extent of the pericolic inflammatory process. Contrast enemas can only indirectly imply the presence of a pericolic inflammatory process when extrinsic mass effect and spiculation of the contour of the colon are demonstrated. In some patients, the pericolic inflammatory process produces little secondary change in the colon and a diagnosis of diverticulitis can be missed (see Fig. 2). Contrast enemas can exclude a perforated cancer when the diseased segment of bowel has tapered contours and preserved mucosal folds. Con-

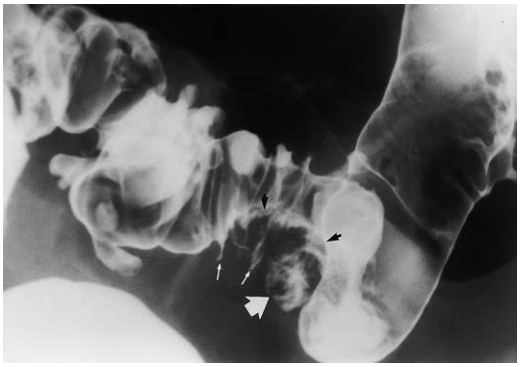

Fig. 15. Diverticulitis in elderly man with chronic left lower quadrant pain. Spot radiograph of proximal sigmoid colon shows barium filling around pericolic collection (*large white arrow*). The lumen of the adjacent sigmoid colon is narrowed by extrinsic mass effect (*black arrows*), but the mucosa is smooth and preserved. Diverticula adjacent to the pericolic abscess are deformed (*small white arrows*). (*From* Rubesin SE. Diverticular disease. In: Levine MS, Rubesin SE, Laufer I, editors. Double contrast gastrointestinal radiology. 3rd edition. Philadelphia: WB Saunders; 2000. p. 471–93, Fig. 14-26.)

trast enemas are superior to CT for differentiating diverticulitis from a perforated colonic carcinoma.

Contrast enemas are also superior to CT for the demonstration of fistulous tracks to the small bowel, urinary bladder, vagina, or abdominal wall. CT can indirectly suggest the presence of fistulas to the bladder and vagina by showing air in these structures with adjacent inflammatory stranding (Fig. 16). In fact, CT is better for suggesting the possibility of fistulas, but contrast studies are better for depicting these fistulas. Finally, contrast enemas performed with barium are potentially dangerous in patients with diverticulitis who have free perforation into the peritoneal cavity. If a contrast enema must be performed in an acutely ill patient with peritoneal signs or symptoms, a water-soluble contrast agent should be used.

Colon cancer

Once a colonic carcinoma has invaded the serosal fat, the possibility of abscess or free perforation or fistula formation is present. A fistula from a transverse colon cancer can spread directly by the transverse mesocolon to the duodenum or by the gastrocolic ligament to the stomach [75]. Rectosigmoid cancers also can form fistulas with the vagina or urinary bladder.

Postoperative colonic perforation

The radiologist may be asked to exclude a leak from a colon that has been partially resected or bypassed. Sites of possible perforation include the stump of a Hartmann's pouch, the stoma of a colostomy or mucus fistula, a colocolic or ileocolic anastomosis, or the diseased colon that was being treated [76]. In general, the radiologist should perform a retrograde contrast enema by the anus or rectum to visualize a suspected leak (Fig. 17). If the site of suspected leak cannot be reached by a contrast enema through the rectum because of the surgical anatomy, the colon can be evaluated by a contrast enema through an ileostomy or colostomy. The authors favor a rectal over a stomal approach when possible, because the rectal approach is safer. Perforations of a stoma have been described during ostomy enemas when the balloon of a Foley catheter is distended in a diseased stoma [77].

When imaging a short segment of bowel, full-strength water-soluble contrast agents can be injected through a Foley catheter insert into the rectum or stoma. The authors prefer Gastroview or Gastrografin to less opaque and less viscous contrast agents, such as Hypaque. When a large volume of contrast must be injected to reach a distant anastomosis, they use a combination of Hypaque (to generate a large enema volume) and Gastroview (to increase the radiographic density). Water-soluble contrast agents instilled into the peritoneal cavity are not deleterious, but the radiologist should remember that in the presence of leak feces is also being swept into the peritoneal space, potentially exacerbating peritonitis or a walled-off abscess. Unlike water-soluble contrast

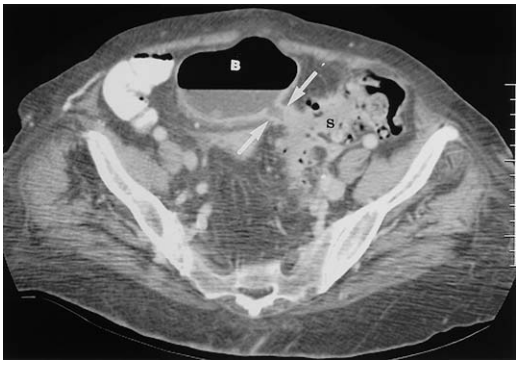

Fig. 16. Colovesical fistula secondary to sigmoid diverticulitis in 83-year-old woman. Axial CT image in the pelvis reveals sigmoid diverticula (s), a fluid-filled fistulous tract to urinary bladder (*arrows*), and large amounts of air in the urinary bladder (B).

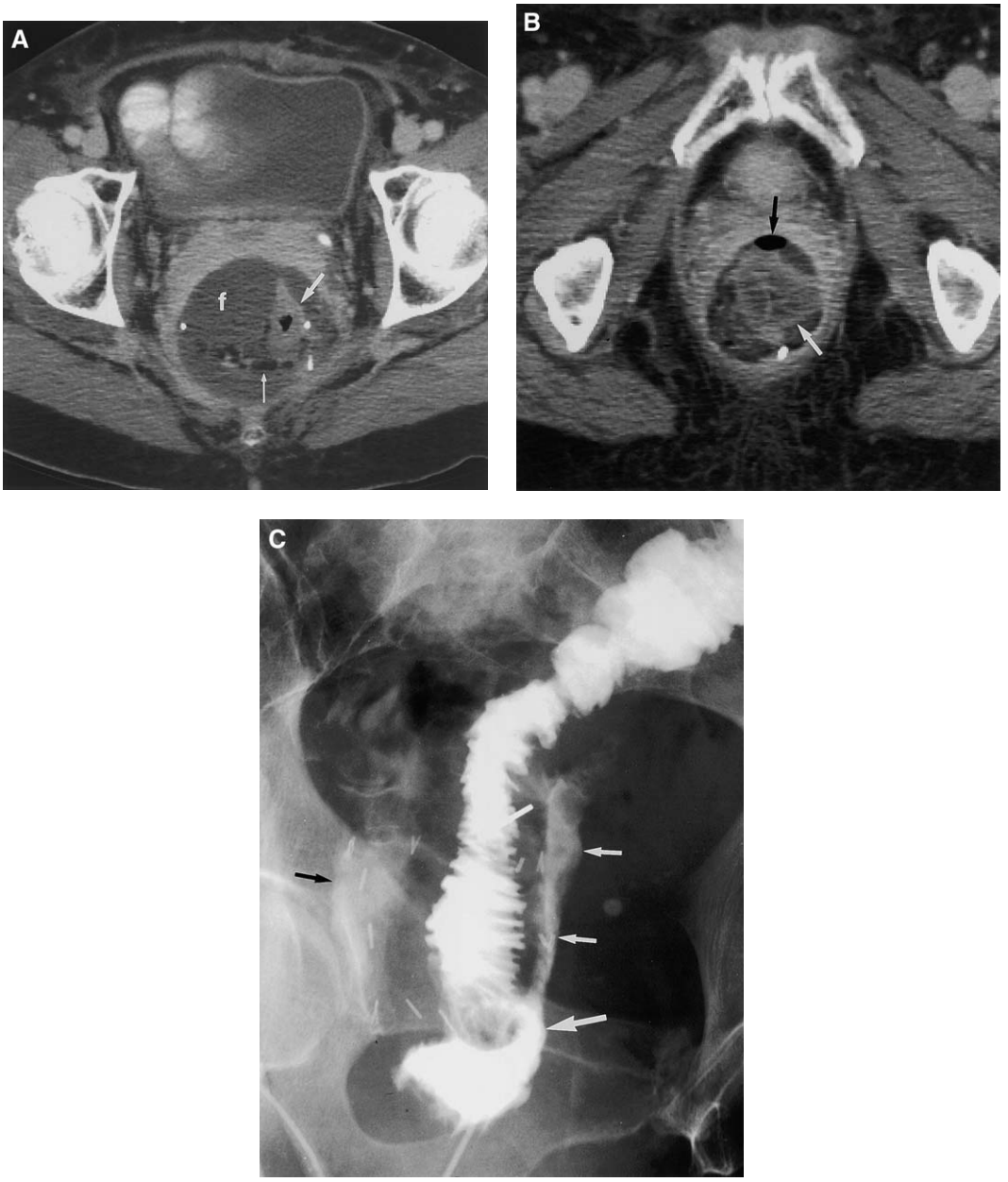

Fig.17. A 68-year-old woman with pelvic pain and history of recent low anterior resection for rectal carcinoma. Pelvic irradiation had been performed before the colectomy. (*A*) CT through the level of the acetabulae shows a large amount of fluid (f) surrounding thick-walled colon (*thick arrow*) and its mesentery (*thin arrow*) that have been pulled into the pelvis to form the colorectal anastomosis. (*B*) CT through the level of the symphysis pubis shows thick-walled distal-most colon with mural stratification (*white arrow*). A bubble of extraluminal gas (*black arrow*) is seen. (*C*) Water-soluble contrast enema performed by a Foley catheter shows a hole near the anastomosis (*large arrow*) with contrast flowing into the right and left pararectal fossae (*small arrows*). Radiation change in the colon proximal to the anastomosis causes the colon to have thick folds mimicking the valvulae conniventes of the small intestine. These images demonstrate how contrast studies often define the site of a perforation better than CT, but CT defines the extraluminal extent of the abnormality.

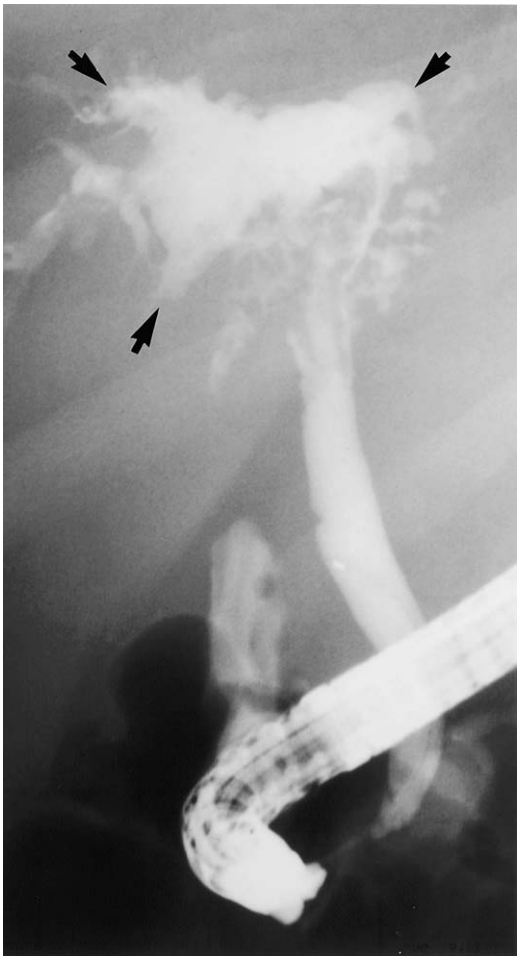

Fig. 18. A 56-year-old woman with fever after liver transplant. Spot radiograph from an ERCP shows a large irregular collection (*arrows*) in the porta hepatis arising from a leak at the choledochocholedochostomy.

studies in patients with suspected upper gastrointestinal perforations, the authors do not follow water-soluble contrast enemas with barium if no leak is initially seen.

Perforations of the biliary tree

Perforations of the biliary tree may be caused by penetrating or blunt abdominal trauma; cholecystitis; or various procedures, such as surgery, percutaneous transhepatic cholangiography, endoscopic retrograde cholangiopancreatography, sphincterotomy, and stent placement. The perforations may result in the development of intrahepatic or extrahepatic bilomas and abscesses; bile peritonitis; or fistulas to the skin, duodenum, or colon.

A biloma is depicted on CT as a fluid collection or thin-walled cyst of low attenuation [78]. On ultrasound, a few septations may be seen within a nonechogenic collection. Although the presence of a bile collection is best demonstrated on CT or ultrasound, the site of biliary perforation is often best demonstrated by endoscopic retrograde cholangiopancreatography, percutaneous transhepatic cholangiography, or T-tube cholangiogram (Fig. 18) [79]. An endoscopic retrograde cholangiopancreatography has the additional advantage of allowing treatment of the bile leak by draining the biliary tree with a stent or nasobiliary tube. A hepatobiliary nuclear medicine scan is a sensitive technique for detecting biliary leaks, but does not demonstrate the site of leak as does contrast injection of the biliary tree.

Bile peritonitis is manifested on CT as ascites associated with diffuse inflammatory changes on the peritoneal surface and mesenteries. Mesenteric vascular engorgement may also be present.

Intrahepatic ductal perforations may occur during extraction of biliary calculi when the surgeon or endoscopist uses guidewires or balloon extraction

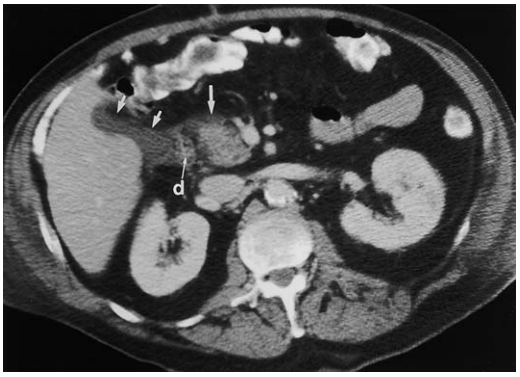

Fig. 19. Small biloma detected only on CT. CT through the level of the pancreatic head and the lower portion of the gallbladder fossa demonstrates a 4 × 2 cm fluid collection (*short arrows*). The fluid spreads anterior to the head of the pancreas (*long arrow*) and to the second portion of the duodenum (*arrow-d*). There was no biochemical evidence of pancreatitis. An ERCP (not shown) did not detect this leak. Cholecystectomy was difficult in this patient with acute cholecystitis infected by *Serratia*. This biloma arose from the gallbladder fossa where accessory cholecystohepatic ducts of Luschka drain a portion of the right lobe of the liver directly into the gallbladder. This case demonstrates that a leak from the gallbladder fossa may be difficult to detect at ERCP or percutaneous transhepatic cholangiography because the ducts that are leaking are at the periphery of the liver.

devices in the biliary tree. CT or endoscopic retrograde cholangiopancreatography may demonstrate irregular collections in a peribiliary location within the liver parenchyma. Most of these biliary perforations are not important [79,80], but some of these collections may develop into abscesses.

The most common site of biliary leakage following cholecystectomy is the cystic duct stump. Leakage from this site may result from slippage of sutures or clips, intraoperative laceration, ischemic necrosis caused by crush injury, or ligation of the arterial blood supply. A biloma may form in the subhepatic space or porta hepatis. Leakage of bile frequently occurs around the insertion site of the T tube, before or after the T tube has been removed. This type of leak may result in a biliary-cutaneous fistula. Leakage from both the cystic duct stump and the T tube entry site may be exacerbated by distal biliary obstruction because of stones, blood clots, or T-tube obstruction.

The accessory cholecystohepatic ducts of Luschka drain a portion of the right lobe of the liver directly into the gallbladder in 25% to 35% of patients [80]. Leakage from these ducts after cholecystectomy may result in the development of a biloma in the gallbladder fossa (Fig. 19). An aberrant right hepatic duct courses along the gallbladder fossa in 5% to 8% of patients. Transection of this aberrant right hepatic duct at cholecystectomy may also result in the development of a biloma in the gallbladder fossa [80].

References

[1] Skucas J. Contrast media. In: Gore RM, Levine MS, editors. Textbook of gastrointestinal radiology. 2nd edition. Philadelphia: WB Saunders; 2000. p. 2–14.

[2] Clavel JP, Lorillot ML, Buthiau D, et al. Absorption intestinale du baryum lors d'explorations radiologiques. Therapie 1987;42:239–43.

[3] Levine MS. What is the best oral contrast material to use for the fluoroscopic diagnosis of esophageal rupture? Question and Answer. AJR Am J Roentgenol 1994; 162:1243.

[4] James AE, Montali RJ, Chaffee V, et al. Barium or Gastrografin: which contrast media for diagnosis of esophageal tears. Gastroenterology 1975;68:1103–13.

[5] Ginai AZ, ten Kate FJW, ten Berg RGM, et al. Experimental evaluation of various contrast agents for use in the gastrointestinal tract in case of suspected leakage: effects on the lungs. Br J Radiol 1984;57:895–901.

[6] Ginai AZ, ten Kate FJW, ten Berg RGM, et al. Experimental evaluation of various contrast agents for use in the gastrointestinal tract in case of suspected leakage: effects on the mediastinum. Br J Radiol 1985;58: 585–92.

[7] Ott DJ, Gelfand DW. Gastrointestinal contrast agents: indications, uses and risks. JAMA 1984;249:2380–4.

[8] Gelfand DW. Complications of gastrointestinal procedures: complications of routine fluoroscopic studies. Gastrointest Radiol 1980;5:293–315.

[9] Chiu CL, Gambach RR. Hypaque pulmonary edema: a case report. Radiology 1974;111:91–2.

[10] Reich SB. Production of pulmonary edema by aspiration of water-soluble nonabsorbable contrast media. Radiology 1969;92:367–70.

[11] Dunbar JS, Skinner GB, Wortzman G, et al. An investigation of the effects of opaque media on the lungs with comparison of barium, Lipiodol and Dionosil. AJR Am J Roentgenol 1959;82:902–26.

[12] Brick SH, Caroline DF, Lev-Toaff AS, et al. Esophageal disruption: evaluation with iohexol esophagography. Radiology 1988;169:141–3.

[13] Gollub MJ, Bains MS. Barium sulfate: a new (old) contrast agent for diagnosis of postoperative esophageal leaks. Radiology 1997;202:360–2.

[14] Rubesin SE, Beatty SM. The postoperative esophagus. Semin Roentgenol 1994;29:401–18.

[15] Rubesin SE, Ruiz C, Levine MS. Principles of performing a barium swallow. Westbury, NY: E-Z-EM; 2003. p. 1–31.

[16] Dodds WJ, Stewart ET, Vlymen WJ. Appropriate contrast media for evaluation of esophageal disruption. Radiology 1982;144:439–41.

[17] Ahga FP, Orringer MB, Amendola MA. Gastric interposition following transhiatal esophagectomy: radiographic evaluation. Gastrointest Radiol 1985;10: 17–24.

[18] Buecker A, Wein BB, Neuerburg JM, et al. Esophageal perforation: comparison of use of aqueous and barium-containing contrast media. Radiology 1997;202: 683–6.

[19] Levine MS, Scheiner JD, Rubesin SE, et al. Diagnosis of pneumoperitoneum on supine abdominal radiographs. AJR Am J Roentgenol 1991;156:731–5.

[20] Mindelzun RE, Jeffrey Jr RB. Unenhanced helical CT for evaluating acute abdominal pain: a little more cost, a lot more information. Radiology 1997;205:43–7.

[21] Derbes VJ, Mitchel RE. Herman Boerhaave's "Atroci nec descripti prius, morbid historia": first translation (from original Latin, 1724) of the classic case report of rupture of the esophagus, with annotations. Bull Med Libr Assoc 1955;43:217.

[22] Mallory GK, Weiss S. Hemorrhages from lacerations of the cardiac orifice of the stomach due to vomiting. Am J Med Sci 1929;178:506.

[23] Levine MS. Miscellaneous abnormalities of the esophagus. In: Gore RM, Levine MS, editors. Textbook of gastrointestinal radiology. Philadelphia: WB Saunders; 2000. p. 465–83.

[24] Isserow JA, Levine MS, Rubesin SE. Spontaneous perforation of the cervical esophagus after an alcoholic binge. Can Assoc Radiol J 1998;49:241–2.

[25] Ghahremani GG, Yaghmai V. Foreign bodies of the alimentary tract. In: Gore RM, Levine MS, editors.

Textbook of Gastrointestinal Radiology. 2nd edition. Philadelphia: WB Saunders; 2000. p. 2196–205.
[26] Velitchkov NG, Grigorov GI, Losanoff JE, et al. Ingested foreign bodies of the gastrointestinal tract: retrospective analysis of 542 cases. World J Surg 1996;20: 1001–5.
[27] Stewart EJ, Miller WM, Hogan WJ, Dodds WJ. Desirability of roentgen esophageal examination after pneumatic dilatation for achalasia. Radiology 1979;130: 589–91.
[28] Ott DJ, Wu WC, Gelfand DW, et al. Radiographic evaluation of the achalasic esophagus immediately following pneumatic dilatation. Gastrointest Radiol 1984; 9:185–91.
[29] Zegel HG, Kressel HY, Levine GM, et al. Delayed perforation after pneumatic dilatation for the treatment of achalasia. Gastrointest Radiol 1979;4:219–21.
[30] Orringer MB. Complications of esophageal surgery. In: Zuidema GE, editor. Shackleford's surgery of the alimentary tract, vol 1. Philadelphia: WB Saunders; 1991. p. 434–59.
[31] Anbari M, Levine MS, Cohen R, et al. Delayed leaks and fistulas after esophagogastrectomy: radiologic evaluation. AJR Am J Roentgenol 1993;160:1217–20.
[32] Kim SH, Lee KS, Shim YM, Kim K, Yang PS, Kim TS. Esophageal resection: indications, techniques, and radiologic assessment. Radiographics 2001;21:1119–40.
[33] Rubesin SE, Williams NN. Postoperative esophagus. In: Gore RM, Levine MS, editors. Textbook of gastrointestinal radiology. 2nd edition. Philadelphia: WB Saunders; 2000. p. 495–508.
[34] Edwards RH, Foster JH. Pneumoperitoneum in perforated duodenal ulcer. Am J Surg 1962;104:551–4.
[35] Jacobsen G, Berne CJ, Meyers HI, et al. The examination of patients with suspected perforated ulcer using water-soluble contrast medium. AJR Am J Roentgenol 1961;86:37–49.
[36] Jeffrey RB, Federle MP, Wall S. Value of computed tomography in detecting occult gastrointestinal perforation. J Comput Assist Tomogr 1983;7:825–7.
[37] Madrazzo BL, Halpert RD, Sandler MA, et al. Computed tomographic findings in penetrating peptic ulcer. Radiology 1984;153:751–4.
[38] Fultz PJ, Skucas J, Weiss SL. CT in upper gastrointestinal tract perforations secondary to peptic ulcer disease. Gastrointest Radiol 1992;17:5–8.
[39] Levine MS, Kelly MR, Laufer I, et al. Gastrocolic fistulas: the increasing role of aspirin. Radiology 1993; 187:359–61.
[40] Laufer I, Thornley GD, Stolberg H. Gastrocolic fistula as a complication of benign gastric ulcer. Radiology 1976;119:7–11.
[41] Travenor T, Smith S, Sullivan S. Gastrocolic fistula: a review of 15 cases and an update of the literature. J Clin Gastroenterol 1993;16:189–91.
[42] Smith CH, Gore RM. Postoperative stomach and duodenum. In: Gore RM, Levine MS, editors. Textbook of gastrointestinal radiology. 2nd edition. Philadelphia: WB Saunders; 2000. p. 682–97.
[43] Blachar A, Federle MP. Gastrointestinal complications of laparoscopic Roux-en-Y bypass surgery in patients who are morbidly obese: findings on radiography and CT. AJR Am J Roentgenol 2002;179:1437–42.
[44] Blachar A, Federle MP, Pealer KM, Ikramuddin S, Schauer PR. Gastrointestinal complications of laparoscopic Roux-en-Y gastric bypass surgery: clinical and imaging findings. Radiology 2002;223:625–32.
[45] Nolan DJ, Herlinger H. Vascular disorders of the small bowel. In: Gore RM, Levine MS, editors. Textbook of gastrointestinal radiology. 2nd edition. Philadelphia: WB Saunders; 2000. p. 838–43.
[46] Smerud MJ, Johnson CD, Stephens DH. Diagnosis of bowel infarction: a comparison of plain films and CT scans in 23 cases. AJR Am J Roentgenol 1990;154: 99–103.
[47] Balthazar EJ, Liebeskind ME, Macari M. Intestinal ischemia in patients in whom small bowel obstruction is suspected: evaluation of accuracy, limitation and clinical implications of CT in diagnosis. Radiology 1997; 205:510–2.
[48] Ha HK, Kiro JS, Lee MS, et al. Differentiation of simple and strangulated small bowel obstruction: usefulness of known CT criteria. Radiology 1997;204:507–12.
[49] Winton TL, Girotti MJ, Manley PN, et al. Delayed intestinal perforation after non-penetrating intestinal trauma. Can J Surg 1985;28:437–9.
[50] Ginaldi S. Small bowel perforation during enteroclysis. Gastrointest Radiol 1991;16:29–31.
[51] Fishman EK, Wolf EJ, Jones B, et al. CT evaluation of Crohn's disease: effect on patient management. AJR Am J Roentgenol 1987;148:537–40.
[52] Pickhardt PJ, Bhalla S, Balfe DM. Acquired gastrointestinal fistulas: classification, etiologies, and imaging evaluation. Radiology 2002;224:9–23.
[53] Greenstein S, Jones B, Fishman EK. Small bowel diverticulitis: CT findings. AJR Am J Roentgenol 1986; 147:271–4.
[54] Rubesin SE, Gilchrist AM, Bronner M, et al. Non-Hodgkin lymphoma of the small intestine. Radiographics 1990;10:985–98.
[55] Pickhardt PJ, Siegel MJ. Abdominal manifestations of posttransplantation lymphoproliferative disorder. AJR Am J Roentgenol 1999;171:1007–13.
[56] Rubesin SE, Furth EE, Birnbaum BA, et al. Ectopic pancreas complicated by pancreatitis and pseudocyst formation mimicking jejunal diverticulitis. Br J Radiol 1997;70:311–3.
[57] Carucci LR, Levine MS, Rubesin SE, Assad S, Herlinger H. Evaluation of patients with jejunostomy tubes: imaging findings. Radiology 2002;223:241–7.
[58] Hrung JM, Levine MS, Rombeau JL, et al. Total proctocolectomy and ileoanal pouch: the role of contrast studies for evaluating postoperative leaks. Abdom Imaging 1998;23:375–9.
[59] Thoeni RF, Fell SC, Engelstad B, et al. Ileoanal pouches: comparison of CT, scintigraphy and contrast enemas for diagnosing postsurgical complications. AJR Am J Roentgenol 1990;154:73–8.

[60] Novy S, Rogers LF, Kirkpatrick W. Diastatic rupture of the cecum in obstructing carcinoma of the left colon: radiologic diagnosis and surgical implications. AJR Am J Roentgenol 1975;123:281–6.
[61] Dodds WJ, Stewart ET, Nelson JA. Rectal balloon catheters and the barium enema examination. Gastrointest Radiol 1989;5:227–34.
[62] Gelfand DW, Ott DJ, Ramquist NA. Pneumoperitoneum occurring during double-contrast barium enema examination. Gastrointest Radiol 1979;4:307–8.
[63] Ott DJ, Gelfand DW, Chen YM, et al. Colonoscopy and the barium enema: a radiologic viewpoint. South Med J 1985;78:1033–5.
[64] Muldorfer SM, Kekos G, Hahn EG, et al. Complications of therapeutic gastrointestinal endoscopy. Endoscopy 1992;24:276–83.
[65] Vallera R, Baillie J. Complications of endoscopy. Endoscopy 1996;28:187–204.
[66] Maglinte DDT, Strong RC, Strate RW, et al. Barium enema after colorectal biopsies: experimental data. AJR Am J Roentgenol 1982;139:693–7.
[67] Harned RK, Consigny PM, Cooper NB. Barium enema examination following biopsy of the rectum or colon. Radiology 1982;145:11–6.
[68] Hulnick DH, Megibow AJ, Balthazar EJ, et al. Computed tomography in the evaluation of diverticulitis. Radiology 1984;152:481–95.
[69] Johnson CD, Baker ME, Rice RP, et al. Diagnosis of acute colonic diverticulitis: comparison of barium enema and CT. AJR Am J Roentgenol 1987;148: 541–6.
[70] Balthazar EJ, Megibow A, Schinella RA, et al. Limitations in the CT diagnosis of acute diverticulitis: comparison of CT, contrast enema, and pathologic findings in 16 patients. AJR Am J Roentgenol 1990;154:281–5.
[71] Cho CK, Morehouse HT, Alterman DD, et al. Sigmoid diverticulitis: diagnostic role of CT comparison with barium enema studies. Radiology 1990;176:111–5.
[72] Balthazar EJ. Diverticular disease of the colon. In: Gore RM, Levine MS, editor. Textbook of gastrointestinal radiology. 2nd edition. Philadelphia: WB Saunders; 2000. p. 915–44.
[73] Chintapalli KN, Esola CC, Chopra S, et al. Pericolic mesenteric lymph nodes: an aid in distinguishing diverticulitis from cancer of the colon. AJR Am J Roentgenol 1997;169:1253–5.
[74] Rubesin SE, Laufer I. Diverticular disease. In: Levine MS, Rubesin SE, Laufer I, editors. Double contrast gastrointestinal radiology. 3rd edition. Philadelphia: WB Saunders; 2000. p. 471–93.
[75] Laufer I, Joffe N. Some Roentgenologic aspects of chronic perforating carcinoma of the colon. Dis Colon Rectum 1973;16:127–35.
[76] Cherukuri R, Levine MS, Maki DD, Rubesin SE, Laufer I, Rosato EF. Hartmann's pouch: radiographic evaluation of postoperative findings. AJR Am J Roentgenol 1998;171:1577–82.
[77] Scholz FJ, Jakomin BV. Postoperative colon. In: Gore RM, Levine MS, editor. Textbook of gastrointestinal radiology. 2nd edition. Philadelphia: WB Saunders; 2000. p. 1151–8.
[78] Pannu HK, Fishman EK. Complications of endoscopic retrograde cholangiopancreatography: spectrum of abnormalities demonstrated with CT. Radiographics 2002; 21:1441–53.
[79] Ghahremani GG, Crampton AR, Bernstein JR, Caprini JA. Iatrogenic biliary tract complications: radiologic features and clinical significance. Radiographics 1991; 11:441–56.
[80] Ghahremani GG, Yaghmai V. Postsurgical and traumatic lesions of the biliary tract. In: Gore RM, Levine MS, editors. Textbook of gastrointestinal radiology. 2nd edition. Philadelphia: WB Saunders; 2000. p. 1395–407.

RADIOLOGIC CLINICS OF NORTH AMERICA

Radiol Clin N Am 41 (2003) 1117–1136

The acute right lower quadrant: CT evaluation

Michael Macari, MD*, Emil J. Balthazar, MD

Department of Radiology, Abdominal Imaging, New York University Medical Center, Medical Center, Tisch Hospital, 560 First Avenue, Suite HW 207, New York, NY 10016, USA

A variety of acute inflammatory conditions may affect the right lower quadrant prompting the patient to seek medical evaluation [1]. The clinical presentation is often confusing. The work-up of a patient with right lower quadrant pain is based on the clinical history and physical examination, laboratory evaluation, and plain-film radiography. In patients with acute right lower quadrant pain (and abdominal pain in general), however, plain-film radiography is often noncontributory (Fig. 1) [2]. A recent study evaluating patients with abdominal pain showed that plain-film radiography was interpreted as nonspecific in 588 (68%) of 871 patients, normal in 200 (23%), and abnormal in 83 (10%). In this study, abdominal radiography had 0% sensitivity for appendicitis, pyelonephritis, pancreatitis, and diverticulitis. Moreover, the clinical history and physical examination in patients with right lower quadrant pain are often nonspecific. Depending on the expertise of the treating physician, abdominal and pelvic CT is often performed to confirm if an inflammatory condition is present and to characterize it further [3]. With the widespread proliferation of multislice CT scanners in emergency departments throughout the country, this trend will likely continue [4]. In most patients with acute right lower quadrant pain, a specific diagnosis of appendicitis can be made with CT leading to prompt surgical intervention [5,6].

Appendicitis is the most common cause of the acute abdomen particularly in young individuals. It is important for the clinician and radiologist to remember, however, that abdominal symptoms and physical signs located in the right lower quadrant may be caused by a variety of other conditions [1,5]. In a review of 10,682 patients with acute abdominal pain, de Dombal [1] found that 28% had appendicitis, 9.7% had cholecystitis, 4.1% had small bowel obstruction, 4% had gynecologic disorders, 2.9% had pancreatitis, 2.9% had renal colic, 2.5% had peptic ulcer disease, 1.5% had cancer, 1.5% had diverticular disease, and 9% a variety of less common conditions. In this review, a specific diagnosis was not established in 34% of cases. It is likely that in many cases where a clinical diagnosis could not be made, CT imaging would have been helpful in establishing a specific etiology.

Furthermore, among the more common acute abdominal conditions enumerated in de Dombal's [1] series, not listed are Crohn's disease; epiploic appendagitis; infectious ileitis; mesenteric adenitis; omental infarction; ileal, cecal, and right-sided colonic diverticulitis; Meckel's diverticulitis; typhlitis; and intestinal ischemia. Although some of these conditions are relatively uncommon, taken as a whole they make up a substantial number of patients who present with acute right lower abdominal pain [5–11]. All of these conditions may be diagnosed with CT.

This article describes the CT imaging findings of patients presenting with acute right lower quadrant pain. The focus is on appendicitis and current imaging techniques and controversies. The remainder of the article evaluates the most common conditions causing right lower quadrant pain other than appendicitis that can be diagnosed with CT.

Appendicitis

Clinical diagnosis and imaging

The diagnosis of appendicitis historically has been made based on clinical signs and symptoms. The

* Corresponding author.
E-mail address: michael.macari@med.nyu.edu (M. Macari).

doi:10.1016/S0033-8389(03)00101-5

classic clinical presentation of appendicitis, however, composed of periumbilical pain migrating to the right lower quadrant with fever and leukocytosis, is not always present. As a result, reported rates of false-positive laparotomies (removal of a normal appendix) in patients with clinically suspected appendicitis ranges from 6.5% to 40% [6]. The highest rates occur when laparotomy or laparoscopy are performed in young women in whom acute gynecologic conditions are common and may mimic appendicitis [12]. When clinical evaluation alone is used for suspected appendicitis, 1 in every 5 to 10 appendices are normal at surgery (Fig. 2).

CT can decrease the false-negative rate for appendectomy. In a study of 146 patients with clinically suspected appendicitis who also underwent CT, the false-negative appendectomy rate was only 4% [13]. Another study evaluating the effect of imaging and the false-negative appendectomy rate in patients with clinically suspected appendicitis showed substantial differences between those who were imaged and those that were not imaged [14]. In this study, the negative appendectomy rate for women was significantly lower for those who underwent preoperative CT (7% [6 of 85 patients, $P = 0.005$]) or ultrasound ([US] 8% [4 of 49 patients, $P = 0.019$]), as compared with 28% (9 of 32 patients) for women who underwent no preoperative imaging. Because of the high false-negative appendectomy rate, and because other acute entities may present with right lower quadrant pain, CT or US is often performed to confirm the diagnosis and to exclude other possible acute abdominal conditions.

A number of different imaging modalities and techniques have been advocated to evaluate the patient with suspected appendicitis. The modalities used include US, CT, and MR imaging. Ultrasound has gained importance in the evaluation of right lower

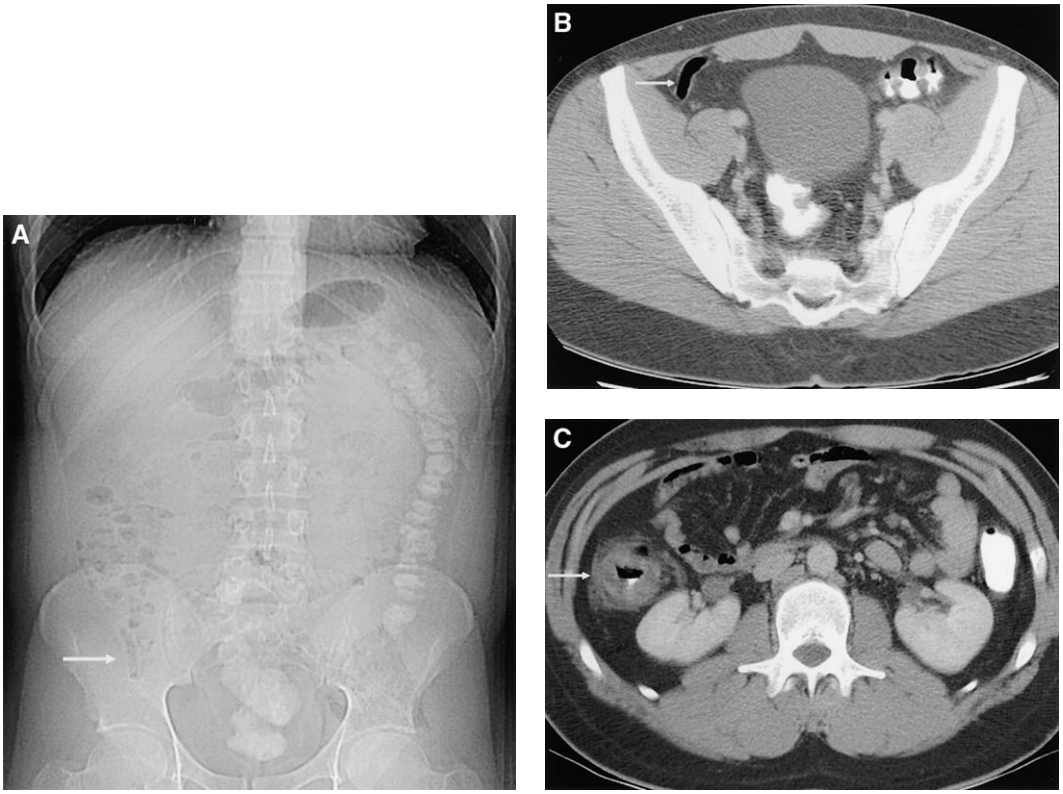

Fig. 1. Improved sensitivity and specificity of CT compared with plain film radiography in evaluating acute right lower quadrant pain. (*A*) Supine scout radiograph shows linear collection of gas (*arrow*) in the right lower quadrant, likely in appendix. Remainder of the image shows no abnormality. (*B*) Axial CT in same patient confirms normal appendix (*arrow*). (*C*) Axial CT image in same patient 10 cm cephalad to *B* shows circumferential thickening of right colon (*arrow*) with associated stranding of the adjacent mesenteric fat. Abnormality extended from the ileocecal valve to the hepatic flexure. Findings are consistent with colitis. In this case, the cause is ischemia.

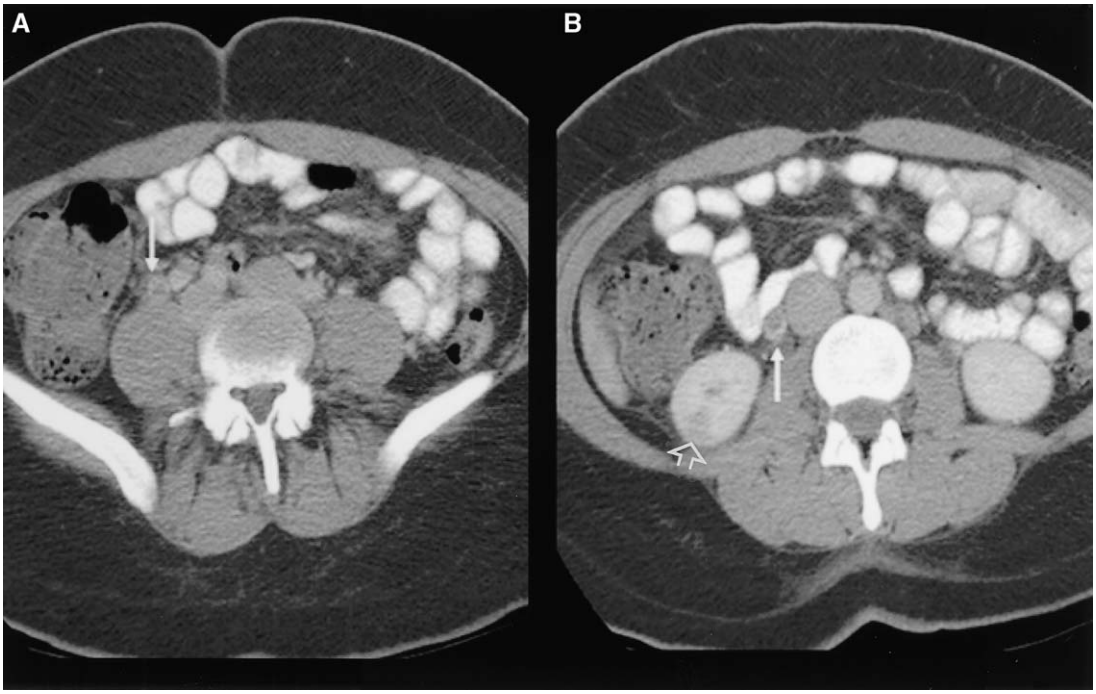

Fig. 2. A 32-year-old woman with right lower quadrant pain, fever, and clinically suspected appendicitis. Axial CT image (*A*) in the upper pelvis shows distended tubular structure with adjacent fat stranding (*arrow*) ventral to the right psoas muscle. Axial CT image (*B*) several centimeters cephalad shows continuation of tubular structure (*arrow*) to the inferior vena cava with central filling defect. Findings are consistent with right gonadal vein thrombosis. Note focal wedge-shaped area of decreased attenuation in right kidney (*open arrow*) consistent with pyelonephritis. Appendix (not shown) was normal.

quadrant pain especially in young women and children [15,16]. The sensitivity and specificity of US in the diagnosis of appendicitis is variable and dependent on a number of factors including patient size and body habitus, and the skill of the examiner. Another technical factor that may make visualization of the normal and abnormal appendix difficult is overlying bowel gas.

Sensitivity rates using US for the diagnosis of appendicitis of up to 90% have been reported [15,17]. A study comparing contrast-enhanced CT with graded compression US, however, showed sensitivity rates of 96% versus 76% for CT and US, respectively [3]. A more recent study showed that the sensitivity of CT and US for diagnosing acute appendicitis was 93% and 77% for the two modalities, respectively [14]. Radiation issues are certainly an important factor to consider in the use of an imaging study, especially in pregnant patients, young women, and children. Conversely, a recent report has showed that helical CT had a significantly higher sensitivity (95% versus 78%, $P = 0.009$) and accuracy (94% versus 89%, $P = 0.05$) compared with graded compression sonography for the diagnosis of appendicitis in children, adolescents, and young adults [18]. At the authors' institution, US is used as the primary imaging technique in pregnant patients, whereas all other individuals undergo CT for evaluation of suspected appendicitis (Fig. 3).

CT

Unenhanced CT

Recently CT has become the primary imaging modality to evaluate patients with clinically suspected appendicitis. There is controversy, however, about how optimally to perform the CT examination in this setting [19–24]. Regarding patient preparation, there are several different techniques that can be used. Some radiologists advocate that the examination be performed without oral or intravenous (IV) contrast as an unenhanced examination [19–21]. The clear benefits of this type of examination are speed with decreased waiting time for the patient, and the examination is noninvasive because iodinated IV contrast material is not administered. Moreover,

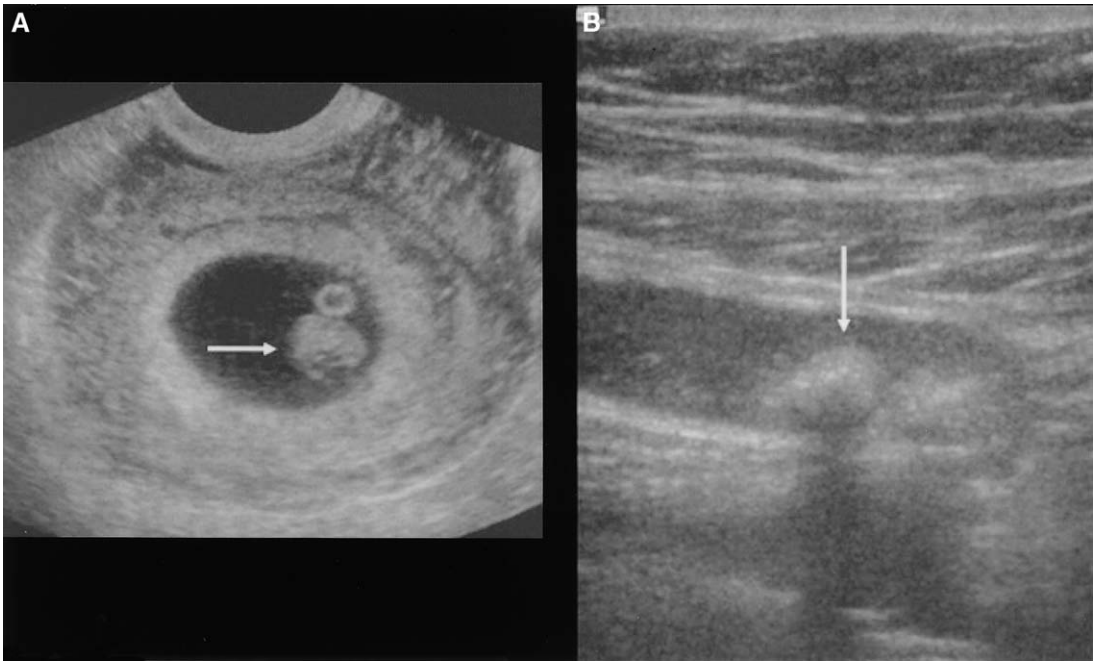

Fig. 3. A 25-year-old woman with right lower quadrant pain. Endovaginal US (*A*) shows single live intrauterine gestation (*arrow*). Compression US (*B*) using 7-MHz transducer shows noncompressible distended tubular structure in right lower quadrant with associated appendicolith (*arrow*). Appendicitis was confirmed at surgery.

reported results have been very encouraging, with one study reporting a sensitivity of 96%, a specificity of 99%, and an accuracy of 97% [21], whereas another study has showed a sensitivity of 96%, specificity of 98%, positive predictive value of 97%, and negative predictive value of 98% [20]. On the basis of these results, the authors recommended that if no definite inflammatory changes are detected with unenhanced CT, the patient could be monitored clinically.

Although appendicitis often can be diagnosed without oral and IV contrast material, a paucity of intraperitoneal and periappendiceal adipose tissue renders the diagnosis more difficult. It is well known that the surrounding periappendiceal fat facilitates recognition of a normal and abnormal appendix. A recent study evaluating the rate of detection of the normal appendix in pediatric patients found that abdominal fat significantly increases the rate of identification of the normal appendix [22]. In women, children, and in patients without intraperitoneal adipose tissue, it is much more difficult to detect a normal appendix and to establish a diagnosis of appendicitis. In these cases, oral and IV contrast facilitates recognition of a normal and abnormal appendix (Fig. 4) [3,6,23]. Moreover, the detection of other offending acute abdominal diseases is greatly enhanced by the use of oral and IV contrast material.

Focused CT

Some investigators have advocated a focused CT examination of the right lower quadrant comprised of imaging only the lower abdomen and pelvis and the use of various combinations of oral, rectal, and IV contrast media [24,25]. A focused CT examination has the advantage of decreasing radiation dose to the patient, which is especially relevant in pediatric patients. A recent pediatric study evaluating a focused technique with scanning beginning below the lower pole of the right kidney and continuing into the entire pelvis, documented a sensitivity of 97%, specificity of 93%, positive predictive value of 90%, and negative predictive value of 98% for the diagnosis of appendicitis [24]. These results were similar to those obtained for CT examination of the entire abdomen and pelvis.

Several recent articles, however, have pointed out some of the limitations of the focused technique in patients suspected of having appendicitis [23,26]. In one comparative study of 100 patients with right lower quadrant pain and clinically suspected appen-

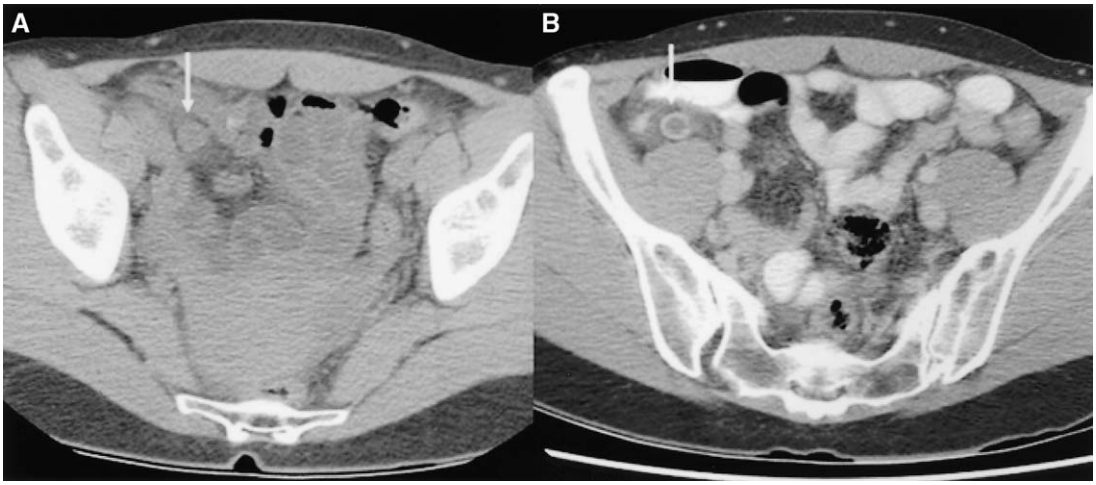

Fig. 4. Appendicitis in 32-year-old woman with clinically suspected kidney stone. Axial CT performed without contrast (*A*) was initially interpreted as normal. There is a paucity of intraperitoneal adipose tissue. In retrospect the appendix (*arrow*) is distended. It is very difficult, however, to differentiate the distended fluid-filled appendix from adjacent loops of unopacified bowel. Patient continued to have pain and underwent repeat CT with oral and intravenous contrast. The enhancing appendix (*arrow, B*) is now easily differentiated from adjacent contrast-filled loops of bowel.

dicitis CT depicted abnormalities in 66 patients (66%). In 59 (59%) patients, the abnormality was located in the pelvis, whereas in seven (7%) patients abnormalities were found outside of the pelvis, a region not scanned during focused appendiceal imaging. Four of these seven patients required surgery. If only a limited CT evaluation had been performed, overall sensitivity for intra-abdominal pathology would have decreased from 99% to 88% ($P < 0.05$) and the sensitivity for cases necessitating surgery would have decreased from 96% to 82% ($P < 0.05$). These authors concluded that both abdominal and pelvic CT examinations are necessary to increase sensitivity and identify the many possible causes of right lower quadrant pain in patients with clinically suspected appendicitis.

Based on the authors' experience they believe that both abdominal and pelvic CT examinations and IV contrast administration are necessary when evaluating patients with right lower quadrant pain [23]. In a study comparing focused with nonfocused CT, three readers evaluated CT scans of the same patient who had two consecutive examinations: an initial focused examination in the right lower quadrant without IV contrast but with oral contrast material, followed by an examination of the entire abdomen and pelvis with oral and IV contrast material. Fifty-one (22.4%) of 228 patients in the study had acute appendicitis. Readers diagnosed appendicitis with 83.3%, 73.8%, and 71.4% sensitivity with focused unenhanced CT and readers diagnosed appendicitis with 92.9%, 92.9%, and 88.1% sensitivity when nonfocused contrast-enhanced CT images were used. Moreover, the level of confidence was higher for all three readers in diagnosing alternative conditions when enhanced CT images were available. In addition, it is worth noting that appendicitis was missed with limited focused CT studies in two patients whose inflamed appendices were located outside the imaging field.

Rectal contrast material

Several studies have pointed improved accuracy of CT for detecting appendicitis in both adults and children after the administration of rectal contrast material [25,27]. Rao et al [25], using a focused appendiceal technique using dilute rectal contrast administration, with or without oral contrast, and no IV contrast, reported a sensitivity of 100%, specificity of 95%, and accuracy of 98% in establishing a diagnosis of appendicitis. It has been suggested that rectal administration of contrast under pressure may force contrast into the appendix that otherwise would not opacify only with oral contrast administration (Fig. 5). For contrast enema, 20 mL of meglumine diatrizoate is mixed with 1000 mL of saline and is instilled by gravity with the use of a rectal catheter.

Another advantage of administration of rectal contrast material is that it is relatively quick so that the patient does not need to wait the 1.5 to 2 hours usually necessary with oral administration of contrast to visualize the terminal ileum and cecum. Limita-

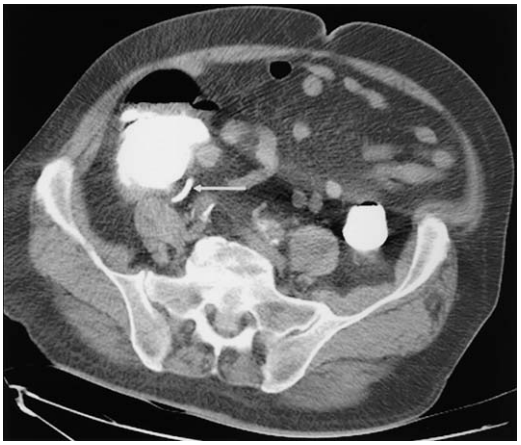

Fig. 5. Administration of dilute iodinated contrast by the rectum in a patient clinically suspected of having appendicitis. Axial CT at level of appendix shows the appendix is filled with contrast material excluding the diagnosis of appendicitis (*arrow*).

tions to the routine use of only rectally administered contrast include patient discomfort, lack of proper visualization of the terminal ileum, and potential spillage of contrast material on the CT table. Perhaps most importantly, IV contrast was not routinely administered using the original protocol. In the authors' opinion, IV contrast material facilitates recognition of not only appendicitis [23] but also of other pathologic entities in the abdomen including processes involving the kidneys, mesentery, vasculature, pancreas, intestinal tract, and other potential sources of acute abdominal pain.

Oral and IV contrast material

In the setting of suspected appendicitis, Balthazar et al [3] documented sensitivity of 98%, specificity of 88%, and overall accuracy of 95% when performing CT with oral and IV contrast material. A survey of academic institutions regarding imaging protocols used in patients with suspected appendicitis showed that IV, oral, and rectal contrast material are routinely given at 79%, 82%, and 32% of institutions, respectively [28]. Twenty-one percent of the institutions routinely use IV, oral, and rectal contrast material simultaneously. Among the numerous options available to scan the patient, CT with oral and IV contrast material continues to be the most commonly used technique. The authors continue to rely on oral and IV contrast-enhanced CT of the abdomen and pelvis to evaluate for suspected acute appendicitis and to diagnose alternative acute abdominal conditions of which it can masquerade.

Regarding the CT technique, it is important to opacify the cecum using oral contrast material (Fig. 6). The authors administer 800 to 1000 mL of oral contrast (dilute meglumine diatrizoate) in small increments over 1.5 to 2 hours before the examination is to be performed. The patient is then placed on the CT table and a scout topogram is obtained to document filling of the cecum. If it is uncertain whether there is filling of the cecum, a single CT slice at the

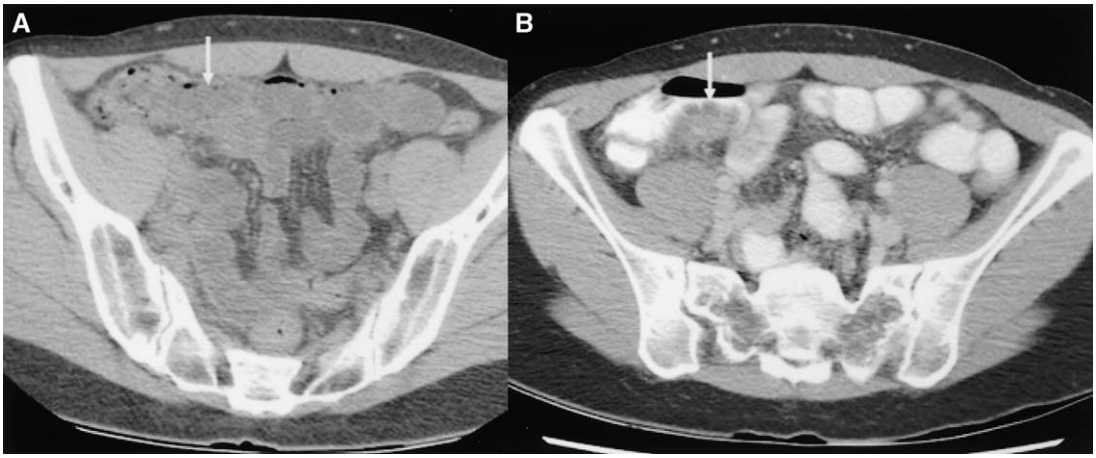

Fig. 6. Appendicitis in a 32-year-old woman with clinically suspected kidney stone, same patient as in Fig. 4. Axial CT performed without contrast (*A*) was initially interpreted as normal. There is a paucity of intraperitoneal adipose tissue. The cecum is unopacified (*arrow*) and appears normal. Patient continued to have pain and underwent repeat CT with oral and intravenous contrast. A focal area of thickening (*B*) is now seen at the base of the cecum (*arrow*) where the appendix arises from the cecum. This focal thickening is an important finding in confirming appendicitis and can only be seen if the cecum is opacified.

level of the sacroiliac joints can be obtained. If the cecum is opacified, the authors begin the examination; otherwise, the patient is taken off the CT scanner, waits an additional 30 minutes, and is then placed back on the CT scanner.

Once the cecum is opacified, helical CT using 5- to 7-mm collimation of the abdomen and 5-mm collimation of the pelvis is performed. Thin-section CT scanning improves sensitivity of CT for the diagnosis of appendicitis [29]. As anticipated, when comparing 5- and 10-mm thick sections in the same patient, the sensitivity for the detection of appendicitis was 99% versus 82%, respectively [29]. If a multidetector CT unit is available, a 4×2.5 mm detector configuration should be used and images routinely reconstructed at 5 mm. If needed, data can then be reconstructed at 2.5-mm thick sections for improved Z-axis resolution. The CT examination is initiated at the dome of the liver and continues in a cranial-caudal direction beginning 60 to 70 seconds after a 100- to 150-mL bolus of iodinated IV contrast material is administered at a rate of 2.5 mL/second. Using either a single detector or multidetector row CT scanner, a pitch of 1.5 provides good trade-off between acquisition time and slice sensitivity profile.

The normal appendix

Using oral and IV contrast material enhanced CT, the normal appendix is filled with positive contrast, fecal matter, gas, or a combination of these materials. Depending on the amount of intra-abdominal adipose tissue, the normal appendix is visualized in approximately 79% of patients with helical CT [30]. When attempting to locate the appendix, the right colon should be followed caudally from the hepatic flexure to the level of the cecum. Once the ileocecal valve is identified, the appendix is usually just caudal to the valve on the same side. It is useful to remember that because the right colon is mobile often attached on a long mesentery, or located in the left abdomen as a result of midgut malrotation, the appendix may not be visualized in its expected location in the right lower quadrant (Fig. 7).

The surgical landmark used to locate the appendix is McBurney's point, situated 1.5 cm medial and cranial from the anterior superior iliac spine, on a line drawn from the umbilicus to the anterior superior iliac spine. A study of 275 double-contrast barium enema examinations showed that only 35% of appendiceal bases were located within 5 cm of McBurney's point, whereas 15% were distant to it by more than

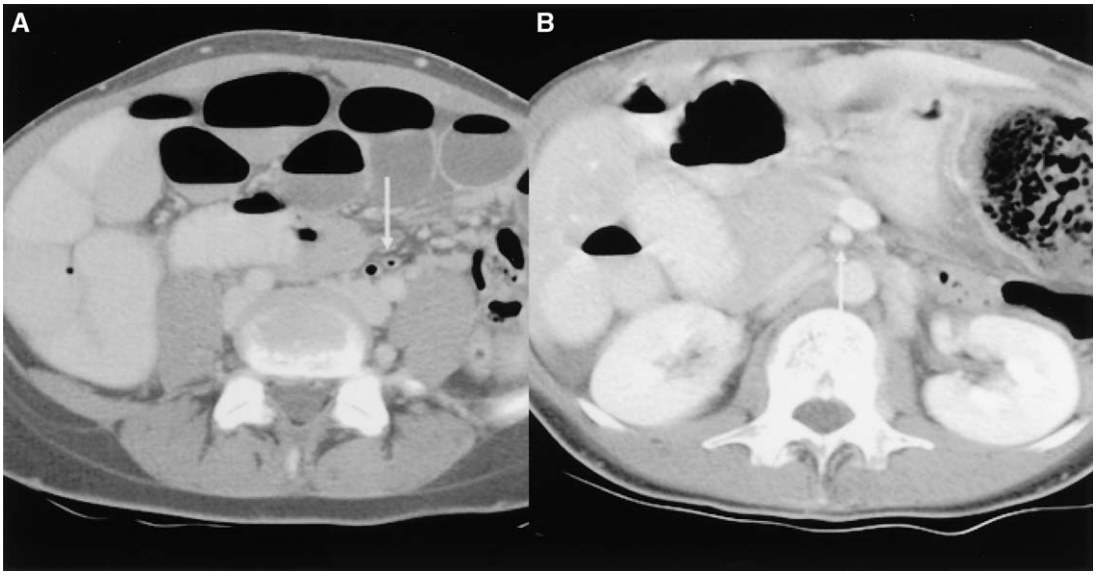

Fig. 7. Normal appendix in the left abdomen. Axial CT image in the lower abdomen (*A*) shows gas-filled tubular structure in left abdomen (*arrow*). Note there is no colon identified in the right abdomen. Axial CT image in same patient at level of superior mesenteric artery and vein (*B*) shows reversal of these vessels with superior mesenteric artery (*arrow*) to the right of the superior mesenteric vein. Findings confirm midgut bowel nonrotation. Patient also has small bowel obstruction related to adhesion from prior cholecystectomy.

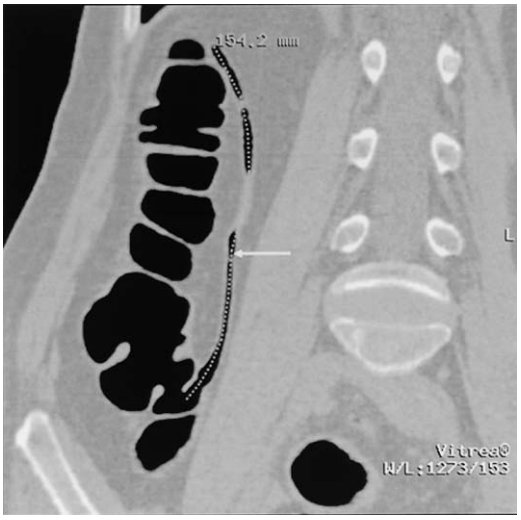

Fig. 8. Long appendix. Coronal reformatted image from CT colonography shows unusually long appendix measuring 15.4 cm (*arrow*). The tip of the appendix is under the right diaphragm.

10 cm [31]. The appendix usually originates 2 to 3 cm below the ileocecal valve and it is positioned between 2 and 6 o'clock relative to the cecum, if the cecum is viewed as a clock on axial images. The appendix is mobile having its own mesentery and it has a variable length of 2 to 20 cm (Fig. 8).

The wall of the normal appendix is thin and when distended with fluid or gas it measures only 1 to 2 mm. After administration of IV contrast it enhances slightly and homogeneously. Occasionally, an appendicolith may be identified in an otherwise normal-appearing appendix. Unless there are other stigmata of appendicitis, such as periappendiceal inflammation, a diagnosis of appendicitis cannot be established. There is some variability in the maximal width of the normal appendix, which in most cases measures less than 7 mm. Even when the appendix measures over 7 mm but is filled with positive contrast material, and there is no periappendiceal inflammation or wall thickening, the patient likely does not have appendicitis.

The abnormal appendix

The inflamed appendix is typically distended with fluid, measuring between 6 and 17 mm in width (Fig. 9). Because it is obstructed at its base, orally or rectally administered contrast material is not present within its lumen. Occasionally, small bubbles of gas may be seen within the abnormal appendix as residual air or from gas-producing bacterial infections. After the IV administration of iodinated contrast material, either a homogeneous or a stratified configuration target appearance of mural enhancement is seen in the wall of the appendix (see Fig. 9) [6]. The wall of the appendix is often mildly thickened. One or several appendicoliths are visualized in 20% to 40% of patients with appendicitis [32]. Recognition of an appendicolith in association with right lower quadrant inflammation or abscess, even if an appendix is not identified, is usually sufficient to establish the diagnosis of appendicitis.

A secondary CT finding that aids in the diagnosis of subtle cases of appendicitis is focal thickening at the tip of the cecum at the expected location of the orifice of the appendix [33]. The cecal bar sign (which represents edema and focal cecal thickening) and the arrowhead sign (which represents oral or rectally administered contrast funneling into the spastic and focally thickened cecum) are important ancillary signs (Fig. 10; see Fig. 9). Sometimes these signs are the only clues that an inflammatory process is present. The arrowhead sign was reported to be present in 17 (30%) of 56 patients with appendicitis and it was not present in patients without appendicitis [34]. The sign is clinically useful but it is not specific because other processes may cause spasticity and focal thickening at the tip of the cecum including cecal diverticulitis, typhlitis, and cecal carcinoma. Whenever focal cecal mural thickening or apical spasticity is identified, consideration of other entities

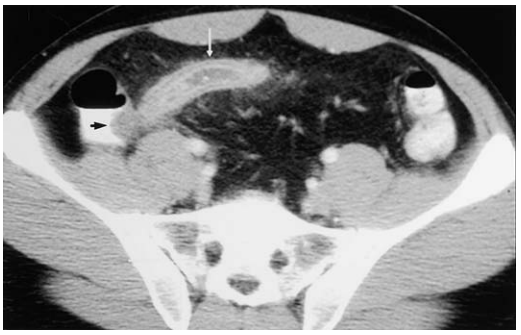

Fig. 9. Acute appendicitis with cecal bar. Axial CT image after the intravenous administration of oral and intravenous contrast material shows distended appendix (*arrow*) with mural stratification to enhancement pattern of inflamed wall. Note also periappendiceal fat stranding and focal thickening of the base of the cecum (cecal bar) (*black arrow*). Visualization of focal thickening is facilitated by the presence of positive contrast material in the cecum.

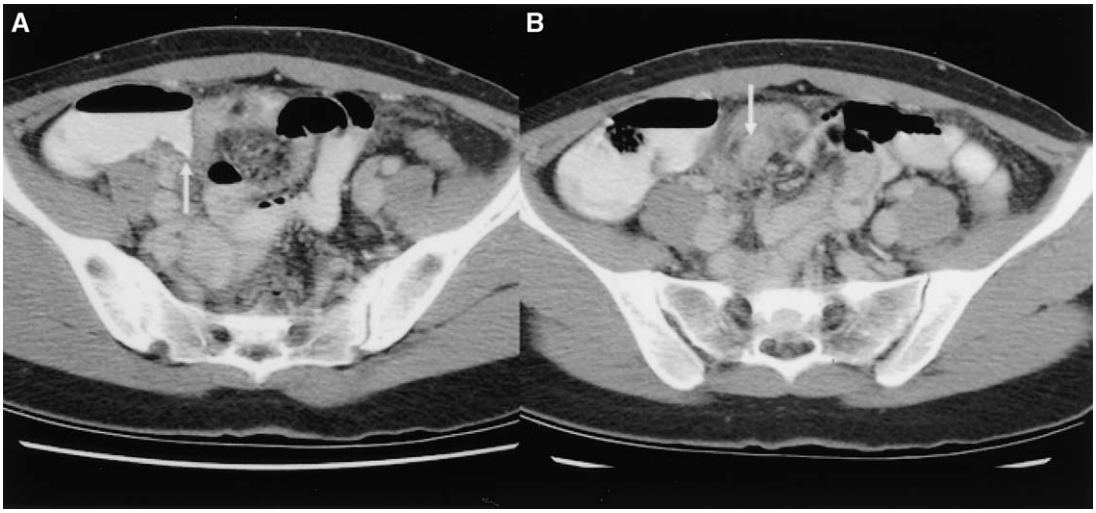

Fig. 10. Arrowhead sign. Axial CT image (*A*) shows positive contrast material in the cecum funneling into abnormal base of cecum (*arrow*). This finding resembles an arrowhead. Axial CT image (*B*) in same patient at a slightly more cephalad area shows nonfilling of inflamed distended appendix (*arrow*).

is paramount especially when an abnormal appendix is not visualized.

Obstruction of the appendiceal lumen leads to appendicitis. When the obstruction occurs distally rather than at its base, the inflammation is confined to the tip of the appendix (Fig. 11). In these cases, the base of the appendix and the cecum are normal. In patients who are undergoing CT for suspected appendicitis, it is imperative that the entire length of the appendix be studied for possible distal or tip appendicitis [34]. If needed, placing the patient in the left lateral decubitus position can aid in detecting the

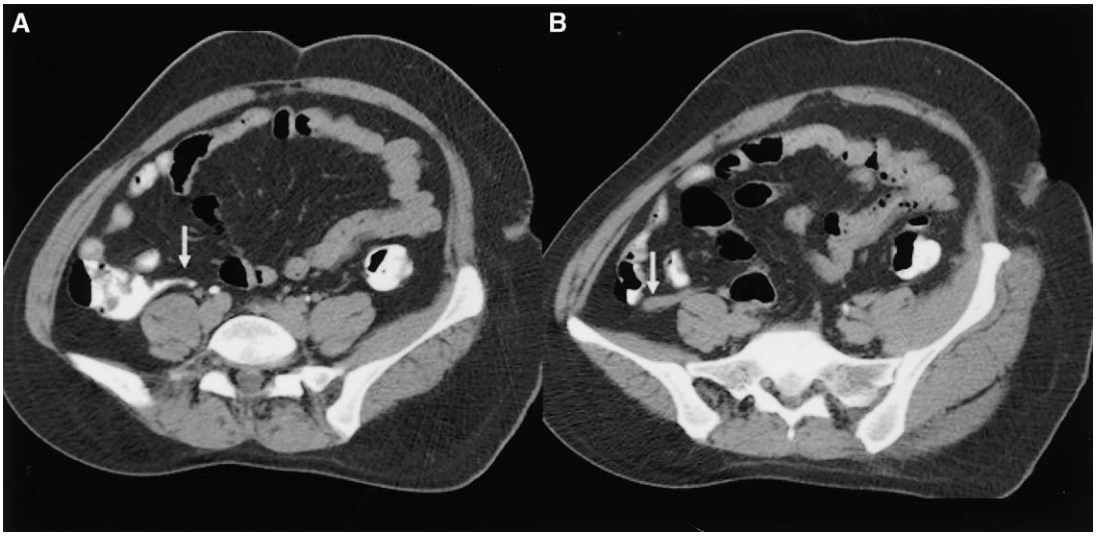

Fig. 11. Tip appendicitis axial CT image (*A*) performed after oral and intravenous contrast material shows normal proximal appendix filled with contrast (*arrow*). Axial CT image (*B*) several centimeters caudal shows distal aspect of appendix (*arrow*) is distended measuring 8 mm and shows no oral contrast material within. Findings suggest distal appendicitis, which was confirmed at surgery.

abnormal appendix by allowing loops of small bowel in the right lower quadrant to be displaced away from the cecum by gravity.

Appendicoliths or noncalcified foreign bodies are the most common causes of appendiceal obstruction and inflammation. Other processes can cause appendiceal obstruction and inflammation, however, including typhlitis, Crohn's disease, cecal carcinoma, and colitis (Figs. 12, 13). In many of these cases, recognizing the underlying cause for an abnormal-appearing appendix can alter the medical or surgical management of the patient. For example, if there is circumferential thickening of the cecum or colon and the wall demonstrates a target appearance after administration of IV contrast material, colitis is most likely present (see Fig. 12). The diffuse inflammatory process in the cecum may secondarily obstruct the orifice of the appendix, leading to an appearance that

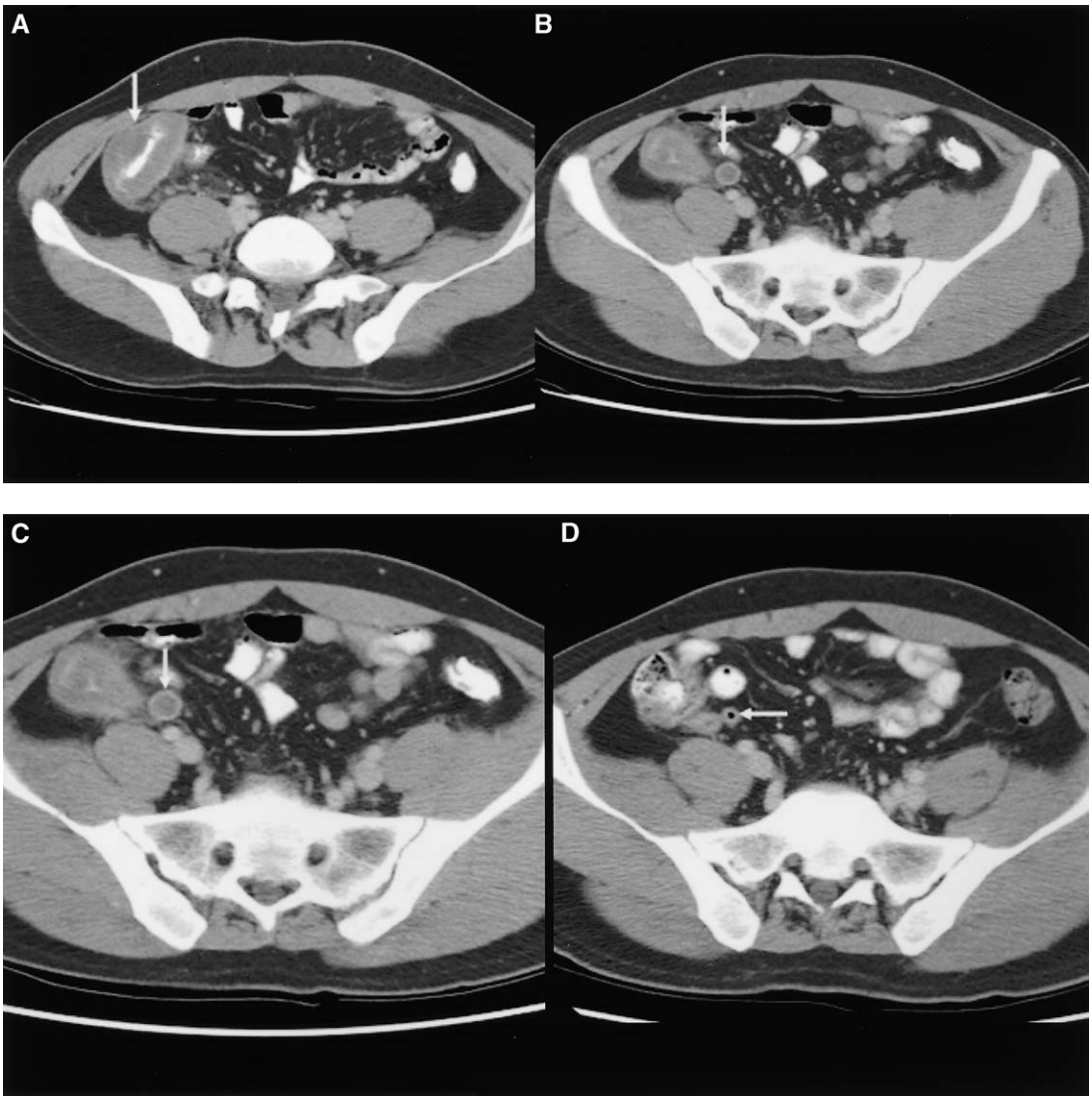

Fig. 12. Infectious colitis causing abnormal appendix. (*A*) Axial CT image performed after oral and intravenous contrast material shows circumferential thickening of the cecum (*arrow*) consistent with colitis. Axial CT image (*B*) several centimeters caudal shows distended appendix (*arrow*) measuring 11 mm and no oral contrast material within. (*C*) The patient was treated with antibiotics. Axial CT image (*C*) same as in *A* again shows abnormal appearance of the appendix (*arrow*) at time of initial presentation. Axial CT image (*D*) after 3 weeks of antibiotic treatment now shows normal-appearing appendix (*arrow*).

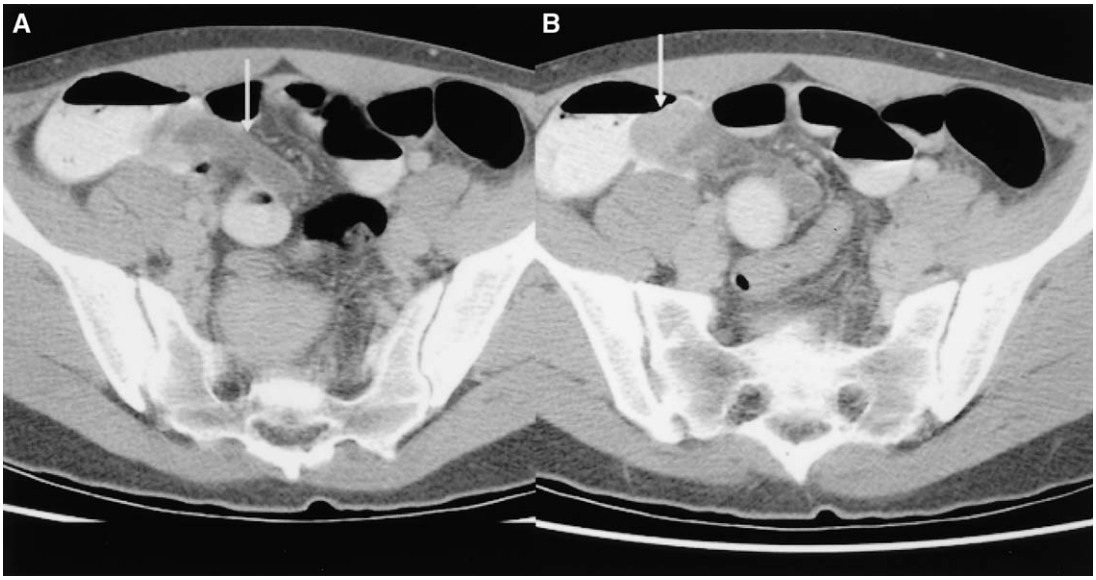

Fig. 13. Cecal carcinoma causing appendicitis. Axial CT image (*A*) performed after oral and intravenous contrast material shows fluid-filled distended appendix consistent with appendicitis (*arrow*). Axial CT image (*B*) several centimeters caudal shows focal thickening at the base of the appendix (*arrow*). At surgery, however, a palpable mass was detected in the cecum and resection revealed cecal carcinoma obstructing the appendix. In this case, it is very difficult prospectively to make the diagnosis of cecal cancer in the setting of appendicitis.

suggests appendicitis. Recognizing that the inflammatory response is circumferential and not localized to the area of the appendix allows differentiation of primary appendicitis and secondarily obstructed appendix, which improve when the primary colonic process is treated.

The major complication of appendicitis is perforation with abscess formation (Fig. 14). The key to prevention of abscess formation is early recognition of appendicitis and early removal of the inflamed appendix. When a large abscess (>4 cm) is present, the preferred treatment is percutaneous drainage. Another complication of appendicitis is small bowel obstruction (Fig. 15). In septic patients who present with distal small bowel obstruction, especially the elderly or those who have not had prior surgery, appendicitis should be considered as a possible etiology of the obstruction. In these cases, the small bowel obstruction is caused by serosal inflammation of the distal small bowel causing spasm, narrowed caliber, and functional obstruction.

Differential diagnosis

Gynecologic and renal causes of acute right lower quadrant pain are common. There are a number of other inflammatory conditions that mimic appendicitis clinically and cause right lower quadrant pain. CT can often detect these other entities and alter the medical or surgical management of the patient. These other processes affecting the right lower quadrant

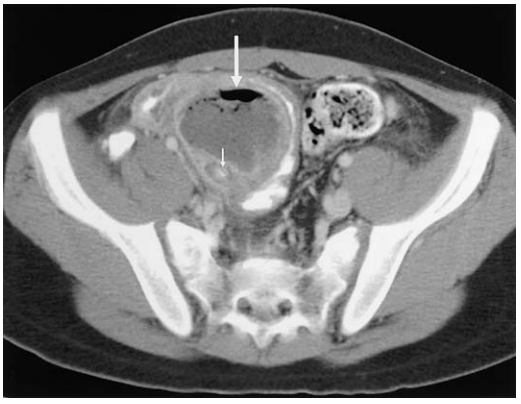

Fig. 14. Abscess complicating appendicitis. Axial CT image after oral and intravenous contrast material shows well-circumscribed gas and fluid collection in the right lower quadrant (*large arrow*). Small bowel is draped over the abscess. Note appendicolith in abscess (*small arrow*). Abscess was treated by percutaneous drainage.

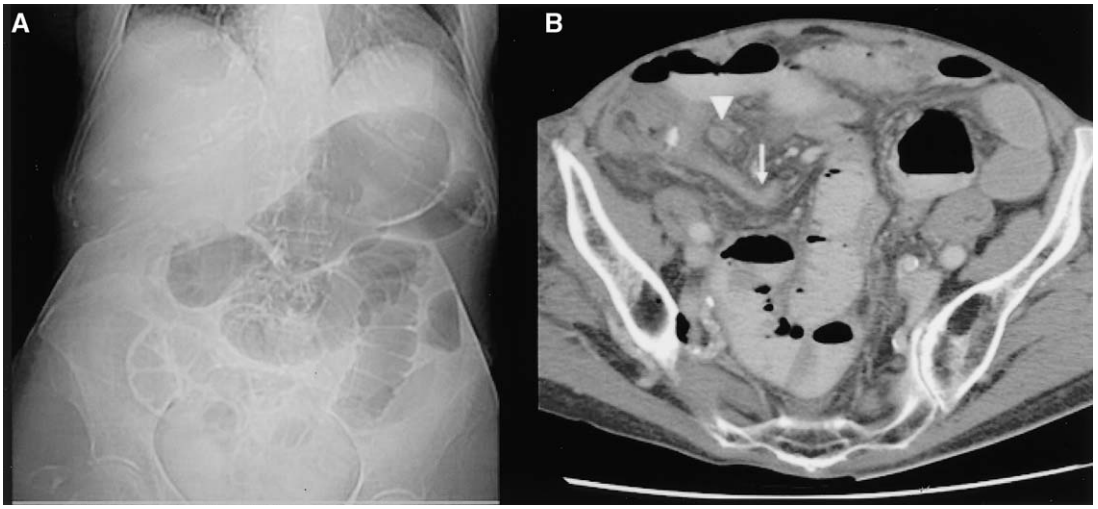

Fig. 15. Appendicitis in a patient presenting with symptoms of small bowel obstruction without prior surgery. Supine scout image (*A*) shows dilated small bowel and paucity of colonic gas consistent with obstruction. Axial CT image in the right lower quadrant (*B*) shows appendicolith in cecum and collapsed distal small bowel (*arrow*). Appendix is distended (*arrowhead*). Surgery confirmed appendicitis with secondary partial small bowel obstruction.

include mesenteric adenitis, Crohn's disease, infectious and ischemic ileitis, cecal and ileal diverticulitis, Meckel's diverticulitis, typhlitis, right-sided acute epiploic appendagitis, and omental infarction.

Mesenteric adenitis

Mesenteric adenitis can be divided into two broad categories: primary and secondary. Primary mesenteric adenitis has been defined as right-sided mesenteric lymphadenopathy without an identifiable acute inflammatory process or with mild (less than 5 mm) wall thickening of the terminal ileum (Fig. 16) [7,35–40]. Enlarged mesenteric lymph nodes, however, have been reported to occur in patients with celiac disease; appendicitis; diverticulitis; Crohn's disease; and neoplastic processes, such as lymphoma and carcinoma [2,10,11,41,42]. In these cases, the mesenteric adenitis can be considered secondary to a specific underlying condition. In most cases of primary mesenteric adenitis, an underlying infectious terminal ileitis is thought to be the etiology [7].

The reported frequency of primary mesenteric adenitis is variable. Puylaert [40] reported 100 consecutive adult patients who underwent compression sonography who were clinically suspected of having appendicitis and found that 14 (14%) had primary mesenteric adenitis with mild terminal ileal thickening. In a study from Rao et al [7], primary mesenteric adenitis was found to be the second most common etiology of right lower quadrant pain after appendicitis, accounting for 7% of the discharge diagnosis in adult and pediatric patients with a clinical suspicion of appendicitis. Kamel et al [26], studying adult patients with acute right lower quadrant pain, found that only 2% of patients had primary mesenteric adenitis. A study evaluating causes of mesenteric adenitis found that the incidence of primary mesenteric adenitis was low, and that when mesenteric adenitis was present, there was usually a specific etiology that could be detected at CT [10]. When enlarged lymph nodes are identified in the small bowel mesentery, an etiology should always be sought. If no associated abnormality is present, and the patient presents with acute right lower quadrant pain, primary mesenteric adenitis is likely present.

Terminal ileitis

Several inflammatory conditions involving the terminal ileum may cause acute right lower quadrant pain. Ileitis may be caused by bacterial, mycobacterial, parasitic, and viral pathogens. These conditions usually cause mild bowel wall thickening (< 5 mm) and

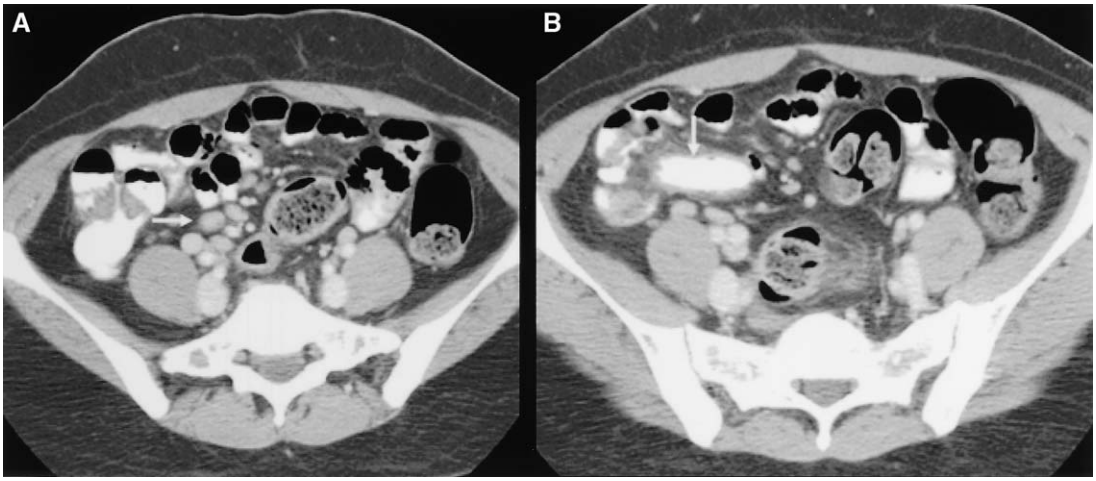

Fig. 16. Patient with right lower quadrant pain and clinically suspected appendicitis. Axial CT image after oral and intravenous contrast material (*A*) shows cluster of lymph nodes in the right lower quadrant mesentery. Axial image in same patient several centimeters caudal (*B*) shows mild thickening of terminal ileum (*arrow*). Findings are consistent with infectious ileitis and mesenteric adenitis.

may be associated with mesenteric adenitis. Other inflammatory entities that may cause terminal ileitis include Crohn's disease, ischemia, and vasculitis.

Crohn's disease

Crohn's disease is a chronic granulomatous inflammatory condition of unknown cause that can affect any segment of the gastrointestinal tract but most commonly involves the terminal ileum and the right colon [11]. Patients who develop acute exacerbations or local complications present often with right lower quadrant pain. CT imaging in these patients can exclude the diagnosis of appendicitis and demonstrate features characteristic of Crohn's disease (Fig. 17). The bowel affected by Crohn's disease usually shows more prominent circumferential wall thickening than in cases of infectious terminal ileitis [43]. In acute and subacute cases, the wall of the bowel shows mural stratification (target sign) after the administration of IV contrast. Occasionally, skip lesions are present characterized by segments of affected bowel separated by intervening normal bowel. Other intraperitoneal findings are often seen including a local proliferation of mesenteric fat around the affected bowel, prominent vessels in the hypertrophied fat, fistulas, sinus tracts, and abscesses [11]. The degree of prominence of the vessels (hyperemia) in the fat adjacent to an affected segment of bowel has recently been reported to correlate with disease activity as assessed both clinically and with barium studies [44].

Ischemia and vasculitis

Ischemia and vasculitis may affect the right colon and distal ileum causing acute right lower quadrant pain [43,45,46]. Small bowel ischemia usually causes long segments of bowel to be affected including the

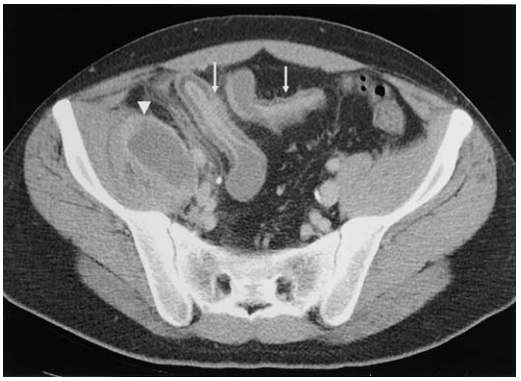

Fig. 17. Patient with right lower quadrant pain and Crohn's disease. Axial CT image after oral and intravenous contrast material shows two separate segmental areas of moderate bowel wall thickening (*arrows*). Note target appearance of bowel wall consistent with an inflammatory process. There is also a proliferation of fat around these affected bowel wall segments characteristic of Crohn's disease. In this patient there is an associated right iliopsoas muscle abscess (*arrowhead*).

terminal ileum. Most cases of small bowel ischemia are caused by either embolus or thrombus formation in the proximal superior mesenteric artery or from low perfusion pressure [46]. Surgical series report the most common cause of mesenteric ischemia to be superior mesenteric artery embolus, accounting for 50% of cases. In clinical practice, however, long segments of the small bowel may demonstrate mild wall thickening in association with a small-caliber superior mesenteric artery at CT. These patients present with pain and elevated lactic acid levels. They are frequently intensive care unit patients with low cardiac output and low perfusion pressure as the cause of their mesenteric ischemia. In either case (superior mesenteric artery embolus or low perfusion pressure), most of the small bowel is at risk. After the administration of IV contrast material, a target appearance of the small bowel wall is seen in many cases [46]. Whenever the small bowel or right colon shows bowel wall thickening with a target appearance, a careful evaluation of the superior mesenteric artery and vein for filling defects or caliber changes is warranted (Fig. 18).

Patients with superior mesenteric artery may present with acute abdominal pain localized in the right lower quadrant. The cause of the pain in these patients is vasculitis affecting the bowel. The small bowel and colon may be involved and often long segments of the bowel are affected [43]. After the IV administration of contrast striking mural stratification may be seen in patients with vasculitis (Fig. 19). In young patients presenting with abdominal pain and diffuse small bowel wall thickening with mural stratification, vasculitis caused by superior mesenteric artery should be high in the differential diagnosis.

Cecal and right-sided colonic diverticulitis

Cecal and right-sided colonic diverticulitis is a well-known entity that causes acute right lower quadrant pain, often mimicking the clinical presentation of appendicitis [47–49]. The importance of making a preoperative diagnosis of cecal diverticulitis is that most of these patients can be treated with antibiotics not requiring surgery [47]. The findings at CT that suggest the diagnosis include focal asymmetric thickening of the colonic wall with adjacent stranding of the pericolonic fat, associated diverticula, and a normal appendix [49]. Often at the center of the inflammatory process the inflamed diverticulum can be identified (Fig. 20). When this is present, a confident diagnosis can be made. When the inflamed diverticulum is not seen, one needs to consider the possibility of colonic carcinoma in the differential diagnosis [48]. In these cases, colonoscopy or barium enema examination are helpful in differentiating the two conditions (Fig. 21) [49].

Meckel's and ileal diverticulitis

A Meckel's diverticulum is a blind sac arising from the distal ileum and is the most common congenital anomaly of the small bowel, occurring in approximately 2% of the population [50,51]. A Meckel's diverticulum is a true diverticulum containing all three layers of the bowel wall. Occasionally a Meckel's diverticulum may become obstructed by a fecalith with resulting diverticulitis and abscess formation. CT may demonstrate an inflammatory process adjacent to a loop of small bowel and occasionally an obstructing calcified fecalith is demonstrated (Fig. 22). A high degree of suspicion is necessary to diagnose this condition on CT because the diverticulum may be small and concealed by adjacent loops of nonopacified small bowel.

In addition to Meckel's diverticulitis, small-acquired diverticula of the ileum may develop. These have been reported in 1% to 2% of small bowel series using spot compression radiography [52]. These diverticula also may become impacted with resultant diverticulitis.

Typhlitis

Typhlitis is an acute inflammatory process usually centered at the level of the cecum. In addition, the terminal ileum, appendix, and right colon may be involved [53]. The condition results from chemotherapy-induced neutropenia. Histologically, combinations of bacterial and fungal overgrowth with superimposed ischemia are present. CT scanning demonstrates marked thickening of the cecum with either heterogeneous areas of decreased attenuation in the wall, or with a target appearance after the administration of IV contrast material (Fig. 23). Therapy is conservative consisting of broad-spectrum antibiotic and antifungal medications.

Primary epiploic appendagitis

Primary epiploic appendagitis is an uncommon condition that may occur in the proximal or distal

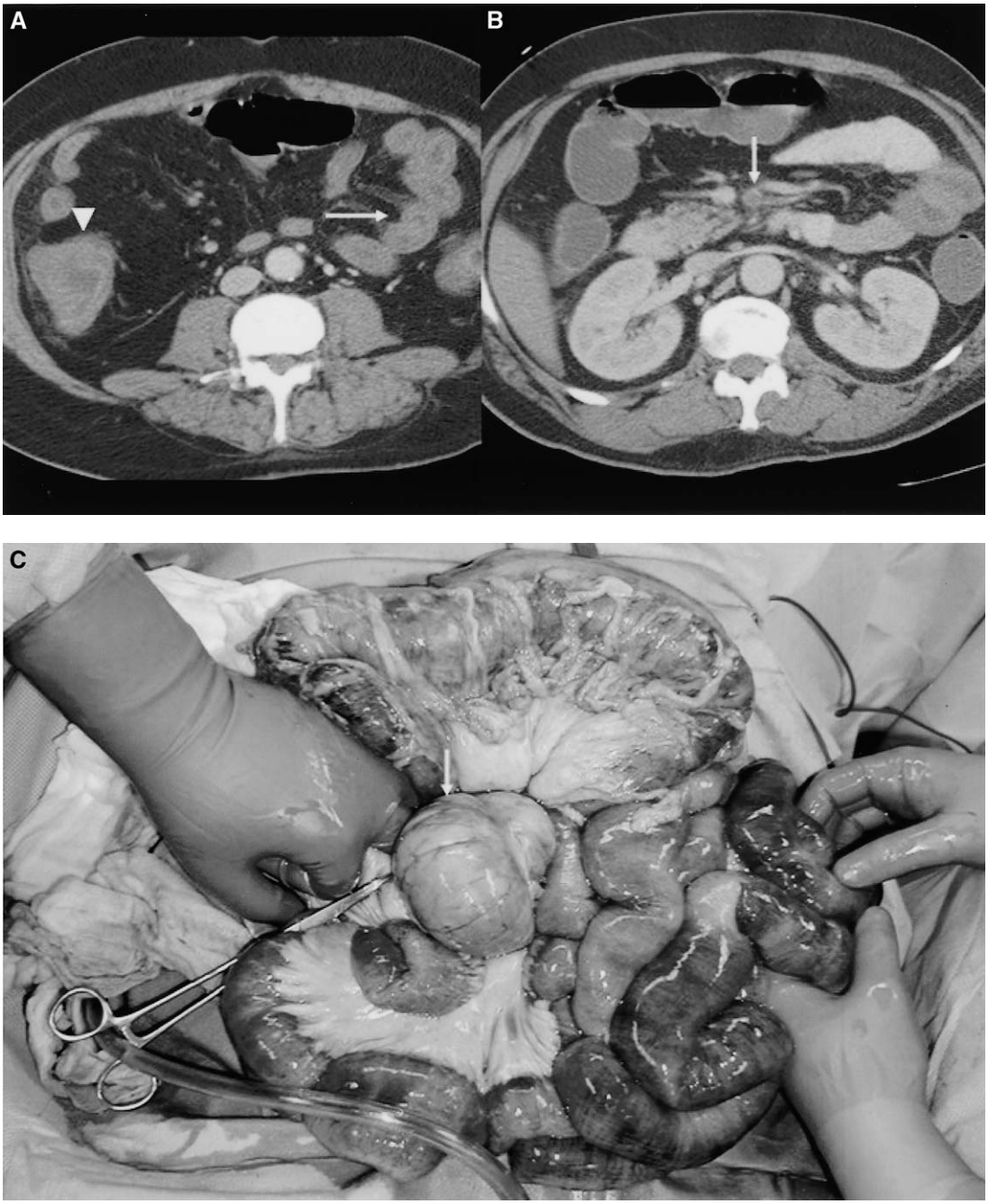

Fig. 18. Patient with acute right lower quadrant and crampy abdominal pain with mesenteric ischemia. (*A*) Axial CT image after oral and intravenous contrast shows multiple mildly thickened small bowel loops (*arrow*) with a target appearance. The right colon also shows circumferential wall thickening and a target appearance (*arrowhead*). Axial CT image (*B*) in same patient at level of superior mesenteric artery shows filling defect in superior mesenteric artery consistent with embolus (*arrow*). (*C*) Surgery confirmed diffuse small bowel and cecal infarction.

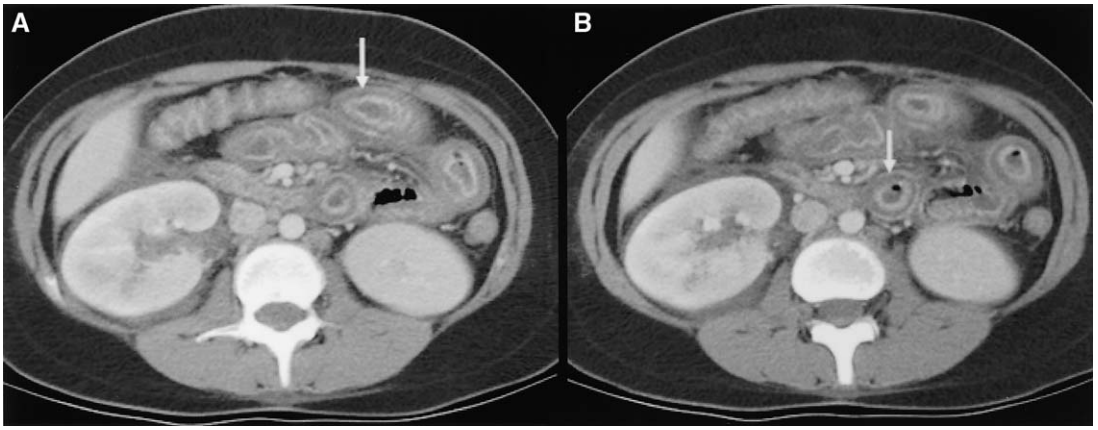

Fig. 19. Patient with acute right lower quadrant pain and superior mesenteric artery. Axial CT image after oral and intravenous contrast (*A*) shows multiple moderately thickened small bowel loops (*arrow*) with a target appearance. Axial CT image (*B*) in same patient 1 cm caudal shows mural stratification in affected loop (*arrow*).

colon. When the condition occurs on the right side, the clinical presentation is one of acute right lower quadrant pain, similar to appendicitis. These patients usually lack associated fever and leukocytosis [54]. The condition is caused by torsion and infarction of the appendage. The CT findings in cases of acute epiploic appendagitis are characteristic and allow for a definitive diagnosis to be made in most cases. At CT, an oval- or round-shaped fatty mass measuring 2 to 4 cm is present with an associated rim

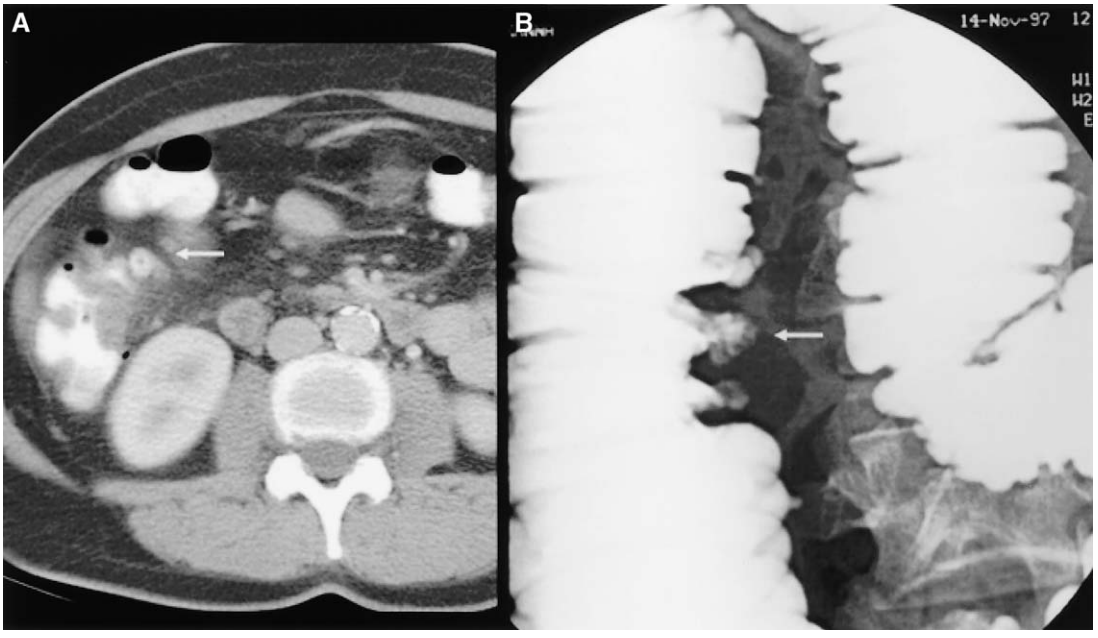

Fig. 20. Right-sided diverticulitis presenting with acute right lower quadrant pain. Axial CT image after oral and intravenous contrast (*A*) shows multiple right-sided diverticulum, focal bowel wall thickening, and adjacent pericolonic stranding (*arrow*). Single-contrast barium enema (*B*) confirms right-sided diverticulum with separation of adjacent diverticula caused by the pericolonic inflammation.

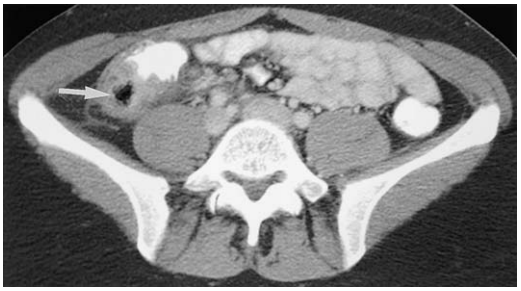

Fig. 21. Cecal diverticulitis in 54-year-old man. Axial CT scan at level of cecum shows focal bowel wall thickening with inflamed enhancing diverticulum at center of process (*arrow*).

of high-attenuation likely representing contrast enhancement around the periphery of the inflamed appendage (Fig. 24). In addition, there is streaking of the adjacent pericolonic fat and occasionally focal thickening of the adjacent colon wall and enhancement of the adjacent parietal peritoneum [54]. Preoperative diagnosis is important because the clinical history is usually suspected appendicitis. Epiploic appendagitis is a self-limited condition that does not require surgery.

Omental infarction

Omental infarction presents as acute abdominal pain. It may occur on the right or left side of the abdomen [55,56]. When it occurs on the right side of the abdomen, the presentation may simulate that of acute appendicitis [55]. The cause is unclear and may be related to anomalies of the arterial or venous system of the omentum, previous surgery, omental

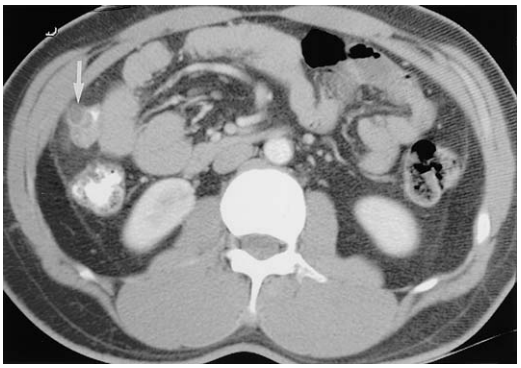

Fig. 22. Meckel's diverticulitis in 38-year-old man with right-sided abdominal pain. Axial contrast-enhanced CT scan shows fluid-filled sac-like structure (*arrow*) adjacent to loop of distal ileum. Surgery confirmed inflamed Meckel's diverticulum with clinically suspected appendicitis.

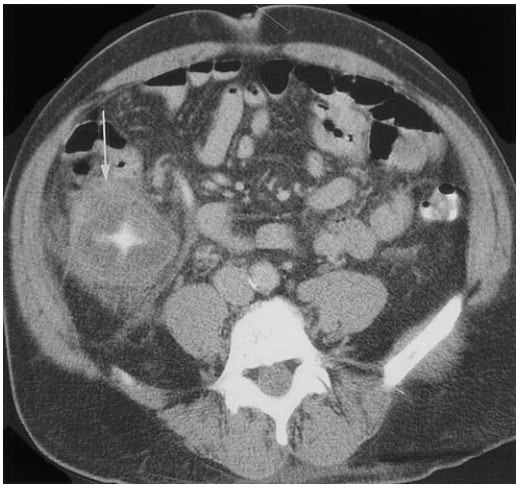

Fig. 23. Typhlitis in a 43-year-old man with acute myelogenous leukemia. Axial contrast-enhanced CT scan shows marked circumferential thickening of the cecum and proximal ascending colon (*arrow*). Patient was neutropenic at the time and was treated with broad-spectrum antibiotics.

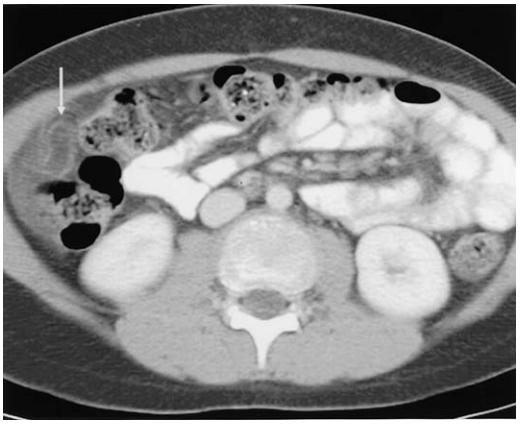

Fig. 24. Epiploic appendagitis presenting with acute right lower quadrant pain. Axial CT image after administration of oral and intravenous contrast material show oval-shaped fatty density with enhancing rim ventral and lateral to the right colon (*arrow*). Note stranding of the adjacent fat. Findings are typical for acute epiploic appendagitis.

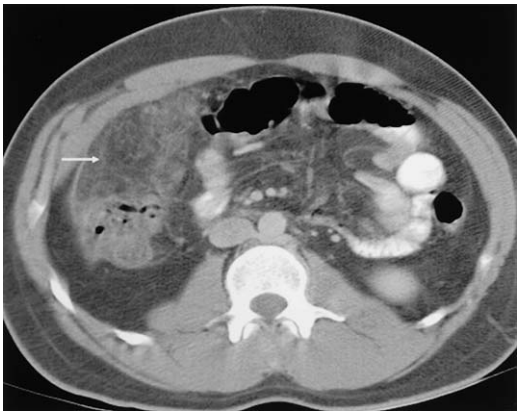

Fig. 25. Omental infarction presenting with acute right lower quadrant pain. Axial CT image after administration of oral and intravenous contrast material shows mass-like, triangular-shaped, infiltration of the omentum (*arrow*) ventral to the right colon. Findings are typical for omental infarction.

torsion, or may be related to prior or recent trauma. The CT findings include triangular or geographic areas of fat stranding in the anterior abdomen at the expected location of the greater omentum [55]. Because of the anterior location of the greater omentum, the infiltrative changes are visualized between the anterior parietal peritoneum and the ventral wall of the ascending or transverse colon (Fig. 25). In most cases the condition is self-limited but occasionally if the symptoms persist or associated abscess occurs, surgery may be indicated. Laparoscopic omentectomy is rarely necessary but has been reported to be successful in the treatment of this condition with rapid resolution of symptoms after surgery [56].

Summary

Acute right lower quadrant pain is a nonspecific but common clinical complaint. Appendicitis is the most common cause of acute right lower quadrant pain and CT has become the most reliable imaging method in the evaluation of these patients. Although there is controversy regarding the best way to perform CT in this setting, oral and IV contrast-enhanced CT remains the most commonly used technique. CT with oral and IV contrast material facilitates diagnosis of appendicitis and the numerous other entities that may cause right lower quadrant pain.

References

[1] de Dombal FT. Diagnosis of acute abdominal pain. 2nd edition. New York: Churchill Livingstone; 1991.
[2] Ahn SH, Mayo-Smith WM, Murphy BL, Reinert SE, Cronan JJ. Acute nontraumatic abdominal pain in adult patients: abdominal radiography compared with CT evaluation. Radiology 2002;225:159–64.
[3] Balthazar EJ, Birnbaum BA, Yee J, et al. Acute appendicitis: CT and US correlation in 100 patients. Radiology 1994;190:31–5.
[4] Novelline RA, Rhea JT, Rao PM, Stuk JL. Helical CT in emergency radiology. Radiology 1999;213:321–39.
[5] Birnbaum BA, Jeffrey RB. CT and sonographic evaluation of acute right lower quadrant abdominal pain. AJR Am J Roentgenol 1998;170:361–71.
[6] Birnbaum BA, Wilson SR. Appendicitis at the millennium. Radiology 2000;215:337–48.
[7] Rao PM, Rhea JT, Novelline RA. CT diagnosis of mesenteric adenitis. Radiology 1997;202:145–9.
[8] Macari M, Balthazar EJ, Krinsky G, Cao H. CT diagnosis of ileal diverticulitis. Clin Imaging 1998;22:243–5.
[9] Rao PM, Rhea JT, Novelline RA. CT diagnosis of mesenteric adenitis. Radiology 1997;202:145.
[10] Macari M, Hines J, Balthazar EJ, Megibow AJ. Mesenteric adenitis: CT diagnosis of primary vs. secondary causes, incidence, and clinical significance. AJR Am J Roentgenol 2002;178:853–8.
[11] Gore RM, Balthazar EJ, Ghahremani GG, Miller FH. CT features of ulcerative colitis and Crohn's disease. AJR Am J Roentgenol 1996;167:3–15.
[12] Bennett GL, Slywotzky CM, Giovanniello G. Gynecologic causes of acute pelvic pain: spectrum of CT findings. Radiographics 2002;22:785–801.
[13] Balthazar EJ, Rofsky NM, Zucker R. Appendicitis: the impact of computed tomography imaging on negative appendectomy and perforation rates. Am J Gastroenterol 1998;93:768–71.
[14] Bendeck SE, Nino-Murcia M, Berry GJ, Jeffrey Jr RB. Imaging for suspected appendicitis: negative appendectomy and perforation rates. Radiology 2002;225:131–6.
[15] Lim HK, Lee WG, Lee SJ, Namgung S, Lim JH. Focal appendicitis confined to the tip: diagnosis at US. Radiology 1996;200:799–801.
[16] Jeffrey Jr RB, Jain KA, Nghiem HV. Sonographic diagnosis of acute appendicitis: interpretive pitfalls. AJR Am J Roentgenol 1994;162:55–9.
[17] Puylaert JB. Acute appendicitis: US evaluation using graded compression. Radiology 1986;158:355–60.
[18] Sivit CJ, Applegate KE, Stallion A, et al. Imaging evaluation of suspected appendicitis in a pediatric population: effectiveness of sonography versus CT. AJR Am J Roentgenol 2000;175:977–80.
[19] Lane MJ, Katz DS, Ross BA, et al. Unenhanced helical CT for suspected acute appendicitis. AJR Am J Roentgenol 1997;168:405–9.
[20] Ege G, Akman H, Sahin A, Bugra D, Kuzucu K. Diagnostic value of unenhanced helical CT in adult

patients with suspected acute appendicitis. Br J Radiol 2002;75:721–5.
[21] Lane MJ, Liu DM, Huynh MD, Jeffrey Jr RB, Mindelzun RE, Katz DS. Suspected acute appendicitis: nonenhanced helical CT in 300 consecutive patients. Radiology 1999;213:341–6.
[22] Grayson DE, Wettlaufer JR, Dalrymple NC, Keesling CA. Appendiceal CT in pediatric patients: relationship of visualization to amount of peritoneal fat. AJR Am J Roentgenol 2001;17:497–500.
[23] Jacobs JE, Birnbaum BA, Macari M, Megibow AJ, Israel G, Maki DD, et al. Helical CT diagnosis of acute appendicitis: comparison of focused appendiceal technique using oral contrast and non focused technique using oral and intravenous contrast. Radiology 2001; 220:683–90.
[24] Fefferman NR, Roche KJ, Pinkney LP, Ambrosino MM, Genieser NB. Suspected appendicitis in children: focused CT technique for evaluation. Radiology 2001; 220:691–5.
[25] Rao PM, Rhea JT, Noveline RA, et al. Helical CT technique for the diagnosis of appendicitis: prospective evaluation of focused appendix technique. Radiology 1997;202:139–44.
[26] Kamel IR, Goldberg SN, Keogan MT, Rosen MP, Raptopoulos V. Right lower quadrant pain and suspected appendicitis: nonfocused appendiceal CT: review of 100 cases. Radiology 2000;217:159–63.
[27] Mullins ME, Kircher MF, Ryan DP, et al. Evaluation of suspected appendicitis in children using limited helical CT and colonic contrast material. AJR Am J Roentgenol 2001;176:37–41.
[28] O'Malley ME, Halpern E, Mueller PR, Gazelle GS. Helical CT protocols for the abdomen and pelvis: a survey. AJR Am J Roentgenol 2000;175:109–13.
[29] Weltman DI, Yu J, Krumenacker Jr J, Huang S, Moh P. Diagnosis of acute appendicitis: comparison of 5- and 10 mm CT sections n the same patient. Radiology 2000;216:172–7.
[30] Benjaminov O, Atri M, Hamilton P, Rappaport D. Frequency of visualization thickness of normal appendix at nonenhanced helical CT. Radiology 2002;225:400–6.
[31] Ramsden WH, Mannion RAJ, Simpkins KC, deDombal FT. Is the appendix where you think it is—and if not does it matter? Clin Radiol 1993;47:100–3.
[32] Rao PM, Rhea JT, Novelline RA. Helical computed tomographic incidence and characterization of appendicoliths in 100 patients with appendicitis. Emergency Radiology 1997;4:55.
[33] Rao PM, Wittenberg J, McDowell RK, et al. Appendicitis: use of arrowhead sign for diagnosis at CT. Radiology 1997;202:363–6.
[34] Lim HK, Lee WJ, Lee SJ, Namgung S, Lim JH. Focal appendicitis confined to the tip: diagnosis at US. Radiology 1996;200:799–801.
[35] Jelloull L, Fremond B, Dyon JF, Orme RL, Babut JM. Mesenteric adenitis caused by *Yersinia* pseudotuberculosis presenting as an abdominal mass. Eur J Pediatr Surg 1997;7:180–3.
[36] Lee JH, Rhea PL, Lee JK, et al. The etiology and clinical characteristics of mesenteric adenitis in Korean adults. J Korean Med Sci 1997;12:105–10.
[37] Garcia-Corbeira P, Ramos JM, Aguado JM, Soriano F. Six cases in which mesenteric lymphadenitis due to non-*typhi* Salmonella caused an appendicitis-like syndrome. Clin Infect Dis 1995;21:231–2.
[38] Koruda MJ, Bell LM, Ross III AJ. Atypical mycobacterial mesenteric lymphadenitis in childhood presenting as an abdominal mass. J Pediatr Surg 1988;23:526–8.
[39] Kunkel MJ, Brown LG, Bauta H, Iannini PB. Menningocoocal mesenteric adenitis and peritonitis in a child. Pediatr Infect Dis 1984;3:327–8.
[40] Puylaert JB. Mesenteric adenitis and acute terminal ileitis: US evaluation using graded compression. Radiology 1986;161:691–5.
[41] Al-Kawas FH, Murgo A, Foshag L, Shiels W. Lymphadenopathy in celiac disease: not always a sign of lymphoma. Am J Gastroenterol 1988;83:301–3.
[42] Heiberg E, Wolverson MK, Sundaram M, Shields JB. Body CT findings in systemic lupus erythematosus. J Comput Tomogr 1988;12:68–74.
[43] Macari M, Balthazar EJ. Computed tomography of bowel wall thickening: significance and pitfalls of interpretation [review]. AJR Am J Roentgenol 2001;176: 1105–16.
[44] Lee SS, Ha HK, Yang SK, Kim AY, Kim TK, Kim PN, et al. CT of prominent pericolic or perienteric vasculature in patients with Crohn's disease: correlation with clinical disease activity and findings on barium studies. AJR Am J Roentgenol 2002;179:1029–36.
[45] Ha HK, Lee SH, Rha SE, Kim JH, Byun JY, Lim HK, et al. Radiologic features of vasculitis involving the gastrointestinal tract. Radiographics 2000;20:779–94.
[46] Macari M, Chandarana H, Balthazar EJ, Babb J. Small intestinal ischemia versus intramural hemorrhage: CT evaluation. AJR Am J Roentgenol 2003;180: 177–84.
[47] Oudenhoven LF, Koumans RK, Puylaert JB. Right colonic diverticulitis: US and CT findings—new insights about frequency and natural history. Radiology 1998; 208:611–8.
[48] Jang HJ, Lim HK, Lee SJ, Lee WJ, Kim EY, Kim SH. Acute diverticulitis of the cecum and ascending colon: the value of thin section helical CT findings in excluding colonic carcinoma. AJR Am J Roentgenol 2000; 174:1397–402.
[49] Balthazar EJ, Megibow AJ, Gordon RB, Hulnick D. Cecal diverticulitis: evaluation with CT. Radiology 1987;162:79–81.
[50] Macari M, Panicek DM. CT findings in acute necrotizing Meckel diverticulitis due to obstructing enterolith. J Comput Assist Tomogr 1995;19:808–10.
[51] Rossi P, Gourtsoyiannis N, Bezzi M, et al. Meckel's diverticulum: imaging diagnosis. AJR Am J Roentgenol 1996;166:567–73.
[52] Macari M, Balthazar E, Cao H, Krinsky G. CT diagnosis of ileal diverticulitis. Clin Imaging 1998;22:243–5.
[53] Wall SD, Jones B. Gastrointestinal tract in the immu-

nocompromised host: opportunistic infections and other complications. Radiology 1992;185:327–35.
[54] Rao PM, Novelline RA. Diagnosis please Case 6: primary epiploic appendagitis. Radiology 1999;210: 145–8.
[55] Grattan-Smith JD, Blews DE, Vrand T. Omental infarction in pediatric patients: sonographic and CT findings. AJR Am J Roentgenol 2002;178:1537–9.
[56] Balthazar EJ, Lefkowitz RA. Left sided omental infarction with associated omental abscess: CT diagnosis. J Comput Assist Tomogr 1993;17:379–81.

RADIOLOGIC CLINICS OF NORTH AMERICA

Radiol Clin N Am 41 (2003) 1137–1151

Adult intussusception: diagnosis and clinical relevance

Benjamin Y. Huang, MD, MPH, David M. Warshauer, MD*

Department of Radiology, University of North Carolina School of Medicine, Campus Box 7510, Chapel Hill, NC 27599–7510, USA

Intussusception occurs when a segment of bowel and its associated mesentery (the intussusceptum) invaginates into the lumen of an adjacent bowel segment (the intussuscipiens). Primarily a disease of childhood, intussusception is the leading cause of intestinal obstruction in children [1]. Although intussusception is rare after childhood, approximately 5% to 16% of intussusceptions in the Western world occur in adults [2–5]. Adult intussusception differs considerably from its pediatric counterpart in its causes, clinical presentation, diagnosis, and treatment.

Pathophysiology

Intussusceptions in both pediatric and adult patients may be caused by an intraluminal, mural, or extraluminal process [6]. The most easily understood mechanism by which intussusception occurs is when an intraluminal mass is pulled forward by peristalsis and drags the attached bowel wall segment with it. Pedunculated tumors, such as adenomatous polyps or lipomas, are the classic prototypes of this group, but a similar mechanism is thought to explain intussusception associated with an inverted Meckel's diverticulum or an inverted appendix. Intussusception secondary to long intestinal tubes may also occur by this mechanism.

Less straightforward but perhaps more common are intussusceptions associated with mural abnormalities. In this group of intussusceptions, a focal area of bowel wall does not contract normally. Peristaltic forces in the adjacent or opposite bowel wall are then able to rotate the abnormal segment inward, causing a kink, which subsequently acts as a lead point for the resulting intussusception. Processes that may cause focal abnormal contraction include sessile malignancies, local inflammation, surgical suture lines, and lymphoid hyperplasia. Intussusceptions associated with celiac disease are also thought to fall under this category. The flaccidity associated with gluten enteropathy produces abnormal or absent contraction allowing for intussusceptions to occur.

Extraluminal factors also may produce intussusception. The classic example is an adhesion that binds one side of the bowel and causes a focal area of abnormal peristalsis or kinking, which then acts as a lead point. An inflamed Meckel's diverticulum or appendix also may cause intussusception in this manner.

Although most intussusceptions occur in the direction of normal peristalsis, retrograde intussusceptions occasionally do occur and have been associated with the presence of long intestinal tubes or a gastroenterostomy [7,8].

Location

Intussusceptions are characterized by their location in the bowel. Enteroenteric intussusceptions involve mesenteric small bowel and can be labeled further by the specific segment involved (eg, jejunojejunal, ileoileal, and so forth). Colocolic intussusceptions involve the colon and similarly can be classified as colocolic and sigmoidorectal intussusceptions. Enterocolic intussusception involves both small and large bowel and can be divided into two types. In the ileocolic type, the lead point resides in the ileum, which prolapses through the ileocecal valve and is drawn into the colon

* Corresponding author.

E-mail address: David_Warshauer@med.unc.edu (D.M. Warshauer).

0033-8389/03/$ – see front matter
doi:10.1016/S0033-8389(03)00116-7

with the cecum and ileocecal valve remaining fixed in the right lower quadrant. In the ileocecal type, the lead point is in the cecum or ileocecal valve itself, which intussuscepts and draws the terminal ileum in as it invaginates. Intussusceptions rarely involve the duodenum, stomach, or esophagus, because these organs are less redundant and more fixed to adjacent structures. Stomal intussusception occurs when there is prolapse of bowel through an existing ileostomy or colostomy. Postoperative intussusception of the excluded segment of a jejunoileal bypass has also been described [2,9,10].

In a large study of 745 surgically diagnosed adult intussusceptions, 52% originated in small bowel, with 39% enteroenteric and 13% ileocolic. Colonic intussusceptions made up 38%, with 17% being ileocecal, 17% being colocolic, and 4% being appendicocecal. Ten percent of cases involved either the stomach or duodenum (6%) or were stomal in origin (4%) [11]. More recent studies have shown similar results with enteric intussusception being slightly more common than those of colonic origin [5,12–14].

In contradistinction to these surgical series, a recent study of adult intussusception detected by CT or MR imaging showed 88% of intussusceptions to be enteroenteric, with only 12% involving the colon. This difference reflects the increased number of transient self-resolving enteroenteric intussusceptions discovered by imaging but not requiring surgical intervention [15].

Etiology

Childhood intussusceptions have been described as idiopathic in up to 95% of cases, but recent epidemiologic data have implicated infection by lymphotropic viruses, such as adenovirus, which produce enlargement of Peyer's patches, as the cause of a substantial number of pediatric intussusceptions [16–18]. In contrast, most adult intussusceptions diagnosed at surgery are secondary to a definable structural lesion or abnormality [2,4,5,11–13,19–21].

Neoplasia is the most common etiology of adult intussusception causing, on average, two thirds of cases in most surgical series. Malignant lesions make up approximately 60% of overall neoplasms. Notably, both percentages are higher in the large bowel. In a review of 1214 cases of adult intussusception published in 1976, 69% of colonic intussusceptions had a neoplastic lead point, with 70% of these tumors being malignant [22]. More recent series have shown similar or somewhat higher numbers [5,12–14,19,21,23,24]. Primary adenocarcinoma is by far the most common colonic malignancy leading to intussusception, with leiomyosarcomas, reticulum cell sarcomas, lymphosarcomas, and metastases also reported (Figs. 1, 2) [4,20,21,23].

In the small bowel, neoplasia and malignancy are less common. In the same review of 1214 cases of adult intussusception from 1976, 57% of intussusceptions in the small bowel were secondary to neoplasm with only 30% of these tumors being malignant [22]. More recent series have shown a similar prevalence of neoplasm and a similar to somewhat higher frequency of malignancy [5,12–14,19,21,23,24]. The most common malignant lead point in small bowel intussusception is a metastasis, with melanoma being the most frequent primary neoplasm. Metastases from squamous cell lung carcinoma, renal cell carcinoma, colon cancer, and myeloma are also seen, as is lymphoma. Primary small bowel adenocarcinomas and leiomyosarcomas and less common malignancies have also been reported [4,5,19–21,23].

Benign tumors are responsible for approximately 25% of adult intussusceptions. In the colon, adenomatous polyps and lipomas are most common, with fibromas, leiomyomas, and mucoceles of the appendix also reported. In the small bowel, Peutz-Jeghers polyps and lipomas are common, with fibromas, leiomyomas, hamartomas, and a variety of other lesions also reported (Fig. 3) [4,5,19–21,23].

Intussusception involving the stomach is usually secondary to a pedunculated benign adenoma. Gastric leiomyomas are also reported along with a number of

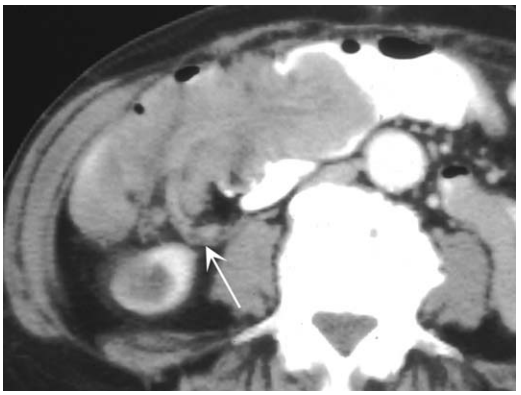

Fig. 1. Colocolic intussusception with a neoplastic lead point. Axial CT scan obtained in an 84-year-old man with colon cancer developing in a villous adenoma shows the longitudinal bowel-in-bowel appearance with mesenteric fat and vessels being drawn into the intussusception (*arrow*). (*From* Warshauer DM, Lee JKT. Adult intussusception detected at CT or MR imaging: clinical imaging correlation. Radiology 1999;212:853–60; with permission.)

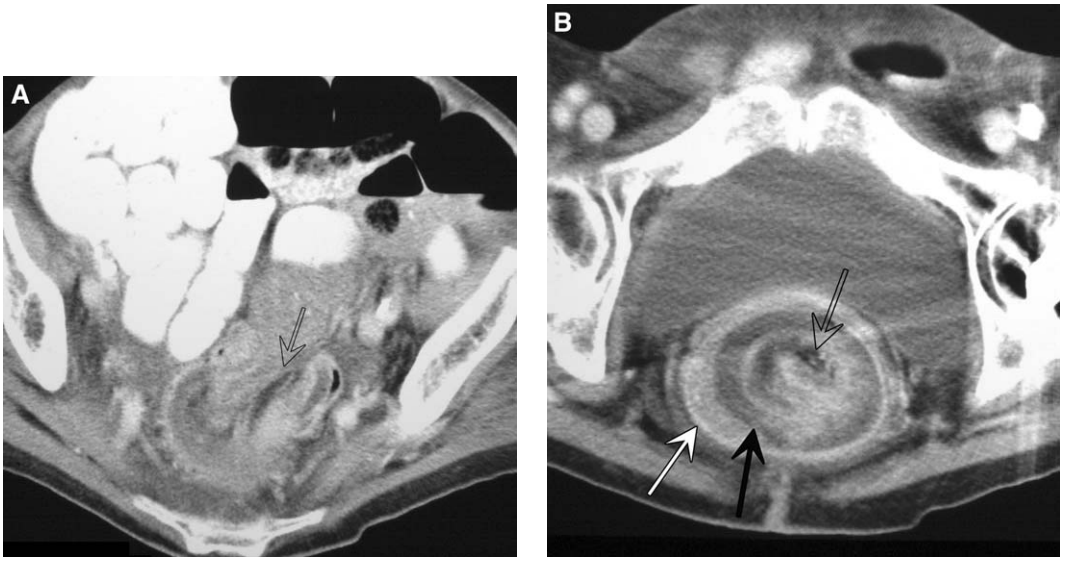

Fig. 2. Sigmoidorectal intussusception with a neoplastic lead point. Axial CT scans obtained in an 85-year-old woman. (*A*) Vessels and fat (*arrow*) being drawn into the intussusceptum. (*B*) Edematous intussusceptum (*black arrow*) within the rectum (*white arrow*). Fat and vessels within intussusceptum (*open arrow*). (Courtesy of Holly J. Burge, MD, Raleigh, NC.)

less common lesions, such as lipomas, hemangiomas, and carcinoids [25]. Gastric malignancy is uncommon as a lead point [26].

Nonneoplastic etiologies account for approximately 30% of colonic intussusceptions [22]. Inflammatory disease in the colon or appendix has been reported to cause colonic intussusception, along with lymphoid hyperplasia, postoperative anastomosis, and suture lines [5,12–14,19,21]. Nonneoplastic etiologies are more common in the small bowel. Postoperative changes and adhesions along with Meckel's diverticula are the two most common nonneoplastic etiologies in recent series [5,12–14,19,21,24]. Less common nonneoplastic causes of small bowel intussusception include lymphoid hyperplasia; scleroderma; cystic fibrosis; celiac disease; Henoch-Schönlein purpura; ileal duplications; abdominal trauma; and inflammatory conditions, such as pancreatitis (Figs. 4, 5) [5,12–14,19–21]. Gastroenterostomies and indwelling intestinal tubes are occasionally associated with gastroenteric intussusceptions (Fig. 6) [8].

Intussusception associated with AIDS has been reported in the last decade [27–31]. In these cases, intussusceptions were most commonly enteric and were secondary to a variety of pathologies including lymphoma, Kaposi's sarcoma, reactive lymphoid hyperplasia, atypical mycobacterial infections, cytomegalovirus colitis, and *Campylobacter* enteritis. The

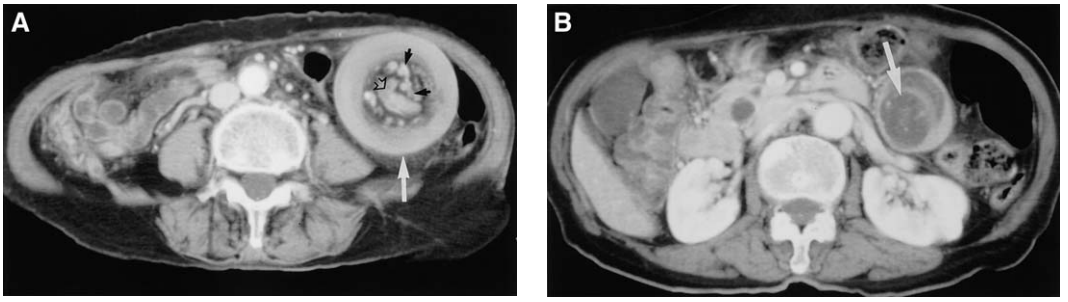

Fig. 3. Enteroenteric intussusception with jejunal lipoma as the lead point. Axial CT image obtained in an 80-year-old woman. (*A*) Intussuscipiens (*long arrow*) and the intraluminal intussusceptum (*open arrow*) on cross-section in the left mid-abdomen. Note the presence of several enhancing vessels (*small arrows*) in the mesentery, which has been drawn adjacent to the intussuscepted intestine. (*B*) Large intraluminal low-attenuated lesion consistent with a jejunal lipoma (*arrow*). Findings proved at surgery.

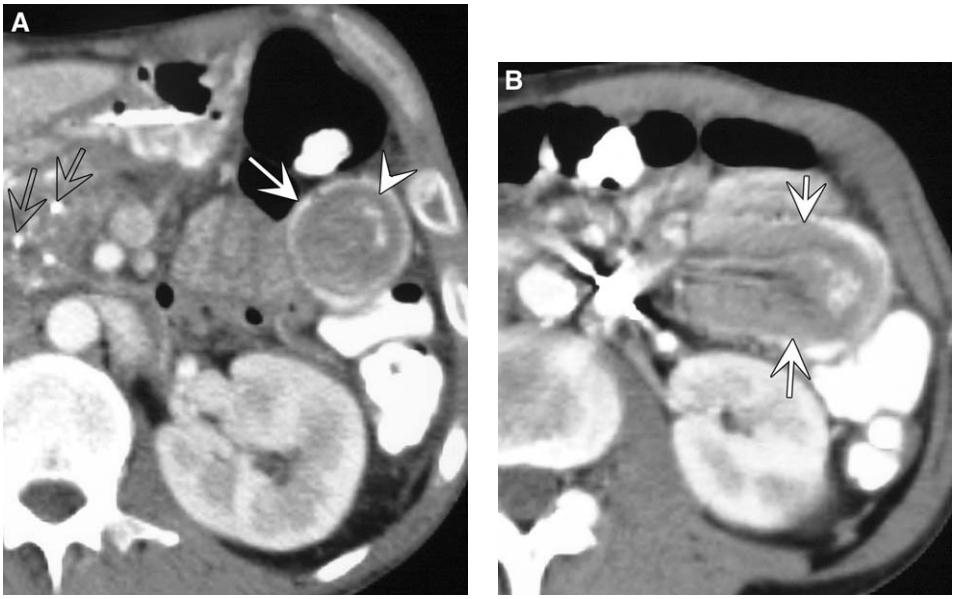

Fig. 4. Transient intussusception associated with local inflammation from pancreatitis. Axial CT scans. (*A*) At the level of pancreatic tail, the intussusceptum (*arrowhead*) is seen within the intussuscipiens (*white arrow*). Note calcifications in region of pancreatic head (*open arrows*) and infiltration of fat in the left anterior pararenal space. (*B*) At 5.2 cm caudal to Fig. 4A, mesenteric vessels, fat, and bowel (*arrows*) can be seen entering the intussuscipiens. Small bowel follow through performed 1 day following CT showed fold thickening in the duodenum and proximal jejunum but no intussusception. CT performed 1 month later also showed no intussusception. (*From* Warshauer DM, Lee JKTL. Adult intussusception detected at CT or MR imaging: clinical imaging correlation. Radiology 1999;212:853–60; with permission.)

frequency of AIDS-associated intussusception is not known, but the diagnosis should be considered in AIDS patients presenting with colicky abdominal pain or symptoms suggesting obstruction (Figs. 7, 8).

Idiopathic primary intussusception is relatively uncommon in recent clinical series making up on average 16% of small bowel etiologies and less than 5% of large bowel etiologies.

It is worth noting that these data are derived from developed nations and are based on series in which symptoms were severe enough to require surgery or major clinical intervention. In tropical regions of the

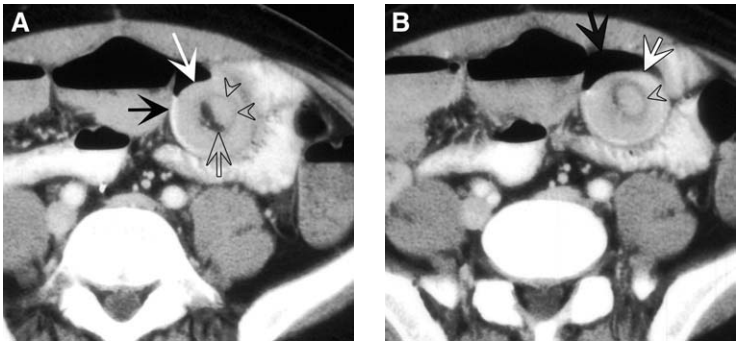

Fig. 5. (*A, B*) Enteroenteric intussusception associated with recent surgery. Three months previously, patient had undergone ileocecectomy for Crohn's disease with ileoascending colon anastomosis. Shown are intussuscipiens (*black arrow*), intussusceptum (*white arrow*), fat within intussusceptum (*open arrow*), and hypodense rim thought to represent muscularis externa of intussusceptum (*arrowheads*). Patient underwent reoperation on the day of the scan. Although an intussusception was not demonstrated at surgery, ischemic changes were seen in the neoterminal ileum. (*From* Warshauer DM, Lee JKTL. Adult intussusception detected at CT or MR imaging: clinical imaging correlation. Radiology 1999;212:853–60; with permission.)

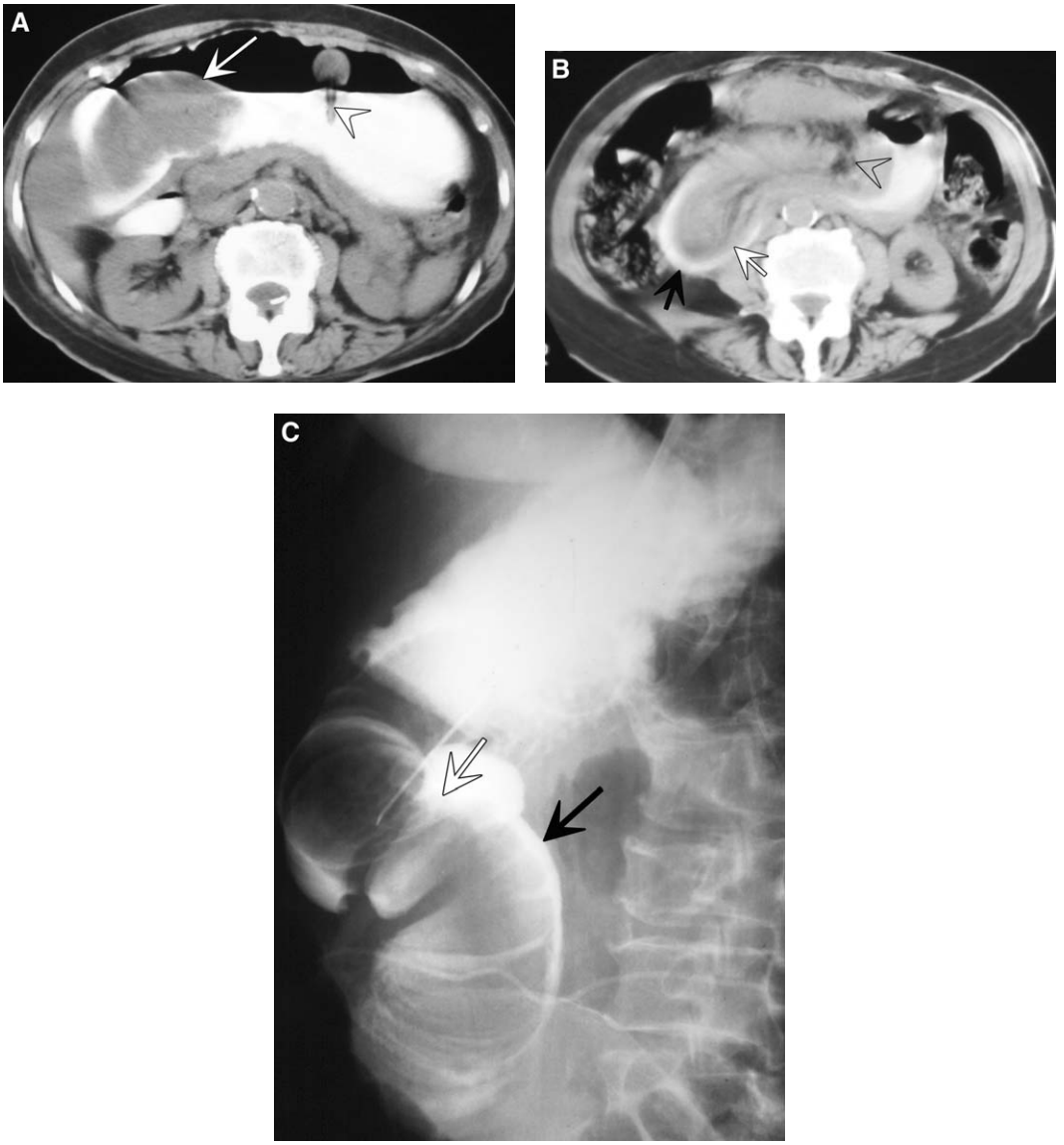

Fig. 6. Retrograde jejunogastric intussusception. Axial CT scans in a 78-year-old nursing home patient. (*A*) Stomach with gastrostomy tube (*arrowhead*) and intussusceptum (*arrow*). (*B*) Duodenum (*black arrow*) containing intussuscepting jejunum (*white arrow*) with fat being pulled in with bowel (*arrowhead*). Image from an upper gastrointestinal exam. (*C*) Intussusceptum (*white arrow*) extending retrograde through duodenum (*black arrow*) and into stomach. Intussusception was presumably related to the gastrostomy tube, which had gotten pulled into the proximal small bowel and was abruptly retracted without balloon deflation. (Courtesy of Scott N. Nadell, MD, Brewster, NY.)

developing world, adult intussusception has been reported with a somewhat higher frequency and with a lower prevalence of malignant causation. The increased prevalence of nonneoplastic adult intussusceptions in these areas is believed to be caused primarily by endemic levels of diarrheal diseases, which may cause disordered peristalsis and predispose to intussusception [24,32–35]. In one study from Papua, New Guinea, two thirds of adult intussusceptions had no associated pathology [34].

A recent series using CT or MR imaging diagnosis of intussusception rather than the surgical diagnosis

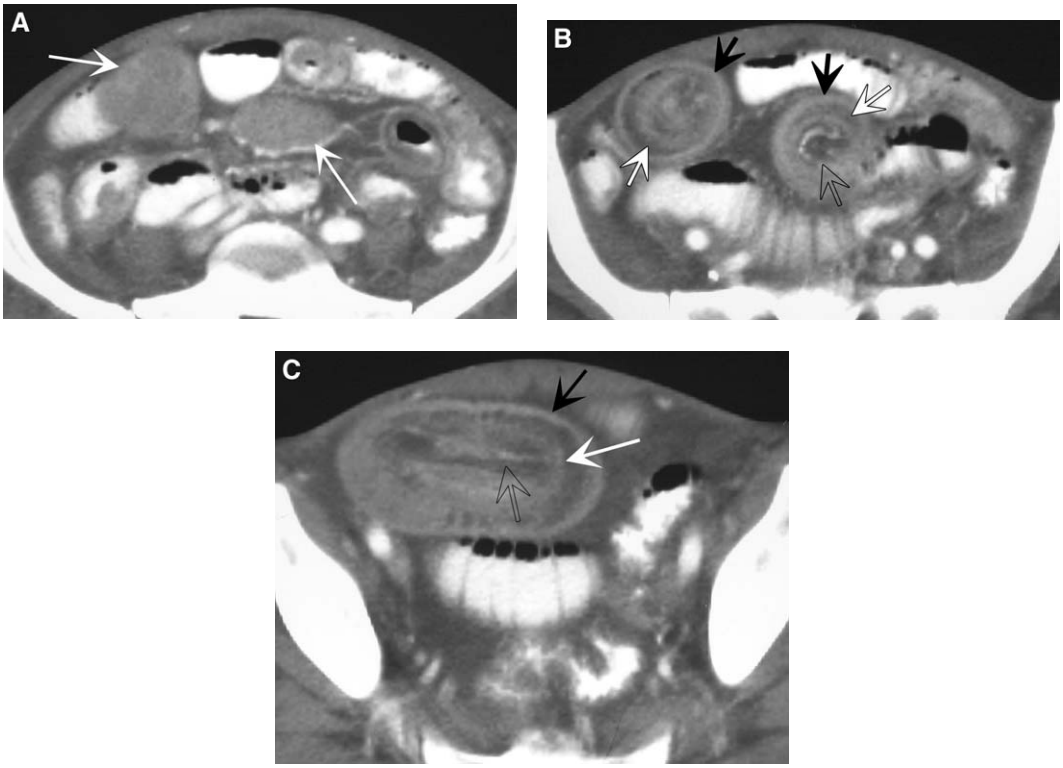

Fig. 7. Enteroenteric intussusception caused by immunoblastic lymphoma. Axial CT scans in a 44-year-old man with AIDS. (*A*) Mesenteric and bowel-associated masses (*arrows*). (*B, C*) Enteroenteric intussusception forming a loop within the pelvis. Intussuscipiens (*black arrows*) and intussusceptum (*white arrows*) are shown. Also shown are mesenteric vessels within intussusceptum (*open arrow*). (*From* Warshauer DM, Lee JKTL. Adult intussusception detected at CT or MR imaging: clinical imaging correlation. Radiology 1999;212:853–60; with permission.)

found an increased rate of idiopathic transient small bowel intussusception approaching 50% [15]. Despite further radiologic investigation and clinical follow-up, no other diagnoses were made in these patients. Furthermore, recurrent abdominal pain was noted in only one patient with transient intussusception, and this patient was thought to have irritable bowel syndrome. The authors concluded that many of these idiopathic enteric intussusceptions were probably caused by transient peristaltic dysfunction and would not have been discovered except for the widespread use of CT (Figs. 9, 10). They suggest that, unlike fixed lesions described in surgical series, these transient intussusceptions do not necessarily require aggressive work-up [15]. A smaller series of five cases of transient intussusception discovered at CT also supports this conclusion [36].

It is important to remember, however, that transient intussusception can be associated with significant disease that should be considered before the imaging finding is dismissed. In one report, at least 20% of patients with known or suspected celiac disease demonstrated evidence for transient intussusception on small bowel follow through (Fig. 11) [37]. Similarly, Crohn's disease has also been associated with transient intussusception [38].

Clinical findings

Adult intussusceptions occur over a wide range of ages extending from the second to the ninth decade of life. The mean age in most series is around 50. There is not a strong sex predilection, with most studies showing a nearly equal male-to-female ratio or a slight male predominance [2,5,12–14,19,21,24,39].

Unlike childhood intussusception, which most commonly presents acutely with episodic, crampy abdominal pain and bloody, currant-jelly stools, adult intussusception often presents with nonspecific

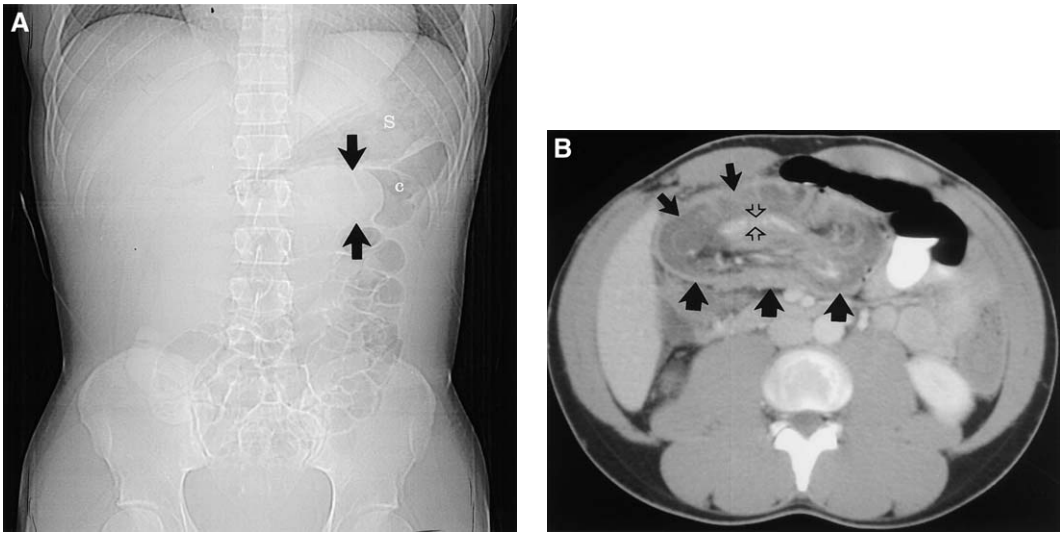

Fig. 8. Ileocolic intussusception caused by *Campylobacter* ileocolitis in a 33-year-old man with AIDS. (*A*) Digital abdomen image demonstrates paucity of air in the upper right abdomen with the crescent configuration of the air column in the distal transverse colon (*arrows*). (*B*) Longitudinal axial section of the transverse colon demonstrates the dilated colon (intussuscipiens, *large arrow*) containing the intussuscepted small bowel (intussusceptum, *open arrows*) and the fat-containing mesentery. At surgery and pathologic examination of the resected bowel, there was evidence of mucosal inflammation but no leading mass.

chronic or subacute symptoms, which may be related to intermittent partial bowel obstruction caused by the intussusception [39]. In several recent reports, only a minority of patients had an acute presentation with over half of patients having symptoms for greater than 1 month [2,21,24]. In one series the mean duration of symptoms was noted to be longer in patients with benign lesions and those with enteric intussusceptions than in those with malignant or colonic intussusceptions [19].

Presenting symptoms are highly variable. The most common presenting symptoms are crampy abdominal pain, which is noted in 75% to 85% of patients, and nausea and vomiting, which occur slightly less frequently. These symptoms reflect the obstructive nature of most intussusceptions. Other less common symptoms include diarrhea and constipation. Bleeding and palpable abdominal mass are observed in only a minority of patients [4,5,13,19,21,22].

Some patients may be completely asymptomatic [14,36]. This is particularly true in the case of celiac disease–associated intussusceptions. In these cases, bowel is believed to be so flaccid that there is insufficient muscular integrity to cause cramping [40].

Some investigators have attempted to stratify symptoms based on etiology and location of intussusception. In one surgical series of 58 adults, it was noted that patients with benign enteric intussusception complained of abdominal pain, nausea, and vomiting most frequently. Patients with malignant colonic intussusceptions were more likely to have melena or guaiac-positive stools [19]. Other series have similarly found nausea and emesis to be more common in small bowel intussusceptions [5,13,21]. Another series of 33 adults with intussusception diagnosed by CT or MR imaging found that patients with intussusceptions caused by neoplasm tended to be older (median age 47.5 years versus 39 years) and to have a significantly lower hematocrit (27.6 versus 39) than those with nonneoplastic intussusceptions [15].

Diagnosis

The clinical diagnosis of adult intussusception remains a challenge, caused in large part by its relative infrequency and by the often vague clinical findings at presentation. In several surgical series, a correct preoperative diagnosis was noted to have been made in only 32% to 50% of cases [12,14,19]. Patients with malignant colonic lesions were more likely to be diagnosed correctly than those with benign enteric lesions (67% versus 22%) [19].

Although the abdominal plain film and barium studies have been used for decades in the diagnosis of intussusception, newer imaging modalities, such as

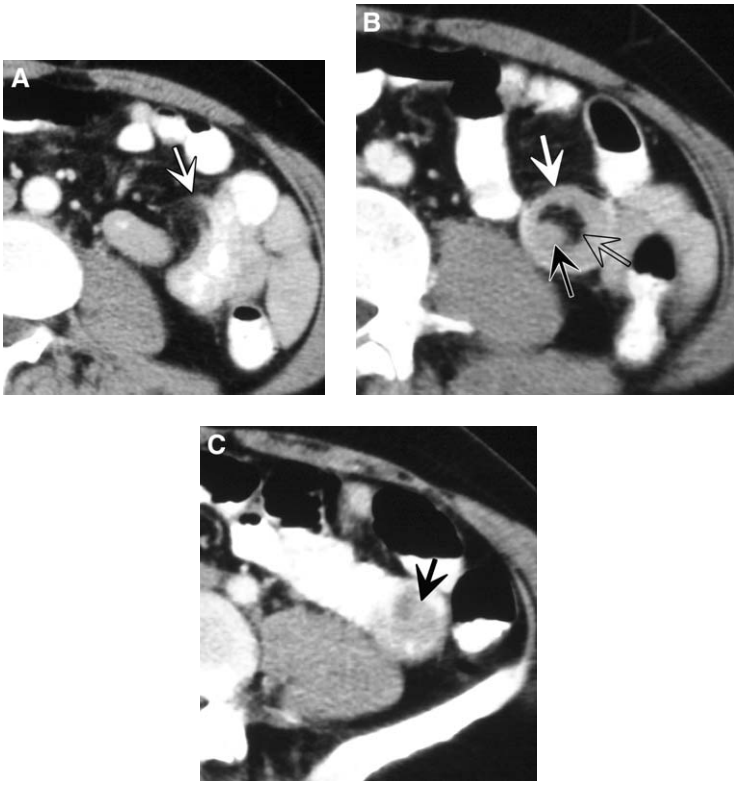

Fig. 9. Idiopathic transient enteroenteric intussusception in an asymptomatic 47-year-old man. Axial CT scans. (*A*) Vessels entering intussusception (*arrow*). (*B*) Fat (*open arrow*) pulled into the intussusception (*white arrow*) adjacent to a portion of the intussusceptum (*black arrow*). (*C*) Image is the last cut on which the intussusceptum is visible (*arrow*) and was obtained 4 cm below Fig. 9B. Results of a small bowel follow through performed 4 days later were unremarkable. Repeat CT 8 months later showed no evidence of bowel lesion or intussusception. (*From* Warshauer DM, Lee JKTL. Adult intussusception detected at CT or MR imaging: clinical imaging correlation. Radiology 1999;212:853–60; with permission.)

ultrasound, CT, and MR imaging, have greatly improved the ability to make a firm diagnosis.

Plain film and barium studies

A plain radiograph of the abdomen is frequently the first imaging study obtained in patients with intussusception. The plain film signs of intussusception, predominantly described in children, lack both sensitivity and specificity [41,42]. In the pediatric population, the presence of a soft tissue mass with decreased colonic gas and a small bowel ileus is the most suggestive appearance. Its value in adults, in whom a palpable mass is uncommon, is unclear. An ‘‘air crescent’’ sign of intraluminal air trapped between the walls of the intussusceptum and the intussuscipiens has also been described (see Fig. 8), but is neither sensitive nor specific. Plain radiography may be useful in assessing and following the degree of bowel obstruction, if present, and in detecting signs of bowel compromise, such as pneumoperitoneum or pneumatosis.

The characteristic finding of intussusception on barium studies is the ‘‘coiled spring’’ appearance with a thin central barium stream with or without a leading mass (Fig. 12). This finding is produced by contrast within the compressed lumen of the intussusceptum (the thin longitudinal central barium stream) and within the narrow intraluminal space between the intussusceptum and intussuscipiens (the coiled spring). A ‘‘stretched spring’’ appearance in which the concentric barium rings are forced apart by increasing edema in the bowel wall and mucosal folds has been suggested as a sign of vascular compromise. All of these signs may be obliterated if there is sufficient bowel edema to prevent influx of contrast into either space. In this eventuality, the intussusception may simply appear as an obstructing intraluminal mass [43].

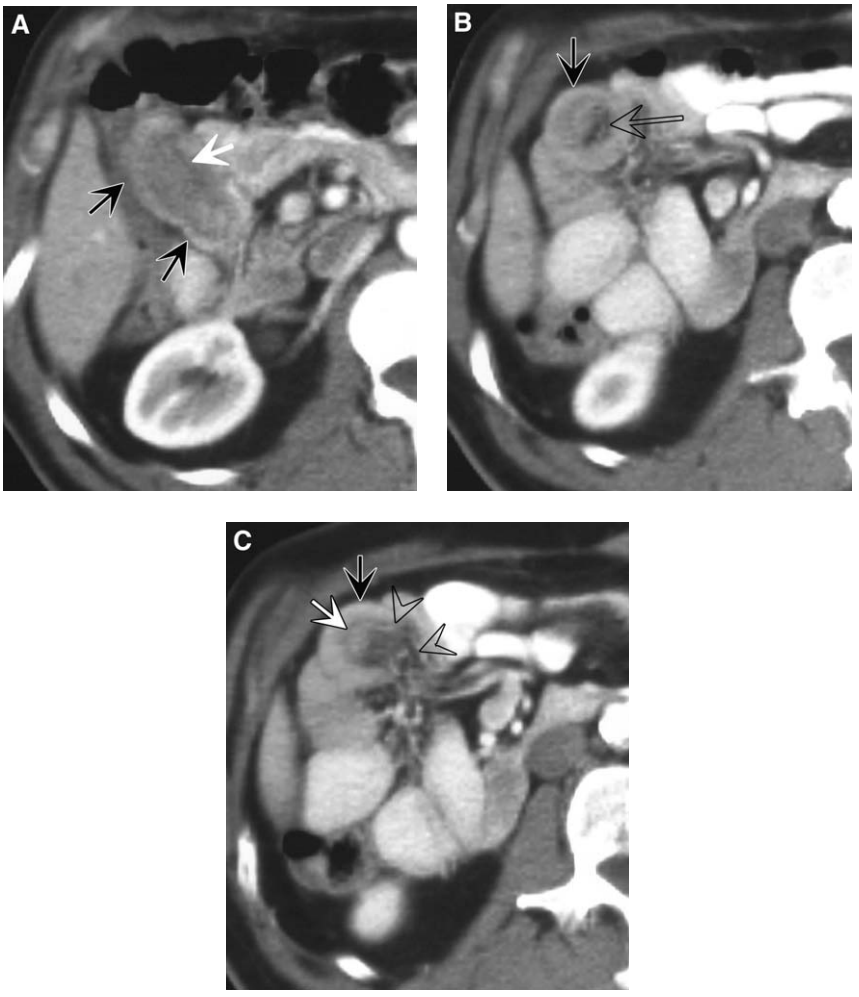

Fig. 10. Idiopathic transient enteroenteric intussusception in a 61-year-old man with back pain. Axial CT scans. (*A*) Intussuscipiens (*black arrows*) containing intussusceptum (*white arrow*) in longitudinal section. (*B*) Intussusception in transverse section with intussuscipiens (*black arrow*) and small amount of mesenteric fat within intussusceptum (*open arrow*). (*C*) Mesenteric vessels and fat entering intussusception (*arrowheads*), and hypodense line thought to correspond to muscularis externa of intussusceptum (*white arrow*). Outer wall of intussuscipiens (*black arrow*). Small bowel follow through 2 days later showed no definite mass or intussusception. Repeat CT 1 month later also showed no small bowel mass or intussusception. Patient has been asymptomatic on subsequent clinical follow-up. (*From* Warshauer DM, Lee JKTL. Adult intussusception detected at CT or MR imaging: clinical imaging correlation. Radiology 1999;212:853–60; with permission.)

Ultrasound

Ultrasound has been used with a moderate degree of success in the diagnosis of childhood intussusceptions, but its role in the diagnosis of adult intussusception is less clear. Several small series and case reports have documented the use of ultrasound to diagnose adult intussusception [44–48]. In many of these cases, ultrasound was performed in the setting of a palpable abdominal mass to which the examination could be targeted [44,46–48].

The ultrasound appearances of intussusception in adults are similar to those reported in the pediatric population. When the ultrasound transducer is oriented transversely relative to an intussusception, the classic appearance is that of a target or doughnut mass with an outer hypoechoic rim (representing the edematous bowel wall of the intussuscipiens) and a central area of increased echogenicity (representing intussusceptum and its invaginated mesenteric fat). In some cases, there may be a central hypoechoic ring representing the wall of the intussusceptum. In the

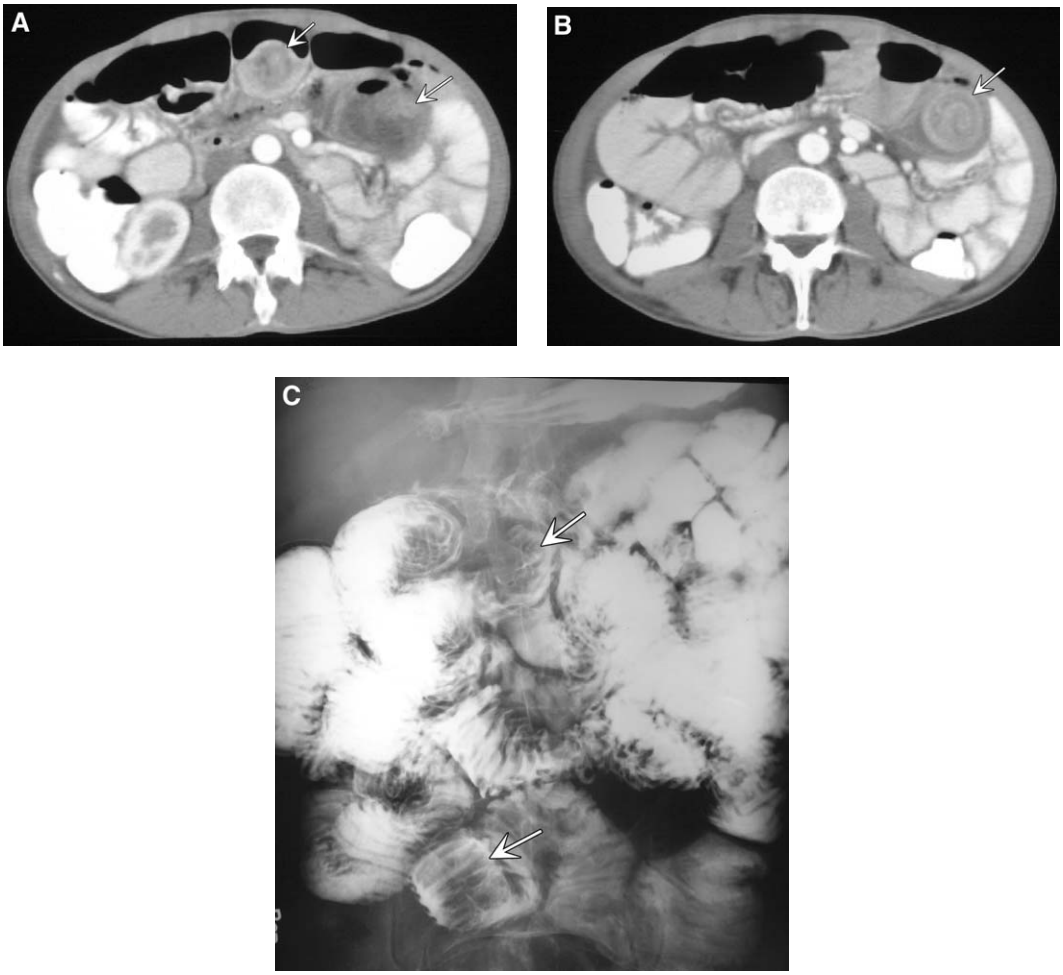

Fig. 11. Multiple asymptomatic enteric intussusceptions in a 43-year-old man with celiac sprue. Axial CT scans. (*A, B*) Mild small bowel dilation with several enteric intussusceptions (*arrows*). (*C*) Small bowel follow through also shows several enteric intussusceptions (*arrows*) along with loss of the normal jejunal fold pattern. Although the patient had significant weight loss and diarrhea, abdominal pain was not noted.

longitudinal plain, the intussusception demonstrates a layering appearance with alternating hypoechoic and hyperechoic layers representing layers of bowel wall and mesentery (Fig. 13) [44]. The appearance has been likened to a hayfork or trident, with the three hypoechoic limbs of the trident made up of the central intussusceptum and the outer walls of the intussuscipiens [49]. When an intussusception is visualized obliquely, the sonographic appearance has been termed the ''pseudokidney'' sign. The edematous bowel wall mimics hypoechoic renal cortex, and the hyperechoic intussusceptum mimics renal sinus fat [44,50]. Although highly suggestive of intussusception, these sonographic appearances are not pathognomonic and may also be seen with other causes of bowel wall edema, including enterocolitis and volvulus [50].

Free peritoneal fluid may be detected on ultrasound, but does not necessarily indicate peritonitis or bowel compromise. Color Doppler may be helpful in determining the degree of vascular compromise of the involved bowel segments. In two small pediatric series, failure to demonstrate blood flow to bowel wall with color Doppler predicted bowel necrosis necessitating surgical resection [51,52]. Although these data are drawn from the pediatric literature, similar concepts likely apply to adults.

Advantages of sonography include its speed, relative lack of expense, and the avoidance of ionizing radiation. Additionally, ultrasound has the advan-

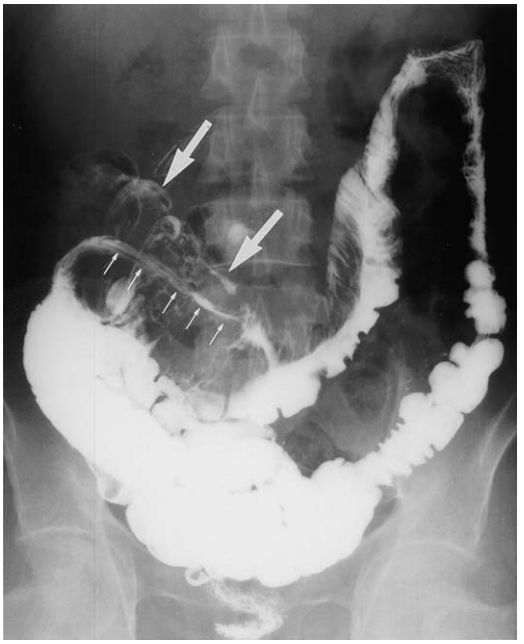

Fig. 12. Ileocolic intussusception caused by carcinoma of the cecum in a 50-year-old man. Antegrade barium examination (small bowel follow through) demonstrates the coilspring appearance of the transverse colon (intussuscipiens, *large arrows*) and the central barium steam.

tage of being able to demonstrate intussusceptions in real time. Disadvantages of ultrasound include operator variability, obscuration by overlying bowel gas, and difficulty imaging patients with an obese body habitus. Although diagnosis of intussusception can be made sonographically, the underlying cause is seldom identified, and pathologic diagnosis is often required to exclude a malignant lead point.

CT

In recent years, CT has become the first imaging study performed, after plain abdominal radiographs, in the evaluation of patients with nonspecific abdominal complaints. It is the modality by which intussusceptions may be first detected. The CT findings of intussusception are virtually pathognomonic [15,53–56]. The intussusception appears as a mass lesion, representing a thickened segment of bowel, which corresponds to the intussusceptum and intussuscipiens and which contains a relatively central area of fat (the intussuscepted mesentery), which may show enhancing vessels (see Figs. 4, 8). If the bowel is oriented transversely to the CT section, the mass is rounded, and the contained fat is crescentic in shape and located centrally or eccentrically, with punctate enhancing structures corresponding to drawn-in mesenteric vessels (see Figs. 2–4). A layered or stratified structure to the mass is frequently seen, giving the appearance of a target. Such stratification may be secondary to fluid trapped between the intussusceptum and intussuscipiens or to edema in the wall of the intussuscipiens.

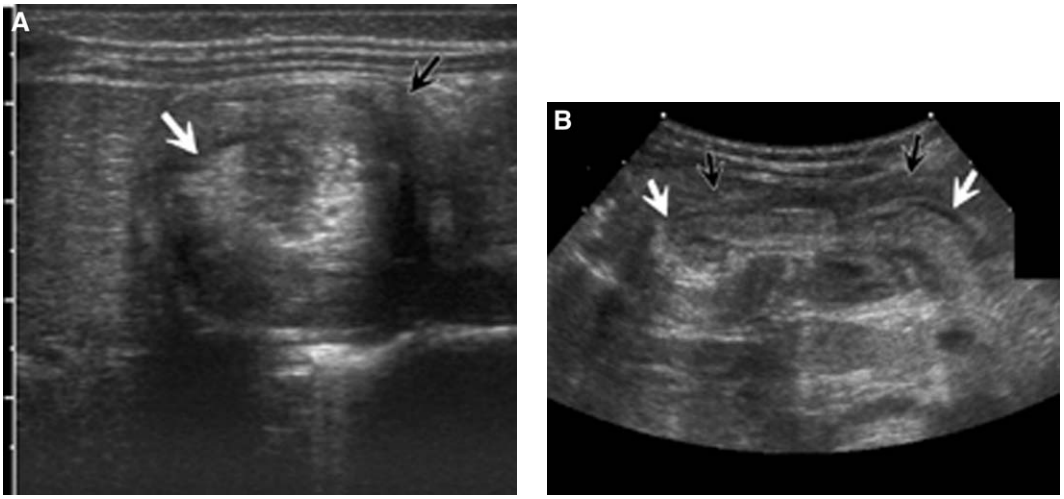

Fig. 13. Ileocecal intussusception. Ultrasound images in a 2-month-old boy. Intussuscipiens (*black arrows*) and intussusceptum (*white arrows*) are shown. (*A*) Target-like appearance of the intussusception on transverse section. (*B*) On longitudinal section the intussusception takes on a layered appearance.

If sectioned longitudinally, the mass and contained fat are more elongated, with the contained vessels appearing more linear in configuration. If sequential images are examined, one may note the continuity with proximal and distal bowel and can often identify a whirling pattern to the mesenteric vessels as they are drawn into the intussusceptum. Varying degrees of proximal bowel dilatation also may be evident, although complete obstruction is rare [53]. Additional findings may include a rim of contrast material sandwiched between the opposing walls of the intussusceptum and intussuscipiens on scans using oral contrast. This finding is analogous to the coiled spring appearance seen on barium studies [53]. Similarly, air bubbles may be seen between the opposed layers of bowel, usually in a nondependent location, which may help to differentiate trapped intraluminal gas from intramural gas.

The CT appearance of intussusceptions depends both on the relationship of the bowel to the CT slice and to the chronicity of the process and degree of vascular compromise. In one experimental study performed in dogs, intussusceptions were produced surgically and were followed with serial CT for up to 30 hours [55]. Four stages were described, each corresponding to a specific point in time following surgery. At stage one (3 hours), the typical target mass was seen with surrounding fascial planes maintained. At stage two (6 to 12 hours), a characteristic mass with alternating bandlike areas of high and low attenuation (the so-called "layered appearance") was seen with a moderate amount of bowel wall thickening and increased intraluminal fluid. At stage three (18 hours), there was severe bowel wall thickening with obscuration of the usual layered appearance caused by bowel and mesenteric edema. At stage four (30 hours), there was severe obstruction, bowel wall thickening, loss of normal bowel wall layers, and obscuration of surrounding fat planes. Stage four was associated with perforation and local peritonitis in two of the dogs. Progression from stage one to stage four reflected increasing degrees of mesenteric strangulation and progressive ischemia.

A recent study in 25 adult patients found three unenhanced CT findings to be related to the degree of vascular compromise in the intussusception: (1) a hypodense layer in the returning wall of the intussusceptum; (2) a fluid collection in the space enclosed by the entering and returning walls of the intussusceptum (bounded by serosa); and (3) a gas collection in the space enclosed by the entering and returning walls of the intussusceptum [57]. The absence of all three findings correlated with minimal vascular compromise and was termed "CT stage 1." The presence of the hypodense layer alone correlated with edema but was usually not severe enough to warrant resection at operation (stage 2), whereas the presence of the hypodense layer plus a fluid collection correlated with sufficient ischemic change to warrant resection (stage 3). The presence of all three of these findings was highly correlated with the presence of bowel necrosis or gangrene (stage 4).

Although the identification of intussusception can be made confidently on CT, the underlying etiology can be difficult to determine [53,56]. With CT alone it is difficult to separate out a neoplastic mass from the mass of the intussuscipiens itself. In a study of 16 patients with intussusception, CT was able correctly to identify the causative pathology in only the two cases where a lipoma acted as a lead point [53]. In these and similar cases, the lipoma can be identified as a fat density mass at the head of the intussuscipiens that does not contain mesenteric vessels (see Fig. 3) [53, 58,59]. Even lipomas, however, can be difficult to diagnose, because infarction and necrosis of the lipoma may result in loss of their typical fat density [58].

Certain CT findings of intussusception may favor a neoplastic process over a nonneoplastic one. In a study of 33 patients with CT-diagnosed intussusception, neoplastic intussusceptions were noted to be significantly longer (average 10.8 versus 4 cm in the nonneoplastic group), larger in diameter (average 4 versus 3 cm), and more likely to be associated with obstruction (present in 50% of cases versus 4.3%) than intussusceptions secondary to nonneoplastic causes. It is of note that all four of the intussusceptions involving the colon in this series were neoplastic in etiology [15].

CT may also provide indirect evidence of a malignant cause of intussusception if there is lymphadenopathy or evidence of metastatic disease to other organs; however, these findings cannot be taken as proof of a malignant lead point. Published reports have described intussusceptions caused by benign etiologies in patients with known malignancies [53,60]. Ultimately, pathologic diagnosis is necessary to determine the actual cause of intussusception in most cases, although in cases of short, transient enteric intussusceptions diagnosed by CT, further evaluation may not be necessary.

MR imaging

Although few reports have described the MR imaging findings of adult intussusception, the general imaging characteristics of intussusception on MR imaging are similar to those on CT [15,61]. In a report of three cases shown on MR imaging, the

intussusceptions were best demonstrated on T2-weighted HASTE sequences, because high signal intestinal fluid contrasted well with the relatively low signal intensity bowel wall of the intussusceptum and intussuscipiens. In one patient, increased T1 and T2 signal intensity was noted in the bowel wall of the intussuscipiens before contrast administration, presumably reflecting the presence of extracellular methemoglobin from mural hemorrhage or necrosis. In this patient, diminished enhancement of bowel wall on postgadolinium T1-weighted images also was noted correlating with necrosis seen at surgery [61].

Treatment

Unlike its childhood counterpart, persistent symptomatic intussusception in adults is nearly always treated surgically, largely because of the high proportion of cases with structural causes and the relatively high incidence of malignancy, particularly in the colon. Attempts at preoperative hydrostatic reduction with barium or air should not be performed in the adult patient [5,21,39,62,63]. In theory, reduction of an intussusception at surgery before resection of the underlying pathologic lesion has the advantage of requiring a smaller resection. Opponents of such preresection reduction, however, point to the risk of potential intraluminal seeding or venous embolization of tumor during manipulation of malignant intussusceptions and to the risk of perforation and peritoneal soiling when there is bowel ischemia [14,21]. Most authors in the surgical literature recommend treating colonic intussusceptions with primary resection without prior reduction, especially if there is a known neoplasm or if the cause of the intussusception is not known [5,21,39].

Appropriate therapy for cases of enteroenteric intussusceptions is more controversial, because of the lower prevalence of malignancy in small bowel intussusceptions. Surgical resection or intervention is not warranted in cases of transient intussusception in the setting of a known benign cause, such as celiac sprue. In these cases, treatment of the underlying process should suffice [37]. A transient, short, nonobstructing intussusception detected incidentally by CT in a relatively asymptomatic patient also may not require any intervention [15]. Fixed or symptomatic intussusceptions of the small bowel, although more likely to be benign in etiology than colonic intussusceptions, may still be malignant in a significant proportion of cases, and in these cases, resection without reduction is generally recommended unless preservation of bowel length is needed [5].

Summary

Intussusception is relatively rare in the adult population and differs substantially from pediatric intussusception. Most adult intussusceptions identified at surgery are caused by a definable structural lesion, a substantial proportion of which are malignant, particularly in the colon. Small bowel intussusceptions, however, have a lower prevalence of malignancy. Diagnosis of adult intussusception can be made reliably with noninvasive imaging techniques. CT is now widely regarded as the modality of choice for diagnosing intussusception in adults, but ultrasound and MR imaging have also been used effectively. Determination of the presence of a malignant lead point remains problematic because an edematous or hemorrhagic intussuscipiens may mimic a mass on each modality. Markers for bowel viability have been described but are not precise. Treatment of the persistent symptomatic intussusception in which neoplasia is suspected is surgical, and preoperative reduction is contraindicated. Transient relatively asymptomatic enteric intussusceptions discovered by imaging may not require intervention.

References

[1] Coran AG. Intussusception in adults. Am J Surg 1969; 117:735–8.
[2] Agha FP. Intussusception in adults. AJR Am J Roentgenol 1986;146:527–31.
[3] Cotlar AM, Cohn Jr I. Intussusception in adults. Am J Surg 1961;101:114–20.
[4] Dean D, Ellis F, Sauer W. Intussusception in adults. Arch Surg 1956;73:6–11.
[5] Eisen L, Cunningham J, Aufses A. Intussusception in adults: institutional review. J Am Coll Surg 1999;188: 390–5.
[6] Reymond RD. The mechanism of intussusception: a theoretical analysis of the phenomenon. Br J Radiol 1972;45:1–7.
[7] Deterling Jr R, O'Malley R, Knox W. Intussusception in the adult, with emphasis on retrograde type. Arch Surg 1953;67:854–64.
[8] Waits JO, Beart Jr RW, Charboneau JW. Jejunogastric intussusception. Arch Surg 1980;115:1449–52.
[9] Billimoria PE, Fabian TM, Schulz EE. Computed tomography of intussusception in the bypassed jejunoileal segment. J Comput Assist Tomogr 1982;6:86–8.
[10] Lo G, Fisch AE, Brodey PA. CT of the intussuscepted excluded loop after intestinal bypass. AJR Am J Roentgenol 1981;137:157–8.
[11] Brayton D, Norris WJ. Intussusception in adults. Am J Surg 1954;88:32–43.
[12] Begos DG, Sandor A, Modlin IM. The diagnosis and

management of adult intussusception. Am J Surg 1997; 173:88–94.
[13] Hamaloglu E, Yavuz B. Intussusception in adults. Panminerva Med 1990;32:118–21.
[14] Reijnen HA, Joosten HJ, de Boer HH. Diagnosis and treatment of adult intussusception. Am J Surg 1989; 158:25–8.
[15] Warshauer DM, Lee JK. Adult intussusception detected at CT or MR imaging: clinical-imaging correlation. Radiology 1999;212:853–60.
[16] Courtney SP, Ibrahim N, Longstaff AJ, Davidson CM. Intussusception in the adult: clinical, radiological and histological features [see comments]. Postgrad Med J 1992;68:449–52.
[17] Hsu HY, Kao CL, Huang LM, et al. Viral etiology of intussusception in Taiwanese childhood. Pediatr Infect Dis J 1998;17:893–8.
[18] Nicolas JC, Ingrand D, Fortier B, Bricout F. A one-year virological survey of acute intussusception in childhood. J Med Virol 1982;9:267–71.
[19] Azar T, Berger DL. Adult intussusception. Ann Surg 1997;226:134–8.
[20] Donhauser JL, Kelly EC. Intussusception in the adult. Am J Surg 1950;79:673–7.
[21] Nagorney DM, Sarr MG, McIlrath DC. Surgical management of intussusception in the adult. Ann Surg 1981; 193:230–6.
[22] Felix EL, Cohen MH, Bernstein AD, Schwartz JH. Adult intussusception; case report of recurrent intussusception and review of the literature. Am J Surg 1976; 131:758–61.
[23] Carter CR, Morton AL. Adult intussusception in Glasgow, UK. Br J Surg 1989;76:727.
[24] Coleman MJ, Hugh TB, May RE, Jensen MJ. Intussusception in the adult. Aust N Z J Surg 1981;51:179–80.
[25] Lin F, Setya V, Signor W. Gastroduodenal intussusception secondary to a gastric lipoma: a case report and review of the literature. Am Surg 1992;58:772–4.
[26] Meyers MA. Gastroduodenal intussusception. Am J Med Sci 1967;254:347–56.
[27] Cappell MS, Hassan T, Rosenthal S, Mascarenhas M. Gastrointestinal obstruction due to *Mycobacterium avium intracellulare* associated with the acquired immunodeficiency syndrome. Am J Gastroenterol 1992; 87:1823–7.
[28] Danin JC, McCarty M, Coker R. Case report: lymphoma causing small bowel intussusception in a patient with the acquired immune deficiency syndrome. Clin Radiol 1992;46:350–1.
[29] Meyerson S, Desai TK, Polidori G, Raval MF, Ehrinpreis MN. A case of intussusception and lymphoid hyperplasia in a patient with AIDS [see comments]. Am J Gastroenterol 1993;88:303–6.
[30] Visvanathan R, Nichols TT, Reznek RH. Acquired immune deficiency syndrome-related intussusception in adults. Br J Surg 1997;84:1539–40.
[31] Wood BJ, Kumar PN, Cooper C, Silverman PM, Zeman RK. AIDS-associated intussusception in young adults. J Clin Gastroenterol 1995;21:158–62.
[32] Ademiluyi SA. Intussusception in Nigerian adults. J Natl Med Assoc 1987;79:873–6.
[33] Atri SC, Singh AK, Naithani YP. Adult intussusception in Allahabad. J Indian Med Assoc 1983;81:155–8.
[34] Hadley GP, Simpson RL. Adult intussusception in the tropics. Br J Surg 1983;70:281.
[35] Otu AA. Tropical surgical abdominal emergencies: acute intestinal obstruction. Afr J Med Med Sci 1991; 20:83–8.
[36] Catalano O. Transient small bowel intussusception: CT findings in adults. Br J Radiol 1997;70:805–8.
[37] Cohen MD, Lintott DJ. Transient small bowel intussusception in adult coeliac disease. Clin Radiol 1978; 29:529–34.
[38] Knowles MC, Fishman EK, Kuhlman JE, Bayless TM. Transient intussusception in Crohn's disease: CT evaluation. Radiology 1989;170:814.
[39] Weilbaecher D, Bolin JA, Hearn D, Ogden WD. Intussusception in adults: review of 160 cases. Am J Surg 1971;121:531–5.
[40] Strobl PW, Warshauer DM. CT diagnosis of celiac disease. J Comput Assist Tomogr 1995;19:319–20.
[41] Levine M, Schwartz S, Katz I, Burko H, Rabinowitz J. Plain film findings in intussusception. Br J Radiol 1964; 37:678–81.
[42] White SJ, Blane CE. Intussusception: additional observations on the plain radiograph. AJR Am J Roentgenol 1982;139:511–3.
[43] Gourtsoyiannis NC, Papakonstantinou O, Bays D, Malamas M. Adult enteric intussusception: additional observations on enteroclysis. Abdom Imaging 1994;19: 11–7.
[44] Boyle MJ, Arkell LJ, Williams JT. Ultrasonic diagnosis of adult intussusception [letter; see comments]. Am J Gastroenterol 1993;88:617–8.
[45] Cerro P, Macrini L, De Angelis O. Sonographic diagnosis of intussusceptions in adults. Abdom Imaging 2000;25:45–7.
[46] Sato M, Ishida H, Konno K, et al. Long-standing painless intussusception in adults. Eur Radiol 2000;10: 811–3.
[47] Sofia S, Casali A, Bolondi L. Sonographic diagnosis of adult intussusception. Abdom Imaging 2001;26: 483–6.
[48] Weissberg DL, Scheible W, Leopold GR. Ultrasonographic appearance of adult intussusception. Radiology 1977;124:791–2.
[49] Alessi V, Salerno G. The "hay-fork" sign in the ultrasonographic diagnosis of intussusception. Gastrointest Radiol 1985;10:177–9.
[50] Anderson D. The pseudokidney sign. Radiology 1999; 211:395–7.
[51] Lagalla R, Caruso G, Novara V, Derchi LE, Cardinale AE. Color Doppler ultrasonography in pediatric intussusception. J Ultrasound Med 1994;13:171–4.
[52] Lam AH, Firman K. Value of sonography including color Doppler in the diagnosis and management of long standing intussusception. Pediatr Radiol 1992; 22:112–4.

[53] Gayer G, Apter S, Hofmann C, et al. Intussusception in adults: CT diagnosis. Clin Radiol 1998;53:53–7.
[54] Gayer G, Zissin R, Apter S, Papa M, Hertz M. Pictorial review: adult intussusception–a CT diagnosis. Br J Radiol 2002;75:185–90.
[55] Iko BO, Teal JS, Siram SM, Chinwuba CE, Roux VJ, Scott VF. Computed tomography of adult colonic intussusception: clinical and experimental studies. AJR Am J Roentgenol 1984;143:769–72.
[56] Merine D, Fishman EK, Jones B, Siegelman SS. Enteroenteric intussusception: CT findings in nine patients. AJR Am J Roentgenol 1987;148:1129–32.
[57] Fujimoto T, Fukuda T, Uetani M, et al. Unenhanced CT findings of vascular compromise in association with intussusceptions in adults. AJR Am J Roentgenol 2001;176:1167–71.
[58] Buetow PC, Buck JL, Carr NJ, Pantongrag-Brown L, Ros PR, Cruess DF. Intussuscepted colonic lipomas: loss of fat attenuation on CT with pathologic correlation in 10 cases. Abdom Imaging 1996;21:153–6.
[59] Donovan AT, Goldman SM. Computed tomography of ileocecal intussusception: mechanism and appearance. J Comput Assist Tomogr 1982;6:630–2.
[60] Lorigan JG, DuBrow RA. The computed tomographic appearances and clinical significance of intussusception in adults with malignant neoplasms. Br J Radiol 1990;63:257–62.
[61] Marcos HB, Semelka RC, Worawattanakul S. Adult intussusception: demonstration by current MR techniques. Magn Reson Imaging 1997;15:1095–8.
[62] Sebbag H, Brunaud L, Marchal F, Collinet-Adler S, Grosdidier G. Intestinal intussusception in adults, treat it like a cancer. Oncol Rep 2000;7:1359–61.
[63] Stubenbord W, Thorbjarnarson B. Intussusception in adults. Ann Surg 1970;172:306–10.

RADIOLOGIC
CLINICS OF
NORTH AMERICA

Radiol Clin N Am 41 (2003) 1153–1169

CT of acute abdominal aortic disorders

Sanjeev Bhalla, MD*, Christine O. Menias, MD, Jay P. Heiken, MD

Mallinckrodt Institute of Radiology, Washington University School of Medicine, 510 South Kingshighway, St. Louis, MO 63110, USA

Abdominal aortic abnormalities may present acutely with pain and signs of hemorrhage including hypotension, tachycardia, cold extremities, hematemesis, hematochezia, or melena. Initial presentation can vary from mild discomfort to hypotensive shock. Understanding the scope of acute abdominal aortic pathology helps to expedite the rapid imaging evaluation and diagnosis of these frequently life-threatening conditions.

The term ''acute abdominal aortic disorder'' includes aneurysm rupture, dissection, acute occlusion, traumatic injury, and postoperative complications. Because of overlap of presentation with other causes of abdominal pain in the emergency setting, the ideal imaging evaluation should be one that is rapid but comprehensive enough to diagnose other acute abdominal conditions. Because many emergency departments have a helical CT scanner within the department or close by, CT has emerged as the primary imaging test for acute aortic conditions. This imaging dominance is bolstered by the rapid image acquisition time (less than 1 minute) and the comprehensive nature of an abdominal CT, which may result in diagnosis of other frequent mimics of acute abdominal aortic disorders, including intestinal ischemia, appendicitis, diverticulitis, and urinary tract stones [1,2].

Although ultrasound may have a limited role in confirming the presence of an aortic aneurysm before surgery, the use of CT as the primary imaging test, especially if the CT scanner is located near the trauma or critical care unit, has resulted in decreased examination times. The added benefit of images readily understood by all members of the clinical team, including vascular surgeons, allows for rapid assessment of the most appropriate treatment, including endovascular repair. MR imaging also is extremely useful for imaging the abdominal aorta; however, in the acute situation it is much more limited than CT. The lack of 24-hour in-house MR imaging technologists combined with the added time of image acquisition and the distance of many emergency departments from an MR imaging machine limits its use for acute aortic emergencies. An additional limitation of MR imaging is the greater difficulty of monitoring acutely ill patients during the imaging examination. Angiography, which images only the vessel lumen, may underestimate aortic pathology (as in the case of dissection, or early aneurysm rupture) and is usually used as a secondary diagnostic tool to clarify a CT finding or plan endovascular therapy. Because CT is the dominant imaging method for diagnosing acute abdominal aortic conditions, this article focuses on CT techniques and manifestations of this group of acute abdominal disorders.

CT technique

The CT techniques recommended in this article include single-detector row helical CT, four-channel multidetector row CT (MDCT), and 16-channel MDCT protocols that are applicable to scanners of all vendors. Helical CT allows for large-volume acquisition during a single breathhold, thereby minimizing respiratory misregistration. Use of rapid table feed and narrow collimation (high pitch) provides excellent z-axis resolution that can be improved while maintaining temporal resolution.

The authors' single-detector CT angiography technique relies on a collimation of 3; a pitch of 2 (table

* Corresponding author.
E-mail address: bhallas@mir.wustl.edu (S. Bhalla).

0033-8389/03/$ – see front matter
doi:10.1016/S0033-8389(03)00136-2

feed 6 mm per gantry rotation); and a reconstruction interval of 2 mm. The ability to reconstruct images retrospectively with overlapping reconstruction intervals enhances multiplanar and three-dimensional reconstructions by helping to eliminate stairstep artifacts. Recent advances with MDCT, first 4 rows then 8 and 16 rows, have further improved spatial and temporal resolution by allowing acquisition of thinner images at faster speeds. Larger volumes can then be covered, using less intravenous contrast material [3–5]. On a 16-row MDCT, the abdominal aorta can be imaged in less than 9 seconds, with images reconstructed using 2-mm slice thickness and 1-mm reconstruction intervals.

The added benefit of MDCT is the ability to reconstruct thinner images retrospectively with overlapping reconstruction as long as the raw-helical data are still available. In the emergency setting this can be quite useful when the study reveals aortic pathology that had been previously unsuspected. With MDCT, however, images cannot be thinner than the detector collimation used to acquire the data. For this reason, the authors recommend that all emergent abdominal CTs be acquired with 4×2.5 mm detector configuration when four-row MDCT is used. The images initially can be reviewed as 5-mm-thick contiguous images. If aortic pathology is encountered or suspected, 3-mm-thick images can be reconstructed at 2-mm intervals. With 16-row MDCT, a 16×1.5 mm detector configuration is recommended, with initial review of 5-mm-thick contiguous images. If aortic pathology is encountered or suspected, 2-mm-thick images can be reconstructed at 1- or 1.5-mm intervals.

When aortic pathology is suspected, no oral contrast material is administered and the patients are brought to the CT scanner as soon as vital signs are stable enough for transport, primary survey has been completed, and intravenous access has been established. Not only does oral contrast material administration result in an unnecessary delay in imaging, but its presence may interfere with three-dimensional postprocessing.

A noncontrast study should always be obtained first, and in some cases may be all that is required. To minimize artifact, both precontrast and postcontrast images are performed with the patient's arms elevated above their head. Noncontrast images are used to identify high attenuation in the aortic wall (ie, intramural hematoma [IMH]), which in the setting of an aneurysm may indicate early or impending rupture [6]. Noncontrast images are also useful in the setting of a surgically repaired abdominal aorta in helping to define high-attenuating structures, such as calcium or metal that may be confused with enhancement on postcontrast images. When rupture is clearly evident on the noncontrast images, communication with the vascular surgeon should be immediate. In most cases, the study is terminated at that point; however, if endovascular therapy is planned, a decision to obtain postcontrast images can be made in conjunction with the vascular surgeon. If endovascular therapy is not planned, intravenous contrast material should not be administered, because it prolongs the imaging procedure and could cause renal damage if the patient becomes hypotensive. Postcontrast images do not provide the surgeon with additional useful information for open operative aneurysm repair. In either case, the patient should be transferred immediately after the study is completed to the emergency room for close monitoring and preparation for surgery.

Some have advocated reducing the radiation dose on the noncontrast images by reducing milliamperes and increasing pitch and collimation (10 mm) [7]. Given that many of these patients are older and that if rupture is encountered, a noncontrast CT may be the sole study obtained, the authors do not routinely change the radiation dose or use thicker images for the noncontrast studies.

The authors routinely review all noncontrast images before administering intravenous contrast medium. They do this to determine whether to terminate the study (as in the case of rupture) and to determine the probability of aortic pathology as the cause of clinical presentation. If a nonaortic cause of abdominal pain is seen, the scan delay is set to coincide with the portal venous phase of enhancement. If the aorta is the likely cause (eg, presence of aneurysm, fat stranding near a graft), arterial-phase imaging is obtained. In this latter situation, the authors use automated bolus-timing software, because of the high incidence of cardiac disease in patients with aortic disease [4,8,9] and the variability of cardiac output and peak arterial enhancement. High injection rates of contrast material are used for suspected aortic pathology (4 to 5 mL/second) by a power injector through a 20-gauge intravenous catheter, usually in the antecubital fossa. A monophasic injection is used routinely, although a biphasic or multiphasic injection may allow for more uniform aortic enhancement [3,10,11]. The authors recommend the use of relatively high concentration (eg, 350 mg I/mL) low-osmolar intravenous contrast material because it is better tolerated than high-osmolar contrast material. Limiting side effects is critical for CT angiography in which patient motion can degrade the examination.

Once the study is completed, images are reviewed on a workstation in the reading room. This allows for

rewindowing of the postcontrast images, on which the vascular contrast is often too dense. The rewindowing is performed so that both the inner and the outer vessel wall can be seen. In this way, a subtle intimal flap can be detected. Use of a narrow window width to view the noncontrast images may allow detection of a subtle IMH or intimal flap. If further postprocessing is required, images are sent to a separate three-dimensional workstation where volume-rendered imaging, multiplanar, and curved planar reconstructions can be performed. These additional techniques are a convenient way of conveying the morphology of the aorta to the referring physicians, but in most cases are not required to diagnose acute aortic pathology.

Abdominal aortic aneurysm

An abdominal aortic aneurysm (AAA) is defined as a focal, irreversible dilation of the abdominal aorta greater than 3 cm [12]. It is relatively common and has been diagnosed with increasing frequency since the early 1950s as a function of both increasing life span and improved, more frequent imaging [13,14]. Ruptured AAAs represent the tenth leading cause of death in men over 55 years of age [15]. Most AAAs are believed to be atherosclerotic in origin. Risk factors include smoking, male gender, advanced age, hypertension, and family history [16]. Interestingly, diabetes is inversely related to the presence of an AAA and hypercholesterolemia as a single risk factor is not associated with increased incidence of an AAA [16]. Less common etiologies of aneurysms include infection; connective tissue disease (eg, Marfan syndrome); arteritis; and sequelae of other aortic pathology, most frequently dissection.

In the abdomen, aortic aneurysms tend to be infrarenal in location. This may be from transmitted pressures near the aortic bifurcation or differences in wall constitution (fewer vasa vasorum, fewer smooth muscle cells) in the infrarenal aorta [17,18]. Isolated suprarenal AAAs are uncommon. Instead, suprarenal aneurysms tend to be part of infrarenal or thoracic aneurysms [19].

Aneurysms less than 4 cm in diameter tend to grow more slowly (1 to 1.5 mm/year) and have a risk of rupture around 8%. Larger AAAs (greater than 4 cm) tend to grow more rapidly (3 mm/year) and have a greater than 25% chance of rupturing, the likelihood of rupture increasing with increasing aneurysm diameter [20,21]. Aortic aneurysm rupture can be catastrophic. Most published series report mortality rates of 70% to 94% for patients with AAA rupture, with more than half of patients dying before getting to the hospital [22–27]. Even among patients who survive long enough to undergo repair, mortality rates hover around 50% as compared with less than 4% for patients undergoing elective AAA repair [28]. Besides absolute size, other risk factors for rupture include increase in aneurysm size of over 18% per year [29], and increase in diameter of over 5 mm in a 6-month period [30].

Classically, patients with ruptured AAA present to the emergency department with abdominal pain, hypotension, and a pulsatile mass. This classical triad, however, is not always seen. As many as 30% of patients with ruptured AAA may be misdiagnosed if they present with only one of the three signs or symptoms [2]. When patients present to general practitioners or internists not familiar with vascular disease, correct diagnosis of rupture is made only 28% to 39% of the time [31,32]. Because the clinical presentation of ruptured AAA mimics other abdominal emergencies, most commonly urolithiasis [31], helical CT should be the first diagnostic test in the evaluation of a potentially ruptured AAA.

CT findings of a ruptured AAA include retroperitoneal hematoma, focal discontinuity in circumferential calcification (Fig. 1), high-attenuating peripheral crescent (Figs. 2, 3), indistinct aortic wall, and frank contrast medium extravasation [33–42]. Retroperitoneal hemorrhage may manifest as subtle stranding of the periaortic fat (Fig. 4) or may be seen as a high-attenuating collection extending into the retroperitoneum (Fig. 5). As with other causes of retroperitoneal hemorrhage, blood from rupture of an aneurysm may be isoattenuating with the psoas and iliacus muscles. The muscles may simply look enlarged or may be

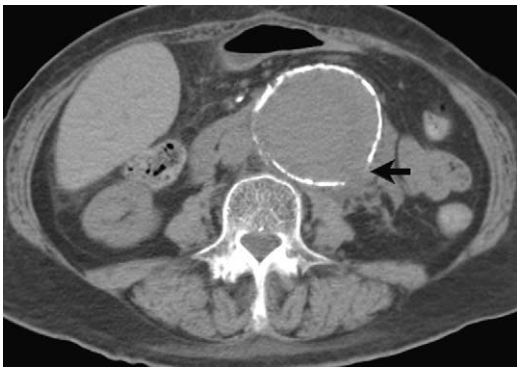

Fig. 1. Abdominal aortic aneurysm rupture. Non–contrast-enhanced CT image shows a heavily calcified abdominal aortic aneurysm. The focal area of discontinuity in the intimal calcification (*arrow*) corresponds to the site of aortic rupture. The stranding within the periaortic fat adjacent to this location indicates early leak.

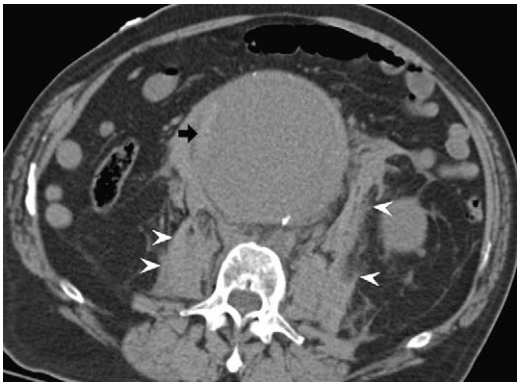

Fig. 2. High-attenuating crescent sign associated with abdominal aortic aneurysm rupture. Non–contrast-enhanced CT image demonstrates a high-attenuating crescent (*arrow*) within the anterior half of an abdominal aortic aneurysm. The high-attenuating crescent represents acute hematoma within the mural thrombus of the aneurysm. Note that the crescent is higher in attenuation than the blood within the aortic lumen, but not as dense as the wall calcification. This attenuation difference can be masked after administration of intravenous contrast medium. Periaortic hematoma (*arrowheads*) indicates that the aneurysm has ruptured.

difficult to distinguish from adjacent structures. Occasionally, the collection of blood is large enough to displace the kidneys anteriorly or laterally.

Calcification in an aneurysm may be within the wall of the vessel or within mural thrombus. Thrombus calcification is seen in 19% to 24% of AAAs and is not correlated with rupture [35,43]. Wall calcification, however, may be useful in predicting AAA rupture. Of the various patterns of aortic wall calcification, the only pattern that has been shown to have a significant association with AAA rupture is focal discontinuity of circumferential mural calcification (see Fig. 1). This pattern is uncommon and is seen in only 8% of ruptured AAAs [35].

Blood from an aortic rupture may extend into the peritoneum. Attenuation values greater than 30 HU can suggest acute hemoperitoneum, but a lower measurement does not exclude hemoperitoneum [44–46]. Other signs, such as a fluid-fluid level or hematocrit effect, may confirm the bloody nature of the fluid. Rarely, iodinated contrast material is seen actively extravasating from the abdominal aorta.

In the absence of frank aneurysm leak, the best sign of early or impending rupture is the high-attenuating peripheral crescent, which is believed to represent acute dissection of blood within the aneurysm wall or mural thrombus (Fig. 6) [6,47–49]. This finding is best appreciated on unenhanced images. A sign that may be seen with contained leak is the "draped aorta sign." This finding refers to the combination of an indistinct posterior aortic wall and the close proximity of the spine and the aortic wall, which follows the contour of the vertebral body on one or both sides [50].

Mycotic aneurysms

Named for their appearance (mushroom-like) and not their causative pathogens, mycotic aneurysms and pseudoaneurysms represent focal aortic dilation from infection and inflammation. The acute inflammatory process results in vessel-wall weakening, possibly from an effect on the vasa vasorum, resulting in necrosis and subsequent vessel enlargement. In the preantibiotic era, the most common cause of mycotic aneurysm was endocarditis from *Streptococcus pyogenes*. Now, *Salmonella* is the most frequently found bacteria species, with *Streptococcus* and *Staphylococcus* less commonly encountered [51–53]. The dominance of *Salmonella* likely relates to the predilection of this organism for diseased tissues, especially atherosclerotic vascular endothelium [54]. Bacterial spread to the aorta may be from direct extension of an adjacent infection (lumbar osteomyelitis, psoas abscess, renal infection) or hematogenous spread of a distant process (gastroenteritis, pneumonia). Iatrogenic or traumatic intimal injury may predispose a particular site to the development of a mycotic aneurysm as can an underlying atherosclerotic plaque.

Mycotic aneurysms are much less frequently encountered than their atherosclerotic counterparts, but

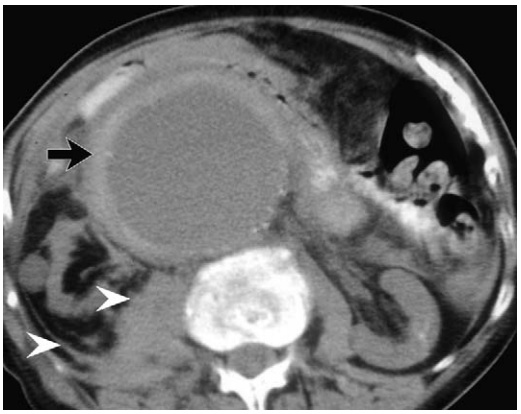

Fig. 3. High-attenuating crescent sign associated with abdominal aortic aneurysm rupture. Non–contrast-enhanced CT image shows a large abdominal aortic aneurysm with a high-attenuating crescent within the thickened aneurysm wall (*arrow*). Retroperitoneal blood (*arrowheads*) adjacent to the right psoas muscle indicates aneurysm rupture.

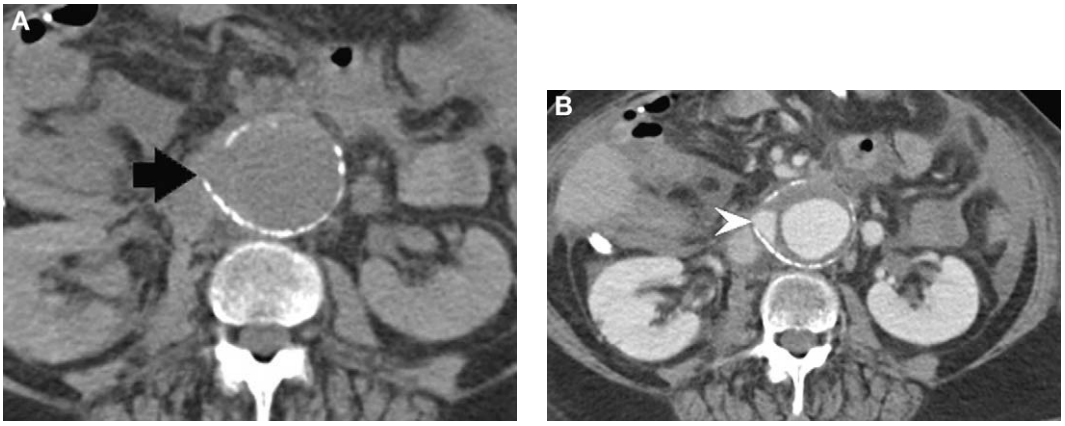

Fig. 4. Abdominal aortic aneurysm rupture. (*A*) Non–contrast-enhanced CT image demonstrates periaortic soft tissue density consistent with blood. Focal aortic contour irregularity and break in intimal calcification (*arrow*) provide clues to the diagnosis. (*B*) Contrast-enhanced image at the same level as Fig. 4A shows blood extending outside the aortic lumen (*arrowhead*), confirming aortic aneurysm rupture.

without surgical intervention, they are more likely to rupture. Besides uncontrollable hemorrhage, they may present with sepsis or fever of unknown origin. Patients with mycotic aneurysms are frequently asymptomatic and present with nonspecific signs, such as fever, leukocytosis, or positive blood cultures. A high-suspicion must be maintained so that patients are imaged expeditiously. As with atherosclerotic aneurysms, mycotic aneurysms tend to be infrarenal. Isolated suprarenal abdominal mycotic aneurysms are rare [51–53].

CT is a very good initial imaging study. Mycotic aneurysms tend to be saccular, eccentric aneurysms with irregularity of outer contour (Fig. 7) [52]. They tend not to have mural calcifications. The presence of gas in the periaortic fat of the retroperitoneum should suggest a mycotic aneurysm in an aorta that has not been surgically repaired [55]. Rarely, gas may be encountered in the wall of the aorta. This location is specific for a gas-forming organism. One such organism, *Clostridium septicum*, has been associated

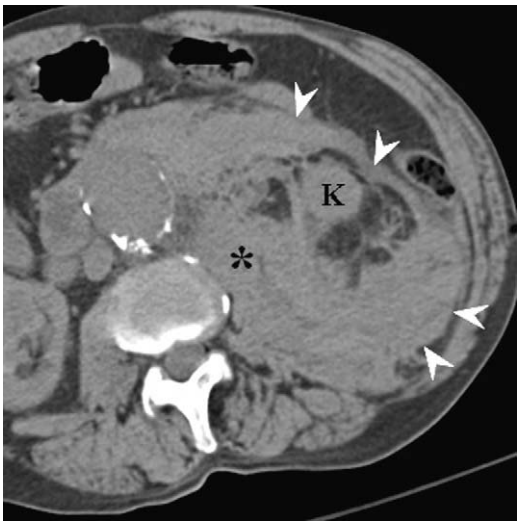

Fig. 5. Abdominal aortic aneurysm rupture. Non–contrast-enhanced CT image shows a large retroperitoneal hematoma (*asterisk*). Note that the hematoma extends along the retroperitoneal fascial planes (*arrowheads*) and displaces the left kidney (K) laterally and anteriorly.

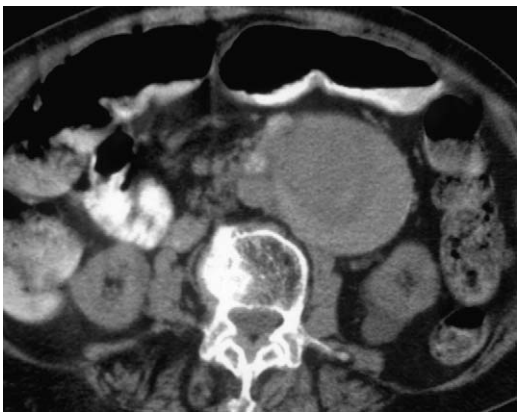

Fig. 6. Impending abdominal aortic aneurysm rupture. Non–contrast-enhanced CT image shows a peripheral high-attenuating crescent within an abdominal aortic aneurysm. Signs of frank aneurysm rupture are absent. At surgery acute hematoma was found within the aneurysm wall.

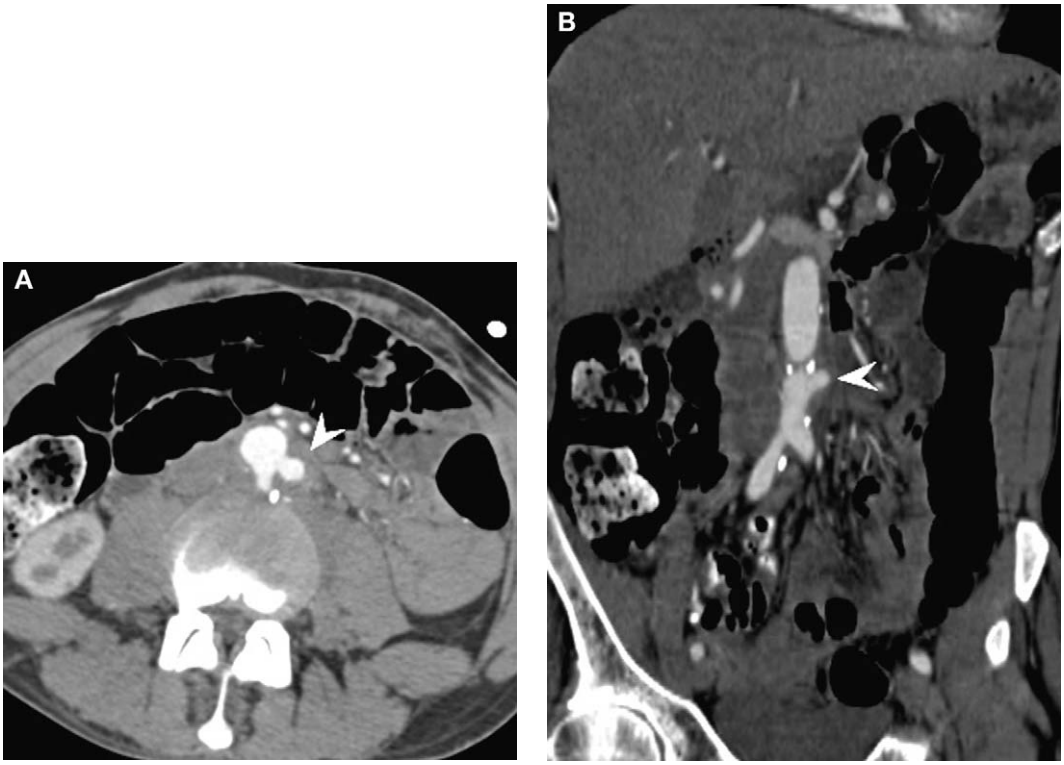

Fig. 7. Mycotic aneurysm. (*A*) Contrast-enhanced CT performed for evaluation of abdominal pain and fever shoes irregularity of the aortic lumen associated with periaortic soft tissue density (*arrowhead*). (*B*) Subsequent coronal reconstruction demonstrates a saccular aneurysm at the same level (*arrowhead*). (*C*) Sagittal reconstruction shows the posterior extension of this aneurysm (*arrowhead*).

with occult gastrointestinal and hematologic malignancies [56].

Mycotic aneurysms tend to expand much more rapidly than atherosclerotic AAAs. For this reason, there may be a role in the use of short-interval serial CTs to document rapid growth in a suspected mycotic aneurysm [57]. Mycotic aneurysms also may be multiple. Any imaging study used should cover the entire abdominal aorta and the iliac arteries [58].

Inflammatory aortic aneurysms

First described in 1972, inflammatory AAA refers to an aortic aneurysm with a wall thickened from chronic inflammatory cells and dense perianeurysmal fibrosis [59]. This fibrous tissue often involves adjacent structures, such as ureters, bowel, and vessels, and may explain why surgical repair of an inflammatory aneurysm is more difficult than repair of conventional atherosclerotic aneurysms [60]. A degree of controversy exists as to whether inflammatory AAA and idiopathic retroperitoneal fibrosis represent variations of the same disease process or entirely different entities [60–64]. Association of an AAA with fibrosis is not controversial, because up to 3% of AAAs are known to be inflammatory [65,66]. Perianeurysmal fibrosis is believed to be secondary to an autoimmune reaction to the antigens in atheromatous plaques. In fact, varying degrees of inflammation can be seen even in noninflammatory AAAs [67]. The term "inflammatory AAA" should be used only for aortic aneurysms that have a thickened wall; usually some degree of periaortic fibrosis is noted.

Patients may present with back pain or abdominal pain and may have an elevated erythrocyte sedimentation rate. More chronic manifestations, such as weight loss, or findings from bowel or ureteral obstruction may be present.

The primary CT finding is the presence of an AAA with a thickened wall (Fig. 8). On precontrast images, the wall tends to be soft tissue attenuation (not high attenuation like the crescent described in impending rupture). After intravenous contrast medium administration, the wall enhances and can be indistinguishable

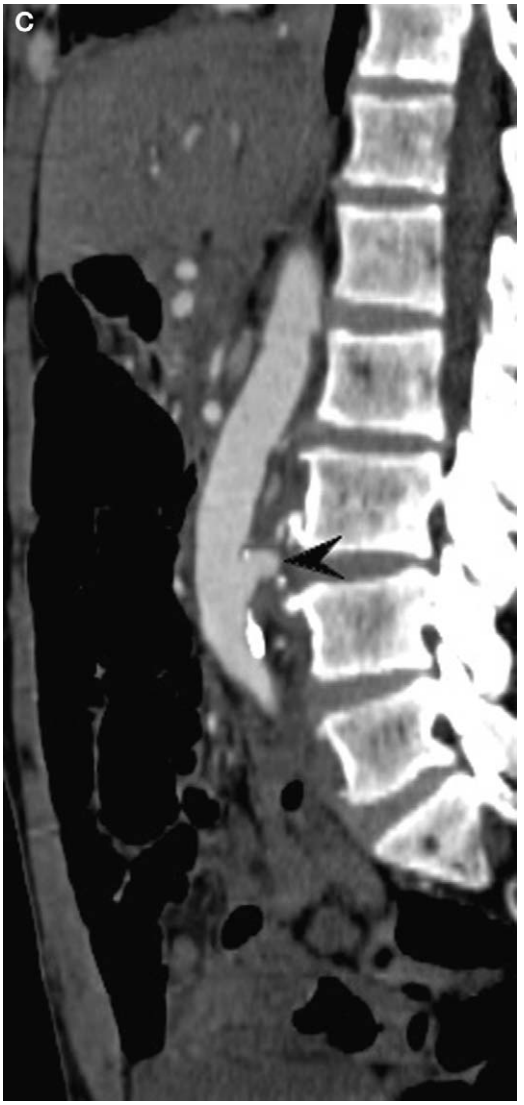

Fig. 7 (*continued*).

from the periaortic fibrosis. Enhancement is most notable on delayed-phase and less pronounced on arterial-phase images [68].

Mimics of inflammatory AAA on CT include lymphadenopathy, periaortic hematoma, and retroperitoneal tumors. The posterior wall of the aorta tends to be less involved than either of the lateral walls or the anterior wall [68]. The lack of anterior displacement of the abdominal aorta from the vertebral column and the retractile nature or lack of mass effect from the soft tissue process helps differentiate this process from retroperitoneal masses [69]. Retroperitoneal lymphadenopathy tends to have a more lobulated contour, may have discrete masses, and is more likely to displace the aorta from the vertebral column.

Abdominal aortic dissection

Isolated abdominal aortic dissections are rare and are much less common than abdominal aortic dissection associated with thoracic aortic dissection [70]. For this reason, whenever an aortic dissection is suspected, the authors' practice is to begin the study above the level of the aortic arch and extend it to the level of the aortic bifurcation. They begin with a noncontrast study and then proceed with intravenous contrast medium administration. Precontrast images are important to look for high attenuation within the aortic wall (ie, IMH) that might be confused with mural thrombus on postcontrast images. In the postoperative aorta, precontrast images may allow for visualization of graft material that might have been confused with enhancement if only postcontrast images had been acquired.

As with AAA, hypertension is believed to be a major risk factor for aortic dissection [71,72]. Cystic medial necrosis, as can be seen with Marfan syndrome, is another important etiology of aortic dissection. In fact, Marfan syndrome accounts for most dissections in patients younger than 40 [73]. Other associations with dissection include chromosomal aberrations (Turner's and Noonan's syndrome); bicuspid aortic valve; aortic dilation; aortitis; Ehlers-Danlos syndrome; cocaine use; pregnancy; and aortic coarctation. Atherosclerosis is not believed to be an independent risk factor for aortic dissection; however, focal dissections may be seen as a complication of a penetrating atherosclerotic ulcer (PAU), and so an association between dissection and atherosclerosis may be found [74–77]. Direct arterial injury from an intravascular catheter may be responsible for up to 5% of aortic dissections, usually in the abdominal and descending thoracic aorta [78].

Two mechanisms are frequently cited as potential etiologies of a dissection. In the first, believed to be the more common cause of dissection, the pathogenesis is described as an intimal injury with blood entering into the aortic wall and creating a false passage within the media [76]. The intima is believed to be more susceptible to sheer stress than the media or adventitia, explaining hypertension as a risk factor. In the second mechanism, the bleeding begins within the aortic wall from cystic medial necrosis and hemorrhage of the vasa vasorum [79]. The blood under pressure creates an entry into the lumen, or an intimal tear. This second mechanism helps to explain how an

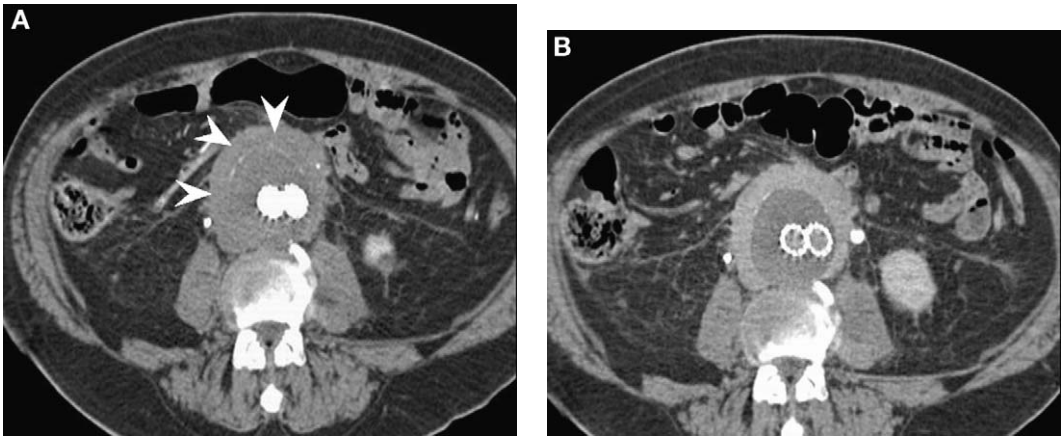

Fig. 8. Inflammatory aortic aneurysm. (*A*) Arterial phase contrast-enhanced CT image shows a soft tissue mantle (*arrowheads*) surrounding most of the circumference of an abdominal aortic aneurysm. Note that the aneurysm has been treated with an endoluminal graft. (*B*) Delayed postcontrast image demonstrates delayed enhancement of the soft tissue mantle, which spares the posterior aspect of the aneurysm adjacent to the vertebrae.

IMH can lead to dissection and also explains the high incidence of dissection in patients with Marfan syndrome [80,81]. Recently a third mechanism has been proposed, which postulates that a dissection may arise from strong smooth muscle contractions, accentuated in patients with hypertension [82].

Patients presenting with an acute aortic dissection most commonly describe unremitting chest pain that radiates to the back, although abdominal pain may be present in up to 33% of cases [70,72]. Pain can occasionally remit in the setting of dissection. The return of pain is an ominous sign and has been linked to impending rupture [83]. Other potential findings include asymmetric blood pressures; symptoms from branch vessel occlusion (neurologic symptoms, renal symptoms, mesenteric ischemia); paraplegia; or hemiplegia [73,84]. Unfortunately, symptoms are not universally present and many times the clinical manifestations may overlap with other diseases that present to an emergency department. High clinical suspicion is important because up to 38% of aortic dissections are initially missed on examination and up to 28% of aortic dissections may go undetected until autopsy [71–73,85].

Although isolated abdominal aortic dissections are rare, the more liberal use of CT in the emergency department has resulted in increased detection [70,86]. A study of 10 patients with isolated abdominal dissection demonstrated that two were completely asymptomatic and five had benign abdominal examinations. In this group of patients, abdominal pain was the most frequent complaint (seven patients). Although hypertension may be a risk factor, isolated abdominal dissections may be related to prior trauma, iatrogenic injury, or PAU [70].

Both CT and MR imaging enable the diagnosis of aortic dissections with a high degree of accuracy [87]. CT is often the first choice because of its close proximity to many emergency departments and its short examination time [72,73,87]. Recent advances in MDCT have improved the ability to perform multiplanar reconstructions and volume-rendered three-dimensional images. Although the postprocessing may help demonstrate the relationship of a complex flap with branching vessels, the authors' experience is congruent with that of others showing that three-dimensional images do not improve the detection of dissection [88,89]. Transaxial images generally suffice in excluding an aortic dissection, and three-dimensional images may prove helpful once a dissection is encountered [88,89].

Because noncontrast CT has no role in the exclusion of an aortic dissection, intravenous contrast medium administration is needed. In patients with renal failure or prior adverse reaction to iodinated contrast material, alternatives to conventional iodine-enhanced CT must be found. In this setting, MR imaging plays an important role in the evaluation of the acute abdominal aorta. The main drawbacks of MR imaging have been the longer examination time and the difficulty in monitoring potentially unstable patients in the long-bore magnet, which is frequently outside the emergency department. With faster MR imaging sequences, patients can be imaged in less than 30 minutes, including MR angiography images that allow multiplanar and three-dimensional processing tech-

niques equivalent to MDCT [87]. Some authors have advocated relying on faster sequences, such as true fast imaging with steady state precession, which can be accomplished in less than 4 minutes and reliably can exclude aortic dissections [90]. Administration of gadolinium could then be reserved for patients in whom a dissection is found. The authors rely on three-plane cardiac-gated black-blood images (usually single-shot fast spin echo or half-Fourier acquisition turbo spin echo sequences) and a three-dimensional MR angiography sequence usually acquired in a sagittal or sagittal-oblique plane. The black-blood images are used to identify an IMH. A precontrast study is obtained for subtraction. With postprocessing, relying mainly on maximum intensity projections, the entire study can be performed in 30 minutes or less. With the faster scanning times of 8- and 16-row MDCT, there may be a role for the use of intravenous gadolinium in the CT examination of patients with contraindications to iodinated contrast material [91,92].

Although transesophageal echocardiography may be equivalent to CT and MR imaging for the detection of aortic dissection, transesophageal echocardiography has little role for the evaluation of dissection in the abdominal aorta. Instead, transabdominal sonography may be used to detect abdominal aortic dissections [93]. In the acute setting, however, the superiority of CT in delineating the extent of the flap and in providing alternative diagnoses makes it preferable to sonography for the evaluation of suspected aortic dissection.

CT and MR imaging findings of an aortic dissection hinge on the identification of an intimal flap that can be seen on more than one transaxial image. Usually a flap isolated to one image (when slice thickness is 8 mm or less) represents artifact. When the dissection arises in the thoracic aorta, the flap in the abdominal aorta usually extends in a spiraling pattern along the left posterolateral wall from about the 3-o'clock to 6-o'clock positions. The result is that the right renal artery, celiac artery, and superior mesenteric artery tend to arise from the true lumen, whereas the left renal artery has a higher chance of originating from the false lumen.

CT findings that may allow distinction of a true from a false lumen include delayed contrast filling, delayed contrast wash out, thrombosis, irregular walls, and the presence of aortic cobwebs within the false lumen [94,95]. The term ''aortic cobwebs'' refers to low-attenuation linear remnants of the media in the false lumen, which are reportedly more common in the abdominal aorta and in the setting of chronic dissection [95].

When an intimal flap is seen, it must be followed throughout its entire course. Although rare, mesenteric ischemia and renal ischemia may complicate abdominal aortic dissections. CT is excellent at depicting the course of a flap into the mesenteric or renal arteries (Fig. 9). The goal is to identify these complications before infarction of the affected organ so that appropriate therapies may be instituted. Renal dissections are more frequently on the left and are more common than mesenteric dissections [96]. Two types of aortic branch occlusion in the setting of acute dissection have been described. In one type, called static obstruction, the dissection flap extends into or intersects the origin of the vessel, compromising flow. In the second type, called dynamic obstruction, the false lumen compresses the true lumen. In this latter entity, the flap is pushed so that it obstructs the origin of the branch vessel [97]. The type of obstruction may lend itself to different treatments with endoluminal stenting used for static obstruction and fenestrations or endoluminal stenting for dynamic obstruction [97].

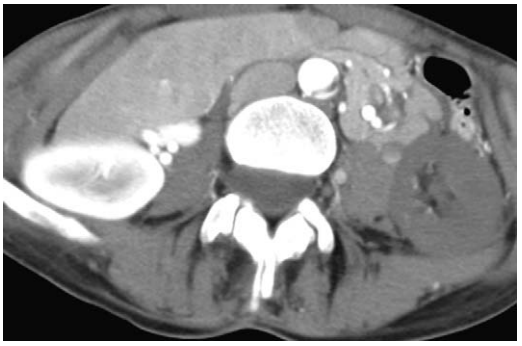

Fig. 9. Aortic dissection with renal involvement. Contrast-enhanced CT image shows an intimal flap within the abdominal aorta. Lack of perfusion of the left kidney was caused by extension of the dissection into the left renal artery.

Aortic rupture represents the most common cause of death in aortic dissection [73]. CT findings of aortic rupture from dissection are identical to those seen with ruptured AAA. Findings include the presence of retroperitoneal hematoma, intraperitoneal hematoma, and discontinuous aortic wall. Rupture is usually from the false lumen with its inherently weaker wall.

Intramural hematoma

Intramural hematoma represents blood in the aortic wall, presumed to be secondary to vasa vasorum rupture, without an intimal tear. As with dissection, hypertension is the major risk factor for the development of an IMH [98]. IMH is believed by many to represent a variant of aortic dissection and is often classified based on its location relative to the left subclavian artery [97,99]. Usually an IMH begins

within the thoracic aorta. Only rarely does it exist in the abdominal aorta alone. When it does, one must exclude trauma, iatrogenic aortic injury, or PAU as an underlying cause. Patients present with complaints that are identical to those seen with aortic dissection.

On precontrast images, a smooth high-attenuating crescent is seen in the aortic wall that displaces any intimal calcifications. Narrow window settings may allow for easier visualization of an IMH [100]. On postcontrast images, the hematoma fails to enhance and appears low in attenuation. If postcontrast images are viewed alone, the IMH may be mistaken for atheromatous plaque or a thrombosed false lumen. In the latter condition, the false lumen tends to spiral around the aorta as it descends, whereas an IMH tends to keep its relationship with a particular portion of the aortic wall circumference (eg, posterolateral) [101]. The CT findings of an IMH should not be confused with wall thickening of an inflammatory AAA, which enhances after contrast medium administration, or with the impending rupture sign, which is seen as a high-attenuating crescent in the wall of an AAA.

Penetrating atherosclerotic ulcer

First described in 1986, penetrating atherosclerotic ulcers have come to be recognized as a distinct entity [74,79]. They represent ulceration of an atheromatous plaque into the media of the aortic wall. Penetrating ulcers can then give rise to a focal IMH, dissection, or even rupture. Over time, a PAU may give rise to a chronic dissection or may resolve [74]. Occasionally, they may give rise to a saccular pseudoaneurysm. Although PAUs are more common in the descending thoracic aorta, they may originate in the abdominal aorta (Fig. 10). Identification of a contrast-filled crater that communicates with the aortic lumen is the key to making the diagnosis of a PAU. The cranial-caudal extent of a PAU, IMH from a PAU, or dissection from a PAU is much shorter than a typical dissection or primary IMH. When a short dissection or IMH is encountered, one should think of a PAU as the likely etiology. Distinction of PAU from dissection or primary IMH is important because treatment for PAU, when necessary, is different from that for the other two entities [102].

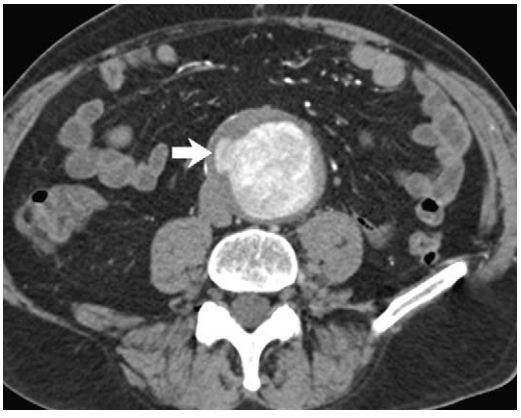

Fig. 10. Penetrating atherosclerotic ulcer. Contrast-enhanced CT image demonstrates a focal outpouching from the aortic lumen (*arrow*), which extends into the aortic wall.

Acute abdominal aortic occlusion

Acute aortic occlusion is a rare vascular catastrophe that can easily escape detection in the emergency department. Patients often present with paralysis that might lead to pursuit of neurologic disease, even when femoral pulses are absent [103]. Acute aortic occlusion should be considered when a patient without atherosclerosis presents with cold extremities and absent femoral pulses. Unlike chronic aortic occlusion (Leriche's syndrome), extensive collateral circulation is not present. Consequently, if acute abdominal aortic occlusion is not treated, mortality is greater than 75% [103].

Acute aortic occlusion may be from a large saddle embolism to the aortoiliac bifurcation, in situ thrombosis of an atherosclerotic aorta, sudden thrombosis of a small aortic aneurysm, or thrombosis related to a traumatic dissection. Rarely, other types of emboli can result in acute aortic occlusion. In endemic areas, even echinococcus has been reported to cause acute aortic occlusion [104].

CT findings of acute aortic occlusion include lack of blood flow in the aorta on postcontrast images and lack of defined collateral vessels (Fig. 11). The absence of collaterals may be appreciated best on multiplanar and three-dimensional images, which tend to highlight these often circuitous vessels. As with dissection, postcontrast images are very important. If iodinated contrast medium administration is contraindicated, MR angiography might be considered. Treatment is embolectomy or bypass if flow cannot be reestablished [103,105].

Abdominal aortic trauma

Blunt traumatic injury of the abdominal aorta is much less common than that of the thoracic aorta, but it

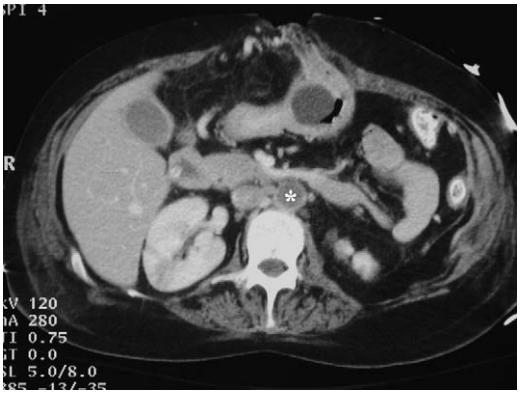

Fig. 11. Acute aortic occlusion. Contrast-enhanced CT at the level of the mid-kidney in a 36-year-old woman with Crohn's disease demonstrates lack of enhancement of the abdominal aorta (*asterisk*). The lack of collateral flow indicates that this is an acute process, which in this case was caused by an embolism from the left atrium.

is no less significant. If left untreated, such injuries may be life-threatening. The spectrum of aortic pathology ranges from IMH to intimal disruption and pseudoaneurysm formation [106,107]. Unlike the thoracic aorta, which is screened easily with chest radiographs, there is no adequate screening examination for the abdominal aorta. Decreased lower extremity pulses may be a finding on physical examination.

CT findings include both direct and indirect signs of aortic injury. As within the thorax, direct signs of aortic injury include the presence of an intimal flap; irregular aortic contour; focal enlargement of the aorta; abrupt change in aortic caliber (traumatic coarctation); and frank contrast medium extravasation (Fig. 12) [108]. Periaortic hematoma is considered an indirect sign. Angiography should be considered when an indirect sign is present but direct signs are absent [108,109].

Traumatic injuries of branch vessels are more common than injury of the abdominal aorta itself. CT findings and physical examination findings stem from ischemia of the affected organ (bowel, spleen, kidney). Perivascular hematoma, vessel thrombosis, traumatic intimal flap, and frank contrast medium extravasation may also be seen.

Postoperative aorta

Occasionally, patients may present acutely with complications from a surgically repaired abdominal aorta. These patients may be clinically challenging, because they often present to the emergency department with nonspecific signs and symptoms, such as fever, abdominal pain, and back pain [110]. Occasionally, a simultaneous groin infection or hematoma may be present.

Postendoaneurysmorrhaphy

To understand the complications of surgical repair one must be familiar with the AAA grafting procedure and its imaging appearance. This procedure, known as ''endoaneurysmorrhaphy,'' requires a longitudinal incision along the course of the aneurysm, removal of mural thrombus from the aneurysm sac, ligation of vessels arising from the aneurysm, suture anastomosis of the graft to the vessels proximal and distal to the aneurysm, and closure of the aneurysm sac around the graft material [111]. Perioperative complications relate to cardiac, renal, or respiratory failure and sepsis [112,113]. Longer-term complications include graft infection, thrombosis, anastomotic aneurysm, dissection, and aortoenteric fistula.

When a graft complication is suspected in a patient who has undergone endoaneurysmorrhaphy, the authors perform an abdominal and pelvic CT with intravenous contrast material but without oral contrast material. Noncontrast images are rarely useful. Initial postcontrast images are reviewed on the scanner console, in case delayed imaging is required to identify the relationship of any encountered complication with venous structures. If iodinated contrast material is contraindicated, the authors may begin with a noncontrast CT (to exclude rupture and to identify gas) and proceed with MR imaging to identify any flow-related complications.

By 3 months after open repair, most of the thrombus within the aortic aneurysm sac surrounding the

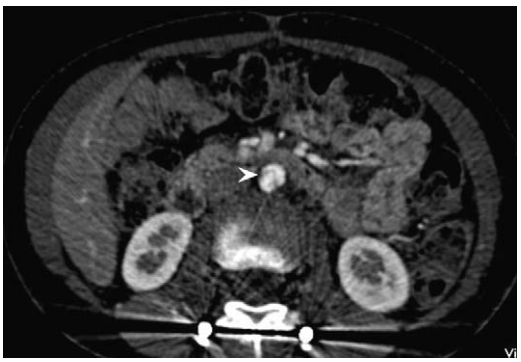

Fig. 12. Traumatic aortic injury from a motor vehicle collision. Contrast-enhanced CT image in a 14-year-old girl shows contour irregularity of the abdominal aortic wall associated with a small flap (*arrowhead*).

graft should have resolved [114,115]. If the collection has increased in size, or if contrast is seen to enter the collection, one should be concerned about graft rupture. Pseudoaneurysm is identified as a focal, eccentric outpouching at the proximal or distal anastomosis and may be associated with graft rupture. Occasionally, graft rupture may be seen as a new or increasing retroperitoneal hematoma.

Graft infection is another complication that may result in acute presentation to the emergency department. CT findings of graft infection include perigraft soft tissue and stranding, gas in the aortic wrap or adjacent to it, and pseudoaneurysm formation (Fig. 13) [115]. Differentiating these findings from normal postoperative findings can be challenging. Knowledge of the interval between the CT and surgery, and the clinical symptoms, is important in making this distinction. Perigraft gas should not be seen more than 14 days after surgery [116]. Unfortunately, not all infected grafts are associated with retroperitoneal gas. When gas is absent but fluid is present and graft infection is suspected, CT may be used to guide needle aspiration to confirm the diagnosis.

Graft thrombosis is diagnosed easily on postcontrast images when the lumen fails to enhance. It may be seen as an isolated condition or can be seen as a complication of graft infection. When thrombosis is present, one must look carefully for gas, retroperitoneal fluid, or other CT signs of infection that have been described previously.

Another life-threatening postoperative complication is an aortic fistula. Fistulae to many structures have been described, but the most commonly observed fistula in the postoperative aorta is an aortoenteric fistula. Aortoenteric fistulae are divided into primary and secondary types. Primary fistulae are much less common. They usually arise from an atherosclerotic aneurysm but may be secondary to a gastric ulcer, bowel carcinoma, foreign body, gallstone, or diverticulitis. Secondary fistulae represent a well-known complication of AAA surgery [117]. Aortoenteric fistula may present with minimal bleeding or catastrophic exsanguination. Although endoscopy can usually uncover a source of frank upper gastrointestinal hemorrhage, it may be negative up to 5% of the time [118]. In these cases, rarer causes of bleeding should be considered, such as Meckel's diverticulum, arteriovenous malformation, small bowel varices, small bowel diverticulum, or aortoenteric fistula. CT may be helpful in these instances. With aortoenteric fistula, the bowel adjacent to the aorta may have a puckered appearance and gas may be present in or near the aortic wall or in the postsurgical wrap. Perigraft soft tissue and bowel wall thickening may be seen (Fig. 14) [115,119]. The fat plane between the aorta and an adjacent bowel loop is often obliterated. Rarely, bowel wall hematoma and frank contrast medium extravasation can be seen [115,119]. Although these findings might suggest an aortoenteric fistula, it is important to keep in mind that a negative CT does not exclude the diagnosis.

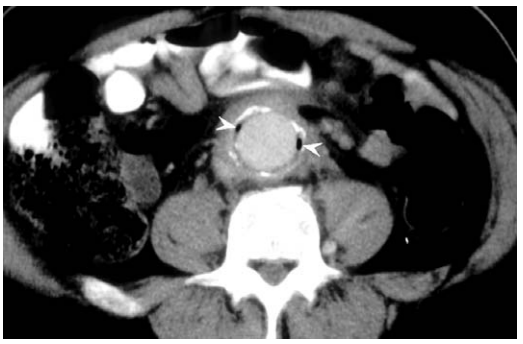

Fig. 13. Aortic graft infection in a patient 4 years after graft repair of an abdominal aortic aneurysm. Contrast-enhanced CT image shows gas (*white arrowheads*) within the native aortic wall wrap adjacent to the graft.

Postendoluminal graft repair

More recently, endoluminal grafts have been used to treat AAAs. These covered stent grafts are deployed intravascularly and share the goal with endoaneurysmorrhaphy of reducing pressure on the aneurysm wall. This is accomplished by creating a graft-covered channel that excludes most of the aneurysm, including the wall, from flowing blood. This endoluminal technique differs from open repair in that aneurysm thrombus is not surgically removed, the stent-graft apposes the normal aorta but is not sutured to it, and branch vessels from the aneurysm sac are not ligated or occluded [111].

Patients with complications of endovascular repair present with symptoms similar to those after open repair, including pain and fever. When complications are suspected, the authors use a different imaging protocol than with open repair. If possible, patients are referred for CT. Images of the abdominal aorta are obtained in three sequences: (1) noncontrast, (2) arterial phase, and (3) a 90-second delayed phase. If the patient is unstable or if the closest scanner does not allow three sequences, the authors begin with a noncontrast study in the emergency department. If that shows no retroperitoneal hematoma or graft migration, contrast-enhanced imaging is deferred until the patient can undergo CT angiography of the abdominal aorta with delayed images. The noncontrast imaging is important

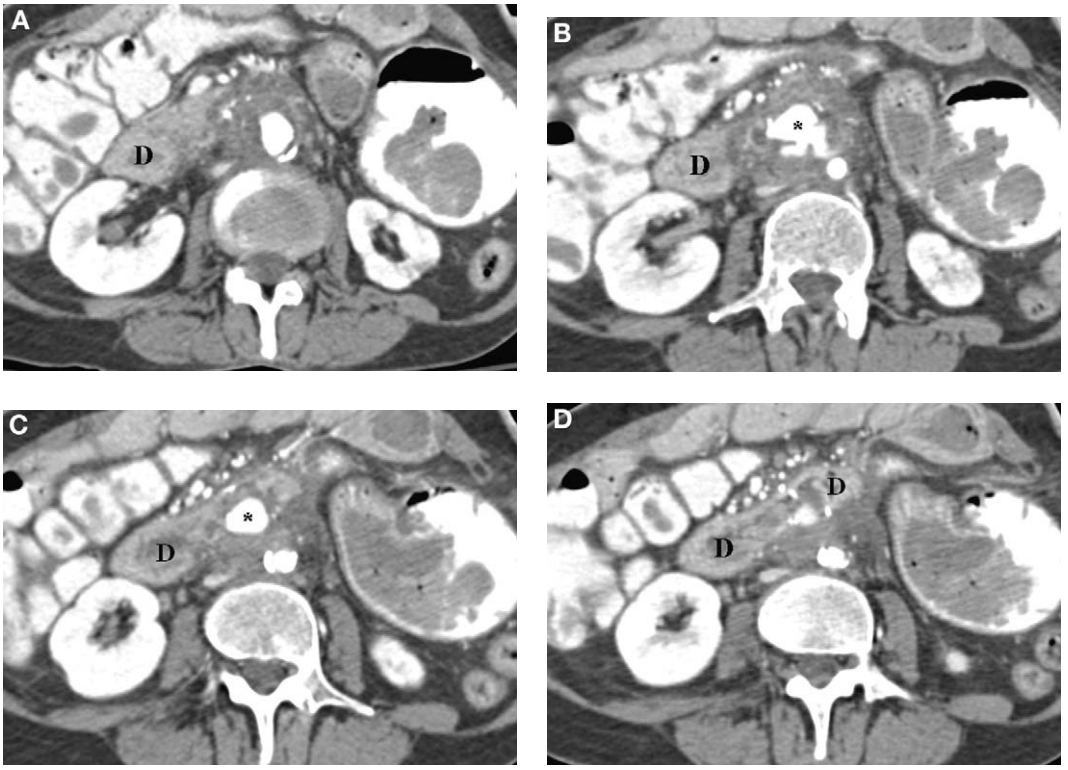

Fig. 14. Aortoenteric fistula in a patient 3 years after graft repair of an abdominal aortic aneurysm. Four sequential images (*A–D*) from a contrast-enhanced CT examination show effacement of the fat between the aorta and the duodenum (*D*) with adjacent irregular contrast-filled structure (*asterisk in B and C*) representing the actual fistula.

to identify the elements of the graft, and the delayed imaging is used to identify delayed endoleak and help confirm flow in the aneurysm sac outside of the graft lumen. Endoleaks represent the most common complication after endoluminal graft deployment. Other complications, which are more likely to cause acute symptoms, include graft thrombosis, graft migration, dissection, branch vessel occlusion, graft kinking, infection, and fistula formation [120,121]. Comparison with an immediate postoperative CT can be very useful in identifying complications of endoluminal graft placement.

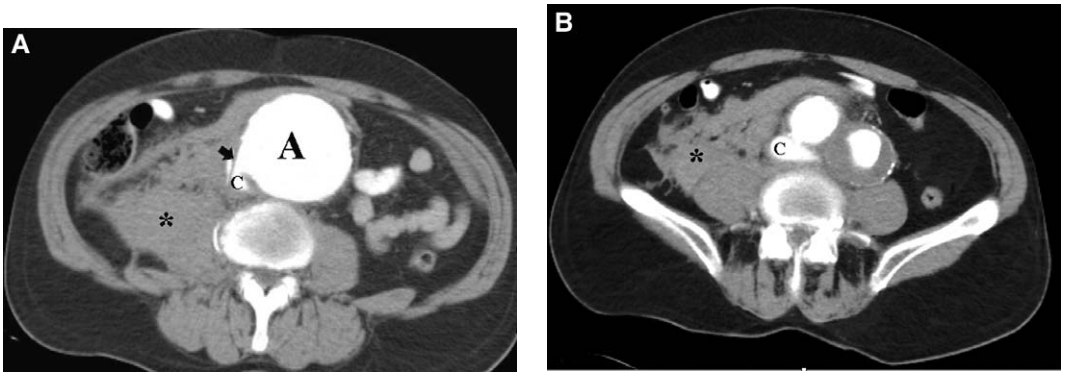

Fig. 15. (*A, B*) Contrast-enhanced CT images demonstrate early, dense contrast enhancement of the inferior vena cava (c) due to communication (*arrow*) between the cava and a large abdominal aortic aneurysm (A). Note large right retroperitoneal hematoma (*asterisk*).

Aortic fistula

Primary aortic fistulae (ie, those involving an unoperated aorta) may complicate AAA (Fig. 15), aortitis, and trauma. Rarely, a foreign body within the bowel lumen may fistulize to the abdominal aorta. Symptoms depend on the organ to which the aorta has fistulized. Aortic fistulae have been reported to bowel, inferior vena cava, renal veins, and ureters [117,122–125].

Summary

Aortic aneurysm rupture, aortic dissection, PAU, acute aortic occlusion, traumatic aortic injury, and aortic fistula represent acute abdominal aortic conditions. Because of its speed and proximity to the emergency department, helical CT is the imaging test of choice for these conditions. MR imaging also plays an important role in the imaging of aortic dissection and PAU, particularly when the patient is unable to receive intravenous contrast material. In this era of MDCT, conventional angiography is used as a secondary diagnostic tool to clarify equivocal findings on cross-sectional imaging. Ultrasound is helpful when CT is not readily available and the patient is unable or too unstable to undergo MR imaging.

References

[1] Borrero E, Queral LA. Symptomatic abdominal aortic aneurysm misdiagnosed as nephroureterolithiasis. Ann Vasc Surg 1988;2:145–9.
[2] Marston WA, Ahlquist R, Johnson Jr G, Meyer AA. Misdiagnosis of ruptured abdominal aortic aneurysms. J Vasc Surg 1992;16:17–22.
[3] Chow LC, Rubin GD. CT angiography of the arterial system. Radiol Clin North Am 2002;40:729–49.
[4] Coulam CH, Rubin GD. Acute aortic abnormalities. Semin Roentgenol 2001;26:148–64.
[5] Rubin GD, Shiau M, Leung A, Kee ST, Logan LJ, Sofilos MC. Aorta and iliac arteries: single versus multiple detector-row helical CT angiography. Radiology 2000;215:670–6.
[6] Mehard WB, Heiken JP, Sicard GS. High-attenuating crescent in abdominal aortic aneurysm wall at CT: a sign of acute or impending rupture. Radiology 1994;192:359–62.
[7] Jeffrey RJ. CT angiography of the abdominal and thoracic aorta. Semin Ultrasound CT MR 1998;19:405–12.
[8] Kishi K, Ito S, Hiasa Y. Risk factors and incidence of coronary artery lesions in patients with abdominal aortic aneurysms. Intern Med 1997;36:384–8.
[9] Rangel A, Albarran H, Solorio S, Hernandez-Gonzalez MA. Angiographic concurrence of coronary artery disease and aortoiliac lesions. Angiology 2002;53:685–92.
[10] Bae KT, Tran HQ, Heiken JP. Mutiphasic injection method for uniform prolonged vascular enhancement at CT angiography: pharmokinetic analysis and experimental porcine model. Radiology 2000;216:872–80.
[11] Fleischmann D, Rubin G, Bankier A, Hittmair K. Improved uniformity of aortic enhancement with customized contrast medium injection protocols at CT angiography. Radiology 2000;214:363–71.
[12] Horejs D, Gilbert P, Burstein S, Vogelzang R. Normal aortoiliac diameters by CT. J Comput Assist Tomogr 1988;12:602–3.
[13] Ashton HA, Buxton MJ, Day NE, et al. The Multicentre Aneurysm Screening Study (MASS) into the effect of abdominal aortic aneurysm screening on mortality in men: a randomised controlled trial. Lancet 2002;360:1531–9.
[14] Melton LI, Bickerstaff L, Hollier L, et al. Changing incidence of abdominal aortic aneurysm: a population-based study. Am J Epidemiol 1984;120:379–86.
[15] Gallagher PJ. Blood vessels. In: Sternberg SS, editor. Diagnostic surgical pathology. Philadelphia: Lippincott Williams & Wilkins; 1999. p. 1256–8.
[16] Blanchard JF, Armenian HK, Friesen PP. Risk factors for abdominal aortic aneurysm: results of a case-control study. Am J Epidemiol 2000;151:575–83.
[17] Powell J, Greenhalgh R. Cellular, enzymatic and genetic factors in the pathogenesis of abdominal aortic aneurysms. J Vasc Surg 1989;9:297–304.
[18] Zatina MA, Zarins CK, Gewertz BL, Glagov S. Role of medial lamellar architecture in the pathogenesis of aortic aneurysms. J Vasc Surg 1984;1:442–8.
[19] Hicks G, Eastland M, DeWeese J, May AG, Rob CG, et al. Survival improvement following aortic aneurysm resection. Ann Surg 1975;181:863–9.
[20] Simoni G, Beghello A, Ermirio D, Caprio J. Growth rate of abdominal aortic aneurysms: ultrasounds study and clinical outcome. Minerva Cardioangiol 2002;50:371–7.
[21] Darling R, Messina C, Brewster D, Ottinger LW. Autopsy study of unoperated abdominal aortic aneurysms: the case for early resection. Circulation 1977;56(3 suppl):161–4.
[22] Ingolby CJH, Wujanto R, Mitchell JE. Impact of vascular surgery on community mortality from ruptured aortic aneurysms. Br J Surg 1986;73:551–3.
[23] Johansen K, Kohler TR, Nicholls SC, Zierler RE, Clowes AW, Kazmers A. Ruptured abdominal aortic aneurysm: the Harborview experience. J Vasc Surg 1991;13:240–7.
[24] Johansson G, Swedenborg J. Ruptured abdominal aortic aneurysms: a study of incidence and mortality. Br J Surg 1986;73:101–3.
[25] Thomas PRS, Stewart RD. Abdominal aortic aneurysm. Br J Surg 1988;75:733–6.

[26] Talbot S, Langman MJS. Epidemiologic features of ruptured dissecting and saccular aneurysms. Postgrad Med J 1972;48:414–6.
[27] Alonso-Perez M, Segura RJ, Sanchez J, et al. Factors increasing the mortality rate for patients with ruptured abdominal aortic aneurysms. Ann Vasc Surg 2001;15: 601–7.
[28] Ernst CB. Abdominal aortic aneurysm. N Engl J Med 1993;328:1167–72.
[29] Limet R, Sakalihassan N, Albert A. Determination of expansion rate and incidence of rupture of abdominal aortic aneurysms. J Vasc Surg 1991;14:540–8.
[30] Brown PM, Pattenden R, Gutelius JR. The selective management of small abdominal aortic aneurysms: the Kingston study. J Vasc Surg 1992;15:21–7.
[31] Acheson AG, Graham AN, Weir C, Lee B. Prospective study on factors delaying surgery in ruptured abdominal aortic aneurysms. J R Coll Surg Edinb 1998;43: 182–4.
[32] Lederle FA, Parenti CM, Chute EP. Ruptured abdominal aortic aneurysm: the internist as diagnostician. Am J Med 1994;96:163–7.
[33] Sagel SS, Siegel MJ, Stanley RJ, Jost GJ. Detection of retroperitoneal hemorrhage by computed tomography. AJR Am J Roentgenol 1977;129:403–7.
[34] Siegel CL, Cohan RH. CT of abdominal aortic aneurysms. AJR Am J Roentgenol 1994;163:17–29.
[35] Siegel CL, Cohan RH, Korobkin M, Alpern MB, Courneya DL, Leder RA. Abdominal aortic aneurysm morphology: CT features in patients with ruptured and nonruptured aneurysms. AJR Am J Roentgenol 1994;163:1123–9.
[36] Sandler CM, Jackson H, Kaminsky RI. Right perirenal hematoma secondary to a leaking abdominal aortic aneurysm. J Comput Assist Tomogr 1981;5:264–6.
[37] Rosen A, Korobkin M, Silverman PM, Moore Jr AV, Dunnick NR. CT diagnosis of ruptured abdominal aortic aneurysm. AJR Am J Roentgenol 1984;143: 265–8.
[38] Clayton MJ, Walsh JW, Brewer WH. Contained rupture of abdominal aortic aneurysms: sonographic and CT diagnosis. AJR Am J Roentgenol 1982;138: 154–6.
[39] Albertyn LE. Perirenal cobwebs: a sign of aneurysm rupture. Australas Radiol 1988;32:98–100.
[40] Gale ME, Johnson WC, Gerzof SG, Robbin AH, Nabseth DC. Problems in CT diagnosis of ruptured abdominal aortic aneurysms. J Comput Assist Tomogr 1986;10:631–41.
[41] Garb M. The CT appearances of ruptured abdominal aortic aneurysms. Australas Radiol 1989;33:154–6.
[42] Raptapoulos V, Cummings T, Smith EH. Computed tomography of life-threatening complications of abdominal aortic aneurysm: the disrupted aortic wall. Invest Radiol 1987;22:373–6.
[43] Torres ME, Maurer DE, Steinberg HV, Robbins S, Bernardino ME. CT of aortic aneurysms: the distinction between mural and thrombus calcification. AJR Am J Roentgenol 1988;150:1317–9.
[44] Federle MP, Jeffrey RB. Hemoperitoneum studied by computed tomography. Radiology 1983;148: 187–92.
[45] Levine CD, Patel UJ, Silverman PM, Wachsberg RH. Low attenuation of acute traumatic hemoperitoneum on CT scans. AJR Am J Roentgenol 1996;166: 1089–93.
[46] Basile KE, Sivit CJ, O'Riordan MA, Marsh E, Grisoni ER. Acute hemoperitoneum in children: prevalence of low-attenuation fluid. Pediatr Radiol 2000;30: 168–70.
[47] Arita T, Matsunaga N, Takano K, et al. Abdominal aortic aneurysm: rupture associated with the high-attenuating crescent sign. Radiology 1997;204:765–8.
[48] Gonsalves CF. The hyperattenuating crescent sign. Radiology 1999;211:37–8.
[49] Pillari G, Chang JB, Zito J, et al. Computed tomography of abdominal aortic aneurysm. Arch Surg 1986; 123:727–32.
[50] Halliday KE, Al-Kutoubi A. Draped aorta: CT sign of contained leak of aortic aneurysms. Radiology 1996; 199:41–3.
[51] Gomes MN, Choyke PL, Wallace RB. Infected aortic aneurysms: a changing entity. Ann Surg 1992; 215:435–42.
[52] Gonda RL, Gutierrez OH, Azodo MVU. Mycotic aneurysms of the aorta: radiologic features. Radiology 1988;168:343–6.
[53] Hsu RB, Tsay YG, Wang SS, Chu SH. Surgical treatment for primary infected aneurysm of the descending thoracic aorta, abdominal aorta, and iliac arteries. J Vasc Surg 2002;36:746–50.
[54] Parsons R, Gregory J, Palmer DL. Salmonella infection of the abdominal aorta. Rev Infect Dis 1983;5: 227–31.
[55] Salzberger LA, Cavuoti D, Barnard J. Fatal salmonella aortitis with mycotic aneurysm rupture. Am J Forensic Med Pathol 2002;23:382–5.
[56] Sailors DM, Eidt JF, Gagne PJ, Barnes RW, Barone GW, McFarland DR. Primary *Clostridium septicum* aortitis: a rare cause of necrotizing suprarenal aortic infection. A case report and review of the literature. J Vasc Surg 1996;23:714–8.
[57] Yasuhara H, Muto T. Infected abdominal aortic aneurysm presenting with sudden appearance: diagnostic importance of serial computed tomography. Ann Vasc Surg 2001;15:582–5.
[58] Donald K, Woodson J, Hudson H, Menzoian JO. Multiple mycotic pseudoaneurysms due to *Yersinia enterocolitica*: a report of a case and a review of the literature. Ann Vasc Surg 1996;10:573–7.
[59] Walker DI, Bloor K, Williams D, Gillie I. Inflammatory aneurysms of the abdominal aorta. Br J Surg 1972; 59:609–16.
[60] Bonamigo TP, Bianco C, Becker M, Faccini FP. Inflammatory aneurysms of infra-renal abdominal aorta: a case-control study. Minerva Cardioangiol 2002;50: 253–8.
[61] Cavallaro A, Sapienza P, di Marzo L, Mosiello G,

Marchetti G, La Fauci M. Inflammatory aneurysm of the abdominal aorta. Review of the literature of the past 30 years. Recenti Prog Med 2001;92(4):290–301.
[62] Debrand-Passard A, Wilhelm H. Ormond's disease or aortic aneurysm? Case reports. Int Urol Nephrol 1996;28:295–304.
[63] Lance NJ, Levinson DJ. Aortitis and periaortic fibrosis. J Rheumatol 1991;18:1095–9.
[64] Leu HJ. Inflammatory abdominal aortic aneurysms: a disease entity? Histological analysis of 60 cases of inflammatory aortic aneurysms of unknown aetiology. Virchows Arch 1990;417:427–33.
[65] Breems DA, Haye H, Meulen JVD. The role of advanced atherosclerosis in idiopathic retroperitoneal fibrosis: analysis of nine cases. Neth J Med 2000; 56:38–44.
[66] Gans RO, Hoorntje SJ, Rauwerda JA, Luth WJ, Hattum LAV, Donker AJ. The inflammatory abdominal aortic aneurysm: prevalence, clinical features and diagnostic evaluation. Neth J Med 1993;43:105–15.
[67] Rijbroek A, Moll FL, Dijk HAV, Meijer R, Jansen JW. Inflammation of the abdominal aortic aneurysm wall. Eur J Vasc Surg 1994;8:41–6.
[68] Iino M, Kuribayashi S, Imakita S, et al. Sensitivity and specificity of CT in the diagnosis of inflammatory abdominal aortic aneurysms. J Comput Assist Tomogr 2002;26:1006–12.
[69] Degesys GE, Dunnick NR, Silverman PM, Cohan RH, Illescas FF, Castagno A. Retroperitoneal fibrosis: use of CT in distinguishing among possible causes. AJR Am J Roentgenol 1986;146:57–60.
[70] Farber A, Wagner WH, Cossman DV, et al. Isolated dissection of the abdominal aorta: clinical presentation and therapeutic options. J Vasc Surg 2002;36:205–10.
[71] Spittell PC, Spittell Jr J, Joyce JW. Clinical features and differential diagnosis of aortic dissection: experience with 236 cases (1980–1990). Mayo Clin Proc 1993;68:642–51.
[72] Hagan PG, Nienaber CA, Isselbacher EM, et al. The International Registry of Acute Aortic Dissection (IRAD): new insights into an old disease. JAMA 2000;283:897–903.
[73] Khan IA, Nair CN. Clinical, diagnostic and management perspectives of aortic dissection. Chest 2002; 122:311–28.
[74] Hayashi H, Matsuoka Y, Sakamoto I, et al. Penetrating atherosclerotic ulcer of the aorta: imaging features and disease concept. Radiographics 2000;20:995–1005.
[75] Larson EW, Edwards WD. Risk factors for aortic dissection: a necropsy study of 161 cases. Am J Cardiol 1984;53:849–55.
[76] Wilson SK, Hutchins GM. Aortic dissecting aneurysms: causative factors in 204 subjects. Arch Pathol Lab Med 1982;106:175–80.
[77] Tamura K, Sugisaki Y, Kumazaki T, Tanaka S. Atherosclerosis-related aortic dissection. Kyobu Geka 2000; 53:194–201.
[78] Archer AG, Choyke PL, Zeman RK, Green CE, Zuckerman M. Aortic dissection following coronary artery bypass surgery: diagnosis by CT. Cardiovasc Intervent Radiol 1986;9:142–5.
[79] Kazerooni EA, Bree RL, Williams DM. Penetrating atherosclerotic aneurysms of the descending thoracic aorta: evaluation with CT and distinction from aortic dissection. Radiology 1992;183:759–65.
[80] Child A. Marfan syndrome: current medical and genetic knowledge. How to treat and when? J Card Surg 1997;12:131–5.
[81] Nienaber CA, Kodolitsch YV. Therapeutic management of patients with Marfan syndrome: focus on cardiovascular involvement. Cardiol Rev 1999;7: 332–41.
[82] Mikich M. Dissection of the aorta: a new approach. Heart 2003;89:6–8.
[83] Meszaros I, Morocz J, Szlavi J, et al. Epidemiology and clinicopathology of aortic dissection. Chest 2000; 117:1271–8.
[84] Kirkorian G, Bonnefoy E, Chevalier P, de Breyne B, Touboul P. Acute dissection of the thoracic aorta. Symptoms and complications. Arch Mal Coeur Vaiss 1997;90 (12 suppl):1793–7.
[85] Bickerstaff LK, Pairolero PC, Hollier LH, et al. Thoracic aortic aneurysms: a population-based study. Surgery 1982;92:1103–8.
[86] Mozes G, Gloviczki P, Park WM, Schultz HL, Andrews JC, et al. Spontaneous dissection of the infrarenal abdominal aorta. Semin Vasc Surg 2002;15: 128–36.
[87] Hartnell GG. Imaging of aortic aneurysm and dissection: CT and MRI. J Thorac Imaging 2001;16:35–46.
[88] Lenz M, Wunderlich AP, Helmberger H, Gross M. Spiral CT in aortic aneurysms. 2D and 3D reconstructions and CT angiography. Rofo Fortschr Geb Rontgenstr Neuen Bildgeb Verfahr 1993;158:393–404.
[89] Huber A, Matzko M, Wintersperger BJ, Reiser M. Reconstruction methods in postprocessing of CT- and MR-angiography of the aorta. Radiologe 2001;41: 689–94.
[90] Pereles FS, McCarthy RM, Baskaran V, et al. Thoracic aortic dissection and aneurysm: evaluation with nonenhanced true FISP MR angiography in less than 4 minutes. Radiology 2002;223:270–4.
[91] Spinosa DJ, Kaufmann JA, Hartwell GD. Gadolinium chelates in angiography and interventional radiology: a useful alternative to iodinated contrast media for angiography. Radiology 2002;223:319–25.
[92] Karcaaltincaba M, Foley WD. Gadolinium-enhanced multidetector CT angiography of the thoracoabdominal aorta. J Comput Assist Tomogr 2002;26:875–8.
[93] Thomas EA, Dubbins PA. Duplex ultrasound of the abdominal aorta: a neglected tool in aortic dissection. Clin Radiol 1990;42:330–4.
[94] Fisher ER, Stern EJ, Goodwin 2nd JD, Otto CM, Johnson JA, et al. Acute aortic dissection: typical and atypical imaging features. Radiographics.
[95] Hayashi H, Onda M, Takagi R, et al. CT analysis of aortic cobwebs in aortic dissection. Nippon Igaku Hoshasen Gakkai Zasshi 1995;55:402–8.

[96] Cambria R, Brewster D, Gertler J, et al. Vascular complications associated with spontaneous aortic dissection. J Vasc Surg 1988;7:199–209.
[97] Sebastia C, Pallisa E, Quiroga S, Alvarez-Castells A, Dominguez R, Evangelista A. Aortic dissection: diagnosis and follow-up with helical CT. Radiographics 1999;19:45–60.
[98] Maraj R, Rerkpattanapipat P, Jacobs E, Makornwattana P, Kotler MN. Meta-analysis of 143 reported cases of aortic intramural hematoma. Am J Cardiol 2000;86:664–8.
[99] Yamada T, Tada S, Harada J. Aortic dissection without intimal rupture: diagnosis with MR imaging and CT. Radiology 1988;168:347–52.
[100] Holden A. The value of narrow CT window settings in the recognition of subtle acute aortic intramural haematoma. Australas Radiol 2000;44:128–9.
[101] Rubin GD. Helical CT angiography of the thoracic aorta. J Thorac Imaging 1997;12:128–49.
[102] Levy JR, Heiken JP, Gutierrez FR. Imaging of penetrating atherosclerotic ulcers of the aorta. AJR Am J Roentgenol 1999;173:151–4.
[103] Surowiec SM, Isiklar HI, Sreeram S, Weiss VJ, Lumsden AB. Acute occlusion of the abdominal aorta. Am J Surg 1998;176:193–7.
[104] Kaynak K, Koksal C, Kazimoglu K, Ozbek C. Vascular echinococcus. Asian Cardiovasc Thorac Ann 2002;10:259–61.
[105] Nobili P, Annolfi B, Giani L, Settembrini PG. Acute occlusion of the abdominal aorta. Il Giornale di Chirurgia 1998;19:112–4.
[106] Reisman J, Morgan A. Analysis of 46 intra-abdominal aortic injuries from blunt trauma: case reports and literature review. J Trauma 1990;30:1294–7.
[107] Brathwaite CE, Rodriguez A. Injuries of the abdominal aorta from blunt abdominal trauma. Am Surg 1992;58:350–2.
[108] Fishman JE. Imaging of blunt aortic and great vessel trauma. J Thorac Imaging 2000;15:97–103.
[109] Dyer DS, Moore EE, Mestek MF, et al. Can chest CT be used to exclude aortic injury? Radiology 1999;213:195–202.
[110] Mark A, Moss AA, Lusby R, Kaiser JA. CT evaluation of complications of abdominal aortic surgery. Radiology 1982;145:409–14.
[111] Kaufman JA, Geller SC, Brewster DC, et al. Endovascular repair of abdominal aortic aneurysms: current status and future directions. AJR Am J Roentgenol 2000;175:289–302.
[112] May J, White G, Yu W, et al. Concurrent comparison of endoluminal versus open repair in the treatment of abdominal aortic aneurysms: analysis of 303 patients by life table method. J Vasc Surg 1998;27:213–21.
[113] Hallett JW, Naesens JM, Ballard DJ. Early and late outcomes of surgical repair for small abdominal aortic aneurysms: a population-based analysis. J Vasc Surg 1993;18:684–91.
[114] Qvarfordt PG, Reilly LM, Mark AS, et al. Computerized tomographic assessment of graft incorporation after aortic reconstruction. Am J Surg 1985;150:227–31.
[115] Low RN, Wall SD, Jeffrey Jr RB, Sollitto RA, Reilly LM, et al. Aortoenteric fistula and perigraft infection: evaluation with CT. Radiology 1990;175:157–62.
[116] O'Hara PJ, Borkowski GP, Hertzer NR, O'Donovan PB, Brigham SL, Beven EG. Natural history of periprosthetic air on computerized axial tomographic examination of the abdomen following abdominal aortic aneurysm repair. J Vasc Surg 1984;1:429–33.
[117] Peck J, Eidemiller L. Aortoenteric fistulas. Arch Surg 1992;27:1191–3.
[118] Rockey DC. Occult gastrointestinal bleeding. N Engl J Med 1999;341:38–46.
[119] Zeppa MA, Forrest JV. Aortoenteric fistula manifested as an intramural hematoma. AJR Am J Roentgenol 1971;157:47–8.
[120] Mita T, Arita T, Matsunaga N, et al. Complications of endovascular repair for thoracic and abdominal aortic aneurysm: an imaging spectrum. Radiographics 2000;20:1263–78.
[121] Magennis R, Joekes E, Martin J, White D, McWilliams RG. Complications following endovascular abdominal aortic aneurysm repair. Br J Radiol 2002;75:700–7.
[122] Quiroga S, Alvarez-Castells A, Hidalgo A, Ruiz-Marcellan C, Castella E, Gifre L. Spontaneous aortocaval fistula: CT findings with pathologic correlation. Abdom Imaging 1995;20:466–9.
[123] Sevastos N, Rafailidis P, Kolokotronis K, Papadimitriou K, Papatheodoridis GV. Primary aortojejunal fistula due to foreign body: a rare cause of gastrointestinal bleeding. Eur J Gastroenterol Hepatol 2002;14:797–800.
[124] Voorhoeve R, Moll F, Letter JD, Bast TJ, Wester JP, Slee PH. Primary aortoenteric fistula: report of eight new cases and review of the literature. Ann Vasc Surg 1996;10:40–8.
[125] Panagiotides H, Kollias V, Limberopoulos C. Case report on primary and secondary aortoenteric fistula in patient. J Cardiovasc Surg 1994;35:437–9.

RADIOLOGIC CLINICS OF NORTH AMERICA

Radiol Clin N Am 41 (2003) 1171–1182

Blunt injury to mesentery and small bowel: CT evaluation

Patrick W. Hanks, MD[a], Jeffrey M. Brody, MD[a,b,*]

[a]*Department of Diagnostic Imaging, Brown Medical School, Providence, RI, USA*
[b]*Clinical Operations, Department of Diagnostic Imaging, Rhode Island Hospital, 593 Eddy Street, Providence, RI 02903, USA*

The availability of high-quality equipment, excellent contrast resolution, and ready depiction of complex anatomy has given CT scanning an important role in the evaluation of trauma patients. In the setting of blunt trauma where a penetrating wound does not indicate the potentially injured organs, CT has the capability of rapidly assessing multiple anatomic regions. In particular, small bowel or mesenteric injury (SBMI) from blunt force may be clinically occult [1–3], but attention to CT signs can point to the correct diagnosis. This was evident in the first papers presented on this subject two decades ago [4,5], but is more commonplace now with the evolution of this technology.

Demographics

In a large series of blunt trauma cases collected from 1991 to 1996 and reported by Frick et al [3], 1.3% of 5303 patients with abdominal injuries had SBMI. Nance et al [6] showed that the greater the number of organs injured the more likely there is associated SBMI and that in one third of patients SBMI coexists with pancreatic or other solid organ injury. Five percent of patients with liver lacerations and 4% with splenic lacerations have major bowel injury according to Buckman et al [7]. Motor vehicle accidents are the most common cause of SBMI [8]. Child abuse, falls from height, sports, industrial accidents, and even the Heimlich maneuver also have been implicated in SBMI [9–11].

Although any fixed object in the car cabin can cause trauma, seat belts are often associated with bowel injury. The presence of discoloration across the abdomen indicative of seat belt abrasion has been associated with small bowel injury in 21% of cases [12]. Seat belts are also a cause of the horizontally oriented vertebral Chance fracture that also has a high association with SBMI [13].

The future distribution of abdominal organ injury in blunt trauma related to motor vehicle accidents is unclear. The passage of mandatory seat belt laws in many states has put more people at risk for seat belt–type injuries. Conversely, the introduction of airbags has changed the spectrum of abdominal injury. Dischinger et al [14] report a 19% decrease in liver injury and a threefold increase in renal injury with airbags in place. The effect on SBMI remains to be seen.

Pathophysiology

The pathophysiology of injury to the small bowel and mesentery was first described in 1890 by Motz [15]. He postulated three types of trauma: (1) crush injury, (2) shearing forces of the bowel and mesentery at fixed points of attachment, and (3) burst injury caused by increased intraluminal pressure. Approximately 25% of patients requiring surgical treatment for bowel trauma have more than one bowel injury

* Corresponding author. Department of Diagnostic Imaging, Rhode Island Hospital, 593 Eddy Street, Providence, RI 02903.

E-mail address: jbrody@lifepan.org (J.M. Brody).

0033-8389/03/$ – see front matter
doi:10.1016/S0033-8389(03)00099-X

[16] and likely more than one mechanism. For example, in cases of seat belt injury, two or more sites of SBMI can be seen in 90% of patients [17].

Crush injury results from the impact of a stationary object on the anterior abdominal wall that catches a loop of bowel between it and the spine or solid organ. The duodenum and transverse colon are at particular risk with this mechanism that results in hematoma, contusion, or transection.

Acquired adhesions and normal points of bowel fixation at the ligament of Treitz and ileocecal junction serve as anchor points in shear injury. Rapid deceleration allows a mobile segment to move rapidly away from fixed points causing the injury. Lacerations of bowel and mesenteric vessels and degloving injuries are seen.

Burst injury occurs when impact with stationary objects reconfigures bowel into closed loops. If compression continues, pressure can rise to the point where bowel wall may burst resulting in full-thickness perforations.

Bowel injury varies from minor hematoma to perforation. Small perforations may go clinically unrecognized [16]. Abdominal pain and peritoneal irritation may be present early after major perforations or develop slowly because bowel contents, particularly jejunal contents, are not enzymatically active and have low pH and bacterial counts [18]. Although mesenteric lacerations can lead to significant hemorrhage and hypotension, there are also secondary effects. One quarter of cases where small bowel requires surgical treatment are the result of devascularization from mesenteric injury [16]. Even delayed internal hernias from untreated mesenteric lacerations and strictures from scar formation can occur [19,16].

Clinical considerations

Penetrating trauma involving the peritoneal cavity is currently diagnosed and treated most often by surgical exploration with little need for preoperative imaging. The radiologist is also likely to have little to do with the initial care of unstable blunt trauma victims with findings suggestive of intra-abdominal hemorrhage. They are often taken from the emergency department directly to urgent laparotomy for control of bleeding. In the past, even stable blunt trauma victims with intra-abdominal hemorrhage shown by diagnostic peritoneal lavage or CT scan went to exploratory surgery. This approach yielded a 20% nontherapeutic laparotomy rate [20,21]. Although CT scanning contributed to the care of these stable patients by identifying solid organ lacerations with hemorrhage, further evaluation of the scans did not affect treatment decisions. Exploration of the abdomen in the operating room allowed the surgeon to evaluate other organs including the bowel and mesentery.

Over the past 5 to 10 years, as more emphasis has been placed on nonoperative management for certain blunt trauma injuries, more complete CT evaluation has been required to help ensure that this treatment path is correct. The treatment of spleen lacerations is an example of this approach. In stable patients with this type of injury, CT scanning shows the extent of laceration and hemoperitoneum and any areas of parenchymal bleeding that can be addressed with percutaneous catheter embolization [22]. The leading cause of failed conservative therapy and delayed laparotomy is the presence of gastrointestinal tract injuries [23]. Although SBMI is uncommon, the clinical consequences related to delayed or missed diagnosis are disproportionately severe [24]. The burden is on CT, clinical signs, and other tests to detect significant SBMI that instead indicates the need for early surgical therapy.

Although physical examination findings, such as abdominal wall contusion, abdominal distention and guarding, or increasing tenderness, can aid in diagnosis and prompt exploration, they can be insensitive in certain situations. Altered levels of consciousness because of closed head injury, distracting injuries, or intoxication can make the physical examination unreliable [25]. Algorithms for diagnosis of SBMI based on the patient's hemodynamic status, associated risk factors, and physical examination are available [3,8,16]. These approaches match the patient's presentation to diagnostic tools including diagnostic peritoneal lavange (DPL), CT, ultrasound, and serial examination and observation. This article concentrates on the use of CT.

CT technique

Full CT evaluation of the abdomen in the blunt trauma victim requires scanning from the diaphragm to the ischial tuberosities. Most trauma centers use helical scanners with intravenous and oral contrast (OC) agents for adults and only intravenous contrast for children. Intravenous iodinated contrast material is administered by rapid injection, at rates of between 1 and 3 mL/second, ideally by a 19-guage antecubital catheter. Children receive 2 to 3 mL of intravenous contrast per kilogram body weight. Approximately 500 to 750 mL of a water-soluble agent diluted to a concentration of 1% to 2% is the standard for OC. This should be administered orally or by nasogastric

tube as soon as the CT is ordered to allow time for bowel transit. Collimation with helical technique is typically 5 to 7 mm. Scanning commences following an arbitrary delay of about 40 to 60 seconds from the start of intravenous infusion to image the liver in the portal venous phase. Because of the rapid nature of helical scanning, delayed, repeat scanning through the kidneys during contrast excretion may be part of the routine protocol to detect collecting system injury.

The necessity of enteric contrast is a topic of contention in the literature. Those opposed to routine use of OC point to the marginal gain in accuracy of diagnosis and delay imposed by waiting for adequate transit through the bowel in those with potentially life-threatening injuries [26]. At least one published, randomized, prospective trial in the setting of blunt abdominal trauma showed equivalent sensitivities for diagnosis of small bowel injuries in those undergoing CT with or without OC [26]. These findings may be related to the limited amount of opacified bowel caused by posttraumatic ileus [27]. Imposing an average 144-minute delay to allow transit of contrast still demonstrated adequate opacification of small bowel in only a slight majority of patients [28].

The presence of enteric contrast extravasation is an uncommon finding. In the setting of bowel perforation, extravasation of OC in the absence of free air has been reported only once in a recent review of the literature [28] again arguing against its routine use. Although extravasation occurs in only a minority of patients, it is a highly specific sign of transmural bowel laceration. It also may help distinguish loops of bowel from hematoma, delineate the mesentery of the small bowel, and accurately assess bowel wall thickness [29]. Identifying abnormal bowel loops is not the only use for OC. At the authors' institution, filling of normal loops also adds certainty to the finding of a negative CT scan.

There is also the concern for aspiration among those opposed to its routine use, but despite the perceived risks related to the administration of water-soluble OC, this injury is an uncommon complication of CT scanning. Studies have shown few documented adverse events, which likely relates to the very dilute nature of the solution used for CT [30,31]. The misconception that this CT contrast is a danger may be caused by parallels drawn with the more concentrated form of this agent that is routinely used for fluoroscopy. It is this high osmolar solution that causes lung injury when aspirated.

Justification for either OC protocol can be found in the literature. The authors have chosen to use OC for their trauma CT scans, but are constantly re-evaluating their protocols as newer data appear. In the future, CT may be used earlier in the treatment algorithm, especially if spine and chest evaluation are done with CT rather than plain film. In that case, the short interval available for bowel transit will likely make the use of OC superfluous.

CT findings of SBMI

The constellation of CT findings related to SBMI include bowel discontinuity; extraluminal air; extravasation of enteric or vascular contrast; intramural gas; bowel wall thickening or enhancement; mesenteric infiltration; and intraperitoneal, retroperitoneal, or mesenteric fluid. Direct visualization of bowel discontinuity and extraluminal oral contrast material are virtually diagnostic of bowel perforation but are relatively insensitive. Conversely, free peritoneal fluid is very sensitive for bowel injury, but almost equally nonspecific. A separate discussion of each CT finding serves to clarify the role each has to play in the diagnosis of SBMI.

Bowel discontinuity

Visualization of bowel discontinuity on CT is a pathognomonic finding of injury. Unfortunately, it is rare to identify clearly the two ends of a disrupted loop. This single primary finding of bowel injury is also uncommonly documented in the literature [32]. One must rely on secondary findings to make the diagnosis of small bowel injury. Mesenteric tears are always suspected on the basis of secondary findings with no literature reports of primary visualization.

Extraluminal air

Depending on the perforated bowel loop's location, extraluminal air can be found in either the peritoneum or retroperitoneum. Free intraperitoneal air is typically seen along the anterior parietal peritoneum, in the perihepatic or perisplenic regions, trapped in leaves of mesentery, or seen outlining retroperitoneal structures. Pneumoperitoneum may be massive and identified easily or more often subtle and easily missed during rapid review of a trauma victim's studies. Viewing the abdominal images at lung window settings (window width 1500, level 100) can assist in identification of free air (Fig. 1). The protocol at film-based institutions generally calls for lung windows only at the diaphragm level where the lung bases are visible. Filming all levels at both soft tissue and lung window settings is prohibitive in terms of film cost and management. Advances in

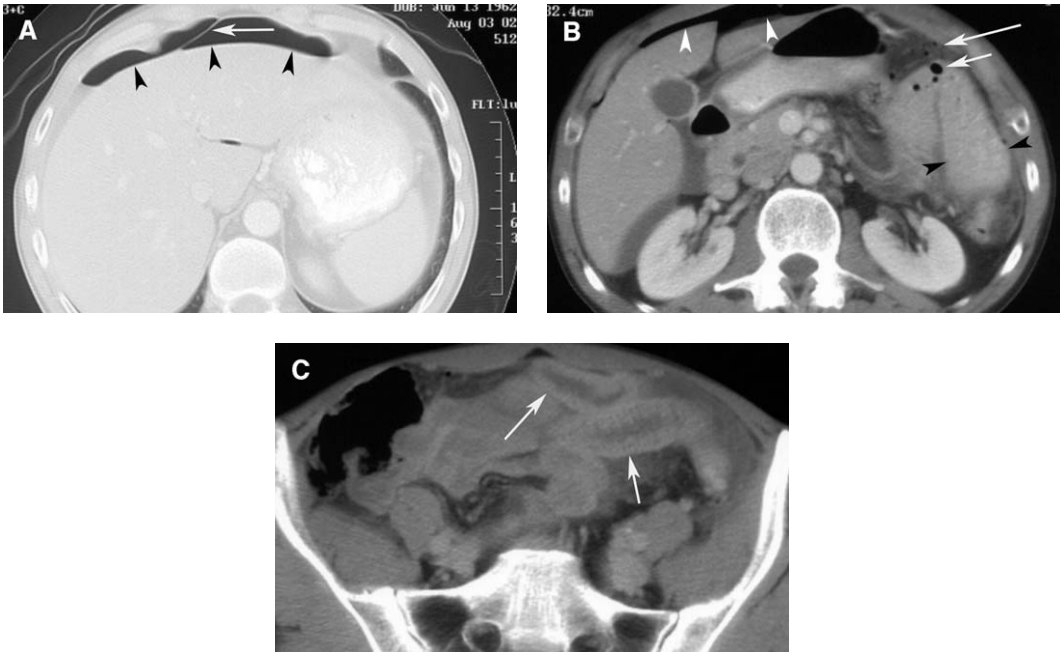

Fig. 1. A 40-year-old bicyclist hit by car with 2-cm jejunal laceration. (*A*) Free air clearly outlines liver surface (*arrowheads*) and falciform ligament (*arrow*) on lung windows (width 1800 level minus 600). (*B*) Large anterior collection of free air (*white arrowheads*), thick-walled jejunum (*black arrowheads*), adjacent subtle mesenteric fold air bubbles (*long arrow*), and intramural air (*short arrow*) are present. (*C*) Thick-walled, enhancing ileum (*arrows*) distal to injury may be localized area of shock bowel.

technology are making it easier to detect free air. Reviewing studies at a PACS or dedicated CT workstation allows one easily to adjust the parameters so the entire study can be viewed with both soft tissue and lung windows.

Because of the normal absence of air in most parts of the small bowel the sensitivity of free intraperitoneal air is approximately 50% to 75% depending on the study [33–36]. Pneumoretroperitoneum can also be identified. Duodenal perforation is often associated with adjacent extraluminal air and fluid [4,37]. The air may also follow fascial planes and can be found some distance from the site of laceration (Fig. 2).

Care must be exercised when incorporating the finding of intraperitoneal or retroperitoneal air into the differential diagnosis. Although bowel perforation is the most likely etiology, there are other sources for the air. Barotrauma and mechanical ventilation have

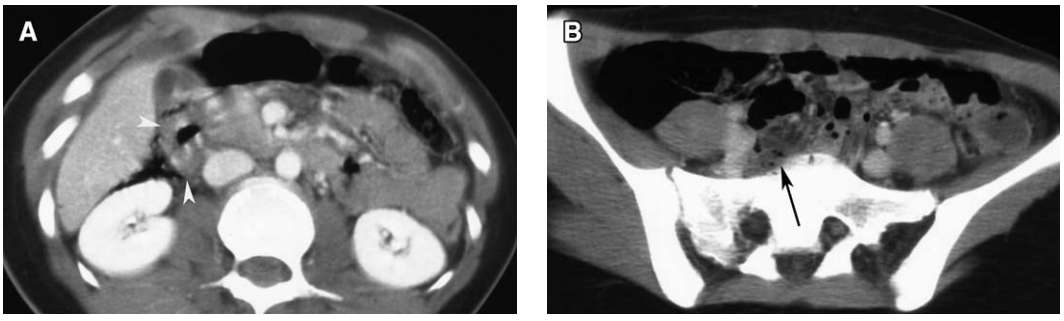

Fig. 2. A 12-year-old girl with second portion duodenal perforation. (*A*) Extraluminal, retroperitoneal air abutting thick-walled duodenum (*arrowheads*). (*B*) Small foci of air distal to perforation at level of sacral promontory (*arrow*). (*From* Brody JM, Leighton DB, Murphy BL, et al. CT of blunt trauma bowel and mesenteric injury: typical findings and pitfalls in diagnosis. Radiographics 2000;20:1527; with permission.)

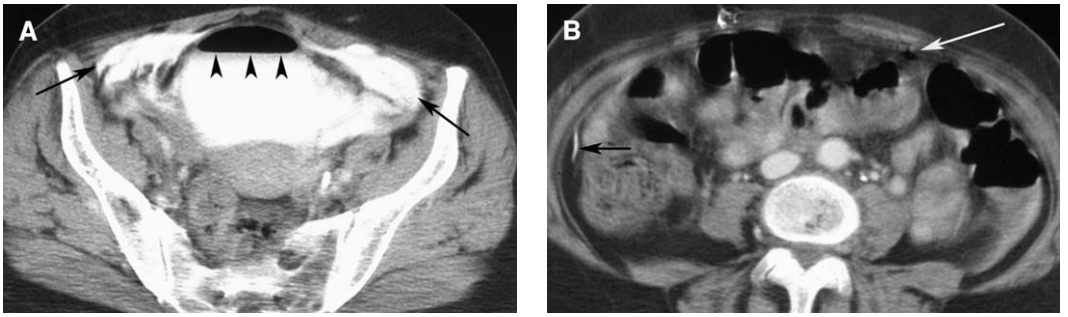

Fig. 3. A 77-year-old woman with intact bowel and mesentery, but extraperitoneal bladder rupture. (*A*) Intravesical air and contrast level (*arrowheads*) and perivesicle, extraperitoneal contrast (*arrows*). (*B*) Abdominal wall motion artifact blurs air in properitoneal space (*white arrow*). Air was introduced retrograde during cystogram. Properitoneal contrast is seen (*black arrow*).

been reported to result in infradiaphragmatic air [37,38]. DPL or bladder rupture with introduction of air during CT cystography can also be misleading in both adults and children (Fig. 3) [39]. Microperforations or pneumatosis cystoides intestinalis, which transmit gas into the peritoneum and then seal off, may be the source of free air in patients with abdominal trauma and none of the aforementioned other causes of extraluminal air. The latter entity is caused by subserosal air-filled cysts, which are the result of microperforation into the intestinal serosa and have been reported in the setting of blunt abdominal trauma [40]. Whenever extraluminal air is identified a diligent search should continue for other secondary signs of bowel injury or other sources of the free air.

Intramural air

Intramural air is seen as discrete bubbles in thickened bowel wall. Despite its intramural nature, this suggests a full-thickness rather than partial thickness injury (Fig. 4) [41]. Along with free intraperitoneal or retroperitoneal air, the finding indicates that surgical therapy is likely required to prevent peritonitis and sepsis as the sequelae of a significant bowel injury [1].

Extraluminal oral contrast material

Extraluminal oral contrast is the one pathognomonic finding of bowel perforation (Figs. 5, 6). The presence of ileus in the victim may preclude significant bowel opacification and subsequent extravasation. This is the likely cause for sensitivities reported in the literature of 12% or less [28,35,36]. False-positive findings may be caused by incorrect interpretation of iodinated contrast from intraperitoneal bladder rupture or vascular hemorrhage from perforated bowel. Other secondary findings and comparing the density of free contrast with that of intra-arterial, intracystic, and enteric contrast should lead one to the correct etiology (see later).

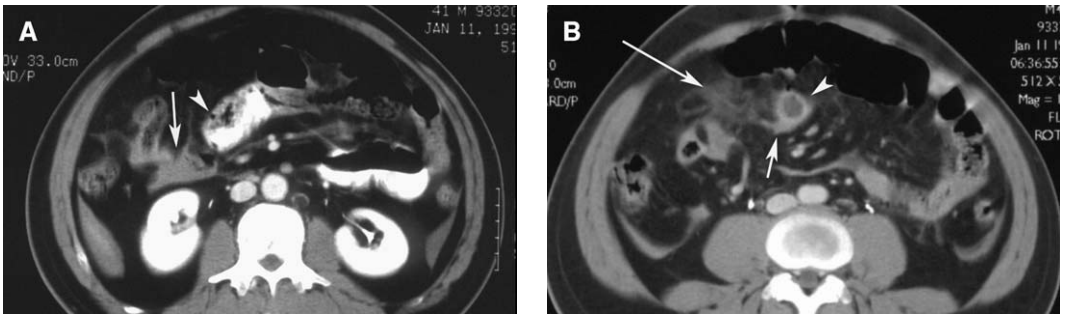

Fig. 4. Proximal ileal perforation in 41-year-old man. (*A*) Intramural air in the ileum (*arrowhead*) with adjacent interloop free fluid (*arrow*). (*From* Brody JM, Leighton DB, Murphy BL, et al. CT of blunt trauma bowel and mesenteric injury: typical findings and pitfalls in diagnosis. Radiographics 2000;20:1528; with permission.) (*B*) Noncontiguous section with bowel wall thickening (*arrowhead*), adjacent fluid (*short arrow*), and mesenteric stranding (*long arrow*).

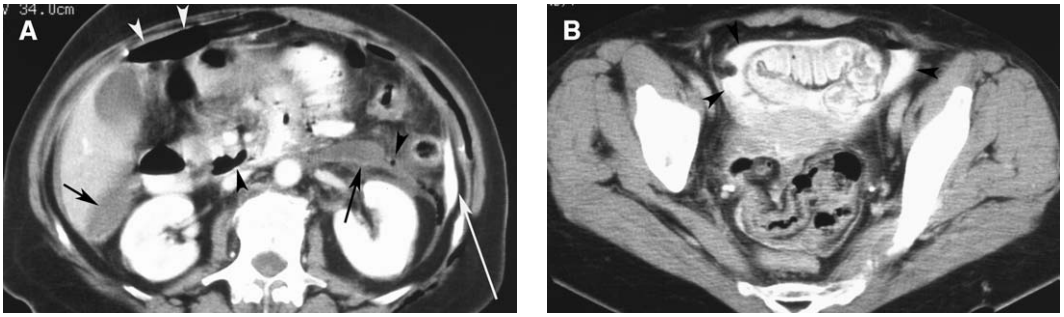

Fig. 5. A 65-year-old woman with duodenal and jejunal perforations. (*A*) Large amount of free intraperitoneal air (*white arrowheads*), oral contrast (*long white arrow*), and fluid (*short black arrow*) from jejunal perforation and retroperitoneal air (*black arrowheads*) and fluid (*long black arrow*) from duodenal perforation. (*B*) Extraluminal intraperitoneal contrast surrounding a pelvic small bowel loop (*black arrowheads*). (*From* Brody JM, Leighton DB, Murphy BL, et al. CT of blunt trauma bowel and mesenteric injury: typical findings and pitfalls in diagnosis. Radiographics 2000;20:1527; with permission.)

Bowel wall thickening

Contusions and lacerations of bowel and isolated mesenteric lacerations that result in ischemia because of disruption of the arterial supply or venous drainage may cause wall thickening. It is reportedly present in up to 61% of SBMI cases [33]. The interpretation of this sign is more subjective than others. Measured wall thickness greater than 3 or 4 mm on at least two contiguous images has been suggested as a way of better quantifying this abnormality [1,29,33,34]. This measurement is not absolute because the degree of luminal distention affects apparent thickness. A combination of observations including disproportionate thickening of the involved segment compared with adjacent bowel loops and circumferential involvement are necessary to identify truly injured segments (see Fig. 6) [41–43].

Rarely, eccentric thickening can be related to injury. It has been described in the presence of intramural hematoma and the authors have seen it with intramural air (see Fig. 4). Care must be taken in evaluating possible eccentric wall thickening because normal bowel with small amounts of air distention may have dependent thickening but demonstrate a normal thin wall outlined by gas along the mucosal surface in the nondependent position. Other secondary findings, such as free air and adjacent free fluid, are indicative of true injury.

Mesenteric infiltration

Mesenteric infiltration or stranding refers to the presence of ill-defined increased attenuation in the normally fatty mesenteric folds caused by perivascular hemorrhage and inflammatory infiltrate [2]. Mes-

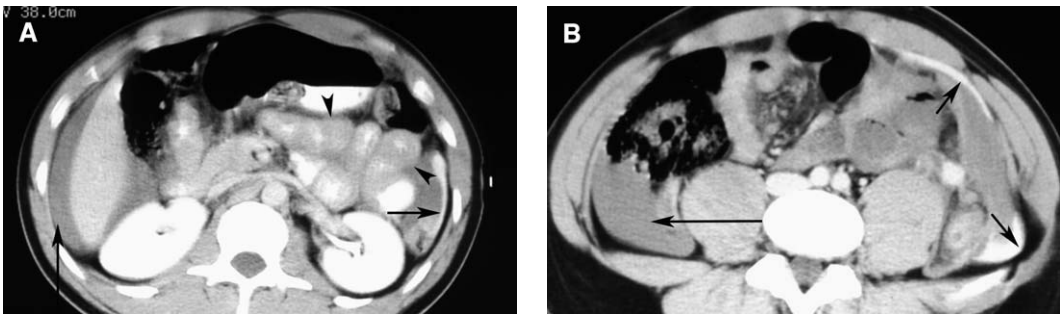

Fig. 6. A 35-year-old man with 10-cm jejunal laceration and descending colon mesentery avulsion. (*A, B*) Thick-walled jejunal loops (*arrowheads*), extraluminal enteric contrast (*short arrow*), and hemoperitoneum (*long arrow*) are seen.

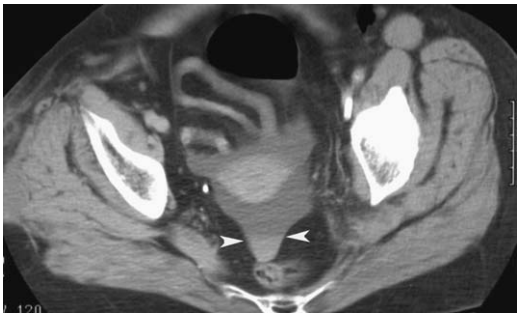

Fig. 7. A 75-year-old woman with multiple mesenteric tears. Fluid-fluid level of hemoperitoneum with dependent clot (*arrowheads*) outlines uterus. (*From* Brody JM, Leighton DB, Murphy BL, et al. CT of blunt trauma bowel and mesenteric injury: typical findings and pitfalls in diagnosis. Radiographics 2000;20:1532; with permission.)

enteric vessels with their tubular appearance and well-defined margins should not be mistaken for stranding, but may be obscured by its presence. Mesenteric tears with or without bowel injury can be associated with mesenteric infiltration. The additional observation of bowel wall thickening increases diagnostic certainty (see Fig. 4) [1,43].

Intraperitoneal fluid

Free intraperitoneal fluid is a common finding in patients with SBMI and in one report was the most frequent sign [44]. It may or may not be hemorrhagic. Succus entericus from small bowel perforation is typically less than 20 Hounsfield units (HU), whereas hemoperitoneum has an intermediate density with a mean of 45 HU [35]. Hemoperitoneum also can manifest as fluid-fluid levels with dependent clot (Figs. 7, 8).

Although hemoperitoneum characteristically has the appearance of high-density ascites, in up to 24% of acute cases it may have attenuation values of less than 20 HU and appear like the simple fluid discussed previously. Intermixing of blood and succus entericus or urine, prolonged delay between the trauma and CT examination, anemia, or addition of peritoneal lavage fluid may cause this low Hounsfield measurement. So as not to mislead clinical staff, radiologists should be

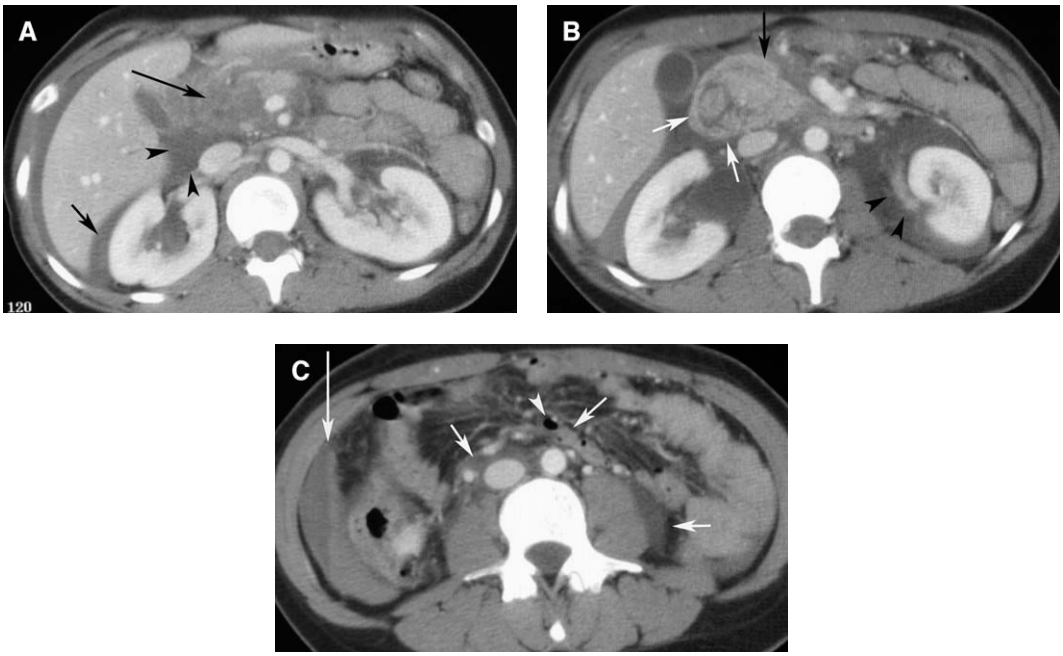

Fig. 8. A 27-year-old woman in motor vehicle accident with 80% circumferential second portion duodenum tear, pancreatic head lacerations, splenic rupture, and renal lacerations. (*A*) Retroperitoneal fluid (*black arrowheads*) around devitalized pancreatic head segment (*long black arrow*) and intraperitoneal blood from spleen injury (*short black arrow*). (*B*) Thick-walled duodenum with intramural hematoma (*short white arrows*) and disrupted, enhancing pancreatic head (*short black arrow*). Hemorrhage from renal laceration (*black arrowheads*). (*C*) Right colic gutter hemoperitoneum fluid-fluid level (*long white arrow*) from spleen injury in vertical orientation caused by victim position at time of clotting. Retroperitoneal fluid (*short white arrows*) and punctuate focus of retroperitoneal air (*arrowhead*) from duodenal, renal, and pancreatic injuries.

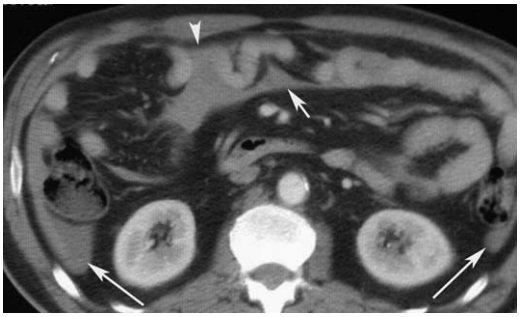

Fig. 9. A 55-year-old man with large mesenteric laceration and hematoma. Blood in polygonal shape between loops of small bowel (*arrowhead*) and mesenteric folds (*short arrow*). Free fluid outlining colic gutters (*long arrows*).

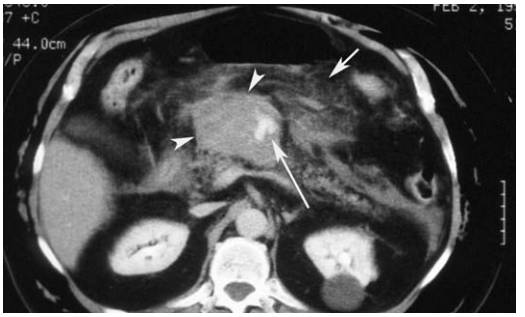

Fig. 11. Mesenteric branch tear in 65-year-old status post motor vehicle accident. High-attenuation extravasation (*long arrow*) surrounded by unopacified blood (*arrowheads*) and mesenteric stranding (*short arrow*).

careful to label fluid as hemoperitoneum only when it is of sufficient density.

Although commonly present in cases of SBMI, free fluid is not diagnostic of SBMI. The false-positive rate in one series was 67% for this single finding. This is likely caused by the frequent presence of fluid related to other injuries [45].

Location may be more important than attenuation in this circumstance. Fluid isolated to the mesentery is an unusual finding in liver or spleen injury and suggests underlying SBMI. Even in the presence of solid organ laceration it should raise the possibility of a SBMI [18,35]. Identifying hematoma in the mesentery has a high specificity (88%) for SBMI [36]. Localized mesenteric hematoma adjacent to bowel wall thickening suggests bowel injury, whereas the absence of bowel abnormality suggests isolated mesenteric injury [46]. Mesenteric fluid manifests as a well-defined, polygonal or triangular shape bordered by loops of bowel or folds of mesentery (Fig. 9). The algorithm outlined by Hughes and Elton [8] and endorsed by others [47] uses DPL to investigate this finding further when the diagnosis remains uncertain.

High-attenuation fluid (> 150 HU) results from escape of OC through a bowel perforation, leak of contrast from an intraperitoneal bladder rupture during CT cystography, or extravasation of intravenous contrast media from active arterial hemorrhage [18]. Hemorrhage is manifest as a blush of increased attenuation that is similar in density to enhanced arteries on the same image. This allows definitive diagnosis of mesenteric vascular injury. The extravasated contrast is often surrounded by a larger area of unopacified clotted blood (Figs. 10,11).

Retroperitoneal fluid

Sources of retroperitoneal fluid include hemorrhage, bowel perforation, renal injury, and pancreati-

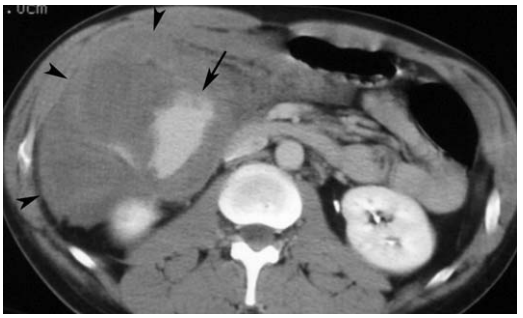

Fig. 10. A 38-year-old man status post head-on car versus snowplow accident with middle colic artery laceration. High-attenuation, active extravasation (*arrow*) with surrounding unopacified blood (*arrowheads*).

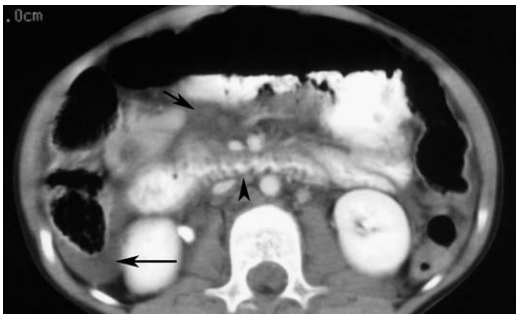

Fig. 12. A 40-year-old man with duodenal hematoma. Thick folds in third portion duodenum (*arrowhead*). Small amount of mesenteric (*short arrow*) and intraperitoneal fluid (*long arrow*).

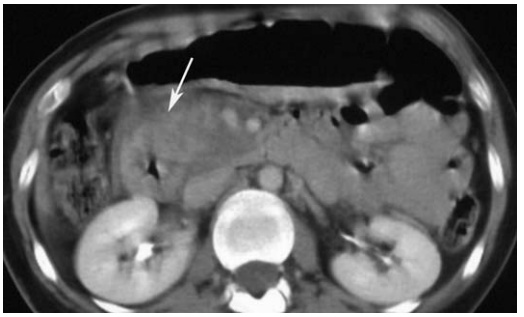

Fig. 13. A 36-year-old woman with pancreatic and duodenal contusion without perforation. Thick-walled duodenum (*arrow*) with blood adjacent to bowel and in mesentery. No free air is seen. Pancreas appeared normal on other images (not shown).

cobiliary laceration. Injuries of the duodenum leading to hematoma or perforation most commonly involve the second (descending) and third (horizontal) segments [40]. The distinction between hematoma and perforation is important because the latter represents a surgical emergency with as high as a 65% mortality rate in the setting of delayed diagnosis [48,49]. Intramural hematoma is seen on CT as diffuse fold thickening or as a high-attenuation mass with narrowing or obstruction of the duodenal lumen. Extraluminal fluid itself cannot be used to differentiate hematoma from perforation (Figs. 12, 13) [42]. Small amounts of fluid may make perforation less likely. In general, when larger amounts of fluid are present duodenal perforation should be suspected [40]. The fluid tends to accumulate in a periduodenal location or in the right anterior pararenal space (Fig. 14) [48]. It can also track caudally along the ascending colon [49]. Pancreatic or biliary injuries may also occur in up to 25% of patients with duodenal injuries and should be considered along with duodenal injury when fluid is present in the retroperitoneum (see Fig. 8) [49].

Bowel wall enhancement

The definition of bowel wall enhancement is attenuation greater than that of the psoas muscle or equal to that of adjacent blood vessels. The observation is often based on empiric assessment [41]. The most striking example was originally described as a diffuse bowel abnormality in young children, particularly those 2 years of age or younger. They presented with severe hemodynamic derangement and most ultimately died of their injuries [50,51]. This enhancement pattern was part of a hypoperfusion complex that included CT findings of diminished aorta and inferior vena cava caliber; intense contrast enhancement of the renal parenchyma; and dilated, thick-walled, fluid-filled small bowel loops. Free fluid also is often present.

Adults can also show diffuse bowel wall enhancement and other signs of hypoperfusion complex, but this does not predict the same potential for fatal outcome seen in the pediatric population (Fig. 15). It has been termed "shock bowel," which also is indicative of the improved clinical course that results from volume resuscitation [52]. The enhancement is related to increased permeability of bowel wall caused by ischemia that leads to wall thickening and increased attenuation from interstitial leak of intravenous contrast material [52].

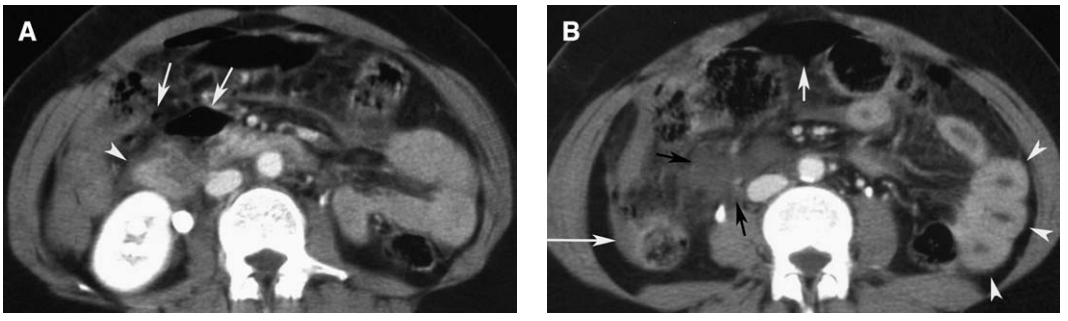

Fig. 14. A 46-year-old woman with second portion duodenum transection and right colon perforation. (*A*) Irregular, thick duodenal wall with adjacent extraluminal fluid (*arrowhead*) and air (*short arrows*). (*B*) Intraperitoneal air (*short white arrow*), periduodenal fluid (*short black arrow*), and gutter fluid (*long arrow*) from the colon perforation and thick-walled small bowel (*arrowheads*) are visible. The small bowel was normal at surgery.

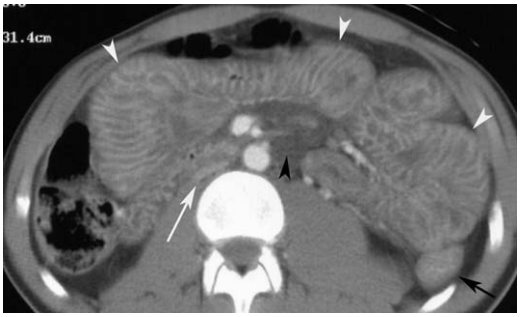

Fig. 15. A 23-year-old man with shock bowel from left femoral head posterior dislocation and acetabular fracture causing hemorrhage. There were no abdominal injuries but severe hypotension and cardiac arrest. He survived after fluid resuscitation. Thick-walled small bowel with enhancement of valvulae conniventes (*white arrowheads*), collapsed inferior vena cava (*long white arrow*), mesenteric fluid (*black arrowhead*), and normal colon (*short black arrow*).

In children and adults the findings are caused by hypoperfusion and not necessarily bowel injury. If bowel or mesenteric damage is present, however, it can contribute to hypotension. Bowel wall thickening of the hypoperfusion complex makes it difficult to make the diagnosis of bowel injury unless other signs, such as free air, are present. Separating those patients with traumatic bowel injury from those with signs of shock bowel on CT becomes important for clinical management of adults because the latter finding alone is not an indication for laparotomy [16]. The authors have not seen classic shock bowel with associated bowel injury at their institution, but did have a situation where there was a more localized region of enhancing, dilated bowel distal to an injured segment (see Fig. 1C).

Performance of CT signs of SBMI

Assessment of the efficacy of CT for SBMI is difficult. These are uncommon injuries and may be present along with other causes of positive CT scans, such as liver laceration. The diagnostic findings of extraluminal OC, free intraperitoneal air, and active hemorrhage are uncommon. Many early studies published on the subject of SBMI were limited by these issues and were based on data from slow, older, nonhelical scanners. These diagnostic impediments have led a recent surgical trauma text to question the role of CT in detecting bowel injury [16]. Recent work using faster helical CT and standardized protocols, however, is more indicative of the role this modality plays in evaluating for SBMI [36,45].

In a retrospective study using trauma radiologists as readers, an accuracy of 86%, a sensitivity of 94%, and a positive predictive value of 92% were achieved for bowel injury [36]. Clinical efficacy also was explored by this group by looking at the ability of CT to predict the need for laparotomy versus simply identifying injury in these patients (ie, those with bowel perforation). Extraluminal air, OC, or free fluid seen on greater than three consecutive CT sections without solid organ injury were used as surgical indicators. Sensitivity of 92%, specificity of 97%, accuracy of 86%, with positive and negative predictive values of 96% was reported. Given the relatively nonspecific finding of free fluid the quantification of greater than three contiguous sections as significant is a helpful observation.

This same report evaluated mesenteric injury as a separate category using typical signs for this injury of mesenteric infiltration or hematoma, active extravasation of vascular contrast, or signs of bowel injury [36]. The sensitivity of 99%, accuracy of 96%, and positive predictive value of 97% point out the value of CT. Predicting the need for surgical therapy was less successful than for bowel injury. Using active extravasation and combined mesenteric hematoma and bowel wall thickening resulted in a sensitivity of 37%, accuracy of 96%, and positive predictive value of 83%.

A study that more likely mirrors actual experience was done by Malhotra et al [45]. They evaluated prospective interpretations by both daytime staff trauma radiologists and overnight on-call residents. SBMI were considered together rather than separately in statistical evaluation and free fluid was not quantified. Sensitivity of 88%, accuracy of 99%, positive predictive value of 53%, and negative predictive value of 99% were reported. The significant finding in this paper was the observation that there was a statistically significant increase in likelihood of injury with an increase in number of findings. This led the authors to suggest a treatment algorithm whereby patients with a single finding should be observed, whereas those with more than one finding suspicious for SBMI should go to laparotomy. An improved true positive rate of 83% results from use of that algorithm.

Summary

Helical CT now allows rapid acquisition of sections through the abdomen and pelvis with optimal vascular opacification and minimal motion artifact. Oral contrast may aid in the identification of subtle

bowel and mesenteric injuries and does not have any significant deleterious effects. CT findings of extraluminal enteric contrast, active hemorrhage, or free intraperitoneal-retroperitoneal air allow accurate diagnosis of SBMI in the setting of blunt abdominal trauma. Mesenteric hematoma in association with bowel wall thickening or the presence of significant amounts of free fluid without solid organ injury is highly suspicious for SBMI requiring laparotomy. CT alone or in concert with DPL and physical examination is a valuable tool in the timely diagnosis and treatment of bowel and mesenteric injury caused by blunt trauma.

References

[1] Dowe MF, Shanmuganathan K, Mirvis SE, Steiner RC, Cooper C. CT findings of mesenteric injury after blunt trauma: implications for surgical intervention. AJR Am J Roentgenol 1997;168:425–8.

[2] Hagiwara A, Yukioka T, Satou M, et al. Early diagnosis of small intestine rupture from blunt abdominal trauma using computed tomography: significance of the streaky density within the mesentery. J Trauma 1995;38:630–3.

[3] Frick Jr EJ, Pasquale MD, Cipolle MD. Small-bowel and mesentery injuries in blunt trauma. J Trauma 1999;46:920–6.

[4] Glazer GM, Buy JN, Moss AA, Goldbert HI, Federle MP. CT detection of duodenal perforation. AJR Am J Roentgenol 1981;137:333–6.

[5] Jeffrey RB, Federle MP, Stein SM, Crass RA. Case report: intramural hematoma of the cecum following blunt trauma. J Comput Assist Tomogr 1982;6:404–5.

[6] Nance ML, Peden GW, Shapiro MB, Kauder DR, Rotondo MF, Schwab CW. Solid viscous injury predicts major hollow viscous injury in blunt abdominal trauma. J Trauma 1997;43:618–22.

[7] Buckman Jr RF, Piano G, Dunham CM, Soutter I, Ramzy A, Militello PR. Major bowel and diaphragmatic injuries associated with blunt spleen or liver rupture. J Trauma 1988;28:1317–21.

[8] Hughes TMD, Elton C. The pathophysiology and management of bowel and mesenteric injuries due to blunt trauma injury. Int J Care Injured 2002;33:295–302.

[9] Cobb LM, Vinocur CD, Wagner CW, Weintraub WH. Intestinal perforation due to blunt trauma in children in an era of increased non-operative treatment. J Trauma 1986;26:461–3.

[10] Scalea T, Goldstein A, Phillips T, et al. An analysis of 161 falls from a height: the jumper syndrome. J Trauma 1986;26:706–11.

[11] Razaboni RM, Braithwaite CEM, Dwyer WA. Ruptured jejunum following Heimlich maneuver. J Emerg Med 1986;4:95–8.

[12] Chandler CF, Lane JS, Waxman KS. Seatbelt sign following blunt trauma is associated with increased incidence of abdominal injury. Am Surg 1997;63:885–8.

[13] Legay DA, Petrie DP, Alexander DI. Flexion-distraction injuries of the lumbar spine and associated abdominal trauma. J Trauma 1990;30:436–44.

[14] Dischinger P, Ho S, Kerns T, Brennan P. Patterns of injury in frontal collisions with and without airbags. In: IRCOBI Conference Proceedings. Bron, France: IRCOBI; 1996. p. 311–9.

[15] Wilson RF, Walt AJ. Injury to the stomach and small bowel. In: Wilson RF, Walt AJ, editors. Management of trauma, pitfalls and practice. 2nd edition. Baltimore: Williams & Wilkins; 1996. p. 497–509.

[16] Wisner DH. Stomach and small bowel. In: Mattox KL, Feliciano DV, Moore EE, editors. Trauma. 4th edition. New York: McGraw-Hill; 2000. p. 713–34.

[17] Slavin RE, Borzotta AP. The seromuscular tear and other intestinal lesions in the seatbelt syndrome: a clinical and pathologic study of 29 cases. Am J Forensic Med Pathol 2002;23:214–22.

[18] Nghiem HV, Jeffrey RB, Mindelzun RE. CT of blunt trauma to the bowel and mesentery. Semin Ultrasound CT MR 1995;16:82–90.

[19] Tsushima Y, Yamada S, Aoki J, Endo K. Ischaemic ileal stenosis following blunt abdominal trauma and demonstrated by CT. Br J Radiol 2001;74:277–9.

[20] Buck III GC, Dalton ML, Neely WA. Diagnostic laparotomy for abdominal trauma: a university hospital experience. Am Surg 1986;52:41–3.

[21] Miller FB, Cryer HM, Chilikuri S, Creech P, Richardson JD. Negative findings on laparotomy for trauma. South Med J 1989;82:1231–4.

[22] Konstantakos AK, Barnoski AL, Plaisier BR, Yowler CJ, Fallon Jr WF, Malangoni MA. Optimizing the management of blunt splenic injury in adults and children. Surgery 1999;126:805–12.

[23] Sorenson VJ, Mikhail JN, Karmy-Jones RC. Is delayed laparotomy for blunt abdominal trauma a valid quality improvement measure in the era of nonoperative management of abdominal injuries? J Trauma 2002;52:426–33.

[24] Fakhry SM, Brownstein M, Watts DD, Baker CC, Oller D. Relatively short diagnostic delays (< 8 hours) produce morbidity and mortality in blunt small bowel injury: an analysis of time to operative intervention in 198 patients from a multicenter experience. J Trauma 2000;48:408–14.

[25] Brownstein MR, Bunting T, Meyer AA, Fakhry SM. Diagnosis and management of blunt small bowel injury: a survey of the membership of the American Association for the Surgery of Trauma. J Trauma 2000;48:402–7.

[26] Stafford RE, McGonigal MD, Weigelt JA, Johnston TJ. Oral contrast solution and computed tomography for blunt abdominal trauma: a randomized study. Arch Surg 1999;134:622–6.

[27] Shankar KR, Lloyd DA, Kitteringham L, Carty HM. Oral contrast with computed tomography in the eval-

uation of blunt abdominal trauma in children. Br J Surg 1999;86:1073–7.
[28] Tsang BD, Panacek EA, Brant WE, Wisner DH. Effect of oral contrast administration for abdominal computed tomography in the evaluation of acute blunt trauma. Ann Emerg Med 1997;30:7–13.
[29] Mirvis SE, Gens DR, Shanmuganathan K. Rupture of the bowel after blunt abdominal trauma: diagnosis with CT. AJR Am J Roentgenol 1992;159:1217–21.
[30] Federle MP, Yagan N, Petizman AB, Krugh J. Abdominal trauma: use of oral contrast for CT is safe. Radiology 1997;205:91–3.
[31] Lim-Dunham JE, Narra J, Benya EC, Donaldson JS. Aspiration after administration of oral contrast material in children undergoing abdominal CT for trauma. AJR Am J Roentgenol 1997;169:1015–8.
[32] Sherck JP, Oakes DD. Intestinal injuries missed by computer tomography. J Trauma 1990;30:1–7.
[33] Rizzo MJ, Federle MP, Griffiths BG. Bowel and mesenteric injury following blunt abdominal trauma: evaluation with CT. Radiology 1989;173:143–8.
[34] Breen DJ, Janzen DL, Zwirewich CV, Nagy AG. Blunt bowel and mesenteric injury: diagnostic performance of CT signs. J Comput Assist Tomogr 1997;21:706–12.
[35] Levine CD, Gonzales RN, Wachsberg RH. CT findings in bowel and mesenteric injury. J Comput Assist Tomogr 1997;21:974–9.
[36] Killeen KL, Shanmuganathan K, Poletti PA, Cooper C, Mirvis SE. Helical computed tomography of bowel and mesenteric injuries. J Trauma 2001;51:26–36.
[37] Kane NM, Francis IR, Burney RE, Wheatley MJ, Ellis JH, Korobkin M. Traumatic pneumoperitoneum: implications of computed tomography diagnosis. Invest Radiol 1991;26:574–8.
[38] Cook DE, Walsh JW, Vick CW, Brewer WH. Upper abdominal trauma: pitfalls in CT diagnosis. Radiology 1986;159:65–9.
[39] Bulas DI, Taylor GA, Eichelberger MR. The value of CT in detecting bowel perforation in children after blunt abdominal trauma. AJR Am J Roentgenol 1989;153:561–4.
[40] Raptopoulos V. Abdominal trauma: emphasis on computed tomography. Radiol Clin North Am 1994;32:969–87.
[41] Brody JM, Leighton DB, Murphy BL, Abbott GF, Vaccaro JP, Jagminas L, et al. CT of blunt trauma bowel and mesenteric injury: typical findings and pitfalls in diagnosis. Radiographics 2000;20:1525–36.
[42] Kunin JR, Korobkin M, Ellis JH, Francis IR, Kane NM, Siegel SE. Duodenal injuries caused by blunt abdominal trauma: value of CT in differentiating perforation from hematoma. AJR Am J Roentgenol 1993;160:1221–3.
[43] Strouse PJ, Close BJ, Marshall KW, Cywes R. CT of bowel and mesenteric trauma in children. Radiographics 1999;19:1237–50.
[44] Halvorsen A, McKenney K. Blunt trauma to the gastrointestinal tract: CT findings with small bowel and colon injuries. Emerg Radiol 2002;9:141–5.
[45] Malhotra AK, Fabian TC, Katsis SB, Gavant ML, Croce MA. Blunt bowel and mesenteric injuries: the role of screening computed tomography. J Trauma 2000;48:998–1000.
[46] Shanmuganathan K, Mirvis SE, Reaney SM. Pictorial review: CT appearance of contrast medium extravasations associated with injury sustained from blunt abdominal trauma. Clin Radiol 1995;50:182–7.
[47] Gonzalez RP, Ickler J, Gachassin P. Complementary roles of diagnostic peritoneal lavage and computed tomography in the evaluation of blunt abdominal trauma. J Trauma 2001;51:1128–34.
[48] Roberts JL, Dalen K, Bosanko CM, Jafir SZ. CT in abdominal and pelvic trauma. Radiographics 1993;13:735–52.
[49] Cox TD, Kuhn JP. CT scan of bowel trauma in the pediatric patient. Radiol Clin North Am 1996;34:807–18.
[50] Taylor GA, Fallat ME, Eichelberger MR. Hypovolemic shock in children: abdominal CT manifestations. Radiology 1987;164:479–81.
[51] Sivit CJ, Eichelberger MR, Taylor GA. CT in children with rupture of the bowel caused by blunt trauma: diagnostic efficacy and comparison with hypoperfusion complex. AJR Am J Roentgenol 1994;163:1195–8.
[52] Mirvis SE, Shanmuganathan K, Erb R. Diffuse small-bowel ischemia in hypotensive adults after blunt trauma (shock bowel): CT findings and clinical significance. AJR Am J Roentgenol 1994;163:1375–9.

RADIOLOGIC CLINICS OF NORTH AMERICA

Radiol Clin N Am 41 (2003) 1183–1201

Spontaneous intraperitoneal hemorrhage: imaging features

Koenraad J. Mortele, MD[a,*], Vito Cantisani, MD[a,b], Douglas L. Brown, MD[a], Pablo R. Ros, MD, MPH[a]

[a]*Division of Abdominal Imaging and Intervention, Department of Radiology, Brigham and Women's Hospital, 75 Francis Street, Boston, MA 02115, USA*

[b]*Department of Radiology, University "La Sapienza", 325 Viale Regina Elena, 00167 Rome, Italy*

Intraperitoneal hemorrhage may result from known conditions, such as bleeding diathesis or blunt abdominal trauma, or may be idiopathic, unrelated to known causes. The latter condition may result from several incidentally discovered etiologies, including rupture of a vascular neoplasm, hemorrhagic cyst, or ectopic pregnancy; perforation of a duodenal ulcer or other gastrointestinal pathologies; and inflammatory erosive processes, such as pancreatitis with subsequent pseudocyst or pseudoaneurysm formation.

The clinical presentation of spontaneous abdominal hemorrhage, although variable, frequently consists of sudden abdominal pain and distention associated with an acute drop in hematocrit. Other less common signs include hypovolemic shock and discoloration around the umbilicus and flanks [1]. Signs and symptoms of abdominal hemorrhage may be equivocal, however, and hematocrit levels obtained acutely may not reflect its diagnosis [2]. Blood is only a minor peritoneal irritant and the intensity of abdominal pain is usually related to the rapidity and volume of extravasation [3]. Nevertheless, clinical signs obtained during physical examination also may be independent from the severity and initiation of the intraperitoneal hemorrhage. For example, subcutaneous hemorrhagic infiltration of the periumbilical area (Cullen's sign) can appear with a variable delay after intra-abdominal hemorrhage [4]. Imaging plays a pivotal role in the diagnosis and assessment of this potentially lethal entity.

* Corresponding author.
E-mail address: kmortele@partners.org (K.J. Mortele).

Intraperitoneal bleeding: general imaging features

Detection and localization of the source of acute intra-abdominal hemorrhage is one of the major challenges in the early diagnostic work-up of acute intraperitoneal bleeding, because it is very helpful to provide hemostasis accomplished by means of transarterial embolization or surgery as soon as possible. CT has been shown to be an effective method for detecting abdominal hemorrhage [5,6], with the diagnosis being based on the high-attenuation value of the peritoneal fluid. In the past, with dynamic incremental scanning, the diagnosis of active hemorrhage resulting from visceral organs often depended on indirect signs rather than direct visualization of extravasation of contrast material [7]. More recently, technologic development has led to the introduction of helical CT, which has been shown to be able to detect even small amounts of contrast material in the peritoneal cavity and to show vascular injuries. A second acquisition may be obtained after a short delay to investigate the distribution of extravasated contrast material. The ability to detect active bleeding with helical CT may be considered a major diagnostic improvement, because it enables a more focused therapeutic approach with either radiologic transcatheter embolization or trauma surgery [8,9]. Recently, with the advent of multidetector-row CT scanners, CT is undergoing further improvement, especially for the evaluation of vascular disease, and subsequently in the evaluation of hemorrhagic complications leading to intraperitoneal bleeding.

The CT appearance of intraperitoneal hemorrhage depends on the location, age, and extent of the bleeding. Immediately after hemorrhage, intraperitoneal

0033-8389/03/$ – see front matter
doi:10.1016/S0033-8389(03)00118-0

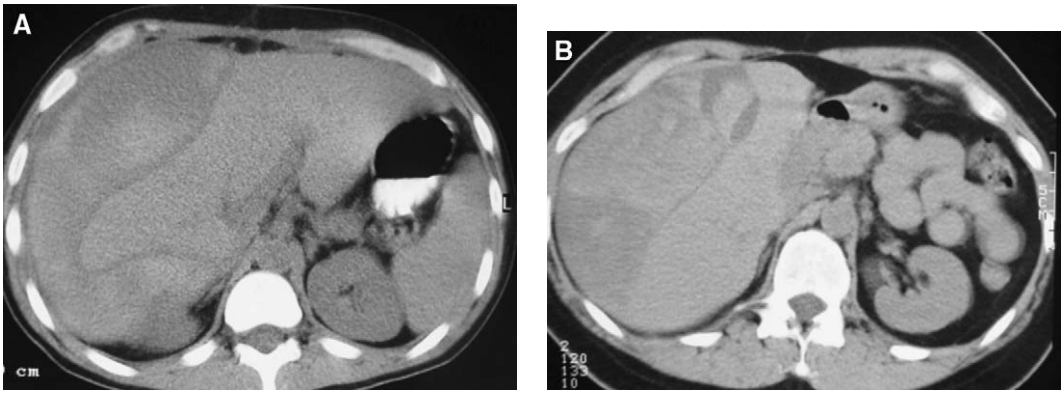

Fig. 1. Axial unenhanced CT images in a patient with spontaneous intraperitoneal bleeding. (*A*) Image obtained at the level of the liver shows increased attenuation of the peritoneal fluid consistent with blood. It appears heterogeneous with nodular areas of high attenuation because of clot formation. (*B*) Image obtained at a lower level again shows the focal areas of clot that are higher attenuation than the free intraperitoneal fluid.

blood has the same attenuation as circulating blood. Within hours, however, the attenuation increases, as hemoglobin is concentrated during clot formation (Fig. 1) [10,11]. In most cases, the attenuation begins to decrease within several days as clot lysis takes place [12]. The attenuation value decreases steadily with time and often approaches that of water (0 to 20 HU) after 2 to 4 weeks [13]. During the hyperacute phase, the attenuation value of intraperitoneal blood ranges from 20 to 90 HU [6,14]. In one large study, all patients with hemoperitoneum less than 48 hours old had fluid collections containing areas of attenuation greater than 30 HU [6]. The morphologic characteristics of recent intraperitoneal hemorrhage are variable. It is important to consider that acute hemoperitoneum can have attenuation values of less than 20 HU [15]. The fluid collections may be homogeneously hypodense or may be heterogeneous with nodular or linear areas of high attenuation surrounded by lower-attenuation fluid. This heterogeneity results from irregular clot resorption or intermittent bleeding [16]. In most cases, intraperitoneal blood contains focal areas of clot that are higher in attenuation than free intraperitoneal blood. These localized clots are helpful in determining the bleeding site, because they usually form adjacent to the organ from which the hemorrhage originated [6]. Occasionally, fresh blood within the peritoneal space may show a hematocrit effect with sedimented erythrocytes producing a dependent layer of high attenuation (Fig. 2). The most common site of blood accumulation on CT scans is Morison's pouch, followed by the right paracolic gutter. With extensive hemorrhage, large collections of blood may fill the pelvis with little blood in upper abdominal sites. It is

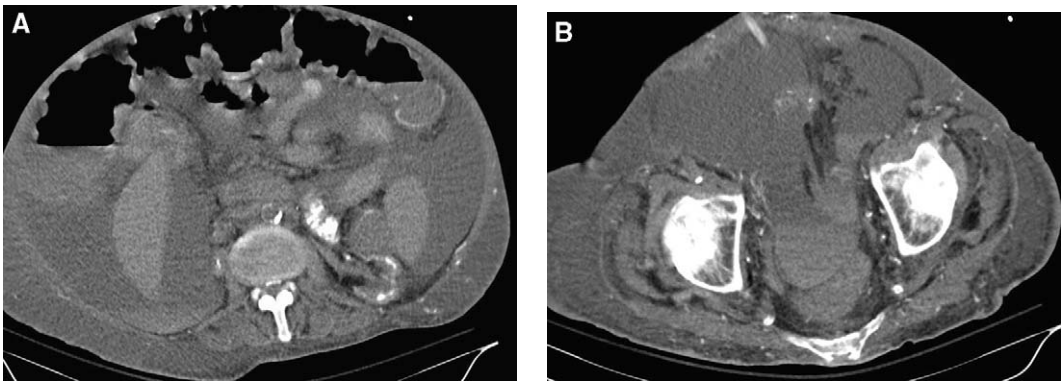

Fig. 2. Axial contrast-enhanced CT images in a patient with spontaneous intraperitoneal bleeding. (*A*) Image obtained at the level of the liver shows fresh blood within the peritoneal space producing a dependent layer of high attenuation (hematocrit effect). (*B*) Image obtained at the level of the pelvis again shows the hematocrit effect indicating fresh hemorrhage.

important to include the pelvis in any CT examination performed for suspected intra-abdominal hemorrhage [6]. Before beginning the examination, adequate oral contrast material should be administered to opacify all abdominal and pelvic bowel loops. If a CT examination without intravenous contrast material has been obtained, viewing the images with a narrow window width is helpful to accentuate the density difference between fresh blood and adjacent soft tissues. In most cases, however, an unenhanced CT examination is unnecessary and one can begin the study with intravenous contrast material administered as a bolus. The contrast enhancement helps to demonstrate abnormality within solid abdominal organs and makes intraperitoneal fluid collections more apparent by increasing the density of surrounding tissues. Extravasation of intravenous contrast material, resulting in an area of fluid whose attenuation is higher than the remainder of the acute hemoperitoneum, is an indicator of significant active bleeding [17].

Although CT is considered the method of choice to diagnose hemorrhage in the upper peritoneal cavity [6], ultrasound (US) has become the modality of choice in evaluating patients for ectopic pregnancy and for detecting hemorrhage in the pelvis. Usually, transvaginal US is favored over transabdominal scanning in these patients [18,19]. Although US is insensitive in detecting injury in solid organs, in these patients it has demonstrated a relatively high sensitivity in detecting free fluid within the lower abdomen. Many different protocols have been used; most include evaluation of perihepatic and perisplenic areas, scans of both paracolic gutters, and the pelvis. Free fluid within the pelvis may be missed if there is no good acoustic

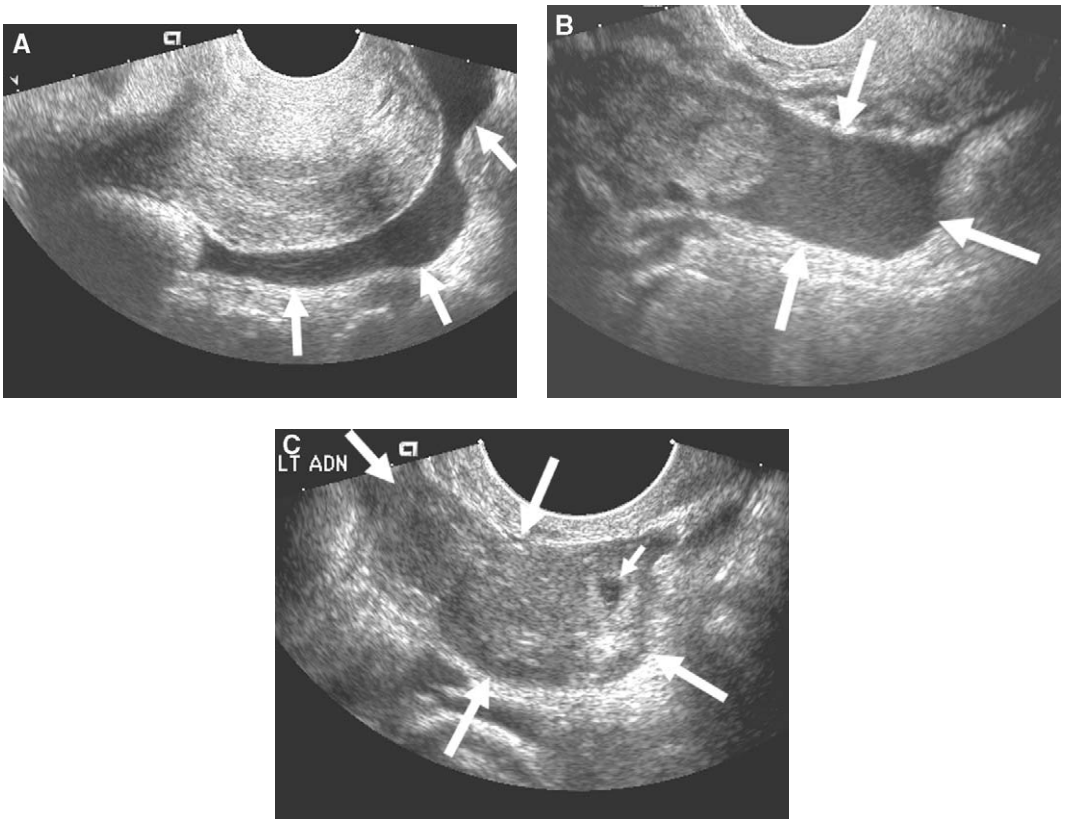

Fig. 3. Transvaginal ultrasound images of a tubal pregnancy with hemoperitoneum. (*A*) Sagittal view shows the cervix with a small amount of fluid (*arrows*) in the cul-de-sac. Low-level internal echoes are present within the fluid. The amount of fluid shown on this image is small, but is slightly more than is typically seen as a normal finding. (*B*) Image of the right adnexa shows more free fluid (*arrows*) with internal echoes, consistent with hemoperitoneum. (*C*) A heterogeneous adnexal mass (*long arrows*) was seen separate from the ovary (not shown). This represented a hematosalpinx, within which there was a small gestational sac (*short arrow*) with a yolk sac.

window, and fluid in the bladder is needed only if transabdominal transducers are used. The sonographic appearance of acute intraperitoneal hemorrhage usually is that of hypoechoic fluid (Fig. 3) [20,21]. There may be mixed echoes in this hypoechoic fluid, isolated echogenic clots, or fluid-fluid interfaces [22]. As clot formation occurs, the US appearance may vary, although the clot is usually hypoechoic compared with solid organs.

MR imaging also can be used to demonstrate intraperitoneal hemorrhage. Many patients referred for suspected intra-abdominal hemorrhage are unstable, however, and require monitoring and supportive equipment, making MR imaging less practical. A hematoma less than 48 hours old may have nonspecific signal intensity features [23]. Intra-abdominal hematoma older than 3 weeks typically has a specific appearance referred to as the ''concentric ring'' sign, in which a thin peripheral rim, dark on all sequences, surrounds a bright inner ring, most distinctive on T1-weighted images [24]. MR imaging can readily distinguish blood from ascites. Acute blood, in the form of deoxyhemoglobin, is low in signal intensity on T2-weighted images. Conversely, subacute blood, in the form of extracellular methemoglobin, has high signal intensity on T1- and T2-weighted images (Fig. 4). The use of fat-suppression techniques accentuates this finding. Hematomas also may demonstrate heterogeneity related to hemoglobin breakdown products admixed with blood. Not infrequently, a high signal intensity rim surrounding a low signal intensity center is seen with subacute hematomas on T1- and T2-weighted images. These imaging characteristics represent extracellular methemoglobin encircling the retracting clot [24]. As hematomas age, a low signal intensity rim develops around the hematoma on both T1- and T2-weighted sequences. This rim corresponds to hemosiderin or fibrosis.

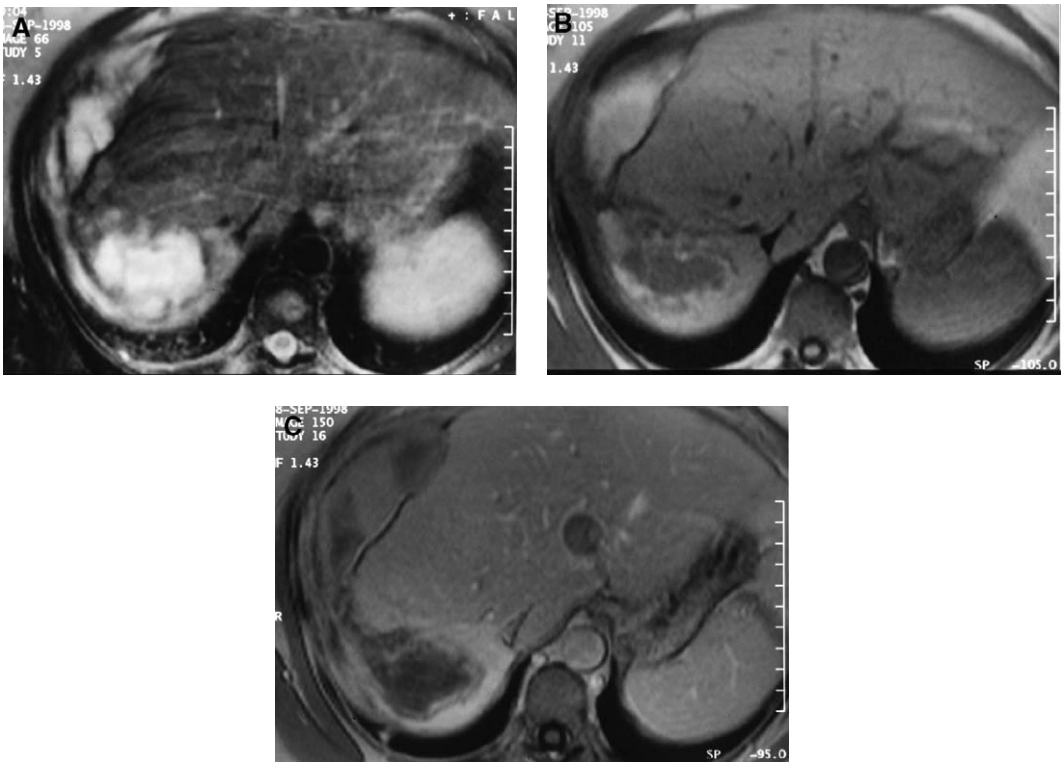

Fig. 4. Axial MR images of a patient with spontaneous intraperitoneal bleeding caused by a ruptured hepatocellular adenoma. (*A*) T2-weighted image obtained at the level of the liver shows the presence of a hyperintense mass in segment 7 of the liver with associated hyperintense fluid in the peritoneal space. (*B*) T1-weighted image obtained at the same level shows a hypointense mass with hyperintense peritoneal fluid. The latter is caused by the presence of extracellular methemoglobin indicating subacute hemorrhage. (*C*) Gadolinium-enhanced T1-weighted image obtained at the same level shows enhancement of the liver mass consistent with a hepatocellular adenoma.

Spontaneous bleeding caused by hepatic conditions

If there is no history of trauma or anticoagulant therapy, spontaneous hepatic bleeding is rare [25]. The most common cause of nontraumatic hepatic hemorrhage is a hypervascular neoplasm, such as hepatocellular carcinoma (HCC) or hepatocellular adenoma (HCA). Other lesions that sporadically can result in intraperitoneal bleeding include focal nodular hyperplasia, hemangioma, metastases, and more rarely HELLP syndrome (*h*emolysis, *e*levated *l*iver enzymes, and *l*ow *p*latelet count), amyloidosis, and cirrhosis with portal hypertension. Other exceedingly rare causes of spontaneous hepatic bleed include peliosis hepatis; angiomyolipoma of the liver; nodular regenerative hyperplasia; connective tissue diseases, such as polyarteritis nodosa and systemic lupus erythematosus; infectious diseases, such as typhoid fever; and parasitic diseases, such as malaria [26,27].

Hepatocellular carcinoma

Hepatocellular carcinoma is the most common solid organ primary malignancy worldwide and most often develops in the setting of chronic hepatic inflammation or cirrhosis [28]. In areas of Asia and Africa, where the prevalence of this cancer is high, rupture is reported to occur in 6.9% to 14% of cases and represents the most common cause of nontraumatic acute hemoperitoneum in male patients; however, ruptured HCC is relatively uncommon in Europe and America [29,30]. The reason for this discrepancy is unclear, but it could be related to the size of the tumor at diagnosis. From 65% to 80% of patients with HCC have established cirrhosis [31], and this association is even higher, ranging from 81% to 93% [13], in patients with ruptured HCC. Clinical diagnosis of ruptured HCC may be difficult because there are no specific symptoms [32]. HCC encompasses a wide spectrum, from relatively minor intrahepatic bleeding, to subcapsular hemorrhage and ultimately rupture through the hepatic capsule into the peritoneum. Subcapsular hepatic bleeding may be revealed by sudden onset of epigastric or right hypochondrial pain because of acute distention of Glisson's capsule. Hepatic rupture may be heralded by hypotension and rapid organ enlargement. Shock is present in 60% to 90% of cases at admission, and 60% to 100% of them have signs of peritonitis [33]. Blood-stained ascites coexists in almost all cases [34]. The mechanisms of spontaneous rupture of HCC are not completely established, although some theories have been proposed, such as (1) rupture of a parasitic artery or vein (eg, inferior phrenic vessel, feeding or draining the tumor) [35]; (2) laceration of a superficial HCC secondary to minor trauma, either from outside the body or from the lesion itself as a result of repeated respiratory movement [36]; (3) vascular invasion with rupture when hepatic vein occlusion is complete [36,37]; (4) tumor necrosis [3]; and (5) portal hypertension caused by associated cirrhosis [3]. Rupture can be predicted in patients with large HCC located in the periphery of the liver, and devoid of overlying normal parenchyma [35]. In patients with cirrhosis, the diagnosis of hemorrhagic HCC is suggested when a hyperechoic mass is seen at US; when a hyperattenuating mass is detected at CT; or when a mass with high signal intensity areas is detected in T1-weighted MR imaging [14,38,39]. It should be considered, however, that only one-third of HCCs have increased signal intensity on T1-weighted images, and this appearance may also be caused by steatosis, intracellular glycogen, or copper deposition [39]. Also, the signal intensity of blood may be increased or decreased depending on the time the hemorrhage is imaged. The high attenuation of acute hematomas is most obvious at unenhanced CT. CT is an effective method of diagnosing hepatic hemorrhage and can often indicate the underlying cause. During the acute stage (24 to 72 hours), the hematoma is hyperattenuating, but it decreases in attenuation and develops a pseudocapsule by 10 to 30 days [14]. A subcapsular hematoma or hemoperitoneum appears as high-attenuation peritoneal fluid around the liver and spleen, sometimes with layering of the clot (hematocrit effect) (Fig. 5). In the presence of major active bleeding, dynamic CT scan can show extravasation of contrast material [40]. Angiography is not required as an additional diagnostic procedure; its sensitivity in detecting HCC is high, but it fails reliably to document active bleeding from a ruptured HCC, showing extravasation of the contrast material from the tumor in only 13% [41] to 23.5% [42] of cases. Another more rarely used diagnostic modality is radionuclide imaging with Tc 99m–labeled red blood cells [43].

Spontaneous rupture of HCC constitutes a critical and life-threatening condition. An aggressive surgical approach, although advocated by several authors, cannot be performed because many patients are poor surgical candidates as a result of underlying cirrhosis and extensive tumor replacement, carrying a high risk of morbidity and mortality [42]. The mortality rate for one-stage hepatic lobectomy, which is often performed under hurried and unfavorable conditions, has been as high as 75% [44]. Embolization therapy is usually attempted as the most effective method of overcoming life-threatening bleeding from a ruptured HCC [42].

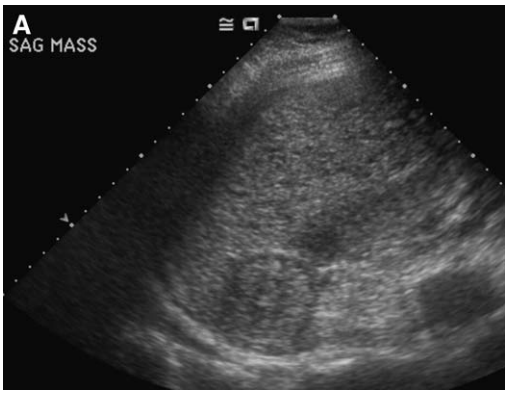
A
SAG MASS

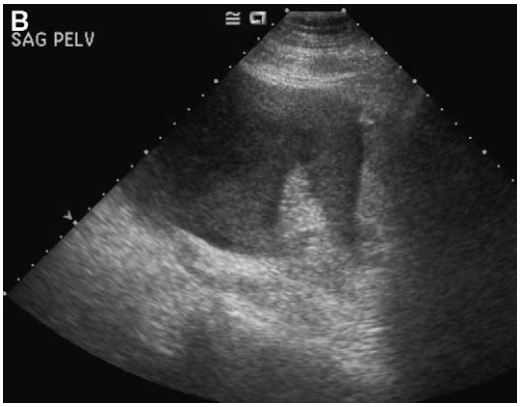
B
SAG PELV

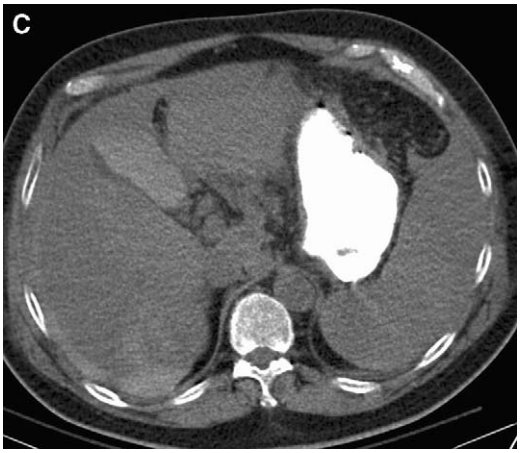
C

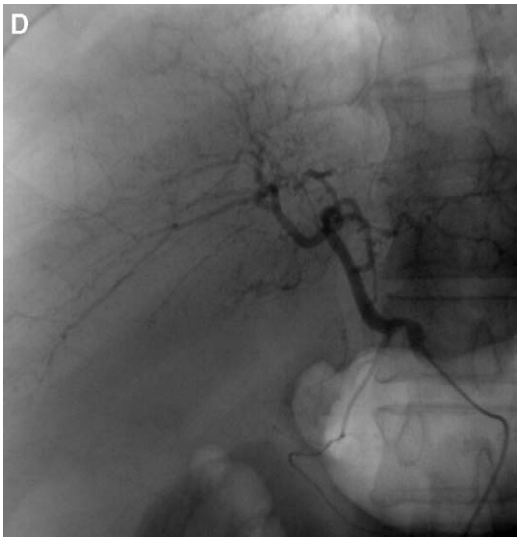
D

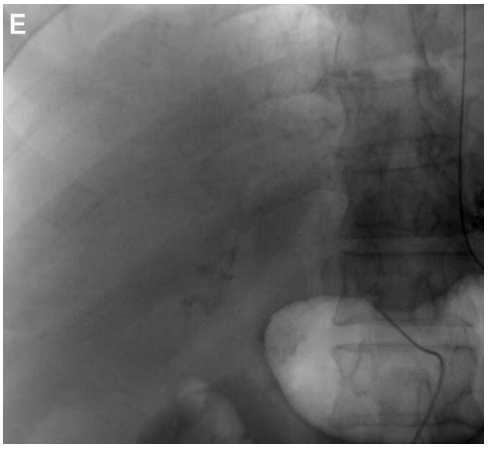
E

Hepatocellular adenoma

Hepatocellular adenoma is a rare, benign liver neoplasm strongly associated with oral contraceptive use and estrogen steroid therapy [45]. HCA is commonly discovered in women of childbearing age who have a history of prolonged use of oral contraceptives [45]. It also can occur spontaneously or be associated with underlying metabolic diseases, such as type 1 glycogen storage disease [46]. Identification of hepatic adenomas is important because of the associated risk of life-threatening hemorrhage [47]. It has the propensity to outgrow its arterial vascular supply, resulting in hemorrhage, necrosis, and occasionally rupture. Withdrawal of estrogen medication may result in the regression of the tumor, although regression may require a period of several months [48].

Hepatic adenomas are reported to be solitary in 70% of cases, but it is not unusual to encounter two or three adenomas in one patient, particularly at multiphasic CT or MR imaging [49,50]. Large adenomas are more prone to spontaneous hemorrhage [51]. The propensity to hemorrhage reflects the histologic characteristics of HCA, which consist of large plates or cords of cells closely resembling normal hepatocytes, with the plates separated by dilated sinusoids. These sinusoids are equivalent to thin-walled capillaries perfused at arterial pressure because adenomas lack portal supply. The extensive sinusoids and feeding arteries constitute the hypervascular nature of HCA. Because the tumor capsule is usually incomplete, hemorrhage may spread into the liver or abdominal cavity (Fig. 6) [52]. Hemorrhage can result in increased echogenicity and heterogeneity at US, and older areas of hemorrhage may appear as hypoechoic or cystic areas (Fig. 7). On CT, hyperattenuating areas corresponding to recent hemorrhage can be noted in 25% of HCAs (Fig. 8) [53]. Old hemorrhage is seen as a heterogeneous, hypoattenuating area within the tumor. On MR imaging, using T1- and T2-weighted images, HCA may appear heterogeneous and hyperintense because of hemorrhage (Fig. 9). The treatment of choice of HCA is resection with a margin of normal liver parenchyma [54].

Focal nodular hyperplasia

Focal nodular hyperplasia is a benign, tumorlike condition that is predominantly diagnosed (80% to 90%) in women during the third to fifth decade of life, although it has been described in women in other age groups and in men [55]. It is the second most common benign liver tumor, after hemangioma. Focal nodular hyperplasia is usually discovered incidentally in asymptomatic patients, but in one third of patients there are clinical symptoms, such as right upper quadrant or epigastric pain, that lead to its discovery. To date, the origin and pathogenesis are still unclear: a congenital vascular malformation or vascular injury has been advocated as the underlying mechanism for secondary hepatocellular hyperplasia [56]. Although oral contraceptive use has been linked to the growth of focal nodular hyperplasia, its real influence is still controversial [46]. A recent study showed that neither the size, number, nor growth rate is influenced by oral contraceptives [57]. Typically, the growth of focal nodular hyperplasia remains proportional to its blood supply, and necrosis or spontaneous rupture and subsequent bleeding are rarely reported [25,46]. Rupture may occur in patients with focal nodular hyperplasia, however, and should be suspected when sudden abdominal pain develops in a young or middle-aged woman [58]. It has been hypothesized that intraperitoneal hemorrhage may occur from erosion of the large vessels present at the periphery or in the central scar [59]. Imaging modalities may detect a subcapsular, heterogeneous fluid collection with hyperechoic or hyperattenuating components at US and CT, respectively [25].

Hemangiomas

Hemangioma is the most common benign hepatic tumor [46] and is found in up to 20% of the population in autopsy series [25]. They are more common in women than in men (ratio 5:1) and can be seen in any age group [60]. Although usually asymptomatic, they can rarely be associated with pain, nausea, or vomiting as a result of extrinsic compression of

Fig. 5. Patient with spontaneous intraperitoneal bleeding caused by hepatocellular carcinoma. (*A*) Axial ultrasound image obtained at the level of the liver shows a well-defined heterogeneous mass in the right lobe of the liver. (*B*) Sagittal ultrasound image obtained at the level of the pelvis shows free fluid with internal echoes, consistent with hemoperitoneum. (*C*) Unenhanced CT image obtained at the level of the liver shows the mass in the right liver lobe and hemoperitoneum. (*D, E*) Digital subtraction angiography (selective hepatic artery) images show abnormal feeding vessels originating from the right hepatic artery and active contrast extravasation. (Ultrasound images courtesy of Donald DiSalvo, MD, Boston, MA.)

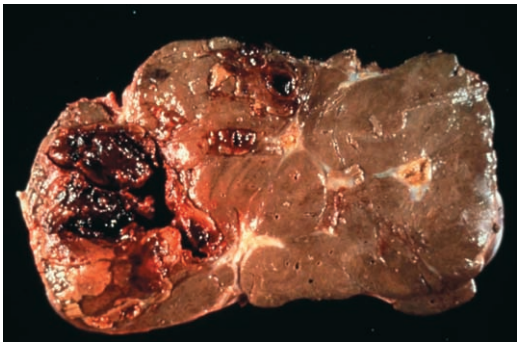

Fig. 6. Gross pathology of a resected ruptured hepatocellular adenoma. Macrophotograph shows a hemorrhagic liver mass bordered by an incomplete capsule.

adjacent structures, rupture, hemorrhage, or thrombosis (Fig. 10) [46,61,62]. Estrogen may cause growth of hepatic hemangiomas, and there are a few reports focusing on the effect of pregnancy with its increased estrogen levels on these lesions [63]. The course of asymptomatic, small, single lesions seems to be

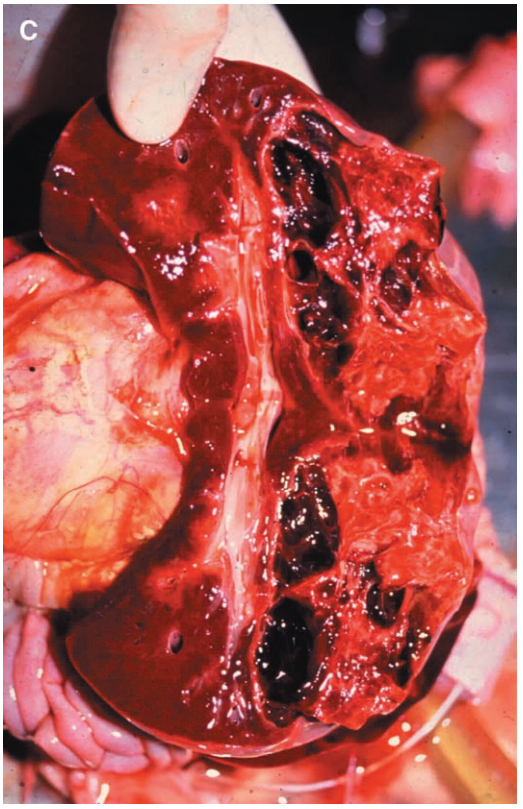

Fig. 10. (*C*) Gross pathology image obtained after resection shows the ruptured hemangioma.

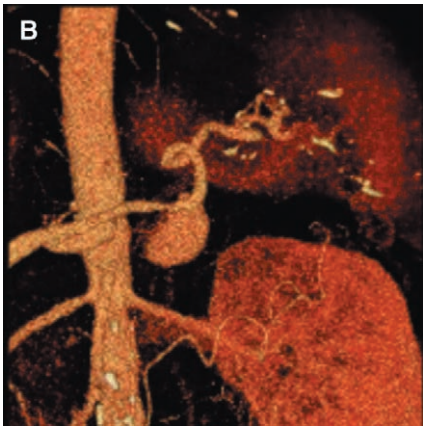

Fig. 14. (*B*) Volume-rendered three-dimensional image illustrates the pseudoaneurysm.

without significant complications during pregnancy. The association of hemangioma with systemic cystic angiomatosis and consumptive coagulopathy with thrombocytopenia, however, has also been reported in pregnancy [64]. Indeed, in pregnancy, hemangiomas have a higher risk of rupture and severe hemorrhage, because of an increase in intravascular volume and intra-abdominal pressure caused by an enlarged uterus. A history of underlying chronic hypertension, preeclampsia, HELLP syndrome, or cocaine abuse may contribute to the increased risk. It must be emphasized that symptoms of impending eclampsia may further confound and challenge the diagnostic process [65]. In patients with known hemangioma, the diagnosis of internal hemorrhage is suggested if the lesion enlarges and shows increased echogenicity by US, increased attenuation by CT, or areas of high signal intensity by T1-weighted MR images [63,66]. Subcapsular hematoma and hemoperitoneum may be associated [25]. Hepatic artery ligation has been suggested as a means of treating ruptured hemangioma. The procedure of choice, however, is subsegmental angiographic embolization [63].

Metastasis

Spontaneous rupture of metastases, although rare, usually results in massive hemoperitoneum, which is life-threatening [34]. There have been reported cases of spontaneous rupture of hepatic metastasis from primary sites including lung [67], kidney [68], colon [69], pancreas [69], gallbladder [69], testicle [70], melanoma [71], and choriocarcinoma [72]. Hepatic metastases from lung and renal carcinomas and melanoma, however, are the most frequent types to cause bleeding [25]. Many contributing factors have been suggested

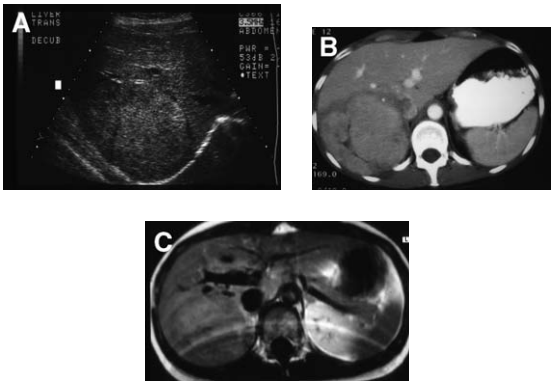

Fig. 7. Ultrasound, CT, and MR images in a patient with hemorrhagic hepatocellular adenoma. (*A*) Ultrasound image obtained at the level of the liver (segment 7) shows increased echogenicity of the liver mass caused by internal hemorrhage. (*B*) Contrast-enhanced CT image obtained at the same level shows the focal areas of pericapsular bleeding. (*C*) T1-weighted MR image shows the hyperintense appearance of the mass caused by the presence of methemoglobin.

and awareness of these factors, some of which are preventable, could conceivably reduce the risk of this complication. Such factors include tumor necrosis, associated or not with chemotherapy; increased abdominal pressure caused by straining, coughing, or forceful abdominal palpation; subcapsular location; local venous congestion resulting from tumor obstruction; and reduced clotting factors [67–69]. At imaging, the diagnosis of hemorrhagic metastasis is suggested if blood is identified in one or more liver lesions in a patient with known hepatic metastases or primary neoplasia elsewhere (Fig. 11) [25]. Treatment of this type of hemoperitoneum depends on the size of the metastasis, its location, and the rate of bleeding. Treatment of hemoperitoneum in patients with metastatic disease is palliative, however, with the goal to control the hemorrhage quickly and effectively [73].

Miscellaneous hepatic conditions

HELLP syndrome

HELLP syndrome was first described by Weinstein [74] in 1982. The small subset of preeclamptic or eclamptic women presenting with findings of hemolysis, elevated liver enzymes, and low platelet count is the cohort of findings known as the ''HELLP syndrome.'' This serious obstetric condition, which occurs either before or immediately after birth, may progress rapidly with complications, such as disseminated intravascular coagulation, hepatic necrosis, and hemorrhagic infarction [74,75]. Early in the clinical course, US is frequently used to exclude gallbladder disease as a cause of right upper quadrant pain. Hematomas (subcapsular and intrahepatic) can be detected with US [76]. CT, however, is the modality of

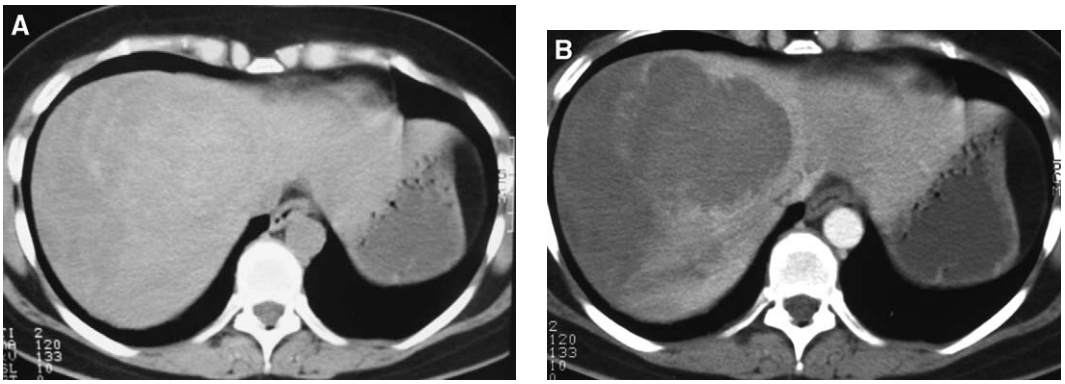

Fig. 8. Axial CT images in a patient with spontaneous intraperitoneal bleeding caused by a ruptured hepatocellular adenoma. (*A*) Unenhanced CT image obtained at the level of the liver (segment 8) shows fresh blood within the peritoneal space and the presence of a mass in the dome of the liver. (*B*) Contrast-enhanced CT image obtained at the same level shows heterogeneous enhancement of the mass bordering the intraperitoneal hemorrhage.

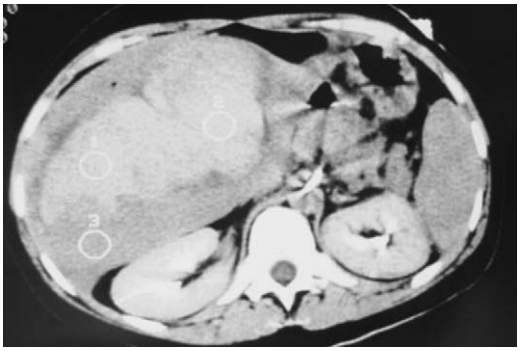

Fig. 9. Axial CT images in a patient with spontaneous intraperitoneal bleeding caused by a ruptured hepatocellular adenoma. Delayed-phase contrast-enhanced CT image at the level of the liver (segment 4) shows the presence of a large mass with presence of hemorrhage in the peritoneal space.

choice for HELLP syndrome because it is able to demonstrate subcapsular hematoma and hepatic rupture with intraperitoneal bleeding. Hepatic infarction can be seen at CT as low-attenuation wedge-shaped areas in the periphery of the liver without mass effect [76].

Amyloidosis

Amyloidosis is defined as extracellular deposition of the fibrous protein amyloid in one or more sites in the body. Organ enlargement, especially of the liver, kidney, spleen, and heart, may be prominent. The liver is frequently involved in amyloidosis; however, hepatocellular rupture is extremely rare [77,78]. Hemoperitoneum or a subcapsular hematoma may be diagnosed with either US or CT.

Patients with cirrhosis and portal hypertension

Hemorrhagic ascites is encountered in only 5% of patients with cirrhosis [3]. Although in most of these cases it is detected incidentally, when present the hemoperitoneum is a poor prognostic sign. Usually it occurs from a ruptured HCC or intraperitoneal varices. In one third of patients, however, no specific cause is found [27]. Long-standing portal hypertension results in the development of extensive collateral circulation. Esophageal varices are the most familiar anatomic sites of hemorrhage [79]. Other sites of variceal bleeding, such as the small intestine, colon, rectum, and vaginal vault, are less common and usually result in intraluminal hemorrhage [80].

Spontaneous bleeding caused by splenic abnormalities

Splenic rupture

The spleen is an abdominal organ commonly involved in hematologic diseases. When rupture occurs

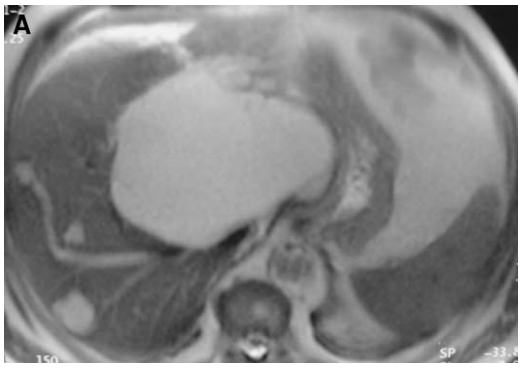

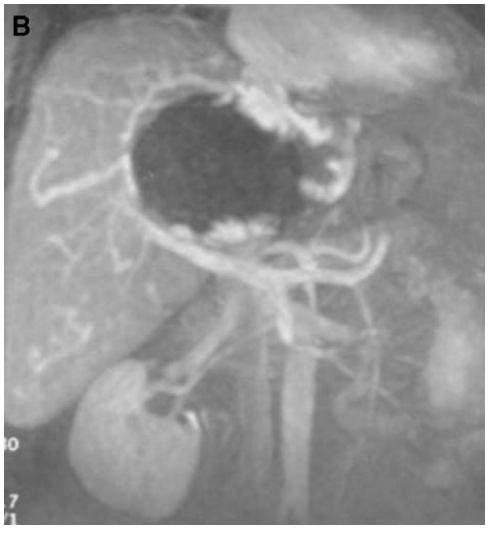

Fig. 10. MR and gross pathology images in a patient with a ruptured giant hemangioma. (*A*) T2-weighted MR image obtained at the level of the liver (segments 3 and 4) shows a giant hyperintense hemangioma and minimal hyperintense bleeding in the adjacent parenchyma. (*B*) Coronal gadolinium-enhanced T1-weighted image shows the characteristic incomplete peripheral nodular enhancement of a hemangioma. (See color Fig. 10C on page 1190.)

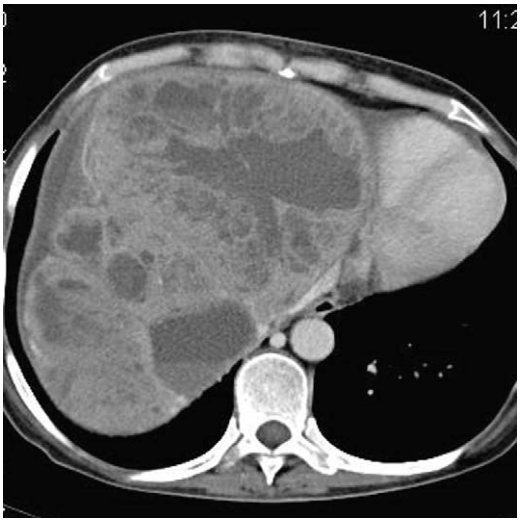

Fig. 11. Axial contrast-enhanced CT image in a patient with metastatic carcinoid shows fluid-fluid level within the hepatic metastases consistent with hemorrhagic necrosis.

without trauma in a spleen involved by disease, the term "pathologic splenic rupture" is used. Pathologic rupture can occur as a complication of infections, such as mononucleosis or malaria; of congenital diseases like cysts; and of metabolic diseases (Gaucher's disease or amyloidosis). Rarely, it is a result of a complication of neoplastic processes diseases, such as hemangiomatosis, angiosarcoma, leukemia, or lymphoma (Fig. 12) [81]. Various diagnostic methods to detect pathologic splenic rupture have been reported. Although Canady et al [82] reported several signs suggestive of splenic rupture by plain abdominal films, both US and CT scan provide a diagnosis with much better sensitivity and specificity. With slow or subacute splenic rupture, liver-spleen scintigraphy has been reported to be of value [83].

Peliosis

Peliosis is a rare disease of unknown cause in which multiple blood-filled cavities are formed in the liver or spleen, and occasionally in other structures, such as lymph nodes and bone marrow [84,85]. The spleen is the site most commonly involved [86]. Peliosis should be differentiated from splenic tumors, particularly hemangioma, which demonstrate contrast pooling on angiograms and also may be complicated with intraperitoneal hemorrhage [87].

Spontaneous rupture of an accessory spleen

Accessory spleens have been reported to occur in 10% to 31% of individuals [88]. Complications, such as hemorrhage or rupture, are well recognized in the primary spleen, but have only rarely been reported in accessory spleens [89,90]. CT and US are the modalities of choice for imaging accessory spleen rupture.

Spontaneous bleeding caused by visceral artery abnormalities

Aneurysms of visceral vessels are an important cause of mortality because they are frequently misdiagnosed and detected only after rupture has occurred, requiring an emergency laparotomy. Nearly 3000 visceral artery aneurysms are reported in the literature, with splenic, renal, and hepatic artery accounting for 60%, 22%, and 10% of them, respectively [91]. The involvement of the mesenteric artery and its branches is less common (Fig. 13) [92]. Spontaneous rupture is the usual clinical presentation of splanchnic artery aneurysms and their presence should be considered during the surgical treatment of hemoperitoneum [91].

Spontaneous rupture occurs in 3% to 10% of patients with splenic artery aneurysm and is associated with a high rate of mortality, estimated around 36% [93]. The risk of rupture, and subsequent mortality, increases dramatically during pregnancy [94]. Regarding superior mesenteric artery aneurysms and pseudoaneurysms, risk of rupture is uncommon but it is also associated with a mortality rate of 30% [95]. Conversely, thrombosis is more frequent, and intra-

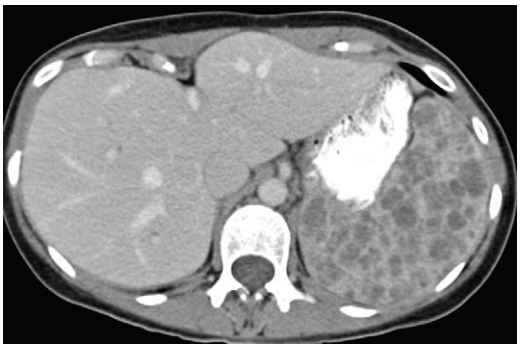

Fig. 12. Axial contrast-enhanced CT image in a patient with splenic hemangiomatosis shows multiple hypoattenuating lesions within the spleen.

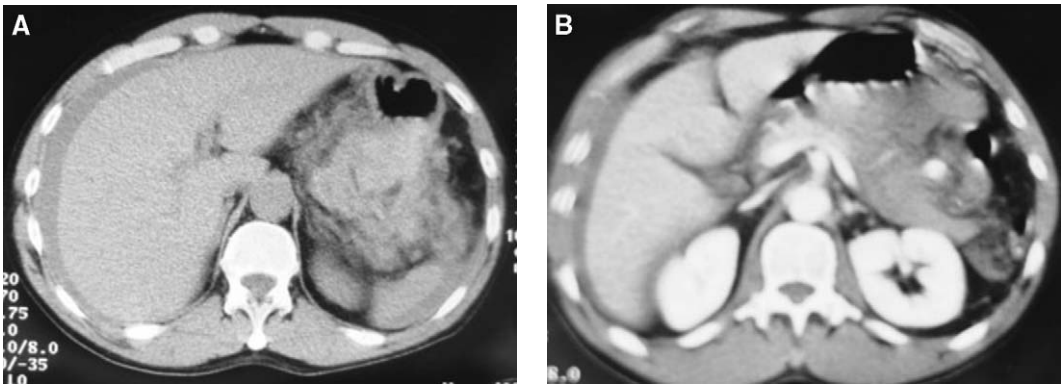

Fig. 13. Axial CT images in a patient with segmental mesenteric artery pseudoaneurysm. (*A*) Unenhanced CT image obtained at the level of the spleen shows hyperattenuating fluid within the lesser sac consistent with hemoperitoneum. (*B*) Contrast-enhanced CT image obtained at the level of the jejunal mesentery shows 1 cm pseudoaneurysm originating from a segmental jejunal artery.

peritoneal bleeding may result from intestinal infarction [96].

The classic description of splenic artery aneurysms on plain films is that of a crescentic calcification with a curvilinear line or ''signet ring'' in the left upper quadrant [97]. Although US color Doppler examination may diagnose an aneurysm or a pseudoaneurysm, CT angiography is considered a viable alternative to selective conventional angiography (Fig. 14). The latter is still considered as the gold standard in the evaluation of splanchnic aneurysms and pseudoaneurysms, offering the possibility to treat them percutaneously and prevent complications, such as thrombosis or rupture.

Spontaneous bleeding caused by other gastrointestinal abnormalities

Peptic ulcer bleeding

When gastric ulcer bleeding is present, abdominal intravenous contrast-enhanced CT without oral contrast medium administration has been reported to be capable to show the extravasation of intravenous contrast material into the gastric lumen [98]. It has been postulated that if radiopaque oral contrast material is given, bleeding can be missed. In addition, adequate gastric distention is essential for successful evaluation of gastric ulcers [99]. Because cases of

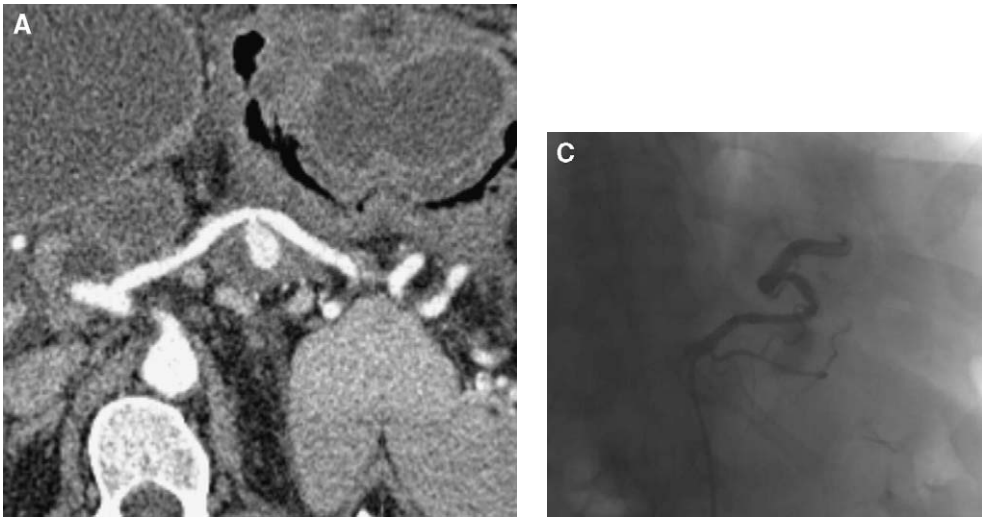

Fig. 14. Contrast-enhanced CT images and digital subtraction angiography image in a patient with splenic artery pseudoaneurysm. (*A*) Oblique contrast-enhanced CT image shows pseudoaneurysm arising from the splenic artery. (*C*) Digital subtraction angiography shows splenic artery pseudoaneurysm and its relation to surrounding vessels. (See color Fig. 14B on page 1190.)

peptic gastric ulcer perforation have been reported [100], this disease should be taken in consideration in the differential diagnosis of acute abdomen with intraperitoneal bleeding.

Pancreatitis

Hemorrhage is an infrequent complication of pancreatitis but it is associated with a high mortality rate that exceeds 50% [101,102]. It usually arises from pancreatitis-related vascular lesions. Pseudoaneurysms, splenic vein thrombosis with segmental portal hypertension, and splenic rupture are recognized vascular complications of pancreatitis that may lead to massive and fatal hemorrhage. Often they occur in association with pancreatic pseudocysts. Massive hemorrhage associated with chronic pancreatitis is very rare, although in some series the incidence was relatively high, ranging from 7% to 9.5% [103]. Development of an arterial pseudoaneurysm related to chronic pancreatitis may result from three mechanisms: (1) severe inflammation and enzymatic autodigestion of a pancreatic or peripancreatic artery; (2) an established pseudocyst may erode into a visceral artery, thereby converting the pseudocyst into a large pseudoaneurysm; and (3) a pseudocyst may erode the wall of the bowel with bleeding from the mucosal surface itself [103]. A pseudocyst may then rupture into the pancreatic ductal system causing hemorrhage into the bile duct and hemobilia. The pseudoaneurysm also may rupture into the free peritoneal cavity or into the gastrointestinal tract. An uncommon but potentially fatal cause of gastrointestinal and intraperitoneal bleeding is pseudoaneurysm formation secondary to pancreatitis [104], which is associated with a high mortality rate of up to 37% [101]. The most frequently involved artery is the splenic artery, followed by pancreaticoduodenal and gastroduodenal arteries [103], although any peripancreatic vessel may be involved. The imaging diagnosis can be accomplished with contrast-enhanced CT, US color Doppler examination, angiography, or MR angiography. With Doppler imaging, blood is seen flowing into the pseudoaneurysm in systole and out in diastole. The amount of flow can wax and wane, depending on the relative amount of formed and lysed clot. Clotting tends to occur at the periphery, where flow is slower and stasis exists. If the entire pseudoaneurysm is filled with clot, no flow is detected, and it is difficult to make the diagnosis with color Doppler [105]. Acute clot tends to be hyperechoic, with older clot becoming hypoechoic. CT scan may reveal features of acute or chronic pancreatitis; demonstrate bleeding into a pancreatic fluid collection or a pseudocyst [106]; or identify vascular complications, such as pseudoaneurysms, venous thrombosis, or varices [101,107,108]. The CT finding of contrast enhancement within or adjacent to a suspected pseudocyst is highly suspicious for pseudoaneurysm formation (Fig. 15) [101]. The enhancement is similar to that of the abdominal aorta. The finding of increased attenuation within a fluid collection on a nonenhanced scan is also suspicious, indicating recent hemorrhage (Fig. 16) [109]. Angiography is considered the gold standard to detect and localize the pseudoaneurysm to a specific vessel [110], aiding in the surgical management, and also

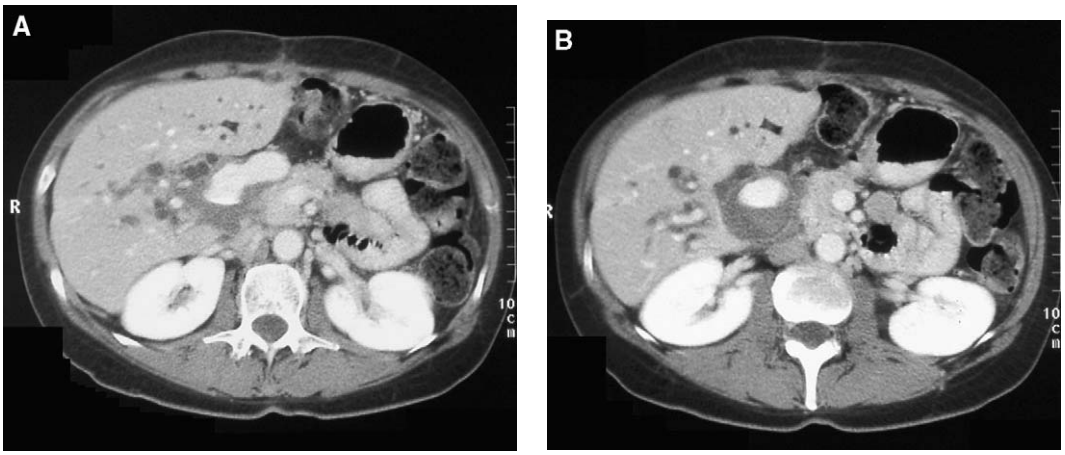

Fig. 15. Axial contrast-enhanced CT images in a patient with hepatic artery pseudoaneurysm caused by pancreatitis. (*A, B*) Consecutive images at the level of the porta hepatis show aneurysmal dilation of the hepatic artery caused by rupture within a peripancreatic pseudocyst in this patient with pancreatitis.

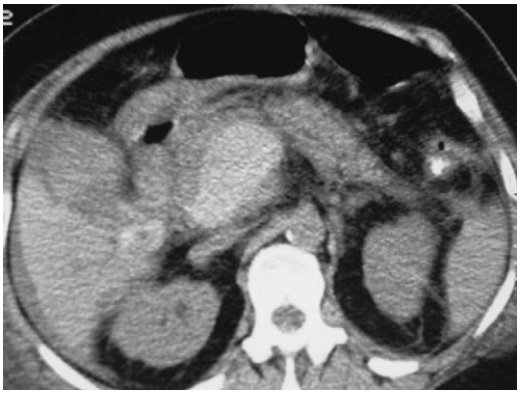

Fig. 16. Axial unenhanced CT image in a patient with gastroduodenal artery pseudoaneurysm.

provides a potential means for treatment by transcatheter embolization.

Spontaneous bleeding caused by gynecologic conditions

The most frequent gynecologic causes of hemoperitoneum are ectopic pregnancy and a ruptured ovarian cyst [111,112]. The authors have seen occasional cases of hemoperitoneum in patients with endometriosis, presumably related to hemorrhage from the endometrial implants, but in their experience this is infrequent. Hemoperitoneum may also be observed with uterine rupture but this is also uncommon. Such rupture may occur intrapartum because of a myometrial defect or may result from placenta percreta.

With hemoperitoneum, the intraperitoneal fluid often has low-level internal echoes. Such echoes are not specific for blood, however, and can be seen with other causes, such as peritoneal metastatic disease. Hemoperitoneum may also appear as anechoic fluid. Whether the fluid is anechoic or contains echoes may vary depending on multiple factors, such as gain settings, transducer type and frequency, use of harmonics, and patient body habitus. Besides seeing fluid, sometimes one may see a more focal heterogeneous area caused by clot. When large, it can be difficult to recognize that such a heterogeneous mass is caused by clot or recognize from where it originates.

One also should realize that small amounts of free fluid in the pelvis are common in premenopausal women and do not indicate hemoperitoneum. It is difficult to quantify the amount of fluid, and the determination of whether the amount of fluid is normal or abnormal is often made on a subjective basis. Such normal fluid is typically anechoic, small in amount, and seen most frequently in the cul-de-sac during transvaginal sonography.

Ectopic pregnancy

In a premenopausal woman with abdominal pain, a positive human chorionic gonadotropin greater than 1000 to 2000 mIU/mL (International Reference Prepa-

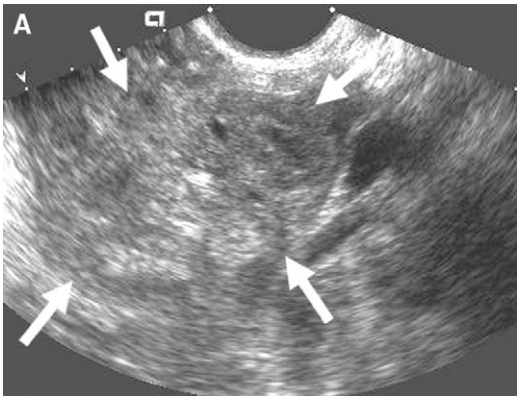

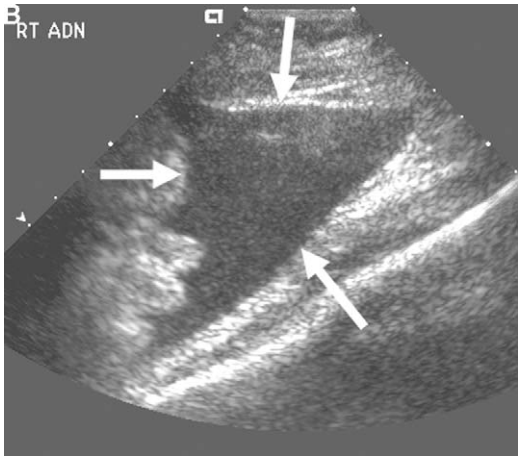

Fig. 17. Ultrasound images of a large pelvic hematoma and hemoperitoneum caused by tubal pregnancy (*A*) Transvaginal ultrasound image of the left adnexa shows a relatively large heterogeneous mass (*arrows*). At surgery, this represented pelvic clot caused by a ruptured tubal pregnancy. (*B*) Transabdominal ultrasound image of the right adnexa shows free intraperitoneal fluid (*arrows*). There are low-level internal echoes within the fluid, although sometimes it is difficult to determine if these are real echoes or noise on transabdominal scanning. (Courtesy of Alejandra Duran-Mendicuti, MD, Boston, MA.)

ration), and no demonstrable intrauterine pregnancy, the sonographic detection of an extraovarian adnexal mass is highly suggestive of an ectopic pregnancy [112]. It is crucial to identify the ovaries and determine the relationship of the adnexal mass to the ovaries. Visualization of the ipsilateral ovary as separate from the adnexal mass increases the likelihood that the mass represents an ectopic pregnancy, whereas visualization of the mass as originating from within the ovary strongly suggests a corpus luteal cyst.

Identification of the extraovarian mass is the most important and useful adnexal feature in diagnosing ectopic pregnancy. One also may see free intraperitoneal fluid in patients with ectopic pregnancy. A small amount of fluid may be normal. Any amount more than small, or fluid with internal echoes, however, likely represents hemoperitoneum (Fig. 17). The presence of hemoperitoneum in patients with ectopic pregnancy does not necessarily indicate tubal rupture [19]. The larger the amount of fluid, the more likely is tubal rupture. Besides tubal rupture, hemoperitoneum may be caused by tubal abortion, bleeding from the fimbriated end of the tube, or a co-existing corpus luteal cyst that has ruptured [111].

Ruptured cyst

A hemorrhagic ovarian cyst is a frequent cause of acute pelvic pain in a woman of childbearing age and is a common indication for referral for US evaluation. The most common underlying etiology is a corpus luteal or follicular cyst [111]. A range of sonographic patterns has been attributed to hemorrhagic ovarian cyst, probably related to the time interval since the hemorrhagic event. Hemorrhagic cysts often have linear to curvilinear internal echoes in a reticular or fishnet pattern that are caused by fibrin strands [112]; however, they can sometimes have other less common appearances [112].

Only a minority of hemorrhagic ovarian cysts rupture and cause hemoperitoneum. The etiology of ovarian cyst rupture is unknown, although it has been

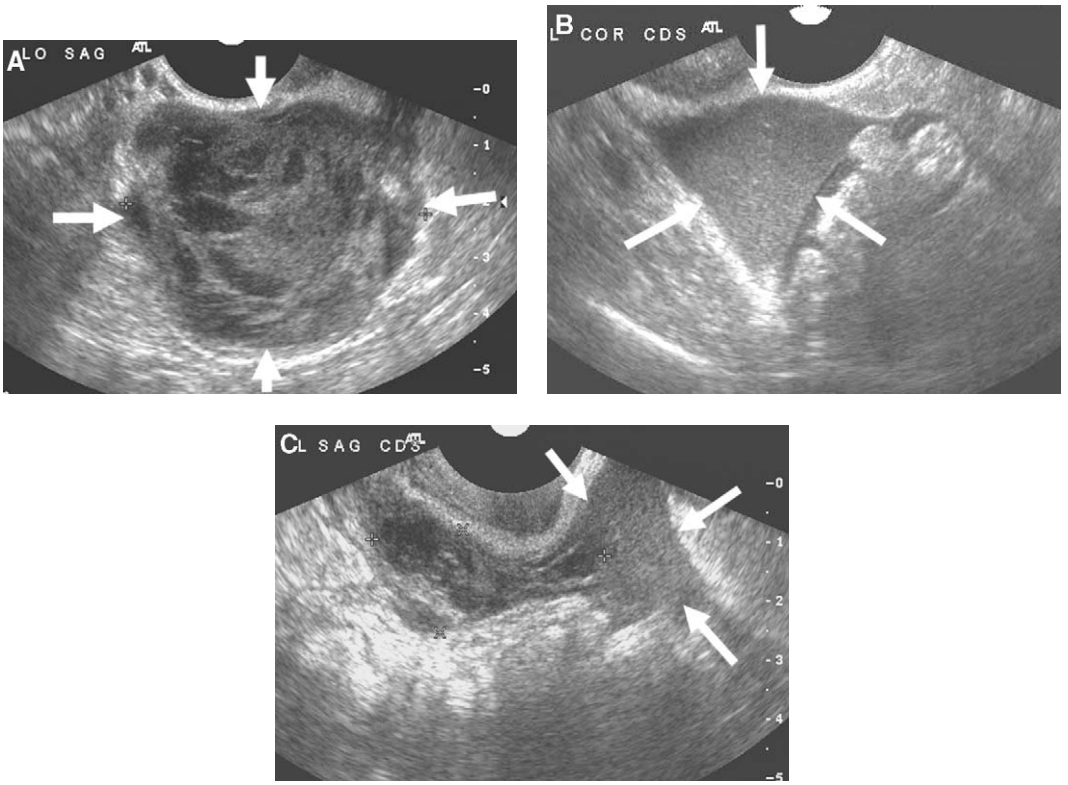

Fig. 18. Transvaginal ultrasound images of hemorrhagic cyst with rupture and hemoperitoneum. (*A*) Image of the left ovary shows a moderate size heterogeneous mass, caused by a hemorrhagic cyst, replacing most of the left ovary. (*B*) Image of the cul-de-sac shows fluid (*arrows*) with internal echoes, consistent with hemoperitoneum. (*C*) Image more to the left side of cul-de-sac again shows the fluid with internal echoes (*arrows*) but also shows a more heterogeneous area (*cursors*), caused by clot.

suggested that the increased vascularity of the ovary in the luteal phase may predispose to rupture of a corpus luteal cyst [111]. One should be aware of this possibility so as not to misdiagnose it as an unrelated gynecologic, urologic, or gastrointestinal disorder [111]. With recent bleeding, fluid with internal echoes or high attenuation can surround the uterus and adnexa [111]. Alternatively, hypoechoic or low-attenuation fluid intermixed with amorphous conglomerations of clotted blood can be seen. The sonographic appearance of echogenic clots may superficially resemble aperistaltic loops of bowel surrounded by ascites [113]. Clots are more amorphous in configuration and echogenicity, and relatively featureless (Fig. 18). When hemoperitoneum extends into the upper abdomen, it may be lower in echogenicity and attenuation than in the pelvis. When CT scanning is performed, the active extravasation of intravenous contrast material may identify the bleeding site. Delayed CT images may show pooling of contrast-enhanced blood in the peritoneal cavity. Ovarian carcinoma may also cause ascites, sometimes of hemorrhagic characteristics, but the clinical setting and identification of peritoneal tumor implants should assist in the correct diagnosis.

Summary

Spontaneous intraperitoneal bleeding can result from a vast array of etiologies. Fortunately, most are uncommon and currently available imaging modalities can be used to differentiate them in almost all cases. Meticulous imaging technique and careful observation of key imaging features are important for accurate characterization of the organ of origin of the spontaneous bleeding. CT is the single most important imaging technique in the detection and characterization of spontaneous intraperitoneal bleeding. Further development in multidetector technology, such as the introduction of new machines with 8 or 16 detectors, should improve the effectiveness of CT further. Sonography and MR imaging are complimentary to CT, especially in patients with pelvic abnormalities or equivocal CT findings.

References

[1] McCott JJ. Intraperitoneal and retroperitoneal hemorrhage. Radiol Clin North Am 1976;14:391–405.
[2] Scott WW, Fishman EK, Siegelman SS. Anticoagulants and abdominal pain: the role of computed tomography. JAMA 1984;252:2053–6.
[3] Akriviadis E. Hemoperitoneum in patients with ascites. Am J Gastroenterol 1997;92:567–75.
[4] Chung MA, Oung C, Szilagyi A. Cullen's sign: it doesn't always mean hemorrhagic pancreatitis. Am J Gastroenterol 1992;87:1026–8.
[5] Pretorius ES, Fishman EK, Zinreich SJ. CT of hemorrhagic complications of anticoagulant therapy. J Comput Assist Tomogr 1997;21:44–51.
[6] Federle MP, Jeffrey Jr RB. Hemoperitoneum studied by computed tomography. Radiology 1983;148:187–92.
[7] Jeffrey Jr RB, Cardoza JD, Olcott EW. Detection of active intraabdominal arterial hemorrhage: value of dynamic contrast-enhanced CT. AJR Am J Roentgenol 1991;156:725–9.
[8] Shuman WP. CT of blunt abdominal trauma in adults. Radiology 1997;205:297–306.
[9] Fishman EK. Spiral CT: applications in the emergency patients. Radiographics 1996;16:943–8.
[10] New PFJ, Aronov S. Attenuation measurements of whole blood and blood fractions in computed tomography. Radiology 1976;121:635–40.
[11] Norman D, Price D, Boyd D, Fishman R, Newton TH. Quantitative aspects of computed tomography of the blood and cerebrospinal fluid. Radiology 1977;123:335–8.
[12] Bergstrom M, Erickson K, Levander B, Svendsen P, Larsson S. Variation with time of the attenuation values of intracranial hematomas. J Comput Assist Tomogr 1977;1:57–63.
[13] Korobin M, Moss AA, Callen PW, DeMartini WJ, Kaiser JA. Computed tomography of subcapsular splenic hematoma: clinical and experimental studies. Radiology 1978;129:441–5.
[14] Swensen SJ, McLeod RA, Stephens DH. CT of extracranial hemorrhage and hematomas. AJR Am J Roentgenol 1984;143:907–12.
[15] Levine CD, Patel UJ, Silverman PM, Wachsberg RH. Low attenuation of acute traumatic hemoperitoneum on CT scans. AJR Am J Roentgenol 1996;166:1089–93.
[16] Wovelson MK, Crepps LF, Sundaram M, Heiberg E, Vas WG, Shields JB. Hyperdensity of recent hemorrhage at body computed tomography: incidence and morphologic variation. Radiology 1983;148:779–84.
[17] Sivit CJ, Peclet MH, Taylor GA. Life-threatening intraperitoneal bleeding: demonstration with CT. Radiology 1989;171:430.
[18] Fleischer AC, Pennell RG, McKee MS, et al. Ectopic pregnancy: features at transvaginal sonography. Radiology 1990;174:375–8.
[19] Frates MC, Brown DL, Doubilet PM, et al. Tubal rupture in patients with ectopic pregnancy: diagnosis with transvaginal US. Radiology 1994;191:769–72.
[20] Healey MA, Simons RK, Winchell RJ, et al. A prospective evaluation of abdominal ultrasound in blunt trauma: is it useful? J Trauma 1996;40:875–83.
[21] McKenney MG, Martin L, Lentz K, et al. 1000 Con-

secutive ultrasounds for blunt abdominal trauma. J Trauma 1996;40:607–10.
[22] Jeffrey RB, Laing FC. Echogenic clot: a useful sign of pelvic hemoperitoneum. Radiology 1982;145: 139–41.
[23] Unger EC, Glazer HS, Lee JKT, Ling D. MRI of extracranial hematomas: preliminary observations. AJR Am J Roentgenol 1986;146:403–7.
[24] Hahn PF, Saini S, Stark DD, Papanicolaou N, Ferrucci Jr JT. Intraabdominal hematoma: the concentric-ring sign in MR imaging. AJR Am J Roentgenol 1987; 148:115–9.
[25] Casillas VJ, Amendola MA, Gaascue A, Pinnar N, Levi JU, Perez JM. Imaging of nontraumatic hemorrhagic hepatic lesions. Radiographics 2000;20: 367–88.
[26] Dachman AH, Ros PR, Goodman ZD, Olmsted WW, Ishak KG. Nodular regenerative hyperplasia of the liver: clinical and radiological observations. AJR Am J Roentgenol 1987;148:717–22.
[27] DeSitter L, Rectors WG. The significance of bloody ascites in patients with cirrhosis. Am J Gastroenterol 1984;79:136–8.
[28] Levy A. Malignant liver tumors. Clin Liver Dis 2002; 6:147–63.
[29] Meyers WC. The liver. In: Sabiston Jr DC, Lyerly HK, editors. Textbook of surgery. 15th edition. Philadelphia: WB Saunders; 1997. p. 1045–116.
[30] Fernandez MP, Redvanly RD. Primary hepatic malignant neoplasms. Radiol Clin North Am 1998;36: 333–48.
[31] Hirai K, Kawazoe Y, Yamashita K, et al. Transcatheter arterial embolization for spontaneous rupture of hepatocellular carcinoma. Am J Gastroenterol 1986;81: 275–9.
[32] Zhu LX, Wang G, Fan ST. Spontaneous rupture of hepatocellular carcinoma. Br J Surg 1996;83:602–7.
[33] Dewar GA, Griffin SM, Ku FW, et al. Management of bleeding liver tumors in Hong Kong. Br J Surg 1991; 78:463–6.
[34] Miyamoto M, Sudo T, Kuyama T. Spontaneous rupture of hepatocellular carcinoma: a review of 172 Japanese cases. Am J Gastroenterol 1991;86: 67–71.
[35] Kanematsu M, Imaeda T, Yamawaki Y, et al. Rupture of hepatocellular carcinoma: predictive value of CT findings. AJR Am J Roentgenol 1992;158:1247–50.
[36] Cheranoi O, Plengavanit U, Asanovich C, et al. Spontaneous rupture of primary hepatoma: report of 63 cases with particular reference to the pathogenesis and rationale of treatment by hepatic artery ligation. Cancer 1983;51:1532–6.
[37] Nagasue N, Inokuchi K, Kobayashi M, et al. Hepatoportal arteriovenous fistula in primary carcinoma of the liver. Surg Gynecol Obstet 1974;145:504–8.
[38] Kim OPN, Kim IY, Bae WK, Lee BH. Computed tomographic findings of ruptured hepatic malignancy. Gastrointest Radiol 1991;16:334–6.
[39] Buetow PC, Midkiff RB. Primary malignant neoplasms in the adult: MR imaging of the liver. Magn Reson Imaging Clin N Am 1997;5:289–318.
[40] Becker CD, Spring P, Glattil A, et al. Blunt splenic trauma in adults: can CT findings be used to determine the need for surgery? AJR Am J Roentgenol 1994;162:343–7.
[41] Okazaki M, Higashikara H, Koganemaru F, et al. Intraperitoneal hemorrhage from hepatocellular carcinoma: emergency chemoembolization or embolization. Radiology 1991;180:647–51.
[42] Hsieh JS, Huang CJ, Huang YS, Sheen PC, Huang TJ. Intraperitoneal hemorrhage due to spontaneous rupture of hepatocellular carcinoma: treatment by hepatic artery embolization. AJR Am J Roentgenol 1987;149: 715–7.
[43] Bajakian RL, Swayne LC, Palace FM. Scintigraphic detection of hemobilia and hemoperitoneum secondary to rupture of hepatic artery aneurysm. Clin Nucl Med 1988;13:831–2.
[44] Lai ECS, Wu KM, Choi TK, et al. Spontaneous ruptured hepatocellular carcinoma: an appraisal of surgical treatment. Ann Surg 1989;210:24–8.
[45] Rabe T, Fiedelman K, Grunwald K, et al. Liver tumors in women on oral contraceptives. Lancet 1994; 3:1568–9.
[46] Mortele KJ, Ros PR. Benign liver neoplasms. Clin Liver Dis 2002;6:119–45.
[47] Meissner K. Hemorrhage caused by ruptured liver cell adenoma following long-term oral contraceptives: a case report. Hepatogastroenterology 1998;45:224–5.
[48] Kawatsu M, Vilgrain V, Erlinger S, et al. Disappearance of liver cell adenoma: CT and MR imaging. Abdom Imaging 1997;22:274–6.
[49] Ichikawa T, Federle MP, Grazioli L, Nalesnik M. Hepatocellular adenoma: multiphasic CT and pathologic findings in 25 patients. Radiology 2000;214: 861–8.
[50] Paulson EK, McClellan JS, Washington K, et al. Hepatic adenoma: MR characteristics and correlation with pathologic findings. AJR Am J Roentgenol 1994;163: 113–6.
[51] Leese T, Farges O, Bismuth H. Liver cell adenomas. Ann Surg 1998;208:558–64.
[52] Molina EG, Schiff ER. Benign solid lesions of the liver. In: Schiff ER, Sorrell MF, Maddrey WC, editors. Schiff's diseases of the liver. 8th edition. Philadelphia: Lippincott-Raven; 1999. p. 1245–67.
[53] Grazioli L, Federle MP, Brancatelli G, Ichikawa T, Olivetti L, Blachar A. Hepatic adenomas: imaging and pathologic findings. Radiographics 2001;21: 877–913.
[54] Flowers BF, McBurney RP, Vero SR. Ruptured hepatic adenoma: a spectrum of presentation and treatment. Am Surg 1990;56:380–4.
[55] Mortele KJ, Praet M, Van Vlieberghe H, Kunnen M, Ros PR. CT and MR imaging findings in focal nodular hyperplasia of the liver: radiologic-pathologic correlation. AJR Am J Roentgenol 2000;175:687–92.
[56] Kondo F. Focal nodular hyperplasia of the liver: con-

troversy over etiology. J Gastroenterol Hepatol 2000; 15:1229–31.
[57] Mathieu D, Kobeiter H, Maison P, et al. Oral contraceptive use and focal nodular hyperplasia of the liver. Gastroenterology 2000;118:560–4.
[58] Becker YT, Raiford DS, Webb L, et al. Rupture and hemorrhage of hepatic focal nodular hyperplasia. Am Surg 1995;61:210–4.
[59] Whelant J, Baugh JH, Chander S, et al. Focal nodular hyperplasia of the liver. Ann Surg 1973;177:150–8.
[60] Semelka RC, Sofka CM. Hepatic hemangiomas. Magn Reson Imaging Clin N Am 1997;5:241–53.
[61] Sewell LJH, Weiss K. Spontaneous rupture of hemangioma of the liver. Arch Surg 1961;83:729–33.
[62] Soyer P, Levesque M. Haemoperitnoeum due to spontaneous rupture of hepatic hemangiomatosis: treatment by superselective arterial embolization and partial hepatectomy. Australas Radiol 1995; 39:90–2.
[63] Graham E, Cohen AW, Soulen M, Faye R. Symptomatic liver hemangioma with intratumor hemorrhage treated by angiography and embolization during pregnancy. Obstet Gynecol 1993;81:813–6.
[64] Bardeguez A, Chatterjee M, Tepedino M, Sicuranza B. Systemic cystic angiomatosis in pregnancy: a case presentation and review of the literature. Am J Obstet Gynecol 1990;163:42–5.
[65] Krasuki P, Poniecka A, Gal E, Wali A. Intrapartum spontaneous rupture of liver hemangioma. J Matern Fetal Med 2001;10:290–2.
[66] Scribano E, Loria G, Ascenti G, Vallone A, Gaeta M. Spontaneous hemoperitoneum from a giant multicystic hemangioma of the liver: a case report. Abdom Imaging 1996;21:418–9.
[67] Mittleman RE. Hepatic rupture due to metastatic lung carcinoma. Am J Clin Pathol 1987;88:506–9.
[68] Wong KT, Khir AS, Noori S, Peh SC. Fatal hemoperitoneum due to rupture of hepatic metastasis from renal cell carcinoma. Aust N Z J Surg 1994;64:128–9.
[69] Urdaneta LF, Nielsen JV. Massive hemoperitoneum secondary to spontaneous rupture of hepatic metastases: report of two cases and review of the literature. J Surg Oncol 1986;31:104–1047.
[70] Fidas-Kamini A, Busuttil A. Fatal haemoperitoneum from ruptured hepatic metastases from testicular teratomas. Br J Urol 1987;60:80–1.
[71] Dousei T, Miyata M, Yamaguchi T, Nagaota M, Takahashi E, Kawashima Y. Rupture of liver metastasis of malignant melanoma-a case of hepatic resection. Jpn J Surg 1991;21:480–4.
[72] Erb RE, Gibler WB. Massive hemoperitoneum following rupture of hepatic metastases from unsuspected choriocarcinoma. Am J Emerg Med 1989;7:196–8.
[73] Murakami R, Taniai N, Kumazaki T, Kobayashi Y, Ogura J, Ichikawa T. Rupture of a hepatic metastasis from renal cell carcinoma. J Clin Imaging 2000;24:72–4.
[74] Weinstein L. Syndrome of hemolysis, elevated liver enzymes, low platelet count: a severe consequence of hypertension in pregnancy. Am J Obstet Gynecol 1982;142:159–65.
[75] Byrd DE, Riely CA. Liver disease in preeclampsia. Gastroenterologist 1996;4:65–9.
[76] Rodriguez D, Velarde R, Cortez E, Hernandez R. Syndrome HELLP hematoma subcapsular e infarto hepaticos, presentacion de dos casos clinicos. Ginecol Obstet Mex 1997;66:4–7.
[77] Bujanda L, Beguiristain A, Alberdi F, et al. Spontaneous rupture of the liver in amyloidosis. Am J Gastroenterol 1997;92:1385–7.
[78] Lucien L, Ooi PJ, Lynch S. Spontaneous liver rupture in amyloidosis. Surgery 1996;120:117–9.
[79] Kosowsky JM, Gibler WB. Massive hemoperitoneum due to rupture of a retroperitoneal varix. J Emerg Med 2000;19:347–9.
[80] Hamlin AN, Morris JS, Lunzer MR, et al. Portal hypertension with varices in usual sites. Lancet 1974;2: 1531–4.
[81] Giagounidis AAN, Burk M, Meckenstock G, Koch AJ, Schneider W. Pathologic rupture of the spleen in haematologic malignancies: two additional cases. Ann Hematol 1996;73:297–302.
[82] Canady MR, Welling RE, Strobel ST. Splenic rupture in leukemia. J Surg Oncol 1989;41:194–7.
[83] Wallace JC. Diagnosis of splenic rupture in malignant lymphoma using radionuclides. Clin Nucl Med 1985; 10:7–8.
[84] Asano S, Wakasa H, Kaise S, Nishimaki T, Kasukawa R. Peliosis hepatis: report of two autopsy cases with a review of literature. Acta Pathol Jpn 1982;32:861–77.
[85] Ichijima K, Kobashi Y, Yamabe H, Fujii Y, Inoue Y. Peliosis hepatis: an unusual case involving multiple organs. Acta Pathol Jpn 1980;30:109–20.
[86] Fujikawa T, Hachiya J, Korenaga T, et al. A case of splenic peliosis. Rinsho Hoshasen 1986;31:115–58.
[87] Tsuda K, Nakamura H, Murakami T, et al. Peliosis of the spleen with intraperitoneal hemorrhage. Abdom Imaging 1993;18:283–5.
[88] Halpert B, Gyorkey F. Lesions observed in accessory spleens of 311 patients. Am J Clin Pathol 1959;31: 165–8.
[89] Richmond R, Humphrey P, Nichols WK. Isolated traumatic accessory splenic rupture: a case report and literature review. Mo Med 1992;89:351–3.
[90] Texeira MB, Hardin WJ. Spontaneous rupture of an accessory spleen. Am Surg 1974;40:491–3.
[91] Borioni R, Garofalo M, Innocenti P, et al. Hemoperitoneum due to spontaneous rupture of an aneurysm of the left gastroepiploic artery. J Cardiovasc Surg 1999;40:63–4.
[92] Stanley JC, Wakefield TW, Graham LM, et al. Clinical importance and management of splanchnic artery aneurysms. J Vasc Surg 1986;3:336–40.
[93] Shanley CJ, Shah NL, Messina LM. Common splanchnic artery aneurysms: splenic, hepatic and celiac. Ann Vasc Surg 1996;10:315–22.
[94] Stanley JC, Thompson NW, Fry WJ. Splanchnic artery aneurysms. In: Rutherford RB, editor. Vascular sur-

gery. 4th edition. Philadelphia: WB Saunders; 1995. p. 1124–39.
[95] Messina LM, Shanley CJ. Visceral artery aneurysms. Surg Clin North Am 1997;77:425–42.
[96] Werner K, Tarashoutchi F, Lunardi W, et al. Mycotic aneurysm of the celiac and superior mesentery artery in a case of infective endocarditis. J Cardiovasc Surg 1991;32:380–3.
[97] Lambert CJ, Williamson JW. Splenic artery aneurysm: a rare cause of upper gastrointestinal bleeding. Am Surg 1990;56:543–5.
[98] Voloudaki A, Tsagaraki K, Mouzas J, Gourtsoyiannis N. Gastric ulcer bleeding: diagnosis by computed tomography. Eur J Radiol 1999;30:245–7.
[99] Fishman EK, Urban BA, Hruban RH. CT of the stomach: spectrum of diseases. Radiographics 1996; 16:1035–54.
[100] Basu AK, Ganguli S, Ghosh H. Spontaneous neonatal gastric perforation causing hemo-pneumoperitoneum. Indian Pediatr 1988;25:690–2.
[101] Stabile BE, Wilson SE, Debas HT. Reduced mortality from bleeding pseudocysts and pseudoaneurysms caused by pancreatitis. Arch Surg 1993;118:45–51.
[102] Burke JW, Erikcson SJ, Kellum CD, et al. Pseudoaneurysms complicating pancreatitis: detection by CT. Radiology 1986;161:447–50.
[103] Bresler L, Boissel P, Grosdidier J. Major hemorrhage from pseudocyst and pseudoaneurysms caused by chronic pancreatitis: surgical therapy. World J Surg 1991;15:649–53.
[104] Gadacz TR, Trunkey D, Kieffer Jr RF. Visceral vessel erosion associated with pancreatitis. Arch Surg 1978; 113:1438–40.
[105] Kahn LA, Kamen C, McNamara MP. Variable color Doppler appearance of pseudoaneurysm in pancreatitis. AJR Am J Roentgenol 1994;162:187–8.
[106] Steckman ML, Dooley MC, Jaques PF, Powell DW. Major gastrointestinal haemorrhage from peripancreatic blood vessels in pancreatitis: treatment by embolotherapy. Dig Dis Sci 1984;29:486–97.
[107] Urban BA, Curry CA, Fishman EK. Complications of acute pancreatitis: helical CT evaluation. Emerg Radiol 1999;6:113–20.
[108] Merckle E, Görich J. Imaging of acute pancreatitis. Eur Radiol 2002;12:1979–92.
[109] Waslen T, Wallace K, Burbridge B, Kwauk S. Pseudoaneurysm secondary to pancreatitis presenting as GI bleeding. Abdom Imaging 1998;23:318–21.
[110] Perez C, Llauger J, Pallardo Y, et al. Radiologic diagnosis of pseudoaneurysm complicating pancreatitis. Eur J Radiol 1993;16:102–6.
[111] Hertzberg BS, Kliewer MA, Paulson EK. Ovarian cyst rupture causing hemoperitoneum: imaging features and potential role for misdiagnosis. Abdom Imaging 1999;24:304–8.
[112] Hertzberg BS, Kliewer MA, Bowie JD. Adnexal ring sign and hemoperitoneum caused by hemorrhagic ovarian cyst: pitfall in the sonographic diagnosis of ectopic pregnancy. AJR Am J Roentgenol 1999;173: 1301–2.
[113] Jain KA. Sonographic spectrum of hemorrhagic ovarian cysts. J Ultrasound Med 2002;21:879–86.

RADIOLOGIC CLINICS OF NORTH AMERICA

Radiol Clin N Am 41 (2003) 1203–1216

Ultrasound and CT evaluation of emergent gallbladder pathology

Genevieve L. Bennett, MD*, Emil J. Balthazar, MD

Abdominal Imaging Division, Department of Radiology, New York University Medical Center, 560 First Avenue, Room HW207, New York, NY 10016, USA

This article provides a review of ultrasound and CT findings in acute conditions of the gallbladder. Although ultrasound or hepatobiliary scintigraphy are usually the initial imaging examinations of choice to evaluate most suspected cases of acute gallbladder pathology, the role of CT in the evaluation of abdominal pain continues to expand. The cause of patient symptoms is often initially unclear because clinical findings may be nonspecific. In this setting, CT allows for more comprehensive evaluation of the abdomen and pelvis and can identify other inflammatory processes that clinically may simulate gallbladder pathology. In many instances, CT may be the initial diagnostic procedure performed; it is important to become familiar with the spectrum of CT findings in emergent gallbladder disorders. Furthermore, CT plays an important role in the evaluation of associated complications of these disorders, facilitating prompt diagnosis and appropriate management.

Acute cholecystitis

Acute cholecystitis results from obstruction of the cystic duct or gallbladder neck with resulting inflammation of the gallbladder wall. In most patients this is caused by gallstones, with acalculous cholecystitis occurring in approximately 5% to 10%. Although most patients present with right upper quadrant pain and tenderness, there may be a diagnostic challenge in the setting of severe advanced inflammation or in elderly patients or those with systemic diseases, such as diabetes. In a patient with suspected acute cholecystitis, ultrasonography or hepatobiliary scintigraphy is usually the initial imaging procedure of choice. CT may be performed initially, however, if the cause of symptoms is unclear or if ultrasound findings are equivocal. Furthermore, CT plays a very useful role in the evaluation of suspected complications of acute cholecystitis, such as emphysematous cholecystitis or gallbladder perforation, as discussed later.

The ultrasound findings in acute uncomplicated cholecystitis are well-described [1–4] and include gallstones, often impacted in the gallbladder neck or cystic duct; a positive sonographic Murphy's sign; gallbladder distention; wall thickening; and pericholecystic fluid (Fig. 1). Of these findings, the first two are considered the most specific. In a study by Ralls et al [3], a positive sonographic Murphy's sign and the presence of gallstones had a positive predictive value of 92% for the diagnosis of acute cholecystitis. A sonographic Murphy's sign is considered positive if maximal tenderness is elicited over the gallbladder visualized at sonography [2]. It may not always be possible to evaluate for this finding, however, if the patient is not responsive or if pain medication has been administered, which may blunt the response. This sign may also be absent in cases of gangrenous cholecystitis (see later) [5]. If it can be demonstrated that a stone is impacted in the gallbladder neck or cystic duct, this is also an important finding that increases the likelihood of acute cholecystitis. To determine that a stone is impacted in the gallbladder neck or cystic duct requires evaluating the patient in the prone or left lateral decubitus position.

* Corresponding author.

E-mail address: genevieve.bennett@med.nyu.edu (G.L. Bennett).

0033-8389/03/$ – see front matter
doi:10.1016/S0033-8389(03)00097-6

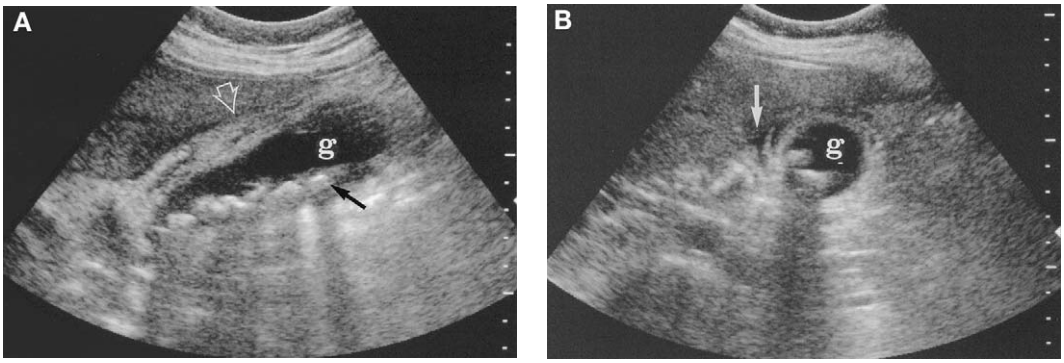

Fig. 1. Acute uncomplicated cholecystitis. Ultrasound of a 45-year-old woman with right upper quadrant pain and fever. (*A*) Ultrasound image of the gallbladder (g) in the sagittal plane demonstrates distention of the gallbladder, which contains multiple shadowing gallstones (*solid arrow*). The gallbladder wall is thickened (*open arrow*) with a striated appearance consistent with edema. (*B*) Transverse image of the gallbladder (g) also demonstrates pericholecystic fluid (*arrow*). There was a positive sonographic Murphy sign. At surgery, acute uncomplicated cholecystitis was confirmed.

The CT findings of acute cholecystitis also have been described [6–8] and include gallstones, gallbladder distention, thickening of the gallbladder wall, pericholecystic inflammation, and fluid (Fig. 2). CT is limited with respect to the detection of gallstones and only approximately 75% are detected [6]. Visualization depends, in large part, on the degree of calcification, although the presence of gas within a noncalcified stone (Mercedes-Benz sign) is often suggestive. An additional useful sign of gallbladder inflammation that may be visualized at CT includes increased enhancement in the liver parenchyma adjacent to the gallbladder secondary to associated hyperemia (Fig. 3) [9,10]. Of all these findings, the presence of pericholecystic inflammatory change is believed to be the most specific [6,8] because other findings, such as gallbladder wall thickening and distention, do not necessarily indicate the presence of inflammation.

Mirvis et al [11] have divided the CT findings of acute cholecystitis into major and minor findings. According to these authors, major criteria include calculi, thickened gallbladder wall, pericholecystic fluid, and subserosal edema. Minor criteria include gallbladder distention and sludge. They concluded that if one major and two minor criteria are present, the diagnosis of acute cholecystitis can be made. In a recent retrospective study at the authors' institution

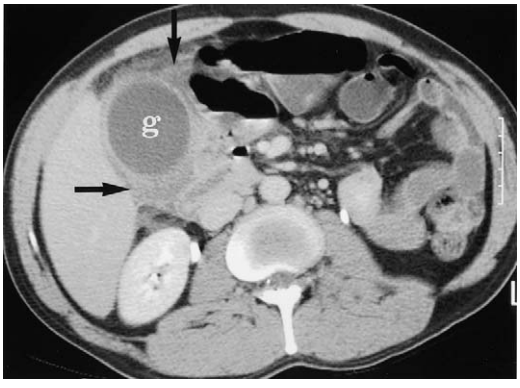

Fig. 2. Acute cholecystitis. CT of a 40-year-old man with right upper quadrant pain and fever. CT with intravenous (IV) contrast demonstrates distended gallbladder (g) with thickened wall, and surrounding pericholecystic fluid and inflammatory change (*arrows*).

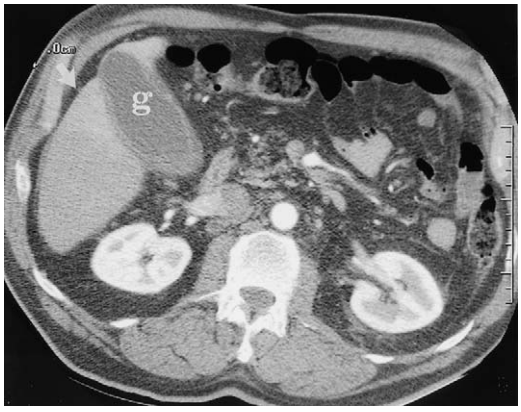

Fig. 3. Acute cholecystitis. CT of a 55-year-old man with right upper quadrant pain and fever. CT with IV contrast demonstrates distended gallbladder (g) with thickened wall. There is increased enhancement of the liver parenchyma in the gallbladder fossa (*arrow*) secondary to hyperemia related to adjacent inflammation.

[12], the overall sensitivity, specificity, and accuracy of CT for the diagnosis of acute cholecystitis were 91.7%, 99.1%, and 94.3%, respectively.

In approximately 5% to 10% of patients, cholecystitis occurs without gallstones (acalculous cholecystitis). This usually occurs in the setting of prolonged illness, such as patients with significant trauma or prolonged stay in the intensive care unit. This is often a difficult diagnosis to make clinically because findings are nonspecific. Many times, ultrasound is equivocal because these patients have distended, thick-walled gallbladders even in the absence of inflammation and the sonographic Murphy's sign is not reliable in these patients. Hepatobiliary scintigraphy is also limited with a significant false-positive rate in severely ill patients. The CT findings are similar with the exception of the absence of gallstones. CT may be more specific in these patients when ultrasound findings or hepatobiliary scintigraphy are nondiagnostic [6,11,13,14].

Gangrenous cholecystitis

Gangrenous cholecystitis is a severe advanced form of acute cholecystitis. The pathogenesis is believed to result from cystic duct obstruction, leading to marked distention of the gallbladder and ultimately ischemic necrosis of the wall [15]. The incidence ranges from 2% to 29.6% in surgical series [16–19]. This is more common in men, patients of advanced age, and those with coexisting cardiovascular disease. Once suspected, patients with gangrenous cholecystitis generally undergo emergency cholecystectomy to avoid life-threatening complications, with a higher conversion rate to open chole-

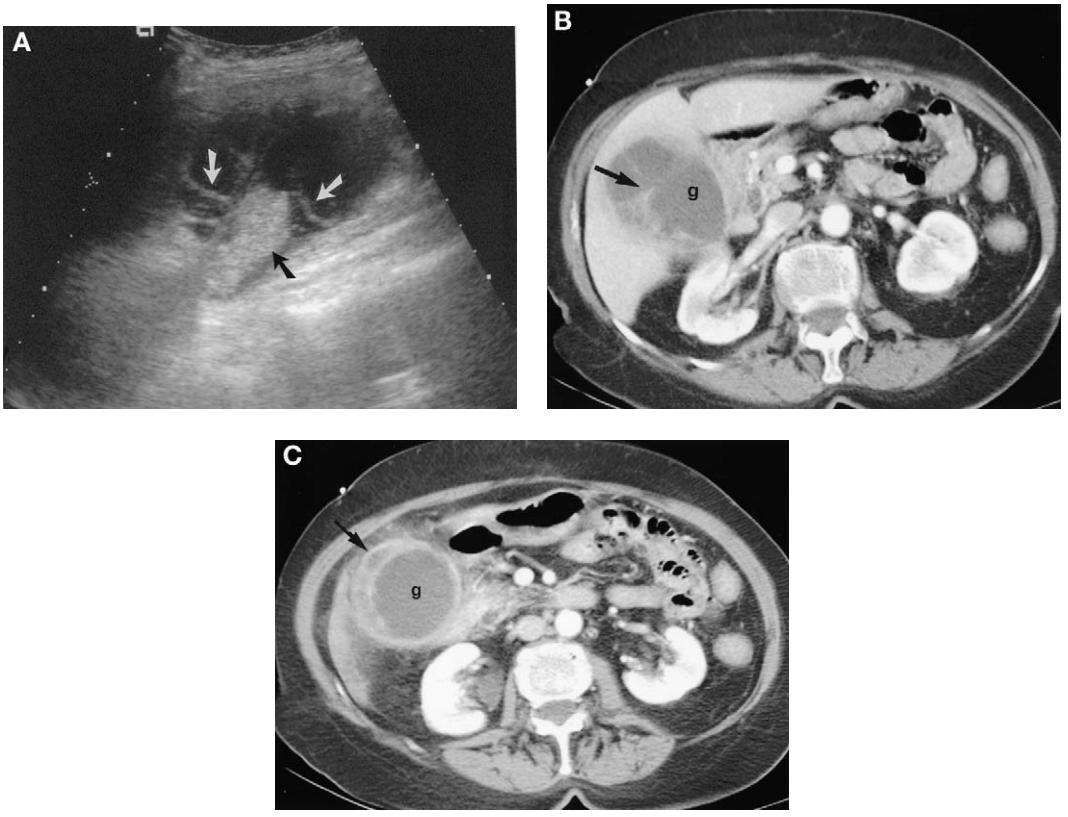

Fig. 4. Acute gangrenous cholecystitis. An 80-year-old woman with fever and abdominal pain. (*A*) Ultrasound image demonstrates linear echogenic foci within the gallbladder lumen (*white arrows*) consistent with intraluminal membranes caused by sloughed mucosa. There is also echogenic material consistent with sludge (*black arrow*). (*B*) CT with IV contrast demonstrates distended gallbladder (g) with intraluminal membranes (*arrow*) and pericholecystic inflammatory change. (*C*) Slightly more inferior image demonstrates irregularity of wall of gallbladder (g) with low-attenuation areas in the wall (*arrow*) representing intramural abscess.

cystectomy than in uncomplicated acute cholecystitis [20–22].

On sonography, the hallmark of gangrenous cholecystitis is the presence of heterogeneous or striated thickening of the gallbladder wall, which is often irregular with projections into the lumen [23,24]. Irregular or asymmetric thickening of the gallbladder wall likely results from ulceration, hemorrhage, necrosis, or microabscesses in the gallbladder wall, and in a series by Jeffrey et al [24] was present in 50% of patients. A striated appearance of the gallbladder wall was reported in 40% of patients by Teefey et al [23] in patients with gangrenous cholecystitis, but this may be seen in other conditions causing gallbladder edema. The presence of intraluminal membranes, which represent desquamated gallbladder mucosa, or fibrinous strands or exudate is a more specific finding, although less common (Fig. 4A). The sonographic Murphy's sign may be absent because of denervation of the gallbladder wall and was positive in only 33% of patients in the series by Simeone et al [5]. Pericholecystic fluid collection or abscess caused by associated gallbladder perforation or intramural abscess may also be observed (Fig. 5).

CT findings of gangrenous cholecystitis include intraluminal membranes, hemorrhage into the lumen, and irregular or absent wall (Fig. 4B,C) [6,8,25–27]. A recent study by the authors [12] evaluated the sensitivity and specificity of CT for the diagnosis of gangrenous cholecystitis. CT was highly specific for identifying acute gangrenous cholecystitis (96%) but had low sensitivity (29.3%). The findings in their series that were most specific for gangrenous cholecystitis were gas in the wall or lumen, intraluminal membranes, irregularity or absence of the gallbladder wall, pericholecystic abscess, and lack of gallbladder wall enhancement (see Fig. 4; Figs. 6, 7). The authors also found that the presence of pericholecystic fluid was predictive of the severity of acute cholecystitis. The greater degree of gallbladder distention in the short axis and the degree of mural thickening also correlated with a higher likelihood of gangrenous cholecystitis. The ability of CT to identify gangre-

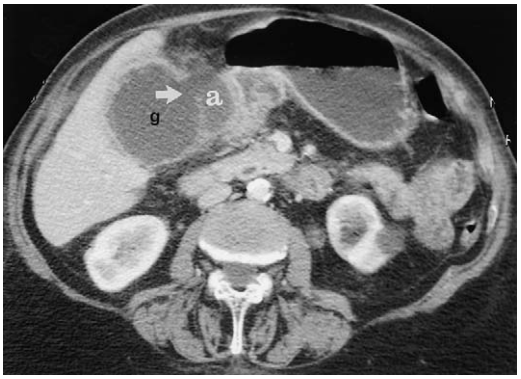

Fig. 6. Acute gangrenous cholecystitis with pericholecystic abscess. CT of a 72-year-old woman with right upper quadrant pain and fever. CT with IV contrast demonstrates distended gallbladder (g) with irregular wall. There is a focal defect in the wall of the gallbladder (*arrow*) with encapsulated pericholecystic fluid collection consistent with abscess (a).

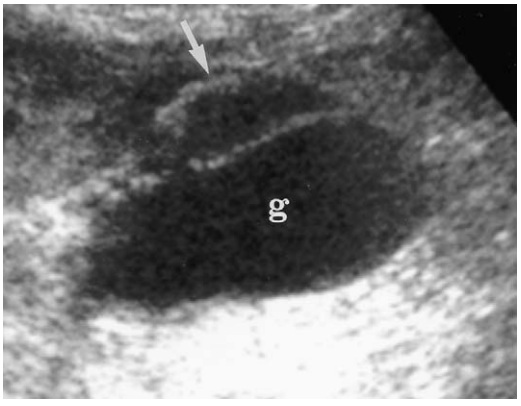

Fig. 5. Acute gangrenous cholecystitis. Intramural abscess in an 80-year-old man with right upper quadrant pain and fever. Ultrasound demonstrates distended gallbladder (g) with thickened wall and hypoechoic area in the wall, consistent with intramural abscess (*arrow*).

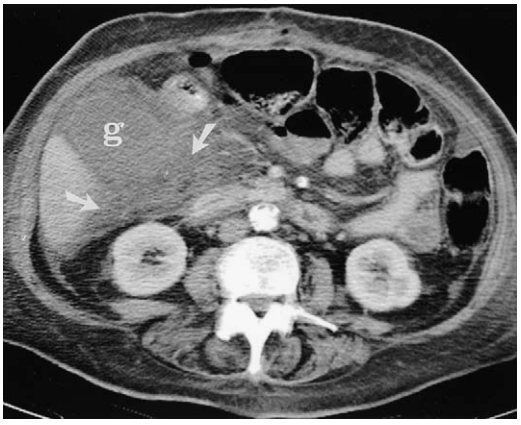

Fig. 7. Acute gangrenous cholecystitis: lack of gallbladder wall enhancement at CT. An 83-year-old woman with sepsis. CT with IV contrast demonstrates distended gallbladder (g) with extensive pericholecystic inflammatory change and fluid (*arrows*). There is no contrast enhancement of the gallbladder wall.

nous cholecystitis is greatest if intravenous contrast is administered because this allows for evaluation of gallbladder wall enhancement and mural contour.

Hemorrhagic cholecystitis

Hemorrhagic cholecystitis is a rare complication of acute cholecystitis and has been reported in both the presence and absence of gallstones [28–30]. It is believed that hemorrhage results from inflammation causing mucosal ulceration and necrosis. Arteriosclerotic change in the gallbladder wall most likely is a predisposing factor [30]. Classically, the clinical presentation includes biliary colic, jaundice, hematemesis, and melena. Occasionally, the patient may present with massive upper gastrointestinal bleeding, hemoperitoneum, or obstruction of the common bile duct [31]. Other etiologies of blood in the gallbladder include neoplasm; vascular abnormalities, such as aneurysms; trauma; anticoagulation; or ectopic pancreatic or gastric mucosa.

At sonography, blood in the gallbladder appears as echogenic material within the lumen, which demonstrates higher echogenicity than sludge (Fig. 8A). This may form a dependent layer; however, blood clots may appear as clumps or masses adherent to the gallbladder wall [28,32]. As the hemorrhage evolves, this may have a cystic appearance [33]. At CT, in addition to other findings of cholecystitis, increased density of bile is also noted (Fig. 8B). A fluid-fluid level may be noted (Fig. 8C). Other conditions that cause high-density bile include recently administered intravenous contrast or milk of calcium, although these do not generally appear echogenic at sonography and do not form a fluid-fluid level. Associated perforation of the gallbladder may lead to hemoperitoneum (Fig. 9). Prompt diagnosis is essential be-

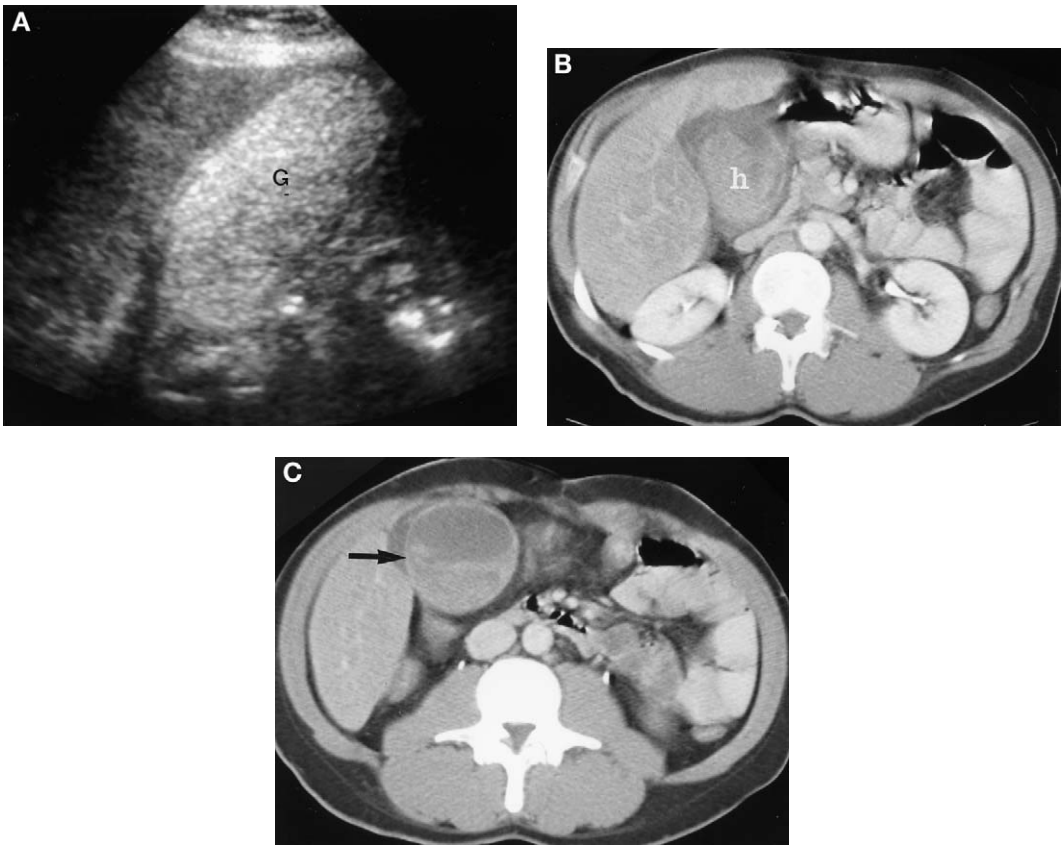

Fig. 8. Acute hemorrhagic cholecystitis. Ultrasound of a 60-year-old man with right upper quadrant pain and fever. (*A*) Ultrasound demonstrates that the gallbladder (G) is distended and is filled with highly echogenic material. (*B*) CT image demonstrates distended gallbladder with high-attenuation material in the lumen consistent with hemorrhage (h). (*C*) Slightly more inferior image demonstrates fluid-fluid level (*arrow*) in the gallbladder lumen secondary to hematocrit effect.

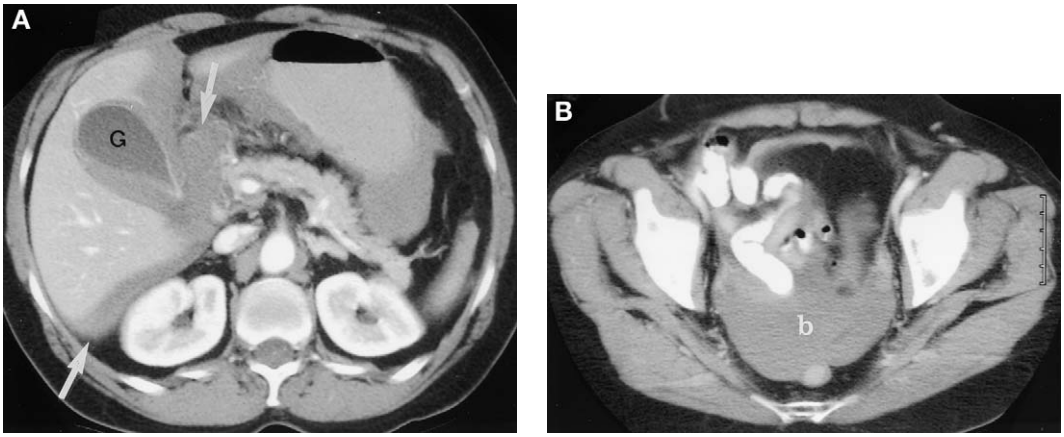

Fig. 9. Acute hemorrhagic cholecystitis with gallbladder perforation. A 50-year-old woman with abdominal pain and hypotension. (*A*) CT with IV contrast demonstrates fluid-fluid level in the gallbladder lumen (G). There is surrounding high-attenuation ascites (*arrows*) consistent with hemoperitoneum caused by associated perforation of the gallbladder. (*B*) A large amount of blood (b) also is present in the pelvis.

cause hemorrhagic cholecystitis is associated with a high mortality rate.

Emphysematous cholecystitis

Emphysematous cholecystitis is a rare life-threatening and rapidly progressive complication of acute cholecystitis. Vascular compromise of the cystic artery is believed to play a role in the development of this complication with proliferation of gas-forming organisms in an anaerobic environment and penetration of gas into the gallbladder wall [34,35]. Commonly isolated organisms include *Clostridium welchii* and *Escherichia coli* [35]. There are distinct differences between emphysematous cholecystitis and acute cholecystitis, which suggest a separate pathogenesis [36]. These include a male preponderance (up to 71%); frequent occurrence in diabetic patients (up to 50%); lack of gallstones in up to one third of patients; and a higher risk of gallbladder gangrene and perforation. On pathologic review, gallbladders with emphysematous cholecystitis have a higher incidence of endarteritis obliterans supporting vascular insufficiency as a causative factor. The mortality rate for emphysematous cholecystitis is 15% versus 4% in uncomplicated acute cholecystitis [36] and prompt surgical intervention is required. The exact incidence is unknown; however, in one recent surgical series, a total of eight cases were seen over a period of 5 years [37].

The clinical presentation of emphysematous cholecystitis is often indistinguishable from that of uncomplicated acute cholecystitis. In particular, symptoms may not be severe in the diabetic patient. The diagnosis should be suspected in the correct clinical setting and relies on imaging findings. Emphysematous cholecystitis may be diagnosed on the basis of abdominal radiographs and is classically described in three stages. Stage 1 includes gas in the gallbladder lumen, stage 2 includes gas in the gallbladder wall, and stage 3 includes gas in the pericholecystic tissues. Either CT or ultrasound is more sensitive in detecting smaller amounts of gas. The ultrasound findings of emphysematous cholecystitis vary depending on the amount and location of gas [1,38,39]. If there is a small amount of gas in the wall, there are echogenic foci in the gallbladder wall with associated ring down or comet-tail artifact. With larger amounts of gas and intraluminal gas, there is a wide curvilinear arc of increased echogenicity with associated "dirty" posterior acoustic shadowing (Fig. 10A) [1]. In these instances, the gallbladder may be difficult to visualize because of the extensive shadowing, and sometimes differentiation from a contracted gallbladder with stones or a porcelain gallbladder with calcified wall may be problematic [38].

CT has a higher sensitivity than sonography for the diagnosis of emphysematous cholecystitis [37]. If emphysematous cholecystitis is suspected at sonography or if there is a high clinical index of suspicion, CT should be performed. CT should also be performed in the patient with suspected acute cholecystitis in whom the gallbladder cannot be visualized adequately at sonography. CT findings include gas within the gallbladder lumen or wall (Figs. 10B, 11)

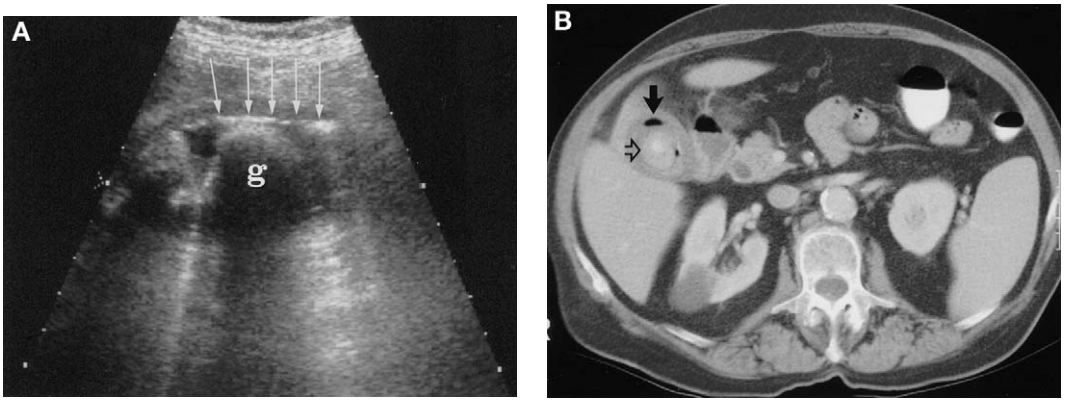

Fig. 10. Emphysematous cholecystitis. A 65-year-old woman with diabetes with right upper quadrant pain and fever. (*A*) Ultrasound demonstrates distended gallbladder (g) with stones and sludge in the lumen. Linear echogenic foci, which parallels the anterior wall of the gallbladder (*arrows*), represents air in the gallbladder wall. (*B*) These findings are confirmed at CT where there is a gallstone (*open arrow*) in the gallbladder and air in the gallbladder wall (*arrow*). (Courtesy of Joseph Yee, MD, New York, NY.)

[40] and extension into the pericholecystic tissues. If free air is identified, this indicates perforation of the gallbladder and urgent surgery is required.

Gallbladder perforation

Gallbladder perforation is most often a complication of severe acute cholecystitis, in one series occurring with an incidence of 11.9% with associated mortality of 24.1% [41]. More recent series suggest an incidence of 8.3% [42]. Perforation of the gallbladder can also occur in the setting of chronic cholecystitis, cholelithiasis, trauma, neoplasm, steroids, or vascular compromise. Niemeier [43] classified gallbladder perforation into three types: (1) acute free perforation into the peritoneal cavity, (2) subacute perforation with pericholecystic abscess, and (3) chronic perforation with cholecystoenteric fistula. In most series, subacute perforation with pericholecystic abscess is the most common type [44]. Abscess formation may be confined to the gallbladder fossa or spread into the peritoneal cavity or rarely extend into the liver [45,46]. A stone impacted in the cystic duct results in obstruction of the gallbladder, which leads to gallbladder distention. Bile salts in the gallbladder lumen produce a chemical inflammatory reaction of the mucosa. Progressive distention leads to vascular compromise followed by gangrene, necrosis, and perforation [42,47]. The fundus is the most frequent site of perforation because of the relatively poor blood supply of this area. Associated life-threatening complications of gallbladder perforation include bacteremia, septic shock, bile peritonitis, and abscess formation, with a wide range of reported mortality rates from 6% to 70% [41,43,44,48,49] depending on the type of perforation. In one series [44], there was a 40% mortality rate associated with type 1 free perforation and a 4% mortality rate for type 2. One third of patients with type 3 perforation present with gallstone ileus, which is discussed further later.

Correct preoperative diagnosis of gallbladder perforation is important to facilitate prompt surgical

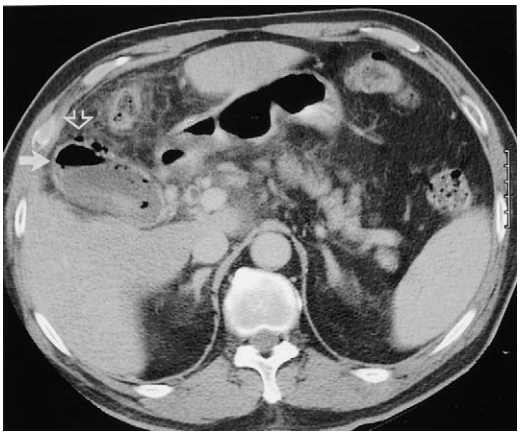

Fig. 11. Emphysematous cholecystitis. A 70-year-old diabetic man with fever and right upper quadrant pain. CT with IV contrast demonstrates air both within the lumen of the gallbladder (*solid arrow*) and within the wall (*open arrow*). There are adjacent inflammatory changes in the pericholecystic fat.

intervention and decrease morbidity and mortality. Clinical signs and symptoms are nonspecific and indistinguishable from uncomplicated acute cholecystitis; imaging plays a vital role in diagnosis. At sonography, which is usually the initial imaging test for evaluation of acute cholecystitis, findings may be nonspecific. The diagnosis may be suspected if the wall of the gallbladder is irregular or ill-defined or if there is a large amount of pericholecystic fluid or loculated fluid collection [47]. A focal defect in the wall is more specific, but not always visualized [50].

If ultrasound findings are equivocal, CT can be performed for further evaluation or to evaluate better the extent of inflammation [45,51,52]. At CT, a gallstone may be visualized outside of the gallbladder lumen [53]. Interruption of the gallbladder wall or a focal defect is an additional finding at CT that indicates gallbladder perforation. Perforation of the gallbladder may be contained and associated with pericholecystic or intrahepatic abscess (Figs. 12, 13). There may also, however, be free perforation associated with free fluid corresponding to bile (Fig. 14).

A study by Kim et al [52] compared ultrasound with CT findings in 13 patients with gallbladder perforation, confirmed at surgery. A defect in the gallbladder wall was visualized in seven patients (53.8%) at CT but no patient on ultrasound. Ultrasound and CT were similar in showing pericholecystic fluid collection, gallbladder wall thickening, and cholelithiasis. Bulging or irregular contour of the gallbladder wall was demonstrated on ultrasound in five cases and on CT in two cases. In all cases, the site of the gallbladder wall defect or bulging on ultrasound or CT corresponded to the site of perforation at the time of surgery. These authors concluded that CT was superior to ultrasound for the diagnosis of gallbladder perforation because of better ability to demonstrate a focal wall defect.

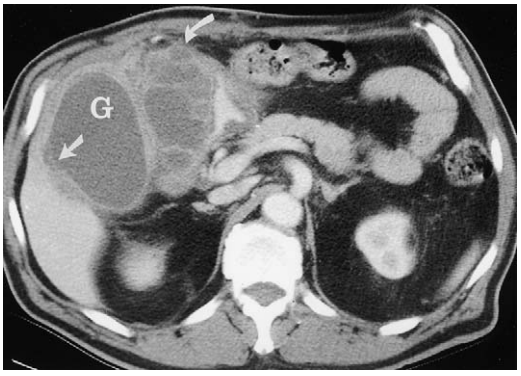

Fig. 12. Contained perforation of the gallbladder with abscess. A 50-year-old woman with sepsis. CT with IV contrast demonstrates that the gallbladder (G) is markedly distended with thickened, irregular wall, which has a focal defect (*straight arrow*). There is a large multiloculated pericholecystic fluid collection consistent with abscess (*curved arrow*).

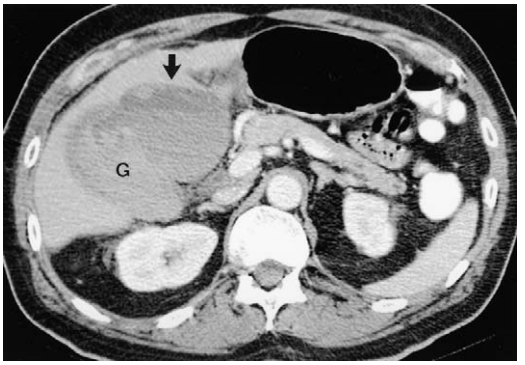

Fig. 13. Contained perforation of the gallbladder associated with hemorrhagic cholecystitis. A 60-year-old man with right upper quadrant pain. CT demonstrates high-attenuation material in the gallbladder (G) lumen consistent with hemorrhage. There is an adjacent pericholecystic fluid collection with fluid-fluid level (*arrow*) consistent with hematoma caused by associated gallbladder perforation.

Gallbladder trauma

Injury to the gallbladder occurs in approximately 2% of blunt abdominal trauma and may include contusion, perforation, and avulsion, with perforation being the most common [54]. Avulsion may be partial in which the gallbladder is partially torn from the liver bed, complete in which the gallbladder is completely torn from the liver bed but with intact cystic duct and artery, or total in which all gallbladder attachments are disrupted and the gallbladder lies free in the abdomen [55]. Prompt diagnosis is essential because delay in diagnosis may lead to substantial morbidity and mortality. The clinical findings are often nonspecific and other injuries may dominate the picture.

The CT findings of gallbladder trauma were reviewed in a series of seven patients [56]. In this series, four patients had gallbladder contusion, one had laceration, and one had intraluminal hemorrhage. CT findings associated with gallbladder injury were nonspecific but included pericholecystic fluid; ill-defined contour of the gallbladder wall; mass effect on the duodenum; high-attenuation material, representing hemorrhage, in the gallbladder lumen; a

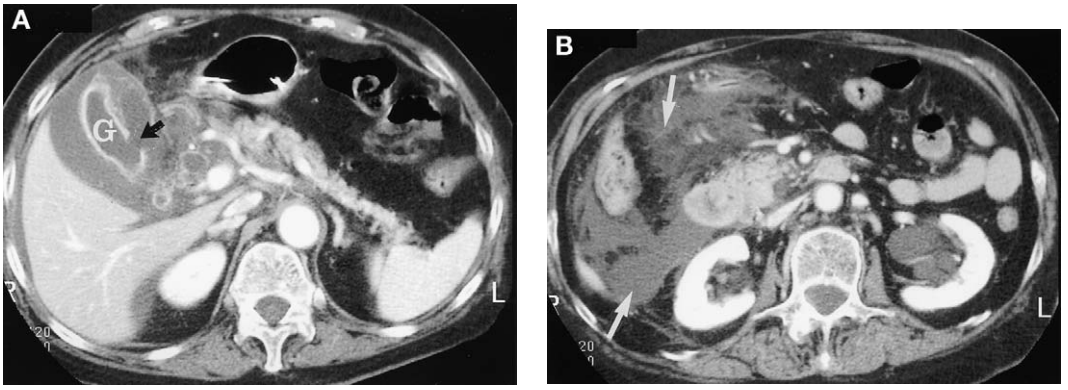

Fig. 14. Free perforation of the gallbladder. A 48-year-old woman with fever and peritonitis. (*A*) CT with IV contrast demonstrates marked thickening of the wall of the gallbladder (G). A focal defect in the gallbladder mucosa is evident (*arrow*). (*B*) More caudad image demonstrates fluid and inflammatory change (*arrows*) in the right paracolic gutter caused by free perforation of the gallbladder.

thickened gallbladder wall; and a nondistended or collapsed gallbladder lumen. Pericholecystic fluid was found in all patients, but is the least specific finding. Pericholecystic fluid associated with a collapsed gallbladder is more suggestive, however, of laceration or avulsion. Associated intra-abdominal injuries were found in six patients and included pericholecystic liver lacerations and duodenal hematoma or perforation. Only one patient had no other evidence of intra-abdominal injury. In other series, the incidence of associated intra-abdominal injuries ranges from 2.7 to 3.3 associated injuries per patient [54], with liver injury the most likely.

In patients with suspected gallbladder injury who do not undergo laparotomy for other reasons, an immediate baseline hepatobiliary scan may be performed to exclude extravasation. Follow-up ultrasound or CT in 3 to 4 weeks after injury to exclude increasing pericholecystic fluid and document resolution of findings also is recommended [56].

Gallstone ileus

Mechanical obstruction of the small bowel caused by an impacted gallstone (gallstone ileus) occurs

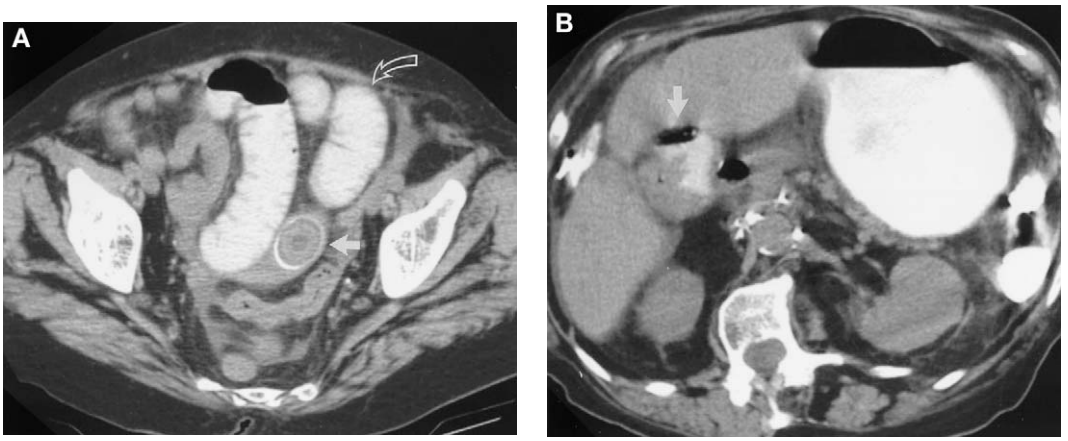

Fig. 15. Gallstone ileus. A 58-year-old woman with small bowel obstruction. (*A*) CT of the pelvis demonstrates dilated fluid-filled loops of small bowel (*open arrow*) with collapsed loops distally, consistent with small bowel obstruction. A calcified gallstone with laminated appearance is present at the transition point (*solid arrow*) and is the cause of obstruction. (*B*) CT image at the level of the gallbladder fossa demonstrates oral contrast and air in the gallbladder fossa (*arrow*) consistent with fistulization between the gallbladder and duodenum.

when a gallstone, usually greater than 2.5 cm, lodges in the small bowel. Overall this condition is responsible for 1% to 5% of cases of nonmalignant small bowel obstruction but increases to 25% in patients over the age of 65 [57]. Gallstone ileus results from perforation of the gallbladder and fistula formation between the gallbladder and adjacent viscus. In a review of 141 cases of cholecystoenteric fistula, Wakefield et al [58] found that in 101 patients the fistulous communication was between the gallbladder and duodenum, in 33 between the gallbladder and colon, and in 7 between the gallbladder and stomach. The most common sites of stone impaction are the ileum (54% to 65%); the jejunum (27%); and the duodenum (1% to 3%) [57]. Duodenal or pyloric obstruction from gallstone impaction is referred to as "Bouveret's syndrome" [59].

Less than half of the patients who present with gallstone ileus may present with a history of preceding gallbladder disease. Patients generally present with nonspecific signs of intestinal obstruction. The plain abdominal radiograph is usually the initial imaging evaluation. Findings include small bowel obstruction, visualization of the obstructing gallstone, and pneumobilia. [60]. This classic triad, however, is only visualized in up to 30% to 35% of patients [61]. CT scanning is increasingly being used to evaluate the patient with small bowel obstruction and not only confirms the presence of obstruction but often defines the site and etiology

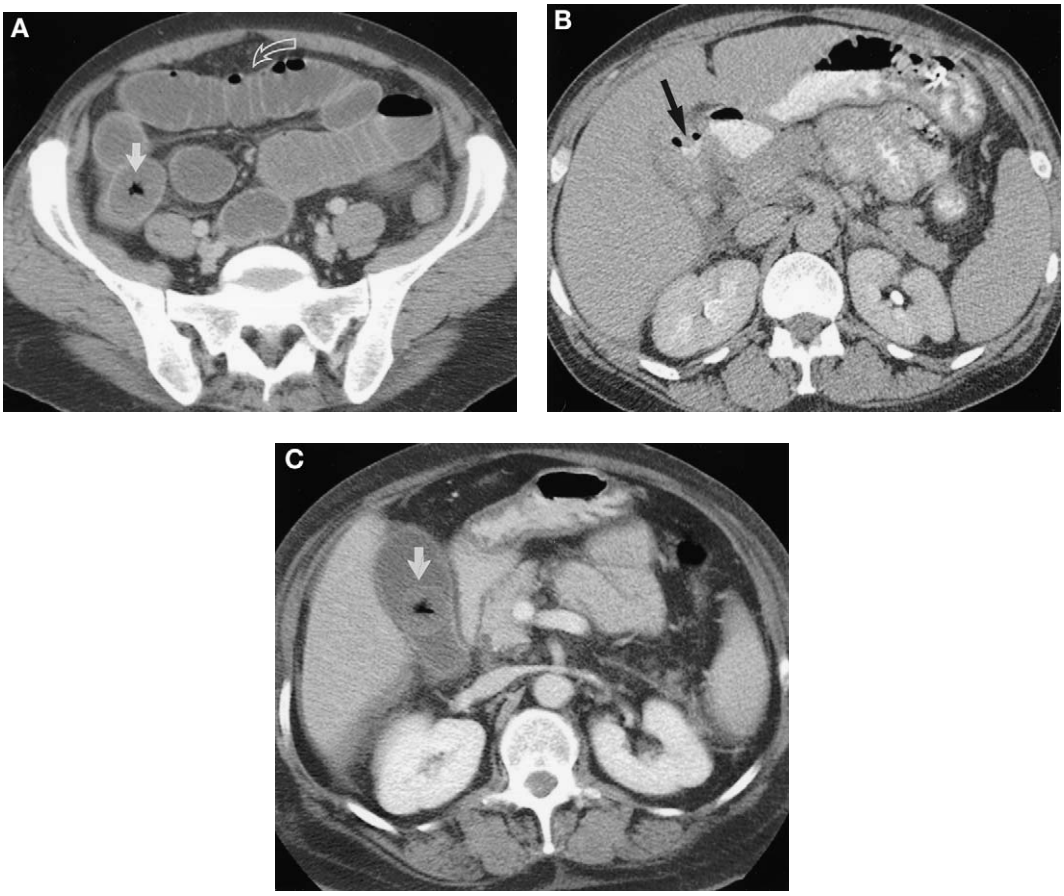

Fig. 16. Gallstone ileus. A 68-year-old man with small bowel obstruction. (*A*) CT of the pelvis demonstrates findings consistent with small bowel obstruction with multiple dilated fluid-filled loops of small bowel (*open arrow*). At the point of transition, there is an unusual collection of air located centrally within a fluid-filled loop of small bowel (*solid arrow*). This represents a low-attenuation cholesterol stone with gas. (*B*) CT image at the level of the gallbladder fossa demonstrates oral contrast in the gallbladder with fistulous tract to the duodenum visualized (*arrow*). (*C*) CT scan performed 1 year earlier demonstrated a noncalcified gallstone (*arrow*) containing gas (Mercedes Benz sign) in the gallbladder lumen. This gallstone is the cause of obstruction on the later scan.

of obstruction. CT offers the advantage over plain radiographs of increased visualization of gallstones at the site of obstruction and detection of small amounts of air in the gallbladder or biliary tree and direct demonstration of the cholecystoduodenal fistula (Fig. 15) [57,62–64]. Even if the gallstone is not calcified, the presence of a stone at the site of obstruction may be evident if there is gas present within the stone (Mercedes-Benz sign) (Fig. 16). A cholecystoenteric fistula may occur in the absence of gallstone ileus, usually a result of chronic gallbladder inflammation. CT findings include air in the gallbladder or biliary tree; contracted appearance of the gallbladder; and visualization of a fistulous tract, usually to the duodenum (Fig. 17) [65].

Mirizzi syndrome

Mirizzi syndrome is a rare complication of long-standing cholelithiasis and was first described by Mirizzi in 1948 [66]. This syndrome results from impaction of a large gallstone in the cystic duct. Associated surrounding inflammation causes narrowing of the common bile duct or there may be extrinsic compression of the common bile duct and obstructive jaundice results. A long or low insertion of the cystic duct into the common bile duct predisposes to this condition [67,68]. In a recent surgical series, this syndrome was found in 1.13% of all cholecystectomies [69]. This has been subclassified into two types by McSherry et al [70]: type I without cholecystocho-

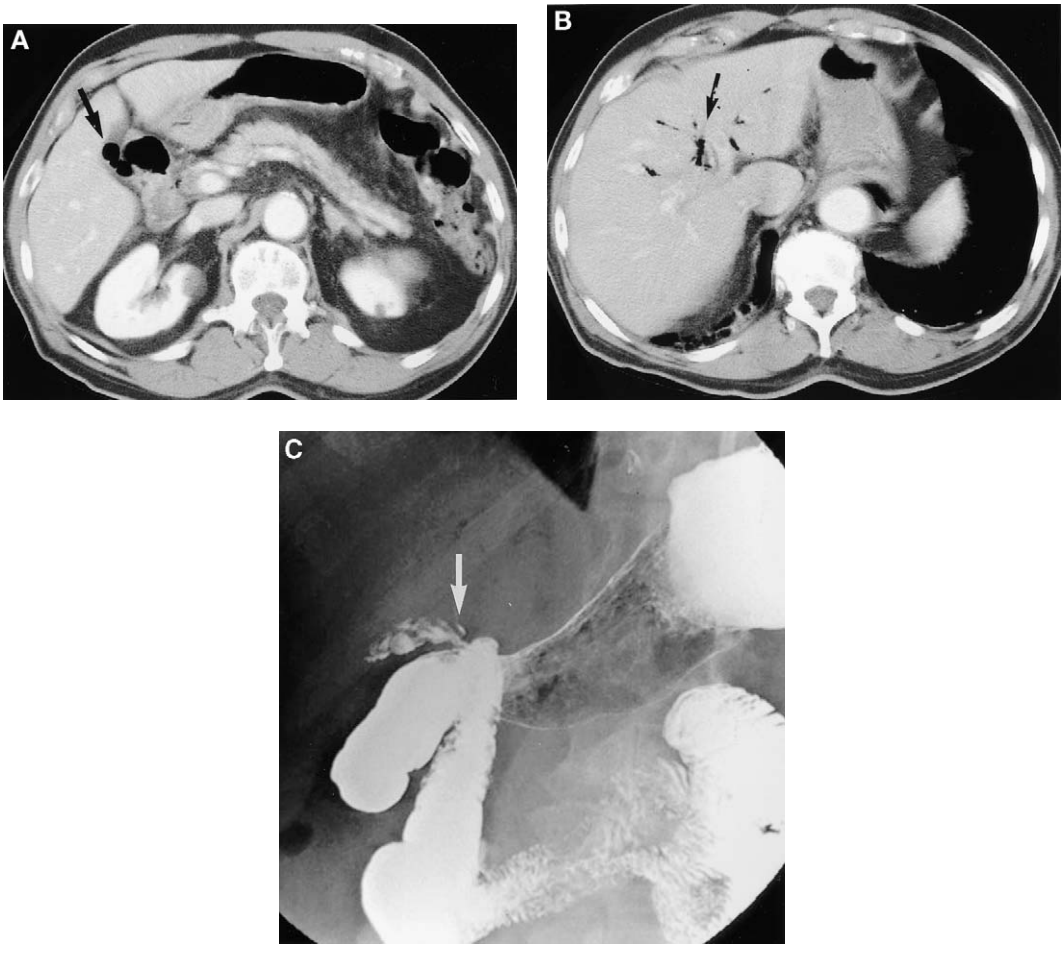

Fig. 17. Cholecystoduodenal fistula secondary to chronic cholecystitis. A 72-year-old man with abdominal pain. (*A*) CT image at the level of the gallbladder fossa demonstrates air in the gallbladder fossa (*arrow*) and air in the adjacent duodenal bulb. (*B*) More cephalad image demonstrates pneumobilia (*arrow*). (*C*) Fistula between gallbladder and proximal duodenum (*arrow*) is demonstrated on upper gastrointestinal series.

ledochal fistula and type II with cholecystocholedochal fistula. Preoperative diagnosis may be challenging; however, choice of surgical therapy may be altered to avoid common bile duct injury, which is increased when standard cholecystectomy is performed. In one series, the diagnosis was made preoperatively in 56% of patients [69]. Endoscopic retrograde cholangiopancreatography confirms biliary obstruction but may not visualize the stone in the cystic duct. Ultrasound confirms the presence of gallstones and common bile duct dilatation, and occasionally helps to visualize the impacted stone in the cystic duct (Fig. 18). More recently MR cholangiopancreatography (MRCP) has been advocated as the best imaging method to confirm this diagnosis because of the ability to demonstrate the level of biliary obstruction and whether stones are intraluminal or extrinsic [71]. CT may be limited because stones may not be radiopaque. Dilatation of the intrahepatic ducts and proximal common bile duct with collapse of the distal

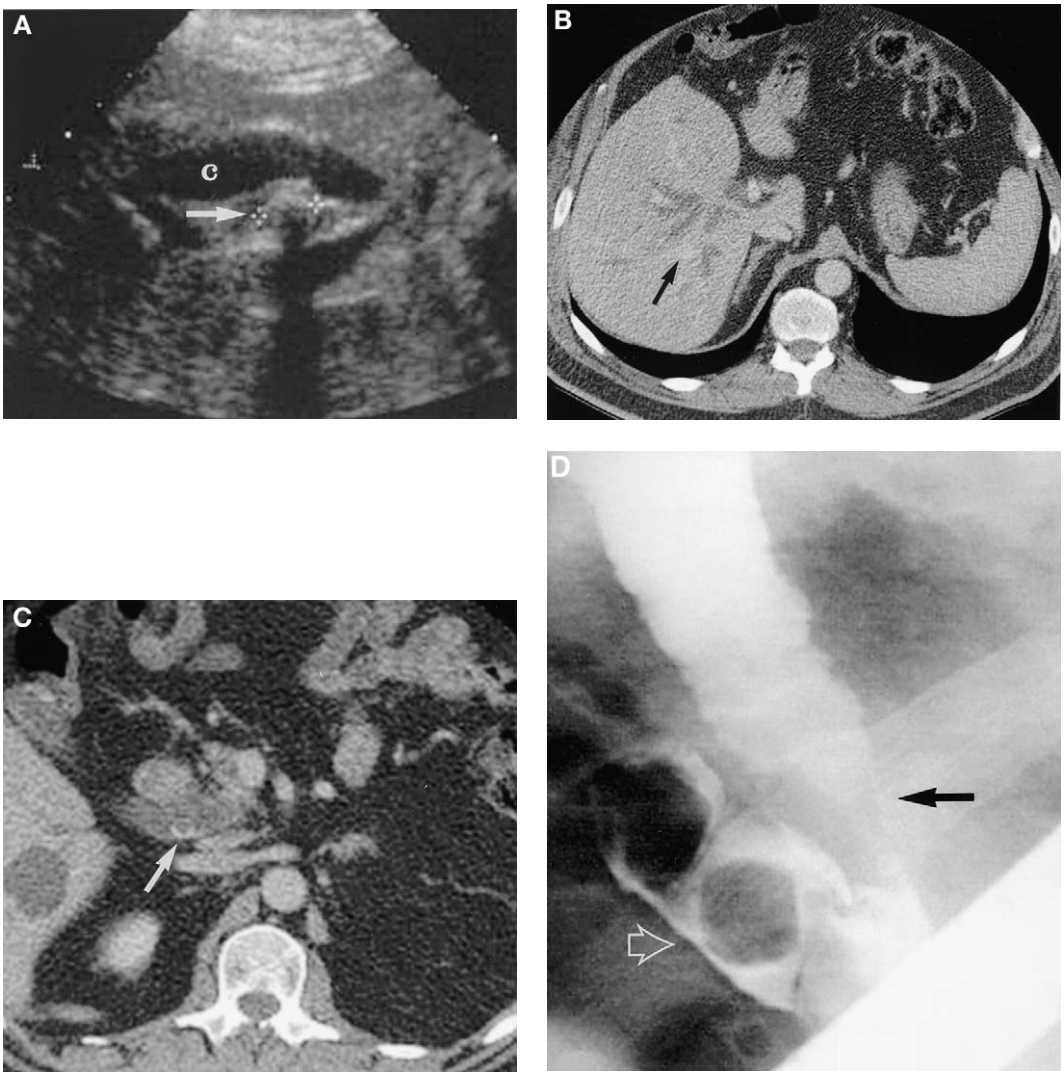

Fig. 18. Mirizzi syndrome. (*A*) Ultrasound demonstrates dilated common bile duct (c) measuring 12 mm, with distal tapering. A shadowing calculus (*arrow*) is visualized adjacent to the common bile duct at the transition point, consistent with a stone impacted in the cystic duct. (*B*) CT demonstrates intrahepatic biliary dilatation (*arrow*). (*C*) A calcified stone is visualized in the cystic duct (*arrow*). (*D*) Multiple stones in the cystic duct (*open arrow*) with narrowing of the distal common bile duct (*solid arrow*) and associated biliary dilatation are confirmed at endoscopic retrograde cholangiopancreatography.

common bile duct and the presence of a stone in the cystic duct, however, is suggestive of this diagnosis.

Summary

Ultrasound is the initial imaging modality of choice for the evaluation of suspected acute gallbladder disorders, and is often sufficient for correct diagnosis. CT also plays a vital role, however, in the evaluation of acute gallbladder pathology. CT is particularly useful in situations where ultrasound findings are equivocal. CT is also extremely valuable in the assessment of suspected complications of acute cholecystitis, particularly emphysematous cholecystitis, hemorrhagic cholecystitis, and gallbladder perforation, which are often very difficult diagnoses to establish at sonography. If CT is the initial imaging test performed in a patient with abdominal pain of uncertain etiology, recognition of the various disorders described in this article may eliminate the need for further imaging and facilitate appropriate management.

References

[1] Laing FC. The gallbladder and bile ducts. In: Rumack CM, Wilson SR, Charboneau JW, editors. Diagnostic ultrasound. 2nd edition. St. Louis: Mosby; 1998. p. 187–93.
[2] Sherman M, Ralls PW, Quinn M, et al. Intravenous cholangiography and sonography in acute cholecystitis: prospective evaluation. AJR Am J Roentgenol 1980; 135:311–3.
[3] Ralls PW, Colleti PM, Lapin SA, et al. Real-time sonography in suspected acute cholecystitis. Radiology 1985; 155:767–71.
[4] Laing FC, Federle MP, Jeffrey RB, et al. Ultrasonic evaluation of patients with acute right upper quadrant pain. Radiology 1981;140:449–55.
[5] Simeone J, Brink J, Mueller P, et al. The sonographic diagnosis of acute gangrenous cholecystitis: importance of the Murphy sign. AJR Am J Roentgenol 1989; 152:289–90.
[6] Paulson EK. Acute cholecystitis: CT findings. Semin Ultrasound CT MR 2000;21:56–63.
[7] Kane RA, Costello P, Duszlak E. Computed tomography in acute cholecystitis: new observations. AJR Am J Roentgenol 1983;141:697–701.
[8] Fidler J, Paulson EK, Layfield L. CT evaluation of acute cholecystitis: findings and usefulness in diagnosis. AJR Am J Roentgenol 1996;166:1085–8.
[9] Yamashita K, Jin MJ, Hirose Y, et al. CT findings of transient focal increased attenuation of the liver adjacent to the gallbladder in acute cholecystitis. AJR Am J Roentgenol 1995;164:343–6.
[10] Ito K, Awaya H, Mitchell DG, et al. Gallbladder disease: appearance of associated transient increased attenuation in the liver at biphasic, contrast-enhanced dynamic CT. Radiology 1997;204:723–8.
[11] Mirvis SE, Vainright JR, Nelson AW, et al. The diagnosis of acute acalculous cholecystitis: a comparison of sonography scintigraphy and CT. AJR Am J Roentgenol 1986;147:1171–5.
[12] Bennett GL, Rusinek H, Lisi V, Israel GM, Krinsky GA, Slywotzky CM, et al. CT findings in acute gangrenous cholecystitis. AJR Am J Roentgenol 2002;178:275–81.
[13] Blankenberg F, Wirth R, Jeffrey RB, Mindelzun R, Francis I. Computed tomography as an adjunct to ultrasound in the diagnosis of acute acalculous cholecystitis. Gastrointest Radiol 1991;16:149–53.
[14] Mirvis SE, Whitley NO, Miller JW. CT diagnosis of acalculous cholecystitis. J Comput Assist Tomogr 1987;11:83–7.
[15] Cotran RS, Kumar V, Robbins SL. Pathologic basis of disease. 4th edition. Philadelphia: WB Saunders; 1989.
[16] Morfin E, Ponka J, Brush B. Gangrenous cholecystitis. Arch Surg 1968;96:567–72.
[17] Wilson AK, Kozol RA, Salwen WA, Manov LJ, Tennenberg SD. Gangrenous cholecystitis in an urban VA hospital. J Surg Res 1994;56:402–4.
[18] Ahmad MM, Macon WL. Gangrene of the gallbladder. Am Surg 1983;49:155–8.
[19] Hunt DRH, Chu FCK. Gangrenous cholecystitis in the laparoscopic era. Aust N Z J Surg 2000;70:428–30.
[20] Merriam LT, Kanaan SA, Dawes LG, et al. Gangrenous cholecystitis: analysis of risk factors and experience with laparoscopic cholecystectomy. Surgery 1999;126: 680–6.
[21] Jacobs M, Verdeja J, Goldstein HS. Laparoscopic cholecystectomy in acute cholecystitis. J Laparoendosc Surg 1991;1:175–7.
[22] Singer JA, McKeen RV. Laparoscopic cholecystectomy for acute or gangrenous cholecystitis. Am Surg 1994;60:326–8.
[23] Teefey SA, Baron RL, Radke HM, Bigler SA. Gangrenous cholecystitis: new observations on sonography. J Ultrasound Med 1991;134:191–4.
[24] Jeffrey RB, Laing FC, Wong W, Callen PW. Gangrenous cholecystitis: diagnosis by ultrasound. Radiology 1983;148:219–21.
[25] Lamki N, Raval B, St. Ville E. Computed tomography of complicated cholecystitis. J Comput Assist Tomogr 1986;10:319–24.
[26] Varma DGK, Faust JM. Computed tomography of gangrenous acute postoperative acalculous cholecystitis. CT: The Journal of Computed Tomography 1988;12: 29–31.
[27] Bridges MD, Jones BC, Morgan DE, Fell SC. Acute cholecystitis and gallbladder necrosis: value of contrast enhanced CT [abstract]. AJR Am J Roentgenol 1999; 172:34–5.
[28] Jenkins M, Golding RH, Cooperberg PL. Sonography and computed tomography of hemorrhagic cholecystitis. AJR Am J Roentgenol 1983;140:1197–8.

[29] Shah VR, Clegg JF. Haemorrhagic cholecystitis. Br J Surg 1979;66:404–5.
[30] Hudson PB, Johnson PP. Hemorrhage from the gallbladder. N Engl J Med 1946;234:438–41.
[31] Polse S, Stoney RJ, Baldwin JN. Hemorrhage from the gallbladder. Calif Med 1967;107:51–3.
[32] Moskos MM, Eschelman DJ. Hemorrhagic cholecystitis. AJR Am J Roentgenol 1991;156:1304–5.
[33] Yiu-Chiu VS, Chiu LC, Wedel VJ. Acalculous hemorrhagic cholecystitis. CT; the Journal of Computed Tomography 1980;4:201–6.
[34] Jacob H, Appelman R, Stein HD. Emphysematous cholecystitis. Am J Gastroenterol 1979;71:325–30.
[35] May RE, Strong R. Acute emphysematous cholecystitis. Br J Surg 1971;58:453–8.
[36] Mentzer Jr RM, Golden GT, Chandler JG, Horsley JS. A comparative appraisal of emphysematous cholecystitis. Am J Surg 1975;129:10–5.
[37] Gill KS, Chapman AH, Weston MJ. The changing face of emphysematous cholecystitis. Br J Radiol 1997;70: 986–91.
[38] Konno K, Ishida H, Naganuma H, Sato M, Komatsuda T, Sato A, et al. Emphysematous cholecystitis: sonographic findings. Abdom Imaging 2002;27:191–5.
[39] Bloom RA, Libson E, Lebensart PD, et al. The ultrasound spectrum of emphysematous cholecystitis. J Clin Ultrasound 1989;17:251–6.
[40] Grayson DE, Abbott RM, Levy AD, Sherman PM. Emphysematous infections of the abdomen and pelvis: a pictorial review. Radiographics 2002;22:543–61.
[41] Diffenbaugh WG. Gangrenous perforation of the gallbladder. Arch Surg 1949;59:743–9.
[42] Strohl EL, Diffenbaugh WG, Baker JH, Chemma MH. Collective reviews; gangrene, and perforation of the gallbladder. Int Abst Surg 1962;114:1–7.
[43] Niemeier OW. Acute free perforation of the gallbladder. Ann Surg 1934;99:922–4.
[44] Fletcher AG, Ravdin IS. Perforation of the gallbladder. Am J Surg 1951;81:178–85.
[45] Peer A, Witz E, Manor H, Strauss S. Intrahepatic abscess due to gallbladder perforation. Abdom Imaging 1995;20:452–5.
[46] Chen JJ, Lin HH, Chiu CT, Lin DY. Gallbladder perforation with intrahepatic abscess formation. J Clin Ultrasound 1990;18:43–5.
[47] Madrazo BL, Francis I, Hricak H, Sandler MA, Hudak S, Gitschlag K. Sonographic findings in perforation of the gallbladder. AJR Am J Roentgenol 1982;139: 491–6.
[48] Heuer GJ. The factors leading to death in operations upon the gallbladder and bile ducts. Ann Surg 1934;99: 881–92.
[49] Cowley LL, Harkins HN. Perforation of the gallbladder. Surg Gynecol Obstet 1943;77:661–8.
[50] Chau WK, Na WT, Feng TT, et al. Ultrasound diagnosis of perforation of the gallbladder: real time application and the demonstration of a new sonographic sign. J Clin Ultrasound 1988;16:358–60.
[51] Fitoz S, Erden A, Karagulle T, Akyar S. Interruption of gallbladder wall with pericholecystic fluid: a CT finding of perforation. Emergency Radiology 2000;7:253–5.
[52] Kim PN, Lee KS, Kim IY, Bae WK, Lee BH. Gallbladder perforation: comparison of US findings with CT. Abdom Imaging 1994;19:239–42.
[53] Mocharla R, Shah HR. Gallbladder perforation with contained empyema diagnosed by CT but missed by sonography and hepatobiliary scintigraphy. AJR Am J Roentgenol 1997;168:283–4.
[54] Sharma O. Blunt gallbladder injuries: presentation of twenty-two cases with review of the literature. J Trauma 1993;39:576–80.
[55] Chen X, Talner LB, Jurkovich GJ. Gallbladder avulsion due to blunt trauma. AJR Am J Roentgenol 2001; 177:822.
[56] Erb RE, Mirvis SE, Shanmuganathan K. Gallbladder injury secondary to blunt trauma: CT findings. J Comput Assist Tomogr 1994;18:778–84.
[57] Chen MYM. Gallstone ileus: CT findings. Appl Radiol 1991;20:37–8.
[58] Wakefield EG, Vickers PM, Walters W. Intestinal obstruction caused by gallstones. Surgery 1939;5:670–3.
[59] Bortoff GA, Chen MYM, Ott DJ, Wolfman NT, Routh WD. Gallbladder stones: imaging and intervention. Radiographics 2000;20:751–66.
[60] Rigler LG, Borman CN, Noble JF. Gallstone obstruction: pathogenesis and roentgen manifestations. JAMA 1941;117:1753–9.
[61] Balthazar EJ, Schechter LS. Air in gallbladder: a frequent finding in gallstone ileus. AJR Am J Roentgenol 1978;131:219–22.
[62] Delabrousse E, Bartholomot B, Sohm O, Wallerand H, Kastler B. Gallstone ileus: CT findings. Eur Radiol 2000;10:938–40.
[63] Loren I, Lasson A, Nilsson A, Nilsson P, Nirhov N. Gallstone ileus demonstrated by CT. J Comput Assist Tomogr 1994;18:262–5.
[64] Swift SE, Spencer JA. Gallstone ileus: CT findings. Clin Radiol 1998;53:451–6.
[65] Shimono T, Nishimura K, Hayakawa K. CT imaging of biliary enteric fistula. Abdom Imaging 1998;23:172–6.
[66] Mirizzi PCJ. Sindrome del conducto hepatico. Int Chir 1948;8:731–77.
[67] Pemberton M, Wells AD. The Mirizzi syndrome. Postgrad Med J 1997;73:487–90.
[68] Koehler RE, Melson GL, Lee JKT, et al. Common hepatic duct obstruction by cystic duct stone: Mirizzi syndrome. AJR Am J Roentgenol 1979;132:1007–9.
[69] Karademir S, Astarcioglu H, Sokmen S, et al. Mirizzi's syndrome: diagnostic and surgical considerations in 25 patients. J Hepatobiliary Pancreat Surg 2000;7:72–7.
[70] McSherry C, Ferstenberg H, Virshup M. The Mirizzi syndrome: suggested classification and surgical therapy. Surg Gastroenterol 1982;1:219–25.
[71] Kim PN, Outwater EK, Mitchell DG. Mirizzi syndrome: evaluation by MR imaging. Am J Gastroenterol 1999;94:2546–50.

RADIOLOGIC
CLINICS OF
NORTH AMERICA

Radiol Clin N Am 41 (2003) 1217–1226

Interventional approach to pancreatic fluid collections

Joseph T. Ferrucci III, MD, Peter R. Mueller, MD*

Division of Abdominal Imaging and Intervention, Department of Radiology, Massachusetts General Hospital, White 270, 55 Fruit Street, Boston, MA 02114, USA

The classification of upper abdominal fluid collections complicating acute and chronic pancreatitis has long been a controversial subject. Each type of collection differs with respect to prognosis and management. Pancreatic fluid collections complicating pancreatitis was advanced by Bradley [1], who convened a panel of international experts in 1992. This group produced a classification of the features of peripancreatic effusions, pancreatic pseudocyst, pancreatic abscess, and pancreatic necrosis. It has long been demonstrated that patients with acute pancreatitis fall into two major groups. Most develop what Bradley termed "mild acute pancreatitis." These patients usually show both clinical and biochemical improvement within 48 to 72 hours. More severe damage leads to several specific local complications variously defined as peripancreatic effusions, pseudocysts, abscess, and pancreatic necrosis (Fig. 1).

Technique

Access route planning

To a significant extent, most pancreatic fluid collections involve or replace a large component of the lesser peritoneal sac and the percutaneous approach to catheter drainage targets that region (Fig. 2). Access routes are chosen to avoid traversing vital intervening structures, especially the colon and stomach. Wherever possible, a retroperitoneal approach through the lateral flank is preferred to an anterior approach across the peritoneal cavity. Collections involving the tail of the pancreas may be approached through the left anterior perirenal space usually behind the descending colon. A similar approach for pancreatic head collections can be designed from the right lateral flank. In both cases, the patient may have to be positioned in a slight posterior oblique on the CT couch. Although it is theoretically possible to use an anterior approach including either through the stomach or through the left liver lobe, these routes are obviously more complex and involve the theoretical disadvantage of antigravity flow or fluid through the drainage catheter. Nevertheless, an anterior approach can be used when it is the only access route (Fig. 3).

Catheter selection and insertion

Drainage catheters chosen are ideally large bore with multiple side holes to maximize drainage efficacy. If the CT appearance suggests more liquid and less viscous contents, a catheter up to 14 to 16F catheter may be used and is often introduced by the trocar technique. When more viscous material is suspected, larger catheter bores are required and are usually best inserted by a Seldinger technique with preliminary dilatation of the catheter tract. Catheters are placed to gravity drainage and are irrigated with normal saline at least daily. A useful general principle is to attempt to lay the length of the catheter transversely into the pancreas from the lateral flank approach so that a maximal number of side holes are in contact with fluid. This is another reason for avoiding the anterior transperitoneal approach because the number of func-

* Corresponding author.
E-mail address: pmueller@partners.org (P.R. Mueller).

0033-8389/03/$ – see front matter
doi:10.1016/S0033-8389(03)00123-4

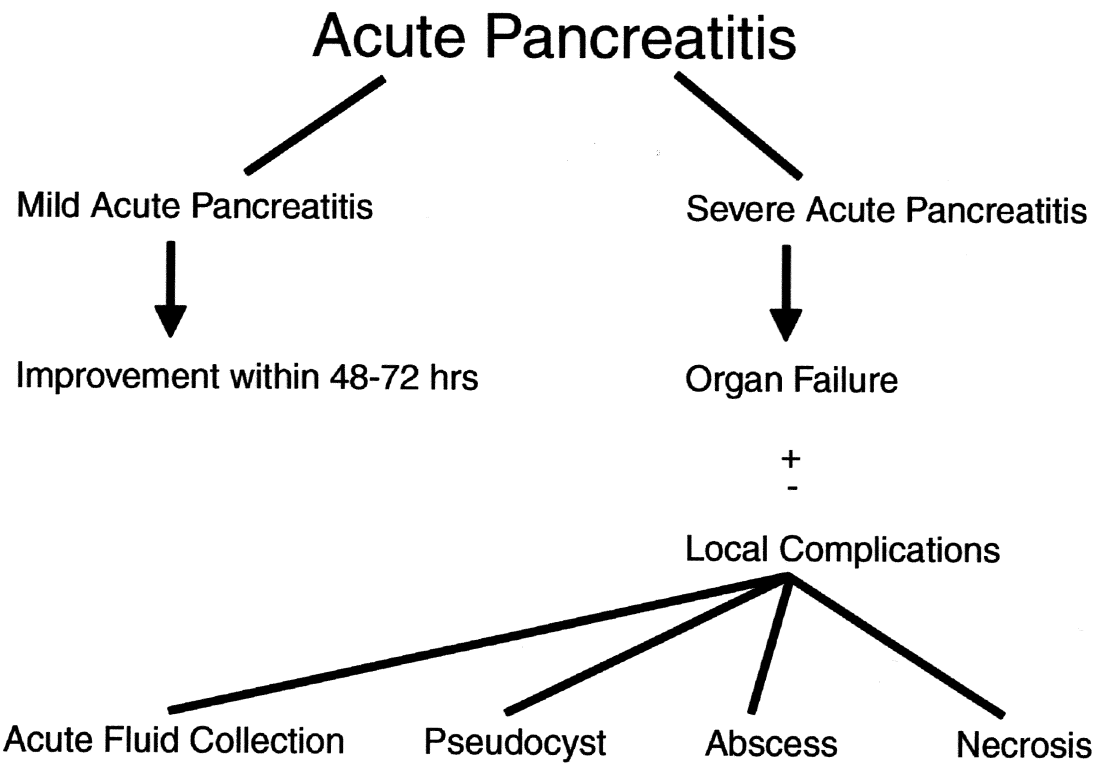

Fig. 1. Schematic detailing the common sequelae of acute pancreatitis.

tioning side holes within the fluid collection is likely to be fewer.

Clinical entities

Peripancreatic effusions

Peripancreatic effusions are a common manifestation of mild acute pancreatitis (Fig. 4). They represent reactive collections typically accumulating around the gland and extending to the anterior pararenal spaces. They are treated conservatively without aspiration or drainage. Failure to resolve within 3 days warrants further evaluation to exclude more serious complications.

Pseudocysts

Patients with acute pancreatitis are at high risk for developing pancreatic pseudocysts. Because of a variety of problems associated with pseudocysts, it is critical to have a team approach when evaluating and treating patients. Pancreatic pseudocysts are collections of pancreatic fluid, inflammatory debris, or blood products surrounded by a nonepithelialzed fibrous capsule. They usually develop 4 or more weeks following an episode of acute pancreatitis and may cause pain, symptoms of obstruction, and occasionally a palpable epigastric mass. Although they are seen anywhere in the abdomen, most are located in the lesser sac or on the anterior surface of the gland with variable retroperitoneal extension. Most pseudocysts are unilocular, but multiple discrete cystlike collections in and around the pancreas are not uncommon. CT is the most accurate mode of defining the location, size, and the association with surrounding structures (Fig. 5). It also provides important information about its evolution. The classic teaching has been pseudocysts that are larger than 6 cm in size and have been present for more than 6 weeks are associated with a low rate of spontaneous resolution and a high rate of complications. They often require drainage by radiologic, endoscopic, or surgical decompression.

The radiologist should understand that some pseudocysts resolve without any treatment. Yeo et al [2] followed 75 patients with pseudocysts of whom 39 resolved without therapy. One needs to review the specific indications for intervention in pseudocyst. Although they are not uniformly accepted, the

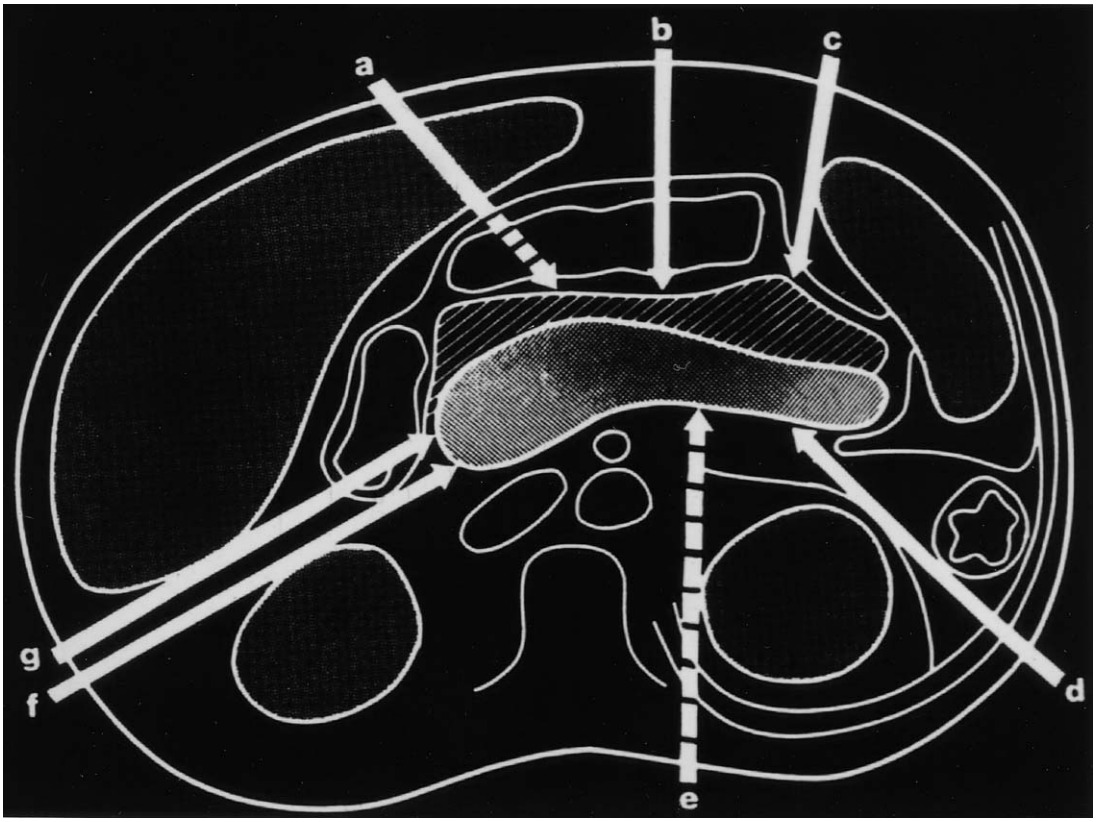

Fig. 2. Access route planning. Schematic showing various potential approaches for interventional access to pancreatic fluid collections. (a) Transhepatic. (b) Transgastric. (c) Transperitoneal. (d) Retroperitoneal. (e) Retroperitoneal posterior paravertebral. (f) Retroperitoneal pararenal. (g) Retroperitoneal by way of Morison's pouch. (*From* Knaus WA, Draper EA, Wagner DP, Zimmerman JE. APACHE II: a severity of disease classification system. Crit Care Med 1985;13:818–29; with permission.)

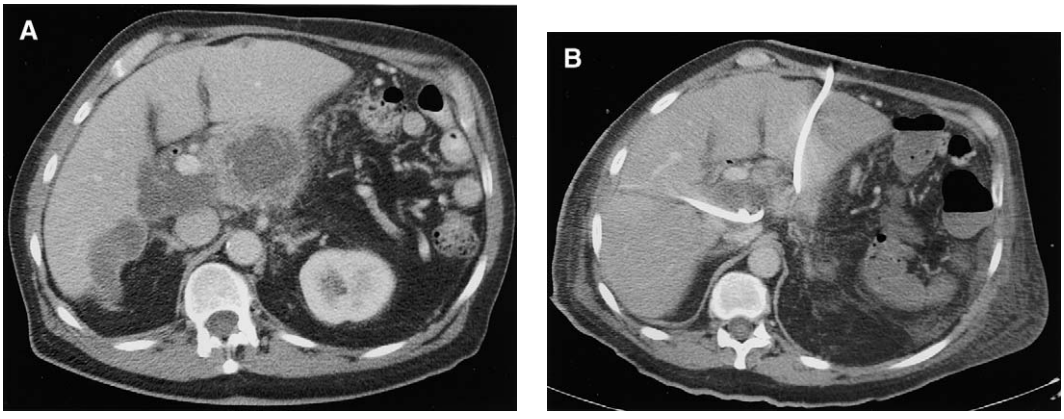

Fig. 3. Anterior transhepatic access routes for separate catheter drainage of multiple subhepatic peripancreatic abscesses. (*A*) Three subhepatic collections are identified under the left lobe, porta hepatis, and right lobe, respectively. (*B*) Two separate catheters have been inserted through the left and right hepatic lobes. The abscess collections have been substantially evacuated.

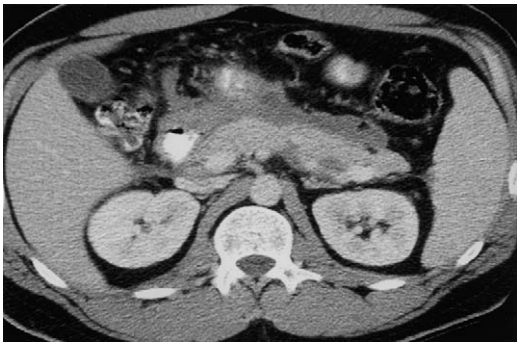

Fig. 4. Peripancreatic effusion. CT scan showing a poorly loculated diffuse anterior lesser sac collection. This collection resolved spontaneously without intervention.

main indications for drainage or intervention are as follows: (1) symptomatic cyst with pain, infection, or compression of adjacent organs; (2) diameter greater than 5 cm; (3) recurrence following surgery or percutaneous aspiration.

Radiologic drainage of pseudocysts may be performed by simple one-step needle aspiration or percutaneous catheter drainage (Figs. 6–8). Dondelinger reviewed articles between 1992 and 1997 comparing aspiration and drainage. He found in a series of over 470 pseudocysts that the success rate for aspiration was only 45% as opposed to a higher success rate for catheter drainage (R. Dondelinger, personal communication, 1992).

Although the general methods for percutaneous drainage of any fluid collection are discussed later, there are certain important requirements for drainage of pseudocysts. Most importantly, the radiologist needs to understand that pseudocysts are the result of disruption of the pancreatic duct either on a macroscopic or microscopic level. This explains why aspiration of pseudocyst may not succeed. If the pseudocyst communicates with the pancreatic duct, and the pancreatic duct is abnormal because of obstruction from stone or stricture, it is likely that there will be a recurrence of the pseudocyst after simple aspiration. Patients who are treated by percutaneous catheter drainage may require long-term catheterization up to 6 months allowing the pancreatic duct to heal. The transgastric approach, an alternative method, enables the pseudocyst to drain into the stomach directly (Fig. 9). In the authors' experience, although transgastric pseudocyst drainage is usually technically possible, it has not been consistently successful in creating a percutaneous cyst gastrostomy. Sacks and Robinson [3] describe a transgastric approach with placement of a double pigtail multisided catheter, which allows one curve of the catheter to lie in the stomach and the second in the pseudocyst.

Endoscopic drainage is another valuable treatment option for critically ill patients. The criteria for endoscopic drainage require the cyst be bulging into the bowel lumen and separated by no more than 1 cm documented by either CT or endoscopic ultrasound. The procedure establishes a direct communication between the pseudocyst and the bowel allowing for direct communication for the fluid to drain until resolution. A third option is surgical management, which is reserved for patients with persistent symptoms, hemorrhage, and obstruction of the gastrointestinal or biliary tracts.

Pancreatic abscess

Pancreatic abscess is a relatively common potentially lethal complication of acute pancreatitis. It is defined as a circumscribed intra-abdominal collection of pus, usually in proximity to the pancreas, containing little or no pancreatic necrosis, which arises as a consequence of acute pancreatitis or pancreatic trauma. Pancreatic abscess can be sequelae of pancreatitis originally caused by anything including alcohol, biliary stone disease, trauma including endoscopic retrograde cholangiopancreatography–related pancreatitis, and even pancreatitis associated with pancreatic cancer. The severity of the initial insult is probably more important than the nature of the precipitating event in determining the likelihood of late abscess formation.

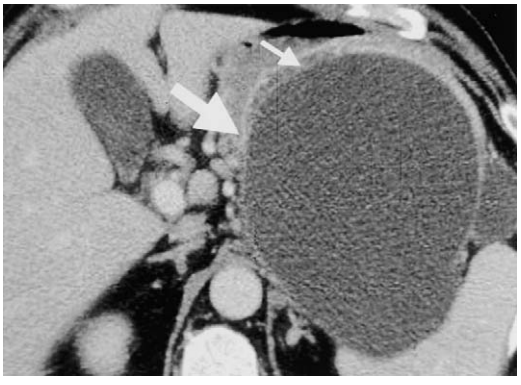

Fig. 5. Pancreatic pseudocyst. CT scan showing a single large loculated pseudocyst in the body of the pancreas with mature, well-visualized walls (*arrows*). This type of collection is amenable to a single stick needle aspiration, percutaneous catheter drainage, either through a lateral flank approach or through a transgastric approach. Endoscopic and surgical drainage also are effective options.

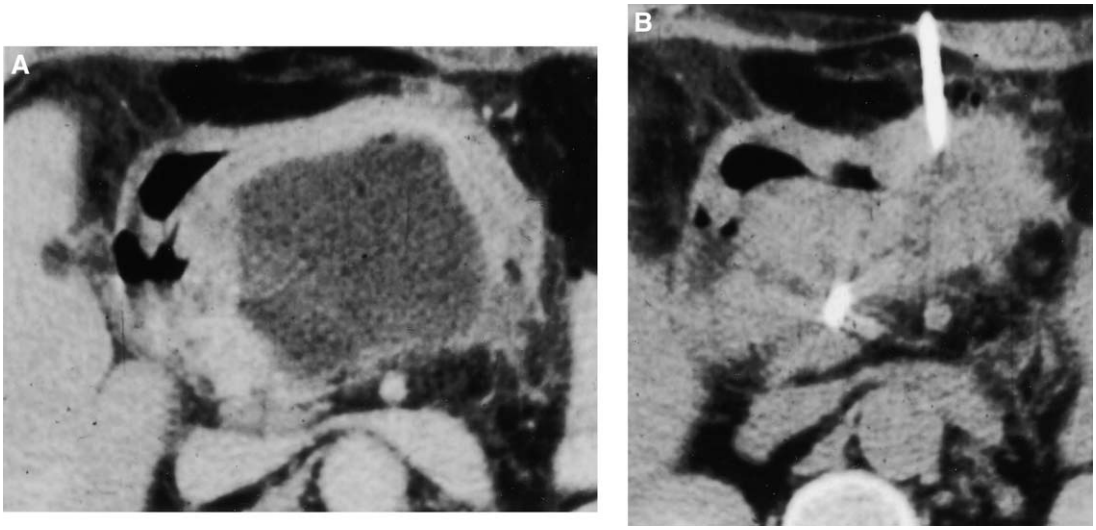

Fig. 6. Percutaneous catheter drainage of a thick-wall pancreatic pseudocyst through an anterior approach. (*A*, *B*) Preimages and postimages showing complete evacuation of the fluid after catheter placement.

In practical terms, this definition translates to a triad of features (eg, a recent episode of acute pancreatitis, the presence of a pancreatic fluid collection on a CT scan, and fever and leukocytosis). Typically, pancreatic abscess is a delayed complication of acute pancreatitis occurring 3 to 4 weeks or more after the initial event. Bacteriologic cultures are often positive and include a vast array of gram-negative and gram-positive organisms. Importantly, super infection with *Candida albicans* (*Monilia*) commonly may occur secondary to bacterial colonization as a result of prolonged indwelling drainage catheters [4–8].

In most cases, pancreatic abscess is diagnosed on the basis of combined clinical and radiographic (CT) features. Imaging studies may include plain radiographs, which can show mottled radiolucent bubbly gas collections or even an air-fluid level in advanced cases. More often, CT demonstrates a diffuse or localized fluid collection in or near the pancreas (Fig. 10). Fluid collections may give a variety of CT appearances from rounded and well marginated to elliptical, mirroring the contours of the lesser sac. Often CT attenuation values of the fluid vary from proteinaceous, purulent, or semi-solid material. Scat-

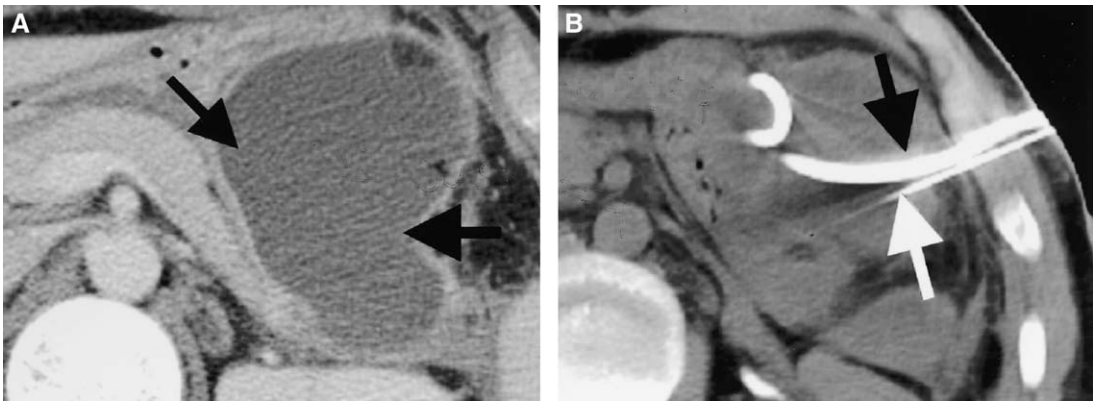

Fig. 7. Percutaneous catheter drainage of a dumbbell-shaped pseudocyst in the pancreatic tail with nearly complete evacuation. Predrainage CT (*A*) showing a dumbbell-shaped cyst (*arrows*). Intraprocedural image (*B*) shows initial diagnostic needle (*white arrow*) and subsequent tandem placed drainage catheter (*black arrow*). Much of the fluid has already been evacuated on the postprocedure image.

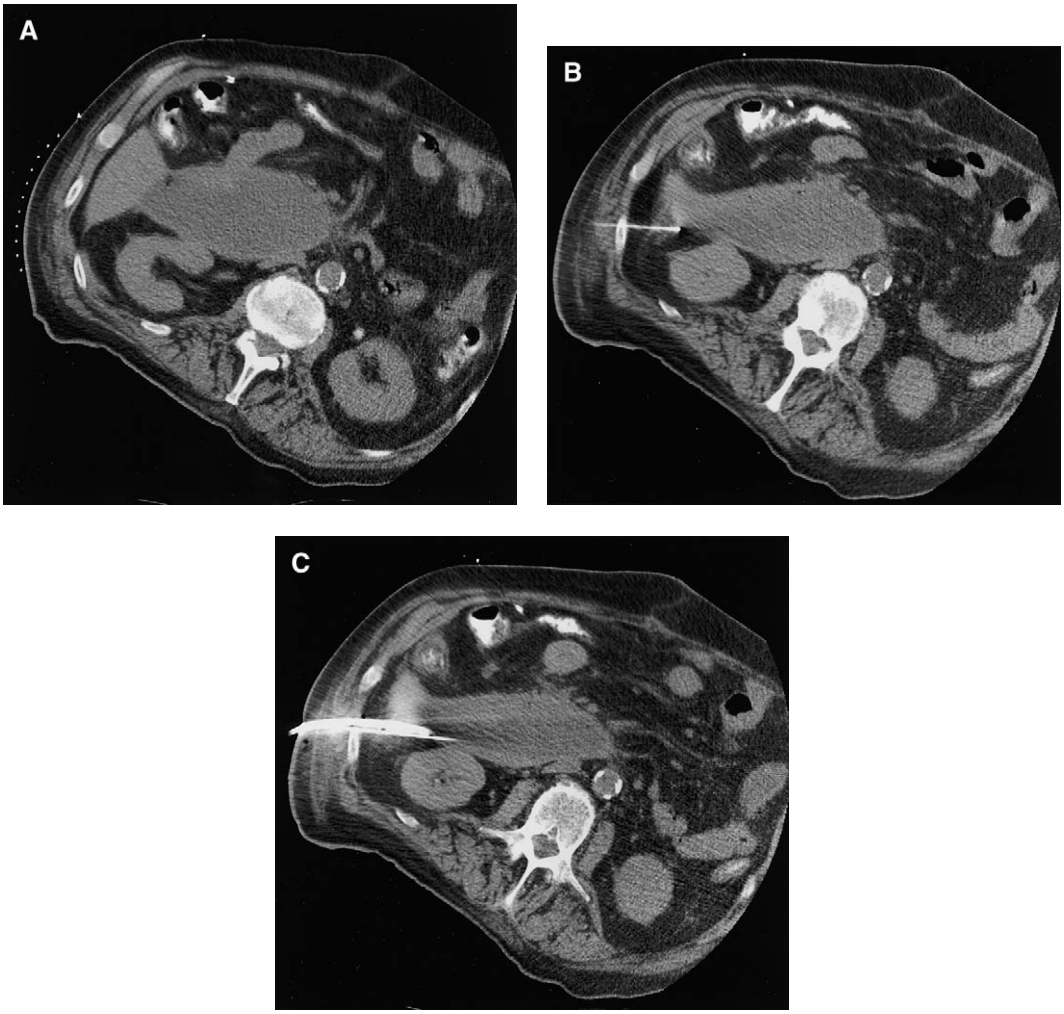

Fig. 8. Retroperitoneal right flank approach for drainage of a pseudocyst involving Morison's pouch and right anterior pararenal space. (*A*) CT scan showing a large well-demarcated oval collection. (*B*) Initial diagnostic needle insertion. (*C*) Tandem introduction of large-bore multihole drainage catheter.

tered gas bubbles are infrequently seen within pancreatic abscesses on CT (Figs. 10, 11), although the presence of gas in the pancreatic bed does not a priori indicate the presence of an active abscess. On occasion, a patient with an indolent or subsiding pancreatic abscess in whom clinical evidence of sepsis has abated may show CT residual evidence of intrapancreatic gas for several weeks. In some cases, the CT attenuation values of the pancreatic fluid collection leave uncertainty as to whether these are recoverable freely drainable fluid content. In such instances, sampling by percutaneous needle aspiration or even diagnostic insertion of a large-bore drainage catheter is necessary to establish whether drainable fluid or pus is present.

CT scanning is the universally accepted standard for image-guided catheter drainage (see Fig. 11). Identification and localization of the fluid collection, the presence of multiple loculations, the response to drainage, appropriateness of catheter position, and undrained collections can all be readily demonstrated. MR imaging has no role in monitoring the results of percutaneous abscess drainage. On occasion, contrast abscessography with fluoroscopic spot filming may be of use in demonstrating the occasional complication of spontaneous fistulization into a neighboring segment of the gastrointestinal tract.

The common theme among modern reviewers in the surgical and interventional radiologic literature is

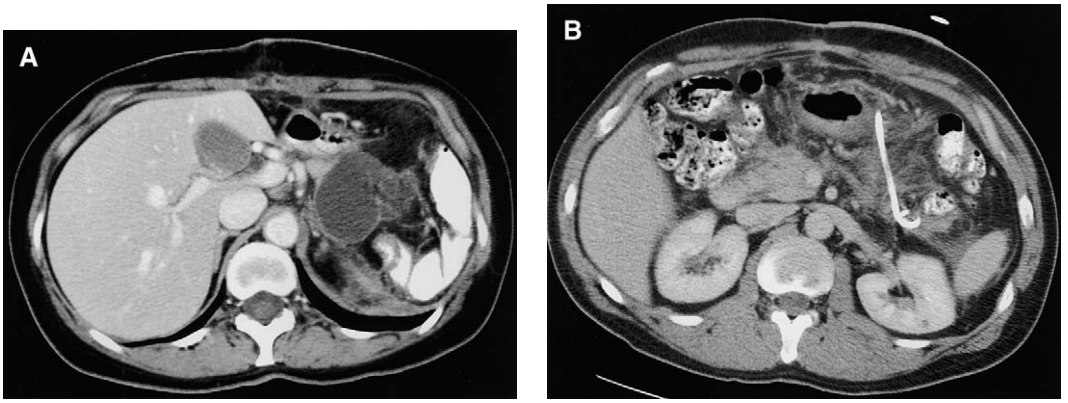

Fig. 9. Pancreatic pseudocyst. Transgastric drainage. (*A*) CT scan showing pseudocyst in the region of the pancreatic tail. (*B*) CT scan after transgastric catheter drainage showing a pigtail loop in the region of the pancreatic tail with the fluid completely evacuated. Transgastric drainage is an effective alternative access method when no safe approach can be found through the retroperitoneal space as shown in the current case. When the transgastric approach is used, the fluid collection may be evacuated either through the catheter lumen to the outside or through multiple side holes placed simultaneously within the gastric lumen for internal drainage.

the complexity of diagnosis and management. Close interdisciplinary cooperation is warranted for success [9–14]. Percutaneous catheter drainage of pancreatic abscess can be an effective life-saving measure. Unlike catheter drainage of most other intra-abdominal abscesses, pancreatic abscesses rarely respond quickly to a single catheter drainage procedure, and the eventual outcome and need for complementary definitive surgical drainage are almost never predictable at the outset. Nevertheless, when surgical drainage is deemed inadvisable because of sepsis, electrolyte imbalance, or multiorgan failure, radiologic catheter drainage can be an effective curative alternative.

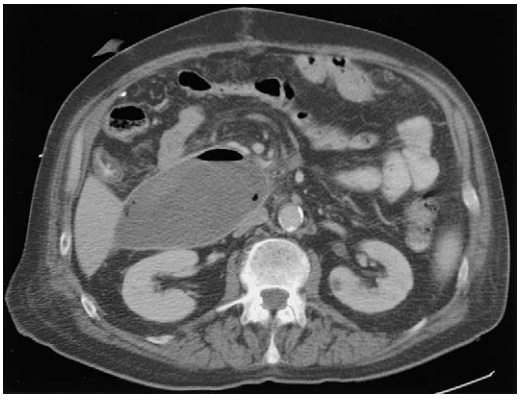

Fig. 10. Pancreatic abscess. CT scan showing a well-demarcated collection with several intracavitary foci of gas. Needle aspiration yielded seropurulent material.

Pancreatic necrosis

Perhaps the most misunderstood complication of pancreatitis is pancreatic necrosis. Pancreatic necrosis occurs early in the course of the pancreatitis, usually at the onset of an acute attack. This clearly distinguishes it from pseudocyst and pancreatic abscess. By definition, pancreatic necrosis is a diffuse or focal area of nonviable pancreatic tissue. Radiologically, pancreatic necrosis is defined as an unenhanced area of pancreatic tissue, which is often greater than 3 cm or more than 30% of the pancreas on an enhanced contrast CT scan. Pathologically, it has been demonstrated that pancreatic necrosis is caused by severe injury with occlusions and thrombosis of the pancreatic microcirculation seen in acute pancreatitis. Bacterial contamination of the infarcted tissue is common and results in high morbidity and mortality. The likelihood of infection increases with the amount of necrosis.

Intervention serves two primary roles in pancreatic necrosis. First, performing diagnostic needle aspiration either to rule in or to rule out infection. The most difficult aspect of this procedure is selecting a safe access route so as not to contaminate either the collection or the aspiration sample. Second, if confirmation of infection is established the necrosis should result in either immediate surgery or percutaneous drainage.

Percutaneous drainage of infected pancreatic necrosis has met with varied results. If the necrotic tissue is solid, which is often the case, percutaneous drainage is not successful. Such patients usually require

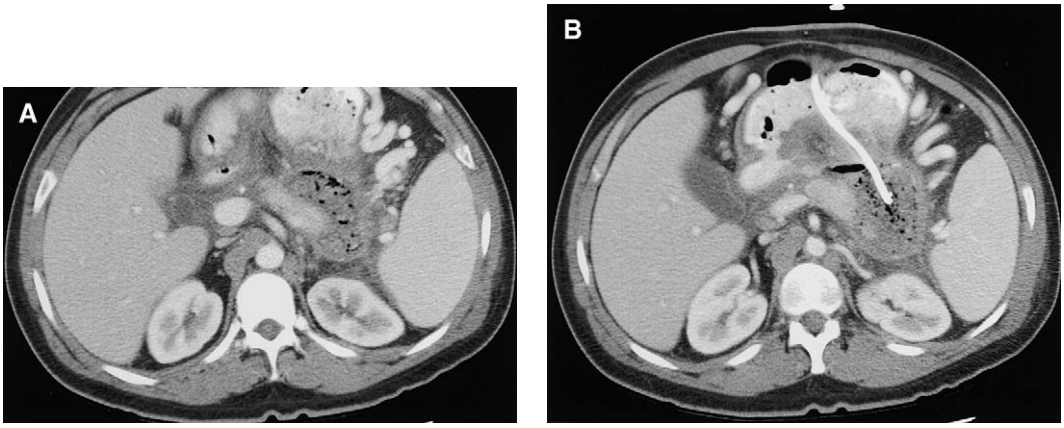

Fig. 11. Pancreatic abscess treated by percutaneous catheter drainage using a transgastric approach. (*A*) Ill-defined collection with numerous mottled gas bubbles involving the body and tail of the pancreas. (*B*) CT scan after percutaneous transgastric insertion. Little or none of the contents have yet been evacuated.

surgical debridement. Liquefied necrotic material, however, may be amenable to percutaneous drainage (Fig. 12). Freeny et al [12] reported a series of 34 patients with pancreatic necrosis of whom 47% were cured. Patients who had central body necrosis were less likely to be cured than patients who had body and tail necrosis. Lee et al [14] demonstrated similar findings with a smaller series of patients. Both authors indicated that success was because of intensive involvement by the interventional radiologist. This included multiple bedside visits, multiple catheter changes, and CT scans.

Assessment and follow-up care

As with any drainage procedure, the classic parameters of fever, white blood cell count, and clinical well-being are assessed daily. Clearly, the importance of the interventionalist is close follow-up and collaboration with the referring physician, usually the surgeons. Periodic CT scans should be obtained for objective evidence of reduction in the collection size and determination of whether catheter drainage is adequate or more catheters should be placed. One of the most important aspects of clinical care is the

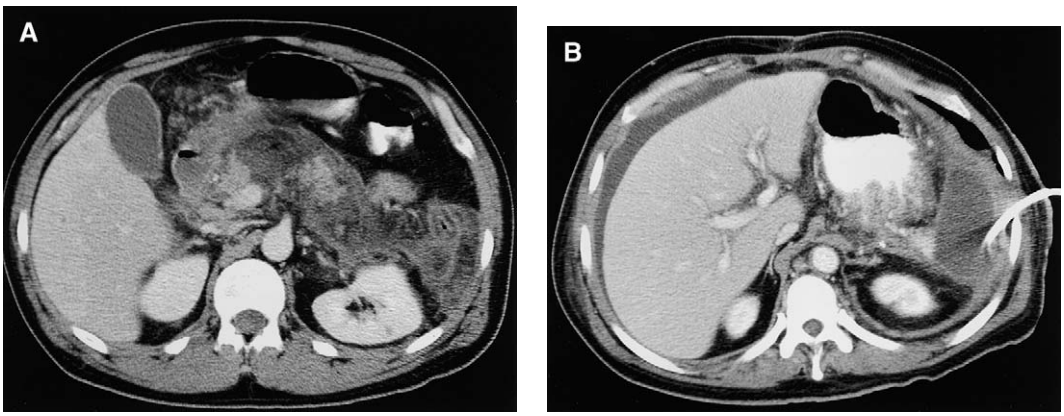

Fig. 12. Percutaneous catheter drainage of liquefied pancreatic necrosis. (*A*) Initial contrast-enhanced CT scan showing multiple regional areas of nonenhanced, nonperfused pancreatic parenchyma. Diffuse pancreatic enlargement with areas of fat necrosis and peripancreatic reaction extending into the left paracolic gutter are also evident. (*B*) CT scan 3 weeks later showing a locule of liquefied necrotic material with a drainage catheter placed percutaneously through the left flank. Marked inflammatory peritoneal thickening is seen along the left paracolic gutter and moderate ascites is also evident around the liver.

assessment of the amount of drainage overtime. This is particularly important in determining if the collection, whether it be a pancreatic pseudocyst, abscess, or infected necrosis, communicates with the pancreatic duct. It is imperative that the interventional radiologist does not simply "leave it up" to the surgeons to determine when the catheter should be withdrawn. Decision making on the basis of imaging also is inappropriate. For example, a CT scan may show complete collapse of the pancreatic collection whether it be an abscess or pseudocyst; however, if there is communication with pancreatic duct the catheter may be draining hundreds of milliliters of fluids a day. If this occurs the interventionalist should determine by direct injection of the catheter the point of communication in the appearance of pancreatic duct. Often in a patient who has either pseudocyst abscess or necrosis that is well drained, communication with the pancreatic duct may show irregularity or areas of narrowing, which result in high drainage amounts. Usually this communication closes over time if the abscess or infected collection is well drained. It is important that the interventional radiologist both practice and preach patience because the catheters in these cases may remain in place for weeks to months. The authors also advocate sinograms to exclude continued communication with the pancreatic duct or with other structures. Patients can usually go home with the catheter in place and be followed-up as an outpatient.

Results

The results of percutaneous drainage of pancreatic fluid collections vary in the literature mostly because of the poor definitions of published articles. In general, success depends on adequate drainage and overall integrity of the pancreatic duct. For example, if the pancreatic duct is obstructed or disrupted the catheter may not maintain adequate drainage for the duct to heal. Generally, results of pancreatic collection drainage are best in pancreatic abscess followed by pancreatic pseudocyst and worst in pancreatic necrosis.

Complications

Principle complications include hemorrhage, inadvertent perforation of the intestine, and fistulization to an adjacent segment of the gastrointestinal tract. The exact percentage and the degree of these complications is actually quite low and probably measures less than 5% in most series. Hemorrhage may be related to the pancreatitis itself, rather than the percutaneous drainage and is actually quite uncommon. Fistulization to adjacent portion to the gastrointestinal tract also may often be attributed to the pancreatitis rather than catheter drainage. Occasionally, inadvertent insertion of the catheter through the colon or small intestine occurs because of poor visualization or opacification at the original time of drainage. In most situations when this occurs surgery is not required and the bowel perforation usually heals.

Causes of failure and management caveats

Most authorities agree that several well-learned caveats pertain to the successful management of pancreatic fluid collections by interventional radiologists. First, the need for multiple catheters in a significant percentage of cases either because of large collections or multiple loculations. Second, many of these catheters require long duration of drainage and hospitalization of such patients. It is not uncommon that successful drainage of pancreatic collections requires several weeks of continued drainage. Third, multiple repeat visits to the radiology department and frequent CT scans may be required to assess response of patients. Lastly, intensive interaction between the radiologist, referring physician, and the patient is necessary to achieve the best possible outcome.

References

[1] Bradley III EL. A clinically based classification system for acute pancreatitis: summary of the International Symposium on Acute Pancreatitis, Atlanta, GA, September 11–13, 1992. Arch Surg 1993;128:586–90.
[2] Yeo CJ, Bastidas JA, Lyncy-Nyhan A, Fishman EK, Zinner MJ, Cameron JL. The natural history of pancreatic pseudocysts documented by computed tomography. Surg Gynecol Obstet 1990;170:411–7.
[3] Sacks D, Robinson ML. Transgastric percutaneous drainage of pancreatic pseudocysts. Am J Radiol 1988; 151:303–6.
[4] Warshaw AL. Current concepts, pancreatic abscesses. N Engl J Med 1972;287:1234–6.
[5] Stanten R, Frey CF. Comprehensive management of acute necrotizing pancreatitis and pancreatic abscess. Arch Surg 1990;125:1269–75.
[6] Fink AS, Hiatt JR, Pitt HA, et al. Indolent presentation of pancreatic abscess: experience with 100 cases. Arch Surg 1998;123:1067–72.
[7] Malangoni MA, Shallcross JC, Seiler JG, Richardson JD, Polk Jr HC. Factors contributing to fatal outcome after treatment of pancreatic abscess. Ann Surg 1986; 203:605–13.

[8] Warshaw AL, Jin G. Improved survival in 45 patients with pancreatic abscess. Ann Surg 1985;202:408–17.
[9] vanSonnenberg E, Wittich GR, Casola G, et al. Complicated pancreatic inflammatory disease: diagnostic and therapeutic role of interventional radiology. Radiology 1985;155:335–40.
[10] vanSonnenberg E, D'Agostino HB, Casola G, Halasz NA, Sanchez RB, Goodacre BW. Percutaneous abscess drainage: current concepts. Radiology 1991;1981: 617–26.
[11] Lee MJ, Rattner DW, Legemate DA, et al. Acute complicated pancreatitis: redefining the role of interventional radiology. Radiology 1992;183:171–4.
[12] Freeny PC, Lewis GP, Traverso LW, Ryan JA. Infected pancreatic fluid collections: percutaneous catheter drainage. Radiology 1998;176:435–41.
[13] vanSonnenberg E, Wittich GR, Chon KS, et al. Percutaneous radiologic drainage of pancreatic abscesses. AJR Am J Roentgenol 1997;168:979–84.
[14] Lee MJ, Wittich GR, Mueller PR. Percutaneous intervention in acute pancreatitis. Radiographics 1998;18: 711–24.

RADIOLOGIC
CLINICS OF
NORTH AMERICA

Radiol Clin N Am 41 (2003) 1227–1242

Ultrasonography of the acute abdomen: gastrointestinal conditions

Julien B.C.M. Puylaert, PhD, MD

Department of Radiology, MCH Westeinde Hospital, The Hague, The Netherlands

Multislice, helical CT is increasingly replacing ultrasonography (US) for the evaluation of patients with acute abdominal pain [1–3]. CT has major advantages over US: it is extremely fast and its time burden is often less than that of a US examination [4]. CT is not disturbed by gas and bone, and obesity is even an advantage. Most of all, CT is not operator-dependent and can be reviewed by others, even at a distance.

With all these advantages, it is not surprising that US is losing field in the evaluation of the acute abdomen. US does, however, have certain specific advantages over CT.

1. US does not require ionizing radiation, which can be important in younger patients and pregnant women [5].
2. The spatial resolution of a high-frequency US image is higher than that of a CT image (Fig. 1). This is only true if the target organ can be approached closely, which requires either a thin patient or the use of graded compression.
3. The dynamic, real-time qualities of US are unique. US can observe fetal movements; peristalsis; and absence of peristalsis (as in paralytic ileus). US can directly visualize blood flow and pulsations, and it is also possible to appreciate the effects of respiration, Valsalva's maneuver (Fig. 2), gravity, and compression. The latter is especially useful to judge whether organs or tissue are soft or rigid (Figs. 3, 4).
4. US allows precise correlation of the area of maximum tenderness or palpable mass with the US findings.
5. US is mobile and flexible. It can be done in the emergency ward, high-care units, and the operating room, and with the present generation of small, battery-assisted, hand-held units, anywhere.
6. In case of intraperitoneal fluid, US-guided puncture is a safe and rapid way to determine if the fluid is blood, pus, bile, amylase, gastric contents, and so forth.
7. The US examination allows a natural and direct form of communication with the patient. Information provided by the patient may lead to a specific search for a US finding, whereas vice versa, certain US findings may lead to a specific question to the patient. This interactive aspect is perhaps the greatest secret of a successful US examination. If performed in this way, US is much more than depicting abdominal organs. As the examination proceeds, it is possible to correlate the US findings with the clinical data, the laboratory results, other imaging studies, and the information provided by the patient. In doing so, the long list of possible differential diagnoses continuously narrows down until a definitive diagnosis is established, or at least direction is given to subsequent imaging studies.

Who does the ultrasound examination ?

Worldwide, there is a large variation of who performs the US examination of the acute abdomen. US is done by technicians, general radiologists, radiologists specialized in US, abdominal radiologists, urologists, gynecologists, and even family doctors.

E-mail address: dr.jbcmpuylaert@wxs.nl

0033-8389/03/$ – see front matter
doi:10.1016/S0033-8389(03)00120-9

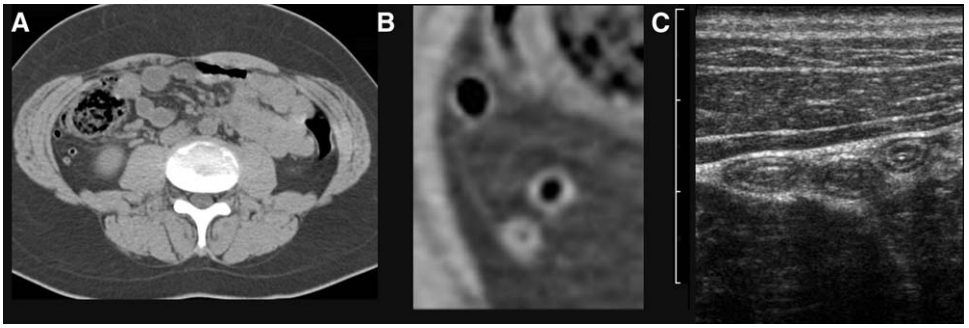

Fig. 1. Visualization of a normal appendix by CT in an obese patient (*A, B*) and by US in a lean patient (*C*). Panel *B* is a magnification of panel *A* to match the centimeter scale as is used in *C*. Note the superior resolution of the US image.

The US examination performed as described previously requires a person with a thorough medical background; knowledge of all possible causative conditions (urologic, gynecologic, gastrointestinal, vascular, and so forth); and with a large expertise in US, CT, imaging-guided puncture, and other radiologic imaging. There is no doubt that the person who meets these conditions best is the radiologist, and preferably a radiologist with special interest in abdominal US and CT. Additional advantages of concentrating all primary, diagnostic abdominal US examinations within the radiology department are obvious. It guarantees integrated imaging, constant quality, around-the-clock coverage, continuity, central archiving, and accurate and early triage of patients with abdominal symptoms [6].

Ultrasound technique

The US examination in patients with acute abdominal pain requires a specific technique of graded compression. In this way fat and bowel are displaced or compressed. This eliminates the disturbing influence of bowel gas and reduces the distance from the transducer to the appendix, allowing the use of a high-frequency probe with better image quality (Fig. 5). This technique also allows assessment of the rigidity of a structure by evaluating its reaction on compression. To avoid pain, the compression should be applied slowly and gently, similar to the classic palpation of the abdomen. The entire abdomen is examined to exclude disease of gallbladder, pancreas, kidney, aorta, stomach, small and large bowel, appendix, uterus, and ovaries. A moderately filled bladder allows better survey of the distal ureters, and of uterus and ovaries in women; however, a full bladder does not allow proper graded compression. Transvaginal US may be used for gynecologic conditions but also for pelvic appendicitis, diverticulitis, and Douglas' abscesses (Fig. 6).

The peritoneal cavity is screened for bowel pathology with five to six vertically oriented, overlapping lanes using a broad-based, high-frequency probe. The author refers to this as "mowing the lawn" (Fig. 7). This form of screening is facilitated by the use of thin-liquid US gel. A fortunate circumstance is that, in

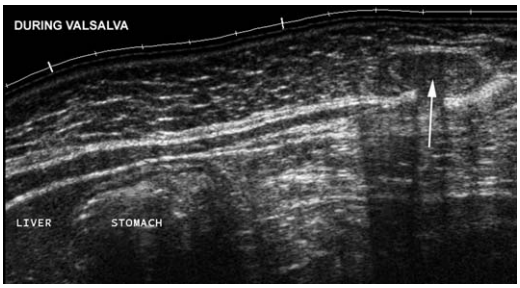

Fig. 2. Real-time US allows one to observe the effects of Valsalva's maneuver. Intra-abdominal fat is pressed into the abdominal wall (*arrow*) through an epigastric hernia.

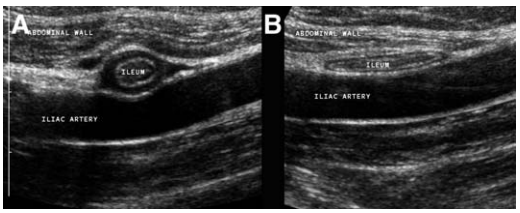

Fig. 3. Real-time US allows one to observe the effect of compression. Compare the contracted normal ileum (*A*) with the relaxed, flattened ileum in the same patient a few seconds later (*B*).

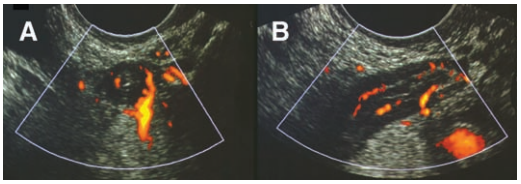

Fig. 6. Acutely inflamed appendix in deep pelvic position. The appendix, visualized here in its transverse (*A*) and longitudinal (*B*) axis, could only be demonstrated with the help of a transvaginal probe.

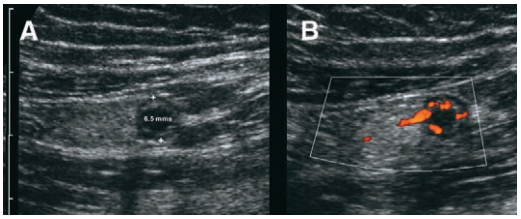

Fig. 20. Pitfall. (*A*) The appendix has a maximal diameter of only 6.5mm; however, there is inflamed fat and an increased Doppler signal (*B*) indicating that it is acutely inflamed.

contrast to normal gas-filled bowel, pathologic bowel usually stands out fairly easily and is readily picked up (Fig. 8). The point of maximum tenderness and a possible palpable mass are correlated with the US findings and in case of free fluid, US-guided puncture can be done (Fig. 9).

Appendicitis

Acute appendicitis is the most common abdominal surgical emergency in the Western world. The diagnosis may be easy but may also be very difficult. The clinical diagnosis of appendicitis is as often wrongly made as it is initially overlooked, leading to unnecessary surgery, respectively to ill advised delay. Using US it is possible to confirm appendicitis by visualizing the inflamed appendix (successful in 90%) or to exclude appendicitis, either by visualization of the normal appendix (successful in 50%) or by demonstrating an alternative condition (possible in 20%). This means that there is always a rather large group of patients in whom the US result is equivocal making further studies necessary. A fortunate circumstance is that most of the patients in the latter group are obese and suitable for CT.

The normal appendix presents as a small, easily compressible, concentrically layered, mobile, blind-ending, sausage-like structure (Fig. 10). The diameter is usually less than 7 mm, but is incidentally large. The normal appendix is mobile, may have a collapsed lumen, but also may contain air or some fecal material, and rarely a little fluid [7]. Power Doppler reveals scarce or no vascular signal and there is no hyperechoic, noncompressible inflamed fat around the appendix.

Ultrasound of appendicitis

The typical appearance of an inflamed appendix is that of a concentrically layered, noncompressible sausage-like structure demonstrated in a fixed position at the site of maximum tenderness (Fig. 11). The average maximum diameter is 9 mm with a variation

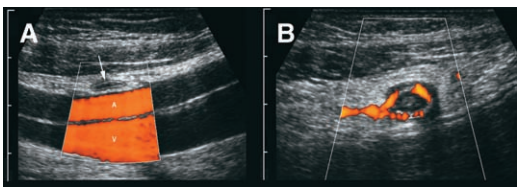

Fig. 11. Axial US image of a normal (*A*) versus an inflamed (*B*) appendix. (*A*) The normal appendix is small, compressible, contains no Doppler signal, and is not surrounded by inflamed fat. A = iliac artery; V = iliac vein. (*B*) The inflamed appendix is large, noncompressible, and hypervascular, and is surrounded by hyperechoic, noncompressible tissue, representing the fatty meso-appendix.

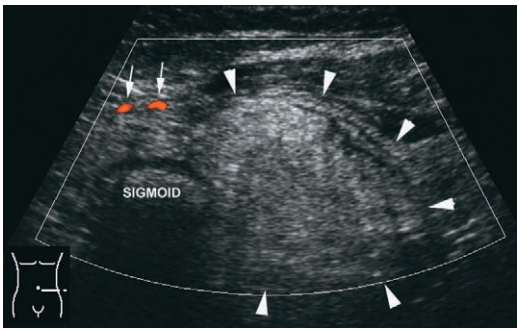

Fig. 35. Epiploic appendagitis in a 48-year-old man with clinical signs of diverticulitis. US reveals an ovoid, noncompressible, avascular fatty mass (*arrowheads*), whereas the adjacent sigmoid has a normal aspect. The neighboring fat shows hyperemia (*arrows*). During respiration the mass, representing the infarcted epiploic appendage, was seen to be adherent to the parietal peritoneum. The patient's symptoms disappeared within a week without treatment.

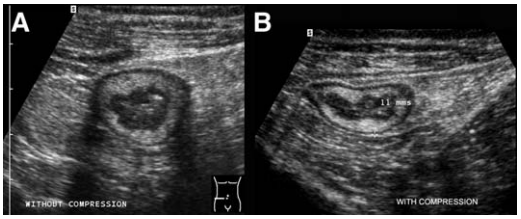

Fig. 4. Decreased compressibility of the ileum in Crohn's disease. Compare the abnormal ileum without compression (*A*) with the image with compression: the diameter is still 11 mm (*B*).

from 7 to 17 mm (Fig. 12). In 30% intraluminal fecalith are found actually obstructing the lumen. Six to 12 hours after the onset of symptoms, the inflammation progresses to the adjacent fat of the mesoappendix, which becomes larger, more hyperechoic, and less compressible. Later on, this fatty tissue tends to increase in volume around the appendix: this represents mesentery and omentum, which have migrated toward the appendix in an attempt to wall-off the imminent perforation (Fig. 13).

Slowly applied intermittent compression is the best way to identify the noncompressible inflamed fat. An irregular, asymmetric contour and loss of the layer structure of the appendix indicate perforation or imminent perforation.

Vascularization of the appendiceal wall is either markedly increased or absent because of high intra-

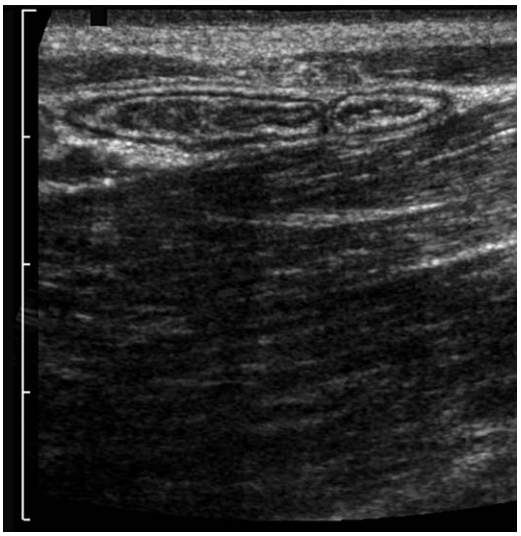

Fig. 5. Normal ileum and appendix during compression. Thin habitus of the patient and the application of compression allow the use of a 13.5-MHz transducer with a high image quality.

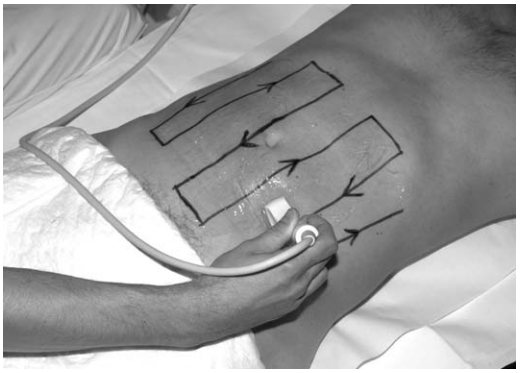

Fig. 7. The "mowing-the-lawn" technique. The peritoneal cavity is screened for bowel pathology by making vertical, overlapping lanes over the abdomen. Bowel pathology is usually conspicuous, because the diseased and empty bowel has a thickened and hypoechoic wall, which contrasts with the surrounding hyperechoic fatty tissue.

luminal pressure with concomitant ischemic necrosis; however, there is always increased vascularization in the directly surrounding fatty tissue. The presence of a generalized, adynamic ileus is suspect for perforated appendicitis, even if the inflamed appendix cannot be visualized.

A small quantity of free intraperitoneal fluid is aspecific. It may be present in both nonperforated and perforated appendicitis and in many other conditions, both surgical and nonsurgical. A large quantity of fluid in the presence of an inflamed appendix may represent pus from perforated appendicitis and then is usually accompanied by paralytic ileus. Larger quantities of free fluid also are found in perforated peptic ulcer (note air and food particles) and gynecologic conditions (puncture usually reveals blood). In most patients with appendicitis inflamed mesenteric lymph nodes can be demonstrated higher up in the mesenterial root.

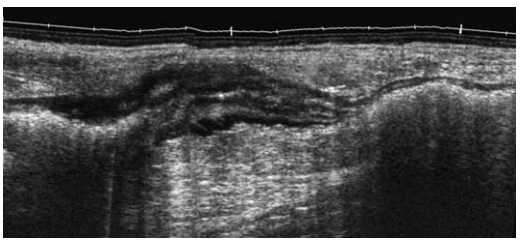

Fig. 8. Segmental colitis caused by Crohn's disease. The pathologic bowel segment is easily picked up using the "mowing-the-lawn" technique.

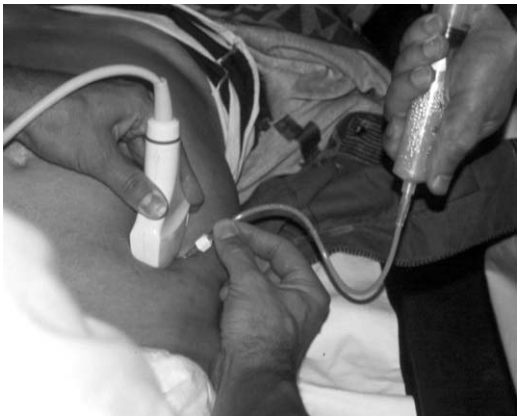

Fig. 9. An US-guided puncture of intraperitoneal fluid reveals purulent nature of the fluid in a patient with perforated appendicitis.

In case of an abnormal position of the inflamed appendix far from where the usual gridiron incision is made, it is useful to indicate the location of the appendix on the skin of the patient with a waterproof marker. This may influence site, size, and orientation of the incision (Fig. 14).

Spontaneous resolving appendicitis

If the clinical symptoms rapidly subside despite the presence of an unequivocally inflamed appendix on US, one should consider the diagnosis of spontaneously resolving appendicitis. These patients initially have the typical clinical signs of appendicitis, but within 12 to 48 hours after the onset of pain the clinical symptoms relatively abruptly subside, probably because of relief of obstruction. On US follow-up, the appendix usually decreases in size in the course of days (Fig. 15). If the patient recalls similar previous attacks, immediate appendectomy is advisable, even if the patient is again completely free of symptoms at that time. Histology in such cases confirms acute inflammation. If conservative management is opted for, keep

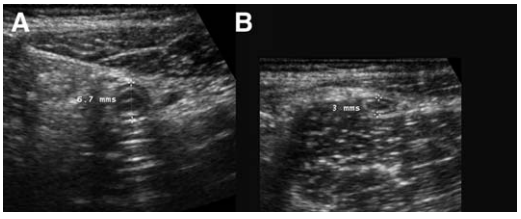

Fig. 10. Transverse US image of the normal appendix without (*A*) and with (*B*) compression.

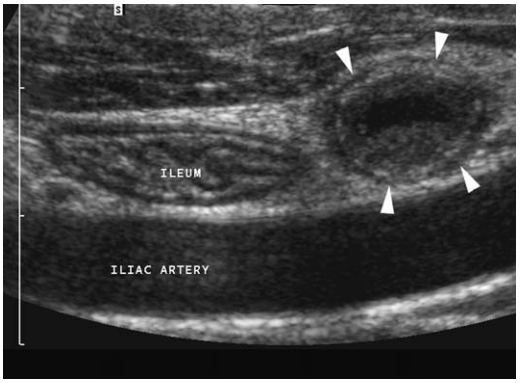

Fig. 12. Acute appendicitis. Noncompressible, inflamed appendix (*arrowheads*) lies next to normal, well-compressible ileum. The appendiceal lumen is dilated and the appendix diameter is 11 by 13 mm. Note a fluid-debris level within the lumen.

in mind that there is a recurrence rate of approximately 40% [8].

Appendiceal mass

Patients who are admitted with considerable delay may present with a palpable mass and relatively mild peritonitis. In these patients, who usually have a high erythrocyte sedimentation rate, US shows a large mass of noncompressible fat around the appendix, interspersed with echolucent streaks. These patients are

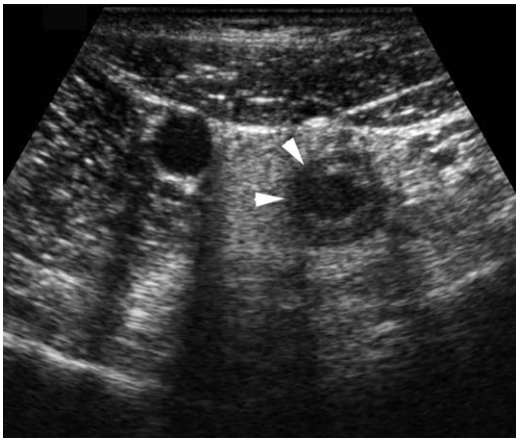

Fig. 13. Acute appendicitis. The inflamed appendix shows local disturbance of the layer structure (*arrowheads*) indicating local transmural progression of the infection. The surrounding inflamed fat probably effectively walls-off the imminent perforation.

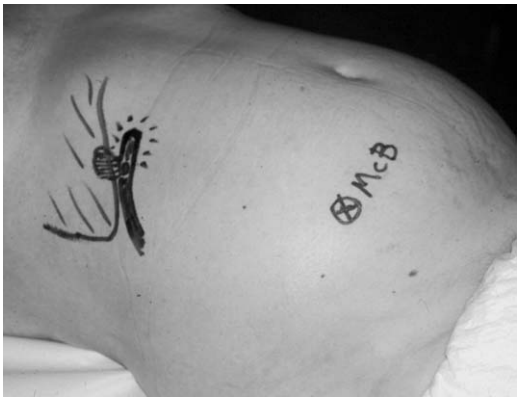

Fig. 14. Inflamed appendix in unusual high position in a patient with clinical signs of cholecystitis. Because of its abnormal position far from McBurney's point (*McB*), the appendix was drawn on the skin with a waterproof pencil. This influenced site, size, and orientation of the incision and facilitated the appendectomy.

diagnosed as "appendiceal phlegmon" and are usually managed conservatively because the surgeon knows that appendectomy in such cases is technically difficult or even impossible [9].

In some patients, the surgeon might be uncertain about the right policy: immediate operation or conservative management. In these cases the clinical symptoms prevail over the US image. If treated conservatively, follow-up US shows a decrease in size of the appendiceal phlegmon within the course of weeks (Fig. 16).

If next to the inflamed appendix a fluid collection is found, this is suggestive for an appendiceal abscess. The collection often contains air and is surrounded by

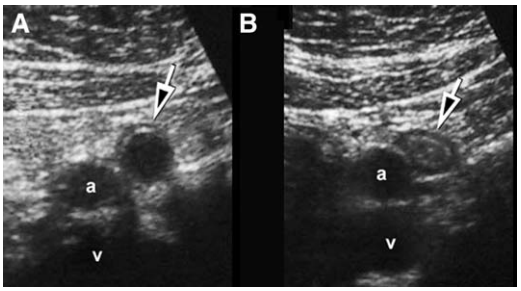

Fig. 15. Spontaneously resolving appendicitis. (*A*) Inflamed appendix (*arrow*) with a dilated lumen and a diameter of 11 mm. The patient experienced rapidly subsiding symptoms and did not undergo operation. (*B*) Two days later the patient was completely symptom free. The appendix (*arrows*) has decreased in size. A = iliac artery; V = iliac vein.

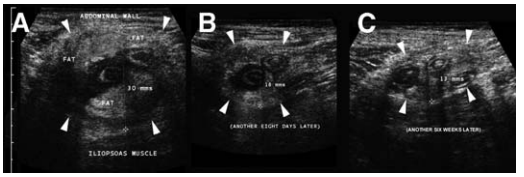

Fig. 16. Resolution of an appendiceal phlegmon. A 35-year-old man with a 10-day history of appendicitis, an erythrocyte sedimentation rate of 65 mm/hour, a palpable mass in the right lower quadrant, and no evidence of peritonitis. (*A*) US reveals large noncompressible inflammatory mass consisting of the inflamed appendix, mesentery, and omentum. The anteroposterior diameter during compression between the abdominal wall and the iliopsoas muscle was 30 mm. The combined clinical-ultrasonographic diagnosis of appendiceal phlegmon was made and the patient was treated conservatively. (*B*) Eight days later the patient was feeling much better. US shows a marked decrease in size of the phlegmon (18 mm). (*C*) Another 6 weeks later the patient was completely symptom free; however, there are still residual abnormalities. There were no recurrent symptoms and the patient did not undergo operation.

inflamed noncompressible hyperechoic tissue representing omentum and mesentery and secondarily thickened neighboring bowel loops, attempting to seal-off the abscess from the peritoneal cavity.

If an appendiceal abscess is demonstrated and there is no frank peritonitis, percutaneous drainage is the treatment of choice (Fig. 17). In stable patients who have no fever and only mild pain, it is wise to await spontaneous drainage of the abscess to neighboring bowel.

Finally, there are some patients with an appendiceal abscess who are better off with immediate surgery: this goes in general for children and for those patients with severe peritonitis, which indicates that the walling-off process is failing. Immediate surgery also is indicated

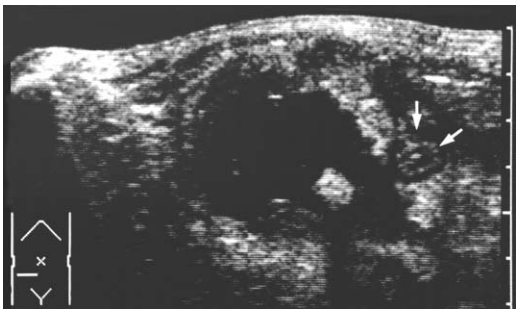

Fig. 17. Appendiceal abscess. Large abscess cavity contains a fecalith. Note the inflamed appendix (*arrows*) lying next to the abscess.

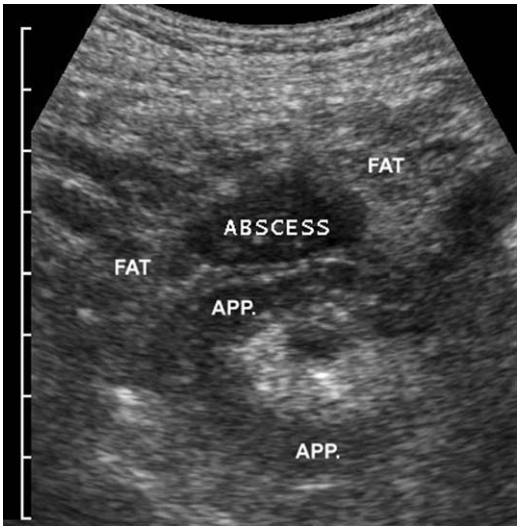

Fig. 18. Acute appendicitis with a small periappendiceal abscess. The patient had a 4-day history of right lower quadrant pain and at physical examination had clear peritonitis. The sedimentation rate was 48 mm/hour. Palpation was unreliable. Subsequent appendectomy with evacuation of the abscess was performed without technical difficulties.

for patients who have a small abscess with a history of only a few days of symptoms, in whom appendectomy with evacuation of the abscess is usually technically easy (Fig. 18).

Before percutaneous drainage, CT is necessary to delineate the extent of the abscess and to determine the safest access route. If expertise is available in US-guided puncture, the combination US plus fluoroscopy has several advantages over CT-guided drainage: it is rapid, allows continuous control, any angulation, and can be performed as a bedside procedure.

Pitfalls in the ultrasound diagnosis of appendicitis

A false-positive diagnosis can be made if the normal appendix is mistaken for an inflamed one. Not infrequently the normal appendix is larger than 7 mm, especially in children when caused by lymphoid hyperplasia and in adults when caused by fecal impaction. Appendiceal compressibility, the absence of a Doppler signal, and the absence of inflamed fat are the most important features in deciding if it is normal or inflamed.

Mistaking a normal appendix for an inflamed one may also occur if there is secondary thickening of the appendix associated with cecal carcinoma. In the latter case, the appendiceal lumen is obstructed giving rise to sterile accumulation of mucus in the lumen. The patient often has remarkably mild symptoms and is managed conservatively under the erroneous diagnosis of an appendiceal phlegmon. If the underlying tumor is small and is not recognized, this may lead to considerable delay in surgical treatment. The combination of a relatively large appendix with paradoxically mild and atypical symptoms should raise suspicion of underlying malignancy. Other conditions with secondary thickening of the appendix are perforated peptic ulcer, Crohn's disease, and sigmoid diverticulitis.

The most important reason for a false-negative ultrasound examination is overlooking the inflamed appendix. In experienced hands the inflamed appendix can be visualized in 90% of patients with acute appendicitis. Generalized peritonitis hampers graded compression, which may account for a lower score in patients with free appendiceal perforation. Air-filled dilated bowel loops from adynamic ileus may hide the appendix from view. Air in the lumen can make it difficult to identify the inflamed appendix (Fig. 19). Another pitfall is demonstration of the normal proximal part of the appendix while the distal inflamed tip is overlooked, because it is obscured by bowel gas. Rarely, the inflamed appendix has a maximal diameter of less than 7 mm. In those cases rigidity, hypervascularity, and the presence of inflamed fat must give the clue (Fig. 20).

Another pitfall is advanced appendicitis where there is secondary wall thickening of the ileum. Often the ileal thickening is more prominent and conspicuous on US than the underlying inflamed appendix. If only the ileum is appreciated and the appendix is overlooked, an erroneous diagnosis of infectious ileocolitis or Crohn's disease can be made, leading to ill-advised surgical delay (Fig. 21). Similarly, if in an adult patient enlarged mesenteric lymph nodes are the sole US finding, one should be cautious to diagnose mesenteric lymphadenitis because these nodes could

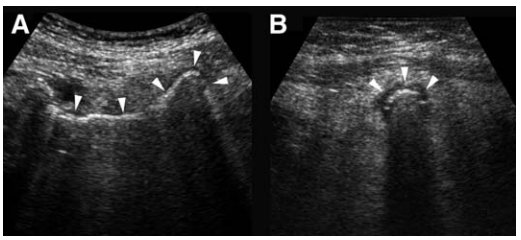

Fig. 19. Pitfall. The inflamed appendix, demonstrated in the longitudinal (*A*) and axial (*B*) plane, has a gas-filled lumen (*arrowheads*), making it difficult to identify. The sausage shape and the inflamed fat are the clue to the diagnosis.

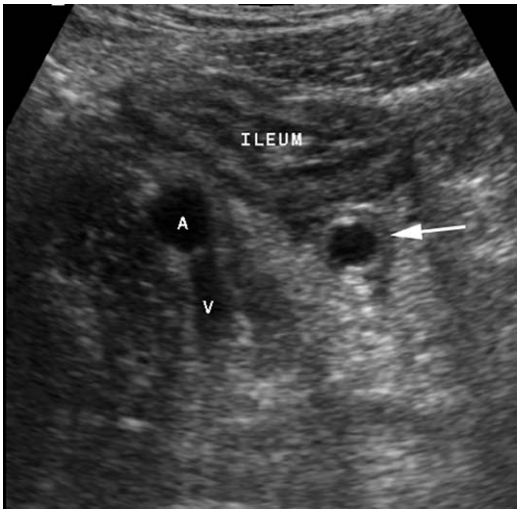

Fig. 21. Pitfall. Secondary thickening of the ileum caused by appendicitis. If the prominent ileum is appreciated, but the inflamed appendix (*arrow*) is overlooked, an erroneous diagnosis of Crohn's disease or infectious ileocolitis can be made, leading to surgical delay.

be secondarily enlarged because of acute appendicitis, while the inflamed appendix is overlooked.

If in a patient with appendicitis only the fecalith in the appendiceal base is visualized and the rest of the appendix is overlooked, this may lead to an erroneous diagnosis of cecal diverticulitis. If in a woman a relatively large right-sided ovarian cyst is found, this is not necessarily the cause of her symptoms and one should still search for appendicitis. Finally, if in advanced appendicitis only the hyperechoic noncompressible inflamed fat of omentum and mesentery is visualized, and the inflamed appendix is overlooked, this may lead to an erroneous diagnosis of omental infarction or epiploic appendagitis [10,11].

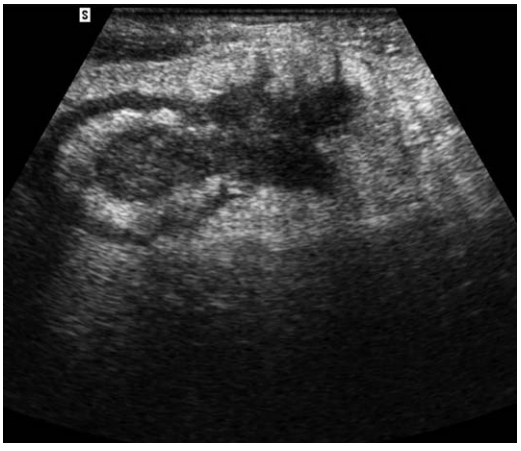

Fig. 22. Crohn's ileitis with abscess formation. US reveals marked wall thickening of the terminal ileum with local disruption of the wall and a small abscess, walled-off by hyperechoic, inflamed fat.

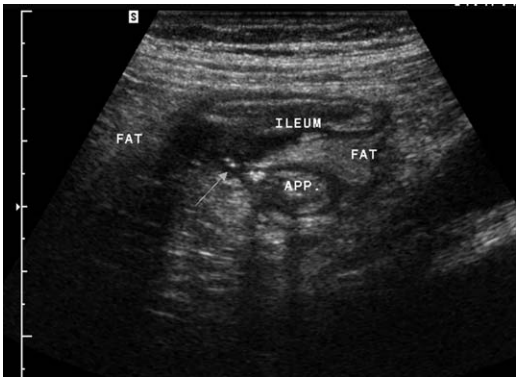

Fig. 23. Crohn's ileitis with fistula (*arrow*) to the adjacent appendix. Note the focal loss of layer structure of the ileal wall and large masses of surrounding inflamed fat.

In patients with equivocal US findings, CT scan is indicated. A fortunate circumstance is that these are often obese patients.

Ileocecal Crohn's disease

Patients with ileocecal Crohn's disease often have protracted and atypical symptoms causing marked diagnostic delay. Crohn's disease may also present with acute, appendicitis-like symptoms and lead to an ill-advised operation. In both scenarios US may play an important role in establishing the initial diagnosis [12,13]. The sensitivity of US for detecting ileocecal Crohn's disease is over 95%.

Sonographically, there is marked mural thickening of the ileum, which shows decreased or no peristalsis and is not compressible. Classically, all layers are involved and layer structure is often locally disturbed, the earliest sign being echolucent changes in the submucosa. There is inflammation of the fatty mesentery and omentum, recognizable as hyperechoic, noncompressible tissue adjacent to the ileum. In the echolucent wall bright eccentric foci may indicate deep ulceration. Echolucent streaks within the hyperechoic tissue indicate liponecrotic tracts, which may herald fistula formation. Cecum and appendix may also show mural thickening. Mesenteric lymph nodes are often markedly enlarged, but hypovascular. In

long-standing Crohn's disease, ''creeping fat'' is found, which is recognized as a large, moderately well-compressible fatty mass encompassing most of the circumference of the ileum and isoechoic to normal fat. Eventually, there are often US signs of prestenotic dilatation, abscess formation, or fistula formation (Figs. 22, 23).

Infectious ileocolitis and infectious ileocecitis

Infectious ileocolitis is a bacterial infection of terminal ileum and colon, which is characterized by diarrhea and abdominal pain. The most frequently cultured bacteria are *Campylobacter*, *Salmonella*, and *Yersinia*. The infection is generally limited to the mucosa, is self-limiting, and rarely poses diagnostic problems.

There is an interesting variant of infectious ileocolitis in which the infection is mainly limited to the ileocecal area and has been termed ''infectious ileocecitis'' [14]. It is usually caused by the same bacteria and the importance of this variant is that its clinical symptoms are dominated by acute right lower abdominal pain, whereas diarrhea is absent or only mild. These symptoms masquerade as the clinical signs of appendicitis and explain why infectious ileocecitis often leads to an unnecessary laparotomy. The symptoms of *Yersinia* are often more protracted and both the clinical symptoms and the US features may mimic those of Crohn's disease. The absence of a transmural component, the self-limiting course, and positive stool cultures or serology yield the correct diagnosis. The frequency of infectious ileocecitis is fairly high and has a ratio of 1 to 8 compared with appendicitis [14].

An US shows fairly characteristic features: there is diffuse thickening of mucosa and submucosa of the terminal ileum and the cecum and enlargement of mesenteric lymph nodes (Fig. 24). The appendix is sonographically normal. In contrast to ileocecal Crohn's disease, in infectious ileocecitis the wall layers are always intact and the muscularis and serosa are never affected. Omentum and mesentery are never involved and there are never signs of bowel obstruction or abscess or fistula formation. The various microorga-

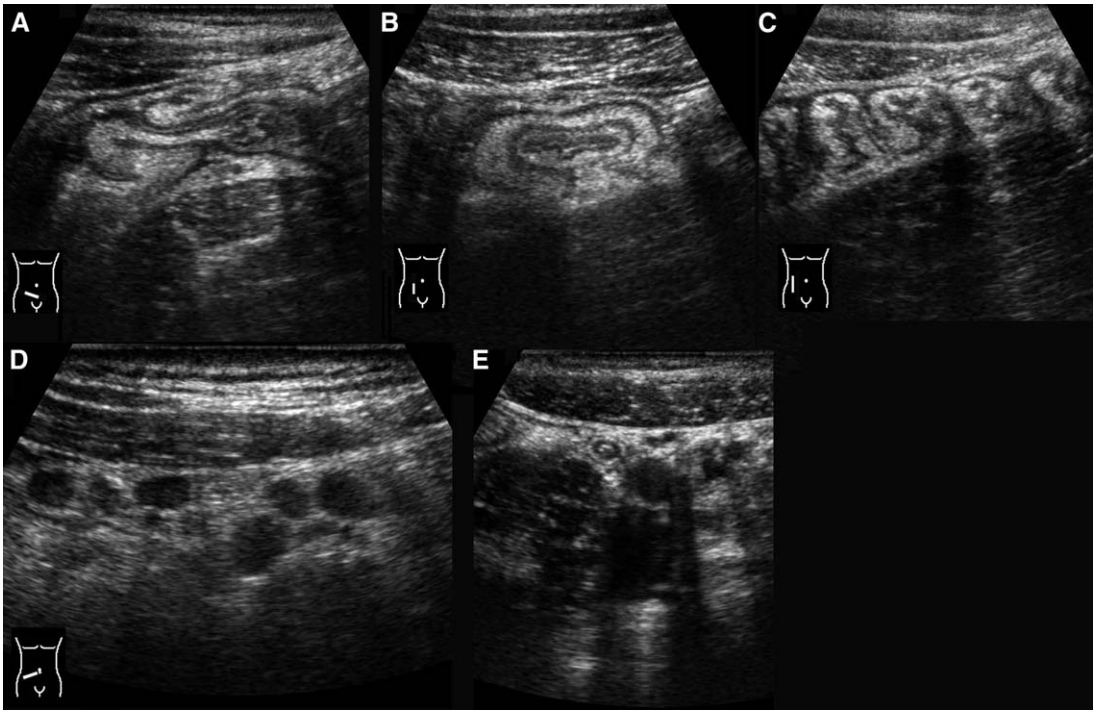

Fig. 24. Infectious ileocecitis in a 26-year-old woman with clinical signs of appendicitis. US shows prominent ileocecal valve in the longitudinal (*A*) and axial (*B*) view caused by marked mucosal and submucosal wall thickening of ileum and cecum. (*C*) Sagittal image of the empty and contracted ascending colon with a prominent haustration pattern caused by mural thickening. (*D*) Enlarged lymph nodes are found in the radix of the mesentery. (*E*) The appendix is normal. Appendectomy was cancelled. The next day the patient developed diarrhea and stool cultures eventually revealed *Campylobacter jejuni*.

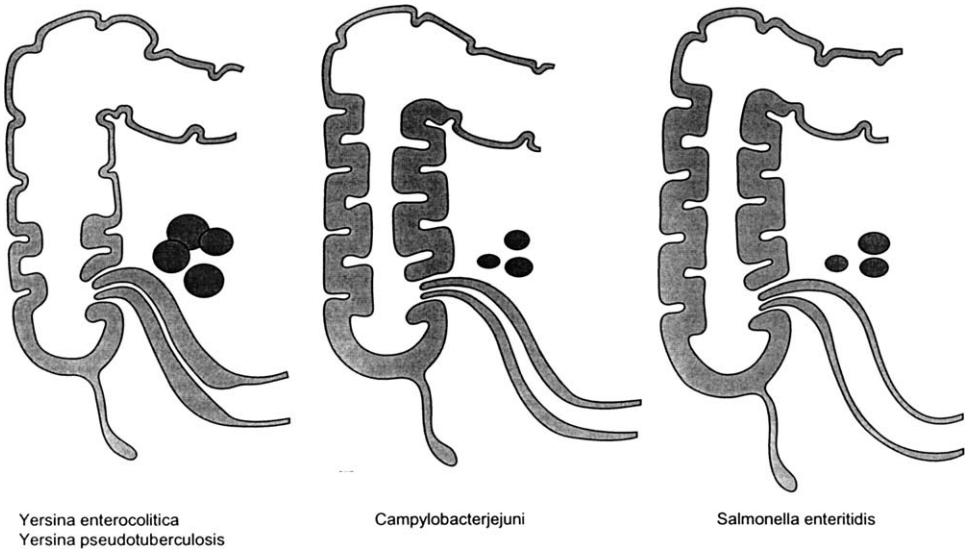

Fig. 25. Infectious ileocecitis. Schematic representation of relative involvement of ileum, cecum, and mesenteric lymph nodes in infectious ileocolitis caused by *Yersinia*, *Campylobacter*, and *Salmonella*. There is some overlap between the different patterns.

nisms have a slightly different pattern of affecting the ileocecal area (Fig. 25).

Mesenteric lymphadenitis

This is an ill-defined entity, probably of viral origin, in which the mesenteric lymph nodes become inflamed and enlarged. It is a typical disease of childhood and is only rarely seen in young adults. It mimics the clinical signs of appendicitis and may lead to an unnecessary appendectomy. The US findings are solely enlarged, hypervascular mesenteric lymph nodes. If these are the only US findings in a symptomatic young adult, however, it is well possible that these nodes are in fact secondarily enlarged because of acute appendicitis and the inflamed appendix is overlooked.

Cecal carcinoma

Patients with cecal carcinoma can present with acute or subacute abdominal symptoms in several ways: the tumor may cause acute small bowel obstruction, the appendix may be involved, the tumor may perforate, and the tumor itself may cause direct pain. The often bulky nature of the tumor and the close proximity of the right colon to the abdominal wall makes cecal carcinoma in most cases fairly conspicuous on US: most present as a hypoechoic, solid, well-vascularized irregular, and asymmetric thickening of the cecal wall (Fig. 26). In the proximity enlarged mesenteric lymph nodes can be found, and in most cases there is also some inflamed fat around the tumor. In a minority the tumor is of the scirrhous type, which

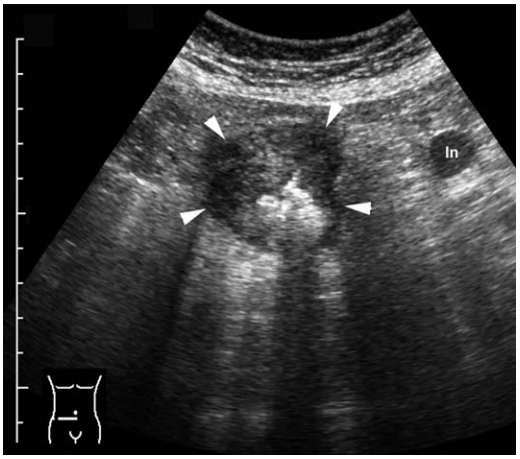

Fig. 26. Cecal carcinoma. US reveals asymmetric, hypoechoic, circumferential wall thickening of the cecum (*arrowheads*) with narrowing of the lumen. There is one pathologically enlarged lymph node (ln).

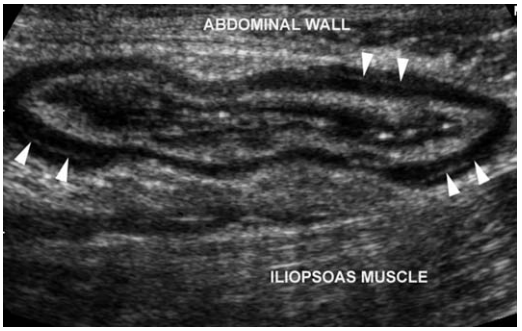

Fig. 27. Normal empty sigmoid. Axial view during relaxation and compression with the transducer shows the colonic anatomy the best. Note the three teniae coli, visible as a focal thickening of the muscularis layer. Note the separation of each tenia from the circular muscular layer by a thin, echogenic layer of connective tissue (*arrowheads*).

is less easy to detect. The finding of liver metastases strongly supports the diagnosis of malignancy.

Ingrowth of the tumor in the appendiceal base only rarely causes a full-blown appendicitis, but rather leads to mucinous dilatation of the appendiceal lumen. On US the enlarged appendix is often more conspicuous than the underlying tumor, and because there is often a palpable mass and protracted symptoms, these patients are often misdiagnosed as to have an appendiceal phlegmon, leading to significant surgical delay. A clue to the correct diagnosis is the discrepancy between the relatively mild and protracted symptoms of intermittent, nagging pain and the impressive size of the appendix and the surrounding tissue. Another helpful sign is markedly enlarged mesenteric lymph nodes (short axial diameter greater than 12 mm). If CT is not helpful and both clinical symptoms and US abnormalities do not resolve within weeks, colonoscopy is indicated.

Sigmoid diverticulitis

The diagnosis of sigmoid diverticulitis is often made on clinical grounds. In the classic case the patient presents with localized pain and guarding in the left lower abdomen, fever, leukocytosis, and later elevation of the sedimentation rate. The diagnosis, however, is not always clear. Clinical signs may be so atypical that initially another diagnosis is considered, such as urinary tract infection; renal colic; perforated peptic ulcer; adnexitis; or in case of diverticulitis in a right-sided loop of sigmoid, appendicitis. The clinician may think, however, of sigmoid diverticulitis, whereas in fact another condition is present, such as sigmoid carcinoma, epiploic appendagitis, a gynecologic or urologic condition, or even a ruptured aortic aneurysm. In all of these cases, US may play a role by making the correct diagnosis at an early point in time.

On US, the normal descending colon and upper part of the sigmoid can reliably be identified in virtually all patients because of its consistent location laterally in the left paracolic gutter. The US appearance of the normal sigmoid is variable: the lumen can be empty or filled with feces, and the sigmoid can be contracted or relaxed (Fig. 27). A third factor influencing the aspect is compression by the transducer, which flattens the colon. The muscularis in diverticulosis is often markedly thickened and fecalith-containing diverticula easily can be recognized as large (4 to 12 mm), strongly reflective, round-ovoid structures casting an acoustic shadow and localized on the outside of the contour of the contracted colon (Fig. 28). If the sigmoid is filled with feces, the diverticula are

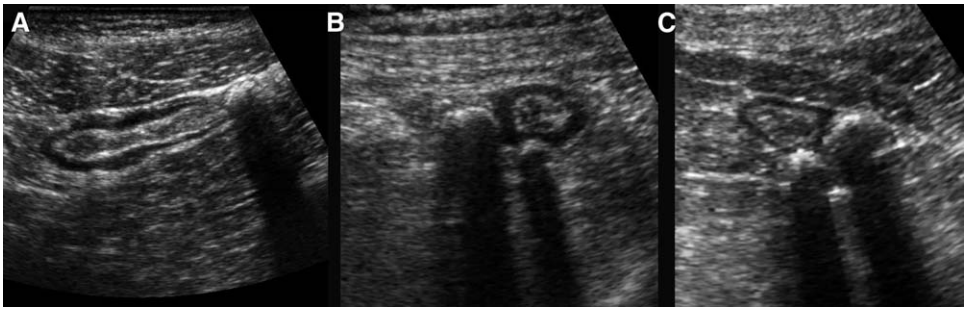

Fig. 28. (*A*, *B*, *C*) Sigmoid diverticulosis in three asymptomatic patients. The fecalith-filled diverticula are recognized as strongly reflective, round structures casting an acoustic shadow and localized at the outer contour of the empty sigmoid. The thin wall of the diverticulum, consisting of mucosa only, is not separately visible.

hardly recognizable. The US appearance of diverticulitis depends on the stage of the disease.

In the earliest stage (stage 0) there is usually local wall thickening of the colon, at first without but later with local blurring of the layer structure. Around the fecalith there is hyperechoic, noncompressible tissue, which represents the inflamed mesentery and omentum trying to seal off the imminent perforation. This inflamed fat, which is best identified during gentle, intermittent compression with the transducer, is obligatory for the diagnosis of diverticulitis [15]. Usually the inflamed diverticulum corresponds with the spot of maximum tenderness. Endovaginal US has an important role in women with deeply located diverticulitis.

An US follow-up in most cases shows the development of a small (often < 1 cm) paracolic abscess and disintegration of the fecalith. In over 80% of patients, after 1 or 2 days the pus and the fecalith evacuate toward the colonic lumen by local weakening of the colonic wall at the level of the original diverticular neck (Figs. 29, 30). Correspondingly, the patient's symptoms resolve. Note that the residual inflammatory

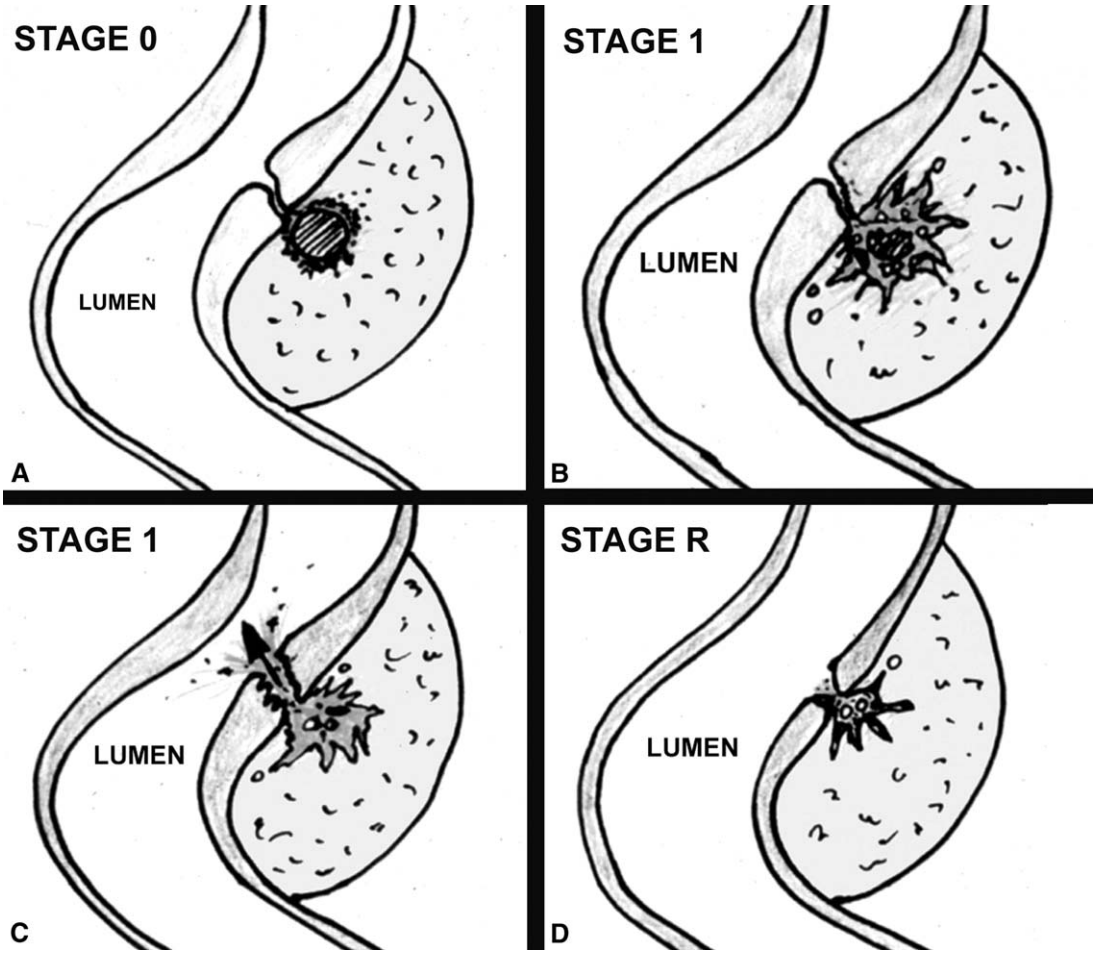

Fig. 29. Schematic presentation of the benign, natural course of sigmoid diverticulitis as it is observed in 80% of patients. (*A*) In stage 0 the neck of the diverticulum becomes obstructed, followed by high intradiverticular pressure and an impaired defense system against the bacteria lodging within the fecalith. Surrounding inflamed fat represents mesentery and omentum attempting to wall-off the imminent perforation. (*B*) Development of a small paracolic abscess, successfully walled-off by mesentery and omentum. The fecalith usually disintegrates and the sigmoid wall is locally weakened. (*C*) Evacuation of pus and residual fecal material through the weakened sigmoid wall into the colonic lumen. (*D*) Residual abnormalities remain fairly long after resolution of the symptoms.

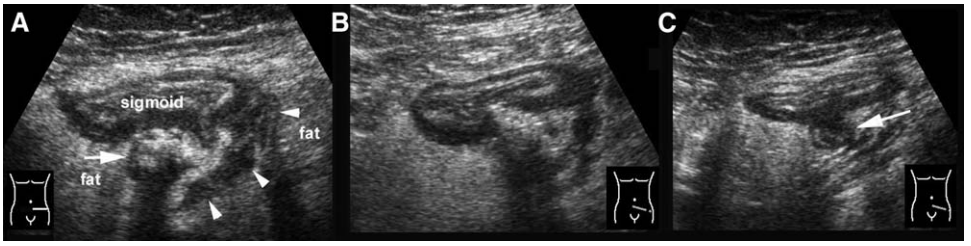

Fig. 30. Natural, benign course of sigmoid diverticulitis. (*A*) US reveals mural thickening of the sigmoid at the level of an inflamed diverticulum (*arrow*) containing a fecalith (stage 0). Note the surrounding hyperechoic, noncompressible tissue representing the omentum and mesentery effectively walling-off the imminent perforation. Within the fat, echolucent linear streaks (*arrowheads*) are visible. (*B*) One day later the patient feels slightly better. The fecalith cannot be recognized as such and the contents of the diverticulum are bulging toward the sigmoid lumen, sign of impending evacuation. (*C*) Another 2 days later, the patient was almost symptom free. Pus and fecal material have completely evacuated to the sigmoid lumen, leaving an empty diverticulum (*arrow*).

changes may remain present for a long time after the evacuation, so the patient can be completely symptom free when there are still considerable US visible abnormalities present. In about 20% of patients, diverticulitis takes a complicated course.

Free perforation without any sealing-off by mesentery or omentum is relatively rare. Spill of fecal material or pus to the peritoneal cavity quickly leads to severe peritonitis rendering laparotomy inevitable. Even in case of a larger diverticular abscess (> 2.5 cm) spontaneous evacuation to the colonic lumen remains the rule (Fig. 31). In some patients, however, the abscess may evacuate in a less favorable direction

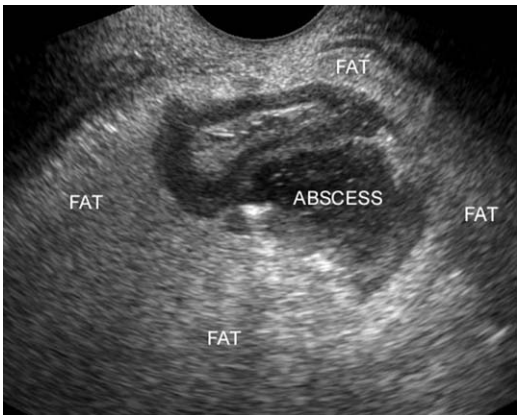

Fig. 31. Paracolic abscess caused by diverticulitis, effectively walled-off by large masses of inflamed fat, representing mesentery and omentum. The abscess eventually evacuated completely, and the patient recovered without surgery.

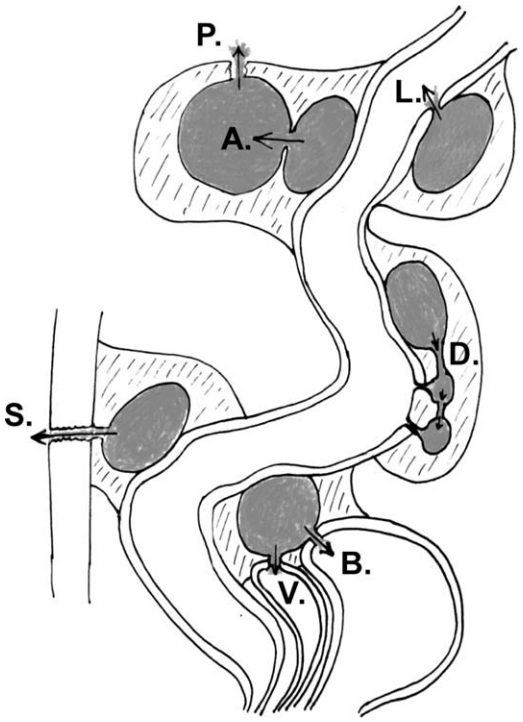

Fig. 32. Schematic presentation of the natural evolution of sigmoid diverticulitis, once a paracolic abscess has developed. The most frequent and most favorable pathway is evacuation to the sigmoid lumen (L). Less favorable is breakthrough to neighboring diverticula (D), giving rise to persistent, longitudinal, cuff-like abscesses. Even worse is the formation of secondary abscesses (A), and eventual perforation to the peritoneal cavity (P). Finally, evacuation to bladder (B), vagina (V), and through the skin (S) leads to fistula formation.

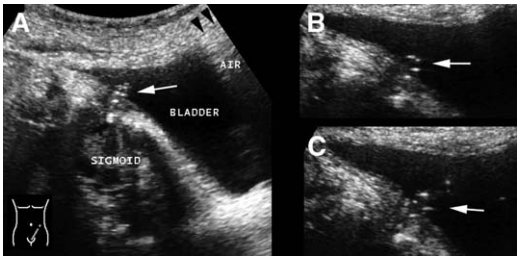

Fig. 33. Colovesical fistula from sigmoid diverticulitis. (*A*) From the lumen of the sigmoid an air-track (*arrow*) can be followed all the way to the bladder. In the dome of the bladder gas (*arrowheads*) is seen. (*B, C*) From the orificium of the fistula, from time to time the passage of air-bubbles (*arrows*) can be witnessed.

(Fig. 32). In the first place, it may find its way to neighboring diverticula, giving rise to more longitudinally oriented abscesses undermining the colonic wall. These abscesses tend to heal badly and often lead to recurrent inflammation with stenosis eventually requiring elective surgery. In rare cases the abscess breaks through to the peritoneal cavity, which may lead to diffuse peritonitis or to secondary abscess formation. If a diverticular abscess evacuates into bladder or vagina, a fistula may result (Fig. 33).

US has an important role in the diagnosis of alternative conditions: ureterolithiasis, sigmoid carcinoma (Fig. 34), ruptured aortic aneurysm, perforated peptic ulcer, appendicitis, and epiploic appendagitis (Fig. 35). Although in lean patients and in women using the transvaginal probe differentiation of diverticulitis from colonic carcinoma is often possible, it is good practice that in every patient with diverticulitis colonoscopy is performed when the inflammatory changes have subsided. Percutaneous drainage of a large diverticular abscess is indicated in case of persistent spiking fever; however, it is only rarely needed. The presence of a persistent, large paracolic abscess should always raise the suspicion of underlying malignancy.

Right-sided colonic diverticulitis

Right-sided colonic diverticulitis in many respects differs from sigmoid diverticulitis. Diverticula of the right colon are usually congenital, solitary, true diverticula containing all bowel layers. The fecalith within these diverticula are larger, the diverticular neck is wider, and there is no hypertrophy of the muscularis of the right colonic wall. Understandably, right colonic diverticulitis, which can occur at any age, almost invariably has a favorable course and never leads to free perforation with peritonitis or large abscesses. Although relatively rare, it is crucial to make a correct diagnosis, because the clinical symptoms of acute right lower quadrant pain may lead to an unnecessary operation for suspected appendicitis. In 40% of patients it even leads to a right hemicolectomy because the surgeon during the operation assumes he or she is dealing with a colonic malignancy. Although much more frequent in Asians, the diagnosis in the Western world is not rare: in a recent study one case of right colonic diverticulitis is seen for every 15 cases of sigmoid diverticulitis, and for every 30 cases of appendicitis [16].

US, if necessary complemented by CT, has characteristic features and prevents unnecessary surgery for this benign and self-limiting condition (Fig. 36).

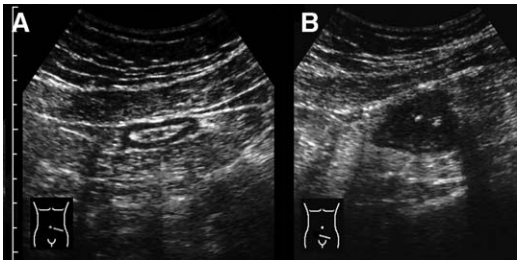

Fig. 34. Sigmoid carcinoma in 39-year-old patient with clinical signs of diverticulitis. (*A*) Transverse image of the sigmoid 5 cm cranial to the tumor: the colon is thin-walled and well-compressible. (*B*) Axial US image of the tumor shows asymmetric, moderately echolucent wall thickening of the sigmoid. There is also noncompressible fat around the tumor, representing a desmoplastic reaction.

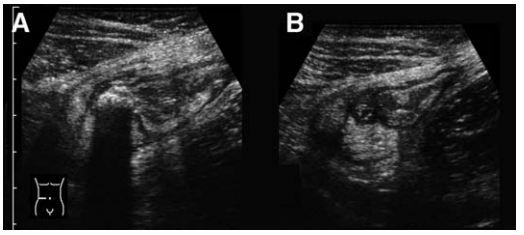

Fig. 36. Cecal diverticulitis in a 23-year-old man with all signs of acute appendicitis. (*A*) US reveals circumferential cecal wall thickening at the level of an inflamed diverticulum, containing a fecalith and surrounded by inflamed fat. The patient was treated conservatively. (*B*) Two days later the patient is almost symptom free. The diverticulum is empty because the fecalith has evacuated to the cecal lumen.

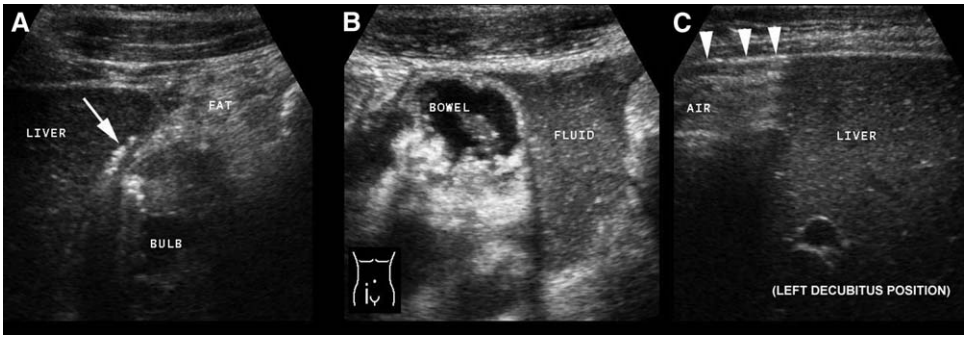

Fig. 37. Perforated duodenal ulcer. (*A*) In the right upper quadrant impressive wall thickening in the duodenal bulb is found. There are both transmural and extramural (*arrow*) gas configurations. The inflamed fat represents mesenterial and omental fat attempting, in vain, to wall off the perforation. (*B*) In the right lower quadrant US a large amount of debris-like peritoneal fluid is found. (*C*) In the left decubitus position free air (*arrowheads*) can be seen to collect between liver and the lateral abdominal wall.

For proper understanding of the US images, it is vital to realize the dynamic sequence of the inflammatory process, where each stage of the disease has its own US image [16]. A dangerous pitfall is to mistake a fecalith in the base of an inflamed appendix for a case of cecal diverticulitis.

Perforated peptic ulcer

The finding of pneumoperitoneum on a standing chest radiograph in combination with severe acute upper abdominal pain is strongly suggestive for perforated peptic ulcer and a laparotomy usually follows without additional imaging. In some cases, however, symptoms of a perforated ulcer may be atypical and mimic those of appendicitis, in which case no chest radiograph is made. In other cases of perforated ulcer free air is not present or not detectable. In all those cases, US and CT may be of help. Free air is detected easier by CT than by US, but US better defines the ulcer, demonstrates the free fluid, and can guide puncture of this fluid (Fig. 37).

In peptic ulcer US visualizes asymmetric thickening of the duodenal wall, which contains a constant air configuration reaching from the duodenal lumen to the periphery of the wall or even penetrating into the adjacent inflamed fat. Right decubitus position allows gastric fluid, which is usually present in peptic ulcer disease, to proceed to the duodenum, enabling a better visualization of the ulcer. In case of perforation, an air-track can be found from the ulcer to the peritoneal cavity usually in ventral or cranial direction. Free air is best demonstrated in the left decubitus position between liver and right abdominal wall. A lot of free fluid is usually present, which contains air bubbles and food particles. Puncture reveals turbid or purulent fluid.

References

[1] Birnbaum BA, Jeffrey Jr RB. CT and sonographic evaluation of acute right lower quadrant abdominal pain. AJR Am J Roentgenol 1998;170:361–71.
[2] Mindelzun RE, Jeffrey Jr RB. Unenhanced helical CT for evaluating acute abdominal pain: a little more cost, a lot more information. Radiology 1997;205:43–5.
[3] Mindelzun RE, Jeffrey Jr RB. The acute abdomen: current CT imaging techniques. Semin Ultrasound CT MR 1999;20:63–7.
[4] Nisenbaum HL, Birnbaum BA, Myers MM, Grossman RI, Gefter WB, Langlotz CP. The costs of CT procedures in an academic radiology department determined by an activity-based costing (ABC) method. J Comput Assist Tomogr 2000;24:813–23.
[5] Jeffrey Jr RB. In patients with right lower quadrant pain, is sonography or CT the preferred imaging technique for initial evaluation? AJR Am J Roentgenol 1995;164:1547–8.
[6] Mindel S. The full potential of ultrasound. Lancet 1988; 1:244.
[7] Rioux M. Sonographic detection of the normal and abnormal appendix. AJR Am J Roentgenol 1992;158: 773–8.
[8] Cobben LPJ, Mol van Otterloo A, Puylaert JBCM. Spontaneously resolving appendicitis: frequency and natural history in 60 patients. Radiology 2000;215: 349–52.
[9] Jeffrey RB. CT and sonography of the acute abdomen. New York: Raven Press; 1996.
[10] Rioux M, Langis P. Primary epiploic appendagitis: clini-

cal, US and CT findings in 14 cases. Radiology 1994; 191:523–6.

[11] Van Breda Vriesman AC, Lohle PNM, Coerkamp EG, Puylaert JBCM. Infarction of omentum and epiploic appendage: diagnosis, epidemiology and natural history. Eur Radiol 1999;9:1886–92.

[12] Sarrazin J, Wilson SR. Manifestations of Crohn's disease at US. Radiographics 1996;16:499–520.

[13] Puylaert JBCM. US of acute GI tract conditions. Eur Radiol 2001;11:1867–77.

[14] Puylaert JBCM, Van der Zant FM, Mutsaers JAEM. Infectious ileocolitis caused by *Yersinia*, *Campylobacter* and *Salmonella*: clinical, radiological and US findings. Eur Radiol 1997;7:3–9.

[15] Wilson SR. Gastrointestinal tract sonography. Abdom Imaging 1996;21:1–8.

[16] Oudenhoven LFIJ, Puylaert JBCM, Koumans RKJ. Right colonic diverticulitis: US and CT findings-new insights about frequency and natural history. Radiology 1998;208:611–8.

RADIOLOGIC
CLINICS OF
NORTH AMERICA

Radiol Clin N Am 41 (2003) 1243–1273

MR imaging in abdominal emergencies

Ivan Pedrosa, MD[a,b,*], Neil M. Rofsky, MD[a,b]

[a]*Department of Radiology, Harvard Medical School, Boston, MA, USA*
[b]*Department of Radiology, WC 090, Beth Israel Deaconess Medical Center, One Deaconess Road, Boston, MA 02215, USA*

Cross-sectional imaging has become an essential part in the diagnostic algorithm of the acutely ill patient. Ultrasound (US) and computed tomography (CT) have been integrated in most diagnostic algorithms in these patients. US is particularly well suited for the evaluation of severely ill patients because it can be performed at bedside, is rapid, and does not require intravenous contrast. CT indications for the assessment of these patients have increased continuously during the last decades as CT scanners have become more accessible and CT examinations faster.

Abdominal-pelvic MR imaging is most often used in a problem-solving capacity. It often is a second-line, alternative imaging modality for those patients with an unclear diagnosis and is not routinely performed in the evaluation of the acutely ill patient. Impediments to a more widespread use in the acute setting include a limited availability of MR imaging scanners, and the complexity, length, and cost of the MR imaging examinations. Multiplanar imaging, lack of ionizing radiation, and safety of the currently available contrast materials, however, are favorable features for MR imaging. Furthermore, if studies can demonstrate a decrease in test redundancy or a more rapid diagnosis and appropriate triage the early treatment, MR imaging may prove to be a cost-effective strategy for imaging in the emergency or urgent setting.

The authors have experienced an increased reliance on MR imaging in this setting and have capitalized on the inherent, excellent soft tissue contrast available and newer techniques that can allow for consistent and rapid diagnoses. This article describes a range of applications for which MR imaging can be of value in the assessment of the patient with acute abdominal emergencies.

MR imaging protocols

MR imaging protocols should be tailored based on the clinical indication. A phase-array body coil is recommended whenever possible because it offers superior signal-to-noise than the built-in body coil. This is particularly important when fast MR imaging acquisitions with high bandwidths are used. The size of the phase-array coil may be a limiting factor when evaluation of the entire abdomen and pelvis is needed. Large phase-array coils or a series of adjacent distinct coils are now available and allow for MR imaging evaluation of the entire abdomen and pelvis with excellent signal-to-noise.

The authors routinely administer oral contrast for MR imaging examinations of the upper abdomen when the biliary tree or pancreas is to be evaluated. The authors use a combination of 150 mL of Gastromark (Mallinckrodt Medical, St. Louis, Missouri) and 150 mL of Readi-cat 2 (EZEM Canada, Westbury, New York). This solution provides negative oral contrast on T1- and T2-weighted images without significant susceptibility effect. Oral contrast also can be useful in patients with suspected bowel pathology. Oral contrast is not mandatory, however, because of the excellent inherent contrast of MR images.

Gadopentetate dimeglumine (Magnevist, Berlex Laboratories, Wayne, New Jersey) is routinely used at the authors' institution for abdominal imaging. MR images are obtained before and after a bolus of gadolinium at the dose of 0.1 mmol/kg (approximately 20 mL) at a rate of 2 mL/second. A flush with saline of 20 mL at the same rate (2 mL/second) is routinely

* Corresponding author. Harvard Medical School, Boston, MA.
E-mail address: ipedrosa@bidmc.harvard.edu (I. Pedrosa).

0033-8389/03/$ – see front matter
doi:10.1016/S0033-8389(03)00102-7

administered. The arterial phase is timed with a bolus test of 2 mL of gadolinium at 2 mL/second with the technique previously described by Earls et al [1]. MR images are then acquired during the arterial, portal (20 seconds after the arterial phase), and delayed venous phases (60 seconds after the arterial phase).

Gadolinium-based contrast agents have been proved to be safe in patients with renal failure [2–4]. In addition, allergic reactions to gadolinium chelates are extremely rare [5]. These characteristics make gadolinium an excellent contrast agent in the assessment of the severely ill patient including patients with a contraindication to the administration of iodinated contrast media

Breathhold imaging

Breathhold imaging acquisitions reduce the total examination time and eliminate respiratory-related artifacts. The authors obtain breathhold acquisitions during end-expiration because this strategy is more reproducible. This is particularly important when subtraction techniques are used. Dual-echo (in-phase and out-of-phase) T1-weighted images are acquired for anatomic information and characterization of fat-containing lesions. Hemorrhagic collections can demonstrate high signal intensity on T1-weighted images. Additionally, these images can be used for detection of susceptibility effects related to air, blood products, and calcium. Blooming effect is readily noted on the in-phase images with a longer echo time at these areas when compared with the out-of-phase images (with a shorter echo time).

Half Fourier single-shot fast spin echo images (SSFSE or HASTE) provide excellent visualization of the biliary tree and are immune to all but the most extreme sources of motion artifact. A combination of axial and coronal thin-slice and coronal thick-slab acquisitions is obtained for assessment of the biliary tree. These images also are used for assessment of the bowel. Bowel wall has intermediate signal intensity on these T2-weighted images. Intraluminal fluid (high signal intensity) or air (signal void) provide an excellent contrast for evaluation of bowel wall pathology.

Dynamic postcontrast images are obtained with a three-dimensional fat-saturated T1-weighted gradient echo sequence. These three-dimensional datasets subsequently can be reconstructed into any plane with almost similar spatial resolution to the original acquisition. In addition, three-dimensional acquisitions can be used for generating MR angiograms that allow for a comprehensive evaluation of the abdomen and pelvis [6,7]. Three volumetric datasets during the arterial, portal, and delayed venous phases are acquired after administration of a bolus of gadolinium.

Although breathhold protocols are desirable, acutely ill patients are frequently unable to sustain long breathhold times. Alternative protocols using short acquisition times are particularly helpful in these patients. Acquisition times can be reduced effectively with the application of parallel imaging techniques. A complete discussion of the principles of parallel imaging is beyond the purpose of this article and the reader is referred to available references [8,9]. Parallel imaging strategies that have been implemented by different MR imaging manufacturers include sensitivity encoding, simultaneous acquisition of spatial harmonics, and array spatial sensitivity encoding technique. With parallel imaging techniques, exploiting spatial information inherent to the geometry of the surface coil allows for faster imaging acquisition without increase of gradient switching rates or radiofrequency (RF) deposition [8]. For each application of a phase-encoding gradient, multiple lines in k-space are generated simultaneously reducing the overall acquisition time [8]. For example, a 20-second acquisition can be reduced to a 10- or 5-second acquisition with acceleration factors of 2x and 4x respectively, with only minimal imaging degradation. Parallel imaging techniques can be applied to both two- and three-dimensional sequences [8].

Non-breathhold imaging

Acutely ill patients are frequently unable to hold their breath. Breathhold-independent acquisitions are crucial in these patients to obtain interpretable images. Fast sequences acquired in a sequential manner are the cornerstone of breathhold-independent examinations. Magnetization-prepared T1-weighted gradient echo images and half-Fourier T2-weighted SSFSE represent the core of the breathhold-independent protocol. Both sequences are obtained on a per-slice basis and each slice is obtained in approximately 1 second. Image quality is not affected by breathing motion when these sequences are used. Slice misregistration can occur with breathing motion, however, and the anatomy can be demonstrated in a nonsequential manner. This approach, however, may represent the only opportunity to acquire interpretable images in these patients.

Magnetization-prepared T1-weighted gradient echo images are acquired before and after administration of a bolus of gadolinium. Timing of the arterial phase is similar to that of dynamic CT examinations with conventional scanners. Images are obtained sequentially from the dome of the liver to the lower

abdomen after arrival of the gadolinium to the upper abdominal aorta. The authors typically obtain three acquisitions during the arterial, portal, and delayed venous phases.

Clinical applications

Liver

Acute infectious diseases of the liver

Hepatic abscesses are most commonly secondary to biliary diseases and those are frequently multiple [10]. Other causes include acute inflammatory processes drained by the portal venous system (acute appendicitis, acute diverticulitis); arterial hematogenous spread in patients with bacteremia; contiguous spread from adjacent organs (pyelonephritis, perforated duodenal ulcer, subphrenic abscess, pneumonia); and blunt and penetrating injury.

Cross-sectional imaging is essential in the diagnosis and management of hepatic abscesses. MR imaging is helpful in the characterization of hepatic lesions in which diagnosis is unclear. Gadolinium-enhanced MR imaging of the liver can be performed in patients with contraindication for administration of iodinated contrast media (eg, allergy, renal insufficiency). There is no specific MR imaging appearance for liver abscess and the MR imaging findings always should be correlated with the clinical findings.

Most pyogenic liver abscesses appear as round, sharply demarcated lesions with low signal intensity on T1-weighted images and high signal intensity on T2-weighted images compared with the hepatic parenchyma [11].

The abscess wall is perceptible in most cases on MR imaging [12]. Gadolinium-enhanced MR images improve the conspicuity of hepatic abscesses because of increased rim enhancement of the abscess wall [13] on multiple phases following contrast administration [11,12]. Larger abscess may demonstrate enhancing thin septations (Fig. 1) [11]. A more uniform appearance of the lesions can be noted on 15 to 60 minutes delayed postgadolinium images because of leakage of the contrast media within the abscess cavity [14]. Because this phenomenon can potentially obscure smaller lesions on delayed postgadolinium MR images [13], dynamic imaging is favored.

Perilesional findings, such as edema with or without transient arterial perilesional enhancement, may be noted and often appear with a wedged shape [11,12]. These findings are nonspecific and can be seen with amebic liver abscesses [15] and in 20% to 30% of primary and secondary hepatic malignancies [11].

Amebic liver abscess is the most common extraintestinal manifestation of the infection caused by *Entamoeba histolytica* [16]. Recent history of travel to an endemic area for amebiasis or impaired patient's immunity is frequent among patients with amebic liver abscesses [16]. Most amebic liver abscesses are

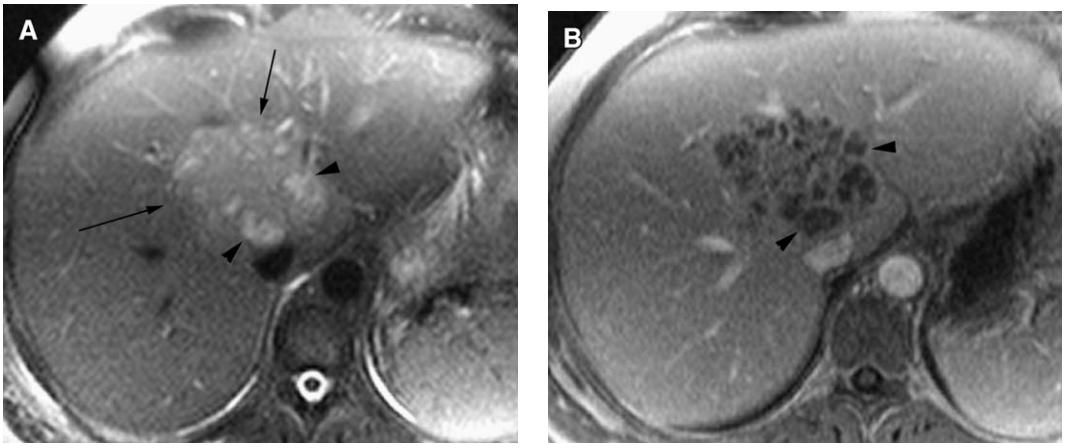

Fig. 1. Hepatic abscess. A 48-year-old man with sepsis and positive blood cultures for *Klebsiella pneumoniae*, assessed with motion-insensitive sequences. (*A*) Axial fat-saturated SSFSE image (TR 1100, TE 64, FA 130, 256 × 190, slice thickness 5 mm) shows a heterogeneous hyperintense mass in the central area of the liver (*arrows*). Note several small markedly hyperintense regions (*arrowheads*). (*B*) Axial T1-weighted turbo fast low angle shot gradient echo image (TR 7.7, TE 4.2, FA 15, 256 × 128, thickness 6 mm) 60 seconds after administration of 20 mL of gadolinium confirms the presence of a heterogeneous mass with multiple nonenhancing areas (*arrowheads*). The mass demonstrates multiple enhancing septae. A small amount of fluid was aspirated from this nonliquefied abscess. Fluid culture was positive for *K pneumoniae*.

located in the right lobe and they are multiple in up to 50% of the cases [16]. Complications of amebic liver abscesses include rupture into the peritoneum, pleural cavity, and pericardium [17]. Pyogenic superinfection has also been described [17].

Most amebic liver abscesses appear on MR images as round or oval lesions with well-defined margins and occasional lobulation [18]. Amebic abscesses are predominantly homogeneously low-signal intensity on T1-weighted images and heterogenous high signal intensity on T2-weighted images [18]. Amebic liver abscesses typically demonstrate one to three concentric rims on MR images [18]. These rings become very prominent after treatment [15]. On dynamic gadolinium-enhanced MR images, the thick wall (5 to 10 mm) of amebic abscesses demonstrates similar enhancement pattern than that of pyogenic abscesses [12].

MR imaging has similar accuracy for detection of amebic liver abscesses than US and CT [18]. MR imaging may be helpful, however, in demonstrating diaphragmatic disruption in patients with thoracic extension of amebic abscesses [18]. Amebic empyema can be differentiated from sympathetic pleural effusion by its high signal intensity on both T1- and T2-weighted images [18]. In addition, MR imaging multiplanar capability can provide valuable information about the relationship of amebic abscesses located in the left lobe of the liver and the heart [18]. Amebic abscess located within the left lobe close to the heart should be drained percutaneously because of its risk for rupture into the pericardium [17]. Finally, MR imaging may be helpful in monitoring the patient's response to treatment [15]. Formation of concentric rings in the wall of the abscess, resolution of perilesional edema (high signal intensity on T2-weighted images), and liquefaction of the abscess center suggest response to treatment [15].

Fungal hepatic abscesses represent an opportunistic infection of immunocompromised patients. *Candida*, *Aspergillus*, *Cryptococcus*, *Histoplasma*, and *Mucormycosis* are responsible for fungal microabscesses in these patients [12]. Hepatic candidiasis is a relatively common infection among patients undergoing chemotherapy for hematologic malignancies [19]. Involvement of the liver, spleen, and kidney occurs in 75%, 94%, and 69% of patients with disseminated candidiasis, respectively [20].

Candida involvement of abdominal visceral organs can be undetected in neutropenic patients because of the lack of inflammatory reaction [19]. Once the patient's neutrophil count recovers, hepatosplenic candidiasis typically presents with small military microabscesses scattered throughout the liver parenchyma. MR imaging is superior to CT in the diagnosis of hepatic candidiasis [20]. Reported MR imaging sensitivity is 100% and specificity 96% [20]. Prospective studies are necessary to confirm these results including patients with low neutrophil counts.

Acute candidal microabscesses are usually less than 1 cm in diameter and oval in shape [20]. Lesions demonstrate high signal intensity on fat-saturated T2-weighted images and low signal intensity on T1-weighted images. Dynamic gadolinium-enhanced T1-weighted images show no enhancement or significant change in appearance of the lesions over time [20]. Gadolinium-enhanced T1-weighted images are the most sensitive for detection of candidal microabscesses, although in some patients these lesions may be seen only on T2-weighted images [20].

Other hepatic infections including echinococcosis, granulomatous infections (tuberculosis, toxoplasmosis, nocardiasis, brucellosis), schistosomiasis, and fascioliasis can present clinically with acute symptoms. Patients with hepatic hydatidosis may present with acute symptoms secondary to cyst rupture into the biliary tree, chest, pleural and peritoneal cavity, or bacterial superinfection [21]. MR imaging findings have been described in these conditions [12,21], although a complete description of these entities is beyond the scope of this article.

Acute hepatitis is the result of an acute inflammation of the liver parenchyma secondary to infection (viral, bacterial), alcohol abuse, drugs, autoimmune reactions, environmental agents, and so forth [22]. Hepatomegaly and periportal edema manifested by bands of high signal intensity paralleling the portal vessels on T2-weighted images are common in patients with severe acute hepatitis [22]. The degree of periportal high signal intensity on T2-weighted images has been correlated with the severity of the disease in acute viral hepatitis [23]. Furthermore, periportal edema decreases on follow-up MR imaging examinations of patients during clinical recovery [23]. Necrosis of the liver parenchyma in patients with fulminant hepatitis is characterized by high signal intensity on T2-weighted images and low-signal intensity on T1-weighted images [24]. Ultrasonographic detection of marked gallbladder wall edema has been previously described in patients with acute hepatitis [25]. Similar findings can be seen on MR imaging examinations. Frequently, marked gallbladder wall edema is associated with lack of distention of the gallbladder, which helps to differentiate from gallbladder wall edema in acute cholecystitis. Gadolinium-enhanced MR images can demonstrate diffuse heterogeneous enhancement of the liver parenchyma during the arterial phase in patients with acute hepatitis from a variety of causes including viral, drug-

induced, alcoholic, and so forth. The liver parenchyma typically becomes homogeneous during the portal phase (Fig. 2).

Acute hepatic vascular conditions

Acute vascular conditions may account for a variety of hepatic emergencies including hepatic infarcts, portal vein thrombosis, Budd-Chiari syndrome, and bleeding. Hepatic infarcts may occur secondary to hepatic artery or portal vein occlusion. Patients can present with nonspecific right upper quadrant pain. Acute hepatic infarcts are typically demonstrated as peripheral wedge-shaped areas of increased signal intensity on T2-weighted images that show no enhancement on gadolinium-enhanced T1-weighted images. Three-dimensional gadolinium-enhanced MR images allow for generation of angiographic-like images that can demonstrate the occlusion of the hepatic artery or portal vein [26,27].

Thrombosis of the portal vein can occur secondary to intra-abdominal infection, hypercoagulable state, trauma, postoperative state, neoplasm, congenital causes, pregnancy, and oral contraceptives [28]. Portal vein thrombosis is idiopathic in approximately 8% to 15% of the cases [28]. Patients can present with abdominal pain, especially when thrombus extends to the superior mesenteric vein [28].

The ability to differentiate between recent and chronic portal vein thrombosis has clinical implications [29]. Patients with recent thrombosis of the portal vein should be treated with early anticoagulation therapy, because they frequently demonstrate recanalization after treatment [29]. Findings suggesting recent thrombosis include recent abdominal pain; no evidence of chronic portal hypertension (gastrointestinal bleeding, ascites, collateral portosystemic circulation, or splenomegaly); and lack of portal cavernous transformation cross-sectional imaging. In the authors' experience, recent thrombus demonstrates high signal intensity on T2-weighted images. High signal intensity on T2-weighted images and increased enhancement after administration of gadolinium in the wall of the portal vein during the acute-subacute stages is probably related to inflammation. These findings have been described as a sign of acute-subacute thrombosis in other anatomic locations [30].

Segmental portal vein occlusion may result in wedge-shaped areas of increased signal intensity on T2-weighted images and decreased signal intensity on T1-weighted images [31]. A transient increased enhancement of the affected hepatic segment can be seen during the arterial phase on dynamic gadolinium-enhanced MR images and is likely related to compensatory increased hepatic arterial blood flow [32,33]. Typically, enhancement of the liver parenchyma becomes homogeneous during the portal and delayed venous phases [33].

Budd-Chiari syndrome is the result of the obstruction of the hepatic outflow secondary to obstruction of the hepatic veins or inferior vena cava. MR imaging findings in Budd-Chiari syndrome include hepatic vein thrombosis, hepatic vein occlusion and narrow-

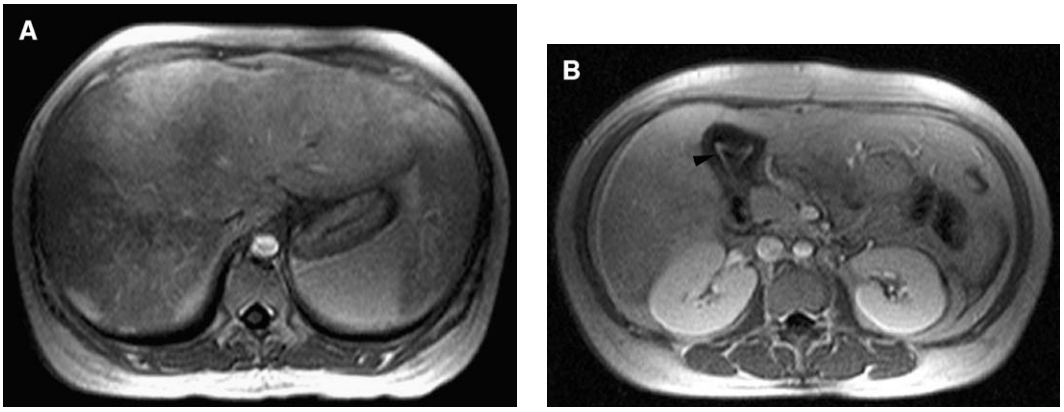

Fig. 2. Acute alcoholic hepatitis. A 40-year-old woman with history of ethanol abuse presenting with nausea, vomiting, elevated bilirubin, and 55,000 white cells in blood. Liver biopsy confirmed acute alcoholic hepatitis. (*A*) Axial T1-weighted turbo fast low angle shot gradient echo image (TR 7.7, TE 4.2, FA 15, 256 × 128, thickness 6 mm) during the arterial phase shows heterogeneous enhancement of the liver parenchyma. Note enlargement of the liver with the left lobe extending around the spleen. (*B*) Same sequence as in Fig. 2A during the portal venous phase at a slightly inferior level shows a collapsed gallbladder with marked wall edema. Note the marked gallbladder wall edema associated with lack of distention of the gallbladder and enhancing mucosa (*arrow*).

ing, and inferior vena cava thrombosis or narrowing [27]. Visualization of the patent central hepatic veins does not exclude Budd-Chiari syndrome, because they may be normal when the obstruction occurs at the level of the small- or intermediate-sized veins. Intrahepatic collaterals can be seen as comma-shaped enhancing vessels [27].

Parenchymal findings on MR imaging during the acute presentation of the Budd-Chiari syndrome include peripheral areas of heterogeneous high signal intensity on T2-weighted images and decreased signal intensity on T1-weighted images with normal signal intensity in the caudate lobe [34]. Increased enhancement in the caudate lobe can be seen during the arterial phase on dynamic postgadolinium images and persists during the delayed venous phase [34]. Perfusion of the caudate lobe is typically preserved because of its independent venous drainage. Heterogeneous peripheral enhancement of the liver parenchyma during the arterial and delayed phases after administration of gadolinium correlates with hepatic ischemia, congestion, and hemorrhage on pathologic examination [34]. Ascites is common because of acute liver failure.

Hepatic hemorrhagic conditions

Nontraumatic acute hemorrhage can occur in different hepatic conditions including neoplastic and nonneoplastic diseases [35]. Patients can present with acute right upper quadrant pain and occasionally with hemodynamic shock. MR imaging should be reserved for hemodynamically stable patients. Solid hepatic lesions including hepatocellular carcinoma and hepatic adenoma are the most common causes [35]. Other lesions, such as focal nodular hyperplasia, hemangioma, and metastasis, can present with acute symptoms related to hemorrhage [35]. Giant hemangiomas (larger than 4 cm in diameter) are more prone to bleed [35]. In general, MR imaging can demonstrate heterogeneous appearance of the lesions with areas of high signal intensity on T1-weighted images consistent with blood products (Fig. 3).

Gallbladder and biliary emergencies

The passage of gallstones through the biliary system produces a spectrum of clinical conditions that varies from the self-limiting biliary colic to the complicated forms of acute cholecystitis. Cross-sectional imaging is a key component in the diagnostic algorithm of the patient with right upper quadrant pain. US is most often the initial evaluation of these patients. CT is favored for those patients with a wider differential diagnosis or those with confusing clinical symptoms and signs. Recently, MR imaging has been shown to be a useful technique in the evaluation of patients with biliary tract disease [36,37]. High-quality MR cholangiography can be performed on most current MR imaging scanners.

Symptomatic cholelithiasis

Patients with gallstones become symptomatic in up to 10% to 25% of the cases in the 10 years following the diagnosis [38], typically with right upper quadrant pain or discomfort. Most stones show low signal intensity on T1- and T2-weighted images. MR imaging appearance of gallstones, however, is variable depending on the lipid and water content [39]. There is poor correlation between the chemical composition and the signal intensity on MR imaging [39]. Central areas of high signal intensity within gallstones on T2-weighted images correspond to fluid-filled clefts [40]. Areas of high signal intensity on T1-weighted images are related to high contents in copper [40].

MR imaging may be helpful for the diagnosis of impacted gallstones in patients with limited US visualization of the gallbladder. MR imaging can demonstrate gallbladder distention caused by an impacted stone but the findings of gallbladder wall edema or pericholecystic fluid suggest cholecystitis.

Acute cholecystitis

Imaging evaluation of the patient with clinical suspicion of acute cholecystitis offers not only confirmation of the diagnosis but also detection of complications, such as gangrene, emphysematous cholecystitis, and perforation. In addition, information about the presence of choledocholithiasis is important before surgery, particularly if laparoscopic cholecystectomy is to be attempted. Imaging studies may reduce the number of surgical explorations by diagnosing a variety of pathologic processes that mimic acute cholecystitis.

Ultrasound, with a sensitivity, specificity, and accuracy greater than 95% for the diagnosis of acute cholecystitis [41], is the initial imaging modality of the patient with right upper quadrant pain Ultrasonographic evaluation of the extrahepatic biliary tree is frequently limited, however, with a sensitivity for detection of common bile duct (CBD) stones as low as 25% [42]. CT and MR imaging are usually performed in those patients with a wider differential diagnosis or with confusing clinical signs and symptoms [41,43].

Initial studies reported decreased signal intensity of the bile within the gallbladder compared with the liver on T1-weighted images in patients with acute chole-

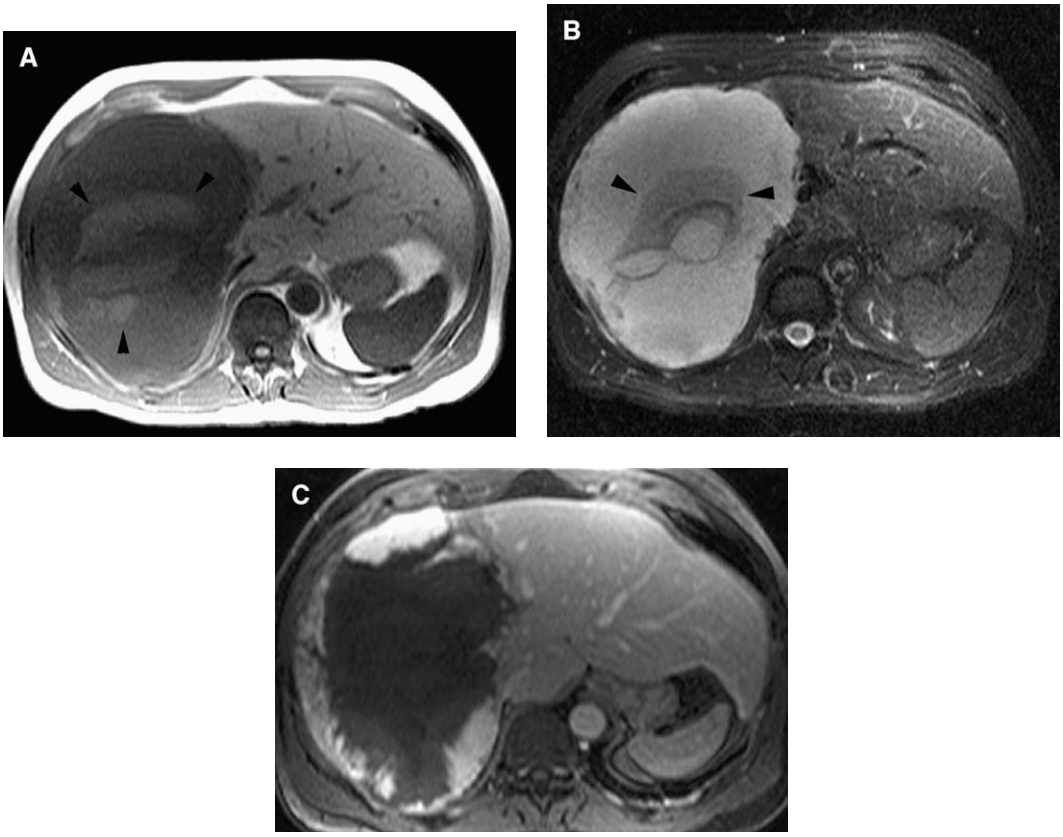

Fig. 3. Giant hepatic hemangioma with acute bleed. A 58-year-old man with known giant cavernous hemangioma in the right lobe of the liver presenting with right upper quadrant pain and dropped hematocrit. (*A*) Axial T1-weighted gradient echo image (TR 170, TE 5.3, FA 80, 256 × 160, thickness 7 mm) shows a large hypointense mass occupying the right lobe of the liver. Centrally areas of high signal intensity are noted, consistent with acute bleed (*arrowheads*). (*B*) Axial STIR (TR 4500, TE 76, FA 150, ETL 33, thickness 7 mm) image shows diffuse high signal intensity within the lesion similar to that of the cerebrospinal fluid. Note the hypointense central area caused by hemorrhage (*arrowheads*). (*C*) Axial three-dimensional fat-saturated T1-weighted gradient echo image (TR 4.5, TE 1.9, FA 12, slice thickness 4 mm, before interpolation) during the portal venous phase after administration of a single dose of gadolinium demonstrates peripheral, discontinuous, nodular intense enhancement, typical for cavernous hemangioma. Pathology confirmed the diagnosis after right hepatectomy.

cystitis [44,45]. This finding may be related to the inability of the gallbladder to concentrate the bile because of the inflammation [45]. The signal intensity of the bile within the gallbladder is variable, however, and false-positive results can occur in the nonfasting patient [46].

Gallbladder wall edema is readily seen with MR imaging [47,48] and this finding, rather than thickening, should be used for the diagnosis of acute cholecystitis. Gallbladder wall thickening is poorly correlated to acute cholecystitis [49–51]. Superior sensitivity (77%) and specificity (78%) have been reported for MR imaging compared with US (27% and 100%, respectively) for detection of gallbladder wall edema [48].

The presence of pericholecystic high signal intensity on SSFSE images has an overall accuracy, specificity, and positive and negative predictive values of 89%, 79%, 87%, and 85%, respectively, for the diagnosis of acute cholecystitis [47]. In the authors' experience, coronal SSFSE images are particularly helpful for differentiating gallbladder wall edema (extending along the entire circumference of the gallbladder wall) from pericholecystic fluid (usually within the gallbladder fossa, between the gallbladder and the inferior surface of the liver). In an article by Loud et al [43], contrast-enhanced T1-weighted images were found to be very useful for the diagnosis of acute cholecystitis. Patients with surgically proved acute cholecystitis had greater than 80% contrast

enhancement of the gallbladder wall [43]. In addition, differentiation between acute and chronic cholecystitis was possible based on the greater enhancement of the gallbladder wall in patients with acute inflammation of the gallbladder [43]. Gallbladder wall thickening was not statistically different in patients with acute or chronic cholecystitis [43].

MR imaging is superior to US for the detection of obstructing calculi in the gallbladder neck and cystic duct [48,52]. Although MR imaging serves as a valuable tool in patients where other imaging results are equivocal, further studies are needed to evaluate the cost-benefit of MR imaging as a primary diagnostic tool in patients with right upper quadrant pain.

A transient increase in hepatic enhancement may be seen around the gallbladder in 70% of the cases during the arterial phase of dynamic imaging [43]. This finding seems to be unique to the arterial phase

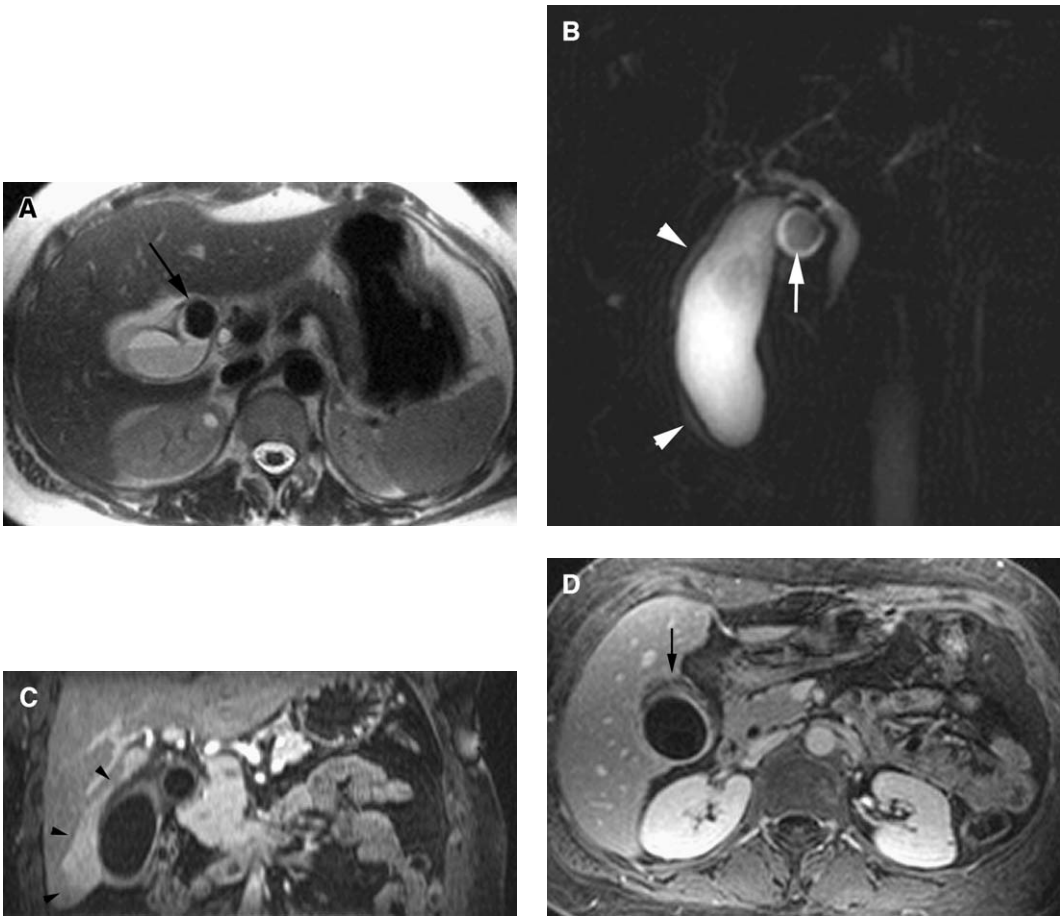

Fig. 4. Acute cholecystitis. A 51-year-old patient with right upper quadrant tenderness and elevated white cell count. (*A*) Axial SSFSE image (TR 1100, TE 64, FA 130, 256 × 190, slice thickness 5 mm) shows an obstructing gallstone impacted in the gallbladder neck (*arrow*). There is a fluid-fluid level within the gallbladder possibly related to biliary sludge. (*B*) Coronal thick-slab SSFSE image (TR 1100, TE 800, FA 130, 256 × 190, slice thickness 50 mm) demonstrates high signal intensity within the gallbladder wall consistent with edema (*arrowheads*). There is no dilatation or filling defect within the biliary tree. The gallstone is noted (*arrow*). (*C*) Coronal reconstruction from an axial three-dimensional fat-saturated T1-weighted gradient echo sequence (TR 4.5, TE 1.9, FA 12, slice thickness 4 mm, before interpolation) obtained during the arterial phase after administration of a single dose of gadolinium. There is increased pericholecystic hepatic enhancement caused by hyperemia secondary to the inflammation from the adjacent gallbladder (*arrowheads*). (*D*) Axial three-dimensional fat-saturated T1-weighted gradient echo image (TR 4.5, TE 1.9, FA 12, slice thickness 4 mm, before interpolation) obtained during the portal phase, 20 seconds after Fig. 4A. The signal intensity of the pericholecystic area has equilibrated with the rest of the liver. There is marked edema of the gallbladder wall (*arrow*) and marked enhancement of the gallbladder mucosa throughout. Patient underwent cholecystectomy and pathology confirmed acute cholecystitis.

(Fig. 4) and also has been described during dynamic CT imaging [53]. It is likely related to increased arterial flow in the pericholecystic liver parenchyma in response to local inflammation [43]. Pericholecystic arterial hepatic enhancement, the MR imaging rim sign, resembles the focal increased flow in the gallbladder region seen in patients with acute cholecystitis on radionuclide angiography with technetium 99m disofenin [54]. Further studies are needed to establish the significance of the MR imaging rim sign and its accuracy to recognize complicated forms of acute cholecystitis.

Gangrenous cholecystitis occurs when ischemia of patchy areas or the complete gallbladder leads to necrosis of the wall. Older men with history of cardiovascular disease and marked leukocytosis (> 17,000 white blood cells/mL) have increased risk of gallbladder gangrene [55]. Gangrenous cholecystitis is present in up to 30% of patients admitted with acute cholecystitis [55]. Preoperative diagnosis of gangrenous cholecystitis is clinically difficult because of lack of specificity of the clinical findings. The normal enhancing gallbladder mucosa easily is appreciated on postcontrast MR images as a hyperintense ring in the inner side of the gallbladder wall. Patients with acute cholecystitis may demonstrate increased enhancement of the gallbladder mucosa making this ring even more apparent [43]. The authors have noted a patchy pattern of mucosal enhancement related to necrosis of the gallbladder wall. This interrupted ring of mucosal enhancement correlated with alternating areas of mucosal necrosis and inflammation on pathologic examination (Fig. 5).

Acalculous cholecystitis is commonly seen in critically ill patients in the intensive care unit. Bedside US is considered the imaging study of choice in these patients. The accuracy of US for the diagnosis of acalculous cholecystitis recently has been questioned in critically ill trauma patients [56]. US findings in these patients include gallbladder wall thickening, pericholecystic abscess, and marked gallbladder distention. These findings can be similarly demonstrated on MR imaging [46].

Hemorrhagic cholecystitis is a rare form of acute cholecystitis in which bleeding occurs within the gallbladder wall or lumen. Mucosal ulcerations and necrosis caused by gallstones have been proposed as causes of hemorrhage and inflammation [57]. Hemorrhagic cholecystitis has been reported in patients with lupus erythematosus [58], metachromatic leukodystrophy [59], hemodialysis [60,61], and anticoagulation therapy [62]. Clinical presentation is similar to other forms of acute cholecystitis with right upper quadrant pain, leukocytosis, and fever [63]. MR imaging provides excellent soft tissue contrast that allows for recognition of blood products within the gallbladder. A heterogeneous high signal intensity hematoma can be seen within the gallbladder lumen on T1-weighted images. Gallbladder contents show moderate to high heterogeneous signal intensity on

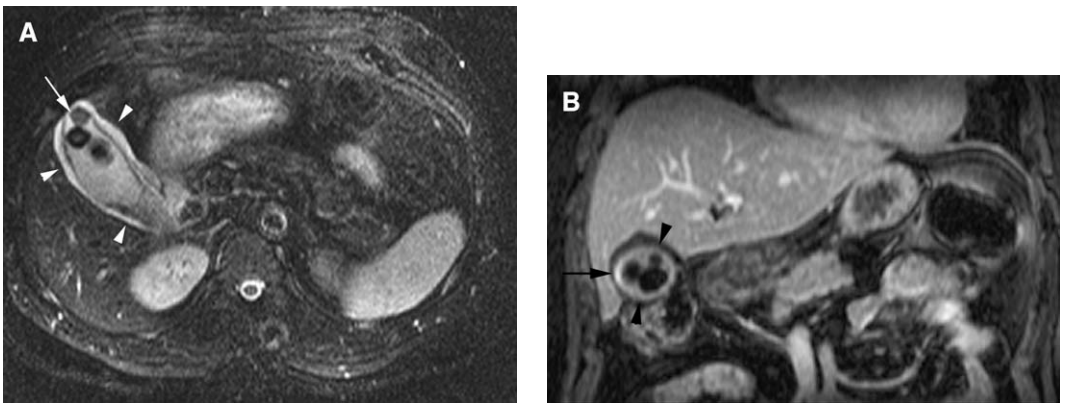

Fig. 5. Acute gangrenous cholecystitis. A 37-year-old woman with right upper quadrant pain and elevated white cell count. (*A*) Axial STIR image (TR 4500, TE 76, FA 150, ETL 33, thickness 7 mm) shows diffuse hyperintense thickening of the gallbladder wall consistent with edema (*arrowheads*). Multiple hypointense filling defects within the gallbladder fundus is consistent with gallstones (*arrow*). (*B*) Coronal reconstruction from a three-dimensional fat-saturated T1-weighted gradient echo acquisition (TR 4.5, TE 1.9, FA 12, slice thickness 4 mm, before interpolation) obtained during the portal phase. Note a focal area of increased enhancement of the gallbladder mucosa secondary to inflammation (*arrow*) alternating with extensive areas of no enhancement (*arrowheads*). This patchy pattern of enhancement, the interrupted rim sign, correlated to the pathology with gangrene of the gallbladder wall.

T2-weighted images. Short-tau inversion recovery (STIR) images can be useful in demonstrating suppression of the signal of the blood products because of its short T1 relaxation time. Both T2-weighted and STIR images can demonstrate high signal intensity within the gallbladder wall secondary to edema. Multiplanar capability of MR imaging may be helpful for differentiating between intraluminal bleeding and hemorrhage within the gallbladder wall. Also, MR angiography can be useful in selected patients when associated vascular pathology is suspected (Fig. 6).

Perforation of the gallbladder occurs in as many as 10% of patients with acute cholecystitis [64]. Most commonly, perforation is localized because it is confined by the omentum [65]. A pericholecystic abscess is usually present [65]. Alternatively, an intrahepatic abscess may be seen. HASTE images are particularly useful for demonstration of the defect in the gallbladder wall and the communication between the gallbladder and the pericholecystic abscess (Fig. 7). MR imaging should be used when perforation is suspected and US or CT are inconclusive [66].

Acute or chronic cholecystitis

Differentiation between new episodes of right upper quadrant pain in patients with chronic cholecys-

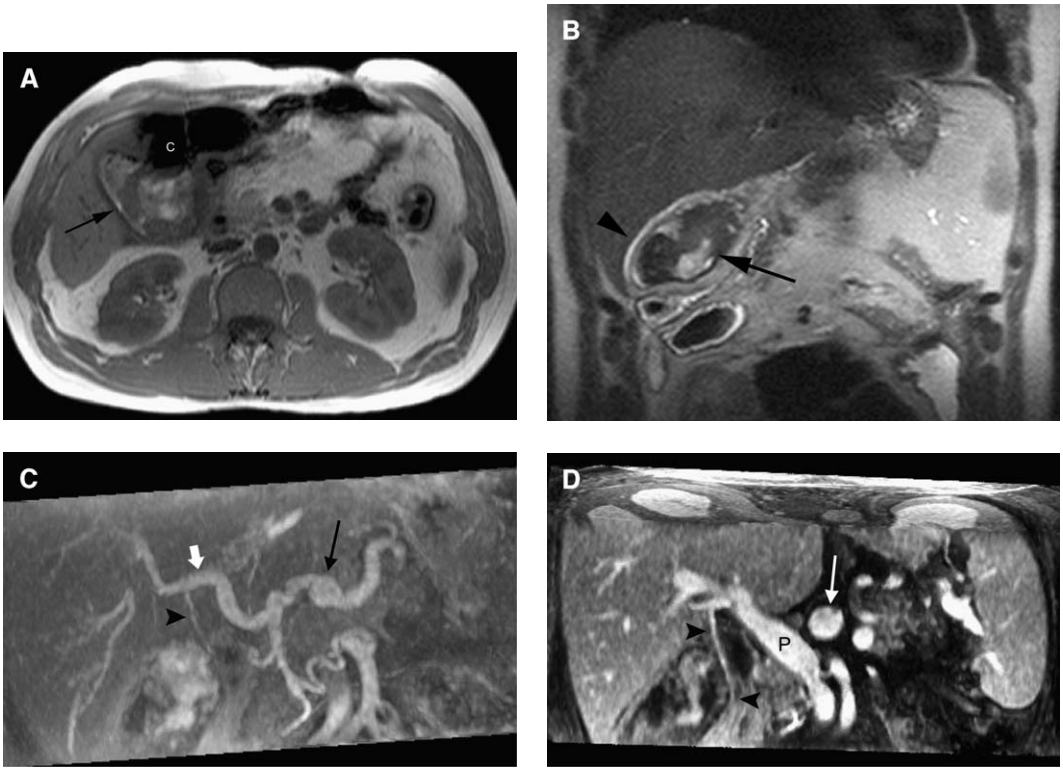

Fig. 6. Acute hemorrhagic cholecystitis. A 40-year-old man with Ehlers-Danlos syndrome type IV and acute right upper quadrant pain and chills. Previous CT showed hemorrhage in the gallbladder fossa and an aneurysm of the celiac artery (not shown). MR imaging performed to confirm blood products within the gallbladder and rule out aneurysm of the cystic artery. (*A*) Axial T1-weighted gradient echo image (TR 170, TE 5.3, FA 80, 256 × 160, thickness 7 mm) shows heterogeneous hyperintense contents within the gallbladder consistent with blood products (*arrow*). Susceptibility artifact anterior to the gallbladder is related to air within the colon (C). (*B*) Coronal HASTE image (TR 1100, TE 64, FA 130, 256 × 190, slice thickness 5 mm) shows heterogeneous contents within the gallbladder (*arrow*). Note mild thickening and hyperintensity of the gallbladder wall (*arrowhead*) secondary to edema. (*C*) Coronal targeted maximum intensity projection reconstruction from an axial three-dimensional fat-saturated T1-weighted gradient echo acquisition (TR 4.5, TE 1.9, FA 12, slice thickness 4 mm, before interpolation) during the arterial phase shows an aneurysm of the celiac axis (*arrow*) and normal appearance of the hepatic artery (*white arrow*) and proximal cystic artery (*arrowhead*). (*D*) Coronal volume-rendering reconstruction from three-dimensional acquisition during the portal venous phase with similar parameters than Fig. 11C confirms the normal appearance of the cystic artery (*arrowheads*). The aneurysm of the celiac artery (*arrow*) and portal vein (P) are also displayed.

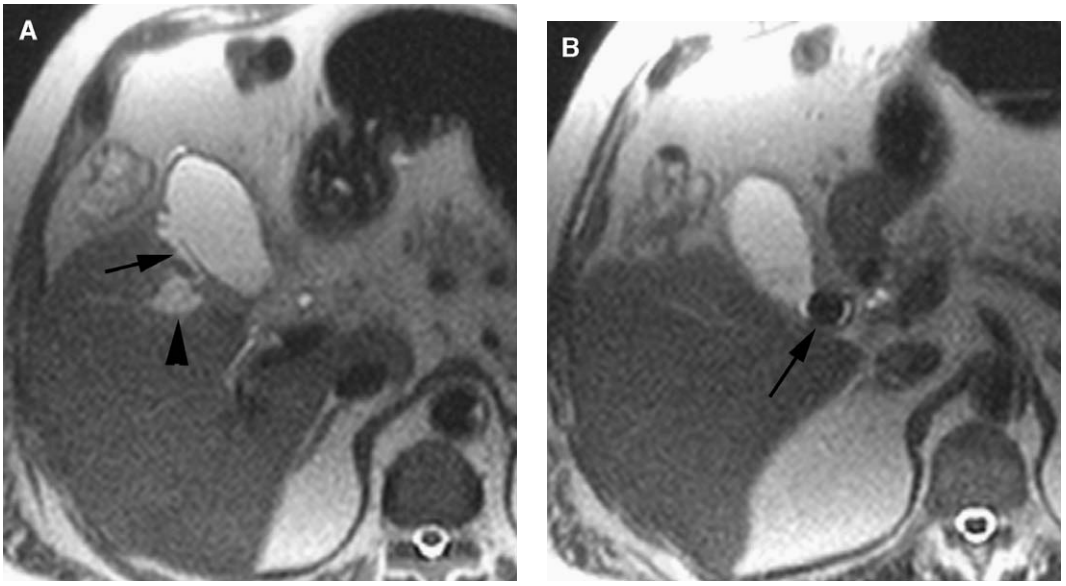

Fig. 7. Perforated acute cholecystitis. A 73-year-old man with right upper quadrant pain, fever, chills, and elevated white count. (*A*) Axial HASTE image (TR 1100, TE 64, FA 130, 256 × 190, slice thickness 4 mm) shows a small fluid collection in the right lobe of the liver (*arrowhead*), connecting to the gallbladder through a thin fluid-filled tract (*arrow*). There is a small amount of pericholecystic fluid. (*B*) Axial SSFSE image at a slightly higher level than Fig. 12A (same imaging parameters) demonstrates the obstructing gallstone impacted in the gallbladder neck (*arrow*). Perforated acute cholecystitis was confirmed at surgery.

titis from superimposed acute cholecystitis can be difficult both clinically and radiologically. MR imaging can demonstrate thickening of the gallbladder wall and gallstones in patients with chronic cholecystitis [67]. Increased enhancement of the gallbladder wall can also be noted. When thickening of the wall is present, the mucosa and muscle usually enhance smoothly in the early phase of the postcontrast dynamic MR imaging examination [67]. In contrast, the subserosa with fibrosis enhances in the delayed phase [67]. Gallbladder wall thickening with low signal intensity in chronic cholecystitis can be differentiated from gallbladder wall thickening caused by edema secondary to acute cholecystitis, typically hyperintense on T2-weighted images. Detection of a transient increase in pericholecystic hepatic enhancement during the arterial phase after administration of gadolinium, the MR imaging rim sign, can be very helpful for the diagnosis of superimposed acute cholecystitis in patients with chronic changes in the gallbladder. In the experience of the authors and others [43], the presence of pericholecystic hepatic enhancement on MR imaging is very specific for acute cholecystitis.

Choledocholithiasis

Choledocholithiasis is present in 7% to 20% of patients undergoing cholecystectomy, although they are usually silent unless they obstruct the CBD [68]. Approximately 10% to 15% of patients with acute cholecystitis have stones in the CBD [69,70]. Clinical, ultrasonographic, and laboratory parameters have a sensitivity of 96% to 98% for recognition of patients with CBD stones [71] but a specificity of only 38% [36]. US sensitivity for detection of CBD stones is limited (18% to 45%), particularly in the distal CBD because of overlying bowel gas [72,73]. Endoscopic retrograde cholangiopancreatography (ERCP) has been recommended in patients with high clinical and laboratory suspicion for choledocholithiasis [74]. If these parameters are used for triaging patients with suspected CBD stones, however, ERCP is positive in only 40% to 70% of the cases [71]. Intraoperative cholangiography is technically challenging in patients undergoing laparoscopic cholecystectomy and it is not routinely performed [75]. Furthermore, intraoperative cholangiography has a false-positive result rate of 2% to 16%, which may increase the number of unnecessary CBD explorations [71]. Several authors have proposed MR cholangiopancreatography as a preoperative diagnostic alternative to ERCP in these patients [36,71,75].

MR cholangiopancreatography has been reported to have an excellent sensitivity (81% to 100%) and specificity (85% to 99%) for the detection of chole-

docholithiasis [75]. The reported positive predictive value (93% to 94%), negative predictive value (77% to 100%), and accuracy (89%) are also excellent [71,75]. MR cholangiopancreatography is more sensitive for the detection choledocholithiasis than both US (20% to 65%) and CT (45% to 85%) [76]. MR cholangiopancreatography allows for selection of patients who may benefit from preoperative ERCP [71]. MR cholangiopancreatography has been recommended in patients with moderate to high suspicion of CBD stones based on clinical, ultrasonographic, and laboratory data [36,75]. MR cholangiopancreatography can rule out CBD stones in up to 48% of patients with high preoperative probability of CBD stones [75].

Common bile duct stones appear as foci of low signal intensity surrounded by bright bile on T2-weighted MR images (Fig. 8). MR cholangiopancreatography can detect stones as small as 2 mm [77,78]. MR cholangiopancreatography, however, tends to underestimate the total number of stones in the CBD [79]. In the experience of the authors and others [80], detection of CBD stones can be challenging in the periampullary region, where impacted stones fill the entire lumen of the intramural segment of the CBD and the classic appearance of the stones surrounded by bile is no longer seen (Fig. 9). Small stones can be missed when thick-slab MR images and maximum intensity projection projections are used because of averaging of the signal intensity of the stones with the surrounding bile. Careful evaluation of the thin-slice source images is mandatory for depiction of small stones. Pneumobilia is frequently seen in patients undergoing MR cholangiopancreatography after ERCP and can be misinterpreted as CBD stones. Air bubbles are readily differentiated from stones on axial HASTE images because the former remain in the nondependent portion of the CBD, whereas stones are typically located in the dependent portion [77]. Bile flow can produce a focal area of low signal intensity in the central portion of the CBD, more frequently seen with CBD dilatation [81]. In general, flow artifacts are less conspicuous, less well defined, less hypointense, and centrally located compared with CBD stones.

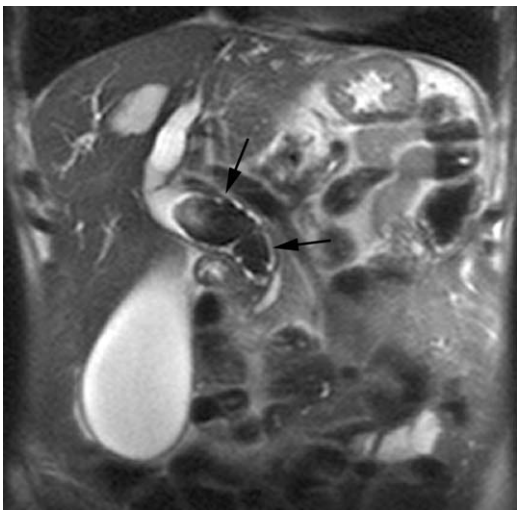

Fig. 8. Obstructive choledocholithiasis. A 72-year-old man with history of Billroth II procedure for perforated ulcer presenting with shortness of breath, jaundice, and fever. Coronal SSFSE image (TR 1100, TE 64, FA 130, 256 × 190, slice thickness 4 mm) shows large stones within the common bile duct (*arrows*) causing proximal dilatation of the biliary tree.

Acute cholangitis

Acute cholangitis refers to the bacterial infection of the bile secondary to obstruction (stones, neoplasm, strictures, and papillary stenosis). Patients with acute cholangitis present with jaundice, biliary colic, and fever with chills (Charcot's triad) in 50% to 100% of the cases [82]. Bile cultures are positive in approximately 80% to 100% of cases [82].

Most patients have a relatively rapid response to antibiotic therapy [68]. The presence of pus under pressure in the biliary system (suppurative cholangitis) secondary to complete occlusion of the CBD, however, has an ominous prognosis with a mortality rate that approaches 100% without treatment [68,83]. Typically, these patients present with multiple hepatic abscesses and poor response to antibiotic therapy [83]. Endoscopic, percutaneous, or surgical decompression of the biliary tree is the treatment of choice in these patients [83,84].

Approximately 80% of patients with cholangitis have an impacted stone in the CBD, a more common cause of cholangitis than malignant obstruction of the biliary tree [68]. The ability of MR imaging to demonstrate direct and indirect signs of cholangitis along with the capacity to demonstrate CBD stones provides an efficient means for diagnosis with appropriate therapeutic guidance.

Dilatation of the biliary tree is the most common MR imaging finding in patients with acute cholangitis [85]. Dilatation is virtually always present, most commonly in the central portion of the liver [85]. Patients without identifiable cause for the cholangitis may demonstrate wedge-shaped areas of ductal dilatation [85]. Proximal ductal stenosis secondary to inflammatory changes has been proposed as the mechanism for the peripheral biliary dilatation seen in these patients [85]. Diffuse concentric thickening of the wall of the CBD (greater than 1.5 mm) has been described in

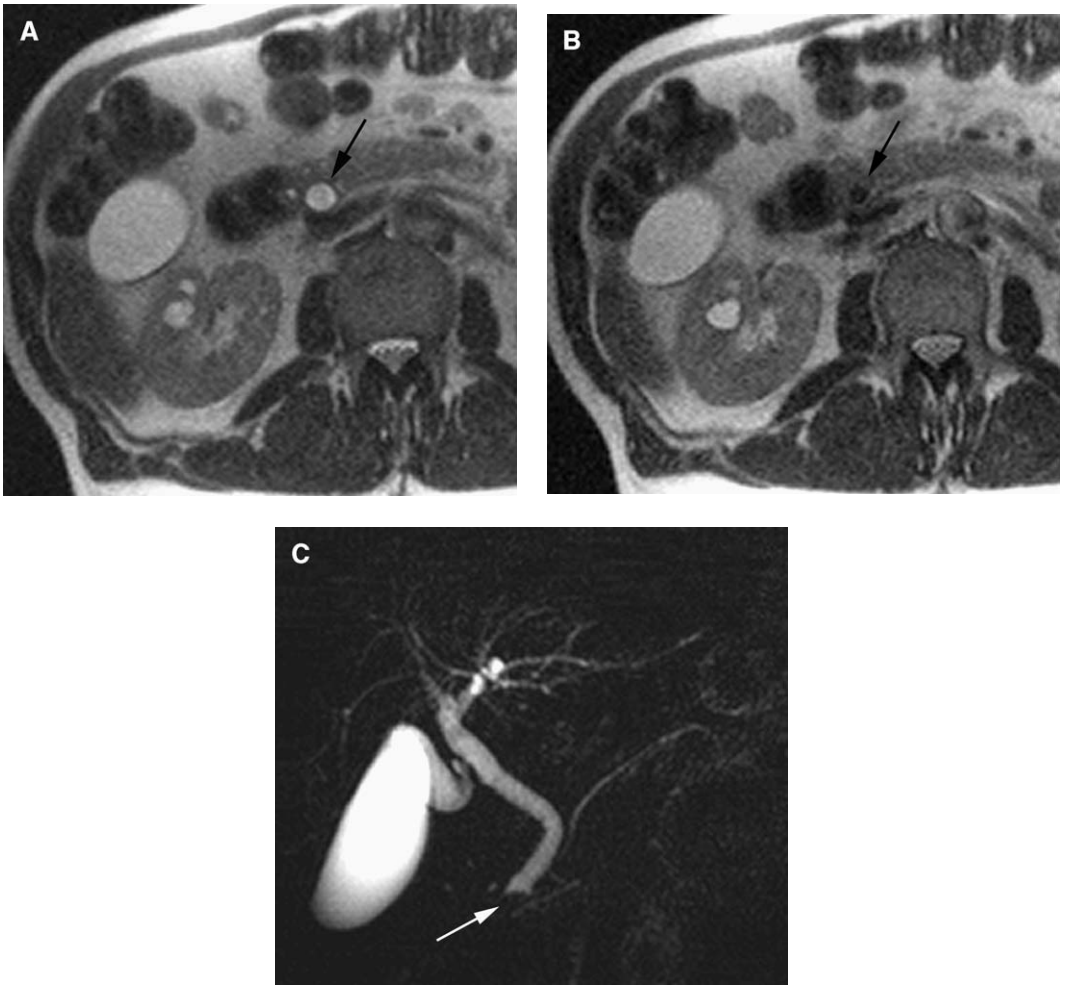

Fig. 9. Impacted ampullary stone. A 64-year-old man with ulcerative colitis presenting with epigastric pain, jaundice, and fever. (*A*) Axial SSFSE image (TR 1100, TE 64, FA 130, 256 × 190, slice thickness 4 mm) shows dilatation of the CBD at the level of the head of the pancreas (*arrow*). (*B*) Axial SSFSE image (TR 1100, TE 64, FA 130, 256 × 190, slice thickness 4 mm) immediately inferior to Fig. 11A demonstrates low signal intensity occupying the entire lumen of the distal CBD suspicious for an impacted stone in ampulla (*arrow*). (*C*) Coronal SSFSE image (TR 1100, FA 130, 256 × 190) confirms dilatation of the biliary tree. Note the meniscus-like appearance of the distal CBD consistent with an impacted stone (*arrow*), which was removed at ERCP.

patients with pyogenic cholangitis on different imaging modalities including US [86], CT [87], and MR imaging [85]. Biliary ductal wall thickening, usually smooth and symmetric, is demonstrated in up to 85% of patients on MR imaging, and is often associated with enhancement of the wall [85]. Parenchymal signal abnormalities (low signal intensity on T1-weighted and high signal intensity on T2-weighted) in regions of biliary dilatation can be seen in up to 70% of patients. These areas are more commonly periportal, although wedge-shaped appearances can be seen [85]. Those wedge-shaped areas may enhance on the arterial phase (Fig. 10). Enhancement along the ducts is also frequent [85]. Band-like irregularities of the duct margins secondary to wall edema have been reported on T2-weighted images [88].

Mirizzi's syndrome

Mirizzi's syndrome occurs when a stone impacted in the cystic duct or the neck of the gallbladder produces extrinsic compression of the CBD causing biliary obstruction and jaundice [89]. Preoperative diagnosis is important to avoid injury of the bile duct particularly in the presence of cholecystocholedochal

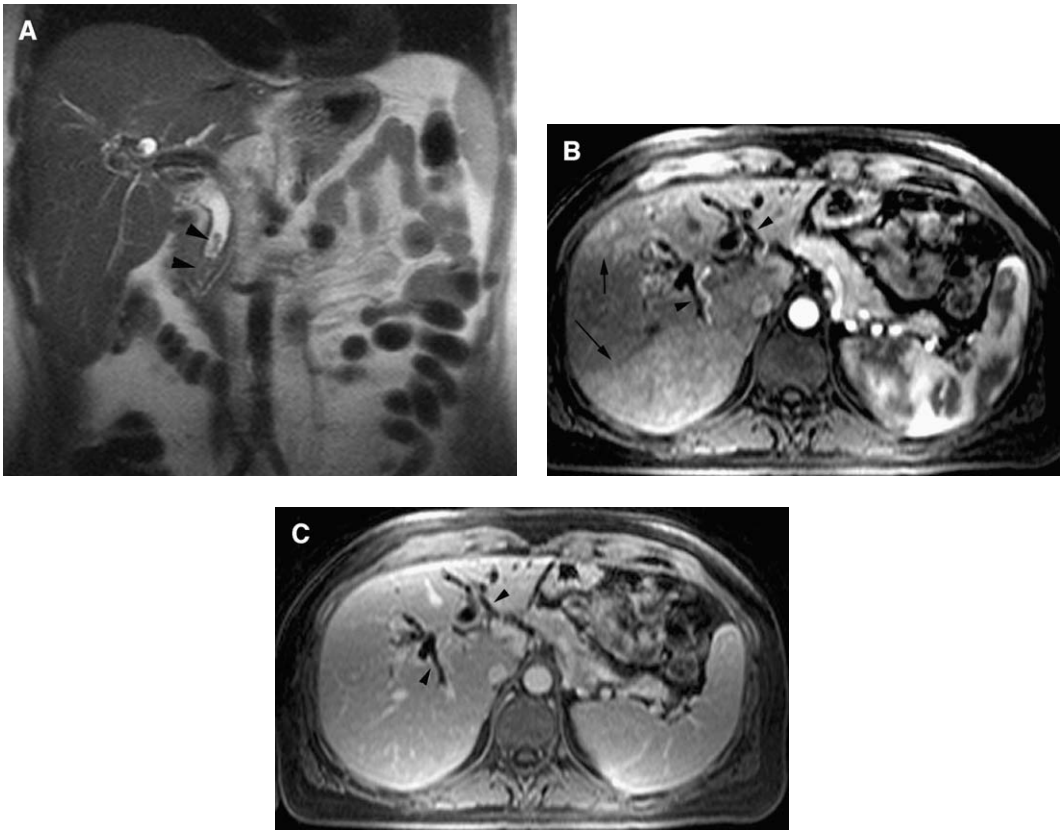

Fig. 10. Acute cholangitis. A 37-year-old woman with recurrent episodes of acute cholangitis presenting with right upper quadrant pain and elevated white cell count. (*A*) Coronal SSFSE image (TR 1100, TE 64, FA 130, 256 × 190, slice thickness 4 mm) shows multiple filling defects in the distal CBD consistent with stones (*arrowheads*). (*B*) Axial three-dimensional fat-saturated T1-weighted gradient echo acquisition (TR 4.5, TE 1.9, FA 12, slice thickness 4 mm, before interpolation) during the arterial phase shows biliary dilatation (*arrowheads*) and heterogeneous appearance of the liver with wedge-shape areas of increased enhancement (*arrows*). (*C*) Axial three-dimensional fat-saturated T1-weighted gradient echo acquisition (TR 4.5, TE 1.9, FA 12, slice thickness 4 mm, before interpolation) during the portal venous phase better distinguishes dilatation of the biliary tree (*arrowheads*) from adjacent vessels. Note the ductal wall enhancement. The liver now shows homogeneous enhancement.

fistulas. MR imaging can demonstrate intrahepatic biliary dilatation, narrowing of the common hepatic duct, the level of the obstruction, and the presence and exact location of the stone within the cystic duct [90]. This information can assist the surgeon in deciding between open or laparoscopic cholecystectomy [91].

Pancreas

MR imaging provides excellent soft tissue contrast of the pancreas and peripancreatic soft tissues that allows for a high sensitivity in the detection of inflammatory conditions of the pancreas. Although CT is still considered the standard of reference in the assessment of patients with acute pancreatitis, the safety of injecting iodinated contrast medium during the early stage has been questioned because of increased renal damage and accentuation of the severity of acute necrotizing pancreatitis in rats [92,93]. The relative safety of gadolinium contrast media has been proved both clinically [94] and experimentally [95] with only one case reported in the literature of gadolinium-induced mild acute pancreatitis [96].

The normal pancreas demonstrates high signal intensity compared with the liver on unenhanced T1-weighted images. The signal intensity and morphology of the pancreas may be preserved in patients with mild episodes of acute pancreatitis [97,98]. More severe forms of acute pancreatitis are usually associated with enlargement of the gland, peripancreatic edema (low signal intensity in the peripancreatic fat), and decreased signal intensity of the gland on

T1-weighted images [99]. Signal intensity of pancreatic necrosis is usually similar to that of the inflamed gland on unenhanced MR images [99].

A superior accuracy of MR imaging in staging the severity of the inflammatory process has been suggested compared with that of CT, based on a higher sensitivity of MR imaging for the detection of hemorrhagic-like peripancreatic collections [100]. Fat saturation facilitates the detection of these hemorrhagic peripancreatic collections and its differentiation from peripancreatic inflammatory changes [100].

Axial STIR images are very helpful for the detection of mild forms of pancreatitis because of its ability to detect subtle increases in signal intensity of the pancreatic parenchyma and small amounts of peripancreatic edema. Additionally, STIR images are helpful in the follow-up of patients with known acute pancreatitis, particularly in those with suspected aggravation of the initial episode (Fig. 11).

Coronal and axial HASTE images are very useful because these images are used to identify choledocholithiasis, one of the most common causes of pancreatitis, and for the assessment of the pancreatic duct. Anatomic variants including pancreas divisum and a dominant dorsal duct can be detected readily with HASTE imaging [101]. Disruption of the pancreatic duct occurs without exception in patients with necrosis affecting the body of the gland [102]. HASTE images may offer additional information about the exact location and extension of the disruption of the pancreatic duct.

Dynamic gadolinium-enhanced fat-saturated acquisitions are necessary for assessment of pancreatic necrosis and ischemia [94]. Moderate to severe acute

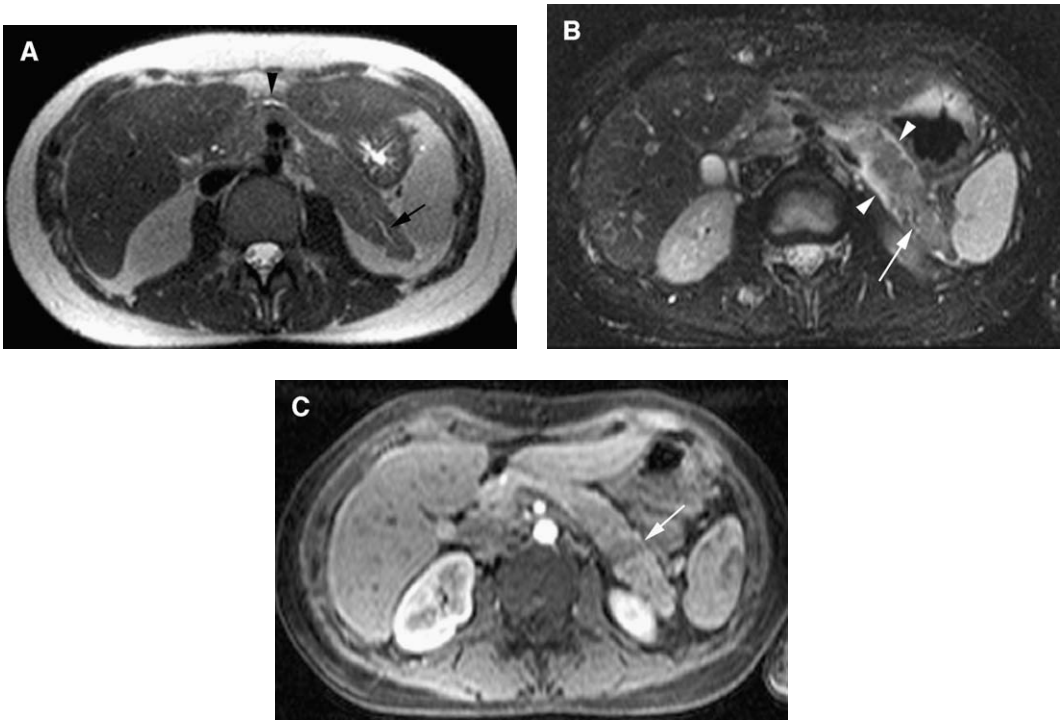

Fig. 11. Acute edematous pancreatitis. A 21-year-old woman with Crohn's disease and acute worsening of symptoms 6 weeks after diagnosis of pancreatitis. (*A*) Axial SSFSE image (TR 1100, TE 64, FA 130, 256 × 190, slice thickness 4 mm) obtained at the time of diagnosis shows slight dilatation of the proximal pancreatic duct within the tail (*arrow*). A trace of fluid is demonstrated anterior to the body of the pancreas (*arrowhead*). (*B*) Axial STIR image (TR 4500, TE 76, FA 150, ETL 33, thickness 7 mm) obtained 6 weeks after Fig. 11A caused by worsening symptoms. There is peripancreatic fluid surrounding the tail of the pancreas (*arrowheads*). There is subtle heterogenicity of the pancreas with increased signal intensity within the tail likely caused by edema. Note the dilated pancreatic duct (*arrow*). (*C*) Axial three-dimensional fat-saturated T1-weighted gradient echo image (TR 4.5 TE 1.9, FA 12, slice thickness 4 mm, before interpolation) during the arterial phase demonstrates heterogeneous enhancement in the tail of the pancreas. The area of increased signal intensity within the tail of the pancreas seen on Fig. 11B demonstrates relative decreased enhancement (*arrow*) consistent with edematous pancreatitis.

pancreatitis correlates with heterogeneous enhancement of the pancreas during the arterial phase and lack of enhancement in a focal area of the gland on postcontrast images indicates necrosis [94]. Subtraction of the precontrast acquisition from the arterial-enhanced acquisition can facilitate the differentiation of ischemia from necrosis. Viable ischemic parenchyma demonstrates some degree of enhancement on subtracted images, whereas pancreatic necrosis shows no enhancement (black signal intensity). High signal on unenhanced images cannot be assumed to be normal parenchyma, because hemorrhagic parenchyma may appear similar. Again, subtraction imaging can help differentiate between viable pancreas and necrotic-hemorrhagic pancreatitis (Fig. 12).

Uncomplicated pseudocysts demonstrate low signal intensity on T1-weighted images and high signal intensity on T2-weighted images [94]. Hemorrhagic fluid collections demonstrate high signal intensity both on T1- and T2-weighted images [94]. Solid necrotic components or clots may be seen in the dependent aspect of complicated pseudocysts and hemorrhagic collections as a layer of low signal intensity on T2-weighted images [94].

Patients with acute pancreatitis are frequently severely ill and their breathhold capacity is limited.

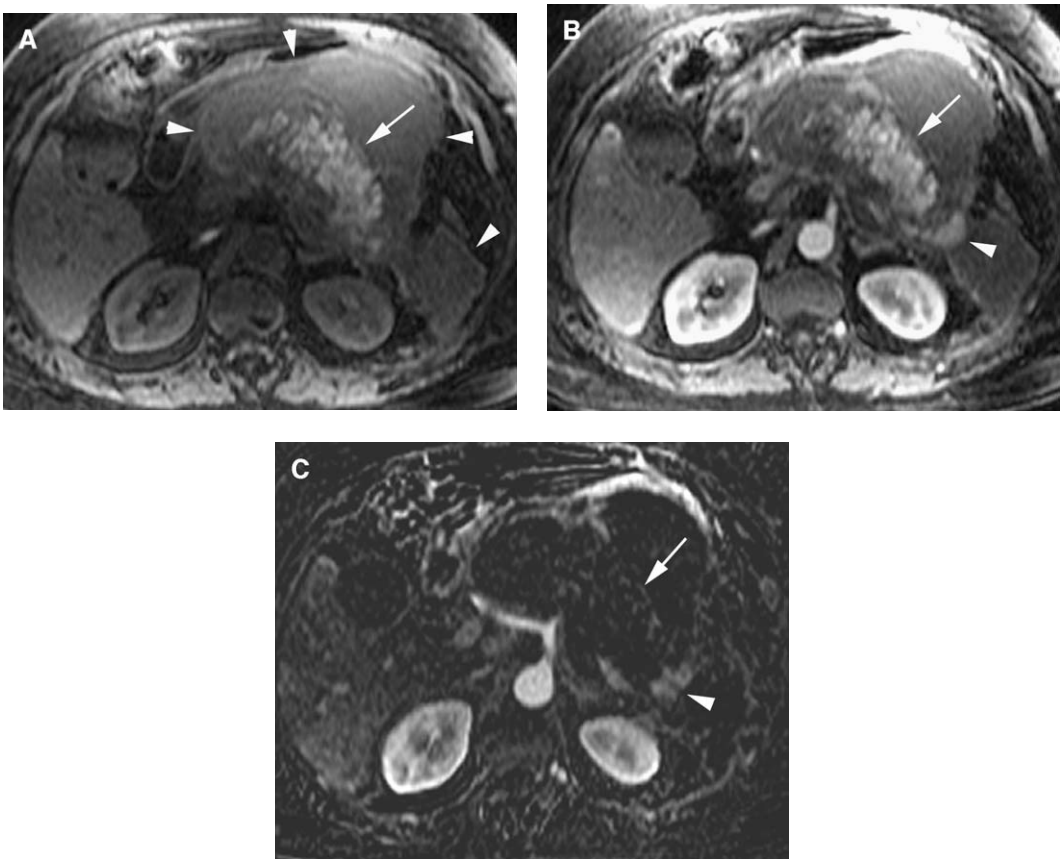

Fig. 12. Acute necrotico-hemorrhagic pancreatitis. A 68-year-old woman with severe upper abdominal pain, nausea, vomiting, and elevated lipase and amylase. (*A*) Unenhanced axial three-dimensional fat-saturated T1-weighted gradient echo image (TR 4.5, TE 1.9, FA 12, slice thickness 4 mm, before interpolation) shows high signal intensity within the body of the pancreas (*arrow*). The tail of the pancreas is not visualized. There is extensive peripancreatic fluid (*arrowheads*). (*B*) Axial three-dimensional fat-saturated T1-weighted gradient echo image (TR 4.5, TE 1.9, FA 12, slice thickness 4 mm, before interpolation) during the arterial phase after administration of a single dose of gadolinium demonstrates normal appearance of the pancreas (*arrow*). Note a small portion of the pancreatic tail not visualized on Fig. 12A (*arrowhead*). (*C*) Subtracted image (Fig 12B minus Fig. 12A) confirms the lack of enhancement in the pancreas consistent with necrotizing pancreatitis (*arrow*). Note the small enhancing region of viable pancreas in the tail (*arrowhead*).

Breathhold-independent imaging strategies (eg, HASTE) are essential in many patients. Fat-saturation can be used with HASTE images to improve visualization of peripancreatic edema and fluid collections. Magnetization-prepared T1-weighted gradient echo sequences are used in these patients for dynamic imaging of the pancreas during administration of a bolus of gadolinium. A two-dimensional true fast imaging with steady-state precession (FISP) sequence provides images with excellent signal-to-noise and free of respiratory-related artifacts. Because the signal intensity on true FISP images is determined by complex contrast (T2/T1 ratio) these images should not be used for evaluation of changes in signal intensity of the pancreas.

Gastrointestinal tract

Small bowel pathology

MR imaging of the bowel traditionally has been limited by long acquisition times and poor image quality related to artifacts secondary to respiratory motion and bowel peristalsis. With the development of ultrafast subsecond MR imaging sequences like HASTE, true FISP, or turbo fast low angle shot, examination of the small bowel is now possible with excellent delineation of the normal and abnormal findings.

The HASTE sequence provides excellent contrast for visualization of the small bowel because the mesenteric fat and the intraluminal fluid (frequently present in ileal and jejunal loops) are hyperintense, whereas the wall and valvulae conniventes are slightly hypointense [103]. The normal thickness of small bowel wall and valvulae conniventes is approximately 2 mm and it should be considered abnormal when it exceeds 3 mm [103]. Thickening of the small bowel wall is a nonspecific finding and can be secondary to inflammation, infection, ischemia, and hypoalbuminemia. The signal intensity of the small bowel wall does not provide insight into the cause of the pathology with the exception of venous ischemia and arterial emboli. In those settings Lee et at [103] reported a signal much

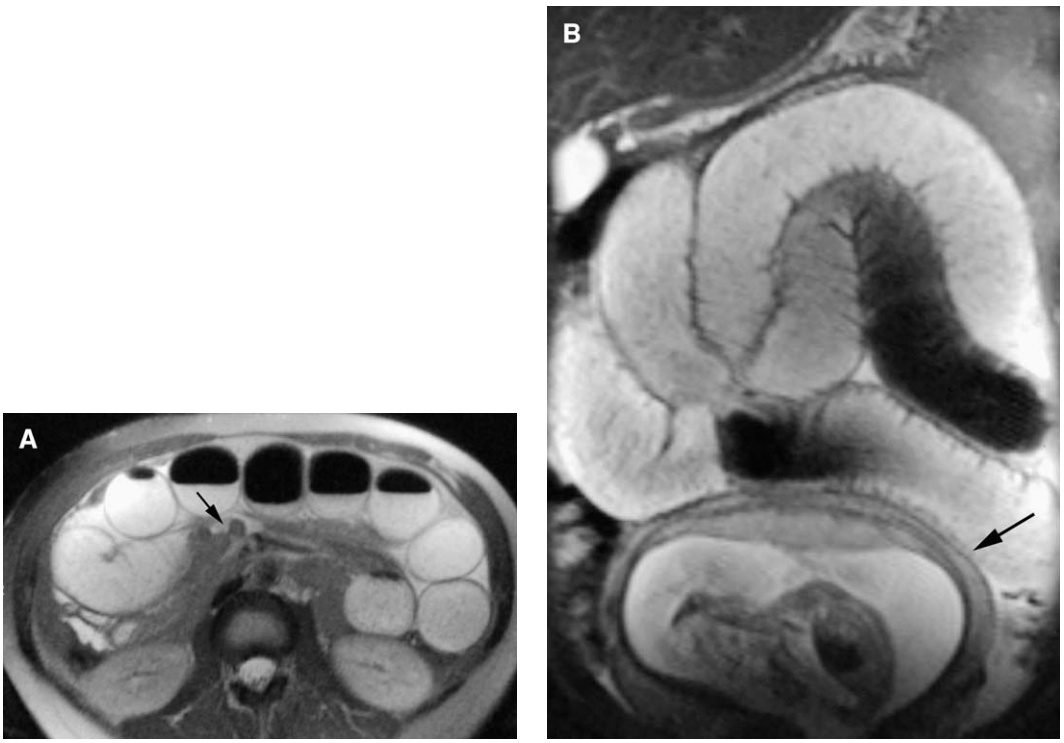

Fig. 13. Small bowel obstruction in pregnancy. A 36-year-old pregnant woman with history of prior pancreatitis and residual peritoneal adhesions. (*A*) Axial SSFSE image (TR 1100, TE 64, FA 130, 256 × 190, slice thickness 5 mm) shows diffuse marked dilatation of the small bowel. A collapsed loop of small bowel is noted in the right lower quadrant consistent with the transition zone (*arrow*). (*B*) Coronal SSFSE image (TR 1100, TE 64, FA 130, 256 × 190, slice thickness 5 mm) shows marked dilatation of small bowel with air (*dark signal*) and fluid (*high signal*). A gravid uterus is demonstrated in the pelvis (*arrow*). Patient symptoms improved with conservative treatment.

higher than the abdominal wall likely caused by intramural hemorrhage.

In the authors' experience, the halo sign described in the CT literature can be seen readily on HASTE images. This finding is demonstrated on HASTE images as increased signal intensity in the bowel wall with a layer of intermediate signal intensity at each side. Similar to the CT halo sign, this finding is not specific and most likely represents wall edema.

MR imaging allows for visualization of changes in caliber of the small bowel and can accurately detect small bowel obstruction. HASTE images are particularly useful in evaluating patients with suspected small bowel obstruction. Oral or intravenous contrast administration is not required with HASTE images because of its inherent contrast. Dilated fluid-filled small bowel loops are detected easily with a hyperintense distended lumen (Fig. 13). Regan et al [104] found the level of obstruction in 73% of the patients with small bowel obstruction using HASTE imaging. Overall sensitivity of HASTE images for detection of small bowel obstruction in this study was 90% and the actual cause of the obstruction was found in 50% [104].

Supplementation of HASTE images with spin echo and short echo train fast spin echo sequences has been advocated to facilitate the detection and characterization of soft tissue pathology and to assist in the visualization of mesenteric fat stranding and inflammation [104]. Similarly, gradient echo sequences with sensitivity to susceptibility effects have value in detecting small amounts of extraluminal air. In this regard the authors find the dual echo T1-weighted gradient echo sequence helpful. In their protocol, T1-weighted images have a longer TE than out-of-phase images. Areas of susceptibility artifact cause a blooming effect on the in-phase images because of the longer echo time. In addition, postcontrast T1-weighted images may help to detect and characterize the obstructing lesion.

Mesenteric ischemia

Acute mesenteric ischemia is a life-threatening condition in which there is insufficient delivery of oxygen to the small bowel or colon [105]. Patients typically present with severe abdominal pain and clinical deterioration occurs in the following hours [106]. Despite the advances in the diagnosis and management of patients with mesenteric ischemia, the clinical outcomes remain poor [107]. Early diagnosis of acute mesenteric ischemia is challenging but critical to initiate promptly the appropriate treatment [106,107]. Approximately 50% of the cases are secondary to embolization of the superior mesenteric artery with occlusion commonly occurring 3 to 10 cm distal to the origin of this vessel, distal to the origin of the middle colic artery branch [106]. In situ thrombosis of a pre-existing atherosclerotic lesion at the origin of the vessel accounts for 25% of the cases [105] and is most frequent at the origin of the superior mesenteric artery [106].

MR imaging provides a noninvasive alternative for the initial evaluation of patients with suspected acute mesenteric ischemia. Gadolinium-enhanced MR angiography provides excellent morphologic information of the proximal mesenteric vasculature [108]. Sagittal three-dimensional acquisitions typically can be obtained in less than 20 seconds. Target acquisition to the abdominal aorta and proximal superior mesenteric artery can be performed in approximately 10 seconds in patients with limited breathhold capacity. In the authors' experience, this technique offers excellent results with administration of 10 to 15 mL of gadolinium.

Although MR imaging assessment of the small mesenteric branches is still limited, additional MR imaging sequences can be obtained to increase the diagnostic yield. MR imaging oximetry with a T2-weighted multiecho sequence can detect differences in oxygen desaturation between the inferior vena cava and superior mesenteric vein after acute segmental mesenteric ischemia in a porcine model [109]. T2 values can be used as a marker of oxygen saturation, although a blood sample is required for calibration [109]. Differences in T2 values between the inferior vena cava and superior mesenteric vein suggest acute mesenteric ischemia [109]. This technique has also been validated in dogs with nonocclusive mesenteric ischemia caused by hemorrhagic shock [110]. Phase contrast imaging allows for determination of flow velocity in the superior mesenteric artery and superior mesenteric vein. This approach is not as valuable as it is in chronic mesenteric ischemia, however, because acutely ill patients cannot be imaged before and after a meal challenge [106].

MR imaging can demonstrate indirect findings in the bowel that suggest mesenteric ischemia. Thickening of the small bowel wall is common [111]. Occasionally, alternating layers of low and high signal in the thickened wall can be a sign on T2-weighted images, similar to the so-called target sign on CT images. Postcontrast images can show lack of enhancement of the bowel wall in the affected segments [112].

Superior mesenteric vein thrombosis is associated with bowel wall thickening and mesenteric congestion on MR imaging [113]. Sensitivity, specificity, and accuracy of MR imaging for the detection of thrombosis in the portal venous system are 100%, 98%, and 99%, respectively [114]. MR venography

can replace conventional angiography for the diagnosis of venous thrombosis in the portomesenteric system [114].

Acute appendicitis

There have been few reports about the use of MR imaging in the diagnosis of acute appendicitis despite the high prevalence of this disease. This is probably related to the excellent accuracy provided by other imaging modalities like US and CT and lack of availability of MR imaging scanners and the time required for MR imaging examinations. US is often preferred in children and young women to minimize exposure to ionizing radiation. Sensitivity and specificity of US are limited, however, in patients with perforated appendicitis [115,116]. For these reason, MR imaging is an appealing alternative to US in those groups of patients where radiation is an important consideration. Although some authors believe that the normal appendix is not visualized with MR imaging, even after administration of gadolinium, because of the lack of appendiceal wall enhancement [117], in the experience of the authors and others [118] the normal appendix is visualized in virtually all patients even without intravenous contrast.

Hörmann et al [118] studied 34 children with MR imaging in whom a clinical diagnosis of acute appendicitis was confirmed by US. MR imaging was performed with T1 and T2 turbo spin echo images. MR imaging showed acute appendicitis in all cases manifested by a distended appendix with fluid-filled lumen (markedly hypointense on T1-weighted images and hyperintense on T2-weighted images); thickened edematous wall (hypointense on T1-weighted images and slightly hyperintense on T2-weighted images); and periappendiceal inflammatory changes (hyperintense on T2-weighted images).

The recent development of ultrafast sequences that allow subsecond imaging has made possible the evaluation of these patients in an expeditious manner with virtually no peristaltic-related or breathing-related artifacts. HASTE images are particularly useful in the visualization of the appendix. The periappendiceal fat is bright and the appendix has a thin hypointense wall in normal conditions. Findings of acute appendicitis on HASTE images are similar to those described by Hörmann et al [118] on T2-weighted fast spin echo images.

Incesu et al [117] evaluated 60 consecutive patients with clinical suspicion of acute appendicitis by US and MR imaging. Gadolinium-enhanced MR imaging can provide excellent results for the diagnosis of acute appendicitis, including complications secondary to appendiceal perforation [117]. In that study MR imaging had a sensitivity of 97%, specificity of 92%, accuracy of 95%, negative predictive value of 96%, and positive predictive value of 94% and was superior to US in revealing appendicitis. Enhancement of the inflamed appendiceal wall was found to be very useful when using fat-suppression technique. Inefficient fat saturation may cause obscuration of the appendiceal wall enhancement by the mesenteric fat [117].

Preoperative diagnosis of acute appendicitis is challenging during pregnancy [119]. Clinical presentation, physical examination, and laboratory analysis are very limited in establishing the diagnosis [119]. Delayed diagnosis is associated with increased fetal mortality. Although US seems to have similar results for the diagnosis of acute appendicitis during the first and second trimester, it is challenging during the third trimester because the size of the gravid uterus limits the use of the graded-compression technique [120,121]. MR imaging is useful in the assessment of the pregnant woman with clinical suspicion of acute appendicitis with inconclusive or negative US. In these patients, MR imaging is an alternative imaging modality that allows for visualization of the appendix, regardless of its location within the abdomen, without administration of contrast media or ionizing radiation (Fig. 14).

The authors perform oral preparation with approximately 600 mL (three cups) of the usual Gastromark/Readicat solution (described previously) during 1 hour. Imaging protocol includes HASTE images in the three orthogonal planes (axial, coronal, and sagittal); axial T1-weighted gradient dual-echo; and axial time-of-flight images. Enlarged gravid uterus during the third trimester may make difficult the visualization of the appendix, although it is usually recognized by careful evaluation of the multiplanar HASTE images. T1-weighted images are useful for recognition of alternative diagnosis, such as subchorionic hematoma and hemorrhagic adnexal cyst. Axial time-of-flight images provide a quick assessment of the patency of the pelvic veins, including the gonadal veins.

Acute diverticulitis

Patients with clinical suspected acute diverticulitis are typically evaluated with CT because of the high incidence of clinical misdiagnosis. CT has excellent sensitivity and specificity for detecting acute diverticulitis. For this reason, MR imaging has not been widely used in patients with suspected diverticulitis. Heverhagen et al [122] studied 20 patients with clinical suspicion of acute diverticulitis by MR imaging with excellent results. In their experience, a limited imaging protocol with STIR and true FISP images is enough to achieve the diagnosis of acute diverticulitis and HASTE images provide no additional information

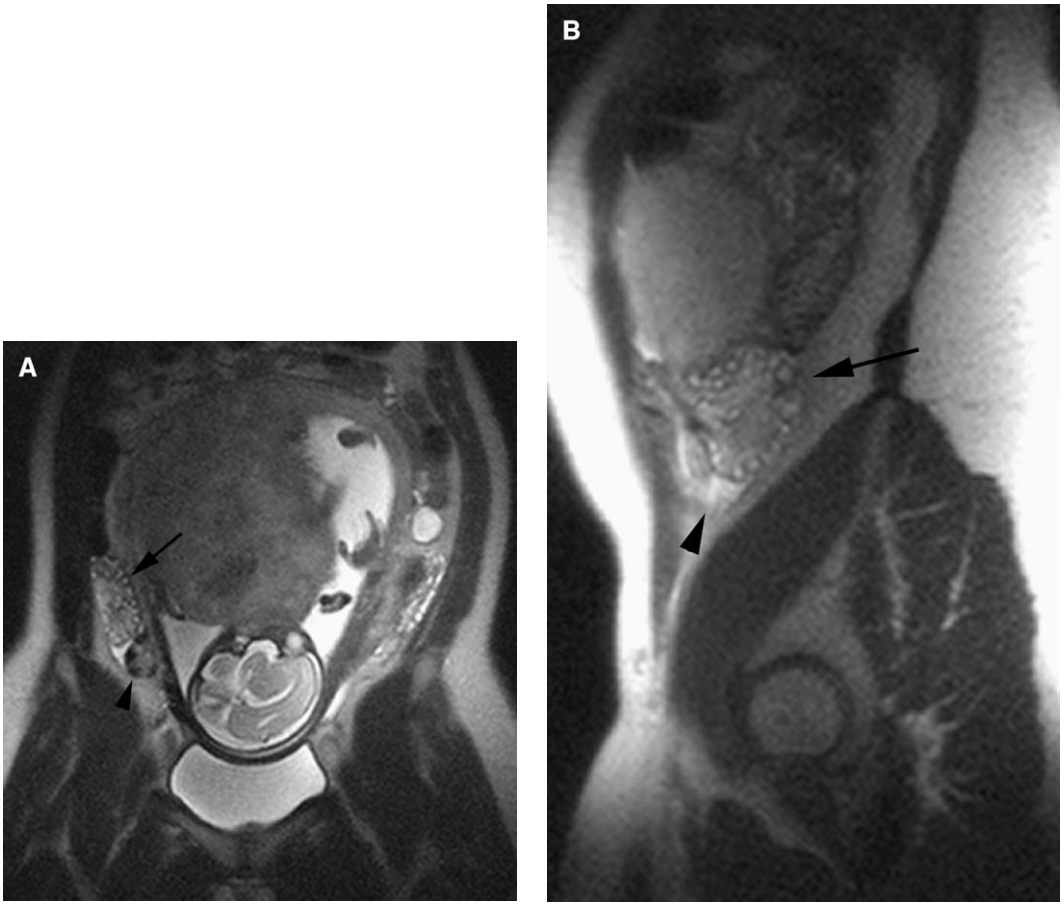

Fig. 14. Ovarian torsion. A 27-year-old pregnant woman with acute right lower quadrant pain. MR imaging performed to rule out acute appendicitis. (*A*) Coronal SSFSE image (TR 1100, TE 64, FA 130, 256 × 190, slice thickness 4 mm) shows a moderately enlarged right ovary with multiple follicles, predominantly located in the periphery (*arrow*). A small amount of free fluid is noted around the inferior aspect of the right ovary. The normal appendix is located just inferior to the ovary (*arrowhead*), and looped on itself. (*B*) Sagittal SSFSE image (TR 1100, TE 64, FA 130, 256 × 190, slice thickness 4 mm) shows the enlarged right ovary (*arrow*) and the free fluid inferiorly (*arrowhead*). Ovarian torsion was confirmed at laparoscopy.

[123]. Edema, pericolic exudation, and ascites are better demonstrated on STIR images [123]. True FISP is superior in showing segmental narrowing of the colon [123]. Abscess formation can be visualized as pericolonic fluid collections that show peripheral rim enhancement (Fig. 15). MR imaging has limited sensitivity for air and small bubbles or collections of extraluminal air can be missed.

Primary epiploic appendagitis

Primary epiploic appendagitis is an acute inflammatory condition caused by torsion or spontaneous venous thrombosis of the appendages epiploicae of the colon [124]. Epiploic appendagitis is a relatively common condition occurring in approximately 1% to 7% of patients with suspected acute diverticulitis and appendicitis [124].

The MR imaging appearance of primary epiploic appendagitis has been reported in two articles [125,126]. Findings are similar to those reported in US and CT with an oval-shaped lesion located anterior or anterolateral to the colon with a central area that follows the signal intensity of fat on T1- and T2-weighted images [125,126]. On MR imaging, the inflamed visceral peritoneum is demonstrated as a low signal intensity rim surrounding the fat-density appendage on T1- and T2-weighted images that enhances after administration of gadolinium [126]. This rim is better demonstrated on fat-suppressed T1-weighted postcontrast images [126]. A hypointense central dot can be

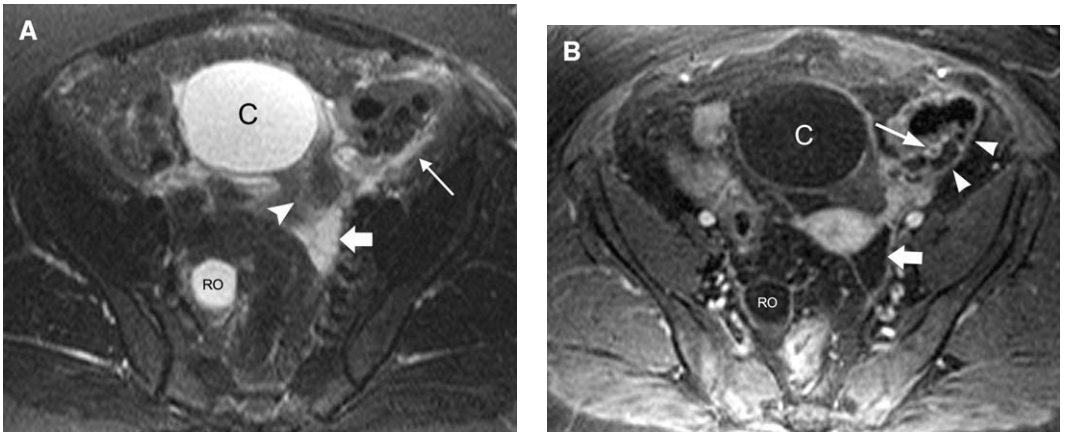

Fig. 15. Acute diverticulitis. A 46-year-old woman with left lower quadrant pain and elevated white cell count. CT showed a left adnexal cyst and no evidence of diverticulitis. (*A*) Axial pelvic STIR image (TR 4500, TE 76, FA 150, ETL 33, thickness 7 mm) shows increased signal intensity posterior to the proximal sigmoid colon consistent with pericolonic inflammation (*arrow*). The left adnexa, which contains a large cystic lesion (c), is visualized medial to the inflammation (*arrowhead*). A second fluid collection is demonstrated posterior to the right adnexa (*short arrow*). Note a small cyst in the right ovary (RO). (*B*) Axial three-dimensional fat-saturated T1-weighted gradient echo acquisition (TR 4.5, TE 1.9, FA 12, slice thickness 4 mm, before interpolation) during the portal venous phase demonstrates peripheral enhancement around the inflammation posterior to the sigmoid colon (*arrowheads*) and the posterior fluid collection (*short arrow*), consistent with abscess formation. Note an enhancing inflamed diverticulum (*arrow*) in the posterior sigmoid colon. The left (*C*) and right adnexal cysts (RO) are again noted. At surgery, perforated diverticulitis with abscess formation was found, which involved the left adnexa and tube.

demonstrated on both T1- and T2-weighted images and correlates with fibrous septa on histopathologic analysis [126]. Fat stranding around the inflamed appendage is common [125].

Acute peritoneal and omental disease

Abnormal peritoneal fluid collections including abscesses, bilomas, hematomas, and pancreatic pseudocysts can be detected readily with MR imaging (Fig. 16) [127]. MR imaging is superior to CT in demonstrating heterogenicity within fluid collections [127]. MR imaging can be used to characterize intra-abdominal fluid collections [128]. Acute hemorrhagic fluid collections demonstrate intermediate signal intensity on T1-weighted images and high signal intensity on T2-weighted images [128]. Patients with diffuse peritonitis can show intraperitoneal fluid and diffuse thickened peritoneum. Increased peritoneal enhancement is usually present on postcontrast T1-weighted images.

Segmental omental infarction typically occurs in the right lower or upper quadrant [129]. US and CT imaging typically reveal a fatty mass anteromedial to the ascending colon [124]. The MR imaging findings of segmental omental infarction have not been reported in the literature. Segmental infarction of the falciform ligament and ligamentum teres represents a rare variant of omental infarction causing acute right upper quadrant pain [130]. To the authors' knowledge, there are no previous reports of this entity describing the MR imaging findings. They have recently evaluated a patient with acute right upper quadrant pain and MR imaging findings consistent with this diagnosis. MR imaging revealed nonspecific inflammatory changes within the falciform ligament with increased signal intensity on STIR images and subtle peripheral enhancement of the inflamed falciform ligament on delayed postcontrast images (Fig. 17). The patient's symptoms improved over time with conservative management.

Genitourinary tract

Renal colic

Acute flank pain is a common complaint in patients seen in the emergency department and frequently leads to referral of imaging studies. In the last decade, unenhanced CT has become the imaging study of choice for demonstration of ureteric obstruction, its cause, level, and size of stones [131] replacing excretory intravenous urography in many institutions. Limitations of CT, however, include the lack of information about the excretory function of the kidneys, the use of ionizing radiation, and the difficulty in differentiating pelvic phleboliths from distal stones [131].

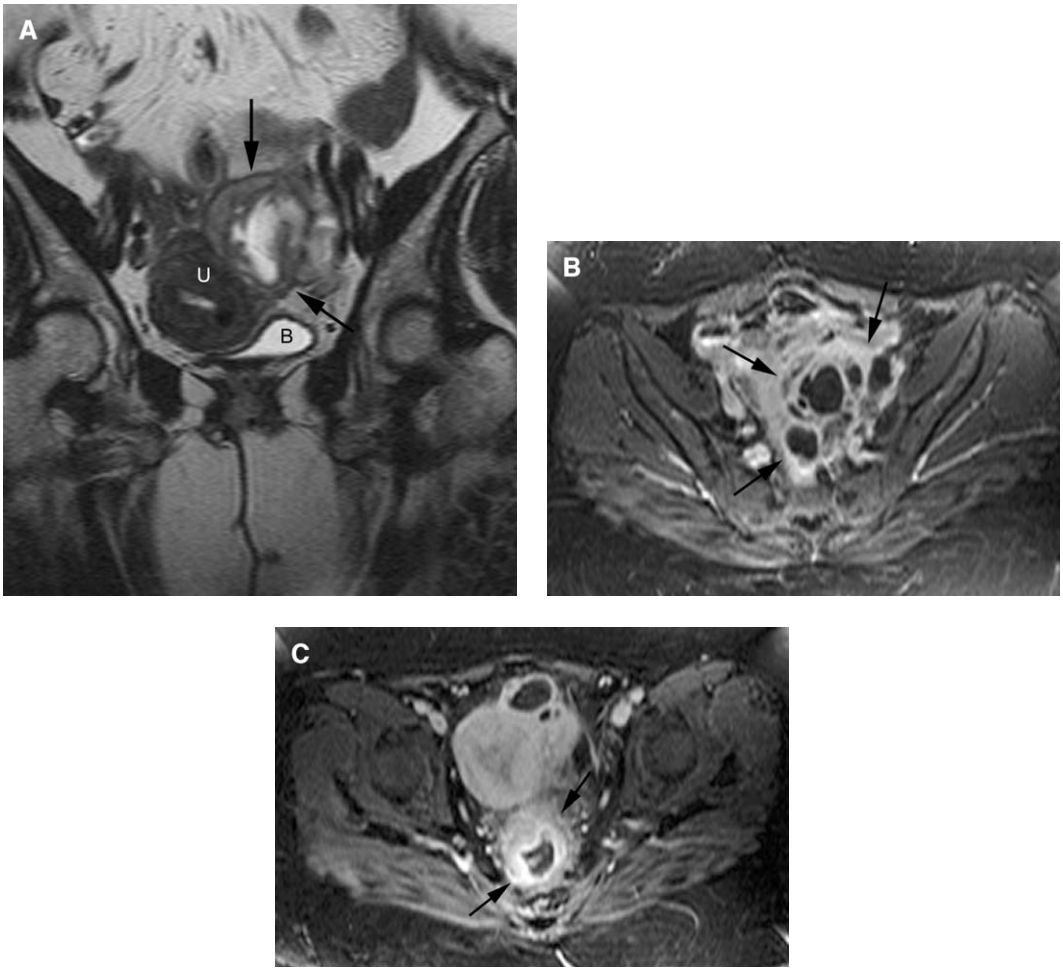

Fig. 16. Crohn's-related abscess. A 59-year-old woman with history of Crohn's disease presenting with fever, chills, and elevated white cell count. (*A*) Coronal T2-weighted fast spin echo image (TR 6350, TE 135, FA 150, ETL 23, thickness 4 mm) shows a thick-walled cystic mass (*arrows*) in the pelvis immediately superior to the uterus (U). B = bladder. (*B*) Axial three-dimensional fat-saturated T1-weighted gradient echo image (TR 4.5, TE 1.9, FA 12, slice thickness 4 mm, before interpolation) during the portal venous phase shows a mass in the left hemipelvis with cystic areas, enhancing rim, and thick septations (*arrows*), indicative of abscess. (*C*) Axial three-dimensional fat-saturated T1-weighted gradient echo image from the same dynamic phase as Fig. 16B at a slightly inferior location shows thickening of the rectal wall and marked mucosal enhancement consistent with inflammation (*arrows*).

MR imaging has been suggested as an alternative imaging technique for patients presenting with acute flank pain [132–135]. MR imaging may be particularly helpful when the use of contrast media or radiation is undesirable (eg, pregnant patients and young adults) [131]. MR imaging detection of ureteric obstruction is based on heavily T2-weighted images and gadolinium-enhanced T1-weighted images.

MR imaging with heavily T2-weighted sequences allows for rapid, safe, and noninvasive detection of urinary tract obstruction [132]. HASTE and rapid acquisition with relaxation enhancement (RARE) sequences provide heavily T2-weighted images that allow for breathhold imaging of the urinary tract without requiring administration of contrast media [134,135]. HASTE thin-slice (thickness of 3 to 6 mm) images are typically obtained in the coronal plane in one breathhold. Patients with large body habitus may require two breathholds to achieve the desired anatomic coverage. Fat saturation can be added and allows for better suppression of the background signal improving the visualization of the collecting systems. Thin-slice HASTE images can be reconstructed further using a maximum intensity projection

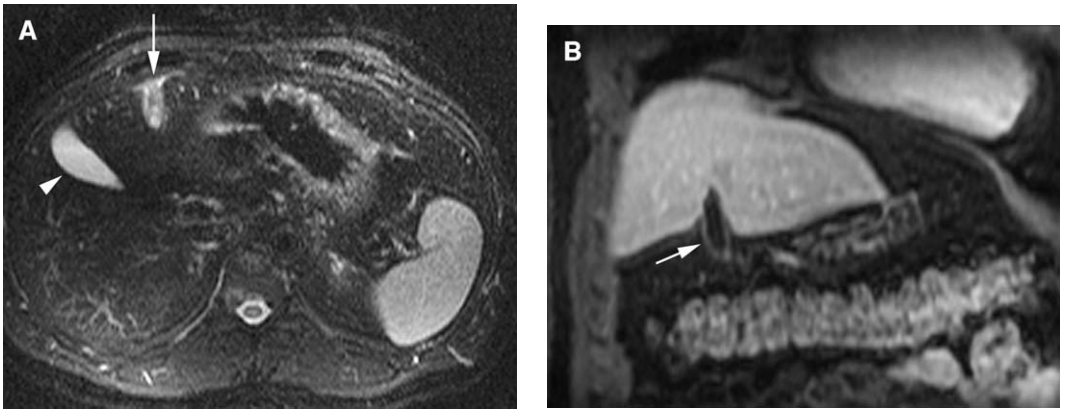

Fig. 17. Falciform ligament infarct. A 31-year-old man with right upper quadrant pain. US and CT were negative. (*A*) Axial STIR image (TR 4500, TE 76, FA 150, ETL 33, thickness 7 mm) at the level of the upper abdomen demonstrates high signal intensity within the falciform ligament (*arrow*) similar to that of the gallbladder (*arrowhead*). (*B*) Coronal reconstruction from an axial three-dimensional fat-saturated T1-weighted gradient echo image (TR 4.5, TE 1.9, FA 12, slice thickness 4 mm, before interpolation) during the portal venous phase shows peripheral enhancement along the falciform ligament (*arrow*). MR imaging findings were consistent with infarction of the falciform ligament. The patient's symptoms subsequently resolved with conservative management and follow-up imaging showed resolution of the inflammatory changes.

algorithm. In general, this strategy does not offer additional information for the diagnosis but it provides urographic-like images that are better accepted by urologists [135].

A coronal thick-slab (thickness of 20 to 60 mm) image can be obtained in one breathhold with a RARE sequence commonly referred to as ''echo train spin echo imaging.'' This approach does not require further postprocessing and includes the entire collecting system in a single image that resembles the conventional excretory urography. Thick-slab RARE can demonstrate both kidneys and ureters in a single image. Multislice technique usually provides better image quality than single thick-slab technique, however, because of the better delineation of background tissues and diminished partial volume effects of the former [134]. A combination of thin-slice HASTE and thick-slab RARE images may increase the confidence of the radiologist for detecting the level of obstruction [132].

The presence of perirenal hyperintense fluid on HASTE and RARE images helps to differentiate between acute and chronic obstruction [136]. Patients with acute obstruction typically present with increased perirenal fluid on T2-weighted images, most likely caused by lymphatic congestion or forniceal rupture [136]. Perirenal fluid can be secondary to any insult to the kidney, however, and should be considered a nonspecific sign [131].

A known limitation of T2-weighted images is their relatively low sensitivity and specificity for small ureteral stones [135]. Thin-slice HASTE images are superior to thick-slab RARE for the detection of small filling defects [134]. Sudah et al [132] found a sensitivity of approximately 54% to 58% in 40 consecutive patients with acute flank pain. The reported specificity was 100%, although all their patients have ureteral stones as a cause of obstruction [132]. Intraluminal clots, debris, or neoplasms can mimic ureteral stones on T2-weighted images because they appear as filling defects [132,135].

Gadolinium-enhanced MR urography is a valuable addition to the T2-weighted images for evaluation of patients with suspected acute renal colic [131]. This technique, first described by Nolte-Ernsting [133], uses a high-resolution T1-weighted sequence after administration of gadolinium contrast media. A low-dose of furosemide (0.1 mg/kg of body weight, for a maximum dose of 10 mg) immediately before the administration of the contrast media (30 to 60 seconds) allows for a complete distention of the collecting system with homogenous distribution of the gadolinium inside the entire urinary tract [133]. Furosemide increases urine volume and results in dilution of the concentrated gadolinium within the collecting system; this decreases the T2* effects and maintains increased signal intensity [133]. Although the first report using this technique used a respiratory-gated T1-weighted spoiled gradient echo sequence [133], recent reports have demonstrated the feasibility of a similar approach combined with a breathhold three-dimensional T1-weighted gradient echo sequence [132].

The entire urinary tract can be visualized with this approach even in the absence of urinary tract obstruction [132]. An increased flip angle (60 to 70 degrees)

allows for excellent visualization of the enhanced collecting systems while the background signal is saturated. Maximum intensity projection reconstructions provide excretory urography-like images with better spatial resolution than thin-slice HASTE or thick-slab RARE images [132]. Source images are essential for the diagnosis, particularly for the detection of small urinary stones (Fig. 18) [132].

In the presence of high-grade obstruction, contrast-enhanced MR urography requires delayed imaging

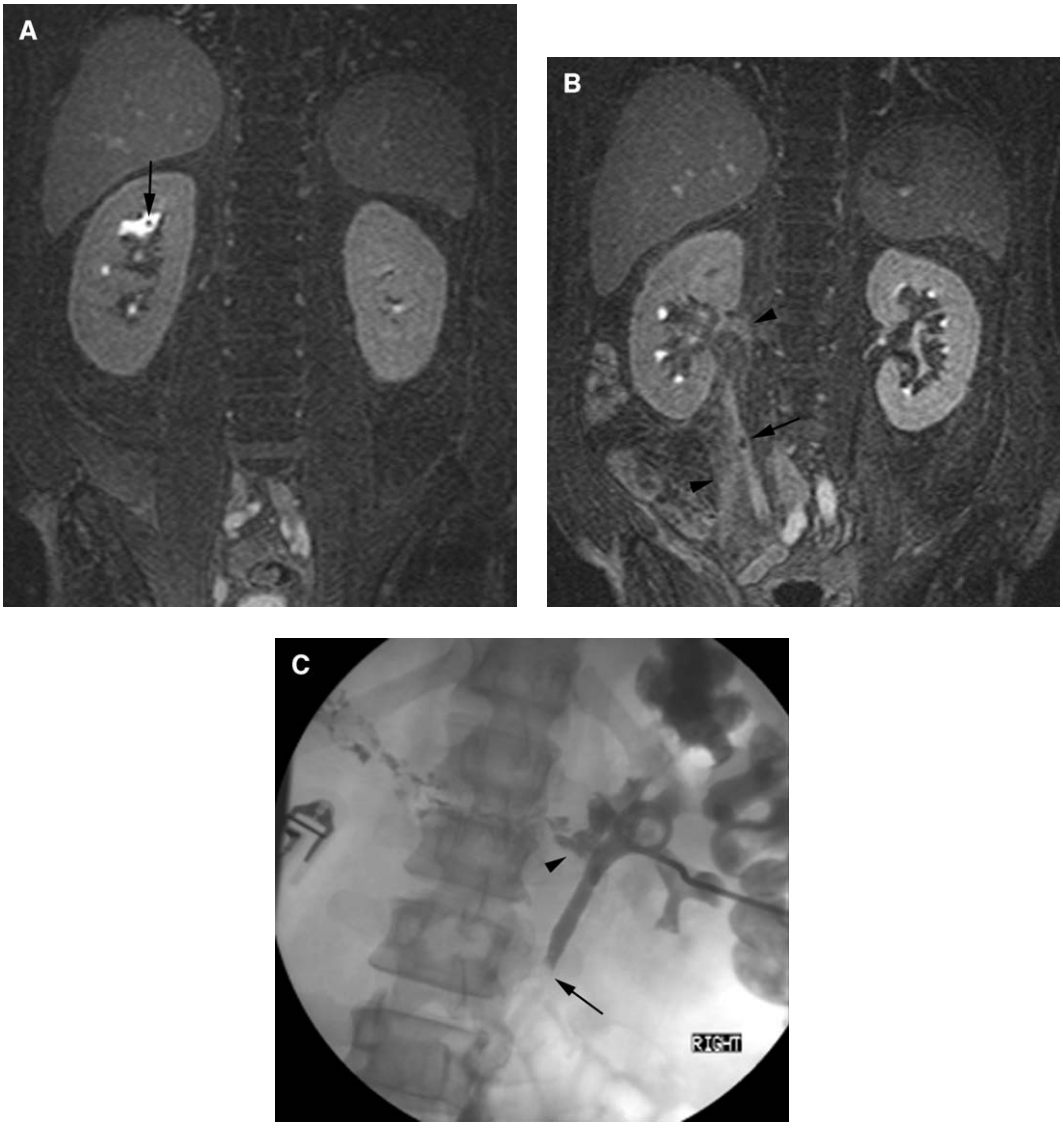

Fig. 18. Obstructive ureterolithiasis. A 54-year-old diabetic man with 2-day history of right back and right lower quadrant pain. (*A*) Coronal three-dimensional fat-saturated T1-weighted gradient echo image (TR 1100, TE 64, FA 30, 256 × 190, slice thickness 4 mm) during the delayed venous phase after administration of a single dose of gadolinium shows a filling defect in the mildly dilated upper calyx of the right kidney (*arrow*). (*B*) Coronal section from the same acquisition than Fig. 18A at a slightly anterior location demonstrates a filling defect in the mid-portion of the right ureter consistent with a stone (*arrow*). Ill-defined, subtly increased signal intensity around the renal pelvis and ureter (*arrowheads*) is consistent with extravasation caused by forniceal rupture. (*C*) Antegrade pyelogram through a nephrostomy tube shows mild dilatation of the collecting system and an obstructing stone in the mid ureter (*arrow*). The patient was imaged in the prone position. There is extravasation of iodinated contrast adjacent to the renal pelvis (*arrowhead*) partially obscured by contrast within the colon (the latter from previous CT examination).

acquisition to allow for sufficient excretion of the contrast media and subsequent filling of the collecting system and ureters [131]. In this situation, the patient may be removed from the MR imaging scanner and subsequent examinations can be repeated until the collecting system is filled and the level and cause of obstruction can be determined [131].

Delayed postcontrast images can be helpful for identification and characterization of intraluminal, intraureteral filling defects. In general, the presence of an intraureteral filling defect with smooth margins that shows no enhancement is considered a ureteral stone [131]. A radiograph of the abdomen to identify a calcification at the same level of the obstruction may be helpful in characterizing a stone. [131]. The presence or absence of postcontrast enhancement of an intraluminal filling defect, however, can be helpful in characterizing a tumor for the former versus a stone or blood clot for the latter. Enhancement must be interpreted with caution because ureteral calculi can produce inflammatory changes in the wall of the ureter leading to increased enhancement. Similarly, increased periureteral high-signal intensity on T2-weighted images has been described in patients with ureteral stones as a confounding finding that may mimic or obscure a neoplastic process [131].

Extravasation of contrast can be seen readily on gadolinium-enhanced MR urography in patients with ruptured fornices [131]. T2-weighted images reveal a hyperintense fluid collection at the same level as the extravasation [131]. These findings correlate well with extravasation of contrast on excretory urography, although small extravasations can be missed at excretory urography [131].

Gadolinium-enhanced MR urography requires a cooperative patient able to perform breathholds of 20 to 25 seconds. Patients unable to perform such breathholds can be studied with T2-weighted half-Fourier SSFSE and RARE images. T1 magnetization-prepared gradient echo images provide nonbreathhold images of the abdomen after administration of gadolinium. Although this sequence offers lower spatial resolution compared with three-dimensional T1-weighted images, patients unable to hold their breaths can be evaluated for the presence and degree of obstruction and the presence of contrast extravasation with this approach.

Pregnant patients with suspected acute renal colic and limited US visualization of the ureters can be assessed with T2-weighted images (HASTE and RARE). This approach allows for identification of the presence and level of obstruction in an expeditious manner. Positioning of the patient in the lateral decubitus (with elevation of the affected side) may help to visualize the distal part of the ureter when compression by the gravid uterus limits its visualization. Gadolinium-enhanced MR urography should be avoided whenever possible in these patients.

Urinary tract infection

Patients with urinary infections may develop bacterial infection of the renal parenchyma and collecting system (pyelonephritis). A patient without rapid improvement after appropriate antibiotic treatment should undergo diagnostic studies including US and CT that may assist in the diagnosis of obstruction, abscess, or emphysematous pyelonephritis [137].

There are few reports in the literature regarding the use of MR imaging in patients with pyelonephritis [138–140]. Majd et al [138] found similar sensitivity and specificity for the diagnosis of acute pyelonephritis in pigs using technetium 99m dimercaptosuccinic acid single photon emission CT, spiral CT, and MR imaging. Sensitivity and specificity of MR imaging for the diagnosis were 89.5% and 87.5%, respectively [138]. Power Doppler US was less accurate in that study than the other three modalities. In a study by Lonergan et al [139] in 37 children with fever and urinary infection, MR imaging depicted more pyelonephritic lesions than renal cortical scintigraphy. In addition, interobserver agreement for the presence of pyelonephritis was superior for MR imaging than for cortical scintigraphy [139].

MR imaging findings in pyelonephritis include renal enlargement with heterogeneous appearance. Perirenal edema is usually present and better seen on T2-weighted images as areas of high signal intensity. T2-weighted images can show heterogenous signal intensity with multiple cortical areas of high signal intensity. Postcontrast images show similar findings to those described on contrast-enhanced CT. The renal parenchyma can show heterogenous striated enhancement, although this is not a specific finding [141]. More advanced cases may show multiple nonenhancing cortical defects, which may represent multiple abscesses or infarctions (Fig. 19).

A method to distinguish pyonephrosis from hydronephrosis has been proposed based on diffusion MR imaging [140]. In a study of 12 patients, pus in the collecting system (pyonephrosis) correlated with marked hyperintense signal, whereas the pelvicalyceal system was hypointense in the hydronephrotic kidney [140]. Furthermore, the apparent diffusion coefficient value of the pyonephrotic kidney was extremely low compared with the hydronephrotic kidney [140]. More studies with larger patient population are needed to confirm these initial findings.

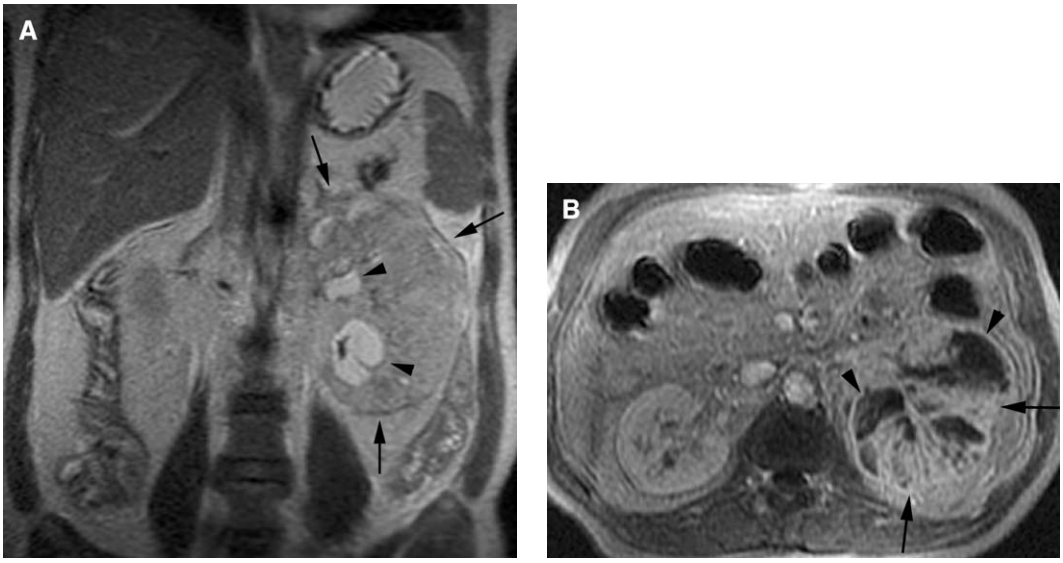

Fig. 19. Acute pyelonephritis. A 54-year-old diabetic man with renal insufficiency; ulcerated skin lesions; and 7-day history of chills, sweats, and urinary frequency. Blood cultures were positive for *Staphylococcus aureus*. A prior unenhanced CT showed enlargement of the left kidney. (*A*) Coronal SSFSE image (TR 1100, TE 64, FA 130, 256 × 190, slice thickness 4 mm) shows a heterogeneous enlarged left kidney (*arrows*) with multiple hyperintense cystic-appearing areas (*arrowheads*) suggestive of acute pyelonephritis. (*B*) Axial T1-weighted turbo FLASH image (TR 1100, TE 64, FA 130, 256 × 190, slice thickness 5 mm) during the delayed venous phase after administration of a single dose of gadolinium demonstrates heterogeneous enhancement of the enlarged left kidney (*arrows*). Multiple nonenhancing areas correspond to the high signal areas on Fig. 19A and can represent infarcts or small abscesses (*arrowheads*). Patient recovered with antibiotic therapy.

Acute renal failure

The corticomedullary differentiation is visualized readily on unenhanced T1-weighted images in the normal kidney [142]. Lack of visualization of the corticomedullary differentiation in the kidneys on unenhanced T1-weighted images has been correlated with elevated creatinine levels (renal insufficiency) [143]. Patients with acute renal failure may have preservation of the corticomedullary differentiation in up to 43% of the cases [144]. Nevertheless, loss of corticomedullary differentiation is a sensitive but nonspecific sign than can be seen in multiple renal pathologies [142]. Low signal intensity along the medulla (especially the outer medulla) on T2-weighted images, possibly representing medullary hemorrhage, is fairly constant and characteristic on MR images of the kidneys in patients with hemorrhagic fever with renal syndrome, an infectious disease caused by different Hantaviruses [145].

Acute vascular conditions

Occlusion or injury to the renal arteries or any of its segmental branches results in ischemia and renal infarction [146]. Patients typically present with acute flank pain. Choo et al [147] correlated the signal intensity of segmental renal infarcts with pathologic examination in 12 rabbits that underwent ligation of a segmental artery of the left kidney. Renal infarcts can demonstrate different signal intensities on T1- and T2-weighted images depending on the time between the onset of the vascular insult and the MR imaging examination [147]. Infarcts had lower signal intensity than the surrounding kidney in the acute stage (< 6 hours) on both T1- and T2-weighted images. As time passes, infarcts become hyperintense on T1-weighted images because of interstitial hemorrhage (24 hours) and hyperintense on both T1- and T2-weighted images (3 days) because of coagulative necrosis [147]. After 2 to 4 weeks organizing fibrosis in the infarcted area accounts for the lower signal intensity on both T1- and T2-weighted images [147]. Gadolinium-enhanced MR angiography allows for exquisite visualization of the renal arteries that can provide important information about the cause for the ischemic renal insult.

Cholesterol embolism is a potential fatal complication of endovascular procedures [148]. Patients present with acute renal failure, eosinophilia, and signs of peripheral ischemia. MR imaging may reveal bilateral renal infarcts and severe atheromatous plaque

formation in the abdominal aorta. Occasionally, a diffuse heterogeneous enhancing pattern may be noted on postcontrast MR images.

Acute renal vein thrombosis may be secondary to different causes including glomerulonephritis, sepsis, lupus nephritis, diabetic nephropathy, amyloidosis, sarcoidosis, sickle cell anemia, malignancy, dehydration, and trauma [149]. Patients with acute renal vein thrombosis can present clinically with acute flank pain. MR imaging shows renal swelling, indistinct corticomedullary differentiation on T1-weighted images, and decreased signal intensity of the renal cortex and medulla [149]. A band of low signal intensity in the outer part of the medulla is typically present, although this finding also can be noted in patients with hemorrhagic fever with renal syndrome [149]. Gadolinium-enhanced MR venography provides excellent visualization of the renal veins. Bland thrombus within the renal vein is shown as a nonenhancing filling defect. Demonstration of thrombus enhancement on postcontrast images is consistent with tumoral thrombus.

Summary

The use of MR imaging in the emergency setting is evolving. Clear indications include situations in need of contrast media when iodinated contrast cannot be administered or to facilitate assessments in pregnant patients and children when exposure to ionizing radiation is considered unacceptable. The availability of rapid, motion-immune sequences now makes MR imaging a feasible study in less cooperative patients extending the range of patients for whom a diagnostic study can be achieved. Capitalizing on the unique benefits of MR imaging there is optimism that MR imaging can eliminate test redundancy and impact patient care in a cost-effective manner. Further investigations are needed to identify the diagnostic algorithms for which this favorable use holds true.

References

[1] Earls JP, Rofsky NM, DeCorato DR, Krinsky GA, Weinreb JC. Hepatic arterial-phase dynamic gadolinium-enhanced MR imaging: optimization with a test examination and a power injector. Radiology 1997; 202:268–73.

[2] Rofsky NM, Weinreb JC, Bosniak MA, Libes RB, Birnbaum BA. Renal lesion characterization with gadolinium-enhanced MR imaging: efficacy and safety in patients with renal insufficiency. Radiology 1991;180:85–9.

[3] Haustein J, Niendorf HP, Krestin G, et al. Renal tolerance of gadolinium-DTPA/dimeglumine in patients with chronic renal failure. Invest Radiol 1992;27: 153–6.

[4] Prince MR, Arnoldus C, Frisoli JK. Nephrotoxicity of high-dose gadolinium compared with iodinated contrast. J Magn Reson Imaging 1996;6:162–6.

[5] Shellock FG, Kanal E. Safety of magnetic resonance imaging contrast agents. J Magn Reson Imaging 1999; 10:477–84.

[6] Rofsky NM, Lee VS, Laub G, et al. Abdominal MR imaging with a volumetric interpolated breath-hold examination. Radiology 1999;212:876–84.

[7] Lavelle MT, Lee VS, Rofsky NM, Krinsky GA, Weinreb JC. Dynamic contrast-enhanced three-dimensional MR imaging of liver parenchyma: source images and angiographic reconstructions to define hepatic arterial anatomy. Radiology 2001;218:389–94.

[8] Sodickson DK, Griswold MA, Jakob PM. SMASH imaging. Magn Reson Imaging Clin N Am 1999;7: 237–54.

[9] Pruessmann KP, Weiger M, Scheidegger MB, Boesiger P. SENSE: sensitivity encoding for fast MRI. Magn Reson Med 1999;42:952–62.

[10] Johannsen EC, Sifri CD, Madoff LC. Pyogenic liver abscesses. Infect Dis Clin North Am 2000;14:547–63.

[11] Mendez RJ, Schiebler ML, Outwater EK, Kressel HY. Hepatic abscesses: MR imaging findings. Radiology 1994;190:431–6.

[12] Balci NC, Sirvanci M. MR imaging of infective liver lesions. Magn Reson Imaging Clin N Am 2002;10: 121–35.

[13] Weissleder R, Saini S, Stark DD, et al. Pyogenic liver abscess: contrast-enhanced MR imaging in rats. AJR Am J Roentgenol 1988;150:115–20.

[14] Schmiedl U, Paajanen H, Arakawa M, Rosenau W, Brasch RC. MR imaging of liver abscesses; application of Gd-DTPA. Magn Reson Imaging 1988;6:9–16.

[15] Elizondo G, Weissleder R, Stark DD, et al. Amebic liver abscess: diagnosis and treatment evaluation with MR imaging. Radiology 1987;165:795–800.

[16] Hughes MA, Petri Jr WA. Amebic liver abscess. Infect Dis Clin North Am 2000;14:565–82.

[17] Ralls PW, Barnes PF, Johnson MB, De Cock KM, Radin DR, Halls J. Medical treatment of hepatic amebic abscess: rare need for percutaneous drainage. Radiology 1987;165:805–7.

[18] Ralls PW, Henley DS, Colletti PM, et al. Amebic liver abscess: MR imaging. Radiology 1987;165:801–4.

[19] Kontoyiannis DP, Luna MA, Samuels BI, Bodey GP. Hepatosplenic candidiasis: a manifestation of chronic disseminated candidiasis. Infect Dis Clin North Am 2000;14:721–39.

[20] Semelka RC, Shoenut JP, Greenberg HM, Bow EJ. Detection of acute and treated lesions of hepatosplenic candidiasis: comparison of dynamic contrast-

enhanced CT and MR imaging. J Magn Reson Imaging 1992;2:341–5.
[21] Pedrosa I, Saiz A, Arrazola J, Ferreiros J, Pedrosa CS. Hydatid disease: radiologic and pathologic features and complications. Radiographics 2000;20: 795–817.
[22] Ros PR, Mortele KJ. Diffuse liver disease. Clin Liver Dis 2002;6:181–201.
[23] Itoh H, Sakai T, Takahashi N, et al. Periportal high intensity on T2-weighted MR images in acute viral hepatitis. J Comput Assist Tomogr 1992;16:564–7.
[24] Murakami T, Baron RL, Peterson MS. Liver necrosis and regeneration after fulminant hepatitis: pathologic correlation with CT and MR findings. Radiology 1996; 198:239–42.
[25] Teefey SA, Baron RL, Bigler SA. Sonography of the gallbladder: significance of striated (layered) thickening of the gallbladder wall. AJR Am J Roentgenol 1991;156:945–7.
[26] Lee VS, Lavelle MT, Krinsky GA, Rofsky NM. Volumetric MR imaging of the liver and applications. Magn Reson Imaging Clin N Am 2001;9:697–716.
[27] Morrin MM, Pedrosa I, Rofsky NM. Magnetic resonance imaging for disorders of liver vasculature. Top Magn Reson Imaging 2002;13:177–90.
[28] Sobhonslidsuk A, Reddy KR. Portal vein thrombosis: a concise review. Am J Gastroenterol 2002;97: 535–41.
[29] Condat B, Pessione F, Helene Denninger M, Hillaire S, Valla D. Recent portal or mesenteric venous thrombosis: increased recognition and frequent recanalization on anticoagulant therapy. Hepatology 2000; 32:466–70.
[30] Froehlich JB, Prince MR, Greenfield LJ, Downing LJ, Shah NL, Wakefield TW. Bull's-eye sign on gadolinium-enhanced magnetic resonance venography determines thrombus presence and age: a preliminary study. J Vasc Surg 1997;26:809–16.
[31] Itai Y, Ohtomo K, Kokubo T, Okada Y, Yamauchi T, Yoshida H. Segmental intensity differences in the liver on MR images: a sign of intrahepatic portal flow stoppage. Radiology 1988;167:17–9.
[32] Yu JS, Rofsky NM. Magnetic resonance imaging of arterioportal shunts in the liver. Top Magn Reson Imaging 2002;13:165–76.
[33] Schlund JF, Semelka RC, Kettritz U, Eisenberg LB, Lee JK. Transient increased segmental hepatic enhancement distal to portal vein obstruction on dynamic gadolinium-enhanced gradient echo MR images. J Magn Reson Imaging 1995;5:375–7.
[34] Noone TC, Semelka RC, Siegelman ES, et al. Budd-Chiari syndrome: spectrum of appearances of acute, subacute, and chronic disease with magnetic resonance imaging. J Magn Reson Imaging 2000;11:44–50.
[35] Casillas VJ, Amendola MA, Gascue A, Pinnar N, Levi JU, Perez JM. Imaging of nontraumatic hemorrhagic hepatic lesions. Radiographics 2000;20:367–78.
[36] Kim JH, Kim MJ, Park SI, et al. MR cholangiography in symptomatic gallstones: diagnostic accuracy according to clinical risk group. Radiology 2002; 224:410–6.
[37] Hochwald SN, Dobryansky MB, Rofsky NM, et al. Magnetic resonance cholangiopancreatography accurately predicts the presence or absence of choledocholithiasis. J Gastrointest Surg 1998;2:573–9.
[38] Greenberger NJPG. Diseases of the gallbladder and bile ducts. In: Braunwald E, Fauci AS, Kasper DL, et al, editors. Harrison's principles of internal medicine. 15th edition. New York: McGraw Hill; 2001. p. 1776–87.
[39] Baron RL, Shuman WP, Lee SP, et al. MR appearance of gallstones in vitro at 1.5 T: correlation with chemical composition. AJR Am J Roentgenol 1989;153: 497–502.
[40] Ukaji M, Ebara M, Tsuchiya Y, et al. Diagnosis of gallstone composition in magnetic resonance imaging: in vitro analysis. Eur J Radiol 2002;41: 49–56.
[41] Harvey RT, Miller Jr WT. Acute biliary disease: initial CT and follow-up US versus initial US and follow-up CT. Radiology 1999;213:831–6.
[42] Gross BH, Harter LP, Gore RM, et al. Ultrasonic evaluation of common bile duct stones: prospective comparison with endoscopic retrograde cholangiopancreatography. Radiology 1983;146:471–4.
[43] Loud PA, Semelka RC, Kettritz U, Brown JJ, Reinhold C. MRI of acute cholecystitis: comparison with the normal gallbladder and other entities. Magn Reson Imaging 1996;14:349–55.
[44] McCarthy S, Hricak H, Cohen M, et al. Cholecystitis: detection with MR imaging. Radiology 1986;158: 333–6.
[45] Pu Y, Yamamoto F, Igimi H, et al. A comparative study usefulness of magnetic resonance imaging in the diagnosis of acute cholecystitis. J Gastroenterol 1994;29:192–8.
[46] Adusumilli S, Siegelman ES. MR imaging of the gallbladder. Magn Reson Imaging Clin N Am 2002; 10:165–84.
[47] Regan F, Schaefer DC, Smith DP, Petronis JD, Bohlman ME, Magnuson TH. The diagnostic utility of HASTE MRI in the evaluation of acute cholecystitis. Half-Fourier acquisition single-shot turbo SE. J Comput Assist Tomogr 1998;22:638–42.
[48] Hakansson K, Leander P, Ekberg O, Hakansson HO. MR imaging in clinically suspected acute cholecystitis: a comparison with ultrasonography. Acta Radiol 2000;41:322–8.
[49] Shlaer WJ, Leopold GR, Scheible FW. Sonography of the thickened gallbladder wall: a nonspecific finding. AJR Am J Roentgenol 1981;136:337–9.
[50] Raghavendra BN, Feiner HD, Subramanyam BR, et al. Acute cholecystitis: sonographic-pathologic analysis. AJR Am J Roentgenol 1981;137:327–32.
[51] Sariego J, Matsumoto T, Kerstein M. Significance of wall thickness in symptomatic gallbladder disease. Arch Surg 1992;127:1216–8.
[52] Park MS, Yu JS, Kim YH, et al. Acute cholecystitis:

comparison of MR cholangiography and US. Radiology 1998;209:781–5.
[53] Yamashita K, Jin MJ, Hirose Y, et al. CT finding of transient focal increased attenuation of the liver adjacent to the gallbladder in acute cholecystitis. AJR Am J Roentgenol 1995;164:343–6.
[54] Colletti PM, Ralls PW, Siegel ME, Halls JM. Acute cholecystitis: diagnosis with radionuclide angiography. Radiology 1987;163:615–8.
[55] Merriam LT, Kanaan SA, Dawes LG, et al. Gangrenous cholecystitis: analysis of risk factors and experience with laparoscopic cholecystectomy. Surgery 1999;126:680–5 [discussion 685–6].
[56] Puc MM, Tran HS, Wry PW, Ross SE. Ultrasound is not a useful screening tool for acute acalculous cholecystitis in critically ill trauma patients. Am Surg 2002; 68:65–9.
[57] Moskos MM, Eschelman DJ. Abdominal case of the day: hemorrhagic cholecystitis. AJR Am J Roentgenol 1991;156:1304–5.
[58] Raijman I, Schrager M. Hemorrhagic acalculous cholecystitis in systemic lupus erythematosus. Am J Gastroenterol 1989;84:445–7.
[59] Vettoretto N, Giovanetti M, Regina P, Baronchelli C, Giulini SM. Hemorrhagic cholecystitis as a likely cause of nontraumatic hemobilia in metachromatic leukodystrophy: report of a case. Ann Ital Chir 2001; 72:725–8.
[60] McFadden DW, Smith GW. Hemodialysis-associated hemorrhagic cholecystitis. Am J Gastroenterol 1987; 82:1081–3.
[61] Iki K, Inada H, Satoh M, Tsunoda T. Hemorrhagic acalculous cholecystitis associated with hemodialysis. Surgery 2002;132:903.
[62] Sogabe M, Hukuno H, Ohkita Y, et al. A case of hemorrhagic cholecystitis during anticoagulant therapy, following surgery of aortic valve replacement, mitral valve plasty and tricuspid valve plasty. Nippon Shokakibyo Gakkai Zasshi 2002;99:974–9.
[63] Chinn DH, Miller EI, Piper N. Hemorrhagic cholecystitis: sonographic appearance and clinical presentation. J Ultrasound Med 1987;6:313–7.
[64] MacDonald JA. Perforation of the gallbladder associated with acute cholecystitis: 8- year review of 20 cases. Ann Surg 1966;164:849–52.
[65] Sherry RM, Gadacz TR. Cholelithiasis and cholecystitis. In: Zuidema GD, editor. Shackelford's surgery of the alimentary tract. 4th edition. Philadelphia: WB Saunders; 1996. p. 229–43.
[66] Sood B, Jain M, Khandelwal N, Singh P, Suri S. MRI of perforated gall bladder. Australas Radiol 2002;46: 438–40.
[67] Demachi H, Matsui O, Hoshiba K, et al. Dynamic MRI using a surface coil in chronic cholecystitis and gallbladder carcinoma: radiologic and histopathologic correlation. J Comput Assist Tomogr 1997;21: 643–51.
[68] Raraty MG, Finch M, Neoptolemos JP. Acute cholangitis and pancreatitis secondary to common duct stones: management update. World J Surg 1998;22: 1155–61.
[69] Pitluk HC, Beal JM. Choledocholithiasis associated with acute cholecystitis. Arch Surg 1979;114:887–8.
[70] Coelho JC, Buffara M, Pozzobon CE, Altenburg FL, Artigas GV. Incidence of common bile duct stones in patients with acute and chronic cholecystitis. Surg Gynecol Obstet 1984;158:76–80.
[71] Liu TH, Consorti ET, Kawashima A, et al. The efficacy of magnetic resonance cholangiography for the evaluation of patients with suspected choledocholithiasis before laparoscopic cholecystectomy. Am J Surg 1999;178:480–4.
[72] Mitchell SE, Clark RA. A comparison of computed tomography and sonography in choledocholithiasis. AJR Am J Roentgenol 1984;142:729–33.
[73] Schwesinger WH, Sirinek KR, Strodel III WE. Laparoscopic cholecystectomy for biliary tract emergencies: state of the art. World J Surg 1999;23:334–42.
[74] Erickson RA, Carlson B. The role of endoscopic retrograde cholangiopancreatography in patients with laparoscopic cholecystectomies. Gastroenterology 1995;109:252–63.
[75] Demartines N, Eisner L, Schnabel K, Fried R, Zuber M, Harder F. Evaluation of magnetic resonance cholangiography in the management of bile duct stones. Arch Surg 2000;135:148–52.
[76] Hartman EM, Barish MA. MR cholangiography. Magn Reson Imaging Clin N Am 2001;9:841–55.
[77] Irie H, Honda H, Kuroiwa T, et al. Pitfalls in MR cholangiopancreatographic interpretation. Radiographics 2001;21:23–37.
[78] Fulcher AS, Turner MA, Capps GW, Zfass AM, Baker KM. Half-Fourier RARE MR cholangiopancreatography: experience in 300 subjects. Radiology 1998;207:21–32.
[79] Varghese JC, Liddell RP, Farrell MA, Murray FE, Osborne H, Lee MJ. The diagnostic accuracy of magnetic resonance cholangiopancreatography and ultrasound compared with direct cholangiography in the detection of choledocholithiasis. Clin Radiol 1999;54:604–14.
[80] David V, Reinhold C, Hochman M, et al. Pitfalls in the interpretation of MR cholangiopancreatography. AJR Am J Roentgenol 1998;170:1055–9.
[81] Hintze RE, Adler A, Veltzke W, et al. Clinical significance of magnetic resonance cholangiopancreatography (MRCP) compared to endoscopic retrograde cholangiopancreatography (ERCP). Endoscopy 1997; 29:182–7.
[82] Hanau LH, Steigbigel NH. Acute (ascending) cholangitis. Infect Dis Clin North Am 2000;14:521–46.
[83] Chock E, Wolfe BM, Matolo NM. Acute suppurative cholangitis. Surg Clin North Am 1981;61:885–92.
[84] Lum DF, Leung JW. Bacterial cholangitis. Curr Treat Options Gastroenterol 2001;4:139–46.
[85] Bader TR, Braga L, Beavers KL, Semelka RC. MR imaging findings of infectious cholangitis. Magn Reson Imaging 2001;19:781–8.
[86] Gaines P, Markham N, Leung J, Metreweli C. The

thick common bile duct in pyogenic cholangitis. Clin Radiol 1991;44:175–7.
[87] Schulte SJ, Baron RL, Teefey SA, et al. CT of the extrahepatic bile ducts: wall thickness and contrast enhancement in normal and abnormal ducts. AJR Am J Roentgenol 1990;154:79–85.
[88] Hakansson K, Ekberg O, Hakansson HO, Leander P. MR characteristics of acute cholangitis. Acta Radiol 2002;43:175–9.
[89] Binmoeller KF, Thonke F, Soehendra N. Endoscopic treatment of Mirizzi's syndrome. Gastrointest Endosc 1993;39:532–6.
[90] Kim PN, Outwater EK, Mitchell DG. Mirizzi syndrome: evaluation by MRI imaging. Am J Gastroenterol 1999;94:2546–50.
[91] Presta L, Ragozzino A, Perrotti P, et al. Detection of Mirizzi syndrome with magnetic resonance cholangiopancreatography: laparoscopic or open approach? Surg Endosc 2002;16:1494–5.
[92] Tervahartiala P, Kivisaari R, Virtanen I. Contrast media-induced renal morphologic changes in rats with acute edematous pancreatitis. Invest Radiol 1992;27: 520–4.
[93] Foitzik T, Bassi DG, Schmidt J, et al. Intravenous contrast medium accentuates the severity of acute necrotizing pancreatitis in the rat. Gastroenterology 1994;106:207–14.
[94] Piironen A. Severe acute pancreatitis: contrast-enhanced CT and MRI features. Abdom Imaging 2001; 26:225–33.
[95] Werner J, Schmidt J, Warshaw AL, Gebhard MM, Herfarth C, Klar E. The relative safety of MRI contrast agent in acute necrotizing pancreatitis. Ann Surg 1998;227:105–11.
[96] Terzi C, Sokmen S. Acute pancreatitis induced by magnetic-resonance-imaging contrast agent. Lancet 1999;354:1789–90.
[97] Piironen A, Kivisaari R, Pitkaranta P, et al. Dynamic high-field MR imaging in experimental porcine acute pancreatitis. Acta Radiol 1995;36:182–7.
[98] Amano Y, Oishi T, Takahashi M, Kumazaki T. Non-enhanced magnetic resonance imaging of mild acute pancreatitis. Abdom Imaging 2001;26:59–63.
[99] Piironen A, Kivisaari R, Kemppainen E, et al. Detection of severe acute pancreatitis by contrast-enhanced magnetic resonance imaging. Eur Radiol 2000;10: 354–61.
[100] Lecesne R, Taourel P, Bret PM, Atri M, Reinhold C. Acute pancreatitis: interobserver agreement and correlation of CT and MR cholangiopancreatography with outcome. Radiology 1999;211:727–35.
[101] Hirohashi S, Hirohashi R, Uchida H, et al. Pancreatitis: evaluation with MR cholangiopancreatography in children. Radiology 1997;203:411–5.
[102] Freeny PC, Hauptmann E, Althaus SJ, Traverso LW, Sinanan M. Percutaneous CT-guided catheter drainage of infected acute necrotizing pancreatitis: techniques and results. AJR Am J Roentgenol 1998;170:969–75.
[103] Lee JK, Marcos HB, Semelka RC. MR imaging of the small bowel using the HASTE sequence. AJR Am J Roentgenol 1998;170:1457–63.
[104] Regan F, Beall DP, Bohlman ME, Khazan R, Sufi A, Schaefer DC. Fast MR imaging and the detection of small-bowel obstruction. AJR Am J Roentgenol 1998;170:1465–9.
[105] McKinsey JF, Gewertz BL. Acute mesenteric ischemia. Surg Clin North Am 1997;77:307–18.
[106] Chow LC, Chan FP, Li KC. A comprehensive approach to MR imaging of mesenteric ischemia. Abdom Imaging 2002;27:507–16.
[107] Boley SJ, Brandt LJ, Sammartano RJ. History of mesenteric ischemia: the evolution of a diagnosis and management. Surg Clin North Am 1997;77:275–88.
[108] Baden JG, Racy DJ, Grist TM. Contrast-enhanced three-dimensional magnetic resonance angiography of the mesenteric vasculature. J Magn Reson Imaging 1999;10:369–75.
[109] Chan FP, Li KC, Heiss SG, Razavi MK. A comprehensive approach using MR imaging to diagnose acute segmental mesenteric ischemia in a porcine model. AJR Am J Roentgenol 1999;173:523–9.
[110] Li KC, Pelc LR, Puvvala S, Wright GA. Mesenteric ischemia due to hemorrhagic shock: MR imaging diagnosis and monitoring in a canine model. Radiology 1998;206:219–25.
[111] Rha SE, Ha HK, Lee SH, et al. CT and MR imaging findings of bowel ischemia from various primary causes. Radiographics 2000;20:29–42.
[112] Klein HM, Klosterhalfen B, Kinzel S, et al. CT and MRI of experimentally induced mesenteric ischemia in a porcine model. J Comput Assist Tomogr 1996;20: 254–61.
[113] Warshauer DM, Lee JK, Mauro MA, White II GC. Superior mesenteric vein thrombosis with radiologically occult cause: a retrospective study of 43 cases. AJR Am J Roentgenol 2001;177:837–41.
[114] Kreft B, Strunk H, Flacke S, et al. Detection of thrombosis in the portal venous system: comparison of contrast-enhanced MR angiography with intraarterial digital subtraction angiography. Radiology 2000;216: 86–92.
[115] Puylaert JB, Rutgers PH, Lalisang RI, et al. A prospective study of ultrasonography in the diagnosis of appendicitis. N Engl J Med 1987;317:666–9.
[116] Borushok KF, Jeffrey Jr RB, Laing FC, Townsend RR. Sonographic diagnosis of perforation in patients with acute appendicitis. AJR Am J Roentgenol 1990; 154:275–8.
[117] Incesu L, Coskun A, Selcuk MB, Akan H, Sozubir S, Bernay F. Acute appendicitis: MR imaging and sonographic correlation. AJR Am J Roentgenol 1997;168: 669–74.
[118] Hormann M, Paya K, Eibenberger K, et al. MR imaging in children with nonperforated acute appendicitis: value of unenhanced MR imaging in sonographically selected cases. AJR Am J Roentgenol 1998;171: 467–70.
[119] Bailey LE, Finley Jr RK, Miller SF, Jones LM. Acute

appendicitis during pregnancy. Am Surg 1986;52: 218–21.
[120] Lim HK, Bae SH, Seo GS. Diagnosis of acute appendicitis in pregnant women: value of sonography. AJR Am J Roentgenol 1992;159:539–42.
[121] Barloon TJ, Brown BP, Abu-Yousef MM, Warnock N, Berbaum KS. Sonography of acute appendicitis in pregnancy. Abdom Imaging 1995;20:149–51.
[122] Heverhagen JT, Zielke A, Ishaque N, Bohrer T, El-Sheik M, Klose KJ. Acute colonic diverticulitis: visualization in magnetic resonance imaging. Magn Reson Imaging 2001;19:1275–7.
[123] Heverhagen JT, Ishaque N, Zielke A, et al. Feasibility of MRI in the diagnosis of acute diverticulitis: initial results. MAGMA 2001;12:4–9.
[124] van Breda Vriesman AC, Puylaert JB. Epiploic appendagitis and omental infarction: pitfalls and look-alikes. Abdom Imaging 2002;27:20–8.
[125] Barbier C, Denny P, Pradoura JM, et al. Radiologic aspects of infarction of the appendix epiploica. J Radiol 1998;79:1479–85.
[126] Sirvanci M, Balci NC, Karaman K, Duran C, Karakas E. Primary epiploic appendagitis: MRI findings. Magn Reson Imaging 2002;20:137–9.
[127] Wall SD, Hricak H, Bailey GD, Kerlan Jr RK, Goldberg HI, Higgins CB. MR imaging of pathologic abdominal fluid collections. J Comput Assist Tomogr 1986;10:746–50.
[128] Terrier F, Revel D, Pajannen H, Richardson M, Hricak H, Higgins CB. MR imaging of body fluid collections. J Comput Assist Tomogr 1986;10:953–62.
[129] Puylaert JB. Right-sided segmental infarction of the omentum: clinical, US, and CT findings. Radiology 1992;185:169–72.
[130] Goti F, Reinhart M, Decurtins M. Idiopathic segmental fatty tissue necrosis of the ligamentum teres hepatis: variation on a theme. Chirurg 2000;71:225–7.
[131] Sudah M, Vanninen RL, Partanen K, et al. Patients with acute flank pain: comparison of MR urography with unenhanced helical CT. Radiology 2002;223: 98–105.
[132] Sudah M, Vanninen R, Partanen K, Heino A, Vainio P, Ala-Opas M. MR urography in evaluation of acute flank pain: T2-weighted sequences and gadolinium-enhanced three-dimensional FLASH compared with urography. Fast low-angle shot. AJR Am J Roentgenol 2001;176:105–12.
[133] Nolte-Ernsting CC, Bucker A, Adam GB, et al. Gadolinium-enhanced excretory MR urography after low-dose diuretic injection: comparison with conventional excretory urography. Radiology 1998;209:147–57.
[134] Tang Y, Yamashita Y, Namimoto T, et al. The value of MR urography that uses HASTE sequences to reveal urinary tract disorders. AJR Am J Roentgenol 1996; 167:1497–502.
[135] Regan F, Bohlman ME, Khazan R, Rodriguez R, Schultze-Haakh H. MR urography using HASTE imaging in the assessment of ureteric obstruction. AJR Am J Roentgenol 1996;167:1115–20.
[136] Regan F, Petronis J, Bohlman M, Rodriguez R, Moore R. Perirenal MR high signal: a new and sensitive indicator of acute ureteric obstruction. Clin Radiol 1997;52:445–50.
[137] Roberts JA. Management of pyelonephritis and upper urinary tract infections. Urol Clin North Am 1999;26: 753–63.
[138] Majd M, Nussbaum Blask AR, Markle BM, et al. Acute pyelonephritis: comparison of diagnosis with 99mTc-DMSA, SPECT, spiral CT, MR imaging, and power Doppler US in an experimental pig model. Radiology 2001;218:101–8.
[139] Lonergan GJ, Pennington DJ, Morrison JC, Haws RM, Grimley MS, Kao TC. Childhood pyelonephritis: comparison of gadolinium-enhanced MR imaging and renal cortical scintigraphy for diagnosis. Radiology 1998;207:377–84.
[140] Chan JH, Tsui EY, Luk SH, et al. MR diffusion-weighted imaging of kidney: differentiation between hydronephrosis and pyonephrosis. Clin Imaging 2001; 25:110–3.
[141] Saunders HS, Dyer RB, Shifrin RY, Scharling ES, Bechtold RE, Zagoria RJ. The CT nephrogram: implications for evaluation of urinary tract disease. Radiographics 1995;15:1069–85 [discussion 1068–88].
[142] Marotti M, Hricak H, Terrier F, McAninch JW, Thuroff JW. MR in renal disease: importance of cortical-medullary distinction. Magn Reson Med 1987;5:160–72.
[143] Semelka RC, Corrigan K, Ascher SM, Brown JJ, Colindres RE. Renal corticomedullary differentiation: observation in patients with differing serum creatinine levels. Radiology 1994;190:149–52.
[144] Chung JJ, Semelka RC, Martin DR. Acute renal failure: common occurrence of preservation of corticomedullary differentiation on MR images. Magn Reson Imaging 2001;19:789–93.
[145] Kim SH, Kim S, Lee JS, et al. Hemorrhagic fever with renal syndrome: MR imaging of the kidney. Radiology 1990;175:823–5.
[146] Tillou A, Romero J, Asensio JA, et al. Renal vascular injuries. Surg Clin North Am 2001;81:1417–30.
[147] Choo SW, Kim SH, Jeong YG, Shin YM, Kim JS, Han MC. MR imaging of segmental renal infarction: an experimental study. Clin Radiol 1997;52:65–8.
[148] Thadhani RI, Camargo Jr CA, Xavier RJ, Fang LS, Bazari H. Atheroembolic renal failure after invasive procedures: natural history based on 52 histologically proven cases. Medicine (Baltimore) 1995;74:350–8.
[149] Jeong JY, Kim SH, Lee HJ, Sim JS. Atypical low-signal-intensity renal parenchyma: causes and patterns. Radiographics 2002;22:833–46.

RADIOLOGIC CLINICS OF NORTH AMERICA

Radiol Clin N Am 41 (2003) 1275–1288

Selective role of nuclear medicine in evaluating the acute abdomen

Lionel S. Zuckier, MD[a,*], Leonard M. Freeman, MD[b]

[a]*Department of Radiology, New Jersey Medical School, 150 Bergen Street, Room H-141, Newark, NJ 07103, USA*
[b]*Department of Radiology and Nuclear Medicine, Albert Einstein College of Medicine/Montefiore Medical Center, 111 East 210th Street, Bronx, NY 10467, USA*

Radiology remains an ever-evolving discipline. Introduction of new modalities frequently impacts on the optimal diagnostic pathway for evaluation of a given clinical symptom or complaint. With respect to evaluating the acute abdomen, much has changed since Nusynowitz [1] embraced radionuclide angiography as a promising screening method for detecting avascular collections, such as pancreatic pseudocysts and retroperitoneal hematomas. Review of the application of nuclear medicine modalities to evaluate patients with acute abdominal pathology is a very worthwhile and timely undertaking.

The value of nuclear medicine studies lies in their ability to evaluate functional and physiologic parameters, often to a greater degree than other radiologic modalities. For anatomic questions, radionuclide methods, such as Tc 99m sulfur colloid scintigraphy for evaluation of the liver and spleen, have largely been supplanted by higher-resolution modalities, such as ultrasound (US), CT, and MR imaging. This article highlights the areas where scintigraphy remains an important tool for the evaluation of patients with acute abdominal disorders. This discussion is organized according to clinical presentation.

Gastrointestinal bleeding

Localization of the site of acute gastrointestinal (GI) bleeding is an important step in patient management [2]. After an upper GI etiology is excluded by evaluation of the nasogastrointestinal aspirate, bleeding scintigraphy has a useful role to play in localizing the bleed to small bowel, right colon, or left colon. This information is of value in determining the initial approach to subsequent angiography, or in directing the surgeon if an emergency hemicolectomy is indicated.

Historically, two radiotracers have been used for bleeding scintigraphy. Tc 99m sulfur colloid was the initial radiopharmaceutical introduced [3] and is still advocated by some as the preferred method of study [4]. Most clinicians have adopted use of Tc 99m red blood cells (RBC), preferably labeled by an in vitro method [5,6], to minimize free pertechnetate. The advantage of Tc 99m RBC is that the radiotracer persists within the blood pool for a prolonged period of time, whereas sulfur colloid is rapidly phagocytosed by reticuloendothelial cells and clears the blood pool over the course of only several minutes. The diagnostic window of time available to detect extravasation with sulfur colloid is limited to approximately 10 minutes, whereas RBC imaging may be performed to 90 minutes or longer. Because GI bleeding tends to be intermittent and episodic [7], the chances of detecting and localizing bleeding are believed to be superior using the RBC technique. Advantages of RBC over sulfur colloid have been confirmed by clinical series that have compared the two techniques [8,9]. Bleeding rates as little as 0.1 mL/minute are detectible using RBC bleeding scintigraphy [10], which is approximately 10-fold as sensitive as angiography.

Typically, static images are acquired at several minute intervals following radiotracer administration throughout the period of observation. Alternatively, multiple sequential dynamic images can be obtained

* Corresponding author.
E-mail address: zuckier@umdnj.edu (L.S. Zuckier).

0033-8389/03/$ – see front matter
doi:10.1016/S0033-8389(03)00098-8

at 15- or 30-second intervals that, on replay in cine mode, provide a movie-type display of extravasation and peristalsis of labeled blood. Cine images are favored by many for detecting and illustrating slow GI bleeds [11]. Dynamic images at 2-second intervals can also be obtained during the injection of radionuclide into the patient to illustrate blood flow, thereby portraying vascular abnormalities. This information can also be of benefit to the angiographer in defining the anatomy of the vasculature before subsequent arteriography [12].

The sine qua nons of a positive examination is the appearance of extravasated blood within the bowel lumen; the process of localizing the bleed can be

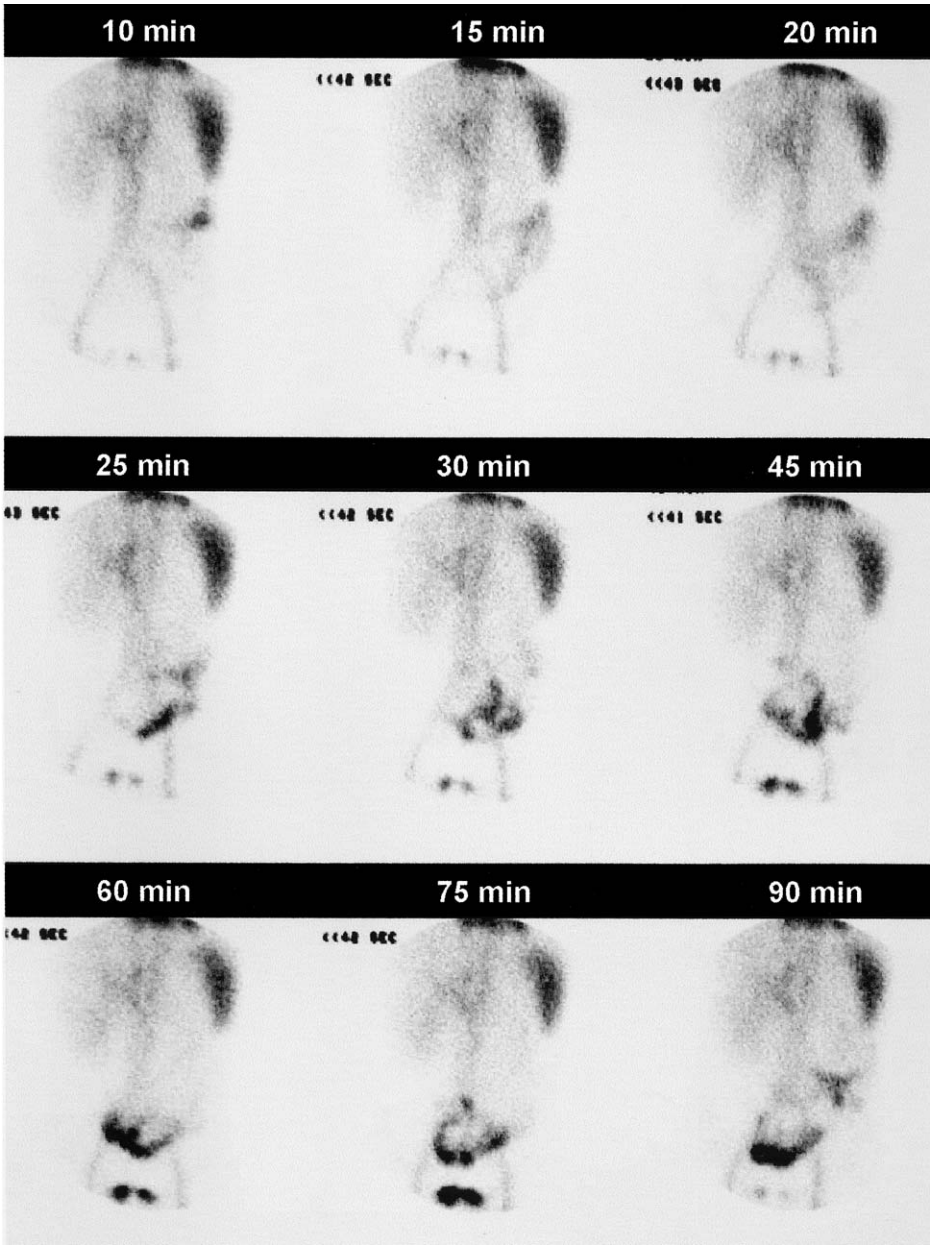

Fig. 1. Small bowel bleed in a 45-year-old man with known cirrhosis. Typical characteristics include central location and rapidly changing appearance of small bowel segments from frame to frame.

broken down to two steps: characterizing the involved bowel as small or large, and subsequently determining the anatomic location within that division.

The key to the first step is identifying the location and pattern of movement of extravasated labeled blood within the bowel lumen. Small bowel is centrally located, and the blood appears to progress rapidly distally through a series of small curvilinear segments on sequential imaging (Fig. 1). In contrast, large bowel bleeding is generally peripheral in location, and progresses in a more elongated pattern on sequential imaging, often with visualization of well-defined haustrations (Fig. 2). Occasionally foci of apparently extravasated blood appear during the course of a study, which do not move on sequential images. Generally, these represent abnormalities other than GI bleeding, such as varices or areas of inflammation [13].

Once the character of the affected bowel is determined to be large or small, one can then identify more precisely the site of bleeding. Blood is an irritant and typically stimulates peristalsis in both the antegrade and retrograde direction; the origin of hemorrhage may therefore not be clear on a delayed image. To identify the actual site of bleeding, one must search for the initial site of appearance of blood, and not the most proximal site visualized. If uncertainty exists, it can often be helpful to trace the motion of extravasated blood backward over time to observe the first frame where abnormality is detected.

Although bleeding scintigraphy is more sensitive than angiography in detecting GI hemorrhage, it only yields a positive test if the patient is actively bleeding during the period of observation. The rate of bleeding also determines the time and degree of scan positivity

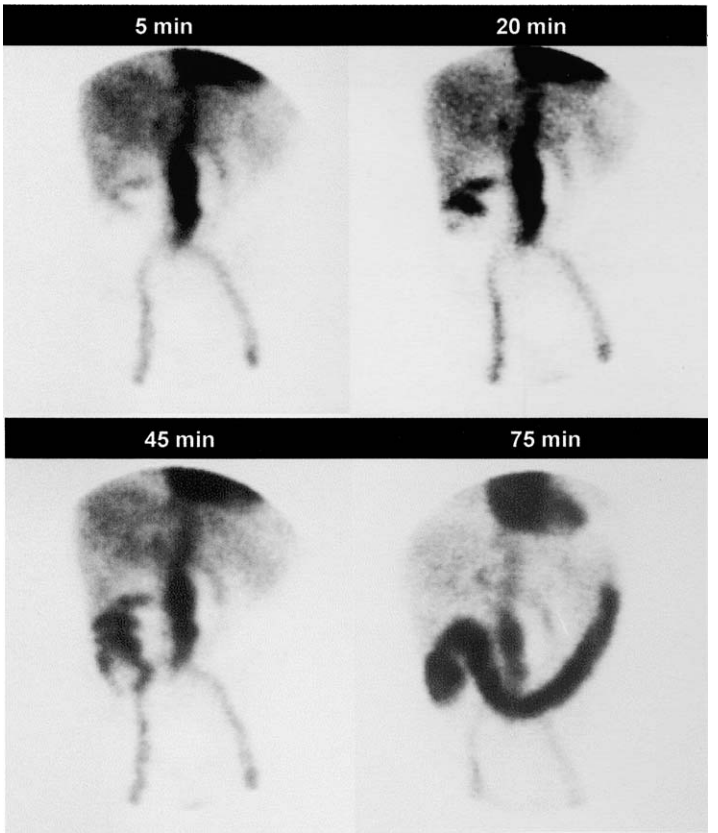

Fig. 2. Large colon bleed in a patient who presented with brisk rectal bleeding. The 5-minute image reveals the bleeding focus to be in the hepatic flexure region. Note that on subsequent frames the blood progresses both antegrade, outlining the transverse colon, and retrograde, extending to the region of the cecum. Characteristics of large bowel bleeding include a peripheral location; variable visualization of haustrations; and visualization of elongated regions of bowel, which slowly change in appearance from frame to frame.

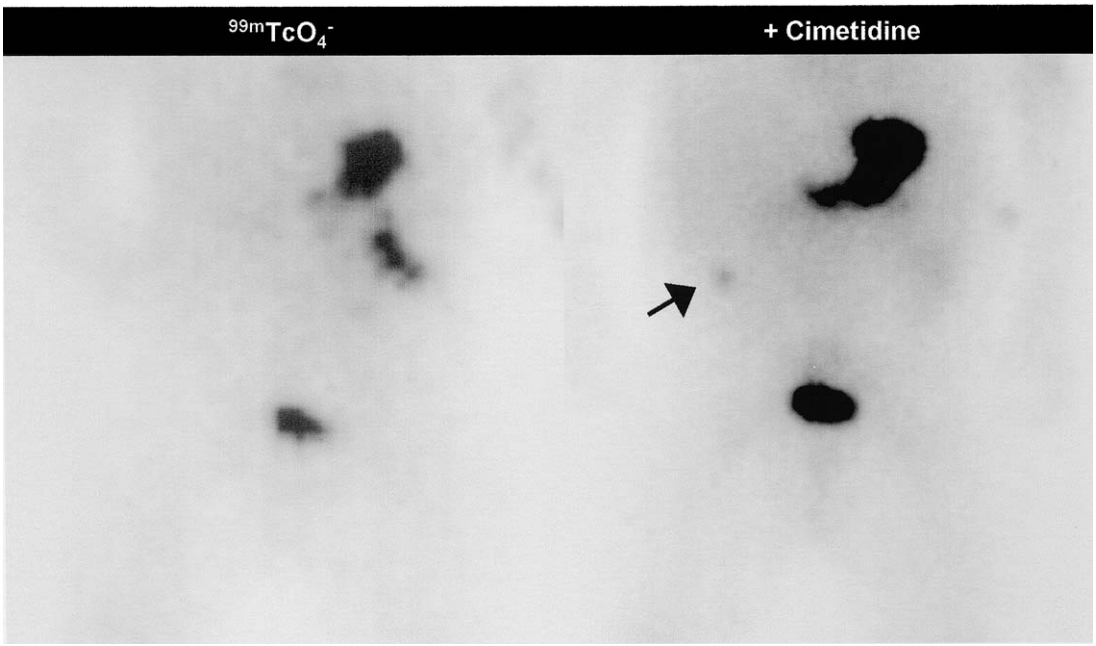

Fig. 3. Representative 40-minute images from pertechnetate studies without (*left panel*) and with (*right panel*) cimetidine pretreatment performed to detect ectopic gastric mucosa in a 7-month-old girl with gastrointestinal hemorrhage. The patient has been placed on cimetidine 3 hours before the study. Representative 40-minute image from initial study (*left panel*) did not reveal presence of the ectopic gastric mucosa. After an additional day of cimetidine treatment, the study was repeated. Corresponding 40-minute image reveals a focus of pertechnetate uptake in the right lower quadrant of the abdomen (*arrow*), in a location typical for Meckel's diverticulum.

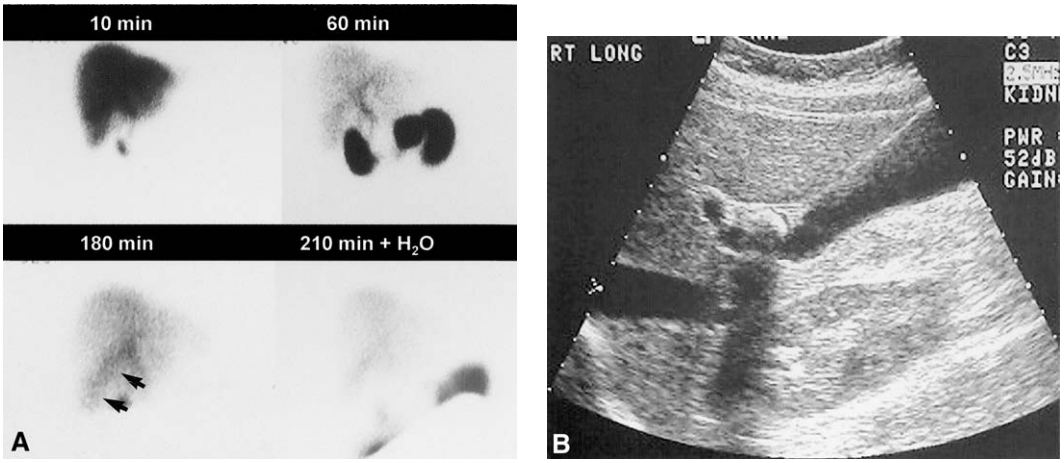

Fig. 4. Acute cholecystitis in a 27-year-old woman who presented with right upper quadrant pain. Biliary excretion study (*A*) reveals prompt uptake by the liver and rapid excretion into the small bowel with no visualization of the gallbladder through 3.5 hours. Of note, there is a suggestion of a faint stripe of activity in the region of the gallbladder fossa (*arrows*), which increases the likelihood of the diagnosis of acute gangrenous cholecystitis. To eliminate the confounding possibility of duodenal activity adjacent to the gallbladder fossa, water was given to the patient between the 3- and 3.5-hour views. Additionally, the bowel is shielded by a lead cape on the 3.5-hour view. Ultrasound study (*B*) demonstrates stones in the region of the neck of the gallbladder.

[14]. The 90-minute imaging period typically used for RBC studies was chosen based on a retrospective review of bleeding studies, where the yield of detecting sites of hemorrhage plateau by this time point [8]. In some bleeding protocols, patients with negative studies have been recalled for an image the following morning (24-hour image). Although on occasion this reveals presence of labeled blood within the bowel, it generally does not contribute clinically useful information because characterization of the site of bleeding is impossible unless the site of actual extravasation is documented during the period of observation and imaging. More productively, patients who are suspected of rebleeding following a return to their clinical ward should be recalled immediately for repeat imaging.

On occasion, GI bleeding may be caused by Meckel's diverticulum (Fig. 3). Most Meckel's diverticulum that bleed have the presence of ectopic gastric mucosa. Gastric mucosa concentrates Tc 99m pertechnetate (TcO_4^-) and this radiopharmaceutical can be used for its detection [15,16]. Typically, 10 mCi of TcO_4^- are administered and sequential anterior abdominal images are obtained over the course of 30 to 60 minutes. Activity appearing in the right lower quadrant of the abdomen, with a similar timing as visualization of the orthotopic gastric mucosa of the stomach, is considered to meet the criteria for positivity. To increase yield, the patient can be pretreated with cimetidine, which is postulated to decrease the release of radiotracer by gastric mucosa and thereby increase lesion-to-background ratios [17].

Right upper quadrant pain

Initial presentation

In previously asymptomatic outpatients presenting with acute right upper quadrant pain, disease of the biliary tree is a prominent consideration. CT and US are often used to assess for acute cholecystitis and common bile duct (CBD) obstruction and may demonstrate morphologic changes, such as edema of the gallbladder (GB) wall, dilatation of the CBD, and presence of pericholecystic fluid. In contrast to the visualization of these secondary phenomena, hepatobiliary scintigraphy can be used more directly to follow the dynamics of bile flow, which may be disrupted at an earlier stage.

In hepatobiliary scintigraphy, 5 mCi of a Tc 99m–labeled hepatobiliary agent is administered, typically either the diisopropyl or trimethylbromo analogue [18]. Patients are generally imaged after a 2- to 4-hour period of fasting. In traditional protocols, imaging extends over 4 hours. Patients without biliary disease exhibit prompt flow of radiolabeled bile into the bowel and GB, both of which are visualized within

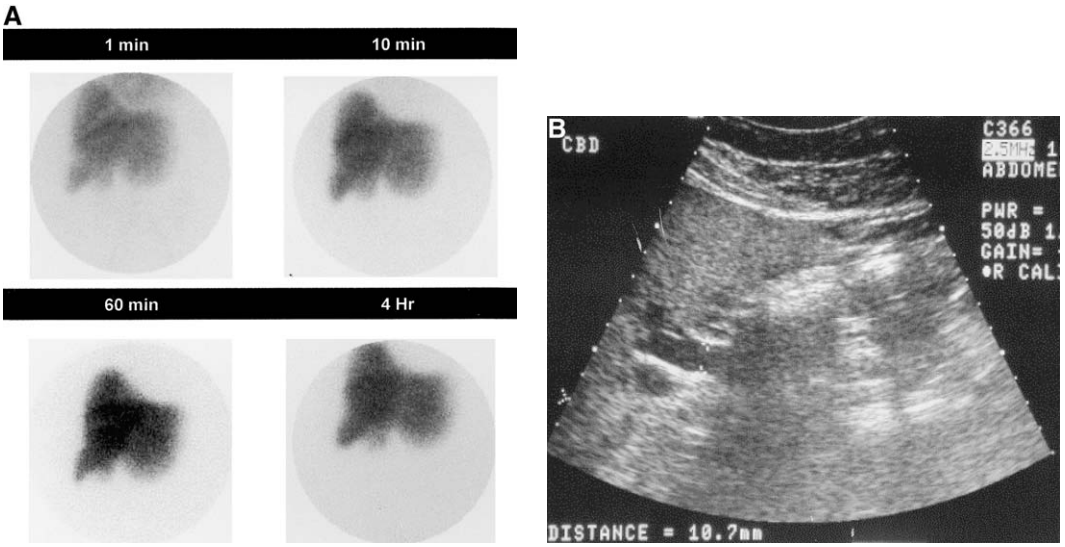

Fig. 5. Common bile duct obstruction in a woman who presented with right upper quadrant pain and was suspected of having acute cholecystitis. Scintigraphic study (*A*) reveals a fixed hepatogram pattern through 4 hours, consistent with the diagnosis of CBD obstruction. Correlative ultrasound performed the following day (*B*) demonstrates mild dilation of the CBD to a diameter of 10.7 mm.

the first hour. Patients with acute cholecystitis (Fig. 4) exhibit prompt flow of bile into the bowel, but nonvisualization of the GB through 4 hours or greater, secondary to cystic duct obstruction [19]. It has been known for over 40 years that 95% of patients with acute cholecystitis have cystic duct obstruction [20]. A related finding that suggests gangrenous cholecystitis is a stripe of increasing activity at the lower margin of the liver (see Fig. 4). Various mechanisms causing this finding have been suggested [21]. One possibility is localized cholestasis of the lower edge hepatocytes caused by inflammation in the adjacent GB, whereas a second proposes actual bile leakage from the perforated GB. When present, the stripe sign is a useful ancillary finding; however, most cases of acute gangrenous cholecystitis only demonstrate the absence of GB visualization.

Cholescintigraphic findings in patients with chronic cholecystitis are variable. The study may be normal if no functional abnormality is associated with sonographically demonstrated calculi. Many cases of chronic cholecystitis demonstrate delayed visualization of the GB, typically between 1 and 4 hours. As the period of scintigraphic observation and GB nonvisualization approaches 3 to 4 hours, it becomes more likely that the patient actually has acute rather than chronic cholecystitis. This should be borne in mind if a full 4 hours of imaging cannot be performed.

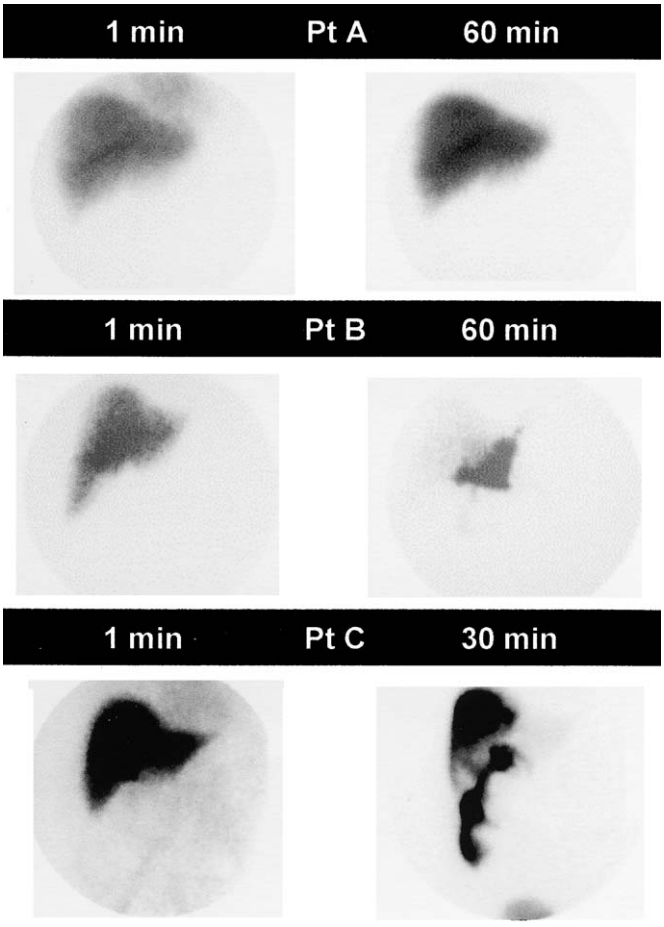

Fig. 6. Representative biliary scintigraphic images in three symptomatic postlaparoscopic cholecystectomy patients. Patient A is a 23-year-old woman, 6 days postprocedure, who has increasing nausea, vomiting, and pain. A CBD obstructive pattern is noted. Patient B is a young woman studied 10 days postprocedure. A relatively confined leak into the lesser sac is noted with negligible activity proceeding into the small bowel. Patient C also evidences a leak, which appears freely flowing down the right paracolic gutter.

If the cause of the patient's acute symptomatology is CBD obstruction, activity is retained in the liver and does not proceed distally into the bowel (Fig. 5). In a study performed at New York's Montefiore Medical Center, this finding occurred in 8.5% of patients who were studied for suspected acute cholecystitis [22]. This correlates well with the surgical literature, which indicates that 11% of patients undergoing cholecystectomy for acute cholecystitis are found to have choledocholithiasis [23]. In the Montefiore study, absent bile flow was caused by CBD obstruction in 63 of the 65 patients in whom the persistent hepato-

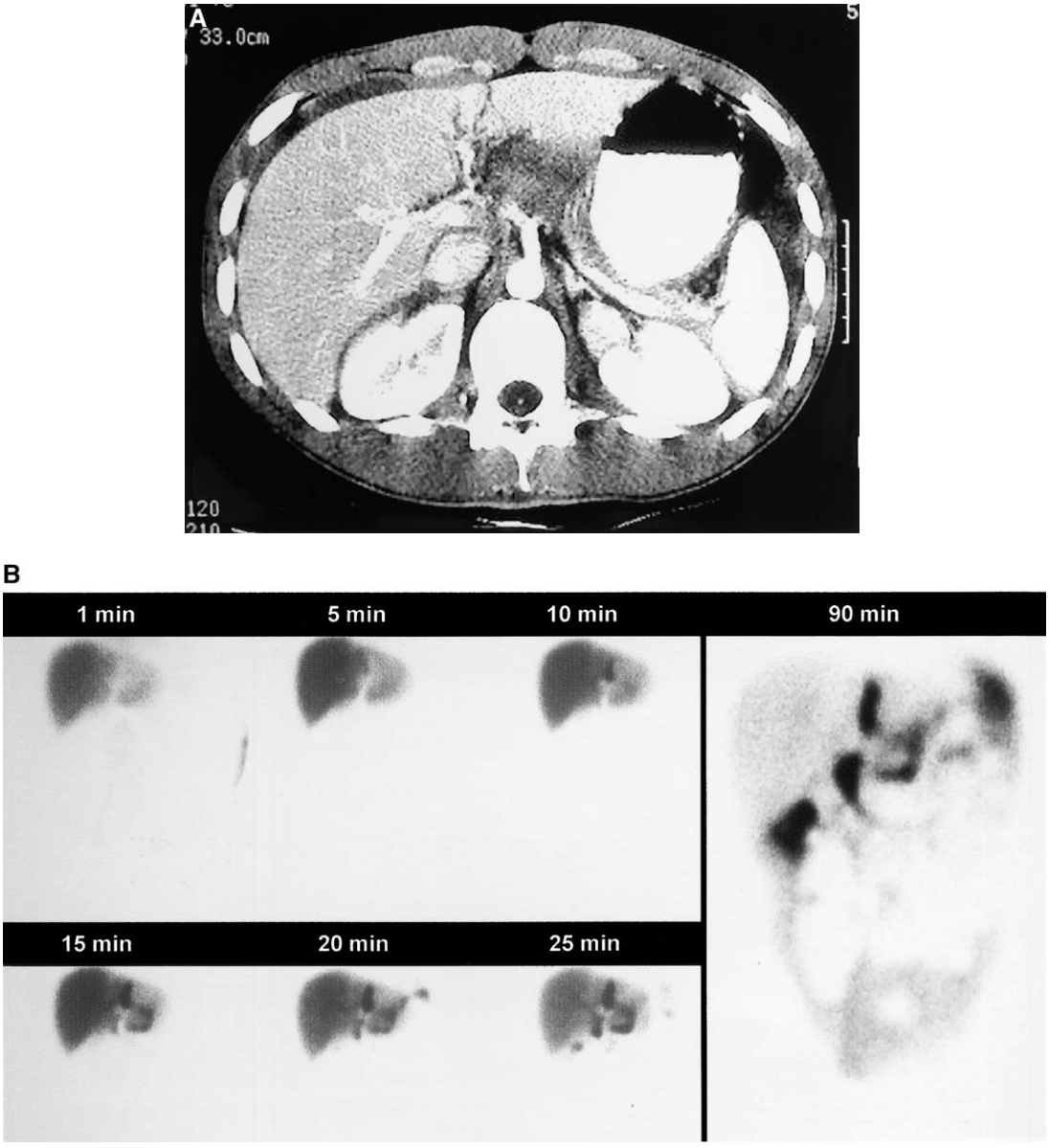

Fig. 7. Utility of biliary scintigraphy in evaluating traumatic injury to the liver and biliary structures in a 25-year-old man who was ejected from a car during a motor vehicle accident. A large liver laceration was noted on CT (*A*) with collection of fluid behind the left lobe. Initial biliary scintigraphy (*B*) demonstrates a large leak with spread of radiotracer throughout the peritoneal cavity by 90 minutes. The bowel loops are visualized as a negative defect. Follow-up scintigraphy performed after 5 days of conservative management (*C*) demonstrates resolution of the leak with progression of activity into the small bowel.

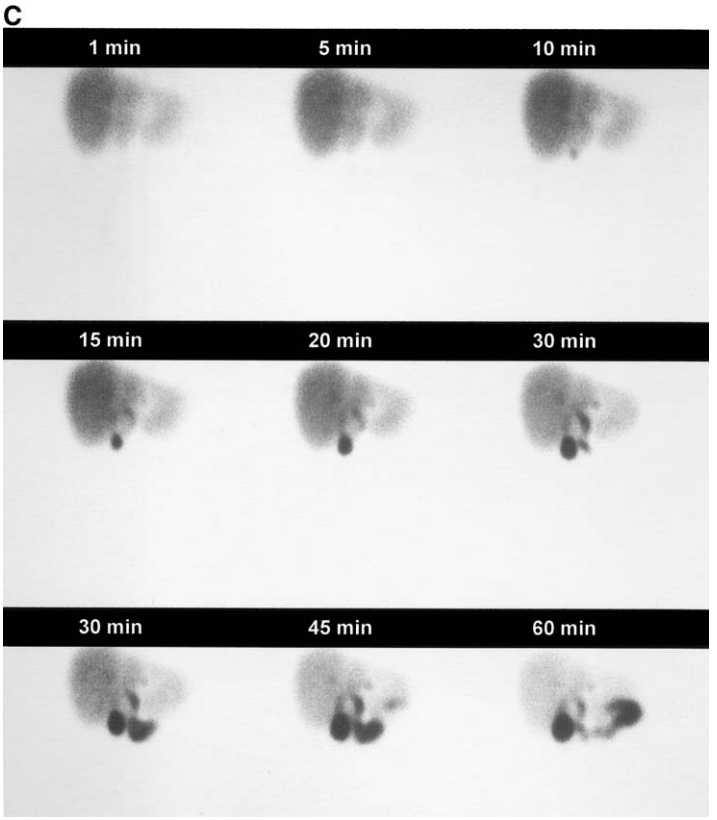

Fig. 7 (*continued*).

gram was demonstrated (positive predictive value of 96%). If CBD obstruction is not relieved, liver uptake becomes increasingly impaired. In patients with severe impairment, the reliability of assessing biliary or cystic duct obstruction is significantly decreased.

An abbreviated method of biliary scintigraphy can be performed, which is especially useful in the emergency setting. Once the duodenum appears but no GB is yet evident, at approximately 1 hour, 1 to 2 mg of morphine can be administered intravenously. This maneuver constricts the sphincter of Oddi and facilitates GB filling through the cystic duct; if filling does not occur then the duct is presumed to be obstructed [24,25]. The morphine-enhanced IDA study shortens the examination time to 1.5 hours instead of the 4 hours needed for completion of a traditional protocol.

Patients who are on total parenteral nutrition or have not eaten for 24 hours or longer require a special preparation before undergoing cholescintigraphy to avoid possible false-positive results from sludge in the GB [26]. A slow intravenous injection of 0.02 μg/kg of sincalide (the terminal octapeptide of cholecystokinin), can be administered, which contracts an otherwise normal GB and allows for the free entry of IDA when administered 20 to 30 minutes later.

The postcholecystectomy patient with pain

A special subset of patients with abdominal pain is those who have had a recent cholecystectomy, especially when performed by laparoscopic technique.

Fig. 8. Biloma following penetrating injury to the abdomen in an 18-year-old man who sustained stab wound to his right flank. CT (*A*) showed a large hemoperitoneum, laceration of the anterior and posterior segments of the right lobe of the liver, and a hematoma in Morison's pouch. Biliary scintigraphy performed the following day (*B*) initially demonstrates presence of a photon-poor collection in the lateral aspect of the right lobe; however, over the hour course of the images, a small focus of bile uptake within the region of the collection is noted (*arrow*). Most of the bile is excreted into the small bowel.

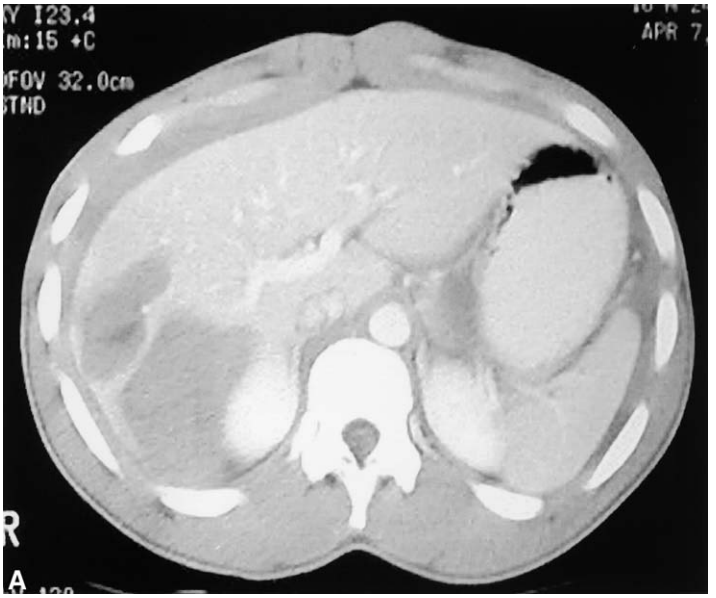
Y 123.4
m:15 +C
FOV 32.0cm
TND
APR 7
R
A

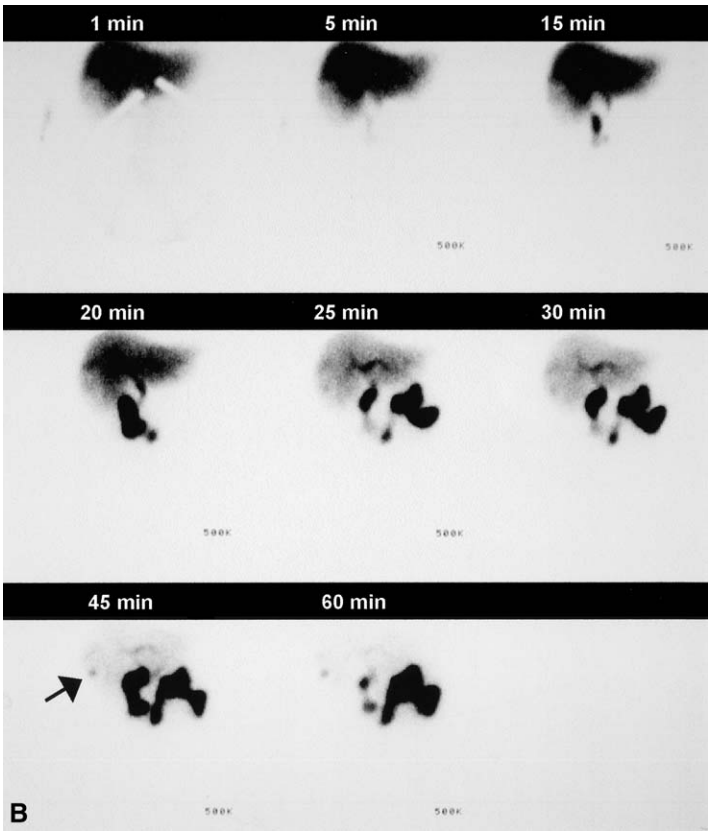
1 min
5 min
15 min
20 min
25 min
30 min
45 min
60 min
B

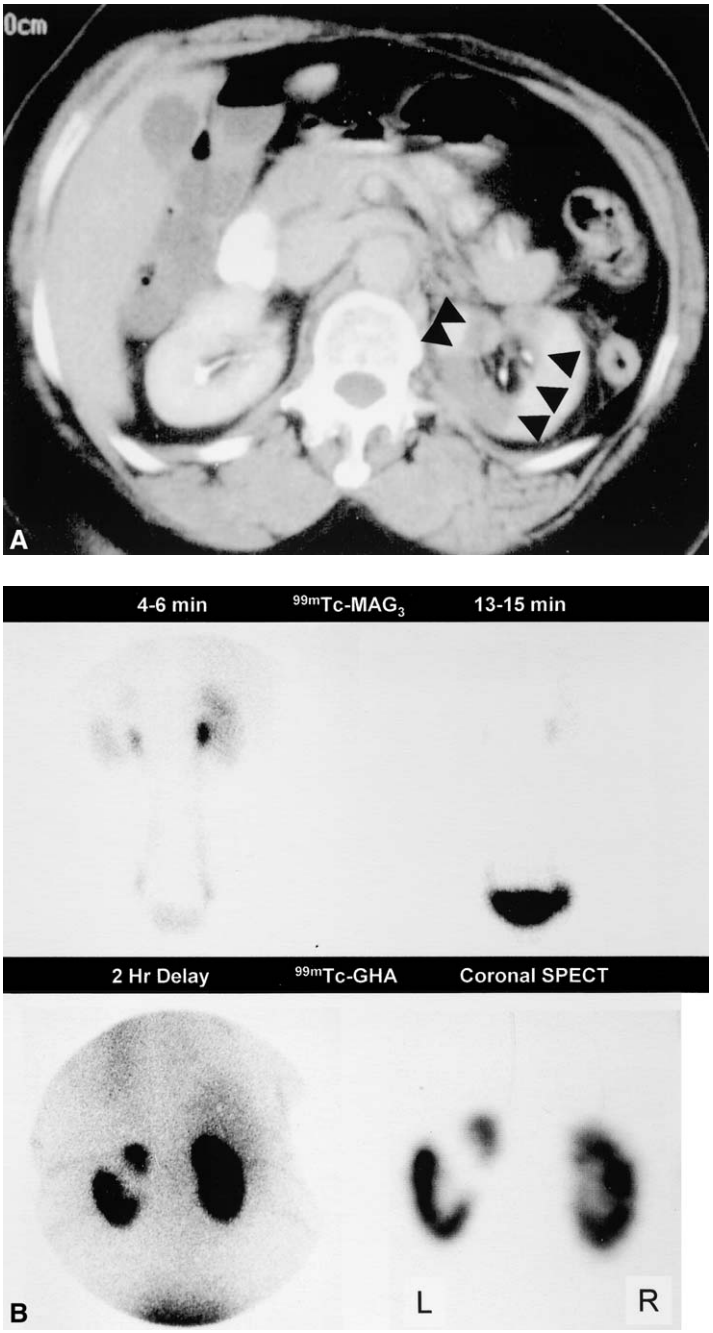

Fig. 9. Left renal infarct in a 68-year-old woman who presented to the emergency room with sudden onset of severe flank pain. CT scan was initially obtained (*A*) demonstrating regions of absent contrast opacification in the left kidney (*arrowheads*). Renal scintigraphy with Tc 99m mercaptoacetyltriglycine was performed 3 days later to evaluate relative and regional function of the kidneys (*B, upper panels*). Representative images demonstrate the suggestion of a cortical defect in the left kidney and an overall diminution of radiotracer concentration on that side. Tc 99m glucoheptonate study was done the following day to define better the extent of infarct (*B, lower panels*). Both planar (*left panel*) and coronal tomographic images (*right panel*) precisely define the extent of the infarct. For the sake of this illustration, the coronal single photon emission CT has been shown in mirror-image to correspond to the other scintigraphic studies.

Common complications of this surgery include presence of bile leak, biliary tree injury, or retained stones [27]. In the postcholecystectomy patient, distorted anatomy or collections may be routinely observed and functional evaluation, as afforded by cholescintigraphy, is especially valuable.

In the case of bile leak, scintigraphy detects the presence, magnitude, and on occasion the approximate location of leak (Fig. 6). The magnitude of leak is judged by comparing the relative flow of bile into the bowel versus into the peritoneum or drains. In the former situation, medical management generally suffices, whereas predominant flow through an artificial pathway likely requires surgical repair. Serial scintigraphy is used to follow resolution of the bile leak, and determine if conservative therapy is sufficient. In cases where the CBD is occluded, biliary scintigraphy visualizes the persistent hepatogram pattern and confirms the diagnosis (Fig. 6A).

Injuries of the solid organs

In the realm of traumatic injuries, scintigraphy may help by providing a functional assessment of damage. As early as 1981, McConnell et al [28] enumerated five organ systems that were effectively studied by radionuclide techniques following blunt trauma: (1) heart, (2) liver, (3) spleen, (4) kidneys, and (5) skeleton [28]. Radionuclide techniques also had a role to play in remotely imaging complications of trauma including infection, cerebrospinal fluid and central nervous system abnormalities, thrombophlebitis, pulmonary emboli, and renal failure. Many of these indications persist today. For example, patients with traumatic injury to the liver may have variable degrees of damage to the biliary tree. US or CT may visualize the primary injury including presence of fluid within the peritoneum; however, the quantitation of bile leak and significance of the injury cannot always be made. Biliary scintigraphy is useful in defining these parameters (Fig. 7) [29]. The injury may be deemed minor if most bile still flows by the common hepatic and bile ducts into the duodenum where the surgeon can adopt a less aggressive stance, conservatively following the injury by repeated scintigraphy and deferring surgical repair. If the leak is major, or no improvement is noted on serial imaging, then surgical repair is needed.

Where a collection of fluid is noted on anatomic imaging in the liver or peritoneal cavity, it can be difficult to differentiate biloma or urinoma from other collections, which can occur in the posttraumatic period. Continuity with the biliary tree can be defined easily on biliary scintigraphy (Fig. 8). Because the relative flow into the collection is typically very small, accumulation of activity into the biloma is slow and minimal, and visualization may only appear on delayed images after maximal wash-out of activity from the normal liver and gradual accumulation of activity within the collection.

Renal scintigraphy is useful in functionally evaluating trauma or vascular insult to the kidney [30,31]. The degree parenchymal disruption may be studied by cortical agents (especially Tc 99m dimercaptosuccinic acid [DMSA]) or the immediate phase of excretory agents (Tc 99m diethylenetriamine pentaacetic acid [DTPA] or Tc 99m mercaptoacetyltriglycine [MAG_3]) (Fig. 9). Collecting system integrity and urodynamics

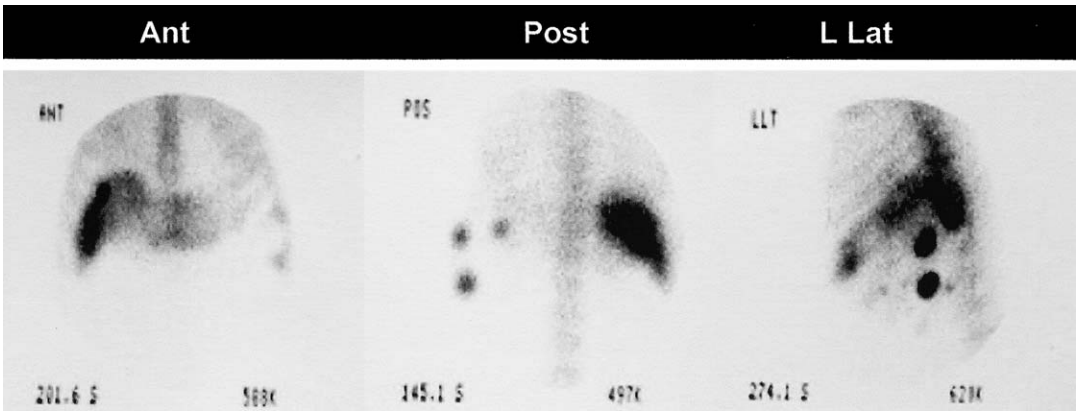

Fig. 10. Splenosis noted on a Tc 99m sulfur colloid study in a patient with cirrhosis and remote history of abdominal trauma and splenectomy. Separation of the lateral aspect of the liver from the rib margin (Helman's sign) is noted, suggesting ascites. A normal spleen is not identified; however, three intense foci of activity in the left upper quadrant of the abdomen represent areas of functioning splenic tissue.

are studied with excreted radiotracers, such as Tc 99m DTPA and Tc 99m MAG_3. Here too, delayed imaging is key to detecting presence of urinoma. Renography has been shown to be of value in identifying the long-term sequellae of renal trauma [32].

In the case of severe trauma to the spleen, a splenectomy may be necessary to prevent exsanguination. As a result of the trauma, or by design of the surgeon, splenic tissue may be distributed within the peritoneum designed to retain phagocytic function and contribute to preserving immunologic defenses [33]. Scintigraphy with Tc 99m sulfur colloid or Tc 99m–labeled crenated RBC can subsequently be used to assess for presence of functional splenic tissue (Fig. 10).

Infection

Radiopharmaceuticals, such as Ga 67 citrate, indium 111 white blood cells, and Tc 99m white blood cells, have become accepted methods of localizing infection in various clinical settings. The limitation of many of these examinations is that they generally require 24 hours or more to complete, which obviates their use in the emergency setting.

One application where these radiotracers can be used successfully is to diagnose suspected appendicitis [34,35]. When using Tc 99m–labeled white blood cells, approximately 2 hours are needed to label the patients' autologous leukocytes and an additional 1 to 2 hours are needed for imaging (Fig. 11). Sensitivity and specificity of the technique have been reported on the order of 98% and 82%, respectively [34].

Because the 2-hour radiopharmaceutical preparation time does delay diagnosis, methods have been developed to use radiolabeled antibodies to label the white blood cells in vivo. Among them, a Tc 99m anti-CD 15 monoclonal antibody (LeuTech, Palatin Technologies, Princeton, New Jersey) is pending approval by the Food and Drug Administration [36]. In this method, the patient is injected with 10 to 20 mCi (adult dose) of Tc 99m–labeled antibody, which binds to leukocytes. Imaging begins immediately, and typically becomes positive within 1 to 2 hours (see Fig. 11). Sensitivity and specificity are reported to be on the order of 90% and 87%, respectively.

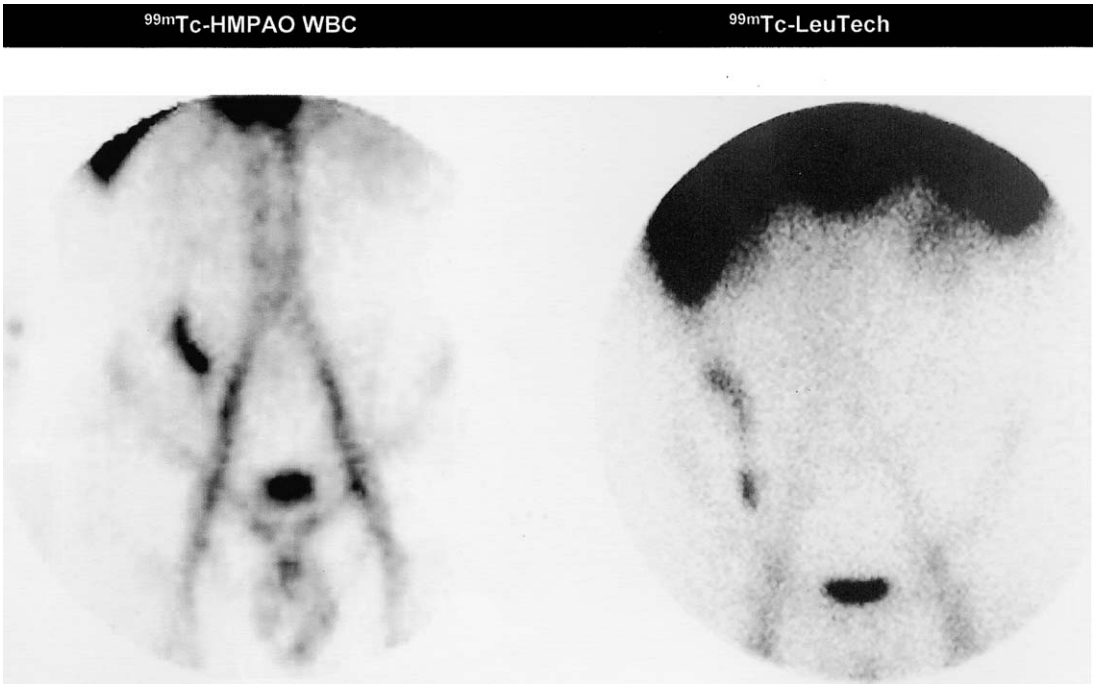

Fig. 11. Representative images in acute appendicitis. In the left panel, Tc 99m hexamethylpropyleneamine oxime–labeled autologous white blood cells have accurately localized an appendiceal abscess in the right lower quadrant of the abdomen. In a different patient injected with Tc 99m LeuTech (*right panel*), appendicitis is also rapidly visualized. The advantage of the latter radiopharmaceutical is that it does not require time and labor-intensive separation and labeling of white blood cells. (Courtesy of Samuel L. Kipper, MD, Oceanside, CA.)

Summary

The imaging evaluation of the acute abdomen has clearly evolved with the introduction of high-resolution imaging techniques, such as CT, US, and MR imaging, leaving scintigraphic examinations an important, though selective, role based on their noninvasive, physiologic, and functional nature. Proper use of these examinations among all the diagnostic methods requires a good understanding of their strengths and limitations.

References

[1] Nusynowitz ML. Radionuclide imaging and acute abdominal disorders [editorial]. JAMA 1974;229:1909.
[2] Ford PV, Bartold SP, Fink-Bennett DM, Jolles PR, Lull RJ, Maurer AH, et al. Procedure guideline for gastrointestinal bleeding and Meckel's diverticulum scintigraphy. Society of Nuclear Medicine. J Nucl Med 1999; 40:1226–32.
[3] Alavi A, Dann RW, Baum S, Biery DN. Scintigraphic detection of acute gastrointestinal bleeding. Radiology 1977;124:753–6.
[4] Ponzo F, Zhuang H, Liu FM, Lacorte LB, Moussavian B, Wang S, et al. Tc-99m sulfur colloid and Tc-99m tagged red blood cell methods are comparable for detecting lower gastrointestinal bleeding in clinical practice. Clin Nucl Med 2002;27:405–9.
[5] McKusick KA, Froelich J, Callahan RJ, Winzelberg GG, Strauss HW. 99mTc red blood cells for detection of gastrointestinal bleeding: experience with 80 patients. AJR Am J Roentgenol 1981;137:1113–8.
[6] Bunker SR, Brown JM, McAuley RJ, Lull RJ, Jackson JH, Hattner RS, et al. Detection of gastrointestinal bleeding sites: use of in vitro technetium Tc 99m-labeled RBCs. JAMA 1982;247:789–92.
[7] Sos TA, Lee JG, Wixson D, Sniderman KW. Intermittent bleeding from minute to minute in acute massive gastrointestinal hemorrhage: arteriographic demonstration. AJR Am J Roentgenol 1978;131:1015–7.
[8] Bunker SR, Lull RJ, Tanasescu DE, Redwine MD, Rigby J, Brown JM, et al. Scintigraphy of gastrointestinal hemorrhage: superiority of 99mTc red blood cells over 99mTc sulfur colloid. AJR Am J Roentgenol 1984;143: 543–8.
[9] Siddiqui AR, Schauwecker DS, Wellman HN, Mock BH. Comparison of technetium-99m sulfur colloid and in vitro labeled technetium-99m RBCs in the detection of gastrointestinal bleeding. Clin Nucl Med 1985;10: 546–9.
[10] Thorne DA, Datz FL, Remley K, Christian PE. Bleeding rates necessary for detecting acute gastrointestinal bleeding with technetium-99m-labeled red blood cells in an experimental model. J Nucl Med 1987;28: 514–20.
[11] Maurer AH, Rodman MS, Vitti RA, Revez G, Krevsky B. Gastrointestinal bleeding: improved localization with cine scintigraphy. Radiology 1992;185:187–92.
[12] Zuckier LS, Patel YD. Incidental abnormalities detected during scintigraphy for gastrointestinal bleeding. Radiographics 1990;10:467–81.
[13] Krynyckyi BR, Zuckier LS, Tatlidil R, Chen WT, Kim CK, Freeman LM. Repeated bleeding scintigraphy may reveal that stationary foci of activity represent sites of active hemorrhage. Clin Nucl Med 2002;27: 25–9.
[14] Smith R, Copely DJ, Bolen FH. 99mTc RBC scintigraphy: correlation of gastrointestinal bleeding rates with scintigraphic findings. AJR Am J Roentgenol 1987;148: 869–74.
[15] Sfakianakis GN, Conway JJ. Detection of ectopic gastric mucosa in Meckel's diverticulum and in other aberrations by scintigraphy: I. Pathophysiology and 10-year clinical experience. J Nucl Med 1981;22:647–54.
[16] Sfakianakis GN, Conway JJ. Detection of ectopic gastric mucosa in Meckel's diverticulum and in other aberrations by scintigraphy: II. indications and methods–a 10- year experience. J Nucl Med 1981;22:732–8.
[17] Sfakianakis GN, Anderson GF, King DR, Boles Jr ET. The effect of gastrointestinal hormones on the pertechnetate imaging of ectopic gastric mucosa in experimental Meckel's diverticulum. J Nucl Med 1981;22: 678–83.
[18] Balon HR, Fink-Bennett DM, Brill DR, Fig LM, Freitas JE, Krishnamurthy GT, et al. Procedure guideline for hepatobiliary scintigraphy. Society of Nuclear Medicine. J Nucl Med 1997;38:1654–7.
[19] Weissmann HS, Frank MS, Bernstein LH, Freeman LM. Rapid and accurate diagnosis of acute cholecystitis with 99mTc-HIDA cholescintigraphy. AJR Am J Roentgenol 1979;132:523–8.
[20] Byrne JJ. Acute cholecystitis. Am J Surg 1959;97: 156–72.
[21] Smith R, Rosen JM, Gallo LN, Alderson PO. Pericholecystic hepatic activity in cholescintigraphy. Radiology 1985;156:797–800.
[22] Kaplun L, Weissmann HS, Rosenblatt RR, Freeman LM. The early diagnosis of common bile duct obstruction using cholescintigraphy. JAMA 1985;254:2431–4.
[23] Pitluk HC, Beal JM. Choledocholithiasis associated with acute cholecystitis. Arch Surg 1979;114:887–8.
[24] Fink-Bennett D, Balon H, Robbins T, Tsai D. Morphine-augmented cholescintigraphy: its efficacy in detecting acute cholecystitis. J Nucl Med 1991;32:1231–3.
[25] Kim CK, Juweid M, Woda A, Rothstein RD, Alavi A. Hepatobiliary scintigraphy: morphine-augmented versus delayed imaging in patients with suspected acute cholecystitis. J Nucl Med 1993;34:506–9.
[26] Saremi F, Jadvar H, Siegel ME. Pharmacologic interventions in nuclear radiology: indications, imaging protocols, and clinical results. Radiographics 2002;22: 477–90.
[27] Estrada WN, Zanzi I, Ward R, Negrin JA, Margouleff D. Scintigraphic evaluation of postoperative compli-

cations of laparoscopic cholecystectomy. J Nucl Med 1991;32:1910–1.
[28] McConnell BJ, McConnell RW, Guiberteau MJ. Radionuclide imaging in blunt trauma. Radiol Clin North Am 1981;19:37–51.
[29] Weissmann HS, Byun KJ, Freeman LM. Role of Tc-99m IDA scintigraphy in the evaluation of hepatobiliary trauma. Semin Nucl Med 1983;13:199–222.
[30] Goldfarb CR, Schoeneman M, Ongseng F, Finestone H. Scintigraphy of renal trauma. Radiology 1990; 174(3 pt 1):896–7.
[31] Lin WY, Wang SJ. Tc-99m DMSA imaging in kidney contusion. Clin Nucl Med 1996;21:144.
[32] Moog R, Becmeur F, Dutson E, Chevalier-Kauffmann I, Sauvage P, Brunot B. Functional evaluation by quantitative dimercaptosuccinic acid scintigraphy after kidney trauma in children. J Urol 2003;169:641–4.
[33] Leemans R, Manson W, Snijder JA, Smit JW, Klasen HJ, The TH, et al. Immune response capacity after human splenic autotransplantation: restoration of response to individual pneumococcal vaccine subtypes. Ann Surg 1999;229:279–85.
[34] Kipper SL. The role of radiolabeled leukocyte imaging in the management of patients with acute appendicitis. Q J Nucl Med 1999;43:83–92.
[35] Colak T, Gungor F, Ozugur S, Bozan H, Yildiz A, Boz A, et al. The value of 99mTc-HMPAO labeled white blood cell scintigraphy in acute appendicitis patients with an equivocal clinical presentation. Eur J Nucl Med 2001;28:575–80.
[36] Rypins EB, Kipper SL, Weiland F, Neal C, Line B, McDonald R, et al. 99m Tc anti-CD 15 monoclonal antibody (LeuTech) imaging improves diagnostic accuracy and clinical management in patients with equivocal presentation of appendicitis. Ann Surg 2002;235: 232–9.

RADIOLOGIC CLINICS OF NORTH AMERICA

Radiol Clin N Am 41 (2003) 1289–1305

Complications of liver transplantation: imaging and intervention

Michael P. Federle, MD*, Vibhu Kapoor, MD

Division of Abdominal Imaging, Department of Radiology, University of Pittsburgh Medical Center, 200 Lothrop Street, Pittsburgh, PA 15213, USA

Orthotopic liver transplantation (OLT) is the accepted treatment for end-stage nonmalignant liver disease. More than 150 centers perform OLT in the United States and the major limitation currently is the lack of an adequate supply of donor organs. As of January, 2003, more than 17,000 people are on a waiting list for liver transplantation and more than 5000 will die while waiting. One- and 3-year survival rates exceed 90% and 80%, respectively, at major transplant centers.

Improvements in surgical techniques and immunosuppressive regimens have reduced substantially the morbidity and mortality of OLT. Nevertheless, OLT recipients are at increased risk for a variety of vascular, biliary, infectious, neoplastic, and other complications. The clinical and laboratory manifestations of post-OLT complications are often nonspecific and may be masked by immunosuppressive drugs. The role of imaging is often critical to diagnosis and prompt treatment of transplant complications. Patients return to their own communities and physicians following recovery from OLT, making it important even for radiologists in smaller communities to become familiar with the spectrum of imaging manifestations of complications of OLT.

Normal posttransplant anatomy

Liver transplantation requires one arterial anastomosis; at least two venous anastomoses (portal vein and inferior vena cava [IVC]); and a biliary anastomosis (Fig. 1). Each of these should be analyzed specifically on post-OLT imaging studies.

The hepatic artery is usually reconstructed using a Carrel patch or "fish-mouth" anastomosis between the donor celiac axis and the recipient vessel at the bifurcation of the right and left hepatic arteries or the branch point of the proper hepatic and the gastroduodenal arteries. Many variations are possible because of congenital anomalies, such as replaced or accessory hepatic arteries, or atherosclerotic narrowing. A donor iliac artery interposition is often used, usually anastomosed to the supraceliac or infrarenal aorta. Communication with the surgeons is vital to ensure proper assessment of posttransplant arterial anatomy.

The portal vein anastomosis is usually end-to-end and is often difficult to identify on imaging. Thrombosis or sclerosis of the portal vein can be identified on pretransplant evaluation and may be addressed by an iliac vein jump graft from the recipient superior mesenteric vein to the donor portal vein (Fig. 2) [1]. Other variations are possible and, again, the radiologist must understand the surgically altered anatomy.

The retrohepatic IVC is often resected during hepatectomy and the donor IVC is anastomosed end-to-end at the suprahepatic and infrahepatic IVC of the recipient. A common variation is the so-called "piggyback" anastomosis in which the recipient retrohepatic IVC is preserved and an anastomosis is created between a common stump of the donor hepatic veins and the recipient IVC [2,3]. On cross-sectional imaging the piggyback donor cava appears as a second intrahepatic IVC; over time the more caudal portion of the donor IVC

* Corresponding author.
E-mail address: federlemp@msx.upmc.edu (M.P. Federle).

0033-8389/03/$ – see front matter
doi:10.1016/S0033-8389(03)00119-2

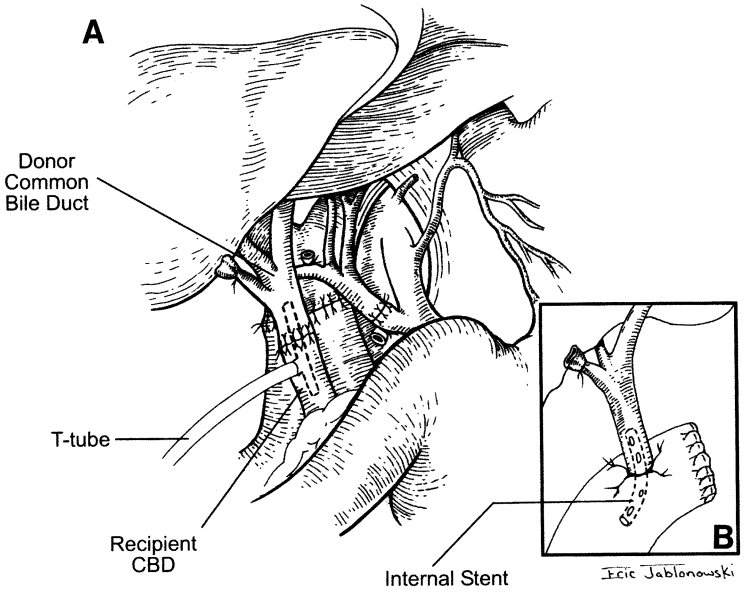

Fig. 1. Standard anastomoses in orthotopic liver transplantation. (*A*) End-to-end anastomoses of donor and recipient bile ducts (over a T tube), portal vein, and between donor celiac artery and recipient vessel (variable). (*B*) If the recipient bile duct is diseased the donor bile duct may be anastomosed to a Roux limb of the bowel over a stent (IVC anastomosis not depicted).

below the hepatic veins often thromboses, usually without clinical sequelae.

The biliary anastomosis is usually (about 70% of the time) end-to-end between the donor and recipient common hepatic ducts (see Fig. 1). Often two cystic ducts are seen on post-OLT cholangiograms and this should not be confused with a biliary leak. The irregular contour of the cystic duct caused by the valves of Heister is a good clue. About 30% of patients have the donor duct anastomosed to a Roux limb of bowel, because of prior disease or scarring of the recipient bile duct. A cholecystectomy is routinely performed as part of the transplant procedure.

Findings that are so common following OLT as to be considered almost normal including the following: right pleural effusion and segmental atelectasis; perihepatic and hepatic fissure fluid including small hematomas [4,5]; right adrenal hematoma (caused by adrenal vein ligation or transection during explantation) [6]; and periportal lymphedema. The latter appears as a lucent halo around portal venous branches and was once thought to be a sign of rejection; subsequent experience indicates that this is caused by disruption of normal lymphatic drainage, and this usually resolves within a few weeks without clinical implications.

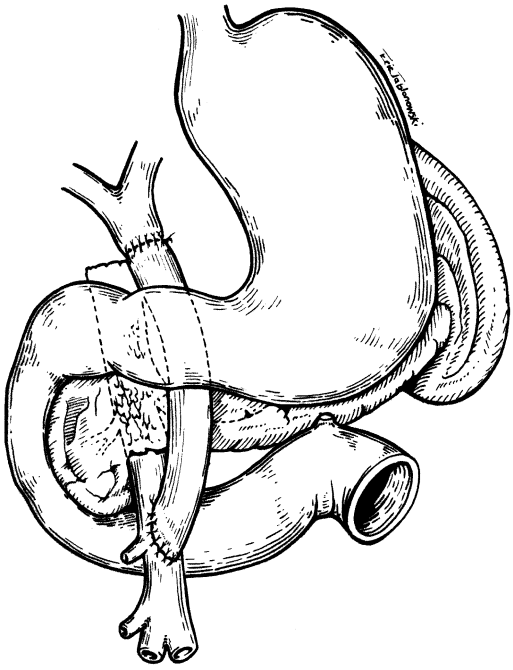

Fig. 2. Iliac jump graft from recipient superior mesenteric vein to donor portal vein. Thrombosis or sclerosis of the portal vein on pretransplant evaluation may necessitate a variation in the usual portal venous anastomosis.

Vascular complications

Vascular complications occur in some 9% of orthotopic whole liver transplantations and a higher percentage of split-liver cases [7–10]. Most are arterial, rather than venous, and these may result in graft failure, bile leak, bleeding, or sepsis. The authors routinely perform Doppler ultrasonography as the initial imaging study to evaluate graft vessels and find the resistive index and systolic acceleration time to be useful parameters (97% sensitivity, 64% specificity) for hepatic artery stenosis or thrombosis [11]. Others have reported less favorable results, and false-positive and false-negative errors can result from rejection, aberrant anatomy, collaterals, and operator inexperience [12].

The authors [13,14] and others [15] have reported excellent results with multislice CT angiography with multiplanar and three-dimensional imaging techniques in patients who have clinical or sonographic findings suggestive of hepatic vascular complications. Water is used as a negative oral contrast material to distend the stomach and duodenum and does not interfere with visualization of the vessels. Depending on the CT scanner being used, axial images are acquired at 1.25- to 3-mm intervals, reconstructed at 1- to 1.3-mm intervals, and are initiated about 25 seconds after beginning the rapid bolus injection (3 to 5 mL/second) of 100 to 125 mL of nonionic contrast media. Newer workstations and software packages allow CT angiographic quality that rivals that of catheter angiography. MR angiography is another alternative for noninvasive diagnosis of vascular complications of OLT [16].

Hepatic artery thrombosis

Hepatic arterial thrombosis is the most common vascular complication of OLT, occurring in 4% to 12% of adult recipients and an even higher percentage of children (Fig. 3) [2,7,11,12]. The clinical manifestations of hepatic artery thrombosis are highly variable, ranging from elevation of hepatic enzyme levels to biliary stricture, necrosis, or leak, to fulminant hepatic necrosis. In adults graft failure and death usually result unless retransplantation is possible. Children and some adults may develop arterial collaterals, which can sustain graft viability, but which

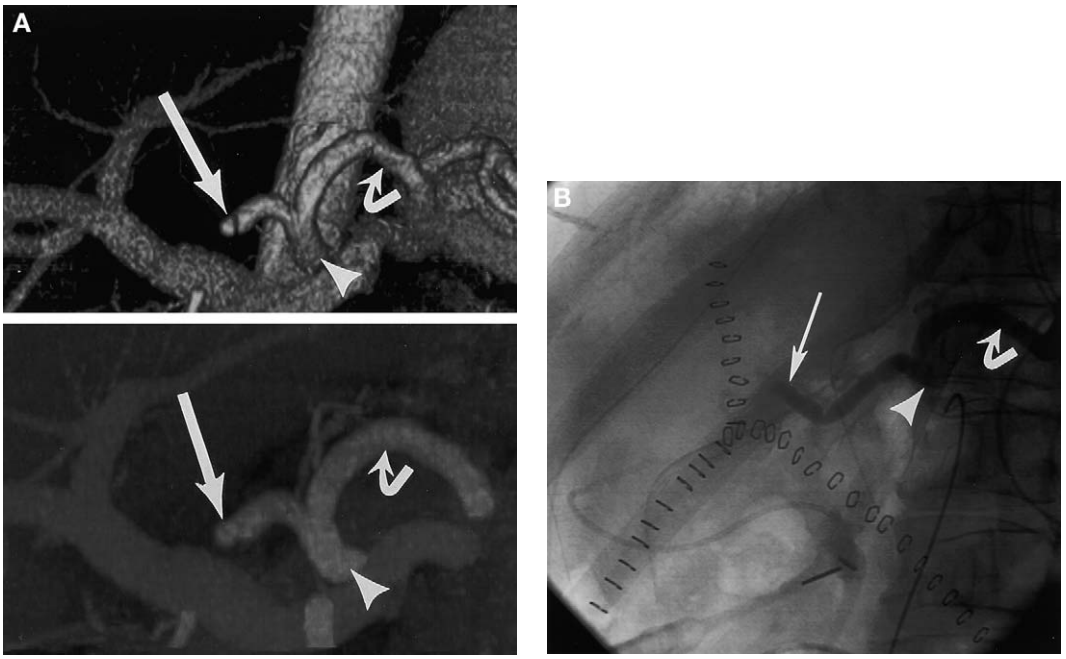

Fig. 3. Hepatic artery thrombosis. (*A*) Shaded-surface reconstruction (*top*) and maximum intensity projection (*bottom*) CT images (anterior view) demonstrate complete occlusion of the hepatic artery at the anastomotic site (*arrow*) 2 days following orthotopic liver transplantation. (*B*) Catheter angiography confirms the hepatic artery occlusion (*arrow*) and the patient underwent retransplantation a day later. Arrowheads mark the celiac artery and curved arrows the splenic artery.

can also lead to false-negative results at Doppler sonography [14,17].

Because the bile ducts are entirely dependent on hepatic arterial supply, thrombosis often results in bile duct necrosis, intrahepatic bilomas, biliary strictures, or hepatic infarct or abscess (Fig. 4). In the setting of transplant dysfunction and any focal hepatic lesion, hepatic artery thrombosis must be considered and evaluated thoroughly.

Intrahepatic bilomas and abscesses can be treated with percutaneous image-guided catheter drainage. In adults such drainage can prolong allograft survival and may uncommonly obviate retransplantation [18]. In children, percutaneous catheter drainage along with antibiotics and hyperoxygenation therapy has been successful in some cases in resolving the intrahepatic collections and avoiding retransplantation. Thrombolytic therapy is not advocated for hepatic artery thrombosis, which frequently occurs in the immediate postoperative period when thrombolytic therapy is contraindicated. By the time of diagnosis of arterial thrombosis hepatic damage is often irreversible.

Hepatic artery stenosis

Arterial stenosis is the second most common vascular complication of OLT, occurring in about 5% of adult cases [7,11,14,16]. The stenosis usually occurs at or near the anastomosis and may result in liver ischemia or biliary stricture [53] and may progress to arterial thrombosis. Stenosis or thrombosis may affect the main hepatic artery or either the left or right branch individually. Sonographic findings depend on the location of the stenosis relative to the sampled site. Peak velocities are increased at the site of stenosis and a peak fellow velocity of more than 2 m/second is very suggestive of stenosis, especially when associated with turbulent flow (spectral broadening of the waveform) [11]. Distal to the arterial anastomosis, a resistive index of less than 0.5 or a systolic acceleration time greater than 0.8 seconds is very suggestive of significant stenosis (Fig. 5). These signs, however, are not reliable indicators of hepatic artery thrombosis for the first 48 hours following transplantation; by several days after OLT, the waveforms are more reliable [11,12,19–21].

CT angiography has proved quite useful in diagnosing arterial stenosis (Fig. 6) [1,14,15]. The ability to rotate in space the three-dimensional arterial anatomy greatly facilitates recognition of the arterial stricture, especially when the hepatic artery is redundant and tortuous.

Catheter angiography remains the standard of reference for diagnosing hepatic arterial complications of OLT and also can be used for therapy [22,23]. Transluminal angioplasty and stent placement have been successful in relieving arterial stenosis with resolution of clinical and biochemical

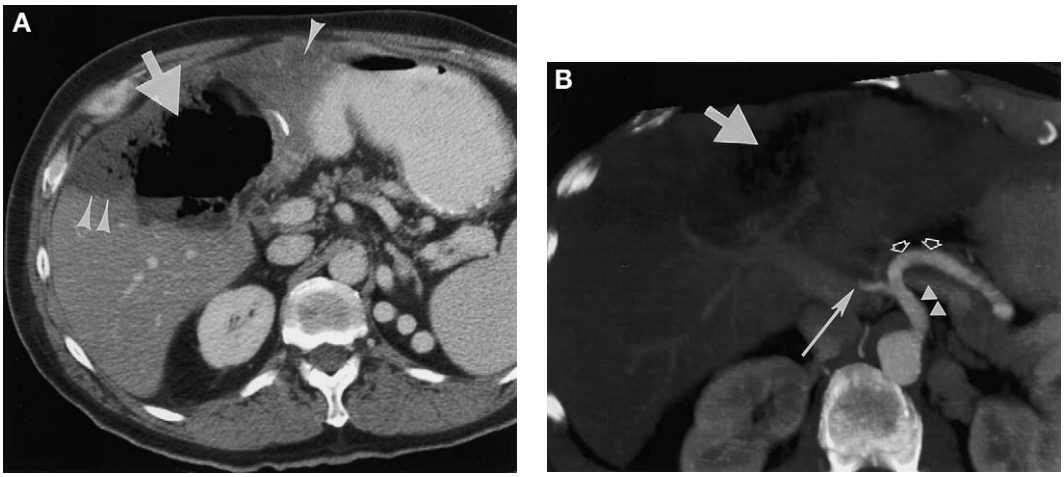

Fig. 4. Hepatic artery thrombosis causing hepatic abscess and infarct. (*A*) Axial CT shows a large gas-containing cavity (*arrow*) with fluid-level in the left hepatic lobe consistent with an abscess. Low-attenuation peripheral areas with sharp straight margins (*arrowheads*) suggestive of infarcts are also evident. (*B*) Maximum-intensity projection CT image 2 days later following percutaneous drainage of the abscess shows occlusion the hepatic artery (*long thin arrow*) with a decrease in size of the abscess cavity (*short solid arrow*) in the left lobe. Arrowheads mark the celiac artery and open arrows the splenic artery.

abnormalities, resulting in graft salvage and avoidance of retransplantation (Fig. 7). Many factors influence the choice of angioplastic versus surgical repair of hepatic arterial stenosis including time of diagnosis following OLT, tortuosity of the artery, and proximity to branch vessels.

Hepatic artery pseudoaneurysm (Figs. 8, 9) is a rare complication of OLT and may result from infection, as a complication of transluminal angioplasty, or after percutaneous liver biopsy [24]. Rupture of the pseudoaneurysm may result in life-threatening intrahepatic or intra-abdominal hemorrhage. Therapeutic options include exclusion by stent graft, coil embolization, and surgical resection.

Portal vein stenosis or thrombosis

Portal vein abnormalities develop in about 1% to 3% of transplant recipients [8,10,16]. Predisposing causes include faulty surgical technique, a mismatch in size between donor and recipient portal veins, and hypercoagulable states. Results include manifesta-

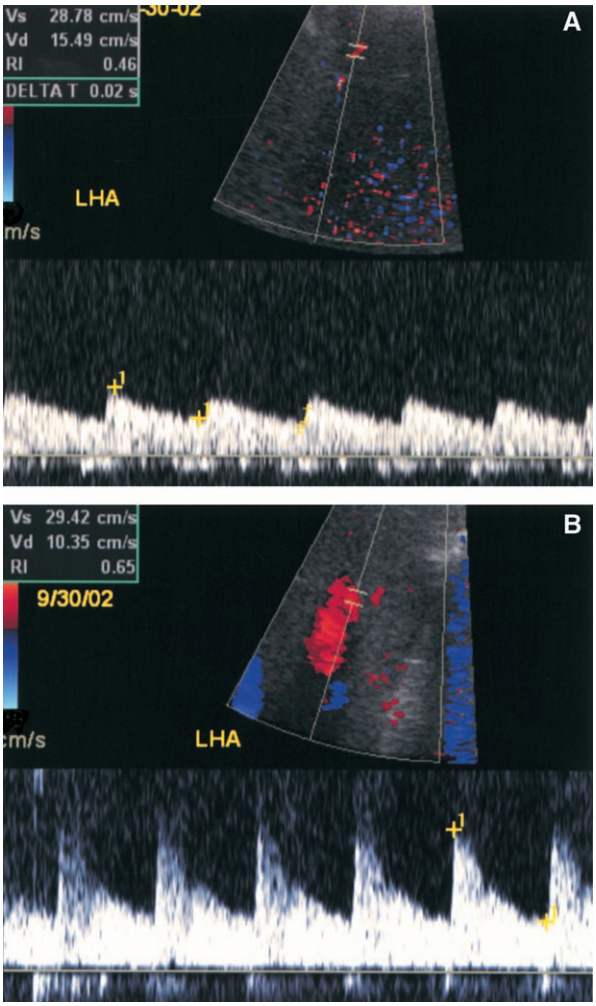

Fig. 5. Color Doppler of hepatic artery stenosis before (*A*) and after (*B*) angioplasty. Duplex Doppler of the left hepatic artery shows a typical low resistive index waveform (RI = 0.46) suggestive of proximal stenosis (*A*) with normalization of the waveform following percutaneous angioplasty (*B*) (RI = 0.65).

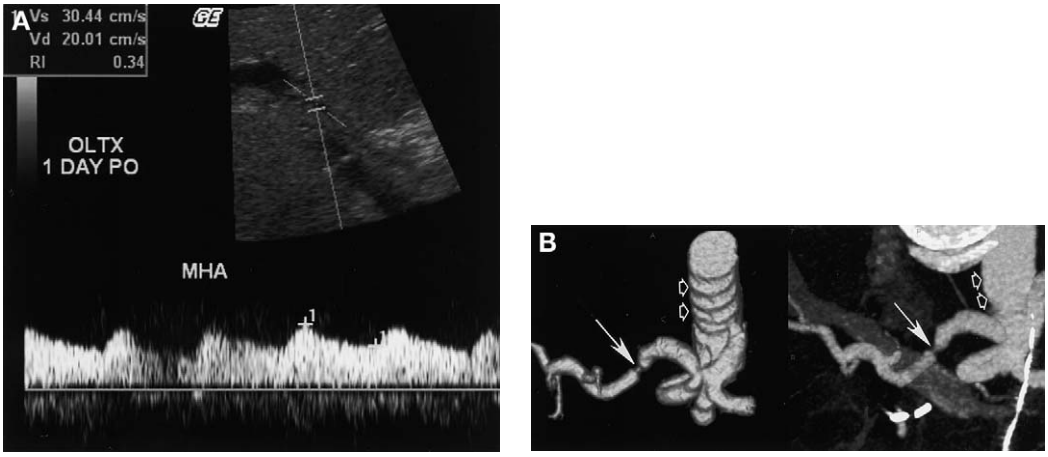

Fig. 6. Hepatic artery stenosis. (*A*) Color Doppler appearance of hepatic artery stenosis with prolonged systolic upstroke (parvus-tardus waveform) and low resistive index (RI = 0.34) for the main hepatic artery. (*B*) Shaded-surface reconstruction (*left*) and maximum intensity projection (*right*) CT images (anterosuperior view) confirm severe stenosis of the hepatic artery at the anastomotic site (*arrow*). Open arrows mark the aorta.

tions of portal hypertension, such as ascites, edema, variceal bleeding, and liver failure.

CT angiography in the portal venous phase has successfully demonstrated portal vein stenosis, thrombosis, and intraluminal clot (Fig. 10) [1,15]. Definitive diagnosis may require transhepatic direct venography, which also allows measurement of the pressure gradient across the venous stenosis (> 5 mm Hg being considered significant) [25]. The transhepatic access also may facilitate thrombectomy, angioplasty, and stent placement.

Inferior vena cava stenosis or thrombosis

Inferior vena cava complications occur in less than 1% of transplant recipients, and usually result from surgical mishaps or hypercoagulable states [10,26]. As noted previously, thrombosis of the donor IVC below the hepatic veins in the setting of a piggyback IVC anastomosis should not be considered a complication or raise clinical concern in most cases. Mere size discrepancy between the donor and recipient IVCs or displacement and compression by graft swelling should not be considered diagnostic of an IVC complication. In the rare event of true stenosis, confirmed by pressure gradient across a stenosis, balloon angioplasty can be considered (Fig. 11) [25].

A rare complication, which may be encountered more frequently with the piggyback technique or with split liver transplantation, is hepatic vein or IVC

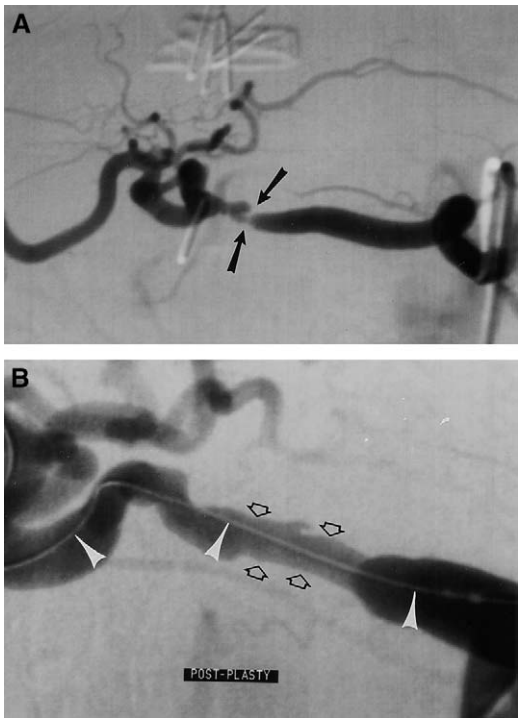

Fig. 7. Hepatic artery stenosis treated with percutaneous angioplasty. Catheter angiography 4 months following liver transplantation (*A*) shows severe hepatic artery stenosis (*arrows*) at the anastomotic site. Following percutaneous balloon angioplasty (*B*) there is marked improvement in the caliber of the stenotic segment of the hepatic artery (*open arrows*). Arrowheads mark the angioplasty catheter.

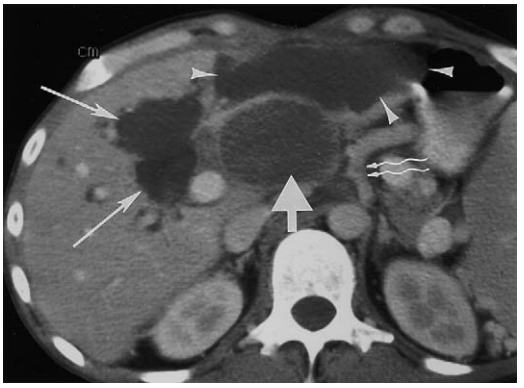

Fig. 8. Thrombosed hepatic artery pseudoaneurysm with bile duct necrosis and hepatic infarct 6 years post–hepatic transplantation. Large, oval, low-attenuation cystic mass at the porta hepatic (*short arrow*) abutting the celiac axis (*curved double arrows*) represents a thrombosed pseudoaneurysm. Sharply defined, low-attenuation, right hepatic lobe lesion (*long thin arrows*) is a characteristic appearance of bile duct necrosis. Also note the large peripheral left lobe infarct (*arrowheads*).

occlusion [2,3,27]. The poor venous drainage of the liver can result in an acute Budd-Chiari syndrome with liver dysfunction and ascites along with mottled perfusion of the liver (Fig. 12).

Arterioportal fistula

Intrahepatic arterioportal fistula is a relatively common complication of percutaneous liver biopsy, whether of the native or transplanted liver (Fig. 13).

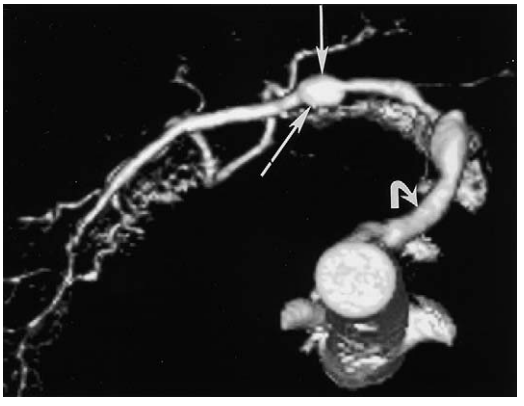

Fig. 9. Hepatic artery pseudoaneurysm. Shaded-surface reconstruction (superior view) CT image of the celiac axis (*curved arrow*) in another patient demonstrates a smaller patent pseudoaneurysm (*straight arrows*) close to the hepatic artery anastomotic site.

The authors believe that this occurs less frequently when sonography is used to guide the biopsy and to avoid large vessels. Most are transient and of little clinical concern, tending to close spontaneously within a few weeks [28]. Fistulas may be mistaken for hypervascular masses on imaging but diagnosis can be made accurately using the following criteria: arterial-phase CT (or MR imaging) demonstrates early filling of peripheral portal venous branches at a time before superior mesenteric and splenic veins are unopacified. There is often a transient hepatic attenuation difference, consisting of a peripheral wedge-shaped area of hyperenhanced liver during the hepatic arterial phase of CT (or MR imaging) that is isoattenuating to liver on nonenhanced and portal venous-phase imaging. The transient hepatic attenuation difference is caused by enhancement of the liver parenchyma that is perfused by contrast medium passing from the high-pressure arterial vessels into the lower-pressure portal venous branches [28]. Absence of a spherical mass accompanying the fistula or shunt is also an important finding.

Biliary complications

Biliary complications following OLT occur in 6% to 34% of patients with the higher rates in children and partial liver recipients, and are the second most frequent cause of graft dysfunction, exceeded only by rejection [29–34]. Most biliary complications become evident during the first 3 months after transplantation, although some strictures and stones develop months to years later.

Patients with a duct-to-duct anastomosis have a T tube in place for several months after OLT that

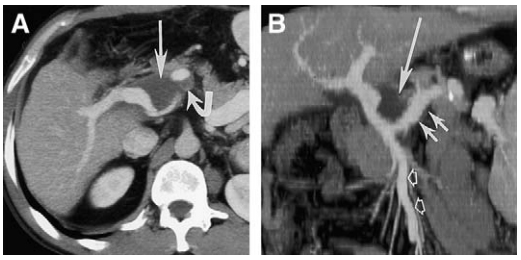

Fig. 10. Portal vein aneurysm with thrombosis. Maximum-intensity projection images, axial (*A*) and coronal views (*B*), in a patient 13 years following liver transplantation show portal vein aneurysm with a large subocclusive thrombus at the portal confluence (*long arrow*) extending into the superior mesenteric vein (*curved arrow*). Double arrows mark the splenic vein and open arrows the superior mesenteric vein.

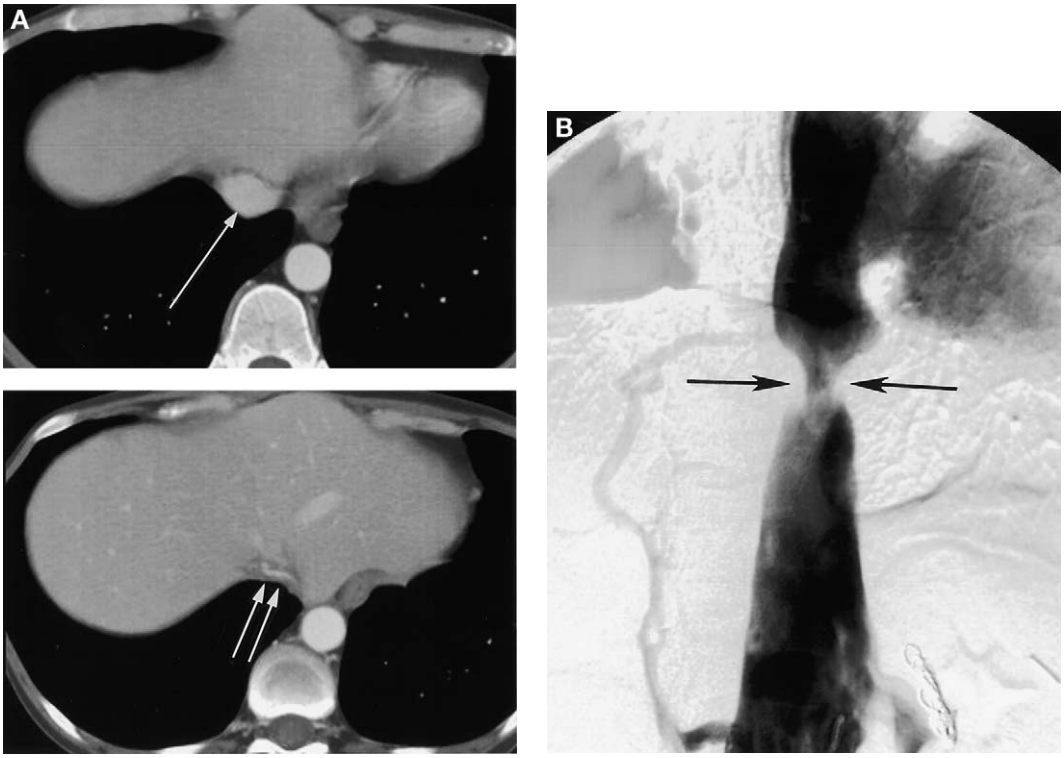

Fig. 11. Inferior vena cava stenosis. (*A*) Axial CT images of the liver demonstrate normal IVC caliber (*single arrow*) cranially with a sudden decrease in diameter (*double arrows*) inferiorly suggesting IVC stenosis at the anastomotic site. (*B*) IVC angiogram confirmed the presence of a hemodynamically significant stenosis (*arrows*) at the anastomotic site.

can be accessed for cholangiography, which is performed routinely at intervals following surgery (12 days, 6 weeks, and 3 months) and immediately if liver dysfunction occurs. Patients who have a duct-enteric anastomosis are evaluated by sonography or MR cholangiopancreatography [35,36]. Intrahepatic biliary dilatation often does not occur within the transplanted liver and its absence does not exclude biliary obstruction.

Some 6% of OLT recipients develop some form of particulate debris with the biliary tree [33]. Nonobstructing concretions on the T tube are of little concern and usually clear with removal of the T tube 3 months following OLT. Necrotic debris or a cast of sloughed mucosa is strongly suggestive of hepatic artery occlusion (Fig. 14). Discreet stones constitute one third of filling defects and require surgical biliary reconstruction in most cases. Some stones can be accessed by transhepatic or endoscopic cholangiography and can either be crushed or retrieved by a metallic stone basket. Some patients with biliary sludge have no apparent underlying etiology and may respond favorably to flushing of the bile ducts or revision of the anastomosis.

Anastomotic biliary strictures are visualized commonly but may not require intervention in the absence of proximal ductal dilatation or liver dysfunction (eg, elevated serum bilirubin or alkaline phosphatase). True strictures are often amenable to endoscopic or transhepatic balloon dilatation, with or without stent placement (Fig. 15) [37,52]. Anastomotic strictures and leaks are substantially more common following partial liver transplantation [30,31].

Nonanastomotic strictures occur in about 10% of patients [29,34,38] and occur at the common hepatic duct bifurcation or peripheral intrahepatic ducts with equal frequency. Among the potential causes are hepatic artery stenosis or thrombosis, ductopenic rejection, infectious cholangitis, and recurrent primary sclerosing cholangitis (Fig. 16) [29,34,39,40]. A search for the etiology should be made but no apparent cause can be identified in up to one-third

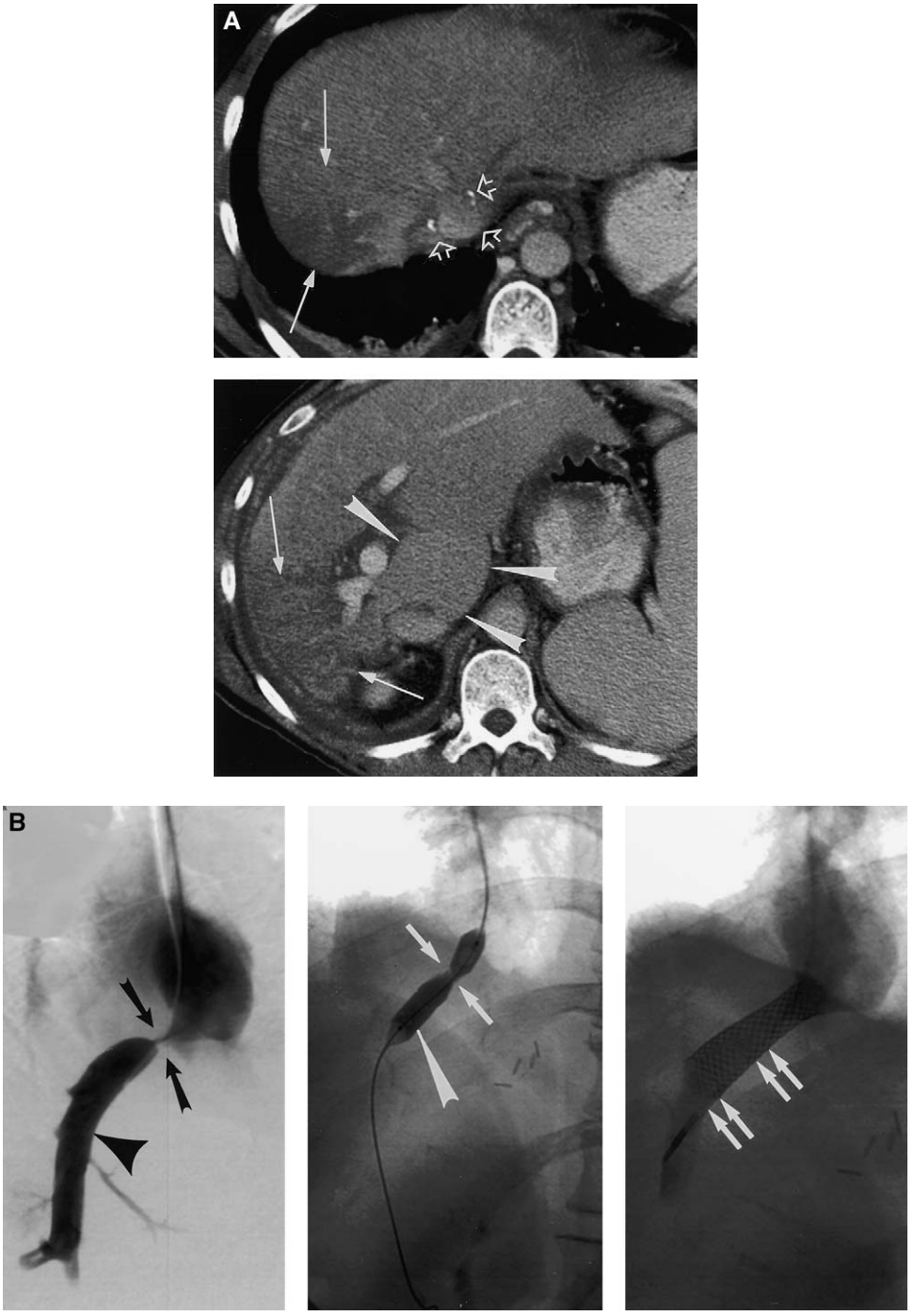

Fig. 12. Budd-Chiari syndrome caused by right hepatic vein stenosis. (*A*) Axial CT images of the liver, during the venous phase, show low-attenuation and atrophy of the right hepatic lobe (*arrows*) with mild caudate lobe hypertrophy (*arrowheads*). Open arrows mark the IVC anastomotic site. (*B*) Selective right hepatic venogram (*black arrowhead*) demonstrates severe stenosis (*black arrows*) of the proximal right hepatic vein. Balloon angioplasty shows marked ''waisting'' (*white single arrows*) of the angioplasty balloon (*white arrowhead*). A stent (*double white arrows*) was placed across the stenosis.

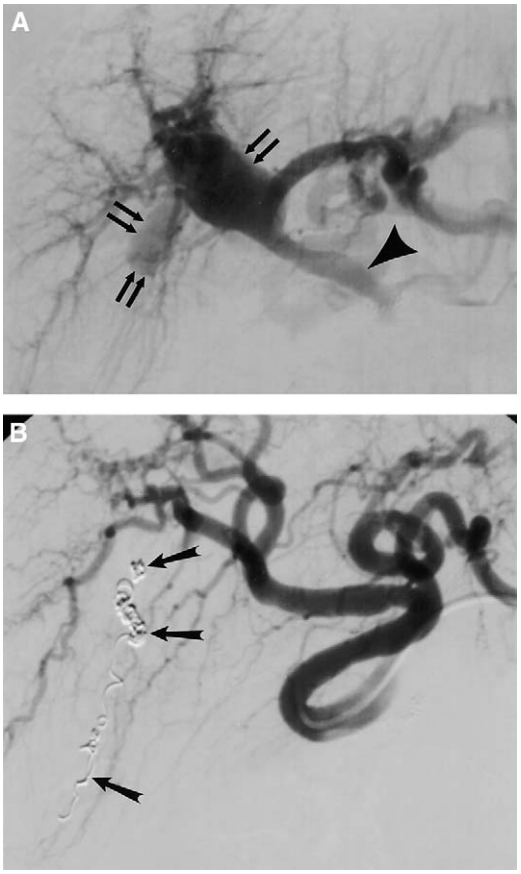

Fig. 13. Arterioportal fistula causing portal hypertension 7 years after liver transplantation. Celiac arteriogram (*A*) demonstrates early filling of a dilated right portal vein (*double arrows*) with reflux into the main portal vein (*arrowhead*) responsible for the patient's portal hypertension. Repeat celiac arteriogram (*B*) following coil embolization of the feeding right hepatic arterial branch (*single arrows*) shows no opacification of the portal venous system.

of cases. Percutaneous or, less commonly, endoscopic stricture dilation affords at least short-term palliation in a minority of patients.

The prevalence of bile leak following OLT is about 4% and the prognosis varies substantially according to its site and etiology [30,32,38,41]. Common clinical signs include fever and signs of cholangitis or peritonitis or increasing bilirubin or liver enzyme levels. Cholangiography is the definitive means of diagnosing bile leak, but is only achieved easily in those with a T tube in place (Fig. 17). Radionuclide (Tc 99m HIDA) and MR cholangiopancreatography are alternative tools; MR imaging diagnosis of leak is demonstrated well following intravenous administration of mangafodipir (Teslascan, Amersham, Princeton, New Jersey), a hepatobiliary contrast agent (Fig. 18). Leak at the site of T-tube entry responds very favorably to endoscopic sphincterotomy and temporary placement of a stent. Anastomotic biliary leaks are more common following duct-enteric, as opposed to duct-duct, anastomosis [41]. These may respond to endoscopic stent placement, but most require surgical revision of the anastomosis. Delays in diagnosis and therapy frequently result in sepsis and death. Nonanastomotic leaks resulting from biliary necrosis indicate hepatic artery thrombosis and usually require retransplantation. Intrahepatic bile leaks may result from biopsy and often resolve following bile duct stenting.

A rare cause of biliary obstruction is mucocele of the cystic duct remnant. Cross-sectional imaging demonstrates a water density spherical lesion adjacent to the common duct, and cholangiography shows extrinsic compression of the common duct [42].

Bowel obstruction

Orthotopic liver transplantation is complicated by bowel obstruction in 1% cases, with adhesions and some form of hernia being the two most common causes, of almost equal frequency [43]. Obstruction caused by adhesions is a diagnosis made after excluding other recognizable causes, such as an incisional hernia or tumor. Patients who have had a biliary-enteric anastomosis are at risk for developing an internal hernia. Creation of the Roux limb results in at least one mesenteric defect which, even after surgical repair, may open to permit herniation and obstruction of small intestinal segments. The herniated bowel may twist and the resulting volvulus is particularly prone to bowel ischemia. The mesenteric whirl sign, clusters of dilated small bowel, and central displacement of colon are among the signs of internal hernia that have been reported [43].

Liver ischemia

Two distinct patterns and causes of graft ischemia are recognized [15,16]. In the postoperative period peripheral subcapsular irregular foci of poor enhancement are seen, which are usually attributed to ischemic injury during the harvesting and preservation period before OLT (Fig. 19). These usually cause no significant graft dysfunction and resolve within a few weeks, only rarely resulting in scars that may calcify.

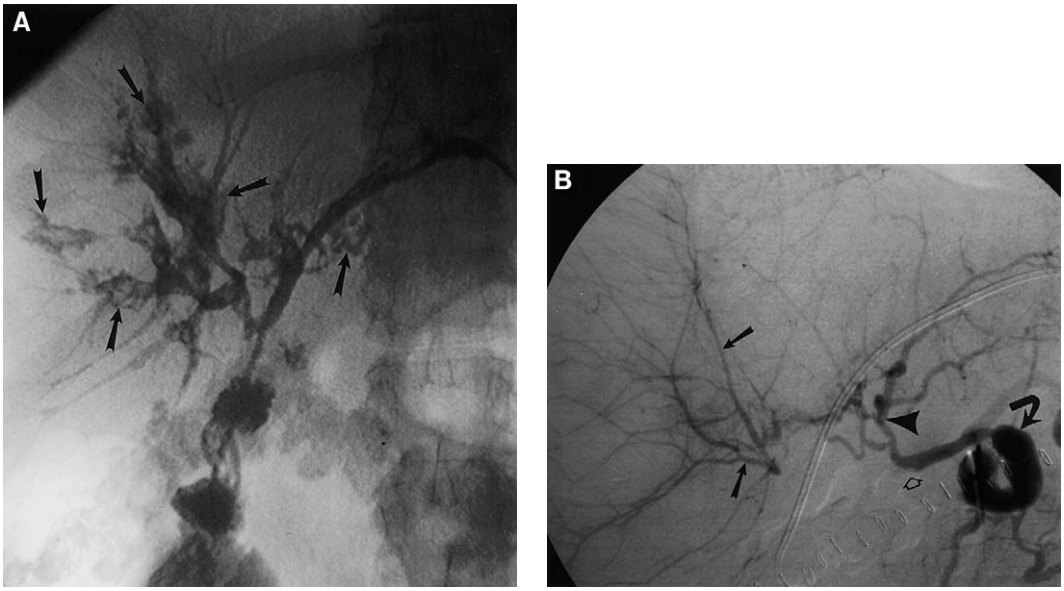

Fig. 14. Hepatic artery thrombosis causing bile duct necrosis. Patient developed fever and elevation of hepatic enzymes 8 months following orthotopic liver transplantation. (*A*) Cholangiography demonstrates marked irregularity of the intrahepatic bile ducts with extravasation of contrast (*arrows*) suggesting biliary necrosis with pericholangitic abscesses. (*B*) Catheter angiography demonstrates recipient splenic (*curved arrow*) to donor hepatic artery anastomosis with occlusion of the right hepatic artery (*open arrow*) at its origin and filling of the distal right hepatic arterial branches (*straight arrows*) through collaterals from the left hepatic artery (*arrowhead*).

Other parenchymal foci of poor enhancement, whether central and irregularly shaped or peripheral and wedge-shaped, raise the concern for liver infarction caused by hepatic artery thrombosis (see Figs. 4, 8) This is often accompanied by bile duct stricture or necrosis. The infarcted liver may liquefy and may become infected, usually accompanied by signs of sepsis and hepatic dysfunction. Percutaneous catheter drainage can prolong allograft survival but retransplantation is usually required [18].

Abscesses and fluid collections

The transplant patient is susceptible to a variety of fluid collections including localized ascites, bilomas, hematomas (Fig. 20), and abscesses. Diagnosis of these fluid collections is usually by CT or ultrasound, but image-guided aspiration is often required for definitive diagnoses and therapy. Frankly purulent collections are treated with indwelling pigtail catheters of a caliber sufficient to drain the fluid, and are usually left in place until daily drainage is less than 20 mL. Smaller and less obviously purulent collections may be treated by needle aspiration. Surgeons sometimes place oxidized cellulose (Surgicel, Johnson and Johnson Medical, Arlington, Texas) at a site of bleeding to achieve hemostasis. This has the appearance of a mottled gas collection (Fig. 21) and can be mistaken for an abscess in the absence of appropriate communication.

Frankly hemorrhagic fluid should always prompt a search for a bleeding source. Catheter angiography and coil embolization are valuable techniques, although hemodynamic instability may require urgent re-exploration to identify and occlude the bleeding site.

Infections

Infectious complications remain the most significant causes of morbidity and mortality in patients undergoing OLT [44]. Predisposing factors include pretransplant infections, such as spontaneous bacterial peritonitis, tuberculosis, and HIV. Posttransplant factors include nosocomial infections, particularly those caused by indwelling central venous catheters, zendotracheal tubes, and Foley catheters.

Immunosuppression is the most critical factor that predisposes patients to infection following OLT. Drug regimens have evolved in an attempt to achieve more specific control of organ rejection with the least impairment of overall immunity.

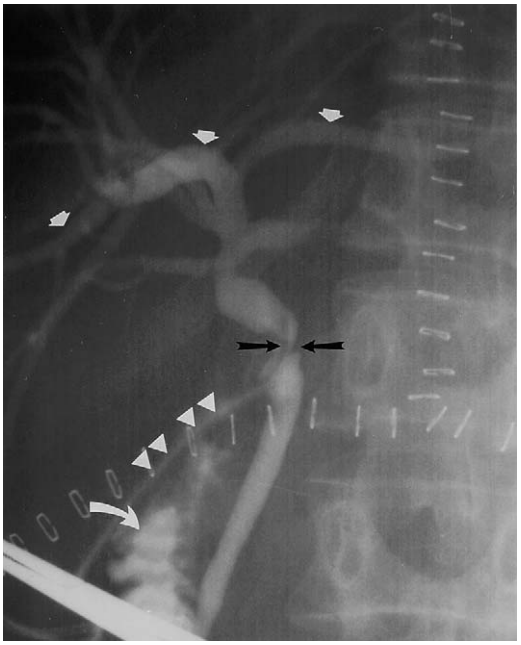

Fig. 15. Biliary stricture. T-tube (*arrowheads*) cholangiography shows severe biliary stricture (*black arrows*) at the anastomotic site during the early postoperative period. There is mild proximal dilatation of the intrahepatic bile ducts (*white arrows*). Curved arrow marks contrast in the small bowel.

In addition to the usual bacterial and fungal agents, several viral infections are of particular importance in OLT patients. Reactivation of hepatitis B or C may infect and damage the transplanted liver. Cytomegalovirus colonization is nearly ubiquitous in immunosuppressed patients; proof of pathogenesis requires biopsy or bronchoalveolar lavage. Cytomegalovirus infection may damage almost any organ; frequent manifestations include cholangitis and enterocolitis (Fig. 22), and these typically develop in the intermediate period after transplantation (30 to 180 days).

Epstein-Barr virus and other herpes viruses are of particular interest, because these account for the striking increase in the prevalence of epithelioid and lymphoid malignancies in transplant recipients (Table 1) [45,46].

Screening of both the potential donor and the recipient is important and many centers obtain serologies for cytomegalovirus; Epstein-Barr virus; herpes simplex virus; hepatitis A, B, and C; and HIV. Knowledge of donor and recipient status for these viruses allows anticipation of infection and complications and helps to identify those who might benefit from prophylactic regimens. Prophylactic regimens vary among transplant centers but these have achieved some success in reducing the prevalence and severity of perioperative and long-term infections by various viral, fungal, protozoan (eg, *Pneumocystis carinii*), bacterial, and mycobacterial agents.

Malignancy

In the early experience with transplantation it was hoped that patients who had malignancy limited to the liver could be cured by OLT. Unfortunately, there was an unacceptably high rate of recurrence for patients with cholangiocarcinoma and hepatocellular carcinoma. More recent studied have shown that careful selection of patients with hepatocellular carcinoma (single tumor $\leq$ 5 cm in diameter or several tumors $<$ 3 cm each) results in graft and patient survival rates no different than for patients with the same degree of liver disease but without tumor [47]. Accurate diagnosis of the presence and extent of tumor has become more important than ever. Multiphasic CT and MR imaging are comparable in this regard. The mean time to recurrence of hepatocellular

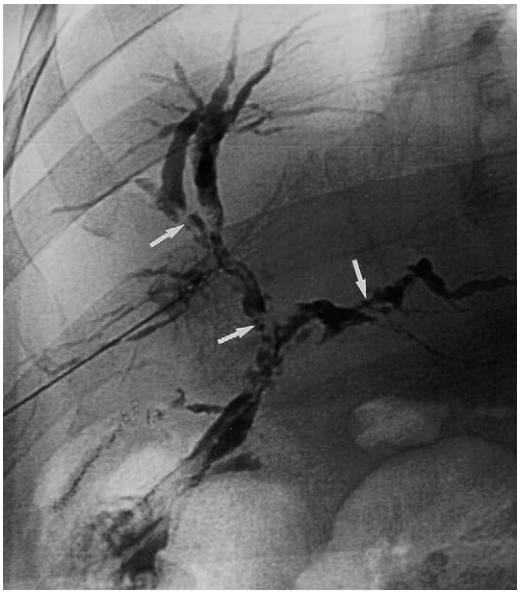

Fig. 16. Recurrent primary sclerosing cholangitis 5 years following hepatic transplantation. Percutaneous transhepatic cholangiography demonstrates scattered, irregular, short-segment narrowing of the intrahepatic bile ducts (*arrows*) with intraluminal filling defects typical of primary sclerosing cholangitis. Similar changes may be seen with bile duct necrosis secondary to hepatic artery thrombosis and biopsy is essential for diagnosis.

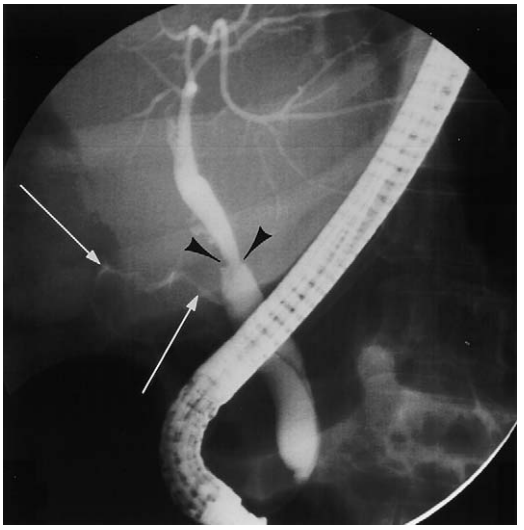

Fig. 17. Bile leak. Endoscopic retrograde cholangiography demonstrates a bile leak along the course of the prior T tube (*arrows*) 4 months following liver transplantation. A change in caliber between the recipient and donor bile ducts (*arrowheads*) is evident, a normal appearance.

carcinoma is 39 months and the most frequent sites are the lung and the liver allograft [47].

Recurrence of hepatocellular carcinoma, cholangiocarcinoma, or any other epithelial malignancy tends to be very aggressive because of the immune-suppressed condition of the patients. Immunosuppression also results in an absolute increased incidence of squamous cell carcinomas (skin, cervix, and so forth) and non-Hodgkin's lymphoma [48]. OLT patients, especially those with hepatitis C, Epstein-Barr virus, or cyclosporine treatment, have a mark-

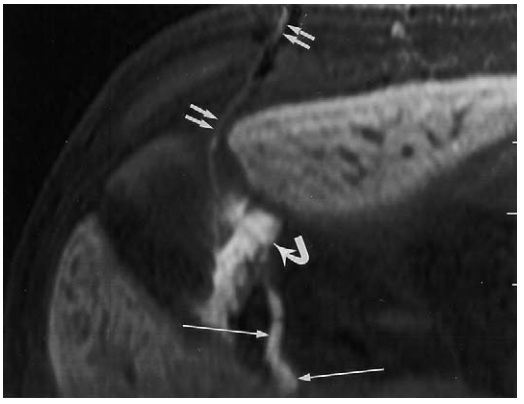

Fig. 18. Bile leak. Axial curved-reformatted mangafodipir trisodium–enhanced cholangiographic MR image shows bile leak (*curved arrow*) in the subhepatic space. The curved-reformatted image shows the entire length of the track from the intrahepatic ducts (*arrows*) to the drainage catheter (*double arrows*).

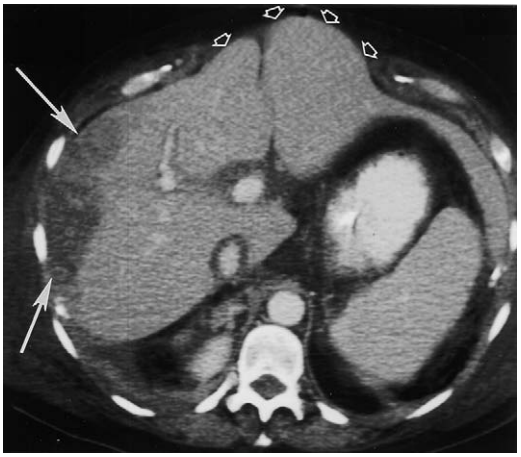

Fig. 19. Pressure necrosis in recipient liver. Axial CT 1 day following liver transplantation shows a peripheral area of low attenuation in the right lobe (*arrows*) caused by injury during transplantation because the transplanted liver was large compared with the abdominal cavity. Note midline herniation of portions of the left lobe (*open arrows*).

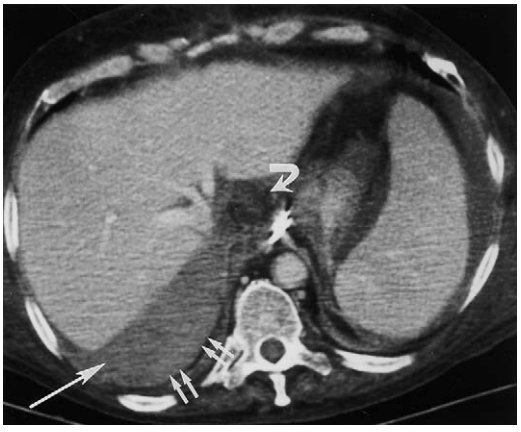

Fig. 20. Perihepatic hematoma. Axial CT of the liver shows a large fluid collection in the posterior perihepatic space (*single arrow*) that had increased in size compared with a prior CT (not shown). Subtle high density seen in the periphery (*double arrows*) suggests it to be a hematoma rather than a simple postoperative serous collection. Oozing from IVC anastomotic site (*curved arrow*) was the cause of the hematoma.

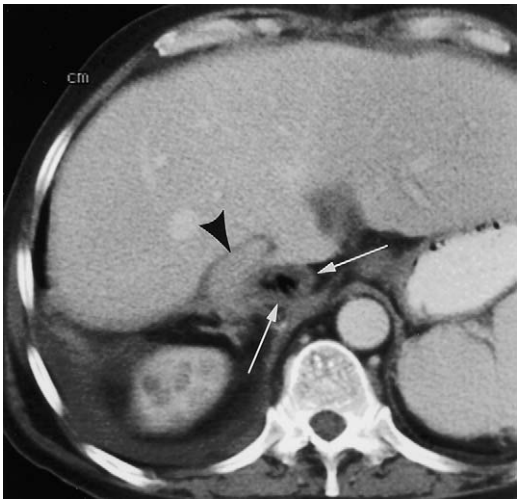

Fig. 21. Oxidized regenerated cellulose or Surgicel (Johnson and Johnson Medical, Arlington, Texas) simulating abscess. Axial CT of the liver shows a small gas collection with surrounding soft tissue thickening (*arrows*) posterior to the IVC (*arrowhead*). This was echogenic on sonography (not shown). Operative notes revealed that surgeons had used Surgicel to achieve hemostasis in this region and this was not an abscess.

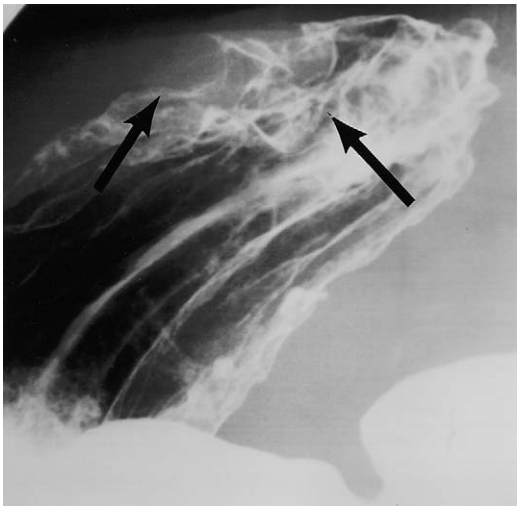

Fig. 22. Cytomegalovirus gastritis following hepatic transplantation. Double-contrast barium study of the gastric fundus demonstrates marked thickening of the mucosal folds (*arrows*). Endoscopic biopsy of this region revealed cytomegalovirus gastritis.

Table 1
Posttransplant malignancies

Tumor type	Relative increase in incidence
Uterine cervix	4 to 14 times
Skin cancer	7 to 40 times
Lip cancer	29 times
Vulva and perineum	100 times
Non-Hodgkin's lymphoma	20 to 350 times
Kaposi's sarcoma	400 to 500 times

From Penn I. The changing pattern of posttransplant malignancies. Transplant Proc 1991;23:1101–3;with permission.

edly increased rate (2% to 2.5% of all OLT recipients) of posttransplantation lymphoproliferative disease (see Table 1) [46,49]. This is a spectrum of disease ranging from a polyclonal proliferation of lymphoid cells, which may respond to titration of the immunosuppressive regimen and antiviral medication, to an aggressive B cell lymphoma. Posttransplantation lymphoproliferative disease may result in lymphadenopathy and visceral masses in any part of the body [51]. Typical abdominal findings are adenopathy, focal bowel masses (Fig. 23), and focal hepatic or porta hepatis masses that are often hypoechoic on sonography and hypovascular or hypoattenuating on CT (Fig. 24). Thoracic manifestations of posttransplantation lymphoproliferative disease include multiple pulmonary nodules, adenopathy, and persistent air space consolidation. Multifocal brain masses, especially in the periventricular white matter, are also a

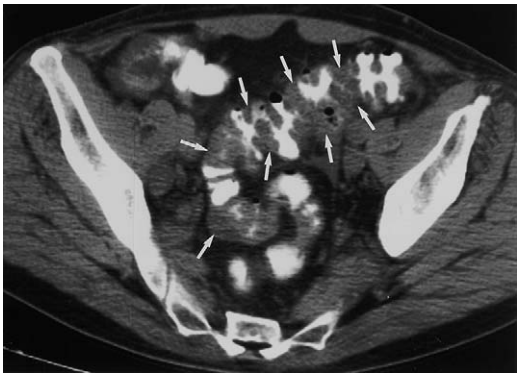

Fig. 23. Colonic posttransplantation lymphoproliferative disorder. Axial CT of pelvis in a patient with severe abdominal pain and rectal bleeding on immunosuppressive therapy shows severe, diffuse, nodular mucosal thickening of the sigmoid colon (*arrows*) that proved to be posttransplantation lymphoproliferative disorder on biopsy. (Similar fold thickening was present throughout the entire colon).

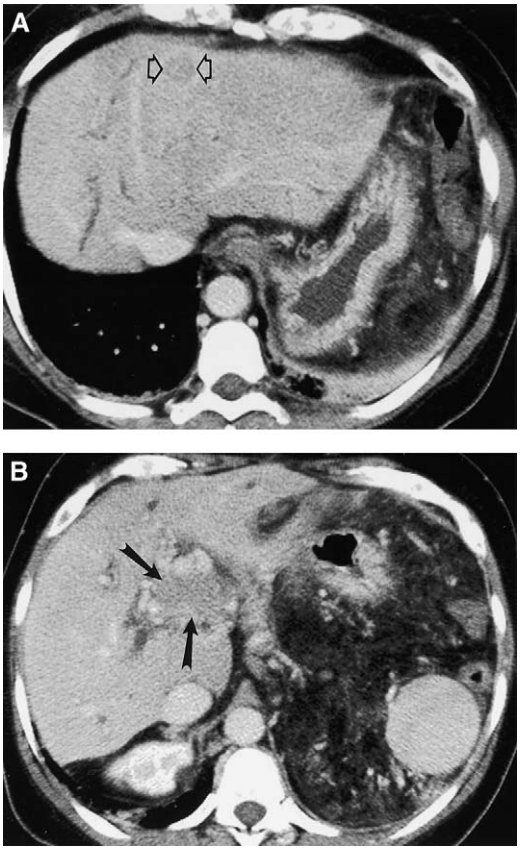

Fig. 24. Hepatic posttransplantation lymphoproliferative disorder. (*A*) Axial CT of the liver demonstrates low-attenuation nodules in the left hepatic lobe (*open arrows*) and (*B*) at the porta hepatis (*arrows*) with compression of the portal vein and bile ducts. Biopsy revealed posttransplantation lymphoproliferative disorder.

recognized pattern of posttransplantation lymphoproliferative disease [50]. Any new mass in a transplant patient should be considered neoplastic and probably lymphoma until biopsy or resection proves otherwise.

Summary

The radiologist can play a key role in diagnosis and management of many of the infectious, inflammatory, and neoplastic processes that affect patients after liver transplantation. Familiarity and skill with the full range of diagnostic and interventional tools are essential for radiologists dealing with transplant patients, even outside the medial centers where the transplantation takes place.

References

[1] Brancatelli G, Federle MP, Pealer K, et al. Portal venous thrombosis or sclerosis in liver transplantation candidates: preoperative CT findings and correlation with surgical procedure. Radiology 2001;220:321–8.
[2] Navarro F, Le Moine MC, Fabre JM, et al. Specific vascular complications of orthotopic liver transplantation with preservation of the retrohepatic vena cava: review of 1361 cases. Transplantation 1999;68:646–50.
[3] Parrilla P, Sanchez-Bueno F, Figueras J, et al. Analysis of the complications of the piggy-back technique in 1,112 liver transplants. Transplantation 1999;67:1214–7.
[4] Ito K, Siegelman ES, Stolpen AH, et al. MR imaging of complications after liver transplantation. AJR Am J Roentgenol 2000;175:1145–9.
[5] Nghiem HV. Imaging of hepatic transplantation. Radiol Clin North Am 1998;36:429–43.
[6] Bowen A, Keslar PJ, Newman B, et al. Adrenal hemorrhage after liver transplantation. Radiology 1990;176:85–8.
[7] Glockner JF, Forauer AR. Vascular or ischemic complications after liver transplantation. AJR Am J Roentgenol 1999;173:1055–9.
[8] Langnas AN, Marujo W, Stratta RJ, et al. Vascular complications after orthotopic liver transplantation. Am J Surg 1991;161:76–83.
[9] Legmann P, Costes V, Tudoret L, et al. Hepatic artery thrombosis after liver transplantation: diagnosis with spiral CT. AJR Am J Roentgenol 1995;164:97–101.
[10] Wozney P, Zajko AB, Bron KM, et al. Vascular complications after liver transplantation: a 5-year experience. AJR Am J Roentgenol 1986;147:657–63.
[11] Dodd III GD, Memel DS, Zajko AB, et al. Hepatic artery stenosis and thrombosis in transplant recipients: Doppler diagnosis with resistive index and systolic acceleration time. Radiology 1994;192:657–61.
[12] Nolten A, Sproat IA. Hepatic artery thrombosis after liver transplantation: temporal accuracy of diagnosis with duplex US and the syndrome of impending thrombosis. Radiology 1996;198:553–9.
[13] Brancatelli G, Katyal S, Federle MP, et al. Three-dimensional multislice helical computed tomography with the volume rendering technique in the detection of vascular complications after liver transplantation. Transplant 2002;73:237–42.
[14] Katyal S, Oliver III JH, Buck DG, et al. Detection of vascular complications after liver transplantation: early experience in multislice CT angiography with volume rendering. AJR Am J Roentgenol 2000;175:1735–9.
[15] Quiroga S, Sebastia MC, Margarit C, et al. Complications of orthotopic liver transplantation: spectrum of findings with helical CT. Radiographics 2001;21:1085–102.
[16] Glockner JF, Forauer AR, Solomon H, et al. Three-dimensional gadolinium-enhanced MR angiography

of vascular complications after liver transplantation. AJR Am J Roentgenol 2000;174:1447–53.
[17] Nghiem HV, Tran K, Winter III TC, et al. Imaging of complications in liver transplantation. Radiographics 1996;16:825–40.
[18] Kaplan SB, Zajko AB, Koneru B. Hepatic bilomas due to hepatic artery thrombosis in liver transplant recipients: percutaneous drainage and clinical outcome. Radiology 1990;174:1031–5.
[19] Flint EW, Sumkin JH, Zajko AB, et al. Duplex sonography of hepatic artery thrombosis after liver transplantation. AJR Am J Roentgenol 1988;151:481–3.
[20] Hall TR, McDiarmid SV, Grant EG, et al. False-negative duplex Doppler studies in children with hepatic artery thrombosis after liver transplantation. AJR Am J Roentgenol 1990;154:573–5.
[21] Platt JF, Yutzy GG, Bude RO, et al. Use of Doppler sonography for revealing hepatic artery stenosis in liver transplant recipients. AJR Am J Roentgenol 1997;168: 473–6.
[22] Abad J, Hidalgo ED, Cantarero JM, et al. Hepatic artery anastomotic stenosis after transplantation: treatment with percutaneous transluminal angioplasty. Radiology 1989;171:661–2.
[23] Abbasoglu O, Levy MF, Vodapally MS, et al. Hepatic artery stenosis after liver transplantation: incidence, presentation, treatment, and long term outcome. Transplantation 1997;63:250–5.
[24] Sheng R, Orons PD, Ramos HC, et al. Dissecting pseudoaneurysm of the hepatic artery: a delayed complication of angioplasty in a liver transplant. Cardiovasc Intervent Radiol 1995;18:112–4.
[25] Zajko AB, Sheng R, Bron K, et al. Percutaneous transluminal angioplasty of venous anastomotic stenoses complicating liver transplantation: intermediate-term results. J Vasc Interv Radiol 1994;5:121–6.
[26] Rossi AR, Pozniak MA, Zarvan NP. Upper inferior vena cava anastomotic stenosis in liver transplant recipients: Doppler US diagnosis. Radiology 1993;187: 387–9.
[27] Margarit C, Lazaro JL, Hidalgo E, et al. Cross-clamping of the three hepatic veins in the piggyback technique is a safe and well tolerated procedure. Transpl Int 1998;11(suppl 1):S248–50.
[28] Chen WP, Chen JH, Hwang JI, et al. Spectrum of transient hepatic attenuation differences in biphasic helical CT. AJR Am J Roentgenol 1999;172:419–24.
[29] Campbell WL, Sheng R, Zajko AB, et al. Intrahepatic biliary structures after liver transplantation. Radiology 1994;191:735–40.
[30] Cheng YF, Chen YS, Huang TL, et al. Biliary complications in living related liver transplantations. Chang Gung Med J 2001;3:174–80.
[31] Egawa H, Inomata Y, Uemoto S, et al. Biliary anastomotic complications in 400 living related liver transplantations. World J Surg 2001;10:1300–7.
[32] Lerut J, Gordon R, Iwatsuki S, et al. Biliary tract complications in human orthotopic liver transplantation. Transplantation 1987;43:47–51.
[33] Sheng R, Ramirez CB, Zajko AB, et al. Biliary stones and sludge in liver transplant patients: a 13-year experience. Radiology 1996;198:243–7.
[34] Ward EM, Wiesner RH, Hughes RW, et al. Persistent bile leak after liver transplantation: biloma drainage and endoscopic retrograde cholangiopancreatographic sphincterotomy. Radiology 1989;171:661–2.
[35] Laghi A, Pavone P, Catalano C, et al. MR cholangiography of late biliary complications after liver transplantation. AJR Am J Roentgenol 1999;172:1541–6.
[36] Fulcher AS, Turner MA. Orthotopic liver transplantation: evaluation with MR cholangiography. Radiology 1999;211:715–22.
[37] Culp WC, McCowan TC, Lieberman RP, et al. Biliary structures in liver transplant recipients: treatment with metal stents. Radiology 1996;199:339–46.
[38] Keogan MT, McDermott VG, Price SK, et al. The role of imaging in the diagnosis and management of biliary complications after liver transplantation. AJR Am J Roentgenol 1999;173:215–9.
[39] Letourneau JG, Day DL, Hunter DW, et al. Biliary complications after liver transplantation in patients with preexisting sclerosing cholangitis. Radiology 1988;167:349–51.
[40] Orons PD, Sheng R, Zajko AB. Hepatic artery stenosis in liver transplant recipients: prevalence and cholangiographic appearance of associated biliary complications. AJR Am J Roentgenol 1995;165:1145–9.
[41] Sheng R, Sammon JK, Zajko AB, et al. Bile leak after transplantation: cholangiographic features, prevalence, and clinical outcome. Radiology 1994;192:413–6.
[42] Zajko AB, Bennett MJ, Campbell WL, et al. Mucocele of the cystic duct remnant in eight liver transplant recipients: findings at cholangiography, CT, and US. Radiology 1990;177:691–3.
[43] Blachar A, Federle MP. Bowel obstruction following liver transplantation: clinical and CT findings in 48 cases with emphasis on internal hernia. Radiology 2001;218:384–8.
[44] Ho M, Jaffe R, Miller G, et al. The frequency of Epstein-Barr virus infection and associated lymphoproliferative syndrome after transplantation and its manifestations in children. Transplantation 1998;45: 719–27.
[45] Opelz G, Henderson R. Incidence of non-Hodgkin lymphoma in kidney and heart transplant recipients. Lancet 1993;342:1514–6.
[46] Starzl TE, Nalesnick MA, Porter KA, et al. Reversibility of lymphomas and lymphoproliferative lesions developing under cyclosporine – steroid therapy. Lancet 1984;1:583–7.
[47] Ferris JV, Baron RL, Marsh Jr JW, et al. Recurrent hepatocellular carcinoma after liver transplantation: spectrum of CT findings and recurrence patterns. Radiology 1994;192:657–61.
[48] Penn I. The changing pattern of posttransplant malignancies. Transplant Proc 1991;23:1101–3.
[49] McLaughlin K, Wajstaub S, Marotta P, et al. Increased risk for posttransplant lymphoproliferative disease in

recipients of liver transplants with hepatitis C. Liver Transpl 2000;6:570–4.

[50] Pickhard PJ, Siegel MJ. Abdominal manifestations of posttransplantation lymphoproliferative disorder. AJR Am J Roentgenol 2000;175:1417–22.

[51] Lee DA, Hartman RP, Trenkner SW, et al. Lymphomas in solid organ transplantation. Abdom Imaging 1998; 23:553–7.

[52] Ward EM, Kidy MJ, Maus TP, et al. Hilar biliary strictures after liver transplantation: cholangiography and percutaneous treatment. Radiology 1990;177: 259–63.

[53] Zajko AB, Campbell WL, Logsdon GA, et al. Cholangiographic findings in hepatic artery occlusion after liver transplantation. AJR Am J Roentgenol 1987; 149:485–9.

RADIOLOGIC CLINICS OF NORTH AMERICA

Radiol Clin N Am 41 (2003) 1307–1335

Cumulative Index 2003

Volume 41

January	BODY MR IMAGING, pages 1–198
March	ADVANCES IN INTESTINAL IMAGING, pages 199–464
May	MULTISLICE HELICAL CT OF THE THORAX, pages 465–662
July	WOMEN'S IMAGING: OBSTETRICS AND GYNECOLOGY, pages 663–862
September	ADVANCES IN RENAL IMAGING, pages 863–1082
November	IMAGING OF THE ACUTE ABDOMEN, pages 1083–1335

Note: Page numbers of article titles are in **boldface** type.

A

Abdomen, multislice CT of, in children. *See* Multislice CT.

Abdominal aorta, CT of, **1153–1169**
- for acute occlusion, 1162
- for aneurysms, 1155–1159
- for dissection, 1159–1161
- for fistulas, 1166
- for inflammatory aneurysms, 1158–1159
- for intramural hematomas, 1161–1162
- for mycotic aneurysms, 1156–1158
- for penetrating atherosclerotic ulcers, 1162
- for trauma, 1162–1163
- postoperative, 1163–1164, 1166
- technique for, 1153–1155

MR angiography of, 124–131, 133
- for acute occlusion, 129–130
- for aneurysms, 127–129
- for dissection, 129
- for renal artery stenosis, 130
- for renal transplant evaluation, 130–131, 133

Abdominal emergencies. *See also* Acute abdominal disease.
MR imaging of, **1243–1273**
- gallbladder and biliary system, 1248–1256
  - cholangitis, 1254–1255
  - cholecystitis, 1248–1253
  - choledocholithiasis, 1253–1254
  - Mirizzi syndrome, 1255–1256
  - symptomatic cholelithiasis, 1248
- gastrointestinal disorders. *See* Gastrointestinal disorders.
- genitourinary tract, 1263–1269
  - acute renal failure, 1268
  - acute vascular disorders, 1268–1269
  - renal colic, 1263–1267
  - urinary tract infections, 1267
- liver, 1245–1248
  - acute infections, 1245–1247
  - acute vascular disorders, 1247–1248
  - hemorrhagic disorders, 1248
- pancreas, 1256–1259
- protocols for, 1243–1245
  - breathhold imaging, 1244
  - non-breathhold imaging, 1244–1245

nuclear medicine studies of, **1275–1288**
- gastrointestinal bleeding, 1275–1277, 1279
- hepatic injuries, 1285
- infections, 1286
- renal injuries, 1285–1286
- right upper quadrant pain, 1279–1282, 1285
  - cholecystitis, 1280
  - common bile duct obstruction, 1281–1282
  - postcholecystectomy, 1282, 1285
- splenic injuries, 1286

Abdominal trauma, and mesenteric ischemia, 337–338
CT of, 337–338

Abdominal wall, ultrasonography of, in first trimester, 683–684

Abscesses, appendiceal, ultrasonography of, 1232
hepatic, liver transplantation and, 1299
MR imaging of, 1245–1246

0033-8389/03/$ – see front matter
doi:10.1016/S0033-8389(03)00150-7

pancreatic, interventional approach to, 1220–1223
tubo-ovarian, MR imaging of, 808–809

Acalculous cholecystitis, MR imaging of, 1251

Acardiac parabiotic twin, radiofrequency ablation of, 721–722
ultrasonography of, 7190722

Acceleration index, in color Doppler imaging, in infants, 933–934

Accessory azygos veins, multislice CT of, 558–559

ACE inhibitor renal scintigraphy, of hypertension, in infants, 939–941
of renal artery stenosis, 913–914

Actinomycosis, ovarian, MR imaging of, 808–809

Acute abdominal disease. *See also* Abdominal emergencies.
multislice CT of, **1083–1093**
abdominal pain, 1088
enhancement phase in, 1091
in children, 1090
liver and bile duct, 1088
pancreas, 1088–1089
pitch and contrast in, 1090–1091
radiation dose in, 1090
technique for, 1083–1086
thinner slices in, 1091
traumatic injuries, 1086–1087
vascular, 1089–1090

Acute right lower quadrant, CT of, **1117–1135**
for abnormal appendix, 1124–1127
for appendicitis, 1117–1123
focused CT, 1120–1121
oral and intravenous contrast agents in, 1122–1123
rectal contrast agents in, 1121–1122
unenhanced CT, 1119–1120
for cecal and right-sided colonic diverticulitis, 1131
for Crohn's disease, 1129
for differential diagnosis, 1127–1128
for ischemia and vasculitis, 1129, 1131
for Meckel's and ileal diverticulitis, 1131–1132
for mesenteric adenitis, 1128–1129
for normal appendix, 1123–1124
for omental infarction, 1133–1134
for primary epiploic appendagitis, 1133
for terminal ileitis, 1129, 1131
for typhlitis, 1132–1133
MR imaging of, for appendicitis, 1261
multislice CT of, for appendicitis, in children, 655–656
ultrasonography of, for appendicitis, 1229–1234
appendiceal masses, 1232–1233
pitfalls in, 1233–1234
spontaneous resolving appendicitis, 1231
technique for, 1230–1231

Acute traumatic aortic injuries, multislice CT of, 479, 541–542, 608–612

Adenitis, mesenteric, CT of, 1128–1129
multislice CT of, in children, 656

Adenocarcinomas, of small bowel, differential diagnosis of, 345
multislice CT of, 209

Adenomas, adrenal, MR imaging of, 153–154
hepatocellular, and intraperitoneal hemorrhage, 1189
MR imaging of, 59–60
serous microcystic, MR cholangiopancreatography of, 107
small bowel, differential diagnosis of, 342, 344

Adenomatous hyperplasia, atypical, multislice CT of, 585–587

Adenomyosis, MR imaging of, 183

Adnexal masses, benign, MR imaging of, 809, 811
in ectopic pregnancy, ultrasonography of, 672–673

Adrenal glands, MR imaging of, 145–146, 152–157
for adenomas, 153–154
for adrenocortical carcinoma, 154–155
for cysts, 156–157
for myelolipomas, 156
for pheochromocytomas, 155–156
for pseudocysts, 156–157
technique for, 145–146

Adrenocortical carcinoma, MR imaging of, 154–155

AIDS, and intussusception, 1139–1140

Air double-contrast enteroclysis, technique for, 220, 222

Airway evaluation, multislice CT in, in children, 649–650

Alcoholic pancreatitis, MR cholangiopancreatography of, 102–103

Aliasing, on fetal MR imaging, 736

Amebic liver abscesses, MR imaging of, 1245–1246

Amniocentesis, to diagnose aneuploidy, 695–696

Amnioreduction, for twin-twin transfusion syndrome, 717–718

Amyloidosis, and intraperitoneal hemorrhage, 1192

Anal fistulas, **443–457**
classification of, 443–444
endosonography of, 445–448
etiology of, 443
fistulography of, 445
management of, 444–445
MR imaging of, 448–452
and surgical outcome, 453–455
versus endosonography, 452–453

Anemia, aortic wall in, multislice CT of, 529–530

Anencephaly, ultrasonography of, in first trimester, 676, 681

Aneuploidy, prenatal diagnosis of, **695–708**
amniocentesis in, 695–696
chorionic villus sampling in, 696
cordocentesis in, 696
maternal serum screening in, 696–697, 704–705
ultrasonography in, 676–677, 697–699, 704
Down syndrome, 699–702
triploidy syndrome, 698–699
trisomy 13, 698
trisomy 18, 697–698, 702, 704
trisomy 21, 697
Turner syndrome, 698

Aneurysms, abdominal aortic, CT of, 1155–1159
MR angiography of, 127–129
mycotic, CT of, 1156–1158
aortic. *See* Aortic aneurysms.
renal artery, and hypertension, 922–923
thoracic aortic, MR angiography of, 35–36
mycotic, multislice CT of, 540–541
visceral, and intraperitoneal hemorrhage, 1193–1194

Angiography, coronary, multislice CT in, 501–504
CT. *See* CT angiography.
intra-arterial, of renal artery stenosis, 919
MR. *See* MR angiography.
of acute mesenteric ischemia, 327
of hypertension, in infants, 935–937
of renal trauma, 1019

Angiomyolipomas, imaging of, ultrasound contrast agents in, 963–965
MR imaging of, 148–150

Angioplasty, for renal artery stenosis, 919, 921

Angioscopy, virtual, of acute thoracic aortic injuries, 611

Anismus, evacuation proctography of, 430

Annular lesions, of small bowel, differential diagnosis of, 345–347

Anorectum, evacuation proctography of, **425–441**
at rest, 427–428
barium trapping in, 431–432
evacuation phase of, 428
for anismus, 430
for descending perineum syndrome and anterior mucosal prolapse, 428–430
for intussusception, 433, 435
for rectal prolapse, 433, 436
for rectoceles, 430–433
for solitary rectal ulcer syndrome, 435–436
recovery phase of, 428
technique for, 426–427

Anterior mucosal prolapse, evacuation proctography of, 428–430

Aortic aneurysms, abdominal. *See* Aneurysms.
growth rate and risk of rupture of, 536–537
multislice CT of, 536–538
thoracic, MR angiography of, 35–36
multislice CT of, 478–479

Aortic dissection, abdominal, CT of, 1159–1161
MR angiography of, 129
MR imaging of, 1160–1161
classification of, 532
etiology of, 532
false versus true lumens in, 535–536
multislice CT of, 479, 533–536
sensitivity and specificity of, 536
thoracic, MR angiography of, 34–35

Aortic occlusion, abdominal, MR angiography of, 129–130

Aortic spindle, multislice CT of, 526

Appendagitis, epiploic, CT of, 1133
MR imaging of, 1262–1263

Appendicitis. *See* Acute right lower quadrant.

Appendix, abnormal, CT of, 1124–1127
normal, CT of, 1123–1124

Arrhythmogenic right ventricular dysplasia, MR imaging of, 21–22

Arterial obstruction, hepatic, MR imaging of, 85

Arterio-arterial anastomoses, in placenta, 712–713

Arteriography, CT, of nonaortic thoracic vascular injuries, 612
intra-arterial digital subtraction, of hypertension, in infants, 936

Arterioportal fistulas, liver transplantation and, 1295

Arteriovenous anastomoses, in placenta, 713

Arteriovenous communications, and hypertension, 923–924

Arteriovenous malformations, CT enteroclysis in, 256–257
pulmonary, multislice CT of, 480
paddle-wheel method in, 627

Atelectasis, of left lower lobe, multislice CT of, 529

Atherosclerotic disease, and renal artery stenosis, 911
coronary, multislice CT of, 504–505
in mesenteric arteries, multislice CT of, 206
MR imaging of, 21
of thoracic aorta, multislice CT of, 531–532

Atherosclerotic ulcers, penetrating, multislice CT of, 539–540, 1162

Atypical adenomatous hyperplasia, multislice CT of, 585–587

Axillary involvement, by breast cancer, ultrasonography of, 847–848

Azygos veins, multislice CT of, 558–559

B

Barium enema, and colon perforation, 1109
double-contrast. *See* Double-contrast barium enema.

Barium studies, of acute mesenteric ischemia, 327
of Crohn's disease, 289
of intussusception, 1144
of small bowel obstruction, 265, 270–271

Barium sulfate, in diagnosis, of gastrointestinal perforation, 1095–1095

Behœt's disease, of small bowel, differential diagnosis of, 357

Bicornuate uterus, MR imaging of, 181–182

Bile ducts, multislice CT of, 1088

Biliary complications, of liver transplantation, 1295–1296, 1298
postoperative, MR cholangiopancreatography of, 92–93

Biliary cystadenomas, MR imaging of, 60

Biliary cysts, MR cholangiopancreatography of, 90–91

Biliary disorders, MR imaging of. *See* Abdominal emergencies.

Biliary tree perforation, diagnosis of, 1112–1113

Biliopancreatic diversion, technique for, 313

Bilomas, diagnosis of, 1112

Biopsy, fine-needle aspiration, of breast cancer, ultrasonography in, 849

Birt-Hogg-Dubé syndrome, imaging of, 1044–1045

Bladder, MR imaging of, **161–177**
anatomy in, 162
for cystoceles, 173–175
for diverticula, 171–172
for endometriosis, 172–173
for lymphomas, 170
for mesenchymal tumors, 170–171
for tumors, 162–170
contrast-enhanced, 167–168
direct spread, 165–167
epidemiology of, 162–163
management and follow-up, 169–170
metastatic to bones, 168–169
metastatic to lymph nodes, 169
primary mass, 163–165
for vesical congestion and inflammation, 172
patient preparation for, 161
planes in, 161–162
pulse sequences in, 161–162

Bleeding, ovarian, MR imaging of, 802
postmenopausal. *See* Postmenopausal bleeding.

Blind loop syndrome, enteroanastomosis and, 309

Blind pouch syndrome, enteroanastomosis and, 308–309

Blood pool agents, in MR angiography, 140

Boerhaave's syndrome, diagnosis of, 1099

Bolus-chase MR angiography, technique for, 134–136, 138

Bone mineral density, definition of, 813
dual x-ray absorptiometry of, 818

Bowel discontinuity, on CT, of small bowel or mesenteric injury, 1173

Bowel herniation, ultrasonography of, in first trimester, 683–684

Bowel wall enhancement, on CT, of small bowel or mesenteric injury, 1179–1180

Bowel wall thickening, on CT, of small bowel or mesenteric injury, 1175–1176

Brachiocephalic veins, multislice CT of, 553–554

Branch vessel infundibula, multislice CT of, 526

Breast cancer, screening for, MR imaging in, 49–50
ultrasonography in, 851

Breasts, MR imaging of, **43–50**
contrast-enhanced, 44–45
for fibroadenomas, 47–48
image analysis in, 45–49
patient preparation for, 44
techniques for, 44
to screen for breast cancer, 49–50
ultrasonography of, *841–856*
contrast-enhanced Doppler, 846–847
for cystic lesions, 842–843
for implants, 851–852
for microcalcifications, 850–851
for solid lesions, 843–846
in males, 852
intraoperative, 849–850
non–contrast-enhanced Doppler, 846
normal anatomy in, 842
screening, for cancer, 851
for known cancer, 848–849
technique for, 841–842
to guide fine-needle aspiration biopsy, 849
to stage cancer, 847–849
nodal involvement in, 847–848
tumor size and grade in, 847

Breathhold imaging, of abdominal emergencies, 1244
of kidneys, 880, 882

Brenner tumors, MR imaging of, 805

Bronchoscopy, virtual. *See* Virtual bronchoscopy.

Brooke ileostomy, creation of, 315

Budd-Chiari syndrome, MR imaging of, 84–85, 1247–1248

Bulk motion, on fetal MR imaging, 734

Bypass graft patency, MR imaging of, 20–21

C

Calcifications, coronary artery, multislice CT of, 497–500
of abdominal aortic aneurysms, 1156
renal, CT of, 867

Candidal microabscesses, hepatic, MR imaging of, 1246

Captopril, in MR imaging, of renal function, 1006–1008

Carcinoid tumors, of small bowel, CT enteroclysis in, 255
differential diagnosis of, 342, 348–349
MR enteroclysis in, 245
multislice CT of, 209

Cardiac function, multislice CT of, 500–501

Cardiac injuries, multislice CT of, 612–613

Cardiac masses, MR imaging of, 24

Cardiac veins, multislice CT of, 554–555, 558

Cardiomyopathies, MR imaging of. *See* Cardiovascular disease.

Cardiovascular evaluation, multislice CT in, in children, 650

Cardiovascular system, MR imaging of, **17–28**
for cardiac masses, 24
for cardiomyopathies, 21–23
arrhythmogenic right ventricular dysplasia, 21–22
dilated, 23
hemochromatosis, 23
hypertrophic, 22
restrictive, 23
for congenital heart disease, 25
for coronary arteries, 19–21
anomalous arteries, 20
atherosclerotic plaque, 21
bypass graft patency, 20–21
Kawasaki disease, 20
MR angiography in, 19–20
for ischemic heart disease, 17–19
contrast-enhanced, 18–19
myocardial viability in, 17
rest imaging, 17
stress imaging, 17–18
for pericardial disease, 23–24
for valvular heart disease, 21

Catheter-associated thromboembolism, angiography of, in infants, 937
ultrasonography of, in infants, 933

Cavitary masses, of small bowel, differential diagnosis of, 344–345

Cecal carcinoma, ultrasonography of, 1236–1237

Cecal diverticulitis, CT of, 1131

Central airways, multislice CT of, **563–578**
axial images in, 563
external three-dimensional rendering in, 571
internal rendering in, 571–573
multiplanar and tree-dimensional images in, 563, 566
optimization of images in, 566–567, 569–570
paddle-wheel method in, 629
three-dimensional reconstruction in, 570–571
two-dimensional multiplanar reformation in, 573–576

Central nervous system, ultrasonography of, in first trimester, 681–682

Central thoracic veins, MR angiography of, 37

Cervical cancer, MR imaging of, 186–187

Cervix, in female infertility, 758

Chemotherapy, and drug-induced enteropathy, 336

Chest, MR angiography of, **29–41**
contrast-enhanced, 29–31
for aortic aneurysms, 35–36
for aortic dissection, 34–35
for central thoracic veins, 37
for developmental anomalies, 36
for pulmonary arteries, 37–39
for thoracic aorta, 34
image analysis in, 34
pulse sequences in, 32–33
techniques for, 29–34

Chest wall, multislice CT of, 486, 488
in children, 650–651

Cholangiocarcinoma, MR cholangiopancreatography of, 93–94
MR imaging of, 62–63

Cholangitis, MR imaging of, 1254–1255

Cholecystectomy, cystic duct stump leakage after, 1113
pain after, nuclear medicine studies of, 1282, 1285

Cholecystitis. *See* Gallbladder disorders.

Cholecystolithiasis, MR cholangiopancreatography of, 91

Choledocholithiasis, MR cholangiopancreatography of, 91–92, 1253–1254

Cholelithiasis, MR imaging of, 1248

Cholesterol embolism, MR imaging of, 1268–1269

Chorionic villus sampling, to diagnose aneuploidy, 696

Chromosome 3, translocation of, and hereditary renal cancer, 1046

Cirrhosis, and intraperitoneal hemorrhage, 1192
MR imaging of, 68–74

Cobblestone mucosa, in Crohn's disease, 286

Colon cancer, and gastrointestinal perforation, 1110
and mesenteric ischemia, 337
CT of, 337
screening for, virtual colonoscopy in. *See* Virtual colonoscopy.

Colon perforation, diagnosis of, 1108–1110, 1112

Colonic diverticulitis, CT of, 1131
ultrasonography of, 1240–1241

Colonoscopy, and colon perforation, 1109
virtual. *See* Virtual colonoscopy.

Color Doppler imaging, of hypertension, in infants, 933–935
of postmenopausal bleeding, 775

Comb sign, in MR enteroclysis, 244–245

Common bile duct obstruction, nuclear medicine studies of, 1281–1282

Computed tomography, in enteroclysis. *See* CT enteroclysis.
multichannel. *See* Multislice CT.
of abdominal aorta. *See* Abdominal aorta.
of abdominal trauma, 337–338
of acute mesenteric ischemia, 327–328
of acute right lower quadrant. *See* Acute right lower quadrant.
of acute thoracic aortic injuries, 609
of colon cancer, 337
of Crohn's disease, 284, 286, 288, 289, 292
of diverticulitis, 1109
of drug-induced enteropathy, 336–337
of gallbladder disorders. *See* Gallbladder disorders.
of gastrointestinal perforation, 1096–1099
of hepatocellular carcinoma, 1187
of intraperitoneal hemorrhage, 1183–1185
of intussusception, 1147–1148
of kidneys. *See* Kidneys.
of pancreatic abscesses, 1221–1222
of pancreatic fluid collections, 1224–1225
of pancreatitis, 1195
of postoperative small bowel, 304, 320–322
of radiation enteritis, 335
of renal trauma. *See* Renal trauma.
of small bowel inflammation, 1106–1107
of small bowel ischemia, 1105–1106

of small bowel obstruction, 271–273, 276–279, 332–333
of small bowel or mesenteric injury. *See* Small bowel or mesenteric injury.
of tracheobronchial injuries, 616
of urinary lithiasis. *See* Urinary lithiasis.
of vasculitis, 333–334
of von Hippel–Lindau disease, 1040
quantitative, of osteoporosis, 820–824

Computer-aided diagnosis, of pulmonary nodules, 593, 595
with virtual colonoscopy, 383–384, 386–387, 391

Congenital heart disease, MR imaging of, 25
ultrasonography of, in first trimester, 684

Congestive heart failure, hepatic efffects of, 85

Conjoined twins, ultrasonography of, 723–724
in first trimester, 691–692

Continent ileostomy reservoir, creation of, 316–317

Contour distortions, of small bowel, differential diagnosis of. *See* Small bowel abnormalities.

Contrast enhancement, of CT, of appendicitis, 1121–1123
of CT enteroclysis, 250
of enteroclysis, 219–220, 222
of MR angiography, of abdominal aorta, 116, 118–131, 133
of chest, 29–31
of MR enteroclysis, 237–238, 244–245
of MR imaging, of bladder tumors, 167–168
of breasts, 44–45
of cardiovascular disease, 18–19
of hepatic tumors. *See* Hepatic tumors.
of multislice CT, of small bowel, 199–200

Contrast esophagography, of esophageal injuries, 613

Contrast ileography, of ileoanal pouch, 317, 319

Contrast studies, of diverticulitis, 1109–1110
of small bowel transplantation, 320

Contusions, renal, imaging of, 1026–1027

Cordocentesis, to diagnose aneuploidy, 696

Coronary angiography, multislice CT in, 501–504

Coronary arteries, MR angiography of, 19–21
multislice CT of, 476–478

Coronary sinus veins, multislice CT of, 554–555, 558

Crohn's disease, barium studies of, 289
classification of, **283–301**
active inflammatory subtype, 284, 286
fibrostenotic subtype, 288–289
fistulizing/perforating subtype, 286, 288
reparative or regenerative subtype, 289
CT enteroclysis in, 252–254, 292
CT of, 284, 286, 288, 289, 292, 1106, 1129
differential diagnosis of, 355–357
MR enteroclysis in, 241–242, 244–245, 286, 288–289, 292, 294
multislice CT of, 206–207
ultrasonography of, 1234

Crossing vessels, renal, CT of, 871

Cryotherapy, for von Hippel–Lindau disease, 1040–1041

CT angiography, in children, 648
of hypertension, in infants, 941
of kidneys, versus CT, 866–867
of nonaortic thoracic vascular injuries, 612
of renal artery stenosis, 918–919
of renal masses, 870–871

CT arteriography, of nonaortic thoracic vascular injuries, 612

CT enteroclysis, **249–262**
contrast-enhanced, 222, 224, 226, 228, 250
CT parameters for, 250–251
disadvantages of, 258–259
in arteriovenous malformations, 256–257
in Crohn's disease, 252–254, 292
in radiation enteritis, 257–258
in small bowel neoplasms, 254–256
in small bowel obstruction, 251–252, 265, 270–273, 278, 279
in unexplained gastrointestinal bleeding, 256–257
technique for, 249–251

CT urography, of abdominal pain, 1088
of hematuria, 944, 946–953
technique for, 944, 946–953
excretory-phase CT with multiplanar reformation, 951–953
scanned projection radiographic technique, 948

Cyclosporine toxicity, and renal transplant dysfunction, MR imaging of, 1013

Cystadenocarcinoma, MR imaging of, 188

Cystadenomas, biliary, MR imaging of, 60

Cystic duct stump, leakage from, 1113

Cystic masses, renal, imaging of, ultrasound contrast agents in, 965–968
ultrasonography of, in infants, 932

Cystoceles, MR imaging of, 173–175
in women, evacuation proctography of, 402–403

Cystourethrography, voiding, of pelvic floor relaxation, 749

Cysts, adrenal, MR imaging of, 156–157
biliary, MR cholangiopancreatography of, 90–91
breasts, ultrasonography of, 842–843
hepatic, MR imaging of, 56–57
ovarian, and intraperitoneal hemorrhage, 1197–1198
MR imaging of, 800, 802–803
renal, MR imaging of, 151–152

D

DeBakey classification, of aortic dissection, 532

Deep venous thrombosis, multislice CT of, 512

Defecography, of female pelvic organ prolapse. *See* Female pelvic organ prolapse.
of pelvic floor relaxation, 749–750

Dermoid cysts, MR imaging of, 185
ovarian, MR imaging of, 808

Descending perineum syndrome, evacuation proctography of, 428–430

Diabetic nephropathy, and hypertension, 925

Diagnostic peritoneal lavage, for renal trauma, 1020

Diaphragm, multislice CT of, 486, 488, 617–618

Diazepam, in enteroclysis, 217

Diffuse hepatic disease, MR imaging of, **67–87**
arterial obstruction, 85
Budd-Chiari syndrome, 84–85
cirrhosis, 68–74
congestive heart failure, 85
fatty liver, 77–79
hemochromatosis, 23, 79–80
hepatitis, 74–75, 77
hepatocellular carcinoma, 62, 81
lymphomas, 81
metastatic disease, 81
mucopolysaccharidoses, 80–81
portal vein thrombosis, 81, 84
technique for, 67–68
vascular disorders, 81

Diffuse lung disease, multislice CT of, 482–484

Digital x-ray radiogrammetry, of osteoporosis, 817

Dilated cardiomyopathy, MR imaging of, 23

Discordant anomalies, in monochorionic twins, 722

Diverticula, bladder, MR imaging of, 171–172
small bowel, CT of, 1106

Diverticulitis, and gastrointestinal perforation, 1109–1110
CT of, 1131–1132
MR imaging of, 1261–1262
ultrasonography of, 1237–1241

Dobutamine stress imaging, of cardiovascular disease, 17–18

Doppler imaging, of breasts, 846–847
of chronic mesenteric ischemia, 330
of pancreatitis, 1195
of postmenopausal bleeding, 775
of renal artery stenosis, 914, 916–917

Double-contrast barium enema, **363–374**
air insufflation in, 367–368
barium thickness in, 367
colon appearance on, 363
enema tip in, 366–367
glucagon in, 367
goals of, 363–364
overhead images in, 368–370
patient preparation for, 364–365
patient selection for, 365–366
scout radiograph in, 365
spot radiographs in, 368
versus virtual colonoscopy, 376
with remote-control fluoroscopy, 370–373
barium-filling phase in, 370–371
carbon dioxide-air distention phase in, 371–372
filming phase in, 372–373

Double decidual reaction sign, in ultrasonography, of gestational sac, 664–665

Double-duct sign, in MR cholangiopancreatography, 105

Down syndrome, maternal serum screening for, in first trimester, 704
ultrasonography of, in second trimester, 699–702

Drug-induced enteropathy, and mesenteric ischemia, 335–337
CT of, 336–337
plain films of, 336

Dual x-ray absorptiometry, of osteoporosis, 818–820

Duct-penetrating sign, in MR cholangiopancreatography, 105

Ductus diverticulum, multislice CT of, 526

E

Echo planar MR imaging, physics of, 9–12

Ectopic pregnancy, and intraperitoneal hemorrhage, 1196–1197
  hematosalpinx and hematocele due to, MR imaging of, 809
  ultrasonography of. *See* Ultrasonography, in first trimester.

Edema, ovarian, MR imaging of, 809, 811

Edward syndrome, ultrasonography of, in second trimester, 696–698

Embolism, cholesterol, MR imaging of, 1268–1269

Embryonic heartbeat, ultrasonography of, 666–667

Embryonic pole, ultrasonography of, 666

Emphysematous cholecystitis, CT of, 1208–1209
  diagnosis of, 1208–1209
  ultrasonography of, 1208

Encephaloceles, ultrasonography of, in first trimester, 681

Endoaneurysmorrhaphy, complications of, 1163–1164

Endoluminal graft repair, complications of, 1164, 1166

Endometrial cancer, MR imaging of, 187–188

Endometriomas, MR imaging of, 803

Endometriosis, and female infertility, 766
  MR imaging of, 172–173, 183, 811

Endometrium, in ectopic pregnancy, ultrasonography of, 673
  in postmenopausal bleeding, ultrasonography of. *See* Postmenopausal bleeding.
  sonohysterography of. *See* Sonohysterography.

Endoscopic retrograde cholangiopancreatography, versus MR cholangiopancreatography, 89, 99–100

Endosonography, of anal fistulas, 445–448, 452–453

Enema, double-contrast barium. *See* Double-contrast barium enema.

Enterectomy, small bowel after. *See* Small bowel, postoperative.

Enteroceles, in women, evacuation proctography of, 398–400
  MR imaging of, 412–413

Enteroclysis, **213–229**
  air double-contrast technique for, 220, 222
  catheters for, 217–219
  contrast delivery in, 219
  contrast media in, 219–220
  CT in. *See* CT enteroclysis.
  enteral infusion in, 220
  in postoperative small bowel, 315
  in small bowel obstruction, 275–276
  intubation technique in, 219
  methylcellulose double-contrast technique for, 222
  MR imaging in. *See* MR enteroclyis.
  patient preparation for, 213
  premedication for, 213, 217

Enteropathy, drug-induced. *See* Drug-induced enteropathy.

Enterostomy, small bowel after, 313–315

Epiploic appendagitis, CT of, 1133
  MR imaging of, 1262–1263

Esophageal injuries, multislice CT of, 613

Esophageal perforation, diagnosis of, 1099, 1101

Evacuation proctography, of anorectum. *See* Anorectum.
  of female pelvic organ prolapse. *See* Female pelvic organ prolapse.

Everting end ileostomy, creation of, 315

Extraluminal air, on CT, of small bowel or mesenteric injury, 1173–1175

Extraluminal oral contrast agent, on CT, of small bowel or mesenteric injury, 1175

F

Fallopian tube, in female infertility, 760–764

Familial renal cancer, imaging of, 1046

Familial renal oncocytomas, imaging of, 1045

Fast imaging with steady-state precession sequence, in MR enteroclysis, 234, 236

Fast low-angle shot sequence, in MR enteroclysis, 234, 237, 245

Fast spin echo MR imaging, physics of, 6–7, 9

Fat saturation, on fetal MR imaging, 742

Fatty liver, MR imaging of, 77–79

Feeding vessel sign, in multislice CT, of pulmonary nodules, 584

Female infertility, **757–767**
  cervix in, 758
  congenital uterine anomalies and, 759–760
  endometriosis and, 766
  fallopian tube in, 760–764
  peritoneal cavity in, 764
  polycystic ovary syndrome and, 764–766
  uterine cavity filling defects and, 758–759
  uterus in, 758
  versus normal ovaries, 764
  versus normal reproduction, 757

Female pelvic organ prolapse, evacuation proctography of, **395–407**
    cystoceles, 402–403
    enteroceles, 398–400
    grading of prolapse in, 396–397
    peritoneoceles, 400
    rectoceles, 397–398
    sigmoidoceles, 401–402
    technique for, 395–396
    vaginal vault prolapse, 402
    versus MR imaging, 404
    versus physical examination, 403–404
  MR imaging of, 404, **409–423**
    advantages of, 410–413, 415–416
      assessment of pelvic floor musculature, 413, 415–416
      assessment of urethra and vagina, 410–412
      assessment of uterine prolapse and enteroceles, 412–413
    appearance of, 418, 420
    diagnostic criteria for, 420–421
    technique for, 416–418

Female pelvis, MR imaging of, **179–192**
    anatomy in, 179–181
    for adenomyosis, 183
    for cervical cancer, 186–187
    for dermoids, 185
    for endometrial cancer, 187–188
    for endometriosis, 183
    for fetal anomalies, 1990–191
    for fibroids, 182–183
    for müllerian anomalies, 181–182
    for ovarian cancer, 188
    for pelvic floor relaxation, 188–189
    for polycystic ovarian disease, 184–185
    for tubo-ovarian complex, 185–186
    in pregnancy, 189–190
    technique for, 179

Fentanyl, in enteroclysis, 217

Ferumoxides, in MR imaging, 53–54

Fetal anomalies, MR imaging of, 190–191
  ultrasonography of, in first trimester, 674–676, 682

Fetal magnetic resonance imaging, **729–745**
  artifacts on, 734–738
    aliasing, 736
    bulk motion, 734
    fluid motion, 734–735
    Gibbs ringing artifact, 738
    motion artifact, 734
    partial volume artifact, 738
    radiofrequency interference, 737
    repeat visualization or nonvisualization, 735–736
    susceptibility artifact, 737
  consent for, 729
  image quality on, 738, 740–742
    fat saturation, 742
    patient body habitus and use of surface coil, 740–741
    signal inhomogeneity, 741–742
    signal-to-noise ration, 738, 740
  indications for, 729
  interpretation of, 730–731
  monitoring during, 730
  patient positioning for, 729–730
  pitfalls in, 742
  protocol for, 730
  versus ultrasonography, 729
  viewing during, 730

Fetal structural abnormalities, ultrasonography of, in first trimester, 676–677

Fibroadenomas, of breasts, MR imaging of, 47–48
    ultrasonography of, 845

Fibroids, uterine, hereditary leiomyoma renal cell carcinoma and, 1043
    MR imaging of, 182–183

Fibromas, ovarian, MR imaging of, 805

Fibromuscular dysplasia, and renal artery stenosis, 911–912

Fine-needle aspiration biopsy, of breast cancer, ultrasonography in, 849

Fistulas, abdominal aortic, CT of, 1164, 1166
  anal. *See* Anal fistulas.

arterioportal, liver transplantation and, 1295
gastrocolic, perforation of, 1102

Fistulography, of anal fistulas, 445

Fluid collections, hepatic, liver transplantation and, 1299
nuclear medicine studies of, 1285
pancreatic. *See* Pancreatic fluid collections.

Fluid motion, on fetal MR imaging, 734–735

Fluoroscopy, MR, in MR enteroclysis, 232–233
of female pelvic organ prolapse, 416–417
with double-contrast barium enema. *See* Double-contrast barium enema.

Focal lung disease, multislice CT of, 482–484

Focal mass lesions, of small bowel, differential diagnosis of. *See* Small bowel abnormalities.

Focal nodular hyperplasia, hepatic, and intraperitoneal hemorrhage, 1189
MR imaging of, 58–59

Foreign body perforation, diagnosis of, 1099–1100

Fractures, osteoporosis and, 814–817
rib, multislice CT of, 603–604
scapular, multislice CT of, 604
sternal, multislice CT of, 606–607

Fungal hepatic abscesses, MR imaging of, 1246

G

Gallbladder disorders, **1203–1216**
acute cholecystitis, 1203–1205
CT of, 1204–1205
nuclear medicine studies of, 1280
ultrasonography of, 1203, 1248
emphysematous cholecystitis, 1208–1209
CT of, 1208–1209
ultrasonography of, 1208
gallstone ileus, 1211–1213
CT of, 1212–1213
gangrenous cholecystitis, 1205–1207
CT of, 1206–1207
MR imaging of, 1251
ultrasonography of, 1206
hemorrhagic cholecystitis, 1207–1208
CT of, 1207
ultrasonography of, 1207
Mirizzi syndrome, 1213–1215, 1255–1256
MR imaging of. *See* Abdominal emergencies.
perforation, 1209–1210
CT of, 1210
ultrasonography of, 1210
trauma, 1210–1211
CT of, 1210–1211

Gangrenous cholecystitis, CT of, 1206–1207
diagnosis of, 1205–1207
MR imaging of, 1251
ultrasonography of, 1206

Gastric perforation, diagnosis of, 1101–1102, 1105

Gastric surgery, small bowel after, 303–305

Gastrocolic fistulas, perforation of, 1102

Gastroileostomy, inadvertent, diagnosis of, 304–305

Gastrointestinal bleeding, nuclear medicine studies of, 1275–1277, 1279
unexplained, CT enteroclysis in, 256–257

Gastrointestinal contrast studies, of small bowel transplantation, 320

Gastrointestinal disorders, and intraperitoneal hemorrhage, 1194–1196
MR imaging of, 1259–1263
appendicitis, 1261
diverticulitis, 1261–1262
mesenteric ischemia, 1260–1261
peritoneal and omental disorders, 1263
primary epiploic appendagitis, 1262–1263
small bowel disorders, 1259–1260
ultrasonography of, **1227–1242**
appendicitis. *See* Acute right lower quadrant.
cecal carcinoma, 1236–1237
Crohn's disease, 1234
ileocolitis and ileocecitis, 1234–1235
mesenteric lymphadenitis, 1235–1236
perforated peptic ulcer, 1241
person performing, 1227–1228
right-sided colonic diverticulitis, 1240–1241
sigmoid diverticulitis, 1237–1240
technique for, 1228–1229

Gastrointestinal perforation, diagnosis of, **1095–1115**
biliary tree perforation, 1112–1113
blunt trauma, 1106
colon cancer, 1110
CT in, 1096–1099
diverticulitis, 1109–1110
during barium enema or colonoscopy, 1109
foreign body perforation, 1099–1100
gastrocolic fistulas, 1102
iatrogenic perforation, 1100–1101
inflammatory conditions, 1106–1107
luminal contrast studies in, 1096–1099
oral contrast agents in, 1095–1096
peptic ulcer disease, 1101–1102, 1241

perforating tumors, 1107
plain films in, 1098
postoperative colon perforation, 1110, 1112
postoperative esophageal perforation, 1101
postoperative gastric perforation, 1102, 1105
postoperative small intestine, 1107–1108
rectal and colonic perforation, 1108–1109
small intestinal ischemia and infarction, 1105–1106
spontaneous esophageal perforation, 1099

Gastrointestinal stromal tumors, multislice CT of, 210–211

Genitourinary tract, ultrasonography of, in first trimester, 684

Genitourinary tract disorders, MR imaging of. *See* Abdominal emergencies.

Germ cell tumors, ovarian, MR imaging of, 808

Gestational sac, ultrasonography of, in first trimester, 663–665

Gibbs ringing artifact, on fetal MR imaging, 738

Glomerular filtration rate, MR imaging of, 1004–1006

Glomerulonephritis, and hypertension, 924–925

Graft infections, abdominal aortic, CT of, 1164

Graft thrombosis, abdominal aortic, CT of, 1164

Gray-scale ultrasonography, in infants, 932–933

Gynecologic disorders, and intraperitoneal hemorrhage, 1196–1198

H

Half-Fourier acquisition single-shot turbo spin echo sequence, in MR enteroclysis, 234, 236–237
in MR imaging, 52, 68

Halo sign, in multislice CT, of pulmonary nodules, 584–585

Hamartomas, renal, MR imaging of, 148–150

Harmonic imaging, of kidneys, 962

Heart, multislice CT of, **493–507**
data visualization in, 495, 497
advanced tools in, 497
maximum intensity projection in, 495
multiplanar reformats in, 495
three-dimensional, 495, 497
for arterial calcifications, 497–500
for cardiac function, 500–501
for vulnerable plaque, 504–505
image acquisition in, 493–495
in coronary angiography, 501–504

Heartbeat, embryonic, ultrasonography of, 666–667

Helical CT, of acute thoracic aortic injuries, 609

HELLP syndrome, and intraperitoneal hemorrhage, 1191–1192

Hemangiomas, hepatic, and intraperitoneal hemorrhage, 1189–1190
MR imaging of, 57–58

Hematoceles, MR imaging of, 809

Hematomas, intramural, multislice CT of, 538–539, 1161–1162
mediastinal, multislice CT of, 611
perinephric, imaging of, 1027
subcapsular, and hypertension, 926–927
imaging of, 1027

Hematosalpinx, MR imaging of, 809

Hematuria, CT of, 867
CT urography of. *See* CT urography.
MR urography of. *See* MR urography.
radiofrequency ablation of, 1068

Hemiazygos veins, multislice CT of, 558–559

Hemochromatosis, MR imaging of, 23, 79–80

Hemorrhage, intraperitoneal. *See* Intraperitoneal hemorrhage.

Hemorrhagic cholecystitis, diagnosis of, 1207–1208
MR imaging of, 1251–1252
ultrasonography of, 1207

Hemorrhagic disorders, hepatic, MR imaging of, 1248

Hemothorax, multislice CT of, 608

Hepatic artery stenosis, liver transplantation and, 1292–1293

Hepatic artery thrombosis, liver transplantation and, 1291–1292

Hepatic disease, diffuse. *See* Diffuse hepatic disease.

Hepatic disorders, and intraperitoneal hemorrhage, 1187, 1189–1192

Hepatic injuries, nuclear medicine studies of, 1285

Hepatic tumors, MR imaging of, **51–65**
biliary cystadenomas, 60
cholangiocarcinoma, 62–63
contrast-enhanced, 52–53
ferumoxides in, 53–54
gadolinium chelates in, 52–53
hepatocyte-selective, 54–55
perfusional, 55–56

cysts, 56–57
focal nodular hyperplasia, 58–59
hemangiomas, 57–58
hepatocellular adenomas, 59–60
hepatocellular carcinoma, 62, 81
metastatic disease, 60–62, 81
T1-weighted sequences in, 51–52
T2-weighted sequences in, 52

Hepatitis, MR imaging of, 74–75, 77, 1246–1247

Hepatocellular adenomas, and intraperitoneal hemorrhage, 1189
MR imaging of, 59–60

Hepatocellular carcinoma, and intraperitoneal hemorrhage, 1187
MR imaging of, 62, 81

Hepatocyte-selective contrast agents, in MR imaging, 54–56

Hereditary renal cancer, **1035–1049**
Birt-Hogg-Dubé syndrome, 1044–1045
familial renal cancer, 1046
familial renal oncocytomas, 1045
histologic subtypes of, 1035, 1037
leiomyoma renal cell carcinoma, 1042–1043
medullary carcinoma, 1045
papillary renal carcinoma, 1041–1042
translocation of chromosome 3, 1046
tuberous sclerosis, 1046
von Hippel–Lindau disease, 1037–1041
cryotherapy for, 1040–1041
CT of, 1040
MR imaging of, 1040
nephron-sparing surgery for, 1040
radiofrequency ablation of, 1040–1041

Herniation, of bowel, ultrasonography of, in first trimester, 683–684

HMO method, of quantifying female pelvic organ prolapse, 420

Hormone replacement therapy, and assessment of postmenopausal bleeding, 777

Human chorionic gonadotropin levels, in ectopic pregnancy, 673–674

Hydrocephalus, ultrasonography of, in first trimester, 682

Hydronephrosis, MR urography of, 1008–1009
versus pyonephrosis, 1267

Hyperreactio luteinalis, MR imaging of, 802

Hypertension, in infants, **929–942**
angiography of, 935–937
CT angiography of, 941
diagnosis of, clinical aspects of, 929–930
imaging of, etiology and, 931
nuclear medicine studies of, 937–941
ultrasonography of, 931–935
portal, and intraperitoneal hemorrhage, 1192
renal causes of, **909–928**
arteriovenous communications, 923–924
chronic pyelonephritis, 925–926
diabetic nephropathy, 925
evaluation of, 927
glomerulonephritis, 924–925
midaortic syndrome, 922
nephroslcerosis, 925
neurofibromatosis, 921–922
polyarteritis nodosa, 923
polycystic kidney disease, 926
posttraumatic stenosis, 924
renal artery aneurysm and dissection, 922–923
renal artery stenosis, 909–914, 916–919, 921
ACE inhibitor renal scintigraphy of, 913–914
atherosclerotic disease in, 911
CT angiography of, 918–919
Doppler ultrasonography of, 914, 916–917
fibromuscular dysplasia in, 911–912
functional versus anatomic imaging of, 913
intra-arterial angiography of, 919
management of, 919, 921
MR angiography of, 917–918
subcapsular hematomas, 926–927
Takayasu'a arteritis, 921
tumors, 926

Hypertrophic cardiomyopathy, MR imaging of, 22

Hysterography, saline infusion.
See Sonohysterography.

Hysteroscopy, of postmenopausal bleeding, 775
versus sonohysterography, 793–794

I

Ileal diverticulitis, CT of, 1131–1132

Ileal pouch, creation of, small bowel after.
See Small bowel, postoperative.
leakage from, 1108

Ileitis, terminal, CT of, 1129, 1131

Ileoanal pouch, creation of, 317, 319

Ileocecal Crohn's disease, ultrasonography of, 1234

Ileocecitis, infectious, ultrasonography of, 1234–1235

Ileocolitis, infectious, ultrasonography of, 1234–1235

Ileostomy, small bowel after, 314–315

Ileus, gallstone, diagnosis of, 1211–1213

Implants, breasts, ultrasonography of, 851–852

Infections, abdominal, nuclear medicine studies of, 1286
liver transplantation and, 1299–1300

Inferior vena cava, multislice CT of, 551–553

Inferior vena cava stenosis, liver transplantation and, 1294–1295

Inferior vena cava thrombosis, liver transplantation and, 1294–1295

Infertility, female. *See* Female infertility.

Inflammatory aortic aneurysms, CT of, 1158–1159

Inflammatory bowel disease, multislice CT of, 657

Inflammatory breast cancer, ultrasonography of, 845

Inflammatory masses, ovarian, MR imaging of, 808–809

Intercostal chest wall, multislice CT of, 559–560

Intestinal gas patterns, in plain films, of small bowel obstruction, 264–265

Intra-abdominal adhesions, and small bowel obstruction, 241, 251–252

Intra-arterial angiography, of renal artery stenosis, 919

Intra-arterial digital subtraction arteriography, of hypertension, in infants, 936

Intradecidual sign, in ultrasonography, of gestational sac, 664

Intraductal papillary mucinous tumors, MR cholangiopancreatography of, 107–110

Intrahepatic duct perforation, diagnosis of, 1112–1113

Intramural air, on CT, of small bowel or mesenteric injury, 1175

Intramural hematomas, multislice CT of, 538–539, 1161–1162

Intraperitoneal fluid, on CT, of small bowel or mesenteric injury, 1176–1178

Intraperitoneal hemorrhage, **1183–1201**
amyloidosis and, 1192
cirrhosis and, 1192
CT of, 1183–1185
ectopic pregnancy and, 1196–1197
focal nodular hyperplasia and, 1189
HELLP syndrome and, 1191–1192
hemangiomas and, 1189–1190
hepatocellular adenoma and, 1189
hepatocellular carcinoma and, 1187
metastatic disease and, 1190–1191
MR imaging of, 1186
pancreatitis and, 1195–1196
peliosis and, 1193
peptic ulcers and, 1194–1195
portal hypertension and, 1192
ruptured ovarian cysts and, 1197–1198
splenic rupture and, 1192–1193
ultrasonography of, 1185–1186
visceral artery abnormalities and, 1193–1194

Intraperitoneal metastases, differential diagnosis of, 345

Intrauterine adhesions, sonohysterography of, 789

Intravenous urography, of renal trauma, 1018

Intussusception, **1137–1151**
clinical features of, 1142–1143
diagnosis of, 1143–1149
barium studies in, 1144
CT in, 1147–1148
MR imaging in, 1148–1149
plain films in, 1144
ultrasonography in, 1145–1147
etiology of, 1138–1142
evacuation proctography of, 433, 435
location of, 1137–1138
management of, 1149
pathophysiology of, 1137

Iron deposition, hepatic, MR imaging of, 79–80

Ischemic heart disease, MR imaging of. *See* Cardiovascular system.

J

Jejunoileal bypass, small bowel after, 310, 312–313

Jejunostomy, small bowel after, 313–314

Jejunostomy tube, misplaced, diagnosis of, 1108

Jugular veins, multislice CT of, 553–554

Juxtaglomerular cell tumors, and hypertension, 926

K

Kaposi's sarcoma, of small bowel, differential diagnosis of, 342

Kawasaki disease, MR imaging of, 20

Kidneys, CT of, **863–875**
compression for distention in, 874
contrast in, 864–866
concentration and total dosage, 864–865
high-concentration contrast, 865–866
injection rates, 865
oral contrast versus water, 865
detectors in, 864
for crossing vessels, 871
for renal masses, 868–871
characterization of, 869
delayed imaging in, 870
nephrographic phase in, 870
staging of, 869–870
versus CT angiography, 870–871
for transplant donor evaluation, 871
for trauma, 868
for urolithiasis, 867–868
molecular imaging in, 874
pitch in, 863–864
radiation dosage in, 872–873
in children, 872, 873
in pregnancy, 872–873
reconstruction in, 864
versus CT angiography, 866–867
volumetric acquisition in, 873–874
devascularized, imaging of, 1030
imaging of, ultrasound contrast agents in. *See* Ultrasound contrast agents.
MR imaging of, 145–152, **877–907**
breathhold technique for, 880, 882
contrast-enhanced dynamic imaging, 895–898
applications of, 895–898
contrast media and volume in, 898
contrast rate in, 898
flush volume and rate in, 898
power injector in, 898
timing of, 898
flow-sensitive imaging, 894–895
for angiomyolipomas, 148–150
for cysts, 151–152
for lymphomas, 150
for metastatic disease, 150–151
for preoperative planning, 152
for renal arteries, 878–880
versus MR angiography, 878–880
for renal cell carcinoma, 146–148
for renal masses, 877–878
for renal veins, 880
for urothelial tumors, 878
image processing in, 898, 900–901
subtraction in, 898, 900
three-dimensional reconstruction in, 900–901
non-breathhold technique for, 882–884
coils and parallel imaging in, 883–884
fast acquisitions in, 882–883
motion compensation strategies in, 883
T1-weighted imaging, 886–888, 890–894
applications of, 886
gradient-echo sequences in, 886–888
in-phase and opposed phase, 888, 890–891
spin-echo sequences in, 892
three-dimensional, 892–894
two- versus three-dimensional, 892
T2-weighted imaging, 884–886
applications of, 884
echo-train imaging in, 885–886
Half-Fourier reconstruction in, 886
spin echo sequences in, 884–885
technique for, 145–146
shattered, imaging of, 1028–1029

Klatskin's tumors, MR cholangiopancreatography of, 93–94

Kock pouch, creation of, 316–317

Krukenberg tumors, MR imaging of, 805

L

Lacerations, renal, imaging of, 1027

Laparoscopic nephrectomy, for renal tumors, 1060, 1061

Laser photocoagulation, for twin-twin transfusion syndrome, 718

Left brachiocephalic vein, multislice CT of, 527

Left inferior pulmonary vein, multislice CT of, 527

Left lower lobe atelectasis, multislice CT of, 529

Left pleural effusion, multislice CT of, 529

Left superior intercostal vein, multislice CT of, 527

Leiomyoma renal cell carcinoma, hereditary, imaging of, 1042–1043

Leiomyomas, bladder, MR imaging of, 170
malignant potential of, 1043
submucosal, sonohysterography of, 787
uterine, and postmenopausal bleeding, ultrasonography of, 773
MR imaging of, 182–183

Leiomyosarcomas, malignant potential of, 1043

Leriche's syndrome, MR angiography of, 129–130

Levator ani muscle complex, in women, MR imaging of, 413, 415

Lithiasis, urinary. *See* Urinary lithiasis.

Liver, multislice CT of, 1088

Liver disorders, MR imaging of. *See* Abdominal emergencies.

Liver transplantation, complications of, **1289–1305**
abscesses and fluid collections, 1299
arterioportal fistulas, 1295
biliary, 1295–1296, 1298
bowel obstruction, 1298
hepatic artery stenosis or thrombosis, 1291–1293
infections, 1299–1300
inferior vena cava stenosis or thrombosis, 1294–1295
liver ischemia, 1298–1299
malignancies, 1300–1303
portal vein stenosis or thrombosis, 1293–1294
normal anatomy after, 1289–1290

Liver tumors. *See* Hepatic tumors.

Luminal contrast studies, of gastrointestinal perforation, 1096–1099

Lung cancer, metastatic to kidneys, MR imaging of, 150–151
screening for, low-dose CT in, 597–598
multislice CT in, 483–484

Lung volume, measurement of, multislice CT in, 483

Lymph nodes, involvement of, by bladder tumors, MR imaging of, 169

Lymphadenectomy, for renal tumors, 1059, 1061

Lymphadenitis, mesenteric, ultrasonography of, 1235–1236

Lymphoid hyperplasia, of small bowel, differential diagnosis of, 355–356

Lymphomas, bladder effects of, MR imaging of, 170
hepatic effects of, MR imaging of, 81
of small bowel, CT enteroclysis in, 255–256
differential diagnosis of, 345
MR enteroclysis in, 245
multislice CT of, 210
renal effects of, MR imaging of, 150

M

Magnetic resonance imaging, fetal. *See* Fetal magnetic resonance imaging.
in enteroclysis. *See* MR enteroclysis.
of abdominal emergencies. *See* Abdominal emergencies.
of acute mesenteric ischemia, 328–329
of adrenal glands. *See* Adrenal glands.
of anal fistulas. *See* Anal fistulas.
of aortic dissection, 1160–1161
of bladder. *See* Bladder.
of breasts. *See* Breasts.
of cardiovascular system. *See* Cardiovascular system.
of diffuse hepatic disease. *See* Diffuse hepatic disease.
of female pelvic organ prolapse. *See* Female pelvic organ prolapse.
of female pelvis. *See* Female pelvis.
of hepatic tumors. *See* Hepatic tumors.
of intraperitoneal hemorrhage, 1186
of intussusception, 1148–1149
of kidneys. *See* Kidneys.
of osteoporosis, 825–827
of ovaries. *See* Ovaries.
of pelvic floor relaxation. *See* Pelvic floor relaxation.
of renal function. *See* Renal function.
of renal trauma, 1021
of trabecular bone structure, in osteoporosis, 830–834
of urinary lithiasis, versus CT, 988, 990
of von Hippel–Lindau disease, 1040
physics of, **1–15**
conventional image acquisition, 3
image data, 2–3
motion artifacts, 3
motion compensation approaches to, 3–5
pulse sequences, 5–7, 9–12, 161–162
echo planar imaging, 9–12
fast spin echo imaging, 6–7, 9
spiral imaging, 9–12
reduction of data collection in, 12–14
requirements and challenges of, 1

Malignancies, and intussusception, 1138
liver transplantation and, 1300–1303

Mallory-Weiss tears, diagnosis of, 1099

Mangafodipir, in MR imaging, 54–55

Maternal serum screening, to diagnose aneuploidy, 696–697, 704

McBurney's point, CT of, 1123–1124

Meckel's diverticulitis, CT of, 1131–1132

Mediastinal evaluation, multislice CT in, in children, 650

Mediastinal hematomas, multislice CT of, 611

Mediastinal masses and adenopathy, multislice CT of, 529

Medullary carcinoma, imaging of, 1045

Melanoma, metastatic to small bowel, CT enteroclysis in, 254–255

Mesenchymal tumors, bladder, MR imaging of, 170–171

Mesenteric adenitis, CT of, 1128–1129
multislice CT of, in children, 656

Mesenteric infiltration, on CT, of small bowel or mesenteric injury, 1176

Mesenteric injury. *See* Small bowel or mesenteric injury.

Mesenteric ischemia, **328–340**
abdominal trauma and, 337–338
bowel obstruction and, 332–333
colon cancer and, 337
drug-induced enteropathy and, 335–337
localized, 331–332
MR imaging of, 1260–1261
multislice CT of, 203–206
non-occlusive, 330–331
radiation enteritis and, 334–335
thromboembolism and, 325–330
angiography of, 327
barium studies of, 327
CT of, 327–328
MR imaging of, 328–329
plain films of, 326
ultrasonography of, 326–327
vasculitis and, 333–334

Mesenteric lymphadenitis, ultrasonography of, 1235–1236

Mesenteric vessels, multislice CT of, 203

Metastatic disease, and intraperitoneal hemorrhage, 1190–1191
from renal cell carcinoma, radiofrequency ablation of, 1068–1070
to bones, MR imaging of, 168–169
to breasts, ultrasonography of, 845
to kidneys, MR imaging of, 150–151
to liver, MR imaging of, 60–62, 81

Methylcellulose, in enteroclysis, 219–220, 222

Metoclopramide, in enteroclysis, 213

Micro-computed tomography, of trabecular bone structure, in osteoporosis, 830–831

Microcalcifications, in breasts, ultrasonography of, 850–851

Midaortic syndrome, and hypertension, 922

Midazolam, in enteroclysis, 217

Minimal aortic injury, multislice CT of, 612

Mirizzi syndrome, diagnosis of, 1213–1215, 1255–1256

Molecular imaging, of kidneys, 874

Monoamniotic twins, ultrasonography of, 724–725

Monochorionic twins, embryology of, 709–710
ultrasonography of, **709–727**
chorionicity and amnionicity in, 710–712
for acardiac parabiotic twin, 719–722
radiofrequency ablation of, 721–722
for conjoined twins, 723–724
for discordant anomalies, 722
for monoamniotic twins, 724–725
for twin embolization syndrome, 719
for twin-twin transfusion syndrome, 714–719
amnioreduction for, 717–718
laser photocoagulation for, 718
for unequal placental sharing, 714
placental vascular anatomy in, 712–713

Motion artifacts, in multislice CT, of thoracic aorta, 531
on fetal MR imaging, 734

MR angiography, contrast-enhanced, 116, 118–124
bolus delivery in, 123–124
pulse sequences in, 121–123
timing of, 119–121
future directions in, 138–140
of abdominal aorta. *See* Abdominal aorta.
of chest. *See* Chest.
of coronary arteries, 19–21
of peripheral arterial occlusive disease, 133–136, 138
bolus chasing in, 134–136, 138
of renal arteries, 878–880
of renal artery stenosis, 917–918
phase-contrast, 115–116
three-dimensional, of kidneys, 892–894
time-of-flight, 115–116

MR cholangiopancreatography, of choledocholithiasis, 1253–1254
of pancreatic diseases. *See* Pancreatic diseases.

MR enteroclysis, **231–248**
advantages of, 246
contrast-enhanced, 237–238, 244–245

disadvantages of, 246
in Crohn's disease, 241–242, 244–245, 286, 288–289, 292, 294
in small bowel neoplasms, 245
in small bowel obstruction, 238, 241, 273
pitfalls of, 245–246
results of, 238, 241–242, 244–245
technique for, 231–234, 236–238
cross-sectional MR imaging in, 233–234, 236–237
MR fluoroscopy in, 232–233

MR fluoroscopy, in MR enteroclysis, 232–233

MR urography, of hematuria, 953–957
gadolinium-enhanced T1-weighted, 955–957
heavily T2-weighted, 953–955
of hydronephrosis, 1008–1009
of renal colic, 1265–1267
technique for, 146

Mucinous cystic neoplasms, MR cholangiopancreatography of, 107

Mucopolysaccharidoses, MR imaging of, 80–81

Mucosal nodularity, of small bowel, differential diagnosis of, 354–358, 360

Müllerian anomalies, MR imaging of, 181–182

Multichannel CT. *See* Multislice CT.

Multidetector row CT. *See* Multislice CT.

Multislice CT, fundamentals of, **465–474**
anatomic coverage, 467, 469–470
detector array configuration, 466–467
image reconstruction, 470–471
isotropic imaging, 467
radiation dose, 471–474
patient exposure to, 473–474
scanners, 465–466
in children, **641–659**
contrast media in, 642
of abdomen, 651, 653–657, 1090
abdominal pain, 655–657
advantages of, 653
appendicitis, 655–656
inflammatory bowel disease, 657
mesenteric adenitis, 656
omental torsion, 656–657
ovarian disorders, 657
urolithiasis, 657
of chest, 645–651
advantages of, 645–646
airway evaluation, 649–650
cardiovascular evaluation, 650
chest wall abnormalities, 650–651
mediastinal evaluation, 650
parameters for, 647
parenchymal disorders, 648–649
parameters for, 643–644
patient preparation for, 642
radiation dose in, 644–645
sequence of, 643
timing of, 642–643
of abdominal aorta, 1154
of acute abdominal disease. *See* Acute abdominal disease.
of central airways. *See* Central airways.
of deep venous thrombosis, 512
of heart. *See* Heart.
of pulmonary embolism. *See* Pulmonary embolism.
of pulmonary nodules. *See* Pulmonary nodules.
of small bowel, **199–212**
for Crohn's disease, 206–207
for mesenteric ischemia, 203–206, 328
for mesenteric vessels, 203
for neoplasms, 208–211
for obstruction, 207–208, 271–273
historical aspects of, 199
intravenous contrast in, 200
normal anatomy in, 201–203
oral contrast in, 199–200
technique for, 199–201
three-dimensional imaging with, 201
versus spiral CT, 200–201
of thoracic aorta. *See* Thoracic aorta.
of thoracic trauma. *See* Thoracic trauma.
of thoracic venous anatomy. *See* Thoracic venous anatomy.
of thorax. *See* Thorax.
of tracheobronchomalacia. *See* Tracheobronchomalacia.
paddle-wheel method in, **621–630**
advantages of, 624–625
disadvantages of, 625
for central airway disorders, 629
for lung nodules, 628–629
for pulmonary vascular disorders, 625–627
image number and lung anatomy in, 621–623
optimization of anatomic detail in, 624
viewing methods in, 624

Mycotic aneurysms, of thoracic aorta, multislice CT of, 540–541

Myelolipomas, MR imaging of, 156

Myocardial viability, MR imaging of, 17

N

Nephrectomy, partial, for renal tumors, 1059–1061
laparoscopic, for renal tumors, 1060, 1061
radical, for renal tumors, 1057–1058, 1060–1061
laparoscopic, for renal tumors, 1060, 1061

Nephron-sparing surgery, for von Hippel–Lindau disease, 1040

Nephropathy, diabetic, and hypertension, 925

Nephrosclerosis, and hypertension, 925

Nephroureterectomy, for renal tumors, 1059

Neurofibromas, bladder, MR imaging of, 170

Neurofibromatosis, and hypertension, 921–922

Nodal involvement, by breast cancer, ultrasonography of, 847–848

Non-breathhold imaging, of abdominal emergencies, 1244–1245
of kidneys. *See* Kidneys, MR imaging of.

Nonaortic thoracic vascular injuries, multislice CT of, 612

Nuchal translucency, ultrasonography of, in first trimester, 674–676, 682, 704

Nuclear medicine studies, of abdominal emergencies. *See* Abdominal emergencies.
of hypertension, in infants, 937–941
of renal artery stenosis, 913–914
of renal trauma, 1021

O

Omental disease, CT of, 1133–1134
MR imaging of, 1263

Omental torsion, multislice CT of, in children, 656–657

Oncocytomas, familial renal, imaging of, 1045

Osteodensitometry, of osteoporosis, 817–818

Osteoporosis, **813–839**
and vertebral fractures, 814–817
definition of, 813–814
dual x-ray absorptiometry of, 818–820
MR imaging of, 825–827
osteodensitometry of, 817–818
plain films of, 816–817
quantitative CT of, 820–824
quantitative ultrasonography of, 824–825
trabecular bone structure in, 827, 829–834
micro-CT of, 830–831
MR imaging of, 830–834
plain films of, 829–830
quantitative ultrasonography of, 830

Ovarian cancer, CT enteroclysis in, 256
MR imaging of, 188

Ovarian cysts, and intraperitoneal hemorrhage, 1197–1198

Ovarian disorders, multislice CT of, in children, 657

Ovarian hyperstimulation syndrome, MR imaging of, 802

Ovaries, MR imaging of, **799–812**
for benign neoplasia, 803–805, 808
germ cell tumors, 808
sex-cord stromal tumors, 805, 808
surface epithelial tumors, 804–805
for bleeding, 802
for endometriomas, 803
for functional cysts, 800, 802–803
for hematosalpinx and hematocele, 809
for inflammatory masses, 808–809
for massive edema, 809, 811
for peritoneal inclusion cysts, 803
for solid endometriosis, 811
for torsion, 809
normal ovaries, 799–800
technique for, 799
normal, versus female infertility, 764

P

Pancreas, multislice CT of, 1088–1089

Pancreas divisum, MR cholangiopancreatography of, 91, 101

Pancreatic diseases, MR cholangiopancreatography of, **89–96, 97–114**
anatomy in, 100–101
biliary congenital variants, 91
biliary cystic diseases, 90–91
cancer, 94
cholangiocarcinoma, 93–94
cholecystolithiasis, 91
choledocholithiasis, 91–92
cysts, 105–110
future directions in, 94–95
pancreas divisum, 91, 101
pancreatitis, 93, 101–104
versus pancreatic cancer, 104–105
postoperative biliary complications, 92–93
primary sclerosing cholangitis, 92
santoriniceles, 101
technique for, 89–90, 97–99

versus endoscopic retrograde cholangio pancreatography, 89, 99–100
MR imaging of, 1256–1259

Pancreatic fluid collections, interventional approach to, **1217–1226**
access route planning in, 1217
assessment and follow-up in, 1224–1225
catheter selection and insertion in, 1217–1218
complications of, 1225
failure of, 1225
pancreatic abscesses, 1220–1223
pancreatic necrosis, 1223–1224
peripancreatic effusions, 1218
pseudocysts, 1218, 1220
results of, 1225

Pancreatitis, and intraperitoneal hemorrhage, 1195–1196
MR cholangiopancreatography of, 93, 101–104
versus pancreatic cancer, MR cholangiopancreatography of, 104–105

Papillary renal carcinoma, hereditary, imaging of, 1041–1042

Paramagnetic contrast agents, in MR angiography, of chest, 30–31

Paraspinal veins, multislice CT of, 559–560

Parenchymal diseases, multislice CT of, in children, 648–649

Partial nephrectomy, for renal tumors, 1059–1061
laparoscopic, for renal tumors, 1060, 1061

Partial volume artifact, on fetal MR imaging, 738

Patau syndrome, ultrasonography of, in second trimester, 698

Peliosis, and intraperitoneal hemorrhage, 1193

Pelvic floor musculature, in women, MR imaging of, 413, 415–416

Pelvic floor relaxation, **747–756**
anatomy of, 747, 749
defecography of, 749–750
MR imaging of, 188–189, 750–755
anatomy in, 751–752
for anterior compartment pathology, 752–753
for middle compartment pathology, 753
for posterior compartment pathology, 753–754
seated imaging in, 754–755
severe cases of, 754
technique for, 751
three-dimensional volumetric analysis in, 755
ultrasonography of, 749
voiding cystourethrography of, 749

Pelvic fluid, in ectopic pregnancy, ultrasonography of, 672

Pelvic organ prolapse, in women. *See* Female pelvic organ prolapse.

Pelvis, female. *See* Female pelvis.

Penetrating atherosclerotic ulcers, of thoracic aorta, multislice CT of, 539–540

Peptic ulcers, and intraperitoneal hemorrhage, 1194–1195
perforation of, 1101–1102, 1241

Percutaneous transluminal renal artery angioplasty, for renal artery stenosis, 919, 921

Percutaneous umbilical cord sampling, to diagnose aneuploidy, 696

Perfusional contrast agents, in MR imaging, 55–56

Periaortic pathology, multislice CT of, 528–529

Pericardial disease, MR imaging of, 23–24

Pericardial effusion, multislice CT of, 529

Pericardial injuries, multislice CT of, 612–613

Pericardial recesses, multislice CT of, 527

Pericardiophrenic veins, multislice CT of, 554–555, 558

Perineal herniation, in women, evacuation proctography of, 398

Perinephric hematomas, imaging of, 1027

Peripancreatic effusions, interventional approach to, 1218

Peripheral arterial occlusive disease, MR angiography of, 133–136, 138

Peritoneal cavity, in female infertility, 764

Peritoneal disease, MR imaging of, 1263

Peritoneal inclusion cysts, MR imaging of, 803

Peritoneoceles, in women, evacuation proctography of, 400

Peritonitis, bile, diagnosis of, 1112

Periurethral soft tissues, MR imaging of, 411–412

Peutz-Jeghers syndrome, small bowel abnormalities in, differential diagnosis of, 344

Phase-contrast MR angiography, technique for, 115–116

Phase ordering with automatic window selection, in MR imaging, 5

Pheochromocytomas, adrenal, MR imaging of, 155–156
bladder, MR imaging of, 170

Phleboliths, versus urinary lithiasis, 980, 982–983

Photocoagulation, laser, for twin-twin transfusion syndrome, 718

Placenta, vascular anatomy of, 712–713

Plain films, of acute mesenteric ischemia, 326
of acute thoracic aortic injuries, 609
of drug-induced enteropathy, 336
of foreign body perforation, 1099
of fracture and deformity, due to osteoporosis, 816–817
of gastrointestinal perforation, 1098
of intussusception, 1144
of postoperative small bowel, 313
of pulmonary contusions, 614
of pulmonary lacerations, 614
of renal trauma, 1018
of scapular fractures, 604
of small bowel obstruction, 264–265, 278
of trabecular bone structure, in osteoporosis, 829–830
of tracheobronchial injuries, 616

Pleural effusion, multislice CT of, 529, 608

Pneumomediastinum, multislice CT of, 607–608

Pneumothorax, multislice CT of, 607–608

Polyarteritis nodosa, and hypertension, 923

Polycystic kidney disease, and hypertension, 926

Polycystic ovarian syndrome, and female infertility, 764–766
MR imaging of, 184–185, 803

Polyps, endometrial, and postmenopausal bleeding, ultrasonography of, 771–772
sonohysterography of, 785–786
in colon, virtual colonoscopy of. *See* Virtual colonoscopy.
in small bowel, differential diagnosis of, 341–342, 344

Portal hypertension, and intraperitoneal hemorrhage, 1192
in cirrhosis, MR imaging of, 74

Portal vein stenosis, liver transplantation and, 1293–1294

Portal vein thrombosis, liver transplantation and, 1293–1294
MR imaging of, 81, 84, 1247

Postmenopausal bleeding, color duplex Doppler imaging of, 775
Doppler imaging of, 775
hysteroscopy of, 775
sonohysterography of, 771–772, 775, 783–784, 791–793
three-dimensional ultrasonography of, 775–776
ultrasonography of, **769–780**
atrophic endometrium in, 770–771
endometrial carcinoma in, 773–775
endometrial hyperplasia in, 772–773
endometrial polyps in, 771–772
in women on hormone replacement therapy, 777
in women on tamoxifen, 776–777
uterine leiomyomas in, 773

Posttraumatic stenosis, of renal artery, and hypertension, 924

Pouchogram, of ileoanal pouch, 317, 319

Pregnancy, appendicitis in, MR imaging of, 1261
ectopic, and intraperitoneal hemorrhage, 1196–1197
hematosalpinx and hematocele due to, MR imaging of, 809
ultrasonography of. *See* Ultrasonography, in first trimester.
MR imaging in, 189–190
normal, ultrasonography of. *See* Ultrasonography, in first trimester.
radiation dosage in, 872–873
renal colic in, MR imaging of, 1267

Primary sclerosing cholangitis, MR cholangiopancreatography of, 92
MR imaging of, 74

Pseudoaneurysms, hepatic artery, liver transplantation and, 1293

Pseudocoarctation, of thoracic aorta, multislice CT of, 526

Pseudocysts, adrenal, MR imaging of, 156–157
pancreatic, interventional approach to, 1218, 1220
MR cholangiopancreatography of, 105–106
MR imaging of, 1258

Pseudosarcomas, bladder, MR imaging of, 171

Pseudotumors, bladder, MR imaging of, 171
renal, imaging of, ultrasound contrast agents in, 968

Pulmonary arteries, MR angiography of, 37–39
multislice CT of, 480, 482

Pulmonary contusion, multislice CT of, 614

Pulmonary embolism, management of, 517–519
multislice CT of, 480, **509–521**
diagnostic accuracy of, 516–517
image interpretation in, 512–516
conditions of, 515
features of acute pulmonary embolism, 512–513
features of chronic pulmonary embolism, 515
new tools in, 515–516
pitfalls in, 513–515
in follow-up, 517
paddle-wheel method in, 625–627
techniques for, 509–512
acquisition protocols, 509–510
impact on image quality, 512
injection protocols, 510–511
optimization of scanning parameters, 511–512
versus other techniques, 517

Pulmonary lacerations, multislice CT of, 614

Pulmonary nodules, multislice CT of, **579–602**
atypical adenomatous hyperplasia, 585–587
computer-aided diagnosis in, 593, 595
contrast enhancement in, 588
densitometry in, 587–588
image registration in, 595–597
in lung cancer screening, 597–598
morphology in, 583–585
nodule growth in, 588–589, 591–592
paddle-wheel method in, 628–629
parameters for, 581–582
techniques for, 579–581
viewing methods in, 582
volume quantification in, 592–593

Pulmonary vascular disorders, multislice CT of, paddle-wheel method in, 625–627

Pulmonary veins, multislice CT of, 480, 482, 560–561
paddle-wheel method in, 627

Pulse sequences, in MR angiography, 32–33, 121–123
in MR imaging. *See* Magnetic resonance imaging.

Pyelography, retrograde, of renal trauma, 1020

Pyelonephritis, chronic, and hypertension, 925–926
imaging of, ultrasound contrast agents in, 972–973
MR imaging of, 1267

Pyonephrosis, versus hydronephrosis, 1267

Q

Quantitative computed tomography, of osteoporosis, 820–824

Quantitative ultrasonography, of osteoporosis, 824–825
of trabecular bone structure, in osteoporosis, 830

R

Radiation enteritis, and mesenteric ischemia, 334–335
CT enteroclysis in, 257–258
CT of, 335

Radical nephrectomy, for renal tumors, 1057–1058, 1060–1061
laparoscopic, for renal tumors, 1060, 1061

Radiofrequency ablation, of acardiac parabiotic twin, 721–722
of renal cell carcinoma. *See* Renal cell carcinoma.
of von Hippel–Lindau disease, 1040–1041

Radiofrequency interference, on fetal MR imaging, 737

Rectal perforation, diagnosis of, 1108–1109

Rectal prolapse, evacuation proctography of, 433, 436

Rectoceles, evacuation proctography of, 430–432
in women, 397–398

Renal arteries, MR imaging of, 878–880

Renal artery aneurysms, and hypertension, 922–923

Renal artery dissection, and hypertension, 923

Renal artery stenosis, and hypertension. *See* Hypertension.
imaging of, ultrasound contrast agents in, 971
MR angiography of, 130

Renal artery thrombosis, ultrasonography of, in infants, 932

Renal cancer, hereditary. *See* Hereditary renal cancer.

Renal cell carcinoma, imaging of, ultrasound contrast agents in, 963
MR imaging of, 146–148

radiofrequency ablation of, **1063–1071**
clinical studies of, 1065–1067
devices for, 1063–1064
for distant metastases, 1068–1070
for recurrent disease, 1068
treatment zone in, 1064
tumor size and, 1065
viable tumor following, 1067

Renal colic, MR imaging of, 1263–1267

Renal cystic diseases, ultrasonography of, in infants, 932

Renal failure, acute, MR imaging of, 1268

Renal function, MR imaging of, **999–1015**
captopril in, 1006–1008
contrast quantification in, 1000–1001
for hydronephrosis, 1008–1009
for renal transplant evaluation, 1009–1013
gadolinium dose optimization in, 1001
glomerular filtration rate in, 1004–1006
image postprocessing in, 1001–1002
perfusion imaging in, 1002–1004
arterial spin labeling technique for, 1003
blood oxygen level–dependent imaging in, 1003–1004
extravascular contrast agents in, 1002–1003
intravascular contrast agents in, 1003

Renal hamartomas, MR imaging of, 148–150

Renal infarcts, MR imaging of, 1268

Renal injuries, nuclear medicine studies of, 1285–1286

Renal masses, CT of. *See* Kidneys, CT of.
cystic, imaging of, ultrasound contrast agents in, 965–968
indeterminate, imaging of, ultrasound contrast agents in, 969, 971
MR imaging of, 877–878

Renal perfusion, imaging of, ultrasound contrast agents in, 971–973

Renal transplantation, donor evaluation for, CT in, 871
postoperative evaluation of, MR angiography in, 130–131, 133
MR imaging in, 1009–1013

Renal trauma, classification of, 1024–1030
grade 1, 1026–1027
grade 4, 1027–1028
grade 5, 1028–1030
grades 2 and 3, 1027
vascular contrast extravasation in, 1030–3031
imaging of, **1017–1033**
angiography in, 1019
CT in, 868, 1021–1024
contrast in, 1021
interpretation of, 1023–1024
technique for, 1021–1023
diagnostic peritoneal lavage in, 1020
intravenous urography in, 1018
MR imaging in, 1021
nuclear medicine studies in, 1021
patient selection for, 1017–1018
plain films in, 1018
retrograde pyelography in, 1020
ultrasonography in, 1019
ultrasound contrast agents in, 973

Renal tumors, cystic, 1052
solid, 1052
surgical management of, **1051–1062**
anatomy in, 1052–1056
blood supply, 1054–1056
lymphatic drainage, 1056
laparoscopic, 1060, 1061
lymphadenectomy in, 1059, 1061
nephroureterectomy in, 1059
partial nephrectomy in, 1059–1061
radical nephrectomy in, 1057–1058, 1060–1061
surgical approaches in, 1056
vena caval extension and, 1058–1059
versus pseudotumors, 1052

Renal vein injuries, imaging of, 1030

Renal vein thrombosis, MR imaging of, 1269
ultrasonography of, in infants, 932

Renal veins, MR imaging of, 880

Reninomas, and hypertension, 926

Resistive index, in color Doppler imaging, in infants, 933–934

Respiratory ordered phase encoding, in MR imaging, 4–5

Rest imaging, of cardiovascular disease, 17

Restrictive cardiomyopathy, MR imaging of, 23

Retained products of conception, sonohysterography of, 789–790

Retrograde pyelography, of renal trauma, 1020

Retroperitoneal fluid, on CT, of small bowel or mesenteric injury, 1178–1179

Retroperitoneal hemorrhage, from abdominal aortic aneurysms, 1155

Rhabdomyosarcomas, bladder, MR imaging of, 171

Rib fractures, multislice CT of, 603–604

Right atrial appendage, multislice CT of, 527

Right lower quadrant, acute. *See* Acute right lower quadrant.

Right upper quadrant pain, nuclear medicine studies of, 1279–1282, 1285

Right ventricular dysplasia, arrhythmogenic, MR imaging of, 21–22

S

Sacculations, of small bowel, differential diagnosis of, 360

Saline infusion hysterography. *See* Sonohysterography.

Salpingitis isthmica nodosa, and female infertility, 762–763

Santoriniceles, MR cholangiopancreatography of, 101

Saphenous veins, multislice CT of, 554–555, 558

Scapular fractures, multislice CT of, 604

Sclerosing stromal tumors, MR imaging of, 805, 808

Seat-belt injuries, and mesenteric ischemia, 338

Secretin-enhanced dynamic MR cholangiopancreatography, technique for, 99

Segmented volume acquisition, in MR angiography, 139

Serous microcystic adenomas, MR cholangiopancreatography of, 107

Serum human chorionic gonadotropin levels, in ectopic pregnancy, 673–674

Sex-cord stromal tumors, MR imaging of, 805, 808

Short-bowel syndrome, enteroanastomosis and, 310

Sickle cell trait, medullary carcinoma in, 1045

Sigmoid diverticulitis, ultrasonography of, 1237–1240

Sigmoidoceles, in women, evacuation proctography of, 401–402

Signal-to-noise ratio, on fetal MR imaging, 738, 740

Single-detector helical CT, of central airways, 566

Single-photon absorptiometry, of osteoporosis, 817–818

Small bowel, multislice CT of. *See* Multislice CT.
  postoperative, **303–324**
    after enterectomy and anastomosis, 305–306, 308–310
      blind loop syndrome in, 309
      blind pouch syndrome in, 308–309
      short-bowel syndrome in, 310
    after enterostomy, 313–315
    after gastric surgery, 303–305
    after ileal pouch construction, 315–317, 319
      continent ileostomy reservoir, 316–317
      ileoanal pouch, 317, 319
    after ileostomy, 314–315
    after jejunoileal bypass, 310, 312–313
    after jejunostomy, 313–314
    after small bowel transplantation, 319–322
    CT of, 304, 320–322
    enteroclysis in, 315
    plain films of, 313
    ultrasonography of, 304

Small bowel abnormalities, differential diagnosis of, **341–362**
  abnormalities in fold size, 352–354
  dilated lumen with normal folds, 350–352
  extrinsic contour distortions, 347–350
    bowel loop separation without tethering, 349–350
    extrinsic mass effect and tethering, 348–349
    tethering of folds, 347–348
  focal mass lesions, 341–342, 344–347
    annular lesions, 345–347
    cavitary masses, 344–345
    multiple polypoid lesions, 342, 344
    solitary polyp, 341–342
  muscular nodularity and irregular fold thickening, 354–358, 360
    distal small bowel, 355–357
    proximal small bowel, 357–358, 360
  sacculations, 360
  tubular bowel, 360

Small bowel disorders, MR imaging of, 1259–1260

Small bowel enteroclysis. *See* CT enteroclysis; Enteroclysis; MR enteroclysis.

Small bowel neoplasms, CT enteroclysis in, 254–156
  MR enteroclysis in, 245
  multislice CT of, 208–211

Small bowel obstruction, **263–282**
  and mesenteric ischemia, 332–333
  barium studies of, 265, 270–271
  closed-loop, 275–278
  conservative management of, 273–275

CT enteroclysis in, 251–252, 265, 270–273, 278, 279
CT of, 271–273, 276–279, 332–333
enteroclysis in, 275–276
etiology of, 263–264
liver transplantation and, 1298
MR enteroclysis in, 238, 241, 273
multislice CT of, 207–208
plain films of, 264–265, 278

Small bowel or mesenteric injury, clinical features of, 1172
CT of, **1171–1182**
efficacy of, 1180
findings on, 1173–1180
bowel discontinuity, 1173
bowel wall enhancement, 1179–1180
bowel wall thickening, 1175–1176
extraluminal air, 1173–1175
extraluminal oral contrast agent, 1175
intramural air, 1175
intraperitoneal fluid, 1176–1178
mesenteric infiltration, 1176
retroperitoneal fluid, 1178–1179
technique for, 1172–1173
demographics of, 1171
pathophysiology of, 1171–1172

Small bowel perforation, diagnosis of, 1105–1108

Snowstorm sign, in ultrasonography, of breast implants, 852

Solitary rectal ulcer syndrome, evacuation proctography of, 435–436

Sonohysterography, **781–797**
catheter insertion for, 782–783
of dysfunctional uterine bleeding, 784–785
of endometrial carcinoma, 788–790
of endometrial hyperplasia, 787–788, 790
of endometrial polyps, 785–786
of intrauterine adhesions, 789
of normal endometrium, 783
of postmenopausal bleeding, 771–772, 775, 783–784, 791–793
of retained products of conception, 789–790
of subendometrial changes, due to tamoxifen, 790–791
of submucosal leiomyomas, 787
patient preparation for, 781–782
versus hysteroscopy, 793–794

Spiral CT, of small bowel, versus multislice CT, 200–201

Spiral MR imaging, physics of, 9–12

Splenic injuries, nuclear medicine studies of, 1286

Splenic rupture, and intraperitoneal hemorrhage, 1192–1193

Stanford classification, of aortic dissection, 532

Steady-state free precession, in MR angiography, 33

Steatosis, MR imaging of, 77–79

Stein-Leventhal syndrome, MR imaging of, 184–185

Stepladder sign, in ultrasonography, of breast implants, 852

Sternal fractures, multislice CT of, 606–607

Streak artifacts, in multislice CT, of thoracic aorta, 531

Stress imaging, of cardiovascular disease, 17–18

Stromal tumors, gastrointestinal, multislice CT of, 210–211

Struma ovarii, MR imaging of, 808

Subcapsular hematomas, and hypertension, 926–927
imaging of, 1027

Subclavian veins, multislice CT of, 553–554

Superior vena cava, multislice CT of, 549–551

Surface epithelial tumors, ovarian, MR imaging of, 804–805

Susceptibility artifact, on fetal MR imaging, 737

T

Takayasu's arteritis, and hypertension, 921

Tamoxifen, and assessment of postmenopausal bleeding, 776–777
subendometrial changes due to, sonohysterography of, 790–791

T-cell lymphomas, of small bowel, CT enteroclysis in, 255–256

Teratomas, ovarian, MR imaging of, 185, 808

Terminal ileitis, CT of, 1129, 1131

Teslascan, in MR imaging, 54–55

Tethering of folds, of small bowel, differential diagnosis of, 347–349

Thecomas, MR imaging of, 805

Thoracic aorta, MR angiography of, 34
multislice CT of, **523–545**
difficulties in, 530–531
kilovoltage and milliampere, 530
motion artifacts, 531

poor contrast enhancement, 530
streak artifacts, 531
for acute traumatic injury, 479, 541–542, 608–612
for aortic aneurysms, 536–538
for aortic dissection, 532–536
for atherosclerotic vascular disease, 531–532
for intramural hematomas, 538–539
for mycotic aneurysms, 540–541
for penetrating atherosclerotic ulcer, 539–540
normal anatomy in, 525–526
normal variants in, 526
pitfalls in, 526–531
anemia, 529–530
left brachiocephalic vein, 527
left inferior pulmonary vein, 527
left lower lobe atelectasis, 529
left pleural effusion, 529
left superior intercostal vein, 527
mediastinal masses and adenopathy, 529
normal anatomic structures, 526
periaortic pathology, 528–529
pericardial effusion, 529
pericardial recesses, 527
right atrial appendage, 527
thymus, 527–528
postoperative, 542–543
techniques for, 523–525
collimation, 523–524
contrast administration, 524–525
field-of-view, 524
kilovoltage and milliampere, 525
pitch, 524
reconstruction increment, 524
tube rotation time, 525

Thoracic cage trauma, multislice CT of, 603–604

Thoracic inlet syndrome, multislice CT of, 479–480

Thoracic outlet syndrome, multislice CT of, 479–480

Thoracic spine trauma, multislice CT of, 604, 606

Thoracic trauma, multislice CT of, **603–620**
diaphragmatic injuries, 617–618
esophageal injuries, 613
nonaortic thoracic vascular injuries, 612
pericardial injuries, 612–613
pleural effusion and hemothorax, 608
pneumomediastinum, 607–608
pneumothorax, 607–608
pulmonary contusions, 614
pulmonary lacerations, 614
sternal injuries, 606–607
thoracic aorta injuries, 608–612
thoracic cage injuries, 603–604
thoracic spine injuries, 604, 606
tracheobronchial injuries, 614–617

Thoracic veins, central, MR angiography of, 37

Thoracic venous anatomy, multislice CT of, **547–562**
advantages of, 547–548
azygos, hemiazygos, and accessory azygos systems, 558–559
inferior vena cava, 551–553
intercostal chest wall and paraspinal veins, 559–560
pericardiophrenic, cardiac, coronary sinus, and saphenous vein grafts, 554–555, 558
pulmonary veins, 560–561
subclavian, jugular, and brachiocephalic veins, 553–554
superior vena cava, 549–551
volume-rendering techniques for, 548–549

Thorax, multislice CT of, **475–491**
in children. *See* Multislice CT.
pulmonary applications, 482–486, 488
chest wall and diaphragm, 486, 488
diffuse and focal lung disease, 482–484
tracheobronchial tree, 484–486
techniques for, 475–476
radiation dose, 476
three-dimensional maximum and minimum intensity projection, 475–476
three-dimensional multiplanar reconstruction, 475
three-dimensional shaded surface display and volume rendering, 476
vascular applications, 476–480, 482
cardiac imaging, 476–478
pulmonary arteries and veins, 480, 482
systemic arteries, 478–480

Three-dimensional imaging, with multislice CT, of small bowel, 201

Three-dimensional ultrasonography, of postmenopausal bleeding, 775–776

Three-dimensional volumetric analysis, in ultrasonography, of pelvic floor relaxation, 755

Thromboembolism, and mesenteric ischemia. *See* Mesenteric ischemia.
catheter-associated, angiography of, in infants, 937
ultrasonography of, in infants, 933
chronic, management of, 517–519

Thrombosis, abdominal aortic, CT of, 1164
portal vein, MR imaging of, 81, 84, 1247

renal artery, ultrasonography of, in infants, 932
renal vein, MR imaging of, 1269
ultrasonography of, in infants, 932

Thymus, multislice CT of, 527–528

Time-of-flight MR angiography, technique for, 115–116

Time-resolved two- and three-dimensional digital subtraction angiography, technique for, 139

Torsion, ovarian, MR imaging of, 809

Trabecular bone structure, in osteoporosis. *See* Osteoporosis.

Tracheobronchial injuries, multislice CT of, 614–617

Tracheobronchial tree, multislice CT of, 484–486

Tracheobronchomalacia, diagnosis of, 631–632
multislice CT of, **631–640**
dynamic imaging in, 632–634
interpretation of, 635, 637–638
techniques for, 634–635
tracheoplasty for, 638–639

Transvaginal ultrasonography, of tamoxifen-induced subendometrial changes, 792

Trauma, abdominal, multislice CT of, 1086–1087
abdominal aortic, CT of, 1162–1163
blunt abdominal, and intestinal perforation, 1106
gallbladder, diagnosis of, 1210–1211
renal. *See* Renal trauma.
solid organ, nuclear medicine studies of, 1285–1286

Triploidy, ultrasonography of, in first trimester, 684, 686, 691

Triploidy syndrome, ultrasonography of, in second trimester, 698–699

Trisomy 13, ultrasonography of, in second trimester, 698

Trisomy 18, ultrasonography of, in second trimester, 696–698, 702, 704

Trisomy 21, ultrasonography of, in second trimester, 696

Tuberculosis, of small bowel, differential diagnosis of, 357
ovarian, MR imaging of, 808–809

Tuberous sclerosis, and hereditary renal cancer, 1046

Tubo-ovarian abscesses, MR imaging of, 808–809

Tubo-ovarian complex, MR imaging of, 185–186

Tubular bowel, differential diagnosis of, 360

Turner syndrome, ultrasonography of, in second trimester, 698

Twin embolization syndrome, ultrasonography of, 719

Twins, monochorionic. *See* Monochorionic twins.

Twin-twin transfusion syndrome. *See* Monochorionic twins.

Typhlitis, CT of, 1132–1133

U

Ulcers, penetrating atherosclerotic, multislice CT of, 539–540, 1162
peptic, and intraperitoneal hemorrhage, 1194–1195
perforation of, 1101–1102, 1241

Ultrasonography, Doppler. *See* Doppler imaging.
fetal, versus fetal MR imaging, 729
in first trimester, **663–679, 681–693,** 704–705
of anterior abdominal wall, 683–684
of central nervous system, 681–682
of congenital heart disease, 684
of conjoined twins, 691–692
of early pregnancy failure, 668, 670
of ectopic pregnancy, 670–674
adnexal mass in, 672–673
endometrium in, 673
free fluid in, 672
management of, 674
serum hCG levels in, 673–674
of fetal abnormalities, 674–676
nuchal translucency, 674–676, 682, 704
of fetal structural abnormalities, 676–677
of genitourinary tract, 684
of normal pregnancy, 663–667
age assessment in, 667
embryonic pole in, 666
gestational sac in, 663–665
heartbeat in, 666–667
yolk sac in, 665–666
of triploidy, 684, 686, 691
of umbilical cord, 682–683
transducer technology in, 663
of acute mesenteric ischemia, 326–327
of aneuploidy. *See* Aneuploidy.
of appendicitis, 1118–1119
of breasts. *See* Breasts.

of cholecystitis, 1248
of gallbladder disorders. *See* Gallbladder disorders.
of gastrointestinal disorders. *See* Gastrointestinal disorders.
of hypertension, in infants, 931–935
of intraperitoneal hemorrhage, 1185–1186
of intussusception, 1145–1147
of monochorionic twins. *See* Monochorionic twins.
of pelvic floor relaxation, 749
of postmenopausal bleeding. *See* Postmenopausal bleeding.
of postoperative small bowel, 304
of renal trauma, 1019
of ruptured ovarian cysts, 1197–1198
of urinary lithiasis, versus CT, 988
quantitative, of osteoporosis, 824–825
of trabecular bone structure, in osteoporosis, 830
transvaginal, of tamoxifen-induced subendometrial changes, 792

Ultrasound contrast agents, in renal imaging, **961–976**
intraoperative, 973
microbubble-specific techniques for, 962–963
of angiomyolipomas, 963–965
of cystic masses, 965–968
of indeterminate masses, 969, 971
of infarcts, 971–972
of pseudotumors, 968
of pyelonephritis, 972–973
of renal artery stenosis, 971
of renal cell carcinoma, 963
of renal perfusion, 971–973
of trauma, 973

Umbilical cord, ultrasonography of, in first trimester, 682–683

Umbilical cord sampling, to diagnose aneuploidy, 696

Unicornuate uterus, MR imaging of, 181

Ureteral complications, of renal transplantation, MR imaging of, 1013

Ureteropelvic junction injuries, imaging of, 1029–1030

Urethra, MR imaging of, 410–412

Urinary lithiasis, CT of, **977–997**
advantages and disadvantages of, 977–978
interpretation of, 980, 982–987
radiation in, 987–988
technique for, 978–980
versus MR imaging, 988, 990
versus ultrasonography, 988
versus phleboliths, 980, 982–983

Urinary tract infections, MR imaging of, 1267

Urography, CT. *See* CT urography.
intravenous, of renal trauma, 1018
MR. *See* MR urography.

Urolithiasis, CT of, 867–868, 872
multislice CT of, in children, 657

Urothelial tumors, MR imaging of, 878

Uterine anomalies, congenital, and female infertility, 759–760

Uterine bleeding, dysfunctional, sonohysterography of, 784–785

Uterine cavity filling defects, and female infertility, 758–759

Uterine fibroids, hereditary leiomyoma renal cell carcinoma and, 1043

Uterine leiomyomas, and postmenopausal bleeding, ultrasonography of, 773

Uterine prolapse, MR imaging of, 412–413

Uterus, in female infertility, 758

Uterus didelphys, MR imaging of, 181

V

Vagina, MR imaging of, 410–412

Vaginal vault prolapse, evacuation proctography of, 402

Valium, in enteroclysis, 217

Valvular heart disease, MR imaging of, 21

Vascular system, multislice CT of, 1089–1090

Vasculitis, and mesenteric ischemia, 333–334
CT of, 333–334

Vena cava, renal tumor extension into, 1058–1059

Ventricular function, MR imaging of, 25

Versed, in enteroclysis, 217

Vesical congestion, of bladder, MR imaging of, 172

Virtual angioscopy, of acute thoracic aortic injuries, 611

Virtual bronchoscopy, of central airways, 572–573
of tracheobronchial injuries, 616–617
of tracheobronchial tree, 486

Virtual colonoscopy, **375–393**
alternate views in, 382–383
computer-aided detection in, 383–384, 386–387, 391
extracolonic findings in, 383
historical aspects of, 375–376
interpretation of, 379–382
primary 2D read, 379–381
primary 3D read, 381–382
MR imaging with, 383
patient selection for, 377, 379
polyp size and flat lesions in, 376–377
radiation dose in, 383
to screen for colon cancer, 376
wall thickening in, 383

Visceral artery abnormalities, and intraperitoneal hemorrhage, 1193–1194

Voiding cystourethrography, of pelvic floor relaxation, 749

von Hippel–Lindau disease. *See* Hereditary renal cancer.

Y

Yolk sac, ultrasonography of, 665–666